Investigating the Design of Bisphosphine Ligands for use in Nickel-catalyzed C(sp^2)-N Cross-Coupling

by

Jillian S. K. Clark

Submitted in partial fulfillment of the requirements
for the degree of Doctor of Philosophy

at

Dalhousie University
Halifax, Nova Scotia
November 2019

Table of Contents

List of Schemes

List of Figures

Abstract

Notwithstanding the matured protocol of palladium-catalyzed C(sp^2)-N cross-coupling (Buchwald Hartwig Amination, BHA), the development of nickel-based catalysts that carry out analogous transformations is motivated both by the benefits of employing Earth-abundant, cost-effective first-row transition-metals, and the potential for nickel catalysts to unveil new modes of reactivity. Over the past five years, significant advances in nickel-catalyzed amination chemistry have led to a widespread interest and expansion of this methodology. Although nickel catalysts are highly effective in the cross-coupling of ammonia, alkylamine, indole, and primary amide nucleophiles with (hetero)aryl electrophiles, these catalytic systems have yet to contend with palladium analogs in terms of exceedingly low catalyst loadings and the turnover of increasingly challenging substrate classes. Whereas BHA benefits from an unambiguous set of criteria that defines optimal ancillary ligand properties for this palladium-catalyzed transformation, structure-reactivity trends for nickel counterparts are ill-defined. Additionally, complex mechanistic details exist for nickel-catalyzed C(sp^2)-N cross-coupling, which may be responsible for the vague guidelines for optimizing ancillary ligands, and the need for higher catalyst loadings.

My thesis work explores ancillary ligand design criteria for nickel-catalyzed C(sp^2)-N cross-coupling by cross-examining top-tier bisphosphine ligand classes with aims of clarifying the apparently divergent properties that exist among state-of-the-art ancillary ligands. Information gathered from the systematic comparisons of these ligand classes results in the development of the new bisphosphine ligand, PAd2-DalPhos, which enables the hitherto unknown nickel-catalyzed C(sp^2)-N cross-coupling of primary heteroarylamines with (hetero)aryl chlorides. This chemical transformation is highly sought-after by pharmaceutical chemists for the synthesis of heteroatom-dense molecular structures, and reveals a new mode of reactivity involving challenging substrates in the context of nickel catalysis.

List of Abbreviations and Symbols Used

Chemical Notation and Abbreviations

Cy	cyclohexyl
***o*-tol**	*ortho*-tolyl
1-nap	1-naphthyl
fur	furanyl
Ar	aryl
Ts	tosyl
dba	dibenzylideneacetone
PTFE	polytetrafluoroethylene
DMSO	dimethylsulfoxide
TMEDA	tetramethylethylenediamine
CPME	cyclopentylmethylether
THF	tetrahydrofuran
COD	1,5-cyclooctadiene
PCg	1,3,5,7-tetramethyl- 2,4,8-trioxa-6-phosphaadamantyl
DME	dimethoxyethane
NHC	N-heterocyclic carbene
NHP	N-heterocyclic phosphine
IPr	1,3-bis(2,6-di-*i*-propylphenyl)imidazole-2-ylidene
DPPF	1,1'-bis(diphenylphosphino)ferrocene
D*i*PPF	1,1′-bis(diisopropylphosphino)ferrocene
DTBPF	1,1′-bis(di-*tert*-butylphosphino)ferrocene
DCPF	1,1′-bis(dicyclohexylphosphino)ferrocene
BINAP	2,2'-bis(diphenylphosphino)-1,1'-binaphthyl
DAIPEN	(2*S*)-(-)-bis(4-methoxyphenyl)-3-methyl-1,2-butanediamine
CyPF-Cy	(R)-(-)-1-[(S)-2-(dicyclohexylphosphino)ferrocenyl]ethyldicyclohexylphosphine

Terms

ee	enantiomeric excess
BHA	Buchwald-Hartwig Amination
NMR	nuclear magnetic resonance
GC	gas chromatography
DFT	density functional theory
S_NAr	nucleophilic aromatic substitution
HRMS	high resolution mass spectrometry
ESI	electrospray ionization
TLC	thin-layer chromatography
UDEFT	uniform driven equilibrium Fourier transform

Miscellaneous

rac	racemic
1°	primary
2°	secondary
etc.	etcetera
i.e.	id est
e.g.	exempli gratia
sec	secondary
t or ***tert***	tertiary
ca.	circa
equiv	equivalents

COMPOUND NUMBERING NOTE: For the purposes of this thesis, ligands are labeled as **L0**, **#-L#**, or $\mathbf{L^X}$, and nickel(II) pre-catalysts labeled as **C0 or #-C#**.

Acknowledgments

I express my sincerest gratitude to my graduate supervisor Dr. Mark Stradiotto for his unwavering support, guidance, and well-founded advice. The generosity and attentiveness he has offered me over the course of my degree cannot be matched. He has played a prominent role in my personal and professional development, and I am incredibly fortunate to have had the opportunity to work with him.

I thank current and past Stradiotto group members Nicolas Rotta-Loria, Carson Wiethan, Alicia Chisholm, Joseph Tassone, Alex Gatien, Ryan Sawatsky, Preston MacQueen, Chris Voth, Carlos Diaz Lopez, Ryan McGuire, Melody (Yue) Shen, and Sam Dudra for their teamwork, advice, and comradery. Utmost gratitude is extended to my mentor Chris Lavoie for his guidance and support during my undergraduate and graduate degree, as well as our continued friendship which I hold dear.

I acknowledge Dr. Mike Lumsden (NMR3) for assistance in conducting NMR experiments, Mr. Xiao Feng for collecting mass-spectrometry data, and Dr. Robert McDonald and Dr. Michael Ferguson (University of Alberta) for X-ray crystallographic data, all of whom have contributed to the work reported herein. I extend gratitude to the members of my thesis committee, Dr. Laura Turculet, Dr. Alex Speed, and Dr. Norm Schepp for their well-received advice and supervision of my thesis progress. The Natural Sciences and Engineering Council (NSERC) of Canada, the Nova Scotia Graduate Scholarship program, the Killam Trusts, the Chemistry Graduate Student Society (CGSS), the Department of Chemistry, and Dalhousie University are thanked for providing funding.

I am grateful to my family and friends who have acted as my support network during my graduate work. My partner Haleigh Atwood has given unconditional support and love throughout the entirety of my degree, and I am wholly grateful and incredibly fortunate for her companionship.

Finally, I extend gratitude to my physical and mental health, which have presented hurdles throughout the course of my studies. They have truly been the greatest teachers in the cultivation of my mental fortitude, and have taken me on an incredible path of mindfulness bordered by meditation, yoga, mountains, and culinary pursuits.

Chapter 1. Introduction

1.1. Introduction to Catalysis

1.1.1. Overview

The widespread use of catalysis in chemical synthesis has opened new avenues in the production of natural products, materials, and pharmaceuticals. The use of sub-stoichiometric amounts of a catalytic reagent to facilitate otherwise challenging reactions under milder conditions has enabled the construction of complex molecules and synthetic building blocks, while demonstrating functional group tolerance and in some cases various forms of selectivity. Catalyst types can range from structurally complex enzymes derived from biological sources, to architecturally designed organocatalysts, to discrete and well-defined transition-metal complexes. Catalytic technologies have improved existing synthetic protocols through enhancement of the overall reaction efficiency by providing a lower energy transition state relative to the uncatalyzed pathway, resulting in an increased reaction rate.[1] For example, the enzyme orotidylate decarboxylase turns over the desired uridine monophosphate product with a half-time of 18 milliseconds, whereas the uncatalyzed reaction would proceed with a half-time of 78 million years.[2]

Catalysts can offer the benefit of selectivity, which alleviates process and purification challenges by creating one enantiomer, diastereomer or regioisomer. In the absence of a catalyst, the same reaction may create an uncontrolled mixture of stereo- or regioisomers which would reduce the yield of the desired product and complicate purification. The Corey-Bakshi-Shibata catalyst (Scheme 1-1) can selectively reduce ketones in high enantiomeric excess (ee), enabled by the intelligent design of a chiral oxazaborolidine organocatalyst that imparts enantioselectivity through the use of a chiral auxiliary and a Lewis acid co-catalyst.[3, 4]

Since catalysts facilitate highly efficient syntheses through improved product yields, shortened reaction times, sensitive functional group tolerance, high selectivity, and milder reactivity, this technology has been exploited to create meaningful amounts of organic products for industrial use. An example is the Takasago-Noyori process for the production of (-)menthol (Scheme 1-2), which is a naturally occurring terpenoid that is commonly used in pharmaceuticals and other consumer products. The catalytic processes involved in the synthesis of (-)-menthol are featured in a five-step modification of the

naturally occurring terpene myrcene. One step employs Noyori's homogeneous BINAP-Rh catalyst to affect an asymmetric isomerisation from achiral geranyldiethylamine to the enantiomerically pure enamine. Subsequent heterogeneous nickel-catalyzed hydrogenation of isopulegol furnishes (-)-menthol.[5, 6] The mass production of this commodity chemical is achieved without the costly and unsustainable task of isolating the terpenoid from the natural source, and accesses higher enantiomeric excess than can be obtained from nature. This process has allowed global production to exceed 19, 000 tonnes, a quarter of which was used for pharmaceuticals.[1]

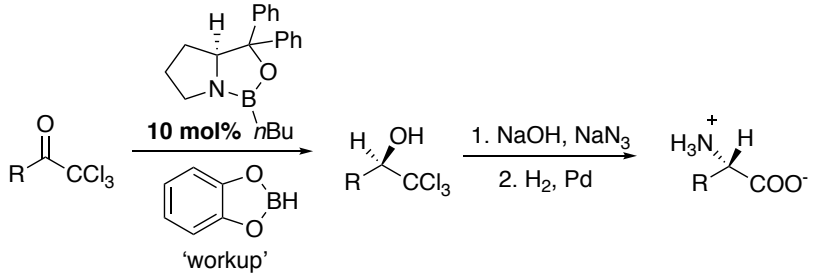

Scheme 1-1. Synthesis of (*S*)-α-amino acids from trichloromethyl ketones using the Corey-Bakshi-Shibata catalyst. The average ee of the intermediate (*R*)-(trichloromethyl)carbinol is ~95% and average yield of (*S*)-α-amino acids is ~93%.[3]

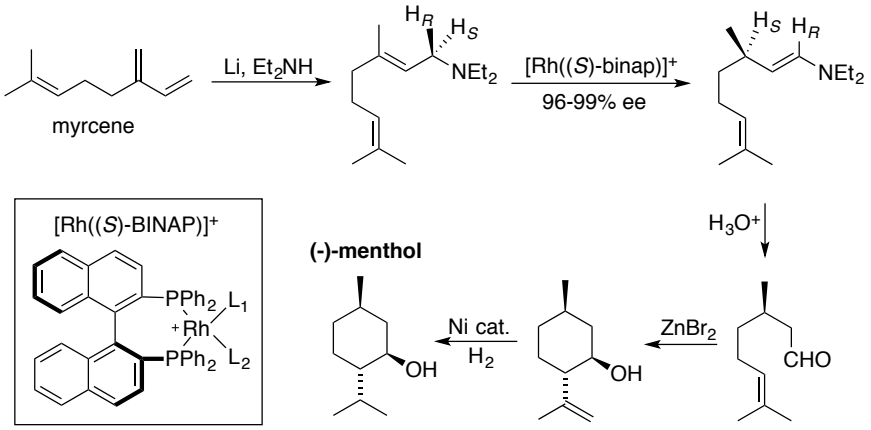

Scheme 1-2. Rhodium-catalyzed asymmetric allylic amine isomerization (Takasago-Noyori process). Ligand assignments for [Rh((*S*)-BINAP)]$^+$: L^1, L^2 = THF, acetone; L^1 = L^2 = COD, (*S*)-BINAP, η^3-enamine; L^1 = L^2 = N-coordinated enamine.[5, 6]

1.1.2. Concepts in Transition-Metal Catalysis

Transition-metal catalysis has moved to the forefront of modern catalytic methods used for organic synthesis. This is due in part to the high degree of modularity associated

with organometallic complex scaffolds which gives access to catalyst complexes with sought-after reactivity characteristics. The judicious choice of transition-metal, concurrent with the ability to fine-tune ancillary ligands, allows for controlled reactivity. Effects of catalyst design may include ligand sterics guiding the orientation of an incoming substrate, an electronic effect conferred by the ligand onto the metal allowing for chemoselectivity and substrate preference, or the choice of metal to optimize metal-substrate interactions. Transition-metal catalysis can offer a myriad of possible transformations, which include, but are not limited to: carbon-carbon and carbon-heteroatom cross-coupling, hydrogenation, small molecule activation, α-arylation, hydroformylation, and polymerization reactions.[7]

The general concept of transition-metal catalysis typically involves modification to a reaction profile that is thermodynamically favourable and features a high activation barrier. The inclusion of a transition-metal catalyst renders the route from starting material to product more kinetically favourable by replacing one energetically taxing reaction pathway with a series of alternative elementary reaction steps comprising an overall lower energy barrier.[8] These alternative steps involve reactions occurring directly at the metal centre with starting reagents, where the d-orbitals of transition-metals can interact with the molecular orbitals of organic molecules to create new organometallic compounds that can further undergo transformations. These elementary reactions that occur at the metal centre include, but are not limited to: oxidative addition, reductive elimination, transmetallation, insertion reactions, and hydride eliminations. Several of these steps are feasible due to the ability of transition-metals to access multiple oxidation states.[9] Transition-metal catalysts increase the rate of a reaction without being consumed due to the propensity for transition-metal catalysts to regenerate after the completion of a catalytic cycle, and as such can be used in sub-stoichiometric amounts.

Transition-metal catalysts can be divided into two categories based on the phase in which they operate in a reaction medium: heterogeneous catalysis, where reactants and catalyst are not in the same phase; and homogeneous catalysis, which allows for interaction between reagents and catalyst in the same phase. There are benefits and disadvantages to each method depending on the desired outcome. Heterogeneous transition-metal catalysts are typically thermally robust and easier to separate from a reaction mixture, which often

allows for recycling of the catalyst; however, the mechanism of heterogeneous catalysts is often poorly understood due to ill-defined reactive sites. Conversely, homogeneous catalysts have well-defined active sites, are highly modifiable, operate under less harsh conditions allowing for thermally sensitive molecules to be crafted, and are relatively well understood from a mechanistic standpoint. Nonetheless, it is challenging to separate the homogeneous catalyst from the reaction mixture,[10] rendering catalyst removal and recovery problematic.

1.2. Ancillary Ligand Design in Transition-Metal Catalysis

Incorporating an appropriate ancillary ligand for a homogeneous transition-metal catalyzed reaction can profoundly influence the outcome of the chemical transformation. Ancillary ligands are molecules that act as adducts to transition-metals and are made up of organic or main-group fragments that bind to metals either through dative or covalent interactions. The ligand can exert both an electronic influence on the metal and steric modification of the spatial environment surrounding the metal centre. Manipulation of the ligand's donor atoms through structural modification of the substituents on the donor atoms or ligand backbone gives rise to these influences. Alteration of the ligand's denticity, a term that denotes the connectivity of the donor atoms within a ligand scaffold to a metal, also modulates the steric and electronic environment of the catalyst.[11] These tunable variables have allowed organometallic chemists to conceive elaborate ligand frameworks that afford highly selective and active catalysts. A rudimentary example of the influence of these modifications is the chelate effect, which describes the inclusion of a second donor atom within a monodentate ligand. The resultant metal-chelate favours ligand-to-metal binding relative to the bis(monodentate) analog,[12, 13] closes up potential reactive sites within the metal coordination sphere, and in most cases, encourages *cis* coordination of incoming substrates, which is often important for certain elementary reaction steps.

Building on the work depicted in Scheme 1-2, Noyori's cooperative hydrogenation of ketones (Scheme 1-3) using meticulously designed ruthenium catalyst systems demonstrates the beneficial effect of appropriately configured ancillary ligands for a specific application. The enantioselectivity imparted by the highly active catalyst *trans*-$RuCl_2$[(*S*)-XylBINAP][(*S*)-DAIPEN] results in part from the chiral pocket that the BINAP derivative generates when bound to ruthenium, which enforces the less sterically hindered

end of the ketone to orient within the metal-ligand pocket. The chiral diamine ligand DAIPEN works in tandem with BINAP to create the chiral environment that dictates which face of the catalyst the substrate approaches. Upon binding, cooperative metal-ligand catalysis transfers the hydridic Ru-H to the electropositive carbonyl carbon and the acidic N-H proton of the diamine to the electronegative oxygen (Scheme 1-3). This catalyst facilitates the hydrogenation of acetophenone to afford near quantitative yield of (*R*)-phenylethanol in 99% ee employing 0.001 mol% catalyst loading.[5, 14, 15]

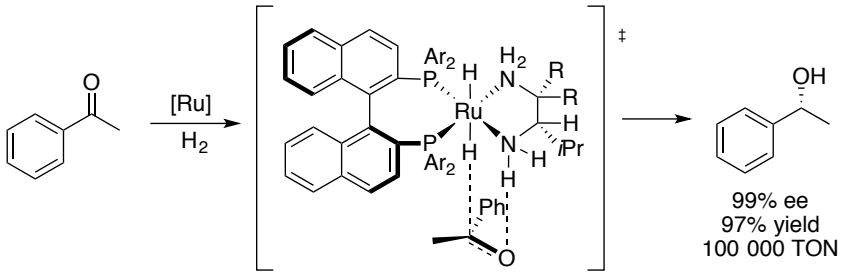

*Scheme 1-3***.** Noyori's asymmetric transfer hydrogenation of acetophenone. [Ru] = *trans*-$RuCl_2$[(*S*)-XylBINAP][(*S*)-DAIPEN], Ar = 3,5-xylyl, and R = *p*-anisyl. Reaction conditions: KO*t*Bu, 2-propanol, 1-10 atm H_2 and room temperature reactivity.[14, 15]

For a specific catalytic reaction, ligand design trends tend to emerge which guide the optimization of catalysts that facilitate more efficient reactions. This is often supplemented by identifying elementary steps within the catalytic cycle that are either rate limiting or off-cycle, followed by rational modification of the ligand framework to enhance that reaction step or deny access to deleterious pathways. Buchwald-Hartwig Amination (BHA), a reaction that generates aniline derivatives from the cross-coupling of an aryl halide with an amine in the presence of base and a palladium catalyst, serves as a useful example. The oxidative addition step can be turnover-limiting in this reaction, whereas the reductive elimination step is typically more facile,[16] although many exceptions do exist.[17] As such, ligands for BHA are often tailored to enhance oxidative addition by creating more electron donating and sterically encumbering ligands. These modifications result in an electron-rich metal that is readily oxidized in the presence of an aryl halide, while simultaneously stabilizing low coordinate reactive intermediates and assisting reductive elimination with enhanced steric bulk.[18] Electrophiles that are more difficult to engage in oxidative addition such as aryl chlorides can be accessed by use of these ligands.[19] The identification of this trend led to the widespread development of 'tailor-made' ligands for

BHA,[11, 20, 21] which in turn enabled chemists to tackle more challenging substrates, achieve continuously diminishing catalyst loadings, and establish mechanistic understanding. This work has collectively developed BHA into a state-of-the-art protocol for C(sp^2)-N bond formation.

1.3. Evolution of Transition-Metal Catalyzed C(sp^2)-N Cross-coupling

Arylamines are ubiquitous molecular fragments in pharmaceutical and natural products chemistry.[1, 20, 22] Traditional means of synthesizing arylamines (outlined below) can be low yielding, unselective, and involve harsh reaction conditions that may decompose organic molecules bearing sensitive functional groups (i.e., mixtures of nitric and sulfuric acids, high reaction temperatures). This can be problematic for multi-step protocols in cases where an amine fragment is installed on a functionalized aromatic ring toward the end of a synthesis. The most common method to make anilines before the advent of modern transition-metal catalysis involved the nitration of benzene using a nitronium ion, followed by reduction to the product aniline which, on a manufacturing scale, typically takes place in the gas phase using heterogeneous nickel or copper catalysts and hydrogen gas at temperatures between 200 - 400 °C.[23]

1.3.1. Overview of Ullmann Amination

In 1903 Ullmann reported the first example of transition-metal mediated aniline formation from aryl halides and amines with the use of stoichiometric copper reagents.[24] Shortly after, Goldberg reported the first copper-catalyzed arylation of amides, and subsequently a protocol for the copper-catalyzed arylation of amines, albeit at reaction temperatures above 200 °C (Scheme 1-4).[25] The role of copper catalysts or reagents for C(sp^2)-N bond formation is ambiguous in the sense that there is not a single discrete catalytic species within the Ullmann amination that is well-behaved in terms of reaction trajectory. Rather, there are several active and inactive copper intermediates caught within productive or cycle-deviating equilibria. This poses issues in understanding the nature of the productive copper species and limits rational catalyst optimization.[19, 26] Given the poor synthetic practicality of the method and mechanistic complexity at this early stage of development, the field of copper-catalyzed arylamine and arylamide formation remained largely undeveloped until transition-metal catalysis rapidly progressed in the latter half of the 20th century.

The use of copper in C(sp^2)-N cross-coupling was revisited in the late 1990s with aims to control the reactivity of the metal using carefully designed ancillary ligands. This lead to the identification of several monodentate and bidentate nitrogen and oxygen based ligands to facilitate cross-couplings employing milder conditions. Studies suggest that the choice of ligand can lead to differentiation between alcohol and amine nucleophiles in copper-catalyzed C(sp^2)-O and C(sp^2)-N cross-coupling, where copper species bearing more electron rich diketone ligands preferentially coordinate amines and electron deficient N,N- donors such as phenanthroline promote the binding of alcohols (Scheme 1-5).[26]

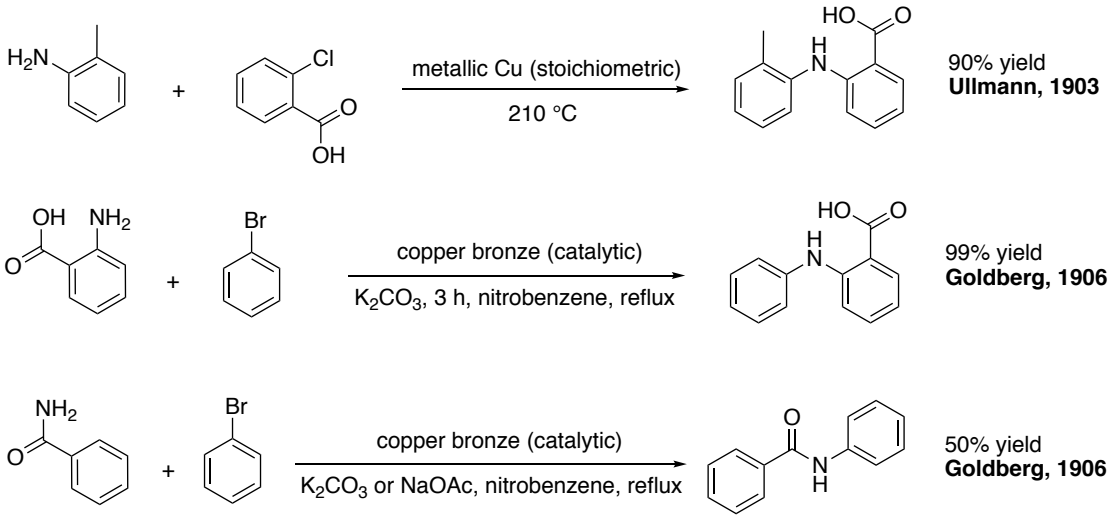

Scheme 1-4. Development of the copper-catalyzed *N*-arylation of amides and anilines.[26, 27]

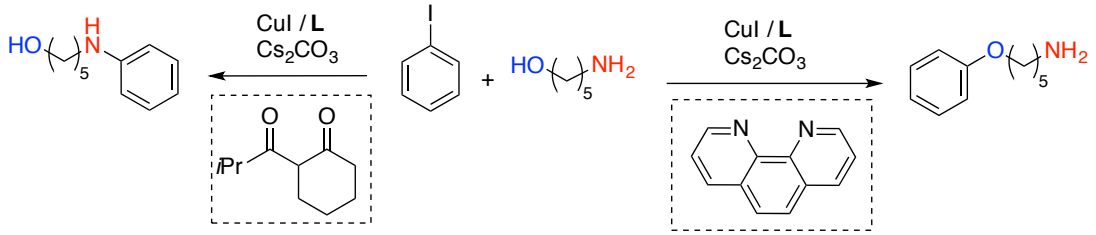

Scheme 1-5. Example of divergent selectivity through the choice of ancillary ligand in the Cu-catalyzed C(sp^2)-heteroatom cross-coupling. This selectivity arises through a reversal in the ordering of elementary steps: coordination of the nucleophile occurs initially when using the phenanthroline ligand with CuI, but oxidative addition is favoured by the neutral diketone ligated copper complex.[28]

Despite this progress, structural trends in terms of ligand design are not clear for these copper-based aminations, but rather several different ligand frameworks bearing the

same donor atom motif appear to work well. It was found that the observed improvement with the inclusion of an ancillary ligand was due to increased solubility of the catalyst and stabilization of coordinatively unsaturated intermediate copper (I) species, which prevents uncontrolled binding of the nucleophile to the metal centre.[19] The revival of the Ullmann reaction has modestly broadened the substrate scope: the formation of secondary and tertiary arylamines and arylamides, *N*-arylation of heterocycles and hydrazides, and inter- and intramolecular heterocycle formations can all be realized with copper catalysts.[26]

1.3.2. The Development of Buchwald-Hartwig Amination

Notwithstanding the benefits of base-metal catalysis, the development of copper-catalyzed amination chemistry was met with several drawbacks. The reactions require relatively high catalyst loadings and temperatures, and suitable substrates are limited to expensive aryl iodides and bromides partnered with a narrow range of amines. Additionally, the outcome of the reaction appears to be sensitive to a delicate balance of various reaction components rather than a dependence on the electronic nature or structure of the ancillary ligand alone. This eliminates the ability to control reaction outcomes in a given catalytic protocol. In fact, there are several examples of ligand-free copper catalyzed amination reactions where the solvent or substrates act as suitable ligands.[19, 26] Palladium-based catalysts are advantageous because specialized ligands that control the metal coordination sphere to form well-defined palladium complexes allow for challenging substrates to undergo amination chemistry with high selectivity and mild reactivity.

Palladium-catalyzed C(sp^2)-N cross-coupling was initiated in 1983 by Migita. This report paired tin amide reagents as nitrogenous nucleophiles with aryl bromides to form N,N-diethylaminobenzene derivatives using 0.1 mol% $PdCl_2(P(o\text{-tolyl})_3)_2$,[29] however the use of toxic and unstable aminostannanes presented a drawback to this method. The independent reports of Buchwald and Hartwig in 1995 featuring the use of free amines in place of tributyl tin amides represented a significant advance. The incorporation of a sterically hindered silyl amide or alkoxide base facilitated formation of the metal-amido intermediate necessary for product-generating C-N reductive elimination, using the same $PdCl_2(P(o\text{-tolyl})_3)_2$ system.[30, 31] Since the inception of this palladium-catalyzed reaction with free amines, coined Buchwald-Hartwig Amination (BHA), the breadth of substrate scope and mild reaction conditions undergo continual improvement, enabled in part by

ongoing ancillary ligand development. After identifying sterically hindered triaryl monophosphines as effective ancillary ligands for the coupling of secondary dialkyl- and arylalkylamines with aryl bromides, independent studies from Buchwald and Hartwig revealed that aromatic bisphosphine ligands (DPPF, *rac*-BINAP, and variants) could couple primary amines and aryl iodides employing catalyst loadings as low as 0.05 mol%.[32, 33] Chelating bisphosphines suppress undesired reactivity at the palladium centre (*β*-hydride elimination of acyclic alkylamines, uncontrolled binding of the nucleophile),[19] and their application has allowed for a near hundred-fold decrease in catalyst loading relative to the previous generation of ligands.[7]

For less activated aryl electrophiles, ligands comprising monodentate, bulky, and highly electron-rich donor atoms were subsequently applied to BHA protocols, including monophosphines such as cataCXium A, Q-Phos, and tri(*t*-butyl)phosphine.[34-36] Following this criteria, Nolan revealed the utility of NHCs for Pd-catalyzed amination. The use of an electron rich and bulky monodentate IPr/Pd based catalyst allowed for the coupling of aryl chlorides, bromides, and iodides with various alkyl and aryl appended primary and secondary amines.[37] Compared to chelating counterparts, monodentate ligands are susceptible to reversible connectivity to the metal centre and resultant isomerization which leads to poor control over the metal catalyst coordination sphere, and in some cases, can lead to undesired reactivity. Additionally, primary amines proved challenging as nucleophiles, and high catalyst loadings were needed in such reactions when using these bulky monophosphines.[38] Further ancillary ligand development led to equally hindered and donating ligands that stabilize low-coordinate palladium complexes through either a second donor atom (strongly coordinating or hemi-labile), *ipso* coordination to aryl portions of ligand backbones, and/or through overly bulky fragments that block open reactive sites.[19] This gave rise to large bite angle bis(dialkyl)phosphines, biaryl mono(dialkyl)phosphines, and mixed donor ligands, such as MorDalPhos;[39] some of these state-of-the-art ligands are depicted in Scheme 1-6. This most recent collection of ligands combines the chelation effect of the second generation aromatic bisphosphines with the steric bulk and highly electron-donating ability of third generation monodentate alkylphosphines to create ideal ligand properties that allow for exceedingly low loadings and/or mild conditions to be employed, even in challenging C(sp^2)-N cross-couplings. In result, the nucleophile scope

has henceforth been extended past primary and secondary alkylamines and anilines to ammonia, hydrazine, sulfoximines, hydrazones, N-H containing heterocycles, carbamates, amidines, (sulfon)amides, oxazolidinones and ureas, and the electrophile scope includes aryl chlorides, bromides, and iodides, heteroaryl halides, and sulfonates.[7, 22]

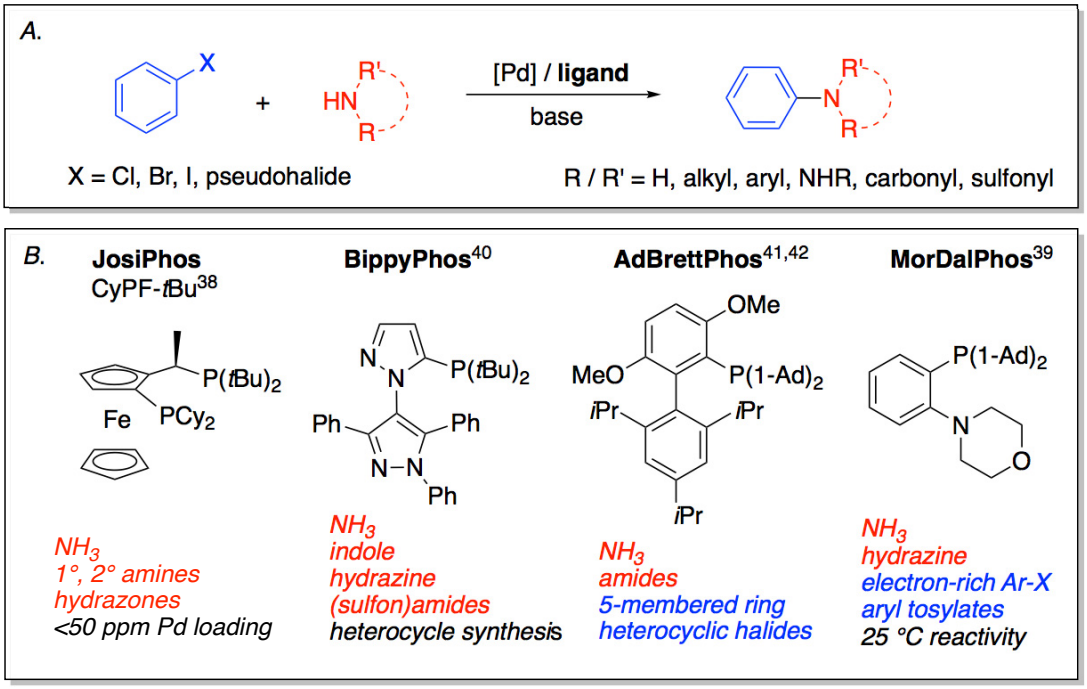

Scheme 1-6. Representative reaction scheme and premier ligands for BHA. *A*. Generic BHA reaction scheme. *B*. Highlights of the respective abilities of selected premier phosphine-based ligands for BHA.[38-42]

Continual advancement of state-of-the-art BHA catalysts is achieved through design improvements based on growing mechanistic data. For example, Buchwald and co-workers recently designed the biaryl monophosphine EPhos to prevent an unwanted metal coordination event involving the competitive binding of an arylmethoxy fragment within an existing ligand framework. Mechanistic details of a top-tier biaryl monophosphine, BrettPhos, identified a deleterious P,O-chelate that is in equilibrium with the productive P,C-chelate, which is formed through coordination of an aryl *ipso*-carbon atom to palladium. The P,O-bound isomer was found to be less efficient in the reductive elimination step relative to the P,C-chelating species. Steric modification of the ligand arising from replacing a methoxy fragment (BrettPhos) with isopropoxy (EPhos) dissuaded P,O-

chelation, allowed for improved reaction rates, and increased product yields with hindered and highly complex heterocyclic substrates.[43]

1.3.3. Nickel-catalyzed C(sp^2)-N Cross-coupling

Using palladium for C(sp^2)-N cross-coupling has inarguably made a substantial impact in the field of transition-metal catalysis, with major contributions spanning from the creation of entirely new libraries of ligands to the enabling of industrial scale syntheses of biologically relevant molecules.[1, 11, 20] Despite these crucial advancements in transition-metal catalyzed C(sp^2)-N cross-coupling, drawbacks associated with the use of palladium exist. Oxidative addition remains challenging for palladium-based catalysts, making economically attractive aryl chlorides and synthetically attractive phenol-derived aryl (pseudo)halides less accessible. The natural abundance of this metal and its reciprocal relationship with market cost renders palladium an unsustainable commodity if intended to maintain industrial demand.[44]

In light of these shortcomings, the development of nickel-based catalysts for use in analogous C(sp^2)-N cross-coupling chemistry has garnered recent interest. Nickel is viewed as a viable stand-in for palladium in BHA-type chemistry because it shares similar chemical properties with its heavier Group 10 analog. Nickel is often purported solely as a sustainable and cost-effective base-metal alternative; however, nickel exhibits a different reactivity profile to palladium, which could reveal complementary catalytic applications. For example, nickel more readily undergoes oxidative addition because it is the least electronegative Group 10 element, which opens up a more expansive scope of challenging electrophiles.[44] Unlike the two electron oxidation and reduction events associated with palladium, the ease of shuttling between one electron oxidation state changes for nickel offers the opportunity for unique catalytic reactivity, such as its role as co-catalyst in iridium-promoted photocatalysis.[45] This potential for radical chemistry may also complicate mechanistic understanding in other catalytic reactions, or even give rise to cycle-ending pathways. In particular, the interaction of nickel(II) and nickel(0) species can lead to comproportionation giving rise to nickel(I) species, which terminate catalytic cycles on a case-by-case basis.[46-52]

A surge of reports on nickel-catalyzed amine arylations have emerged in recent years, however the initial breakthrough surfaced seventy years ago[53] followed by sparse

reports appearing until the debut of BHA in the 1990s. Although high loadings of nickel(II) salts and nickel(0) complexes were employed at elevated temperatures, these early reports collectively demonstrated the propensity for nickel to cross-couple a limited scope of aryl electrophiles with piperidine and methylamine.[54] A promising insight into the divergent modes of reactivity between nickel and palladium was exposed in a 1995 study by Cristau and Desmurs. Comparison of nickel and palladium catalysts in the cross-coupling of aliphatic amines and aryl bromides revealed the exclusive formation of C-N cross-coupled product when using the former, whereas the latter readily formed hydrodehalogenated by-products, albeit using an inconsistent ligand motif.[55] In an effort to improve reaction efficiency and to expand the substrate scope, Buchwald and Wolfe reported *in situ* generated DPPF and 1,10-phenanthroline ligated nickel catalysts that facilitated cross-couplings of (hetero)aryl chlorides with primary and secondary (alkyl/aryl)amines using an alkoxide base and relatively lower catalyst loadings.[56] This seminal report provided the basis for later nickel amination catalyst development, involving catalysts featuring NHCs, simple tertiary phosphines, and bipyridine-type ancillary ligand scaffolds in the cross-coupling of alkylamines and anilines with (hetero)aryl (pseudo)halides.[54] Notably, transformations involving room temperature reactivity, low catalyst loadings (<1% Ni), and reactivity with challenging electrophiles such as aryl tosylates, anisoles, and aryl carboxylates were achieved by 2010.[57-61]

A 2014 report from Hartwig and co-workers details the cross-coupling of primary amines and unactivated (hetero)aryl chlorides using a *rac*-BINAP ligated nickel(0) catalyst that is stabilized by an η^2-coordinated benzonitrile ligand. The report also serves as a model study of the catalytic cycle for nickel-based amination chemistry.[51] It was proposed that the arylation of primary amines with the (BINAP)Ni(0) species follows a cross-coupling pathway akin to BHA (Scheme 1-7, where M = Pd). Cleavage of the carbon-halogen bond of an aryl halide affords the oxidative addition nickel(II) intermediate, which was shown to be the turnover-limiting step in the case of an aryl chloride; nucleophile binding in a dative fashion occurs, followed by a base-mediated transmetallation event to form a nickel(II) amido; lastly, C-N reductive elimination yields the product arylamine (Scheme 1-7, where M = Ni). Off-cycle pathways were identified, such as the formation of BINAP bis-ligated nickel(0), P-C cleavage of the BINAP backbone to generate P,C-chelated and

triarylphosphine-bound nickel, and extrusion of the bisphosphine by excess amine to yield an amine-ligated nickel(II) intermediate. Additionally, the nickel(I) dimer [(BINAP)Ni(μ-Cl)]$_2$ was catalytically incompetent in the cross-coupling of 4-chlorobenzotrifluoride and octylamine.

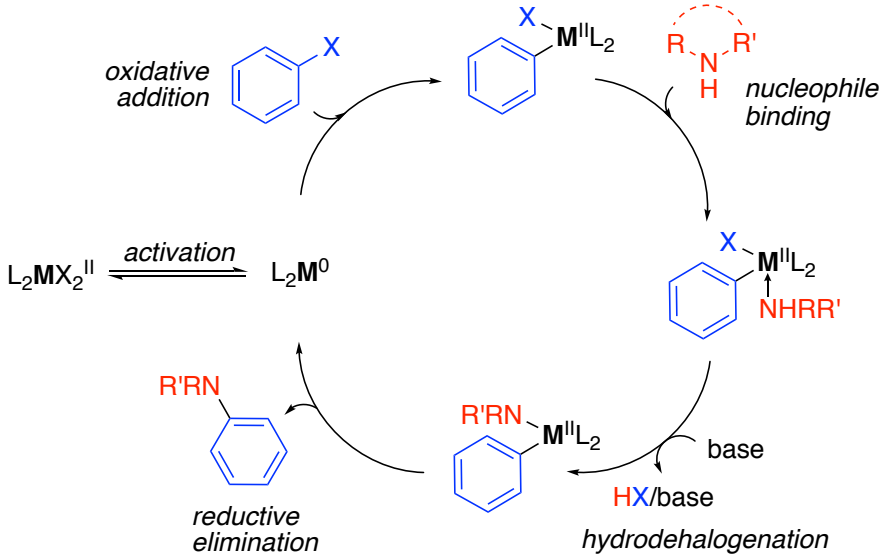

Scheme 1-7. Generic catalytic cycle for the transition-metal catalyzed C(sp^2)-N cross-coupling involving a redox cycle of $\mathbf{M}^0/\mathbf{M}^{II}$. **M** is nickel or palladium;[51,62] alternative postulated mechanistic pathways exist for the overall transmetallation step.[62-64]

In the same vein, Nicasio and co-workers recently explored the mechanistic details of the cross-coupling of 2-chloropyridine derivatives with indole using an IPr-supported nickel catalyst.[65] Stoichiometric reactions of isolated nickel(II) complexes that presumably lie on an operative Ni(0)/Ni(II) cycle (i.e., (NHC)Ni^{II}ArX, (NHC)Ni^{II}ArNHR) generated desired product, supporting an even electron manifold. Unlike Hartwig's report, this NHC-ligated system experiences a slow reductive elimination step and a nickel(II) amido resting state which was validated through kinetic, experimental, and computational analyses.

Although these reports currently represent a widely accepted Ni(0)/Ni(II) mechanism for the amination of aryl halides using nickel-based catalysts, recent reports have shown that some NHC-ligated[66] and bisphosphine-bound[67] nickel(I) pre-catalysts are competent (and sometimes better than nickel(II) pre-catalysts) in select C(sp^2)-N cross-coupling applications. A recent study from the Stradiotto group describes a viable competing Ni(I)/Ni(III) cycle for the amination or amidation of aryl chlorides.[67] In this

report, computational analysis supports the odd electron manifold *via* an initial net transmetallation sequence involving the amine nucleophile, followed by oxidative addition of the electrophile. Comparative experiments between bisphosphine ligated Ni^{I} and Ni^{II} pre-catalysts reveal case-specific catalytic competencies of each in select pairings of aryl chlorides with amides or amines, suggesting a delicate interplay between the choice of ligand, substrates, and catalyst oxidation state.

Since Hartwig's 2014 report,[51] disclosures of new nickel catalysts accessing increasingly challenging substrates frequently appear. In the same year, Buchwald reported a nickel(II) pre-catalyst resembling an oxidative addition intermediate (i.e., (DPPF)Ni(*o*-tolyl)Cl) that arylates primary and secondary amines, and N-H heterocycles such as carbazole and indole.[68] In 2015, the use of $(IPr)Ni^{0}(styrene)_2$ for the N-arylation of carbazole and indole derivatives was disclosed by Nicasio and co-workers.[69] The first mono-arylation of ammonia and ammonium salts using JosiPhos-ligated Ni^{II} and Ni^{0} catalysts was simultaneously reported by the groups of Hartwig and Stradiotto.[70, 71] In an effort to both circumvent the use of the expensive JosiPhos ligand class and access ammonia mono-arylation chemistry employing room-temperature conditions, the Stradiotto group developed the new bisphosphine ligand PAd-DalPhos. When used within a pre-catalyst scaffold ([PAd-DalPhos]Ni(*o*-tolyl)Cl), not only ammonia but a wide range of primary amines, amides, and lactams were coupled with a comprehensive scope of (hetero)aryl chlorides and phenol derived electrophiles.[72, 73] PAd-DalPhos has since been expanded into its own ligand class which has broadened the substrate scope for nickel-catalyzed amination methods.

Beyond these thermally driven nickel-based transformations exist newer catalytic technologies, namely electrochemically driven (i.e., E-amination)[74, 75] and photoredox catalysis.[45, 76] These two methods rely on the generation of a high energy Ni^{III} catalytic intermediate that experiences a favourable C-N reductive elimination. This is achieved *via* anodic electrochemical oxidation of a nickel(II) aryl amido species in the case of E-amination, and through a single electron transfer event between a triplet photoexcited state iridium(III) species and a nickel(II) arylamido in the case of photoredox catalysis. These methods collectively encompass a substrate scope of amino acid esters, protected oligopepitides and nucleosides, a sulfonamide, aliphatic amines, and (hetero)aryl bromides

and chlorides. Both of these methods circumvent the methodical design of ancillary ligands that promote challenging C-N reductive elimination through exogenous manipulation of the transition-metal oxidation state to effect energetically favoured elementary steps.

1.4. Approach to Ligand Design for Nickel-catalyzed C(sp^2)-N Cross-Coupling

For nearly a decade the approach to discovering an optimal ligand for a nickel-catalyzed C(sp^2)-N cross-coupling reaction was reliant on a trial and error system. This involves screening a collection of ligands made for BHA in a nickel-catalyzed amination reaction using controlled reaction parameters. Whichever ligand(s) give rise to the highest yield of aniline product within an allotted reaction time are selected for further reaction optimization (i.e. varying the solvent, concentration, base, nickel source, additives, etc.). Subsequently, the scope of the optimized catalyst system is examined. This protocol that repurposes palladium ligands for use in nickel catalysis, while in some cases effective, neglects the nuanced effects that the ligand imparts on the nickel catalytic system. This may exclude possible effects on the elementary steps of the catalytic cycle, and/or favoured nickel oxidation state. For example, in Stradiotto and co-workers report on the use of a JosiPhos-ligated nickel catalyst for the mono-arylation of ammonia, two variants of the ferrocenyl ligand were similarly competent and superior to the other BHA ligands and JosiPhos variants; however, one JosiPhos variant featured a less bulky electron-poor bis(trifluoromethyl)phenylphosphino fragment and the other featured moderately hindering electron-rich dicyclohexylphosphino donors (CyPF-Cy).[71] The divergent nature of the electronic properties of these ligand variants complicates our understanding of the donor requirements for this nickel-catalyzed reaction, and provides little insight for furthered improvement of this ligand class in such applications. The ambiguity that is associated with the current 'ligand repurposing' method calls for a re-examination of how to effectively advance the development of nickel-based amination catalysts. Particularly promising are approaches based on rational catalyst design, efficient identification, and mechanistic understanding of ancillary ligands and their function with nickel catalysts.

The first example of a ligand that was designed specifically for a nickel-catalyzed amination application is the bisphosphine PAd-DalPhos (Scheme 1-8, where R = *o*-tolyl).[72] Its structural features reflect the assumption of an operative Ni^0/Ni^{II} cycle (Scheme 1-7). Envisioning reductive elimination to be slow relative to analogous palladium chemistry

(Section 1.3.3), the phosphino substituents of PAd-DalPhos are less electron-rich than typical BHA alkylphosphines (Scheme 1-6) and are sterically hindered to better facilitate the reduction of nickel(II) arylamidos to low-valent nickel(0) species. These phosphino groups include a secondary dialkylphosphine that is constrained in a cage-like structure tethered by electronegative alkoxy linkages, and a somewhat electron poor yet hindered di-*ortho*-tolyl phosphino fragment. The (PAd-DalPhos)Ni(*o*-tolyl)Cl pre-catalyst forms a five-membered ring chelate through the bisphosphine connectivity. Despite being relatively electron-poor, challenging oxidative additions such as deactivated aryl chlorides and sulfonates are feasible with this catalyst. It also boasts selectivity for the mono-arylation of ammonia. A striking similarity in catalytic performance exists between nickel catalysts supported by PAd-DalPhos and CyPF-Cy despite the contrasting characteristics of the two ligands, apart from the denticity and donor motif. This convolution reinforces the subtle and poorly understood nature of ligand design for nickel-catalyzed amination.[77]

Since the inception of PAd-DalPhos, few reports of new ligands designed to enable nickel-catalyzed aminations have surfaced. In 2016, a bis-silylene ligand with a carborane linker was developed for the arylation of secondary amines and aniline using 0.5 mol% catalyst loading at elevated temperatures.[78] In the following three years CyPAd-DalPhos,[79] PhPAd-DalPhos,[80] and NHP-PAd-DalPhos[81] were added to the PAd-DalPhos family, which enable the arylation of cyclopropylamine, bulky primary amines, and the amination of heteroaryl chlorides with primary alkylamines, respectively. Although not directly pertaining to C(sp^2)-N cross-coupling, in 2017 Doyle and co-workers developed a specialized monophosphine for nickel-based Suzuki cross-coupling of acetals with aryl boroxines to form benzylic ethers.[82] This work was inspired by the ineffectiveness of repurposed ligands intended for palladium, and was supported by ligand parameterization studies to identify the key characteristics of superior ancillary ligands in this reaction. Ligands that worked well exhibited remote steric bulk, a term that describes a relatively small percent buried volume and a large Tolman cone angle. This characteristic serves as a key ligand guideline in the development of nickel-based catalysts due to the shorter bond lengths of organonickel complexes versus palladium or platinum. Since these ideal parameters were adjusted in response to the properties of the metal, Doyle proposes these

ligand characteristics may be more broadly applicable to other nickel-catalyzed cross-couplings.

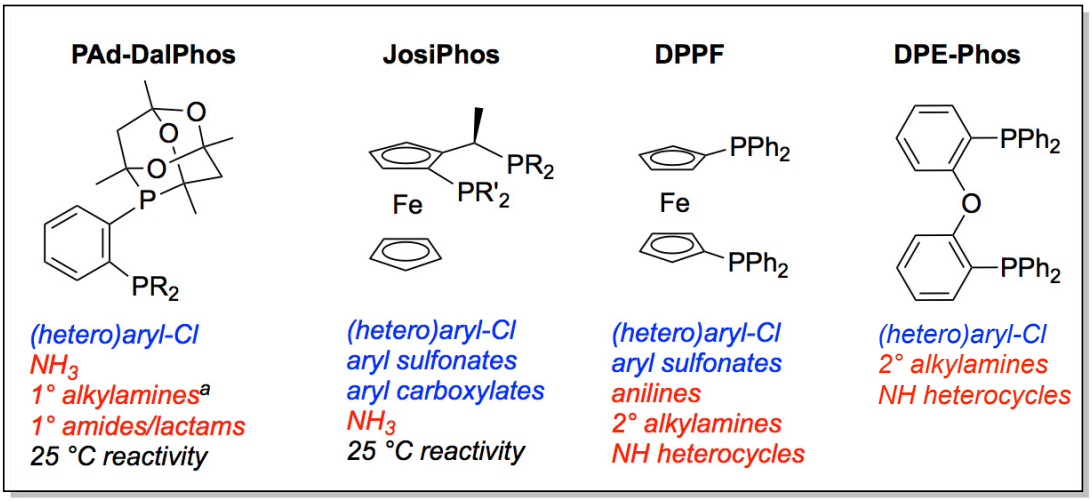

Scheme 1-8. Characteristic abilities of the most effective and commonly used bisphosphines for nickel-catalyzed C(sp^2)-N cross-coupling. [a] Includes cyclopropylamine and bulky 1° amines. From left to right: PAd-DalPhos ligand class, R = *o*-tolyl, phenyl, or cyclohexyl;[72, 73, 79, 80] JosiPhos family, R = cycloxhexyl or *t*-butyl, R' = cycloxhexyl or phenyl;[70, 71, 83, 84] DPPF;[56, 68, 85-89] and DPE-Phos.[90]

A high-throughput method of ligand identification was reported by Weix and collaborators at Pfizer,[91] which involves the mining of pharmaceutical compound libraries comprising 2.8 million N and O-containing heterocyclic substructures through successive refinement (i.e. specified core-structure searching; low molecular weight and non-propriety parameters) to identify effective ligands for nickel-based cross-electrophile coupling. This led to a significantly smaller library of *in silico* identified ligands derived from complex pharmaceutical compounds or building blocks that might not conventionally be considered as ancillary ligands for transition-metal catalysis. Catalytic screening of this narrowed ligand library led to the discovery of several pyridyl carboxamidines as superlative ligands for the cross-electrophile coupling of functionalized alkyl bromides with (hetero)aryl bromides compared to commonly used bipyridine-type ligands such as 4,4'-dimethoxybipyridine. Whereas the identification of exemplary ligands is often approached either through the design of new ligands or the variation of existing ligands, this complementary approach serves to accelerate the discovery of effective new ligand classes.

It is evident that repurposing BHA ligands is no longer a reliable method for developing effective nickel catalysts for C(sp^2)-N cross-couplings. Now that the field has a solid foundation with several reaction challenges addressed and a handful of effective ligand scaffolds, we can think about more rational ways to implement ligand design. In this regard, my thesis research focusses on a careful evaluation of the ligand properties (i.e., ligand backbone, donor substituents) of bisphosphine classes that have been successfully employed in nickel catalysis (i.e., DPPF, PAd-DalPhos). The data gathered from these surveys led to the development of PAd2-DalPhos, a ligand featuring ideal structural characteristics that give rise to robust catalytic performance and novel modes of reactivity in the context of nickel catalysis.

1.5. Overview of Thesis Work

This body of work involves the assessment of ligand frameworks that feature a common donor atom motif and are highly effective for nickel-based amination catalysis, with the intention of identifying trends in reactivity through either direct comparison of ligand classes or systematic variations within a ligand class. This selection of ligands includes the JosiPhos variant CyPF-Cy, the PAd-DalPhos family, and 1,1'-bis[di(alkyl/aryl)phosphino]ferrocenyl ligands (Scheme 1-8). The overarching goal of this work is to identify key ligand design trends that effect newfound or superlative reactivity in the context of nickel-based amination chemistry.

This work was initiated through an evaluation of the differences in catalytic performance between CyPF-Cy, PAd-DalPhos, and DPPF by means of comparative reactivity surveys. These involved C(sp^2)-N cross-couplings of representative substrate classes (i.e., furfurylamine as a linear primary alkylamine, *sec*-butylamine as a branched primary alkylamine) using competitively low nickel catalyst loadings to allow for differentiation of the ligands in terms of product yield. The selectivities of the ligands were also evaluated, such as preferences for (hetero)aryl (pseudo)halides and types of amines. The general theme of this research phase was to either identify a superior ligand among the three surveyed, or to establish abilities that are unique to each catalyst system. The results of this investigation are presented in Chapter 2.

Subsequently, a narrowed investigation into the effect of altering phosphino substituents within the 1,1'-bis[di(alkyl/aryl)phosphino]ferrocene framework was

conducted. This allowed for the elucidation of structure-reactivity trends within the DPPF ligand class. Steric and electronic variations of the phosphino fragments generated a small library of diverse alkyl- and arylphosphino ligands, which were compared in reactivity surveys between (hetero)aryl chlorides and amine substrates that are compatible with the parent bisphosphine (i.e., DPPF). Identification of the ineffective and superior variants allowed for further examination of the latter, with the intention of determining the specific properties of the phosphino substituents that give rise to desirable catalytic performance. This work is outlined in Chapter 3

The following phase of my research involves a systematic evaluation of both the phosphino donor substitution pattern and ligand backbone of PAd-DalPhos. This survey explored the effects on catalytic outcome when the parent ligand is spanned by various heteroaryl backbones that give rise to electronic differences, and compares regioisomers of the parent phosphino motif. The ligands whose properties offered superlative performance were carried forward in pre-catalyst syntheses for further competitive screening reactions versus PAd-DalPhos. The goal of this second round of screening was to identify structure-reactivity trends that will improve the current state-of-the-art for nickel-catalyzed amine arylations. These results are disclosed in Chapter 4.

The final research chapter of this thesis details the development of a new class of PAd-DalPhos ligands whose design was guided by the data generated in the preceding chapters. The tetramethyltrioxaphosphaadamantyl (PCg) moiety that is unique to the parent was doubly incorporated into a ligand set comprising (hetero)aryl backbones, whose catalytic abilities were shown to greatly outperform that of the parent in primary alkylamine couplings. Further exploration of the phenylene bridged ligand revealed a new mode of reactivity in the context of nickel catalysis. The ligand, coined PAd2-DalPhos, is capable of catalyzing the mono-arylation of primary heteroarylamines when used in a nickel pre-catalyst scaffold, which opens up a new class of substrates for this branch of catalysis.

Experimental details for Chapters 2-5 are provided in Chapter 6, and concluding remarks and proposals for future projects stemming from this work are found in Chapter 7. Supplementary experimental details and data are provided in the Appendix.

Chapter 2. Comparison of PAd-DalPhos, CyPF-Cy, and DPPF

2.1. Chapter 2 Overview

While collectively CyPF-Cy (**1-L1**), PAd-DalPhos (**L0**), and DPPF cover a broad scope of NH substrates, individually the successful application of each of these ancillary ligands in nickel-catalyzed C(sp^2)-N cross-coupling chemistry is demonstrated only for selected substrate classes (Scheme 1-8). In an effort to learn more about the relative abilities of these three ligands in nickel-catalyzed C(sp^2)-N cross-couplings, head-to-head reactivity comparisons were carried out employing a representative selection of aryl electrophiles and structurally varied NH substrates. Given the efficacy of catalysts based on either the electron-rich ligand **1-L1** or the comparatively electron-poor ligand **L0** in rather challenging nickel-catalyzed ammonia monoarylation chemistry, direct comparison of the reactivity behavior of structurally analogous nickel pre-catalysts featuring these electronically divergent ancillary ligand sets was of particular interest. In the case of **1-L1**, this required preparation of the hitherto unknown pre-catalyst (**1-L1**)Ni(*o*-tol)Cl (**1-C1**). In this chapter the synthesis and characterization of **1-C1** is reported, as well as the results of a comparative reactivity survey of (**L0**)Ni(*o*-tol)Cl (**C0**), **1-C1**, and (DPPF)Ni(*o*-tol)Cl (**1-C2**) in representative nickel-catalyzed C(sp^2)-N cross-coupling reactions.

2.2. Synthesis and Characterization of the Pre-catalyst (CyPF-Cy)Ni(o-tol)Cl

From a practical perspective, there is considerable interest in the development of air-stable nickel(II) pre-catalysts that can be reduced to the requisite nickel(0) species under catalytic conditions, without the required addition of an exogenous reductant. Given the utility of pre-catalysts of the type $\mathbf{L}_n$NiArX in this regard,[92, 93] including **C0**[72] and **1-C2**,[68] the complex **1-C1** was prepared. Combination of **1-L1** with $NiCl_2$(DME) to give the putative intermediate (**1-L1**)$NiCl_2$, followed by treatment with (*o*-tolyl)MgCl afforded **1-C1** in 76% overall isolated yield (Scheme 2-1, eq 1). The diamagnetic, air-stable complex **1-C1** was characterized by use of NMR spectroscopic and single-crystal X-ray diffraction techniques (Scheme 2-1). The crystal structure of **1-C1** reveals a distorted square planar geometry at nickel (Σ_{angles} at Ni ~ 360º), whereby the κ^2-*P*,*P*-(**1-L1**) ligand features chloride *trans* to the trialkylphosphine donor fragment. The *cis*-chelating bisphosphine in **1-C1** exhibits a P-Ni-P bite angle (~97.8º) that is intermediate between those found in the crystal structures of **C0** (~86.5º)[72] and **1-C2** (~102.0º).[68] Broadened signals are observed in the

NMR spectra of **1-C1** at 300 K, a characteristic that may be attributed to restricted rotation involving the Ni-C(*o*-tolyl) moiety. In the $^{31}P\{^{1}H\}$ NMR spectrum of **1-C1** at ambient temperature there exists an apparent doublet at 7.9 ppm and a broad signal at 47.3 ppm that does not exhibit splitting; however, at 200 K, the latter signal sharpens to a well-defined doublet with a mutual coupling constant to the signal at 7.9 ppm. Akin to the postulation made in the observed dynamics of **C0**,[72] this dynamic phenomenon may be attributed to hindered rotation of the Ni-C(sp^2) bond of the pre-catalyst at ambient temperature.

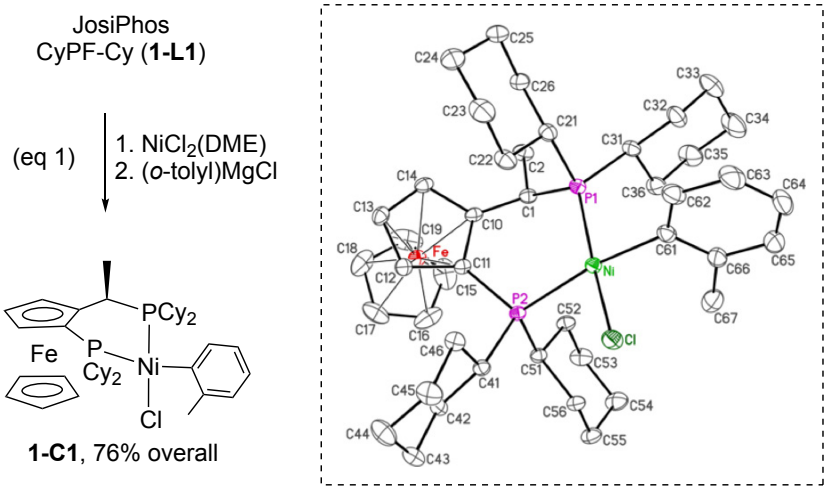

Scheme 2-1. Synthesis and single-crystal X-ray structure of **1-C1**. X-ray structure is shown with 30% thermal ellipsoids and with hydrogen atoms omitted for clarity. Selected interatomic distances (Å) and angles (°) for **1-C1**: Ni-P1 2.1774(8), Ni-P2 2.2721(8), Ni-Cl 2.2078(8), Ni-C(aryl) 1.925(3), P1-Ni-P2 97.84(3), P1-Ni-C(aryl) 89.16(10), P2-Ni-C1 89.54(3), Cl-Ni-C(aryl) 84.34(10).

2.3. Catalytic Survey of PAd-DalPhos, CyPF-Cy, and DPPF Pre-catalysts

2.3.1. Mono-arylation of Ammonia using Ni(II) Catalysts

Ammonia is one of the most widely produced commodity chemicals, and as such represents an attractive synthon in the synthesis of nitrogen-containing organic molecules.[94, 95] However, the selective monoarylation of ammonia with (hetero)aryl electrophiles has proven to be a significant challenge, due in part to the fact that for most catalyst systems the sought-after primary (hetero)aniline products are often better substrates than ammonia itself, leading to uncontrolled polyarylation.[96] In this regard, ammonia monoarylation provides a useful testing ground for ancillary ligand design in

metal-catalyzed C(sp^2)-N cross-coupling chemistry. Whereas palladium-based catalysts have traditionally offered optimal performance for the cross-coupling of ammonia with (hetero)aryl chlorides,[97] the scope of reactivity exhibited by **C0**, both in terms of the breadth of electrophilic partners and the varied reaction conditions tolerated including room temperature transformations, was found to exceed that achieved by use of any known catalyst system.[72] Mixtures of $Ni(COD)_2$/**1-L1** were previously demonstrated as effective in ammonia monoarylation chemistry conducted at elevated temperatures (Section 1.3.3.); under analogous conditions, the performance of $Ni(COD)_2$/DPPF was found to be comparatively poor.[71] Given the potential for catalyst inhibition by COD,[47, 98] this work directly compares the performance of **C0**, **1-C1**, and **1-C2** in ammonia monoarylation chemistry at both 25 and 110 ºC, involving 1-chloronaphthalene, 3-chloroanisole, 4-chloroanisole, and 5-chlorobenzo[*b*]thiophene as representative *ortho*-substituted, electron-poor, electron-rich, and heterocyclic aryl chlorides, respectively (Scheme 2-2). For these transformations as well as related cross-couplings involving alternative amine substrates (Schemes 2-3 to 2-4), somewhat challenging reaction conditions (e.g., low catalyst loading) were intentionally selected in an effort to differentiate the catalytic abilities of the pre-catalysts. For the majority of the transformations reported herein, poor product formation was accompanied by low conversion of the electrophile.

The room temperature monoarylation of ammonia employing 1-chloronaphthalene leading to **1.1a** was readily achieved by use of either **C0** or **1-C1** (1 mol%, 90%); however, in both cases efforts to reduce the catalyst loading to 0.5 mol% resulted in <20% conversion to **1.1a** under analogous conditions (Scheme 2-2). In monitoring the rate of formation of **1.1a** in such reactions employing **C0** or **1-C1** (25 ˚C, 1 mol%), 50% conversion to **1.1a** was observed after 20 minutes with **C0**, whereas 20% conversion was achieved by use of **1-C1**; after 1 h, 60% conversion to **1.1a** was achieved with each of **C0** and **1-C1**. Without ascribing definitive mechanistic significance to these limited observations, it appears that **C0** is more easily activated under the specific reaction conditions employed. Notably, **1-C2** proved ineffective for ammonia monoarylation involving 1-chloronapthalene and the other electrophiles examined in the survey.

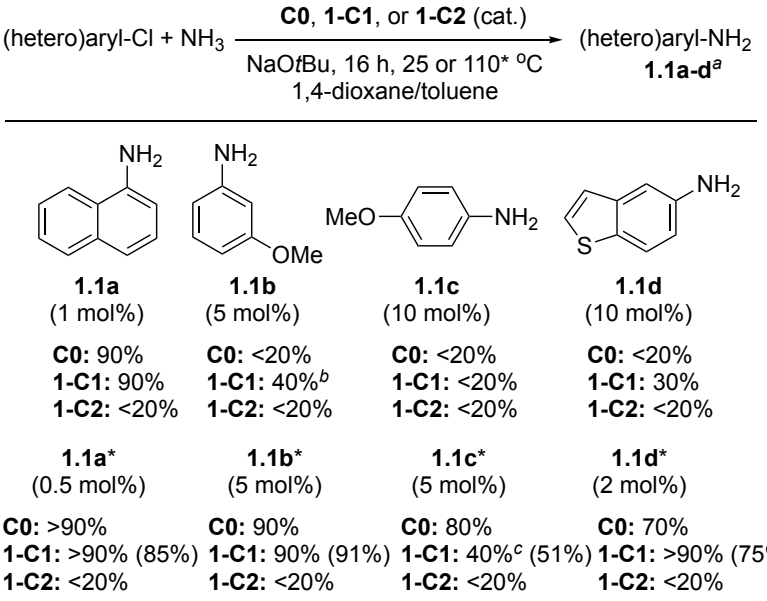

Scheme 2-2. Comparative catalytic screening of **C0**, **1-C1**, and **1-C2** in the nickel-catalyzed mono-arylation of ammonia. Unless otherwise noted, poor product formation was accompanied by low conversion of the electrophile. [a] Estimated conversion to product after 16 h (unoptimized) is based on GC data, with product yield based on ^{1}H NMR data in parantheses. Reactions using 0.5 M stock solution of NH_3 in 1,4-dioxane, employing the mol% pre-catalyst as indicated. Conditions: 0.10 M 1-chloronaphthalene (25 °C, 3 eq. NH_3; 110 °C, 5 eq. NH_3), otherwise 0.07 M Ar-Cl and 7 eq. NH_3; [b] 80% conversion to **1.1b** employing 10 mol% **1-C1**; [c] Significant amounts of higher molecular weight by-products observed. Asterisk indicates 110 °C reaction temperature.

Related room temperature reactions involving more challenging test electrophiles leading to **1.1b-d** were less successful (Scheme 2-2). In the transformation of relatively electron-poor 3-chloroanisole, 40% conversion to **1.1b** was achieved by use of **1-C1** (5 mol%); in doubling the catalyst loading, 80% conversion to **1.1b** was achieved. Under analogous conditions using **C0** (25 ˚C, 5 mol%), <20% conversion to **1.1b** was observed. This trend was retained in the monoarylation of ammonia with electron-poor 4-chlorobenzonitrile under analogous conditions (25 °C, 5 mol% pre-catalyst); >90% conversion to 4-aminobenzonitrile was achieved with **1-C1**, whereas poor conversion to 4-aminobenzonitrile was observed when using **C0**, along with the formation of higher molecular weight by-products.

Improved catalytic performance in ammonia monoarylation was observed for **C0** and **1-C1** at 110 ºC, with each of these pre-catalysts affording synthetically useful conversions to **1.1a**, **1.1b**, and **1.1d**. Divergent performance was noted in reactions involving the relatively electron-rich substrate 4-chloroanisole, whereby selectivity for conversion to **1.1c** with **C0** (80%) exceeded that achieved by use of **1-C1** (40%). Collectively, these results provide preliminary evidence that the catalytic performance of **1-C1** is competitive with, and in some ways complementary to, **C0** in otherwise challenging ammonia monoarylation chemistry.

2.3.2. Mono-arylation of Alkylamines using Ni(II) Catalysts

The selective monoarylation of primary alkylamines with (hetero)aryl (pseudo)halides remains a relatively challenging class of transformations in nickel-catalyzed C(sp^2)-N cross-coupling chemistry.[54] Notwithstanding two isolated entries involving the arylation of *n*-hexylamine with aryl chlorides by use of $Ni(COD)_2$/DPPF catalyst mixtures at 110 °C that are present in Wolfe and Buchwald's[56] pioneering paper, the first broadly useful nickel pre-catalyst for the selective monoarylation of primary alkylamines, (*rac*-BINAP)Ni(η^2-NC-Ph), was disclosed in 2014 by Hartwig and co-workers (Section 1.3.3.).[51] Use of this (*rac*-BINAP)Ni(0) pre-catalyst enabled the cross-coupling of a range of functionalized primary alkylamines with (hetero)aryl chlorides and bromides under relatively mild conditions (1-4 mol% Ni; 50-80 °C). Stewart and co-workers[99] subsequently reported on analogous transformations employing (*rac*-BINAP)Ni($P(OPh)_3)_2$ as a pre-catalyst. The effectiveness of **C0** in promoting the cross-coupling of a broad spectrum of electron-rich and electron-poor (hetero)aryl (pseudo)halides with linear and branched primary alkylamines has been demonstrated, including the first examples of nickel-catalyzed room temperature transformations of this type.[72] Encouraged by the efficacy of **1-C1** in nickel-catalyzed ammonia monoarylation (Scheme 2-2), a reactivity comparison of the three pre-catalysts in the cross-coupling of furfurylamine or *sec*-butylamine with 1-chloronaphthalene, 3-chloroanisole, 4-chloroanisole, or 5-chlorobenzo[*b*]thiophene was initiated.

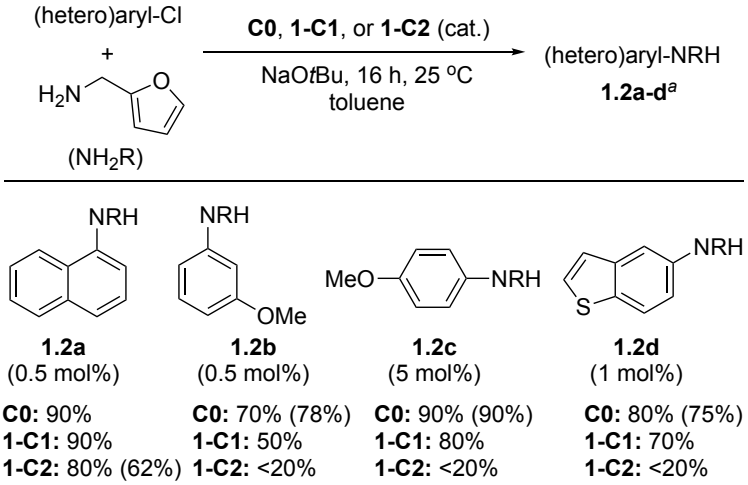

Scheme 2-3. Comparative catalytic screening of **C0**, **1-C1**, and **1-C2** in the nickel-catalyzed mono-arylation of furfurylamine. Poor product formation was accompanied by low conversion of the electrophile. [a] Estimated conversion to product after 16 h (unoptimized) is based on GC data, with isolated yields in parantheses. Reactions: 1.1 eq. furfurylamine; 0.16 M 5-chlorobenzo[*b*]thiophene, otherwise 0.24 M Ar-Cl; employing the mol% pre-catalyst as indicated.

Whereas all three pre-catalysts proved effective for the monoarylation of furfurylamine and 1-chloronaphthalene under mild conditions (25 ˚C, 0.5 mol%) leading to **1.2a**, related transformations involving the other electrophiles proved challenging for **1-C2** (Scheme 2-3). Conversely, under the screening conditions employed each of **C0** and **1-C1** provided useful levels of conversion to the target monoarylation products **1.2b-d** at room temperature, with slightly higher conversions to the target aniline achieved in each transformation by use of **C0**. The efficacy of **C0** and **1-C1** as pre-catalysts in the monoarylation of ammonia (Scheme 2-2) and the primary alkylamine furfurylamine (Scheme 2-3) prompted the examination of the relative preference of these pre-catalysts for such substrates within a competition scenario (Scheme 2-4). Interestingly, in cross-couplings employing equal amounts of ammonia and methylamine with limiting 1-chloronaphthalene (25 °C, 5 mol%), **1-C1** exhibited a marked preference for ammonia monoarylation leading to **1.1a**, whereas preferential monoarylation of methylamine leading to **1.2e** was achieved by use of **C0**. The observed **1.1a**:**1.2e** selectivity drops to 2:1 (for **1-C1**) and 1:2 (for **C0**) for analogous reactions conducted at 110 °C. While it is plausible to conclude that the less electron-donating nature of PAd-DalPhos (**L0**), versus CyPF-Cy (**1-**

L1), gives rise to reactive nickel intermediates that favour binding and turnover of more basic amines (e.g. methylamine over ammonia), the scenario is likely more nuanced; for example, the contribution of steric differences between **L0** and **1-L1** on the observed selectivity outlined in Scheme 2-4 is also likely to be important.

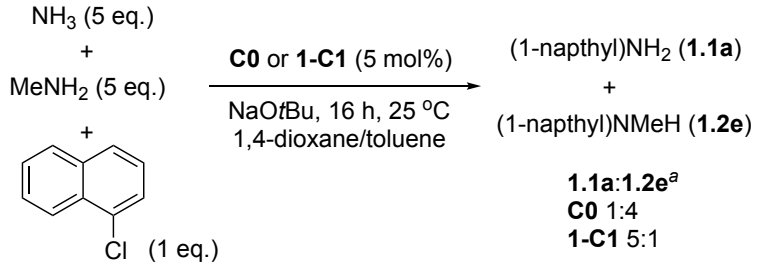

Scheme 2-4. Competitive mono-arylation of ammonia and methylamine with 1-chloronaphthalene using **C0** and **1-C1**. [a] Estimated product ratio on the basis of GC data; full conversion of the aryl chloride observed.

The monoarylation of the more sterically demanding *sec*-butylamine was subsequently examined (Scheme 2-5). Pre-catalyst **C0** proved effective in the cross-coupling of 1-chloronaphthalene leading to **1.3a** (80%) at room temperature; under analogous conditions the performance of each of **1-C1** (40%) and **1-C2** (20%) was inferior. Whereas related room temperature transformations involving 3-chloroanisole, 4-chloroanisole, and 5-chlorobenzo[*b*]thiophene, leading to **1.3b-d**, also proved feasible with **C0** and **1-C1**, it is apparent that the cross-coupling of *sec*-butylamine with 4-chloroanisole to give **1.3c** is challenging in comparison to reactions involving the less hindered furfurylamine (Scheme 2-3). Efforts to improve catalytic performance by conducting reactions at 110 °C, albeit at lower catalyst loadings, were met with some success, with the improved formation of **1.3a** and **1.3c** by use of **1-C1** being notable.

The cross-coupling of morpholine and either 4-chlorobenzonitrile or 5-chlorobenzo[*b*]thiophene by use of the pre-catalysts, leading to **1.4a** or **1.4b**, was examined in an effort to briefly compare the abilities of these pre-catalysts in the *N*-arylation of a prototypical secondary dialkylamine (Scheme 2-6). The reaction conditions employed were based on those described by Buchwald and co-workers[68] in their report pertaining to the use of **1-C2** in related cross-couplings. Moderate conversion to **1.4a** (60%) was achieved by use of **1-C1**; otherwise **C0** and **1-C1** proved ineffective in such transformations.

Conversely, the use of **1-C2** enabled high (>90%) conversion to **1.4a** and **1.4b** under analogous conditions, in keeping with the literature.[68]

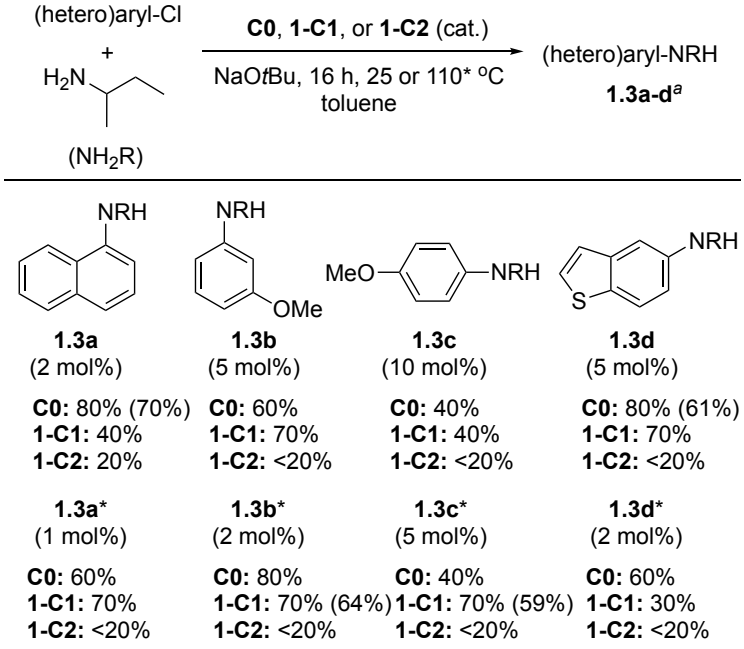

Scheme 2-5. Comparative catalytic screening of **C0**, **1-C1**, and **1-C2** in the nickel-catalyzed mono-arylation of *sec*-butylamine. Estimated conversion to product after 16 h (unoptimized) on the basis of GC data, with isolated yields in parentheses. Poor product formation was accompanied by low conversion of the electrophile; [a] Reaction conditions: 1.1 eq. *sec*-butylamine; at 25 °C, 0.16 M 1-chloronaphthalene, otherwise 0.12 M Ar-Cl; at 110 °C, 0.32 M 1-chloronaphthalene or 0.12 M 4-chloroanisole, otherwise 0.24 M Ar-Cl; employing mol% catalyst loadings as indicated. Asterisk indicates 110 °C conditions.

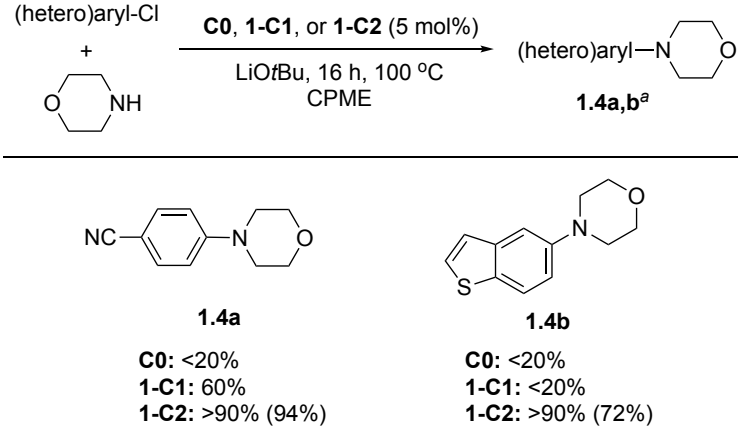

Scheme 2-6. Comparative catalytic screening of **C0**, **1-C1**, and **1-C2** in the nickel-catalyzed *N*-arylation of morpholine. [a] Estimated conversion to product after 16 h (unoptimized) on

the basis of GC data, with isolated yields in parantheses. Poor product formation was accompanied by low conversion of the electrophile. Reactions using morpholine (1.5 eq.), LiO*t*Bu (1.5 eq.), and 0.5 M in Ar-Cl in CPME.

2.3.3. Selectivity Studies of PAd-DalPhos and CyPF-Cy Ni(II) Pre-catalysts

In an effort to learn more about the electrophile tolerance and selectivity preferences of **C0** and **1-C1** beyond the (hetero)aryl chlorides examined thus far, room temperature cross-couplings of furfurylamine and aryl bromides were subsequently examined (Scheme 2-7). Whereas high conversion to the target aniline **1.5a** was achieved when using **C0** or **1-C1** in combination with 4-chlorotoluene, comparatively poor catalytic performance was displayed by **1-C1** in analogous reactions employing 4-bromotoluene. This trend was retained in analogous cross-couplings employing 1-bromo-4-butylbenzene, leading to **1.5b**; whereas modest conversion to **1.5b** (40%) occurred by use of **1-C1**, clean conversion to **1.5b** (>90%) was achieved with **C0** under analogous conditions.

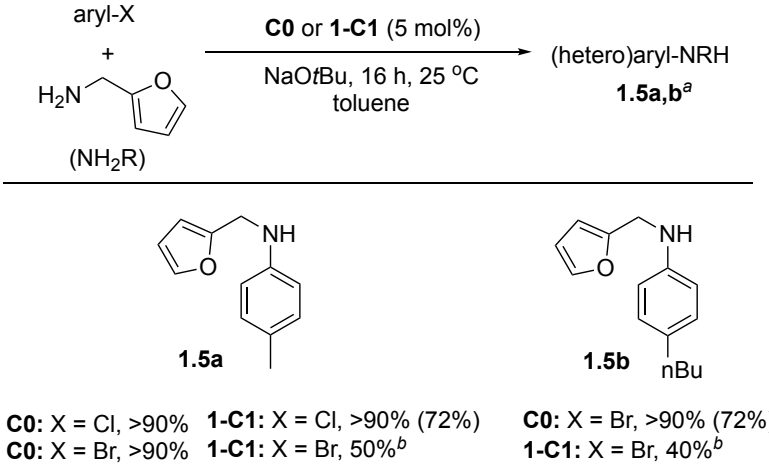

Scheme 2-7. Halide compatibility in the arylation of furfurylamine using **C0** and **1-C1** at room temperature. [a] Estimated conversion to product after 16 h (unoptimized) on the basis of GC data, with isolated yields in parentheses. Unless otherwise noted, poor product formation was accompanied by low conversion of the electrophile; [b] Significant quantities of by-products detected.

The competitive preference of **C0** and **1-C1** for chloride versus bromide or tosylate electrophiles in room temperature cross-couplings employing limiting furfurylamine was examined subsequently (Scheme 2-8). In keeping with challenging aryl bromide reactivity involving **1-C1**, incomplete conversion of furfurylamine was observed, accompanied by a

modest preference for uptake of the aryl chloride. Conversely, complete consumption of the amine occurred when using **C0**, with the aryl bromide being the preferred electrophile. In analogous competitions involving 4-chlorotoluene and 4-ethylphenyl tosylate, modest and inverted electrophile selectivity was exhibited by **C0** and **1-C1**.

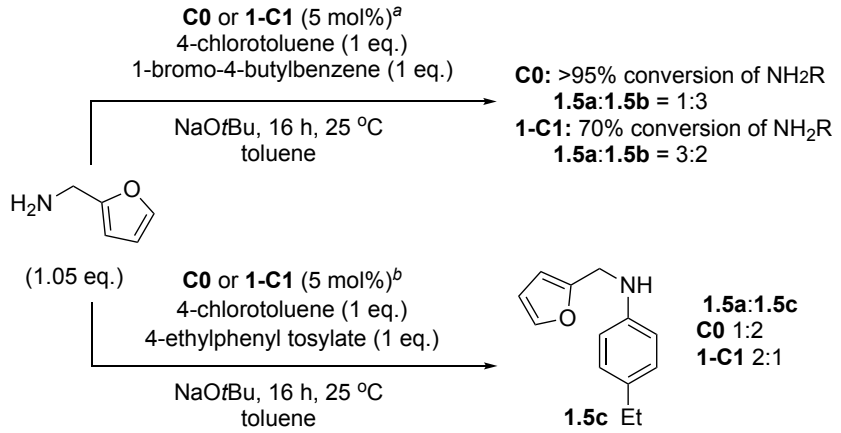

Scheme 2-8. (Pseudo)halide competition in the arylation of furfurylamine using **C0** and **1-C1** at room temperature. Poor product formation was accompanied by low conversion of the electrophile. [a] Estimated conversion to product after 16h (unoptimized) on the basis of ^{1}H NMR data; [b] Estimated conversion to products after 16h (unoptimized) on the basis of GC data.

2.4. Chapter 2 Summary

In summary, the comparative catalytic survey of **C0**, **1-C1**, and **1-C2** in selected representative nickel-catalyzed C(sp^2)-N cross-coupling reactions establishes the new air-stable pre-catalyst **1-C1** as being competitive with, and in some cases complementary to, **C0** in challenging transformations including the room temperature monoarylation of ammonia and primary alkylamines with (hetero)aryl chlorides. Although **1-C2** proved ineffective for such transformations, this DPPF-based pre-catalyst was found to be superior to **C0** and **1-C1** in combination with the secondary dialkylamine test substrate, morpholine. The comparable reactivity of **C0** and **1-C1** in the monoarylation of ammonia and primary alkylamines is intriguing in light of the differing electronic characteristics of the ligand sets featured in these pre-catalysts, with **1-C1** featuring much more electron-rich phosphorus donor groups relative to those in **C0**; the comparatively poor performance of **1-C2** with such substrates suggests that significant steric demand is a pre-requisite for successful ancillary ligands in these difficult cross-coupling applications. However, in the absence of

additional data, definitive proposals regarding the manner in which these structurally varied ancillary ligands give rise to the differences observed herein with regard to substrate compatibility cannot be put forth. Notwithstanding the generally similar reactivity profile exhibited by **C0** and **1-C1**, competition experiments revealed a differing preference for ammonia versus methylamine monoarylation, with **1-C1** favoring ammonia monoarylation. Furthermore, (pseudo)halide comparison studies at room temperature revealed that **1-C1** is less effective than **C0** in transformations of aryl bromides.

In the context of bisphosphine ligation it is evident that **C0**, **1-C1**, and **1-C2** represent a complementary and useful set of pre-catalysts for use in addressing a broad spectrum of NH nucleophiles in nickel-catalyzed C(sp^2)-N cross-coupling chemistry. Given the important role of ancillary ligand design in promoting elementary catalytic steps, as well as in controlling desired oxidation states of derived catalytic intermediates, further investigations of bisphosphine ancillary ligand motifs for use in nickel-catalyzed C(sp^2)-N cross-coupling are explored in the ensuing chapters.

2.5. Statement of Contributions for Chapter 2

Experimental work and manuscript preparation was conducted by J. S. K. Clark. Dr. C. M. Lavoie and Dr. P. M. MacQueen acted as mentors to the lead author. Single crystal X-ray diffraction analysis was conducted by Dr. Michael Ferguson. Prof. Dr. Mark Stradiotto acted as graduate supervisor for the lead author, and co-wrote the published manuscript. This work has been published: J. S. K. Clark, C. M. Lavoie, P. M. MacQueen, M. J. Ferguson, M. Stradiotto. *Organometallics*, **2016**, *35*, 3248-3254.

Chapter 3. Investigating the DPPF Framework

3.1. Chapter 3 Overview

The apparently similar catalytic abilities of the structurally divergent **L0** and **1-L1** (as seen in Chapter 2) prompted a narrowed investigation into the variation of phosphino substituents within a single ligand framework, and the resultant effects on reactivity in the context of nickel-based amination chemistry. Owing to the number of existing variants of the priveleged DPPF ($\mathbf{L^{Ph}}$) ancillary ligand and its high degree of modularity, the work in Chapter 3 examines the performance of structurally varied 1,1'-bis(di(alkyl/aryl)phosphino)ferrocene ancillary ligand variants of $\mathbf{L^{Ph}}$ in nickel-catalyzed C(sp^2)-N cross-coupling chemistry. A conceptually related study involving the palladium-catalyzed amination of aryl bromides with selected primary alkylamines appeared approximately twenty years ago;[100] nonetheless, the influence of 1,1'-bis(di(alkyl/aryl)phosphino)ferrocene ligation on the performance of nickel in C(sp^2)-N cross-couplings is likely to be distinct from analogous transformations involving palladium, given the differing size, electronegativity, and redox properties of these metals.[44, 101, 102] The comparison of $\mathbf{L^{Ph}}$ analogues in nickel-catalyzed C(sp^2)-N cross-couplings is limited to a single report by Stewart and co-workers[88] involving a relatively small number of $\mathbf{L^{Ph}}$ variants in the cross-coupling of 4-chloroanisole and *p*-toluidine. The results of a competitive reactivity survey involving ten variants of $\mathbf{L^{Ph}}$ (Scheme 3-1) in the nickel-catalyzed C(sp^2)-N cross-coupling of the test nucleophiles furfurylamine, morpholine, and indole in combination with structurally varied (hetero)aryl chlorides are reported in this chapter.

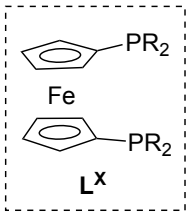

$\mathbf{L^{iPr}}$: R = iPr
$\mathbf{L^{Cy}}$: R = Cy
$\mathbf{L^{tBu}}$: R = *t*Bu
$\mathbf{L^{Ph}}$: R = Ph
$\mathbf{L^{o\text{-}tol}}$: R = *o*-tolyl
$\mathbf{L^{1\text{-}nap}}$: R = 1-napthyl
$\mathbf{L^{CF3}}$: R = 3,5-(bis-CF_3)phenyl
$\mathbf{L^{fur}}$: R = 5-methyl-2-furanyl
$\mathbf{L^{OMe}}$: R = 4-OMe-3,5-dimethylphenyl
$\mathbf{L^{Me}}$: R = 3,5-dimethylphenyl

Scheme 3-1. Ligand assignments for $\mathbf{L^X}$ variants.

3.2. Selection of Ancillary Ligand Variants and Test Substrates

While definitive mechanistic data pertaining to nickel-catalyzed C(sp^2)-N cross-couplings employing $\mathbf{L^{Ph}}$ and related variants are lacking, it is possible that the use of

relatively electron-rich ancillary ligands might promote (hetero)aryl chloride oxidative addition; conversely, relatively electron-poor ancillary ligands may facilitate product-forming C-N reductive elimination. Furthermore, sterically demanding ancillary ligands may enhance catalytic performance both by driving C-N reductive elimination,[103] dissuading comproportionation, and by discouraging the formation of putative off-cycle $(\mathbf{L^X})_2$Ni-type intermediates.[51, 104] In this context, and in viewing $\mathbf{L^{Ph}}$ as the parent ancillary ligand prototype, the use of variants featuring (Scheme 3-1): electron-rich alkylphosphines of varying steric bulk (D*i*PPF, $\mathbf{L^{iPr}}$; DCPF, $\mathbf{L^{Cy}}$; DTBPF, $\mathbf{L^{tBu}}$); an electron-rich arylphosphine ($\mathbf{L^{OMe}}$); electron-poor arylphosphines ($\mathbf{L^{CF3}}$ and HiersoPHOS-3, $\mathbf{L^{fur}}$); a modestly electron-rich *meta*-substituted arylphosphine ($\mathbf{L^{Me}}$); and bulky *ortho*-substituted arylphosphines ($\mathbf{L^{o\text{-}tol}}$ and $\mathbf{L^{1\text{-}nap}}$) were targeted.

Encouraged by the established utility of $\mathbf{L^{Ph}}$ in the nickel-catalyzed C(sp^2)-N cross-coupling of alkylamines, furfurylamine and morpholine were included as test substrates.[56, 68, 85-89, 105-107] Whereas (NHC)Ni catalysts have proven to be particularly effective in the cross-coupling of a range of (hetero)aryl chlorides and indole derivatives,[69] the application of $\mathbf{L^{Ph}}$-ligated nickel catalysts in analogous transformations of aryl chlorides is limited to the cross-coupling of 4-chlorobenzotrifluoride and carbazole at 110 °C;[68] at the outset of this work, no examples of nickel-catalyzed indole *N*-arylation at room temperature were known. In this context, indole was selected as a potentially more challenging nucleophile for the reactivity survey. 1-Chloronaphthalene, 4-chlorobenzonitrile, 3-chloroanisole and 5-chlorobenzo[*b*]thiophene were employed initially as representative *ortho*-substituted, *para*-substituted electron poor, *meta*-substituted electron poor, and heterocyclic test electrophiles, respectively. A selection of successful $\mathbf{L^X}$ variants was then carried forward in potentially more challenging cross-couplings involving 4-chloroquinaldine (at room temperature), 1-bromo-4-*tert*-butylbenzene, hindered 2-chloro-1,4-dimethylbenzene, and/or electron-rich 4-chloroanisole. Throughout, this work focused on efficiently identifying $\mathbf{L^X}$ variants that afforded high conversion to the target monoarylation product of interest. While for the most part low yields of the target compound were accompanied by substantial quantities of unreacted starting materials, in some cases non-negligible amounts of by-products possibly arising from hydrodehalogenation, diarylation, and/or aryl transfer from the $\mathbf{L^X}$ ligand[100] were observed, but were neither identified nor quantified. To

expedite the catalytic screen, catalyst mixtures of $Ni(COD)_2$/$\mathbf{L^X}$ were employed, which mandated the use of inert-atmosphere conditions owing to the air-sensitive nature of $Ni(COD)_2$. While the requirement of inert-atmosphere instrumentation has in the past represented a barrier to the implementation of protocols that make use of $Ni(COD)_2$, Garg and co-workers[108] have recently demonstrated that employing paraffin-coated $Ni(COD)_2$ capsules allows for the use of more simple bench-top techniques.

3.3. Reactivity Surveys of L^X in Nickel-Catalyzed C(sp^2)-N Cross-Couplings

3.3.1. Nickel-Catalyzed Monoarylation of Furfurylamine

The relative ability of the $\mathbf{L^X}$ ancillary ligand variants in Scheme 3-1 to promote the nickel-catalyzed monoarylation of furfurylamine was explored initially (Scheme 3-2). In cross-couplings with 1-chloronapthalene or 4-chlorobenzonitrile, the use of $\mathbf{L^{iPr}}$, $\mathbf{L^{Cy}}$, $\mathbf{L^{Ph}}$, $\mathbf{L^{CF3}}$, $\mathbf{L^{OMe}}$, or $\mathbf{L^{Me}}$ in each case afforded high conversion to the target products **2.1a** and **2.1b**. Conversely, the application of $\mathbf{L^{tBu}}$, $\mathbf{L^{o\text{-}tol}}$, $\mathbf{L^{1\text{-}nap}}$, or $\mathbf{L^{fur}}$ in all of the furfurylamine cross-couplings examined gave minimal conversion to product. The superiority of the diarylphosphino variants $\mathbf{L^{Ph}}$, $\mathbf{L^{CF3}}$, $\mathbf{L^{OMe}}$, and $\mathbf{L^{Me}}$, relative to the dialkylphosphino derivatives $\mathbf{L^{iPr}}$ and $\mathbf{L^{Cy}}$, was apparent in transformations involving 3-chloroanisole and 5-chlorobenzo[*b*]thiophene leading to **2.1c** and **2.1d**. Collectively, these observations suggest that for the nickel-catalyzed monoarylation of primary alkylamines, a range of electronically diverse $\mathbf{L^X}$ variants are competent, including dialkylphosphino ($\mathbf{L^{iPr}}$ and $\mathbf{L^{Cy}}$), electron neutral ($\mathbf{L^{Ph}}$ and $\mathbf{L^{Me}}$), electron poor ($\mathbf{L^{CF3}}$), and electron rich ($\mathbf{L^{OMe}}$) diarylphosphino derivatives. However, $\mathbf{L^X}$ derivatives featuring sterically demanding phosphorus donor groups (e.g., $\mathbf{L^{tBu}}$, $\mathbf{L^{o\text{-}tol}}$, or $\mathbf{L^{1\text{-}nap}}$), are incompatible with such transformations. Similar trends were observed by Stewart and co-workers[88] in their study of $\mathbf{L^{Ph}}$ variants in the nickel-catalyzed cross-coupling of 4-chloroanisole and *p*-toluidine. The poor performance of $\mathbf{L^{tBu}}$ and $\mathbf{L^{o\text{-}tol}}$ may be related to difficulty in accessing putative ($\mathbf{L^X}$)NiArCl intermediates, in keeping with the inability to synthesize ($\mathbf{L^X}$)Ni(*o*-tolyl)Cl pre-catalysts derived from these ancillary ligands (see Section 3.3).

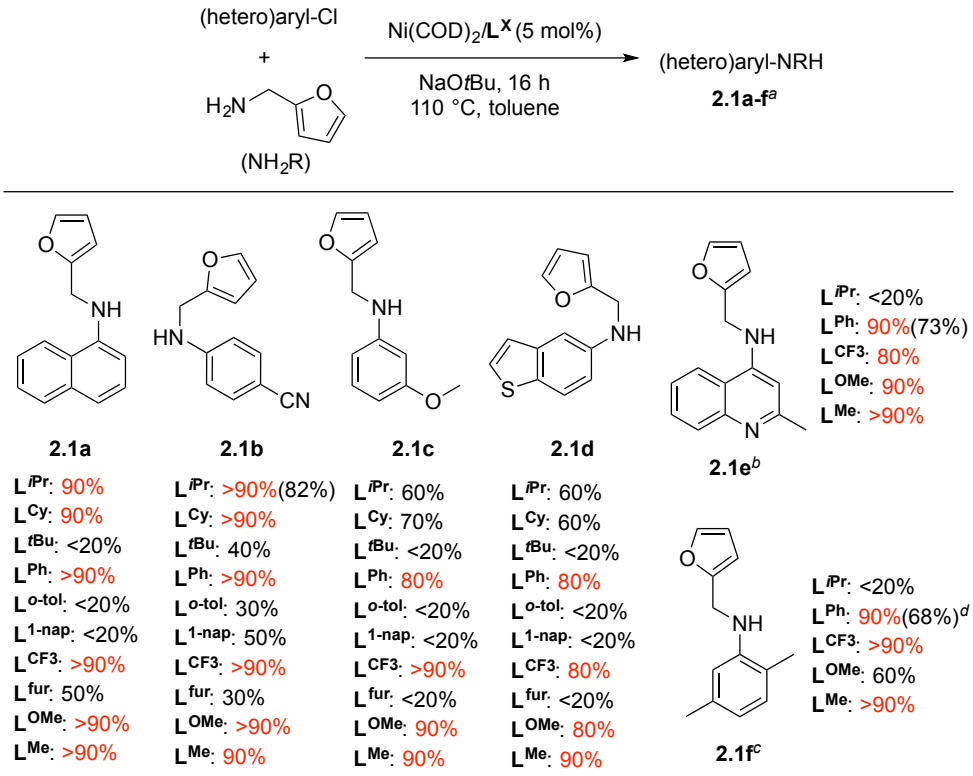

Scheme 3-2. Comparative catalytic screening in the nickel-catalyzed mono-arylation of furfurylamine. [a] Estimated conversion to product after 16 h (unoptimized) on the basis of calibrated GC data, with isolated yield in parentheses (unless otherwise indicated); [b] Conducted at 25 °C; [c] Using 10 mol% Ni/$\mathbf{L}^{\mathbf{X}}$; [d] Calculated on the basis of ^{1}H NMR data.

Potentially more challenging nickel-catalyzed cross-couplings of 4-chloroquinaldine (at room temperature) and *ortho*-substituted 2-chloro-1,4-dimethylbenzene with furfurylamine leading to **2.1e** and **2.1f** were subsequently pursued, employing $\mathbf{L}^{\mathbf{X}}$ variants that performed well in the formation of **2.1a-d** (Scheme 3-2). Whereas $\mathbf{L}^{i\mathbf{Pr}}$ gave low conversion to products **2.1e** and **2.1f**, the arylphosphine derivatives $\mathbf{L}^{\mathbf{Ph}}$, $\mathbf{L}^{\mathbf{CF3}}$, $\mathbf{L}^{\mathbf{OMe}}$, and $\mathbf{L}^{\mathbf{Me}}$ in general performed well (>80%); modest deviation from this trend was observed in the lower conversion to **2.1f** (60%) that was achieved by use of $\mathbf{L}^{\mathbf{OMe}}$.

To place these observations in the context of some related palladium-catalyzed C(sp^2)-N cross-coupling chemistry involving primary alkylamines, Hamann and Hartwig[100, 109, 110] noted that while the use of $\mathbf{L}^{o\text{-}\mathbf{tol}}$ in place of $\mathbf{L}^{\mathbf{Ph}}$ in some instances improved selectivity for monoarylation over diarylation, increased hydrodehalogenation also occurred. They also established that electronic perturbations arising from arylphosphine substitution in variants of $\mathbf{L}^{\mathbf{Ph}}$ are less pronounced than in simple

monodentate triarylphosphines, in keeping both with the observation that electron poor ($\mathbf{L}^{\mathbf{CF3}}$) and electron rich ($\mathbf{L}^{\mathbf{OMe}}$) diarylphosphino derivatives performed similarly to the parent ligand $\mathbf{L}^{\mathbf{Ph}}$ in palladium-catalyzed amination chemistry,[100] and with observations using nickel herein. Conversely, whereas the use of $\mathbf{L}^{\mathbf{tBu}}$ afforded negligible conversion in this survey of nickel-catalyzed cross-couplings of furfurylamine with (hetero)aryl chlorides (Scheme 3-2), Hamann and Hartwig[109, 110] found $\mathbf{L}^{\mathbf{tBu}}$ to be highly effective in analogous palladium-catalyzed arylations of primary anilines and alkylamines, as well as secondary cyclic dialkylamines such as morpholine. This latter observation further underscores the concept that the application of ancillary ligands that perform well in palladium-catalyzed BHA chemistry is not a universally effective strategy for the development of effective nickel-catalyzed C(sp^2)-N cross-couplings (Section 1.4).[71, 72]

3.3.3. Nickel-Catalyzed N-Arylation of Morpholine

Morpholine was employed subsequently, under established literature conditions,[68] as a prototypical secondary dialkylamine test substrate in the survey of $\mathbf{L}^{\mathbf{X}}$ variants in nickel-catalyzed amine arylation (Scheme 3-3). Whereas in transformations involving 1-chloronaphthalene leading to **2.2a** the relatively unhindered diarylphosphino derivatives $\mathbf{L}^{\mathbf{Ph}}$, $\mathbf{L}^{\mathbf{CF3}}$, $\mathbf{L}^{\mathbf{OMe}}$ and $\mathbf{L}^{\mathbf{Me}}$ proved most effective, a much larger collection of the $\mathbf{L}^{\mathbf{X}}$ ancillary ligands surveyed performed well in cross-couplings of 4-chlorobenzonitrile leading to **2.2b**. Indeed, the cross-coupling of morpholine and 4-chlorobenzonitrile represents the only substrate pairing throughout the entire study in which $\mathbf{L}^{\mathbf{tBu}}$, $\mathbf{L}^{\mathbf{o\text{-}tol}}$ and $\mathbf{L}^{\mathbf{1\text{-}nap}}$ perform in a competitive manner relative to other effective $\mathbf{L}^{\mathbf{X}}$ variants. In moving to 3-chloroanisole, a different collection of ligands afforded ≥80% conversion to **2.2c** ($\mathbf{L}^{\mathbf{iPr}}$, $\mathbf{L}^{\mathbf{Cy}}$, $\mathbf{L}^{\mathbf{Ph}}$, and $\mathbf{L}^{\mathbf{Me}}$), with $\mathbf{L}^{\mathbf{CF3}}$ and $\mathbf{L}^{\mathbf{OMe}}$ proving somewhat less effective. A similar trend was observed in the cross-coupling of 5-chlorobenzo[*b*]thiophene to give **2.2d**, with the exception that $\mathbf{L}^{\mathbf{OMe}}$, but not $\mathbf{L}^{\mathbf{CF3}}$, proved competitive with $\mathbf{L}^{\mathbf{iPr}}$, $\mathbf{L}^{\mathbf{Cy}}$, $\mathbf{L}^{\mathbf{Ph}}$, and $\mathbf{L}^{\mathbf{Me}}$.

A selection of effective $\mathbf{L}^{\mathbf{X}}$ variants were then carried forward and applied in nickel-catalyzed cross-couplings of morpholine with more challenging electrophiles, leading to products **2.2e-h** (Scheme 3-3). While in all cases $\mathbf{L}^{\mathbf{Ph}}$ and/or $\mathbf{L}^{\mathbf{Me}}$ provided optimal catalytic performance, it is worthy of note that the hindered and modestly electron-rich 2-chloro-1,4-dimethylbenzene proved particularly challenging (≤50% conversion to **2.2g** for all $\mathbf{L}^{\mathbf{X}}$ variants).

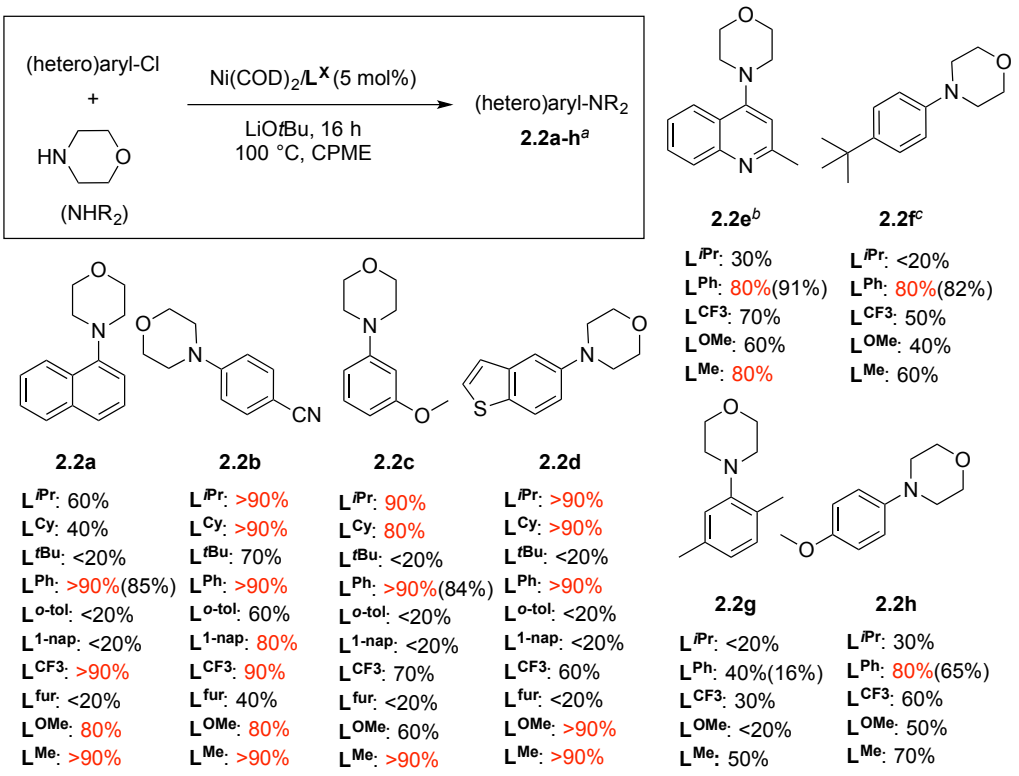

Scheme 3-3. Comparative catalytic screening in the nickel-catalyzed *N*-arylation of morpholine. [a] Estimated conversion to product after 16h (unoptimized) on the basis of calibrated GC data, with isolated yield in parentheses; [b] Conducted at 25 °C; [c] From the aryl bromide.

3.3.4. Nickel-Catalyzed N-Arylation of Indole

The nickel-catalyzed *N*-arylation of indoles and related derivatives continues to represent a particularly challenging transformation.[54] The most broadly effective nickel catalyst for such reactions is (IPr)Ni(styrene)$_2$ (5-10 mol% Ni, 110 °C) which has been shown to accommodate a range of (hetero)aryl chlorides (Section 1.3.3).[69] Conversely, the feasibility of conducting such aryl chloride aminations employing $\mathbf{L^X}$ ancillary ligands is restricted to a single entry involving the cross-coupling of the unhindered and electronically activated electrophile 4-chlorobenzotrifluoride with carbazole using $\mathbf{L^{Ph}}$ at elevated temperatures.[68] As such, the nickel-catalyzed cross-coupling of indole with sterically and electronically varied (hetero)aryl chlorides leading to **2.3a-f** offered an intriguing context in which to compare the catalytic utility of $\mathbf{L^X}$ variants (Scheme 3-4).

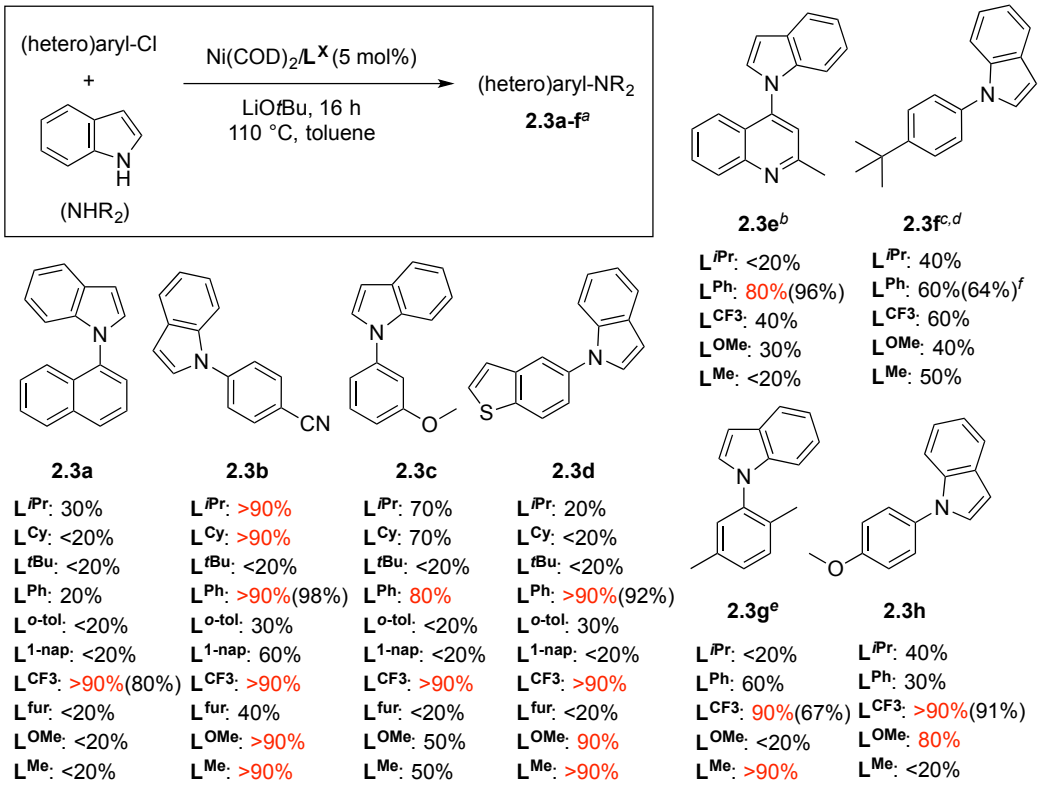

Scheme 3-4. Comparative catalytic screening in the nickel-catalyzed *N*-arylation of indole. [a] Estimated conversion to product after 16h (unoptimized) on the basis of calibrated GC data, with isolated yield in parentheses; [b] Conducted at 25 °C; [c] From the aryl bromide; [d] Using 2.5 mol% Ni/$\mathbf{L}^{\mathbf{X}}$; [e] Using 10 mol% Ni/$\mathbf{L}^{\mathbf{X}}$; [f] Using 5 mol% Ni/$\mathbf{L}^{\mathbf{X}}$.

The remarkable utility of the electron-poor ancillary ligand $\mathbf{L}^{\mathbf{CF3}}$ in the nickel-catalyzed *N*-arylation of indole was apparent in reactions involving 1-chloronaphthalene, whereby only this variant afforded the target product **2.3a** in high yield. In contrast, cross-couplings employing less challenging 4-chlorobenzonitrile, leading to **2.3b**, proceeded effectively with several $\mathbf{L}^{\mathbf{X}}$ variants, including $\mathbf{L}^{\mathbf{iPr}}$, $\mathbf{L}^{\mathbf{Cy}}$, $\mathbf{L}^{\mathbf{Ph}}$, $\mathbf{L}^{\mathbf{CF3}}$, $\mathbf{L}^{\mathbf{OMe}}$, and $\mathbf{L}^{\mathbf{Me}}$. In keeping with previous reaction surveys involving furfurylamine and morpholine (Schemes 3-2 and 3-3), consistently inferior performance was noted for $\mathbf{L}^{t\mathbf{Bu}}$, $\mathbf{L}^{o\text{-}\mathbf{tol}}$, $\mathbf{L}^{\mathbf{1\text{-}nap}}$, and $\mathbf{L}^{\mathbf{fur}}$ in each of the indole cross-couplings examined.

Amination of 3-chloroanisole to form **2.3c** was brought about most successfully by use of $\mathbf{L}^{\mathbf{CF3}}$, followed by $\mathbf{L}^{\mathbf{Ph}}$ and the two dialkylphosphine derivatives $\mathbf{L}^{i\mathbf{Pr}}$ and $\mathbf{L}^{\mathbf{Cy}}$; the observation that $\mathbf{L}^{\mathbf{OMe}}$ and $\mathbf{L}^{\mathbf{Me}}$ afforded comparatively lower conversion to **2.3c** was somewhat surprising, given the otherwise competitive nature of these ligands relative to

$\mathbf{L}^{\mathbf{Ph}}$ and $\mathbf{L}^{\mathbf{CF3}}$ in the formation of **2.3b**. Formation of **2.3d**, derived from 5-chlorobenzo[*b*]thiophene, in ≥90% yield was achieved by use of $\mathbf{L}^{\mathbf{Ph}}$, $\mathbf{L}^{\mathbf{CF3}}$, $\mathbf{L}^{\mathbf{OMe}}$ or $\mathbf{L}^{\mathbf{Me}}$ exclusively.

A focused set of ancillary ligands (i.e., $\mathbf{L}^{\mathbf{i Pr}}$, $\mathbf{L}^{\mathbf{Ph}}$, $\mathbf{L}^{\mathbf{CF3}}$, $\mathbf{L}^{\mathbf{OMe}}$, and $\mathbf{L}^{\mathbf{Me}}$) was employed in subsequent reactivity studies involving more challenging transformations of 4-chloroquinaldine, 1-bromo-4-*tert*-butylbenzene, 4-chloroanisole, and 2-chloro-1,4-dimethylbenzene, leading to **2.3e-h**, respectively. The parent ligand $\mathbf{L}^{\mathbf{Ph}}$ proved superior in the formation of **2.3e**; this transformation represents the first room-temperature *N*-arylation of indole employing an aryl chloride electrophile by any catalyst (i.e., Cu, Pd, Ni, or other). With the exception of transformations employing $\mathbf{L}^{\mathbf{CF3}}$ or $\mathbf{L}^{\mathbf{Me}}$ in the formation of **2.3g**, and $\mathbf{L}^{\mathbf{CF3}}$ or $\mathbf{L}^{\mathbf{OMe}}$ in the formation of **2.3h**, modest conversion to **2.3f-h** (≤60%) was achieved throughout. The successful nickel-catalyzed cross-coupling leading to **2.3g** observed herein warrants further commentary. The only analogous C(sp^2)-N cross-coupling reaction leading to **2.3g** was claimed by Buchwald and co-workers,[111] whereby 2-bromo-1,4-dimethylbenzene was employed in the presence of a Pd_2dba_3/binaphthylmonophosphine catalyst system (5 mol% Pd, 120 °C, 87% isolated yield **2.3g**). In this regard, the first high-yielding formation of **2.3g** from an aryl chloride by use of $Ni(COD)_2$/$\mathbf{L}^{\mathbf{CF3}}$ and $\mathbf{L}^{\mathbf{Me}}$ (10 mol% Ni, 110 °C) is noteworthy.

3.4. Attempted Pre-Catalyst Syntheses

In addition to the benefits outlined in Section 2.2 on the use of well-characterized $\mathbf{L}_n$NiArX pre-catalysts in place of $Ni(COD)_2$/$\mathbf{L}_n$ mixtures, the potentially inhibiting effect of COD is avoided by use of such Ni^{II} precursors.[47, 98] In the context of the ancillary ligand survey herein, Buchwald and co-workers have demonstrated that ($\mathbf{L}^{\mathbf{Ph}}$)Ni(*o*-tolyl)Cl is particularly effective in nickel catalyzed C(sp^2)-N cross-couplings.[68] In this vein, the preparation of new ($\mathbf{L}^{\mathbf{X}}$)Ni(*o*-tolyl)Cl variants was attempted so as to compare directly their catalytic abilities. The synthetic methods envisioned as potentially effective in this regard included: formation of ($\mathbf{L}^{\mathbf{X}}$)$NiCl_2$ followed by treatment with (*o*-tolyl)MgCl;[93] ligand displacement by $\mathbf{L}^{\mathbf{X}}$ starting from (TMEDA)Ni(*o*-tolyl)Cl[107, 112] or $(PPh_3)_2$Ni(*o*-tolyl)Cl;[68] or exposure of $\mathbf{L}^{\mathbf{X}}$ to $Ni(COD)_2$ followed by addition of 2-chlorotoluene. Preliminary efforts employing the first of these methods proved suitable for the synthesis of diamagnetic ($\mathbf{L}^{\mathbf{i Pr}}$)Ni(*o*-tolyl)Cl, which was obtained as an air-stable analytically pure solid. The single-

crystal X-ray structure of ($\mathbf{L}^{i\mathbf{Pr}}$)Ni(*o*-tolyl)Cl is presented in Figure 3-1 and features what is best described as a distorted square planar geometry, involving a *trans*-spanning $\mathbf{L}^{i\mathbf{Pr}}$ ligand; the *trans*-coordination of $\mathbf{L}^{i\mathbf{Pr}}$ is consistent with the observation of a single ^{31}P NMR resonance. Whereas the structural features of ($\mathbf{L}^{i\mathbf{Pr}}$)Ni(*o*-tolyl)Cl mirror those in ($\mathbf{L}^{\mathbf{Cy}}$)Ni(*o*-tolyl)Cl,[93] ($\mathbf{L}^{\mathbf{Ph}}$)Ni(*o*-tolyl)Cl[68] features *cis*-ligated bisphosphine ligation. Unfortunately, attempts to prepare analogous complexes featuring $\mathbf{L}^{t\mathbf{Bu}}$ and $\mathbf{L}^{o\text{-}\mathbf{tol}}$ were unsuccessful, despite exhaustive efforts employing the synthetic protocols outlined above. The inability to synthesize ($\mathbf{L}^{\mathbf{X}}$)Ni(*o*-tolyl)Cl complexes of $\mathbf{L}^{t\mathbf{Bu}}$ and $\mathbf{L}^{o\text{-}\mathbf{tol}}$, and their poor performance seen in Schemes 3-2 to 3-4, may arise due to the poor ligating properties of these sterically demanding ligands with nickel, and/or their inability to support putative ($\mathbf{L}^{\mathbf{X}}$)Ni(0) species that undergo oxidative addition of (hetero)aryl chlorides. The problematic nature of preparing alternative (bisphosphine)Ni(*o*-tolyl)Cl complexes featuring sterically demanding P(*o*-tolyl)$_2$ or P(*t*Bu)$_2$ donor fragments has been described.[93]

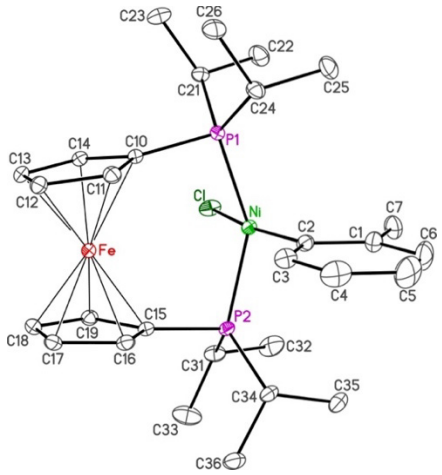

Figure 3-1. Single-crystal X-ray structure of ($\mathbf{L}^{i\mathbf{Pr}}$)Ni(*o*-tolyl)Cl. X-ray structure shown with 30% thermal ellipsoids and with hydrogen atoms omitted for clarity. Selected interatomic distances (Å) and angles (°): Ni-P1 2.1888(4), Ni-P2 2.1927(4) Ni-Cl 2.2462(4), Ni-C(aryl) 1.8993(13), P1-Ni-P2 144.863(16), P1-Ni-C(aryl) 91.99(4), P2-Ni-Cl 90.57(4), Cl-Ni-C(aryl) 166.54(4).

Difficulties were also encountered in the preparation of ($\mathbf{L}^{\mathbf{X}}$)Ni(*o*-tolyl)Cl pre-catalysts using $\mathbf{L}^{\mathbf{CF3}}$ or $\mathbf{L}^{\mathbf{OMe}}$. The most promising, albeit low-yielding (<30%), results were obtained by treatment of $\mathbf{L}^{\mathbf{CF3}}$ with (TMEDA)Ni(*o*-tolyl)Cl, or *via* formation of the putative intermediate ($\mathbf{L}^{\mathbf{OMe}}$)NiCl$_2$ followed by exposure to (*o*-tolyl)MgCl. In both cases, yellow-

orange solids were obtained that proved competent in a selection of the C(sp^2)-N cross-couplings presented herein. Nonetheless, the remarkably poor solubility of these presumed ($\mathbf{L^X}$)Ni(*o*-tolyl)Cl complexes derived from $\mathbf{L^{CF3}}$ or $\mathbf{L^{OMe}}$ in a range of solvents thwarted any efforts to properly characterize these materials.

3.5. Chapter 3 Summary

The comparative reactivity survey involving ten structurally varied 1,1'-bis(di(alkyl/aryl)phosphino)ferrocene ancillary ligands ($\mathbf{L^X}$) in the nickel-catalyzed C(sp^2)-N cross-coupling of furfurylamine, morpholine, or indole with various (hetero)aryl halides using $Ni(COD)_2$ revealed some informative structure-reactivity trends. Whereas *ortho*-substituted diarylphosphino ($\mathbf{L^{o\text{-}tol}}$ and $\mathbf{L^{1\text{-}nap}}$), sterically demanding dialkylphosphino ($\mathbf{L^{tBu}}$), and difuranylphosphino ($\mathbf{L^{fur}}$) variants proved ineffective, the parent ligand $\mathbf{L^{Ph}}$, less sterically demanding dialkylphosphino ($\mathbf{L^{iPr}}$ and $\mathbf{L^{Cy}}$), and *meta*-substituted diarylphosphino ($\mathbf{L^{CF3}}$, $\mathbf{L^{OMe}}$, and $\mathbf{L^{Me}}$) ancillary ligands proved competent in several of the test reactions employed. Particularly challenging cross-couplings such as the room-temperature amination of 4-chloroquinaldine, or reactions involving *ortho*-substituted electrophiles revealed the superiority of the diarylphosphino ancillary ligand sub-class ($\mathbf{L^{Ph}}$, $\mathbf{L^{CF3}}$, $\mathbf{L^{OMe}}$, and $\mathbf{L^{Me}}$); in the case of indole *N*-arylation, the electron-poor variant $\mathbf{L^{CF3}}$ proved particularly effective. The comparable catalytic performance of $\mathbf{L^{Ph}}$, $\mathbf{L^{CF3}}$, and $\mathbf{L^{OMe}}$ in several of the nickel-catalyzed C(sp^2)-N cross-couplings examined herein suggests that any electronic perturbations arising from arylphosphine substitution do not markedly influence the behavior of nickel in this chemistry, in keeping with prior observations in related metal-catalyzed aminations. Rather, it appears as though the common *meta*-disubstitution pattern is responsible for their similar catalytic competencies. The poor performance of $\mathbf{L^{tBu}}$ in the nickel-catalyzed transformations reported herein contrasts the outstanding ability of this ancillary ligand in enabling palladium-catalyzed arylations of primary anilines and alkylamines, highlighting the sometimes divergent ancillary ligand preferences of nickel and palladium in C(sp^2)-N cross-couplings.

Whereas the synthesis of ($\mathbf{L^{Ph}}$)Ni(*o*-tolyl)Cl and related nickel(II) compounds has been described previously in the literature, efforts to prepare analogous $\mathbf{L^X}$ ancillary ligand derivatives were met with limited success. Whereas ($\mathbf{L^{iPr}}$)Ni(*o*-tolyl)Cl was prepared straightforwardly and crystallographically characterized, the use of $\mathbf{L^{CF_3}}$, $\mathbf{L^{tBu}}$, $\mathbf{L^{o\text{-}tol}}$, or

$\mathbf{L}^{\mathbf{OMe}}$ under similar conditions resulted in poor conversion to product and/or the formation of highly insoluble materials. Notwithstanding the utility of $\mathbf{L}_n$NiArX pre-catalysts, these results bring to light practical limitations of this design strategy.

The successful identification of structure-reactivity trends of ancillary ligands in this chapter prompted a similar experimental study using a best-in-class ligand framework, PAd-DalPhos (**L0**). The results of this work will be disclosed in Chapter 4.

3.6. Statement of Contributions for Chapter 3

Experimental work involving syntheses of new ligands, (attempted) pre-catalyst syntheses, and catalyst screening experiments was partitioned equally between C. N. Voth and J. S. K. Clark. Manuscript preparation was undertaken by J. S. K. Clark. Single crystal X-ray diffraction analysis was conducted by Dr. Michael Ferguson. Prof. Dr. Mark Stradiotto acted as graduate supervisor for the lead author, and co-wrote the published manuscript. This work has been published: J. S. K. Clark, C. N. Voth, M. J. Ferguson, M. Stradiotto. *Organometallics*, **2017**, *36*, 679-686.

Chapter 4. Investigating the PAd-DalPhos Framework

4.1. Chapter 4 Overview

Motivated by the ligand design trends that emerged in Chapter 3, efforts to better understand the superlative catalytic performance offered by PAd-DalPhos (**L0**) in a range of nickel-catalyzed aminations were made using a similar experimental design. Chapter 4 systematically examines the aryl backbone and phosphino substitution pattern of **L0** through the comparison of new regioisomeric **L0** variants comprising various heteroaryl backbones.

In the initial development of **L0**,[72] a rigid *ortho*-phenylene backbone group was selected to span the two phosphorus donor fragments. The incorporation of heteroaryl backbone spanning units could influence ancillary ligand binding in terms of the enforced bite angle, *via* modulation of the donicity of the phosphorus donor groups, and possibly even by providing alternative chelation modes involving coordination to the heteroaryl unit,[11] thus potentially leading to new or improved catalytic performance. One particularly noteworthy example of such reactivity trends in nickel catalysis was reported by Yamaguchi, Itami, and co-workers in 2014,[113] whereby 3,4-bis(dicyclohexylphosphino)thiophene (DCYPT) out-performed both 1,2-bis(dicyclohexylphosphino)benzene (DCYPBz) and 1,2-bis(dicyclohexylphosphino)ethane (DCYPE) in the α-arylation of ketones with phenol-derived electrophiles. A subsequent report by Pringle and co-workers[114] established that both 2,3- and 3,4-bis(diphenylphosphino)thiophene ancillary ligands afforded superior catalytic performance relative to structurally related 1,2-bis(diphenylphosphino)benzene in iron-catalyzed Negishi cross-couplings.

The synthesis of heteroaryl analogues of **L0** and related bis(di(*o*-tolyl)phosphino) ancillary ligand variants (each based on a pyridine or thiophene backbone), the preparation of air-stable Ni(II) pre-catalysts derived from a selection of these new ligands, and a comparative catalytic survey versus **L0** in selected nickel-catalyzed C(sp^2)-N cross-couplings are reported herein.

4.2. Synthesis of PAd-DalPhos Variants

To complement the known ligands PAd-DalPhos (**L0**),[72] *o*-(P(*o*-tolyl)$_2$)$_2$benzene (**2-L1**),[115] and 3,4-(P(*o*-tolyl)$_2$)$_2$-thiophene (**2-L9**),[114] a small library of *ortho*-bisphosphine

ancillary ligands featuring either two di(*o*-tolyl)phosphino fragments, or tetramethyltrioxaphosphaadamantane (CgP) and di(*o*-tolyl)phosphino fragments, were prepared in synthetically useful yields by using the modular protocol outlined in Scheme 4-1. The new ligands **2-L2** to **2-L8** were fully characterized on the basis of NMR spectroscopic and high-resolution mass spectrometric data, and in the case of **2-L2** also by use of single-crystal X-ray methods (Figure 4-1).

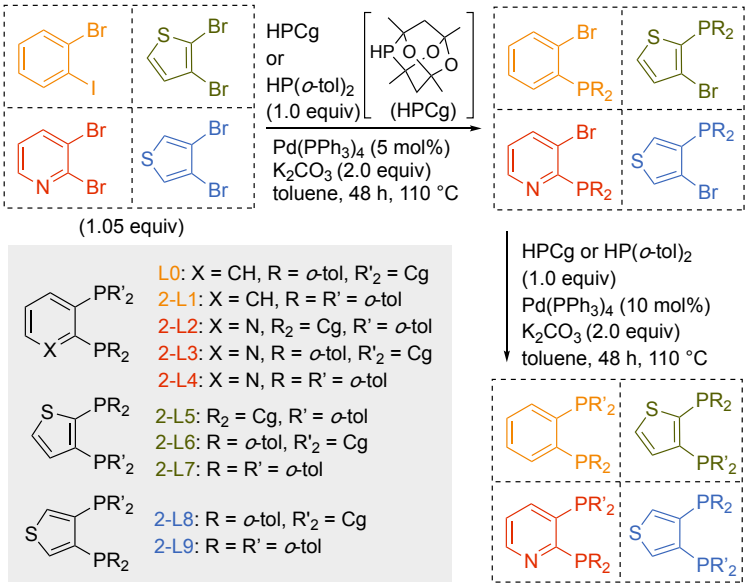

Scheme 4-1. Ancillary ligands examined in this study. These include **L0** to **2-L9** where **2-L8** = ThioPAd-DalPhos. Reaction scheme depicts the general synthetic protocol used in the preparation of **2-L1** to **2-L9**.

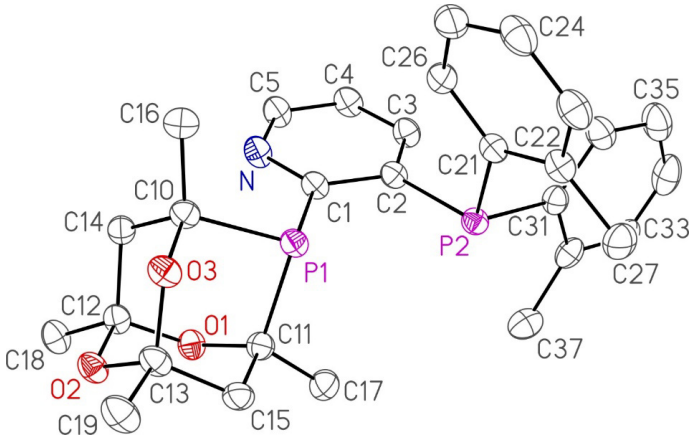

Figure 4-1. Single-crystal X-ray structure of **2-L2**. Perspective view showing the atom labelling scheme. Non-hydrogen atoms are represented by Gaussian ellipsoids at the 30% probability level. Hydrogen atoms are not shown.

4.3. Reactivity Surveys of PAd-DalPhos Variants

4.3.1. Preliminary In-Situ Catalyst Screens

In a preliminary effort to assess the relative catalytic performance of **L0** to **2-L9**, a selection of nickel-catalyzed C(sp^2)-N test cross-couplings involving aryl chlorides was examined, employing 5 mol% $Ni(COD)_2$ and featuring nucleophiles (i.e., furfurylamine, ammonia, and benzamide) that had each proven compatible with the parent, **L0**,[72, 73] but herein under relatively challenging reaction conditions (Scheme 4-2). In the cross-coupling of 1-chloronaphthalene with furfurylamine to give **3.1a** at 25 °C, very poor (≤30%) conversion of the starting materials was noted with each of the ligands examined except for 3,4-(P(*o*-tolyl)$_2$)$_2$-thiophene (**2-L9**), whereby 60% conversion to **3.1a** was achieved. In switching to transformations of the electronically deactivated electrophile 4-chloroanisole at 65 °C, the isomeric thiophene-derived ligands **2-L5**, **2-L6**, and **2-L8** (ThioPAd-DalPhos) featuring CgP and di(*o*-tolyl)phosphino donor groups proved unique in their ability to enable ≥80% conversion to the target cross-coupling product **3.1b** under the reaction conditions employed. However, in examining either ammonia monoarylation with 1-chloronapthalene at 110 °C to give **3.1c**, or benzamide cross-coupling with 4-chlorobenzonitrile at 90 °C to give **3.1d**, none of the ancillary ligand variants examined out-performed **L0**.

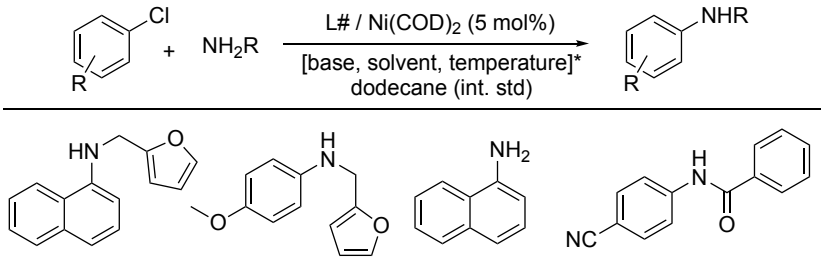

3.1a [25 °C][b]	**3.1b** [65 °C][b]	**3.1c** [110 °C][c]	**3.1d** [90 °C][d]
L0: 10%[g]	L0: 50%	L0: 70%	L0: 60%
2-L1: <10%[f]	2-L1: 10%[e]	2-L1: 20%[h]	2-L1: 10%[f]
2-L2: 10%	2-L2: 70%	2-L2: 60%[e]	2-L2: 30%
2-L3: 10%[e]	2-L3: 50%	2-L3: 50%[f]	2-L3: 40%
2-L4: 10%	2-L4: 30%	2-L4: 40%	2-L4: 10%
2-L5: 20%[g]	2-L5: 80%	2-L5: 60%	2-L5: 50%
2-L6: 30%[e]	2-L6: 80%	2-L6: 60%[e]	2-L6: 30%
2-L7: 20%	2-L7: 60%	2-L7: 30%[e]	2-L7: 10%
2-L8: 10%[e]	2-L8: 90%	2-L8: 50%	2-L8: 40%[e]
2-L9: 60%	2-L9: 40%	2-L9: 20%	2-L9: <10%

Scheme 4-2. Ancillary ligand screen in selected nickel-catalyzed C(sp^2)-N cross-couplings. [a] Estimated conversion to the target product after 16 h (unoptimized time) on the basis of

calibrated GC data using dodecane and authentic products as an internal standard, and unless stated where the mass balance corresponds to unreacted starting materials; [b] NaO*t*Bu (2.0 equiv), toluene (0.12 M Ar-Cl); [c] NH_3 (3.0 equiv, 0.5 M solution in 1,4-dioxane), NaO*t*Bu (2.0 equiv), toluene (0.07 M Ar-Cl); [d] K_3PO_4 (1.5 equiv), *t*-butanol (0.12 M Ar-Cl); [e] Accompanied by 10% higher molecular weight by-products; [f] Accompanied by 20% higher molecular weight by-products; [g] Accompanied by 30% higher molecular weight by-products; [h] Accompanied by 40% higher molecular weight by-products.

4.3.2. Pre-catalyst Syntheses of 3,4-Thiophenyl Ligands

Encouraged by the observation that the 3,4-disubstituted thiophene ligands **2-L8** and **2-L9** apparently offer improved performance relative to the parent **L0** in the nickel-catalyzed C(sp^2)-N cross-coupling of primary alkylamines, the synthesis of (**L**)NiCl(*o*-tolyl) pre-catalysts were pursued.[92] In keeping with the synthesis of (**L0**)NiCl(*o*-tolyl) (**C0**),[72] treatment of $NiCl_2$(DME) with either **2-L8** or **2-L9**, followed by exposure of the putative (**L**)$NiCl_2$ intermediates to (*o*-tolyl)MgCl, afforded the desired analytically pure and crystallographically characterized (**L**)NiCl(*o*-tolyl) complexes **2-C1** (71%) and **2-C2** (73%), respectively (Scheme 4-3). In the crystal structure of **2-C1**, the chloride is positioned *trans* to the CgP group within a distorted square-planar setting, as in **C0**.[72] However, the complex NMR features of **2-C1** (and **2-C2**) arising from a combination of second-order coupling, hindered Ni-C(*o*-tolyl) and/or P-C(*o*-tolyl) bond rotation, and dynamic equilibria involving tetrahedral and square planar species do not preclude the co-existence of isomers whereby the chloride is positioned *cis* to the CgP group, as was observed definitively in (CyPAd-DalPhos)NiCl(*o*-tolyl).[79] While overall the structural features of **C0**[72] and **2-C1** are rather similar, including P-Ni-P bite angles of 86.52(3)° and 87.92(3)° respectively, the Ni-P(*o*-tolyl)$_2$ distances (**C0**: 2.2263(8) Å; **2-C1**: 2.2724(9) Å) differ in a statistically significant manner. Complex **2-C2** features a P-Ni-P bite angle (86.20(3)°) similar to that found in **C0** and **2-C1**, and in keeping with the stronger *trans*-directing character of aryl relative to chloride, the Ni-P1 contact (2.1606(9) Å) *trans* to chloride is significantly shorter than the analogous Ni-P2 distance (2.2879(9) Å).

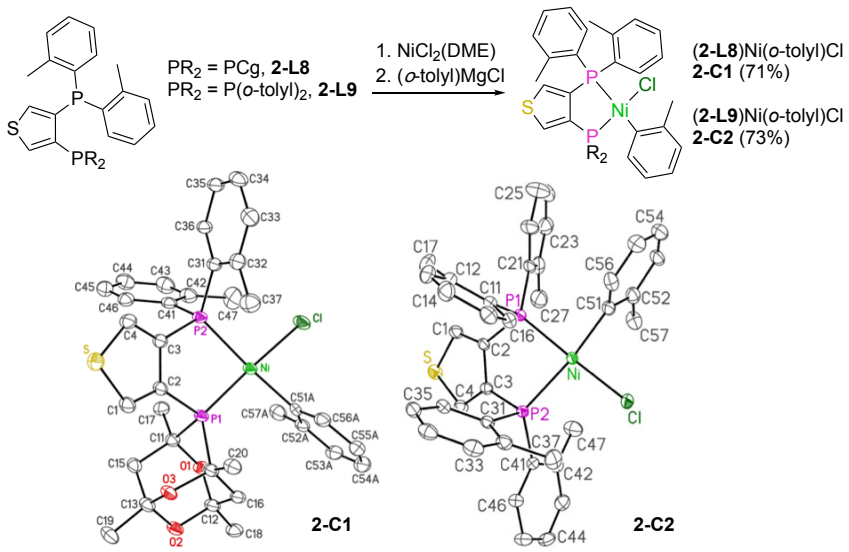

Scheme 4-3. Synthesis and single-crystal X-ray structures of **2-C1** and **2-C2**. X-ray structures are represented with thermal ellipsoids at the 30% probability level, and with hydrogen atoms omitted for clarity. Selected interatomic distances (Å) for **2-C1**: Ni-P1 2.1752(8); Ni-P2 2.2724(9); Ni-Cl 2.1957(9); Ni-C51 1.954(13). Selected interatomic distances (Å) for **2-C2**: Ni-P1 2.1606(9); Ni-P2 2.2879(9); Ni-Cl 2.1874(10); Ni-C51 1.939(4).

4.3.3. Catalytic Comparison of Pre-catalysts

With **2-C1** and **2-C2** in hand, subsequent tests were conducted to determine whether these new pre-catalysts might out-perform the parent **L0** pre-catalyst **C0** in cross-couplings involving primary alkylamines (Scheme 4-4). While **L0** remains one of the most effective ancillary ligands known for such nickel-catalyzed C(sp^2)-N cross-couplings,[72] an unmet challenge in the field is the identification of catalysts that can function effectively at room temperature and/or at low catalyst loadings (<0.5 mol%). With this in mind the cross-coupling of 1-chloronaphthalene with furfurylamine at 25 °C employing only 0.25 mol% of **C0, 2-C1** and **2-C2** was examined. Notably, while 60% conversion to **3.1a** was achieved by use of **C0** or **2-C2** under these conditions, the use of **2-C1** afforded 80% conversion to **3.1a**. While high conversion (≥70%) to **3.1a** was similarly achieved by use of **2-C1** with the analogous tosylate or bromide, efforts to employ **2-C1** at even lower catalyst loadings (0.125 mol%, 25 or 80 °C) afforded lower conversion to **3.1a** (≤50%).

The superiority of **2-C1** over **C0** and **2-C2** was further revealed in other challenging test cross-couplings conducted at 25 °C involving furfurylamine with 4-chlorobenzonitrile,

4-chloroanisole, or 4-chloroquinaldine, leading to **3.2a-c**. In a brief examination of substrate scope, the use of **2-C1** at low catalyst loadings (0.25-0.50 mol%) proved effective in cross-couplings involving primary alkylamines with (hetero)aryl chlorides featuring quinaldine, quinoxaline, and quinoline core structures, as well as naphthyl tosylate, affording **3.3a-d** in high isolated yield (68-91%).

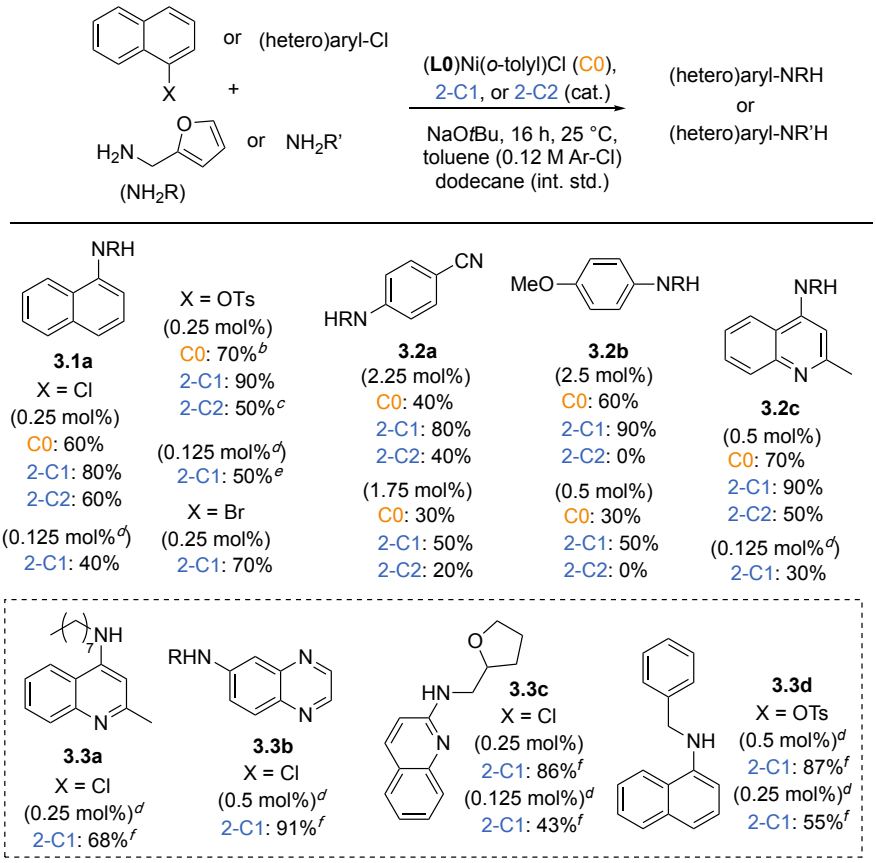

Scheme 4-4. Ancillary ligand screen in selected nickel-catalyzed C(sp^2)-N cross-couplings. [a] Estimated conversion to the target product after 16 h (unoptimized time) on the basis of calibrated GC data using dodecane and authentic products as an internal standard, and unless stated where the mass balance corresponds to unreacted starting materials; [b] <10% ArOH; [c] 20% ArOH; [d] Conducted at 80 °C; [e] 50% ArOH; [f] Isolated yield.

4.3.4. Computational Analysis of ThioPAd-DalPhos and PAd-DalPhos

In an effort to better understand the improved catalytic performance of **2-C1** versus **C0**, additional experimentation and computational analysis was undertaken. In monitoring the early formation of **3.1a** resulting from the cross-coupling of furfurylamine and 1-chloronaphthalene employing **C0** or **2-C1** (0-80 minutes, 0.25 mol%, 25 °C), no significant

difference in the reaction profiles was noted for these two pre-catalysts, and neither catalytic system displayed a pronounced induction period.

Stradiotto and co-workers have previously reported on the application of density functional theory (DFT) computational methods in evaluating complete catalytic cycles for nickel-catalyzed C(sp^2)-N cross-coupling reactions involving bisphosphines including PAd-DalPhos (**L0**);[67, 81] throughout, C(sp^2)-N bond reductive elimination from (**L**)Ni(aryl)(NHR) intermediates was found to be rate-limiting within a presumptive Ni^0/Ni^{II} cycle. With this knowledge, the cross-coupling of chlorobenzene and furfurylamine was examined by use of DFT calculations, focusing exclusively on comparing C(sp^2)-N bond reductive elimination from (**L**)Ni(Ph)(NH(CH_2-furyl)) (**IN-1**) intermediates *via* **TS-1** to afford (**L**)Ni(η^2-*N*-phenyl-furanmethanamine) (**IN-2**), for each of PAd-DalPhos (**L0**) and ThioPAd-DalPhos (**2-L8**) (Scheme 4-5). The methodology used to determine these calculations was implemented as per these previous reports.[67, 81]

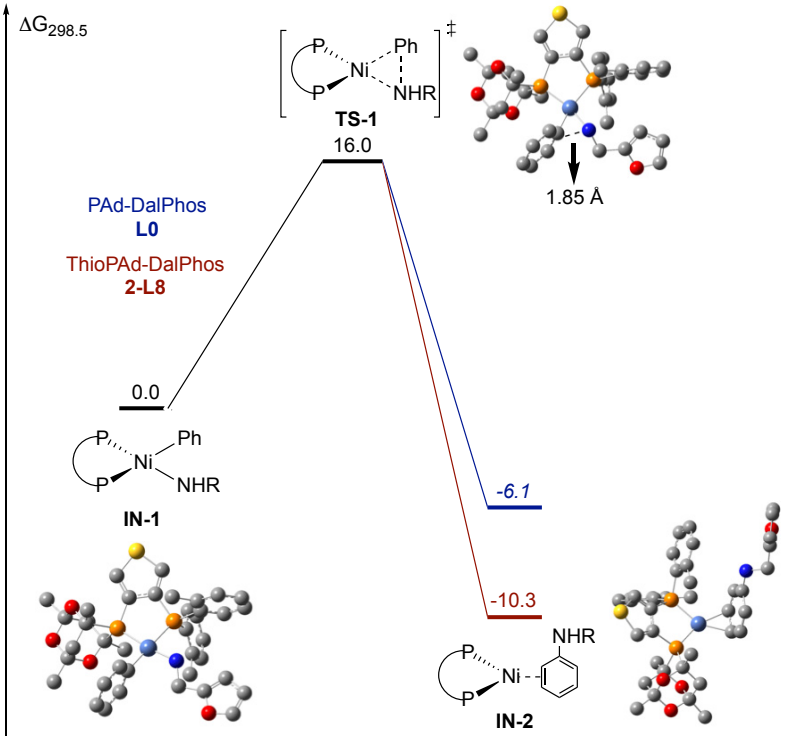

Scheme 4-5. Comparative reaction profile (relative free-energies, kcal mol^{-1}). Calculated by use of DFT methods for the nickel-catalyzed C(sp^2)-N cross-coupling of chlorobenzene and furfurylamine involving (**L0**/**2-L8**)Ni species (R = CH_2-furyl). Presented structures feature **2-L8**.

Notably, while the barrier to C(sp^2)-N bond reductive elimination commencing from **IN-1** was found to be identical (16.0 kcal mol^{-1}) when involving either **L0** or **2-L8**, the resultant **IN-2** species were found to have significantly differing energies (**L0**: -6.1 kcal mol^{-1}; **2-L8**: -10.3 kcal mol^{-1}; Scheme 4-5). It is plausible that the greater stability afforded to **IN-2** from **2-L8**, relative to **L0**, may contribute in part toward the improved catalytic performance of **2-L8** in nickel-catalyzed C(sp^2)-N cross-couplings involving primary alkylamines.

4.4. Chapter 4 Summary

The performance of newly prepared heteroaryl analogues of PAd-DalPhos and related bis(di(*o*-tolyl)phosphino) ancillary ligand variants based on pyridine or thiophene backbone structures was examined in selected challenging nickel-catalyzed C(sp^2)-N cross-coupling reactions. In the course of this investigation, the pre-catalyst (**2-L8**)NiCl(*o*-tolyl) (**2-C1**), featuring the thiophene-derived ancillary ligand ThioPAd-DalPhos (**2-L8**), was found to offer improved performance versus the related PAd-DalPhos-derived pre-catalyst **C0** in the nickel-catalyzed C(sp^2)-N cross-coupling of primary alkylamines with (hetero)aryl-X electrophiles (X = Cl, Br, OTs) under unprecedentedly mild reaction conditions (0.25-0.50 mol% Ni), including examples conducted at room temperature. In monitoring the early progress of representative reactions involving **C0** or **2-C1**, neither significant variation in the reaction profiles nor a pronounced induction period was noted. Given that the geometrical parameters associated with **C0** and **2-C1** also do not vary significantly, the observed benefit of employing ThioPAd-DalPhos in such transformations may arise from a subtle combination of steric and electronic factors that provide increased longevity versus the analogous PAd-DalPhos catalyst system. DFT studies suggest that ThioPAd-DalPhos is more efficient at stabilizing catalytic species formed following rate-limiting C-N bond reductive elimination from (**L**)Ni(aryl)(NH(alkyl)) intermediates, which may contribute to improved catalytic performance versus PAd-DalPhos.

The data generated from the direct comparison of **C0**, **2-C1**, and **2-C2** suggests that both a 3,4-thiophenyl linker and the inclusion of the PCg moiety improves catalytic performance. Considering this, Chapter 5 focuses on the evaluation of **L0** variants comprising both (hetero)aryl backbones and twofold incorporation of the unique PCg fragment.

4.5. Statement of Contributions for Chapter 4

Ligand and pre-catalyst syntheses (Schemes 4-1 and 4-3), pre-catalyst screening and aniline product isolation (Scheme 4-4), and manuscript preparation were conducted by J. S. K. Clark. *In-situ* catalytic screening (Scheme 4-2) was conducted by R. T. McGuire. DFT analysis and interpretation (Scheme 4-5) was executed by Dr. C. M. Lavoie. Single crystal X-ray diffraction analysis was conducted by Dr. Michael Ferguson. Prof. Dr. Mark Stradiotto acted as graduate supervisor for the lead author, and co-wrote the published manuscript. This work has been published: J. S. K. Clark, R. T. McGuire, C. M. Lavoie, M. J. Ferguson, M. Stradiotto. *Organometallics*, **2019**, *38*, 167-175.

Chapter 5. The Development of PAd2-DalPhos

5.1. Chapter 5 Overview

The unique tetramethyltrioxaphosphaadamantane (PCg) moiety serves as the commonality that links the PAd-DalPhos family of ligands (Section 1.3.3, Chapter 4). It is clear that this substituent, when used in ancillary ligand frameworks, imparts characteristics that give rise to excellent catalytic performance. The size of the PCg fragment has been described by Pringle and co-workers as related to a P*t*Bu$_2$ fragment, and its σ/π-bonding characteristics as similar to a diphenyl phosphonate,[116, 117] which collectively represent unusual attributes for alkylphosphines. In the context of catalysis, the bulky nature of PCg may dissuade comproportionation,[46-50, 52] formation of $(P_2)_2Ni^0$ species,[51, 104] or drive C-N reductive elimination.[103] The reduced electron-donating character compared to classic alkylphosphines may further assist the final C-N bond forming step.[103] Furthermore, Hazari suggested that arylphosphines enhance comproportionation of Ni^{II} species arising from η^2-coordination of approaching Ni^0 species with phosphino aryl rings, which could pose an additional benefit to the use of aliphatic PCg in ligand scaffolds.[50]

Encouraged by the success of PCg-containing PAd-DalPhos ligands, the work described in Chapter 5 explores the utility of analogous chelating bisphosphines featuring two PCg donor groups. In this chapter, the syntheses and characterization of new 'double cage' ancillary ligands comprising various (hetero)aryl backbones are reported, including PAd2-DalPhos (**3-L1**). Syntheses of (*o*-tolyl)nickel(II) chloride pre-catalysts bearing the double cage ligands are reported, followed by comparative catalytic screenings versus the analogous PAd-DalPhos (**L0**) complex, **C0**, in primary alkylamine couplings with (hetero)aryl chlorides employing challenging conditions. The results of these studies led to the application of air-stable (**3-L1**)Ni(*o*-tol)Cl, **3-C1**, which allows for previously unknown and sought-after Ni-catalyzed cross-couplings of primary five- and six-membered ring heteroarylamines and (hetero)aryl chlorides to be achieved with synthetically useful scope.

5.2. Synthesis of 'Double Cage' Ligands and Nickel Pre-catalysts

New double cage $(PCg)_2$(hetero)arene variants of **L0** based on phenyl (**3-L1**), pyridyl (**3-L2**), or quinoxalyl (**3-L3**) linking fragments were prepared in synthetically useful yield (Scheme 5-1A). Owing to the chiral (racemic) nature of the HPCg starting material, ~1:1 diastereomeric mixtures of air-stable *meso* (*RS*,*SR*) and *rac* (*RR*,*SS*) **3-L1**, **3-**

L2, and **3-L3** were obtained when using the sequential P-C cross-coupling approach outlined in Scheme 5-1A; in the case of **3-L1** and **3-L2**, the *meso* and *rac* diastereomers could be separated in air by use of column chromatography.[118] The isolated diastereomers of **3-L1** and **3-L2**, and the *meso*/*rac* mixture of **3-L3**, were characterized on the basis of solution NMR spectroscopic data and high-resolution mass spectrometric analysis. Furthermore, single-crystal X-ray data were successfully obtained for each of the *meso* and *rac* isomers of **3-L1**, **3-L2**, and **3-L3** (Section 6.4). The performance-enhancing ability of a 3,4-thiophenyl backbone (Chapter 4) warranted the exploration of a similar framework in this study; however, the synthesis of a variant starting from 3,4-dibromothiophene under otherwise analogous conditions to those found in Scheme 5-1A proved to be low-yielding and thus unsuitable for further investigation.

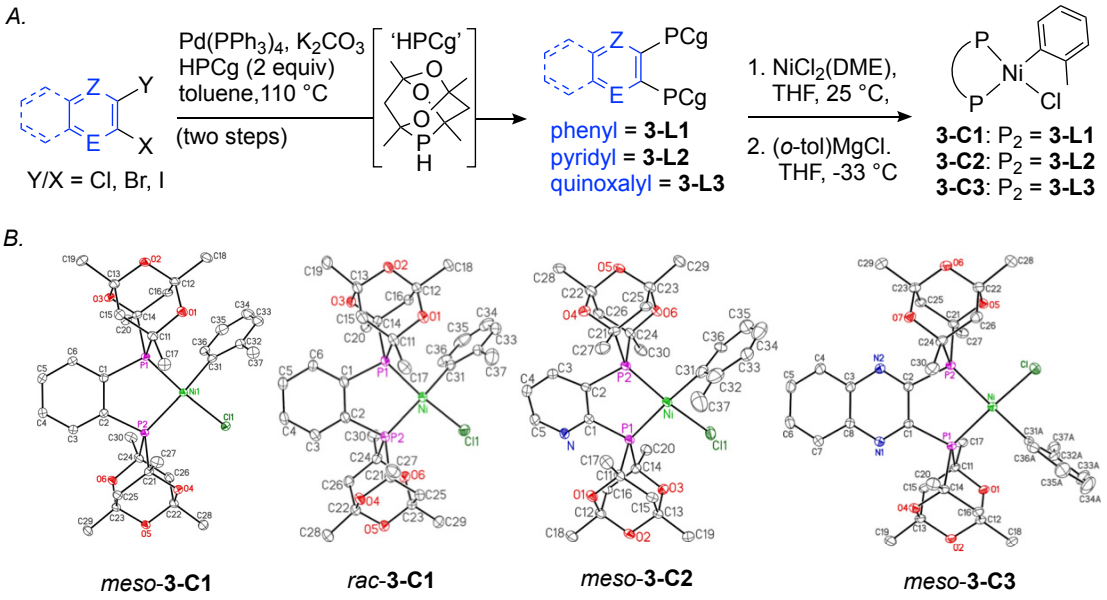

Scheme 5-1. Development of new 'double cage' ligands and respective Ni(II) pre-catalysts. *A*. Synthesis of **3-L1** to **3-L3** using sequential Pd-catalyzed P-C cross-coupling protocols, as well as **3-C1** to **3-C3**. *B*. Single-crystal X-ray structures of *meso*-**3-C1**, *rac*-**3-C1**, *meso*-**3-C2**, and *meso*-**3-C3**, each represented with thermal ellipsoids at the 30% probability level, and with hydrogen atoms omitted for clarity. Selected interatomic distances (Å) and angles (°): for *meso*-**3-C1**: Ni-P1 2.1791(7), Ni-P2 2.2458(7), Ni-Cl1 2.2177(8), Ni-C31 1.925(3), P1-Ni-P2 87.99(2); for *rac*-**3-C1**: Ni-P1 2.1679(10), Ni-P2 2.2402(10), Ni-Cl1 2.1893(11), Ni-C31 1.923(3), P1-Ni-P2 87.34(4); for *meso*-**3-C2**: Ni-P1 2.2266(16), Ni-P2

2.1629(17), Ni-Cl1 2.1968(17), Ni-C31 1.948(7), P1-Ni-P2 87.79(6); for *meso*-**3-C3**: Ni-P1 2.1634(6), Ni-P2 2.2253(6), Ni-Cl 2.1897(6), Ni-C31A 1.947(5), P1-Ni-P2 89.24(2).

Complexes of the type (**L**)Ni(*o*-tolyl)Cl featuring **3-L1**, **3-L2**, and **3-L3** were prepared via treatment with $NiCl_2$(DME), followed by transmetallation of the putative intermediates (**L**)$NiCl_2$ with (*o*-tolyl)MgCl, to afford **3-C1**, **3-C2**, and **3-C3** as analytically pure, air-stable solids (Scheme 5-1A). In addition to the solution NMR spectroscopic characterization of these complexes, single-crystal X-ray diffraction data were obtained for *meso*-**3-C1**, *rac*-**3-C1**, *meso*-**3-C2**, and *meso*-**3-C3** (Scheme 5-1B). In each case, a distorted square planar geometry is observed at Ni, with the Ni-P distance *trans* to chloride being shorter than the Ni-P distance opposite to the more strongly *trans*-directing *o*-tolyl group.

5.3. Catalytic Screening of 'Double Cage' Pre-catalysts

The catalytic competence of the new complexes **3-C1**, **3-C2**, and **3-C3**, versus **C0**, was assessed initially in challenging room temperature Ni-catalyzed C(sp^2)-N cross-couplings of the heteroaryl-containing substrate furfurylamine with aryl chlorides at low catalyst loadings, leading to products **4.1a-c** (Scheme 5-2). Employing 1.75 mol% of each complex with 4-chlorobenzonitrile to give **4.1a** revealed the superiority of **3-C1** to **3-C3** (>88% yield) versus **C0** (26% yield) in this reaction. In cross-couplings of 1-chloronaphthalene using 0.25 mol% Ni, the exceptionally high conversion to **4.1b** achieved when using **3-C1** or **3-C2** (>93% yield) was contrasted by the lower productivity of **C0** and **3-C3** (61% and 66% yield, respectively). These entries involving **3-C1** and **3-C2** represent the first examples of such high-yielding (>90%), Ni-catalyzed C(sp^2)-N cross-couplings of aryl chlorides conducted at room temperature using only 0.25 mol% Ni, in result outperforming ThioPAd-DalPhos (**2-L8**, Section 4.3.2). Similar trends were noted in cross-couplings involving 4-chloroanisole using 0.5 mol% catalyst, whereby **3-C1** and **3-C2** (>95% yield of **4.1c**) outperformed **C0** (24%). Having established **3-C1** and **3-C2** as offering comparably high catalytic efficiency, for simplicity subsequent examination of $(PCg)_2$(hetero)arene-based pre-catalysts was narrowed to the use of **3-C1**. In examining further cross-couplings leading to **4.1a** using only 0.5 mol% **C0** or **3-C1**, excellent productivity was attained with **3-C1** (78% yield), whereas no turnover was achieved using **C0**. Collectively, this survey establishes **3-C1** (and **3-C2**) as having the potential to offer

superior catalytic performance in these transformations versus otherwise best-in-class Ni pre-catalysts, such as **C0** and related variants.

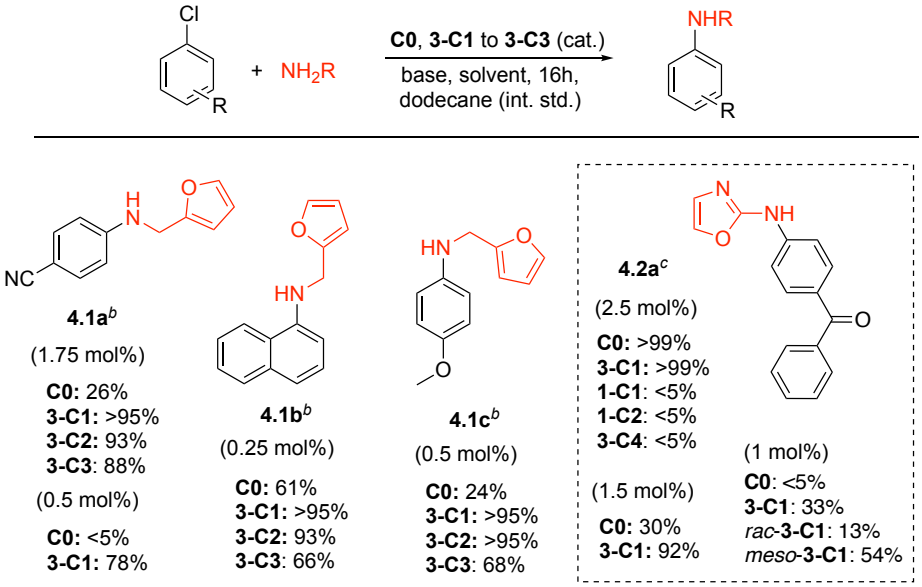

Scheme 5-2. Pre-catalyst screening. [a] Estimated conversion to the target product after 16 h (unoptimized time) on the basis of calibrated GC data using dodecane and authentic samples of **4.1a-c** as standards; mass balance corresponds to unreacted starting material; [b] NaO*t*Bu (2 equiv), toluene (0.12M ArCl), 25 °C; [c] NaOPh (1.2 equiv), 2-MeTHF (0.25M ArCl), 80 °C.

Encouraged by the outstanding catalytic performance of **3-C1** in known transformations leading to **4.1a-c**, application of this pre-catalyst in a desirable class of C(sp^2)-N cross-couplings for which no broadly effective base-metal catalyst is known was pursued. In this regard, the base-metal cross-coupling of primary five- or six-membered ring heteroarylamines with (hetero)aryl chlorides to afford unsymmetrical di(hetero)arylamines represents an attractive route to heteroatom-dense, biologically active compounds that exploit relatively inexpensive starting materials.[119] Heteroaromatic rings are found commonly in active pharmaceutical ingredients, owing to their roles as bioisosteres[120] and enhanced binding affinity with polar functional groups of proteins. The di(hetero)arylamine motif in particular, formally derived from primary five-membered ring heteroarylamines, is featured in a number of commercialized pharmaceuticals, including dasatanib (leukemia). However, metal-catalyzed C(sp^2)-N cross-coupling involving such NH nucleophiles has proven to be significantly more challenging than transformations

involving alkylamines or simple anilines, due in part to the increased acidity of the amine as a result of adjacent heteroatoms, which can lead to poor substrate binding and/or slow C-N reductive elimination.[103, 121] Prior to this work, no base-metal catalyst capable of effecting the cross-coupling of primary five-membered ring heteroarylamines and (hetero)aryl chlorides with synthetically useful scope had been disclosed in the literature. In the context of Pd catalysis, a 2017 report from Buchwald and co-workers[43] describing the C(sp^2)-N cross-coupling of (hetero)aryl chlorides and bromides with 2-aminooxazole and 4-aminothiazole using a Pd/EPhos catalyst (2.0-7.5 mol% Pd; 100 °C) represents the state-of-the-art for this type of transformation (Section 1.3.2.). In light of these considerations, the performance of **C0** and **3-C1**, as well as related pre-catalysts featuring CyPF-Cy (**1-C1**, Chapter 2),[71, 83] DPPF (**1-C2**, Chapter 2),[68] or XantPhos (**3-C4**),[93] which have each been employed successfully in alternative C(sp^2)-N cross-coupling applications, were compared in the cross-coupling of 2-aminooxazole and 4-chlorobenzophenone to give **4.2a** (2.5 mol% Ni, 80 °C; Scheme 5-2). Under these conditions, **C0** and **3-C1** afforded quantitative conversion to **4.2a**, whereas negligible catalytic turnover was achieved by use of the other Ni pre-catalysts. In lowering the loading to 1.5 mol% Ni, 92% yield of **4.2a** was achieved with **3-C1**, whereas use of **C0** afforded only 30% yield of **4.2a**. A significant drop-off in conversion was noted upon lowering the catalyst loading to 1 mol% Ni, whereby negligible conversion of the starting materials was achieved with **C0**, and 33% yield of **4.2a** was observed when using **3-C1**. Notably, further screening of this C(sp^2)-N cross-coupling reaction leading to **4.2a** employing diastereomerically pure *meso*-**3-C1** or *rac*-**3-C1** (1 mol% Ni) revealed the former to be more effective than the latter (with both being superior to **C0**) in this particular transformation.

5.4. Substrate Scope of PAd2-DalPhos

Encouraged by the utility of **3-C1** in the cross-coupling of 2-aminooxazole leading to **4.2a**, the scope of reactivity with other heteroarylamines and (hetero)aryl chlorides (Scheme 5-3) was explored. To avoid substrate-specific optimization, the diastereomeric mixture of **3-C1** (*meso* and *rac*) was employed at 5 mol% (i.e., the mid-point loading of the Pd/EPhos catalyst employed by Buchwald and co-workers[43]). 2-Aminooxazole, 2-aminothiazole, 5-amino-1,3-dimethyl-1H-pyrazole, and 2-aminopyridine were each employed successfully as nucleophiles in combination with **3-C1**, affording products **4.2a**-

l in synthetically useful isolated yield. Aryl chlorides containing ketone (**4.2a**) and cyano (**4.2e**) functionality proved to be suitable reaction partners, as did electrophiles featuring extended or linked aromatic hydrocarbon groups (**4.2j**, **4.2k**). Heteroaryl chlorides based on quinoxaline (**4.2b**, **4.2d**), quinoline (**4.2c**, **4.2h**), benzothiazole (**4.2g**), and quinaldine (**4.2f**, **4.2i**) core structures proved to be suitable reaction partners, and the successful cross-coupling of 2-bromo-4-phenylthiazole leading to **4.2l** confirmed the compatibility of heteroaryl bromides in this chemistry. In keeping with the trends in Scheme 5-2, inferior catalytic performance was observed for **C0** versus **3-C1** under analogous conditions in cross-couplings leading to **4.2b** or **4.2l**. For convenience, the experimental setup employed in the cross-coupling reactions leading to **4.2a**-**l** involved handling of the air-stable pre-catalyst **3-C1** on the benchtop, followed by reaction setup within an inert-atmosphere glovebox. To evaluate the chemoselectivity of **3-C1**, and to establish that glovebox/Schlenk methods are not required for the chemistry reported herein, the cross-coupling of 4-chloro-*N*-methylpicolinamide and aminopyrazine was conducted under nitrogen using benchtop-only protocols. The targeted unsymmetrical di(hetero)arylamino product **4.2m** was obtained in 83% isolated yield.

Control experiments were conducted to confirm that the transformations reported in Scheme 5-3 proceed negligibly in the absence of **3-C1** under the conditions employed. For the reaction leading to **4.2g**, exclusion of **3-C1** resulted in the formation of substantial quantities of the C-O coupled product arising from reactivity with the phenoxide base. These results notwithstanding, reactions involving ethyl 2-chlorooxazole carboxylate, 2-chlorobenzoxazole, 2-chlorobenzothiazole, 2-chloro-4,6-dimethoxypyrimidine, and 4-chloro-6,7-dimethoxyquinazoline afforded C-N coupled (and other) products in selected reactions with 2-aminothiazole, 2-aminooxazole, and 2-aminopyridine under the conditions in Scheme 5-3, but in the absence of **3-C1**. These observations underscore the importance of conducting control experiments in developing metal-catalyzed cross-coupling methodologies

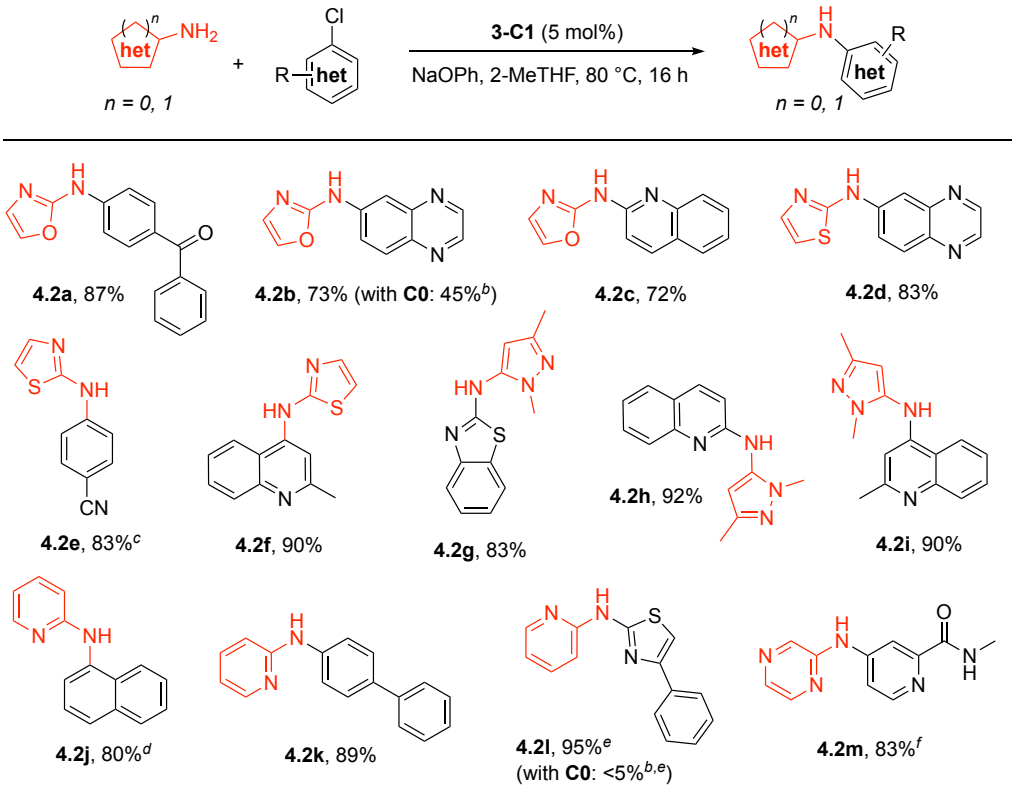

Scheme 5-3. Scope of the Ni-catalyzed C(sp^2)-N cross-coupling of primary heteroarylamines with (hetero)aryl electrophiles using **3-C1**. [a] Reaction conditions: **3-C1** (5 mol%), electrophile (1 equiv), amine (1.2 equiv), NaOPh (1.2 equiv), 2-MeTHF (0.25M ArX), 80 °C, 16h (unoptimized time). Isolated yields are reported, unless otherwise indicated; [b] NMR integrated yield using ferrocene as an internal standard in DMSO-d_6; [c] THF used as solvent, mixture of NaO*t*Bu, PhOH (1.2 equiv each) used as base; [d] NMR integrated yield using dodecane as an internal standard in $CDCl_3$; [e] Starting from the corresponding heteroaryl bromide; [f] in THF.

5.5. Limitations of PAd2-DalPhos and Other Synthetic Challenges

Some substrate scope limitations were encountered when employing **3-C1**, including unsuccessful cross-couplings of 5-amino-3-methylisoxazole or 2-amino-5-phenyl-1,3,4-thiadiazole with 4-halobenzonitrile (X = Cl or Br), or 3-chloropyridine with 4-aminopyridine, under conditions outlined in Scheme 5-3. Efforts to accommodate more complex diamine substrates, including the cross-coupling of 2,3-diaminopyrazine or 3,4-diaminopyridine with 4,6-dichloro-2-methylaniline, as well as electrophiles lacking activating groups (i.e., 4-chlorobiphenyl, 5-chlorobenzothiophene, 2-

chlorobenzothiophene, or 4-chloroanisole with 2-aminothiazole; 5-chloro-1,3-benzodioxole with 2-aminopyridine), were similarly unsuccessful.

Efforts to employ a transition-metal free synthesis of **3-L3** were unsuccessful. The synthetic route that accesses the similarly hindered *o*-(P*t*Bu$_2$)$_2$-benzene was envisioned to be directly applicable in the synthesis of double cage ligands reported herein, which makes use of a lithiated boronium bisphosphine salt to effect S_NAr-type reactivity on the ligand backbone.[122] Bridging of the phosphino groups in this manner creates an intramolecular scenario upon initial nucleophilic attack, which may favour the installation of two adjacent hindered fragments over sequential additions of monophosphine borane lithium salts.[123] Attempts to employ (HPCg)$_2$BH$_2$Br as shown in Scheme 5-4 afforded trace product and liberated HPCg. The lower basicity of HPCg relative to HP*t*Bu$_2$ may lead to a weaker adduct in the formation of the boronium bisphosphine salt, which is likely responsible for its decomposition upon lithiation.

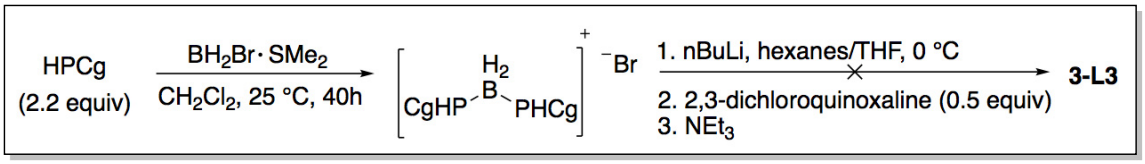

Scheme 5-4. Alternative (albeit unsuccessful) transition metal-free synthesis of **3-L3** employing (HPCg)$_2$BH$_2$Br.

5.6. Chapter 5 Summary

The success of PCg containing PAd-DalPhos ligands prompted the development of a new class of double cage bisphosphine ligands (i.e., *o*-PCg$_2$-(hetero)arene), including PAd2-DalPhos (**3-L1**) to address outstanding challenges in Ni-catalyzed C(sp^2)-N cross-coupling. Double cage ligands bearing phenylene (**3-L1**), pyridine, and quinoxaline backbones were examined in reactivity surveys versus the state-of-the-art parent PAd-DalPhos (**L0**) in their respective (**L**)Ni(*o*-tolyl)Cl pre-catalyst forms. Building on the observation that **3-L1** systematically outperformed **L0** in selected challenging test cross-couplings involving furfurylamine and 2-aminooxazole as nucleophiles, the **3-L1** derived Ni pre-catalyst **3-C1**was employed successfully in establishing the first base-metal cross-coupling of (hetero)aryl chlorides and primary five- or six-membered ring heteroarylamines, with synthetically useful scope. Application of **3-L1** in this context has

expanded the substrate scope for Ni-catalyzed amination methods, allowing for more elaborate organic molecules that are pharmaceutically and biologically relevant to be constructed. Notably, the catalytic performance of the Ni pre-catalyst **3-C1** in enabling the assembly of sought-after heteroatom-dense, unsymmetrical di(hetero)arylamines is competitive with state-of-the-art Pd catalysis, in terms of catalyst loading and substrate scope, while operating effectively at milder reaction temperatures.

5.7. Statement of Contributions for Chapter 5

Experimental work and manuscript preparation was conducted by J. S. K. Clark. Single crystal X-ray diffraction analyses were conducted by Dr. Michael Ferguson and Dr. Robert McDonald. Prof. Dr. Mark Stradiotto acted as graduate supervisor for the lead author, and co-wrote the published manuscript. M. Yue Shen and J. P. Tassone contributed to catalyst screening. Repare Therapeutics provided chemicals and instrumentation time during the revision phase of this work. This work has been published: J. S. K. Clark, M. J. Ferguson, R. McDonald, M. Stradiotto. *Angew. Chem. Int. Ed.*, **2019**, *58*, 6391-6395.

Chapter 6. Experimental Details

6.1. General Considerations

Unless otherwise indicated, all experimental procedures were conducted in a nitrogen-filled, inert-atmosphere glovebox using oven-dried glassware and purified solvents, with the exception of the workup of catalytic reaction mixtures which was conducted on the bench-top in air using unpurified solvents. For solvents used within the glovebox, the following purification methods were used: toluene, hexanes, and pentane were deoxygenated by sparging with nitrogen gas followed by passage through an mBraun double column solvent purification system packed with alumina and copper-Q5 reactant; tetrahydrofuran and diethyl ether were dried over Na/benzophenone followed by distillation under an atmosphere of nitrogen gas; *tert*-butanol was dried over CaH_2 followed by distillation under an atmosphere of dinitrogen; anhydrous cyclopentyl methyl ether (CPME), 2-methyltetrahydrofuran (2-MeTHF) and dichloromethane were sparged with nitrogen gas and stored over 4 Å molecular sieves for 24 h prior to use. All solvents used within the glovebox were stored over activated 4 Å molecular sieves. All other commercial solvents, reagents, and materials were used as received. Each of 4-ethylphenyl tosylate,[124, 125] 1-naphthyltosylate,[126] *N*-methylnaphthalen-1-amine,[72] 2-(1,3,5,7-tetramethyl-2,4,8-trioxaphosphaadmantyl)-3-bromobenzene (**P1**),[72] (PAd-DalPhos)Ni(*o*-tolyl)Cl (**C0**),[72] and (DPPF)Ni(*o*-tolyl)Cl (**1-C2**),[68] were prepared using literature procedures. With the exception of bis(3,5-dimethyl-4-anisyl)chlorophosphine,[127] which was prepared as per literature methods, all chlorophosphines as well as **1-L1**, $\mathbf{L^{Ph}}$, $\mathbf{L^{iPr}}$, $\mathbf{L^{Cy}}$, $\mathbf{L^{tBu}}$, and $\mathbf{L^{fur}}$ were obtained from Strem Chemicals. The known ligands $\mathbf{L^{o\text{-}tol}}$,[100] $\mathbf{L^{CF3}}$,[100] and $\mathbf{L^{1\text{-}nap}}$[128] were synthesized in a manner analogous to that described for $\mathbf{L^{OMe}}$ and $\mathbf{L^{Me}}$, via quenching of dilithiated ferrocene prepared *in situ* using literature methods[128] with two equivalents of the appropriate $ClPR_2$ reagent, employing modified literature protocols.[100] All other chemicals were obtained from commercial suppliers and were used as received. GC data were obtained on an instrument equipped with a SGE BP-5 column (30 m, 0.25 mm i.d.). Flash column chromatography was carried out using Silicycle Siliaflash 60 silica (particle size 40 - 63 μm; 230-400 mesh). In the case of **4.2m**, purification was carried out in air employing reverse-phase flash chromatography using an Isco Gold-C18 50g cartridge, followed by lyophilization using a FreeZone 4.5 Liter Benchtop Freeze Dry System,

operating at a collector temperature of -50 °C. ^{1}H NMR (500 and 300 MHz), ^{13}C{^{1}H} NMR (125.8 and 75.5 MHz), and ^{31}P{^{1}H} NMR (202.5 and 121.4 MHz) spectra were recorded at 300 K in $CDCl_3$ with chemical shifts expressed in parts per million (ppm). Splitting patterns are indicated as follows: br, broad; s, singlet; d, doublet; t, triplet; q, quartet; m, multiplet. Mass spectra were obtained using ion trap (ESI) instruments operating in positive mode.

6.2. Synthetic Procedures and Characterization Data for Nickel Complexes and Bisphosphine Ligands

Synthesis of 1,1'-(bis(di-(3,5-dimethyl-4-anisyl))-phosphino)ferrocene (**L^{OMe}**):

Within a glovebox, a vial containing a magnetic stir bar was charged with ferrocene (167 mg, 0.9 mmol), tetramethylethylenediamine (283 µL, 1.89 mmol), and hexanes (3.74 mL), and magnetic stirring was initiated. To the vial was added dropwise *n*-butyllithium (2.5 M in hexanes, 756 µL, 1.89 mmol) and the resulting mixture was allowed to stir at ambient temperature for 12 h. In a separate vial, bis(3,5-dimethyl-4-anisyl)chlorophosphine (637 mg, 1.89 mmol) was treated with tetrahydrofuran (1.2 mL); we found this chlorophosphine to be poorly soluble in this and other common solvents. Both the chlorophosphine mixture and the dilithioferrocene mixture were cooled to -33 °C. To the stirring dilithioferrocene mixture the chlorophosphine mixture was added dropwise, and the resulting mixture was then stirred until full consumption of the chlorophosphine was confirmed on the basis of ^{31}P{^{1}H} NMR data obtained from a reaction aliquot (ca. 2 h). The reaction mixture was then concentrated *in vacuo* and purified by flash column chromatography on silica gel using a gradient eluent: starting with hexanes (~200 mL), 49:1 hexanes/ethyl acetate (~200 mL), 24:1 hexanes/ethyl acetate (~400 mL) and finishing with 15.7:1 hexanes/ethyl acetate. The product was isolated in 30% yield (210 mg, 0.27 mmol) as a light orange solid. ^{1}H NMR (500 MHz, $CDCl_3$): δ 6.97-6.96 (m, 8H), 4.20 (m, 4H), 4.03 (m, 4H), 3.71 (s, 12H), 2.22 (s, 24H). ^{13}C{^{1}H} NMR (125.8 MHz, $CDCl_3$): δ 157.6, 134.1 (d, J = 20.1 Hz), 135.5, 130.7, 130.6, 73.6 (d, J = 13.8 Hz), 72.3, 59.8, 16.3. ^{31}P{^{1}H} NMR (202.5 MHz; $CDCl_3$): δ -19.1. HRMS *m/z* ESI^{+} found 787.2763 $[M + H]^{+}$ calculated for $C_{46}H_{53}FeO_4P_2$ 787.2769.

Synthesis of 1,1'-(bis(3,5-xylyl)phosphino)ferrocene (**L^{Me}**): A protocol directly analogous to that described for the synthesis of **L^{OMe}** was employed (above), using ferrocene (148 mg, 0.85 mmol), tetramethylethylenediamine (268 µL, 1.79 mmol), *n*-

butyllithium (2.5 M in hexanes, 714 μL, 1.79 mmol), and bis(3,5-xylyl)chlorophosphine (494 mg, 1.79 mmol). The reaction mixture was then concentrated *in vacuo* and purified by flash column chromatography on silica gel using a gradient eluent: starting with hexanes (~200 mL), 99:1 hexanes/ethyl acetate (~200 mL), 49:1 hexanes/ethyl acetate (~200 mL), 32.3:1 hexanes/ethyl acetate (~200 mL), and finishing with 24:1 hexanes/ethyl acetate. The product was isolated in 35% yield (221 mg, 0.30 mmol) as a light orange solid. ^{1}H NMR (500 MHz, $CDCl_3$): δ 6.97-6.94 (m, 12H), 4.27-4.26 (m, 4H), 4.04-4.03 (m, 4H), 2.27 (s, 24H). $^{13}C\{^{1}H\}$ NMR (125.8 MHz, $CDCl_3$): δ 138.7 (d, J = 7.6 Hz), 137.8 (d, J = 6.3 Hz), 131.7, 131.5, 130.7, 74.0 (d, J = 13.8 Hz), 72.8, 21.8. $^{31}P\{^{1}H\}$ NMR (202.5 MHz, $CDCl_3$): δ -16.9. HRMS *m/z* ESI^+ found 667.2340 $[M + H]^+$ calculated for $C_{42}H_{45}FeP_2$ 667.2346.

General procedure for the synthesis of *ortho*-PR_2-halo(hetero)arene precursors (**P2**-**P9**); In a dinitrogen filled glovebox, a vial containing a magnetic stir bar was charged with $Pd(PPh_3)_4$ (0.05 equiv), K_2CO_3 (2.0 equiv), *ortho*-dihalo(hetero)arene (2,3-dibromopyridine, 1,2-bromoiodobenzene, 2,3-dibromothiophene, 3,4-dibromothiophene 2-chloro-3-bromopyridine, or 2,3-dichloroquinoxaline, 1.05 equiv), toluene (0.15 M aryl halide; 0.3 M aryl halide for **P8**-**P9**), and the appropriate phosphine (1,3,5,7-tetramethyl-2,4,8-trioxaphosphaadamantane (HPCg) or di-*o*-tolylphosphine (HP(*o*-tol)$_2$), 1.0 equiv). The vial was sealed with a cap containing a PTFE septum, removed from the glovebox and placed in a temperature-controlled aluminum heating block set to 110 °C for 48 h under the influence of magnetic stirring. The reaction mixture was subjected to purification according to Workup Method D (1-P(*o*-tol)$_2$-2-bromobenzene, **P2**: 19:1 hexanes/dichloromethane eluent; 2-PCg-3-bromopyridine, **P3**: 19:1 hexanes/ethyl acetate eluent; 2-P(*o*-tol)$_2$-3-bromopyridine, **P4**: 19:1 hexanes/ethyl acetate eluent; 2-PCg-3-bromothiophene, **P5**: 24:1 hexanes/ethyl acetate eluent; 2-P(*o*-tol)$_2$-3-bromothiophene, **P6**: 49:1 hexanes/ethyl acetate eluent; 3-P(*o*-tol)$_2$-4-bromothiophene, **P7**: 7:3 hexanes/dichloromethane eluent; 2-chloro-3-PCg-pyridine, **P8**: hexanes/ethyl acetate eluent gradient (19:1, 500 mL; 17:3, 300 mL); 2-chloro-3-PCg-quinoxaline, **P9**: 23:2 hexanes/ethyl acetate eluent) and subsequently dried *in vacuo* to afford the desired arylphosphine as a white to off-white solid (**P2**: 69% (268 mg, 0.73 mmol); **P3**: 68% (1.27 g, 3.42 mmol); **P4**: 83% (1.54 g, 4.15 mmol); **P5**: 66% (498 mg, 1.32 mmol); **P6**: 73% (1.10 g, 2.92 mmol); **P7**: 87% (327 mg, 0.87 mmol); **P8**: 48% (365 mg, 1.11 mmol); **P9** (yellow solid): 57% (1.31 g, 3.45 mmol)). While **P2** is a

known compound that was prepared *via* lithiation and quench of *o*-dibromobenzene using bis(2-methylphenyl)chlorophosphine, an alternative synthesis is reported herein; spectral data are in agreement with literature.[129] Data for **P2**-**P9** can be found in the Appendix.

Procedure for the synthesis of *o*-(P(*o*-tolyl)$_2$)$_2$benzene (**2-L1**): In a dinitrogen filled glovebox, **P2** was dissolved in diethyl ether (1.0 equiv, 0.5 M) within a vial containing a magnetic stir bar. The vial was sealed with a cap containing a PTFE septum, and cooled to -33 °C. Under the influence of magnetic stirring, *n*-butyllithium (1.2 equiv, 2.5 M in hexanes) was added dropwise to the solution, and the resulting mixture was left to stir at ambient temperature. After 30 minutes, a solution of di(*o*-tolyl)chlorophosphine dissolved in diethyl ether (1.1 equiv, 0.55 M) was added dropwise to the stirring solution. The resulting solution was left to stir for 48 h (unoptimized) at ambient temperature. At this point the reaction mixture was purified according to Workup Method D, using a hexanes/dichloromethane eluent gradient (9:1, 300 mL; 17:3, 300 mL; 4:1, 400 mL). The resultant material was dried *in vacuo* to afford **2-L1** in 85% yield (295 mg, 0.59 mmol). While **2-L1** is a known compound that was prepared *via* addition of excess (*o*-tolyl)MgBr to 1,2-bis(dichlorophosphino)benzene, an alternative synthesis is reported herein; spectral data are in agreement with literature.[115] ^{1}H NMR (300 MHz, $CDCl_3$): δ 7.24-7.13 (m, 10H, ArH), 7.01-6.92 (m, 6H, ArH), 6.76-6.74 (m, 4H, ArH), 2.21 (s, 12H, CH_3). $^{13}C\{^{1}H\}$ UDEFT NMR (125.8 MHz, $CDCl_3$): δ 145.1-144.7 (m, ArC), 144.2-143.9 (dd, $J_{1\ C\text{-}P}$ = 8.4 Hz, $J_{2\ C\text{-}P}$ = 24.3 Hz, ArC), 142.3-142.0 (m, ArC), 135.9 (d, $J_{C\text{-}P}$ = 10.1 Hz, ArC), 135.6 (d, $J_{C\text{-}P}$ = 8.8 Hz, ArC), 133.8 (m, ArC), 132.7-132.6 (m, ArC), 131.7 (ArC), 129.9 (m, ArC), 128.7 (ArC), 128.3 (ArC), 125.8 (ArC), 21.2-21.0 (overlapping signals, CH_3). $^{31}P\{^{1}H\}$ NMR (121.5 MHz, $CDCl_3$): δ -27.8 (s). HRMS *m/z* ESI$^+$ found 503.2052 $[M + H]^+$ calculated for $C_{34}H_{33}P_2$ 503.2057. The corresponding NMR spectra are found in the Appendix.

General procedure for the synthesis of 2-PR_2-3-PR'_2-(hetero)arene ligands: In a dinitrogen filled glovebox, a vial containing a magnetic stir bar was charged with the appropriate arylphosphine precursor (**P1**, or **P3**-**P9**, 1.0 equiv), $Pd(PPh_3)_4$ (0.07 (for **3-L#**) or 0.1 (for **2-L#**) equiv), K_2CO_3 (2.0 equiv), toluene (0.15 M aryl halide; 0.3 M aryl halide for **3-L1** to **3-L3**), and the appropriate phosphine (1,3,5,7-tetramethyl-2,4,8-trioxaphosphaadamantane or di-*o*-tolylphosphine, 1.0 equiv). The vial was sealed with a

cap containing a PTFE septum, removed from the glovebox and placed in a temperature-controlled aluminum heating block set to 110 °C for 48 h under the influence of magnetic stirring. The reaction mixture was then subjected to purification according to Workup Method D (2-PCg-3-P(*o*-tol)$_2$-pyridine, **2-L2**: 93:7 hexanes/ethyl acetate eluent; 2-P(*o*-tol)$_2$-3-PCg-pyridine, **2-L3**: 93:7 hexanes/ethyl acetate eluent; 2,3-(P(*o*-tol)$_2$)$_2$pyridine, **2-L4**: 3:2 hexanes/dichloromethane eluent; 2-PCg-3-P(*o*-tol)$_2$-thiophene, **2-L5**: 7:3 hexanes/dichloromethane eluent; 2-P(*o*-tol)$_2$-3-PCg-thiophene, **2-L6**: 24:1 hexanes/ethyl acetate eluent; 3,4-(P(*o*-tol)$_2$)$_2$-thiophene, **2-L7**: 9:1 hexanes/dichloromethane eluent; 3-PCg-4-P(*o*-tol)$_2$-thiophene, **2-L8**: 7:3 hexanes/dichloromethane eluent; 3,4-(P(*o*-tol)$_2$)$_2$-thiophene, **2-L9**: hexanes/dichloromethane eluent gradient (9:1, 300 mL; 17:3, 500 mL); *o*-PCg$_2$-benzene, PAd2-DalPhos, **3-L1**: 19:1 hexanes/ethyl acetate eluent; 2,3-PCg$_2$-pyridine, **3-L2**: hexanes/ethyl acetate eluent gradient (9:1, 400 mL; 17:3, 400 mL; 4:1, 400 mL); 2,3-PCg$_2$-quinoxaline, **3-L3**: 23:2 hexanes/ethyl acetate eluent) and subsequently dried *in vacuo* to afford the desired bisphosphine as a white to off-white solid (**2-L2**: 41% (276 mg, 0.55 mmol); **2-L3**: 64% (324 mg, 0.64 mmol); **2-L4**: 63% (278 mg, 0.55 mmol); **2-L5**: 70% (357 mg, 0.70 mmol); **2-L6**: 51% (347 mg, 0.68 mmol); **2-L7**: 46% (206 mg, 0.41 mmol); **2-L8**: 71% (364 mg, 0.71 mmol); **2-L9**: 31% (148 mg, 0.29 mmol); **3-L1**: 62% (543 mg, 1.07 mmol); **3-L2**: 66% (276 mg, 0.54 mmol); **3-L3** (yellow solid): 61% (170 mg, 0.30 mmol)). Separation of *meso*-**3-L1** (R_f = 0.20, 9:1 hexanes/ethyl acetate eluent) from *rac*-**3-L1** (R_f = 0.28, 9:1 hexanes/ethyl acetate eluent), and *meso*-**3-L2** (R_f = 0.29, 4:1 hexanes/ethyl acetate eluent) from *rac*-**3-L2** (R_f = 0.51, 4:1 hexanes/ethyl acetate eluent) was achieved *via* chromatographic purification. An attempt to synthesize **3-L1** in one step using 2.1 equiv HPCg, 1.0 equiv 1,2-bromoiodobenzene, and 0.1 equiv Pd(PPh$_3$)$_4$ afforded the desired bisphosphine in a 20% isolated yield (0.053 mg, 0.10 mmol), which is lower than the 53% net yield when using the two-step protocol outlined herein (86% yield **P1**,[72] 62% yield **3-L1**). Data for *rac*-**3-L1** and *meso*-**3-L1** are found in Section 6.5, NMR spectra for *meso*-**3-L1** are found in Section 6.5, and NMR spectra for *rac*-**3-L1** are found in the Appendix. Data and spectra for **2-L3** to **2-L9**, **3-L2**, and **3-L3** are found in the Appendix.

Synthesis of (**L**)Ni(*o*-tolyl)Cl Pre-catalysts: Within an inert atmosphere glovebox a vial containing a magnetic stir bar was charged with NiCl$_2$(DME) (1.0 equiv) and either **1-**

L1 (CyPF-Cy, 0.95 equiv), **2-L8**, **2-L9** (1.1 equiv), 1,1'-(bis(diisopropyl)phosphino)ferrocene (**L**$^{i\mathbf{Pr}}$), *meso*-**3-L1**, *rac*-**3-L1**, **3-L1**, **3-L2**, or **3-L3** (1.05 equiv). To the solid mixture was added THF (0.1 M; 0.2 M with **1-L1**), and the resulting heterogeneous mixture was stirred magnetically at room temperature for 2 h. The reaction vial was removed from the glovebox, and in air the reaction mixture was treated with pentane (4 mL) thereby generating a precipitate. The solid was isolated *via* suction filtration, washed with pentane (3 × 2 mL), and dried *in vacuo* to afford the putative intermediates (**1-L1**)$NiCl_2$ as a dark purple solid , (D*i*PPF)$NiCl_2$ as a dark green solid, and PAd-DalPhos variant containing (**L**)$NiCl_2$ complexes as purple solids, which were used without further purification. Within an inert atmosphere glovebox, each of the isolated (**L**)$NiCl_2$ (1.0 equiv) were transferred to a vial containing a magnetic stir bar, followed by the addition of THF (0.1 M). The resultant heterogeneous mixture was cooled to −33 °C for 0.5 h, followed by the addition of precooled (*o*-tol)MgCl (−33 °C, 1.0 M in THF, 1.2 equiv); the mixture was allowed to warm to room temperature under the influence of magnetic stirring. After 4 h, the reaction vial was removed from the glovebox, and the reaction mixture was treated with methanol (0.5 mL) and pentane (4 mL) thereby generating a precipitate. The solid was isolated *via* suction filtration and washed with cold methanol (3-4 × 1 mL) followed by cold pentane (3-5 × 2 mL). The resulting material was dried *in vacuo* to afford desired products **1-C1** (0.32 mmol, 78%), (**L**$^{i\mathbf{Pr}}$)Ni(o-tolyl)Cl (0.20 mmol, 57%), **2-C1** (0.38 mmol, 71%), **2-C2** (0.33 mmol, 73%), *meso*-**3-C1** (0.02 mmol, 44%), *rac*-**3-C1** (0.13 mmol, 71%), **3-C1** (0.65 mmol, 78%), **3-C2** (0.10 mmol, 50%), and **3-C3** (0.08 mmol, 59%) as analytically pure light to dark orange solids. A single crystal suitable for X-ray diffraction was obtained *via* vapor diffusion of diethyl ether into a dichloromethane solution in the case of **1-C1** and (**L**$^{i\mathbf{Pr}}$)Ni(o-tolyl)Cl, pentane into a dichloromethane solution in the case of **2-C1**, **2-C2**, *rac*-**3-C1, 3-C2**, and **3-C3**, and pentane into a deuterated chloroform solution in the case of *meso*-**3-C1**. Typically, the ^{1}H and $^{13}C\{^{1}H\}$ solution NMR spectra for these complexes are sufficiently complex so as to preclude meaningful assignment, arising from a combination of: diastereomeric mixtures of Ni(II) complexes in the case of **3-C1, 3-C2**, and **3-C3**; second-order coupling; dynamic behavior arising from hindered rotation in the case of **1-C1**, **2-C1** and **2-C2**; and the potential for dynamic equilibria involving Ni-(*o*-tolyl) rotamers and/or between tetrahedral

and square planar species. Where feasible, NMR assignments are provided. Data for **3-C1** and NMR spectra for *meso*-**3-C1** is found in Section 6.5, and NMR spectra for **3-C1** and *rac*-**3-C1** is found in the Appendix. Data and NMR spectra for **1-C1**, (**L**$^{i\mathbf{Pr}}$)Ni(o-tolyl)Cl, **2-C1**, **2-C2**, **3-C2**, and **3-C3** are provided in the Appendix.

6.3. General Catalytic Procedures and Workup Methods

General procedure for the mono-arylation of primary amines with (hetero)aryl (pseudo)halides (**GP1**): Within a glovebox, either bis(cyclooctadiene)nickel(0) (0.05 eq.) and **L**$^{\mathbf{X}}$ or **2-L#** (0.05 eq.), or pre-catalyst **C0**, **1-C1**, or **1-C2** (0.005-0.10 eq.) were added to a screw capped vial containing a magnetic stir bar, followed by the addition of NaO*t*Bu (2.0 eq.), aryl (pseudo)halide (1.0 eq.), and toluene (0.12 M of aryl (pseudo)halide; when using **2-L#**, bis(cyclooctadiene)nickel(0) (0.05 equiv) was pre-dissolved in toluene), followed by the addition of the primary amine (1.1 eq.). When using **2-C1**, **2-C2**, **3-C1**, **3-C2**, or **3-C3** in competition experiments versus **C0**, the catalyst was delivered *via* an aliquot from a freshly prepared stock solution (0.025-0.00125 equiv, 2.5 g/L in dichloromethane) to a screw capped vial and evaporated to dryness *in vacuo*, and the vial was then transferred into a nitrogen-filled glovebox for subsequent reagent addition. The vial was sealed with a cap containing a PTFE septum, removed from the glovebox and placed in a temperature-controlled aluminum heating block set to either 25 °C or 110 °C for 16 hours. After cooling to room temperature, reactions were monitored using both TLC and GC methods. The product was isolated or analyzed by using one of Workup Methods A-C.

General procedure for the mono-arylation of ammonia with aryl chlorides (**GP2**): Within a glovebox, **2-L#** (0.05 equiv) or pre-catalyst **C0**, **1-C1**, or **1-C2** (0.005-0.10 equiv), NaO*t*Bu (2.0 equiv), aryl chloride (1.0 equiv), and toluene (0.06-0.1 M aryl chloride; when using **2-L#**, bis(cyclooctadiene)nickel(0) (0.05 equiv) was pre-dissolved in toluene) were added to a screw capped vial containing a magnetic stir bar, followed by the addition of ammonia (0.5 M in 1,4-dioxane, 3.0-7.0 eq.). The vial was sealed with a cap containing a PTFE septum, removed from the glovebox and placed in a temperature-controlled aluminum heating block set to either 25 °C or 110 °C for 16 hours. After cooling to room temperature, reactions were monitored using both TLC and GC methods. The product was isolated or analyzed by using one of Workup Methods A-C.

General procedure for the *N*-arylation of morpholine with aryl halides (**GP3**): Within a glovebox, bis(cyclooctadiene)nickel(0) (0.05 eq.) and $\mathbf{L^X}$ (0.05 eq.), or pre-catalyst **C0**, **1-C1**, or **1-C2** (0.05 eq.), LiO*t*Bu (1.5 eq.), aryl halide (1.0 eq.), cyclopentyl methyl ether (0.5 M in aryl halide), were added to a screw capped vial containing a magnetic stir bar, followed by the addition of morpholine (1.5 eq.). The vial was sealed with a cap containing a PTFE septum, removed from the glovebox and placed in a temperature-controlled aluminum heating block set to 25 °C or 100 °C for 16 hours. After cooling to room temperature, reactions were monitored using both TLC and GC methods. The product was isolated or analyzed by using Workup Method A or B.

General procedure for the *N*-arylation of indole with aryl halides (**GP4**): Within a glovebox, bis(cyclooctadiene)nickel(0) (0.05 eq.), $\mathbf{L^X}$ (0.05 eq.), LiO*t*Bu (1.5 eq.), aryl halide (1.0 eq.), toluene (0.12 M of aryl halide), were added to a screw capped vial containing a magnetic stir bar, followed by the addition of indole (1.1 eq.). The vial was sealed with a cap containing a PTFE septum, removed from the glovebox and placed in a temperature-controlled aluminum heating block set to 25 °C or 110 °C for 16 hours. After cooling to room-temperature, reactions were monitored using both TLC and GC methods. The product was isolated or analyzed by using Workup Method A or B.

General procedure for the *N*-arylation of benzamide with 4-chlorobenzonitrile (**GP5**): In a nitrogen-filled glovebox, **2-L#** (0.05 equiv), tripotassium phosphate (1.5 equiv), benzamide (1.1 equiv), and 4-chlorobenzonitrile (1.0 equiv) were added to a screw capped vial containing a magnetic stir bar, followed by the addition of bis(cyclooctadiene)nickel(0) (0.05 equiv) dissolved in *tert*-butanol (0.12 M aryl halide). The vial was sealed with a cap containing a PTFE septum, removed from the glovebox and placed in a temperature-controlled aluminum heating block set to 90 °C for 16 h under the influence of magnetic stirring. After cooling to room-temperature, dodecane (0.12 mmol) was added to the reaction mixture, which was subsequently analyzed by use of GC methods following Workup Method B.

General procedure for the mono-arylation of primary heteroarylamines with (hetero)aryl halides (**GP6**): On the benchtop, an aliquot from a freshly prepared stock solution of **C0** or **3-C1** (0.025-0.010 equiv, 2.5 g/L in dichloromethane) was delivered to a screw capped vial and evaporated to dryness *in vacuo*, and the vial was then transferred

into a nitrogen-filled glovebox; when employing 0.05 equiv **C0** or **3-C1**, the vial was charged with the pre-catalyst as a solid within a nitrogen-filled glovebox. To the vial was added a magnetic stir bar, NaOPh (1.2 equiv), 2-methyltetrahydrofuran (0.24 M aryl halide), (hetero)aryl halide (1.0 equiv), and primary heteroarylamine (1.2 equiv). The vial was sealed with a cap containing a PTFE septum, removed from the glovebox and placed in a temperature-controlled aluminum heating block set to 80 °C for 16 h under the influence of magnetic stirring. After cooling to room-temperature, dodecane (1.0 equiv, 0.12 mmol) was added to the reaction mixture when 0.025-0.010 equiv pre-catalyst was used, which was subsequently analyzed by use of GC methods following Workup Method B; when 0.050 equiv pre-catalyst was used, the reaction mixture was subjected to purification according to Workup Method A.

Procedure for aryl (pseudo)halide competition studies (**GP7**): Pre-catalyst **C0** or **1-C1** (0.006 mmol, 0.05 equiv), furfurylamine (46.4 μL, 0.525 mmol, 1.05 equiv), NaO*t*Bu (96.1 mg, 1.0 mmol, 2.0 equiv), 4-chlorotoluene (59.1 μL, 0.5 mmol, 1.0 equiv), and 1-butyl-4-bromobenzene or 4-ethylphenyl tosylate (0.5 mmol, 1.0 equiv) were added to a screw capped vial containing a magnetic stir bar, followed by the addition of toluene (4.2 mL). The vial was sealed with a cap containing a PTFE septum, removed from the glovebox and placed in a temperature-controlled aluminum heating block set to 25 °C for 16 hours. After cooling to room temperature, the reaction mixture was diluted with ethyl acetate (ca. 30 mL), washed with brine (3 × ca. 30 mL) and the organic layer was dried over sodium sulfate. The resultant mixture was adsorbed onto silica gel to form a dry pack and eluted with hexanes (200 mL) on a silica plug to remove the residual starting materials. The product was then eluted through the dry pack with ethyl acetate (200 mL), the eluent was collected and the solvent was removed *in vacuo* via rotary evaporation. Ferrocene was subsequently added to the dry reaction mixture as an internal standard (18.6 mg, 0.1 mmol, 0.2 equiv), and the reaction mixture was taken up in $CDCl_3$ (3 mL). A drop of D_2O was added to the sample to eliminate the exchangeable NH proton peak in the spectrum. The resultant solution was subjected to NMR analysis.

Procedure for the monitoring of reaction progress via NMR analysis (**GP8**): Pre-catalyst **C0** or **1-C1** (0.006 mmol, 0.01 equiv), 0.5 M ammonia in 1,4-dioxane (3.6 mL, 1.8 mmol, 3.0 equiv), NaO*t*Bu (115.3 mg, 1.2 mmol, 2.0 equiv), and 1-chloronaphthalene (81.7

μL, 0.6 mmol, 1.0 equiv) were added to a screw capped vial containing a magnetic stir bar, followed by the addition of toluene (2.4 mL). The procedure was repeated individually eight times, one for each designated time interval. The vials were sealed with caps containing PTFE septa, removed from the glovebox and placed in a temperature-controlled aluminum heating block set to 25 °C. Each reaction vial was removed from the heating block after incremental time intervals of 15 minutes, was diluted with ethyl acetate (ca. 30 mL), washed with brine (3 × ca. 30 mL), and the organic layer was dried over sodium sulfate. The solvent was removed *in vacuo* via rotary evaporation, and dodecane was subsequently added to the dry reaction mixture as an internal standard (13.6 μL, 0.06 mmol, 0.1 equiv), and the reaction mixture was taken up in $CDCl_3$ (3 mL). The resultant solution was subjected to NMR analysis.

General procedure for monitoring the reaction progress of the mono-arylation of furfurylamine with 1-chloronaphthalene using GC methods (**GP9**): On the benchtop, an aliquot from a freshly prepared stock solution of **C0** or **2-C1** (0.0025 equiv, 2.5 g/L in dichloromethane) was delivered to a screw capped vial and evaporated to dryness *in vacuo*. The vial was then transferred into a nitrogen-filled glovebox, where a magnetic stir bar, NaO*t*Bu (2.0 equiv), toluene (0.12 M aryl halide), dodecane (1.0 equiv) and 1-chloronaphthalene (1.0 mmol, 1.0 equiv) were added, followed by the addition of furfurylamine (1.1 equiv). The vial was sealed with a cap containing a PTFE septum and magnetic stirring was initiated, all within the glovebox. Aliquots of the reaction mixture were taken at 10 minute intervals and analyzed using Workup Method B.

Workup Method A (purification of aniline products *via* chromatography): Following **GP1**-**GP4** or **GP6** (employing between 0.6-1.0 mmol (hetero)aryl halide), after cooling to room temperature, the reaction mixture was diluted with ethyl acetate (ca. 30 mL) and washed with brine (3 × ca. 30 mL) and the organic layer was dried over sodium sulfate. For compounds **4.2a-m**, the organic layer was not washed with brine but was adsorbed directly onto silica, unless otherwise noted. The solvent was removed *in vacuo* and the compound was purified by flash column chromatography on silica gel.

Workup Method B (procedure for the preparation of GC samples): Following **GP1**-**GP6** (employing 0.12 mmol aryl halide), after cooling to room temperature, the reaction mixture was diluted using 9:1 ethyl acetate/methanol mixture and was passed through a

Kimwipe filter containing a Celite/silica gel pad into a GC vial. Calibrated GC estimates are given by comparison to authentic samples. For products **3.1a-d**, **3.2a-c**, **3.3a-d**, **4.1a-c**, and **4.2a**, dodecane (0.12 mmol) was added to the reaction mixture prior to filtration, and was subsequently analyzed by use of response-factor calibrated GC methods employing authentic samples.

Workup Method C (procedure for the preparation of samples for NMR quantification): Following **GP1**, **GP2**, or **GP6** (employing between 0.48-0.6 mmol aryl chloride), after cooling to room temperature, the reaction mixture was diluted with ethyl acetate (ca. 30 mL) and washed with brine (3 × ca. 30 mL) and the organic layer was dried over sodium sulfate. The solvent was removed *in vacuo*, followed by the addition of the internal standard (dodecane or ferrocene, 10-20 mol% or 1 equiv) to the vial containing the product mixture. The resultant mixture was taken up in either DMSO-d_6 or $CDCl_3$ and was then subjected to NMR spectroscopic analysis. In select cases where the resultant aniline was volatile and thus subject to evaporation *in vacuo*, the reaction mixture was not dried exhaustively, resulting in residual solvent impurity peaks in the NMR spectra.

Workup Method D (Purification of (hetero)arylphosphines *via* chromatography): Following ligand (**2-L1** to **2-L9** and **3-L1** to **3-L3**) and ligand precursor syntheses (**P1**-**P9**), the reaction mixture was cooled to room temperature and subsequently diluted with dichloromethane (ca. 30 mL). The organic layer was washed with brine (3 × ca. 30 mL) and dried over sodium sulfate. The solvent was removed *in vacuo* and the compound was purified by use of flash column chromatography on silica gel.

6.4. Supplementary X-ray Crystal Structures

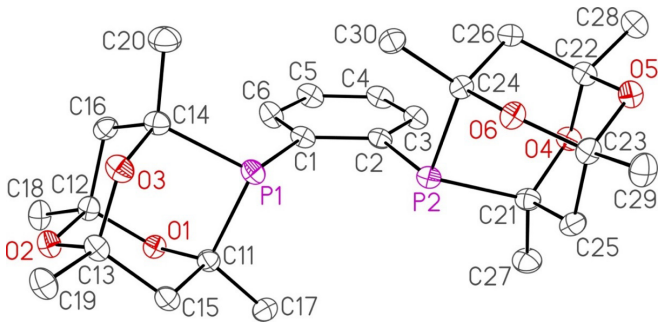

Figure 6-1. Single-crystal X-ray structure of *meso*-**3-L1**. Perspective view showing the atom labelling scheme. Non-hydrogen atoms are represented by Gaussian ellipsoids at the 30% probability level. Hydrogen atoms are not shown.

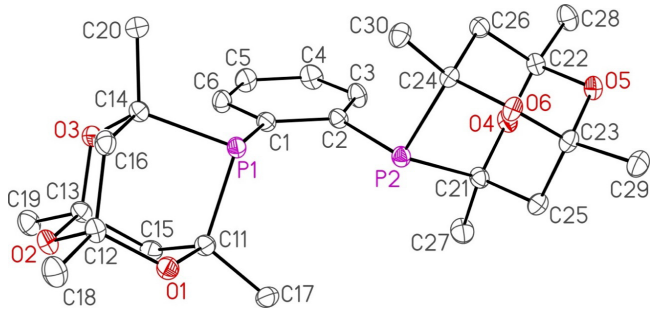

*Figure 6-2***.** Single-crystal X-ray structure of *rac*-**3-L1**. Perspective view showing the atom labelling scheme. Non-hydrogen atoms are represented by Gaussian ellipsoids at the 30% probability level. Hydrogen atoms are not shown.

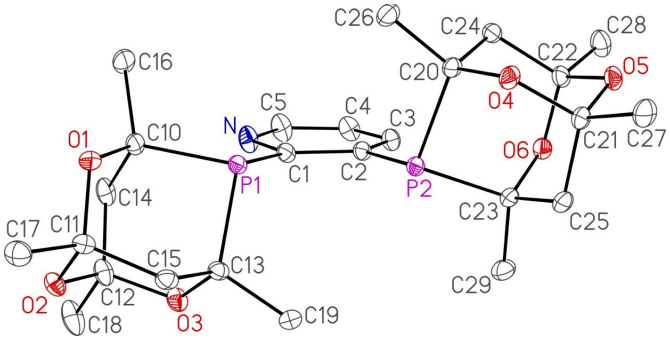

*Figure 6-3***.** Single-crystal X-ray structure of *meso*-**3-L2**. Perspective view showing the atom labelling scheme. Non-hydrogen atoms are represented by Gaussian ellipsoids at the 30% probability level. Hydrogen atoms are not shown.

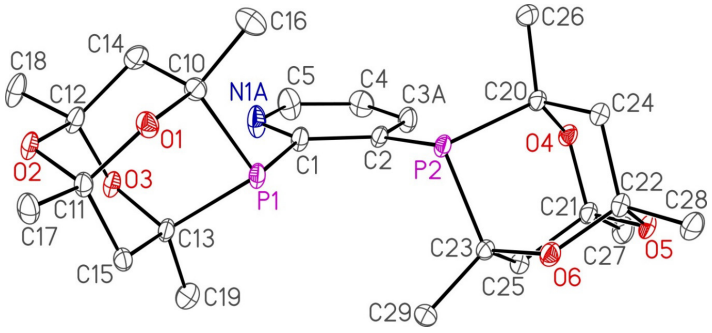

*Figure 6-4***.** Single-crystal X-ray structure of *rac*-**3-L2**. Perspective view showing the atom labelling scheme. Non-hydrogen atoms are represented by Gaussian ellipsoids at the 30% probability level. Hydrogen atoms are not shown.

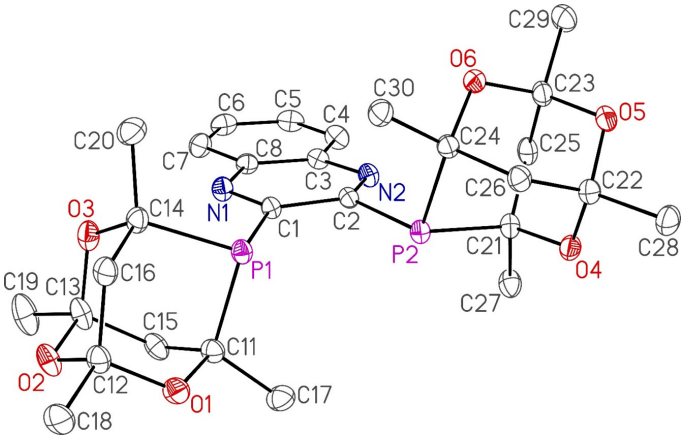

*Figure 6-5***.** Single-crystal X-ray structure of *meso*-**3-L3**. Perspective view showing the atom labelling scheme. Non-hydrogen atoms are represented by Gaussian ellipsoids at the 30% probability level. Hydrogen atoms are not shown.

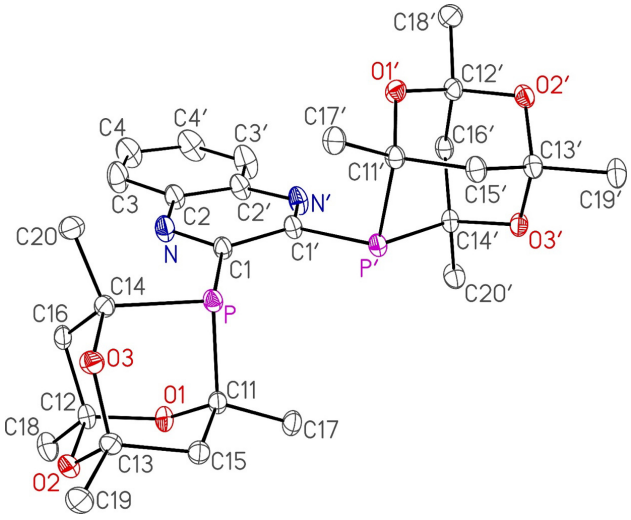

*Figure 6-6***.** Single-crystal X-ray structure of *rac*-**3-L3**. Perspective view showing the atom labelling scheme. Non-hydrogen atoms are represented by Gaussian ellipsoids at the 30% probability level. Hydrogen atoms are not shown.

6.5. Representative Characterization Data for Anilines, (Hetero)Aryl Phosphines, and Nickel Complexes

Data for 4-((furan-2-ylmethyl)amino)benzonitrile (**2.1b**): The title compound was synthesized from the corresponding chloride according to **GP1**, conducted at 110 °C using 5 mol% 1,1'-bis(diisopropylphosphino)ferrocene (**L**$^{i\mathbf{Pr}}$), and purified according to Workup Method A. Purified by flash column chromatography on silica gel using 19:1 hexanes/ethyl

acetate which afforded the title product in 82% isolated yield (163 mg, 0.82 mmol) as a yellow solid. ^{1}H NMR (500 MHz; $CDCl_3$): δ 7.39-7.35 (m, 3H), 6.63-6.61 (m, 2H), 6.32-6.31 (m, 1H), 6.24 (m, 1H), 4.81 (br. s, 1H), 4.33-4.32 (d, J = 5.9 Hz, 2H). ^{13}C{^{1}H} NMR (125.8 MHz; $CDCl_3$): δ 151.3, 150.9, 142.3, 133.6, 120.5, 112.5, 110.5, 107.6, 99.0, 40.4. HRMS *m/z* ESI^{+} found 221.0685 $[M + H]^{+}$ calculated for $C_{12}H_{10}N_2NaO$ 221.0691.

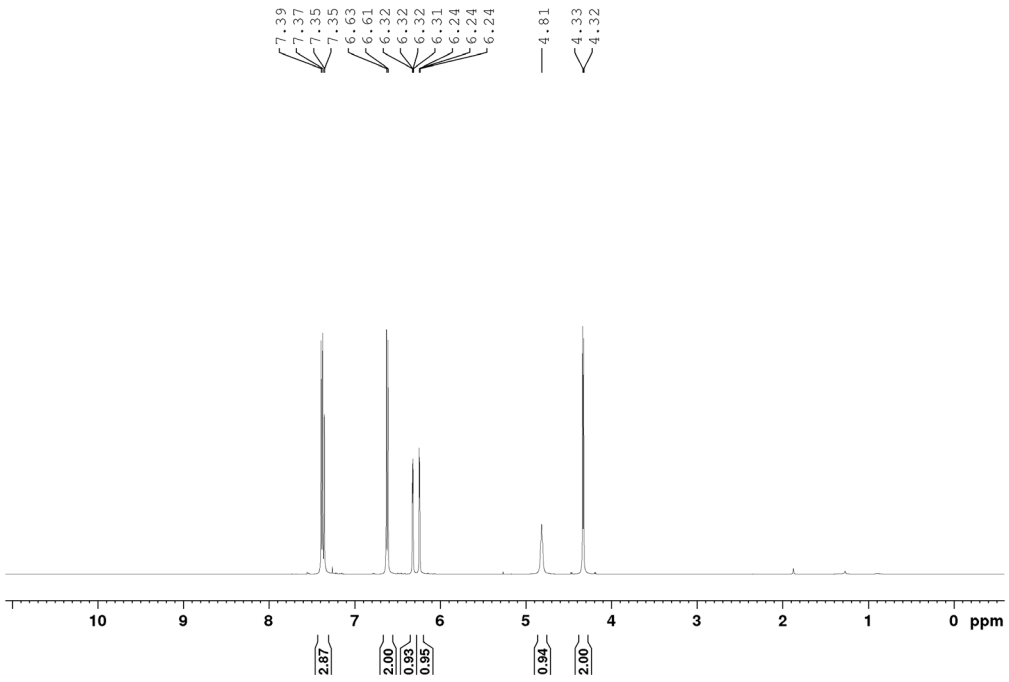

Figure 6-7. ^{1}H NMR Spectrum of ***4-((furan-2-ylmethyl)amino)benzonitrile***, **2.1b** ($CDCl_3$, 500 MHz).

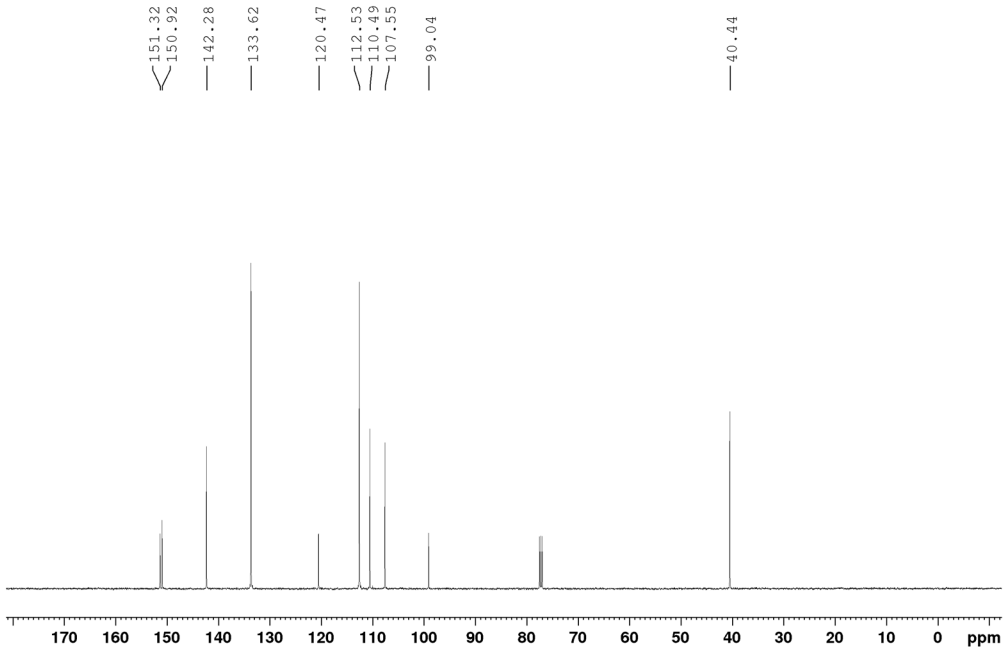

Figure 6-8. $^{13}C\{^{1}H\}$ NMR Spectrum of **2.1b**, ($CDCl_3$, 125.8 MHz)

Data for **3-L1** (*o*-PCg_2-benzene, PAd2-DalPhos): *rac*-**3-L1**: ^{1}H NMR (300 MHz, $CDCl_3$): δ 8.34-8.29 (m, 2H, ArH), 7.39-7.33 (m, 2H, ArH), 2.16-2.10 (m, 2H, CgP), 2.04-1.86 (m, 4H, CgP), 1.44-1.37 (m, 26H, CgP). $^{13}C\{^{1}H\}$ UDEFT NMR (125.8 MHz, $CDCl_3$): δ 143.8 (ArC), 134.0 (ArC), 129.0 (ArC), 96.8 (CgP), 96.0 (CgP), 74.8-74.7 (m, CgP), 73.9-73.8 (m, CgP), 46.2-46.1 (m, CgP), 36.0 (CgP), 28.1 (CgP), 27.8-27.7 (m, CgP), 26.5-26.4 (m, CgP). $^{31}P\{^{1}H\}$ NMR (202.5 MHz, $CDCl_3$): δ -40.2. HRMS *m/z* ESI^+ found 529.1879 $[M + H]^+$ calculated for $C_{26}H_{36}NaO_6P_2$ 529.1885. NMR spectra for *rac*-**3-L1** are found in the Appendix. *meso*-**3-L1**: ^{1}H NMR (300 MHz, $CDCl_3$): δ 8.29-8.24 (m, 2H, ArH), 7.45-7.40 (m, 2H, ArH), 2.29-2.21 (m, 4H, CgP), 2.06-1.88 (m, 2H, CgP), 1.70-1.64 (m, 2H, CgP), 1.51 (s, 6H, CgP), 1.42-1.35 (m, 12H, CgP), 1.27-1.22 (m, 6H, CgP). $^{13}C\{^{1}H\}$ UDEFT NMR (125.8 MHz, $CDCl_3$): δ 144.0 (ArC), 134.4 (ArC), 129.3 (ArC), 97.1 (CgP), 95.9 (CgP), 74.6-74.5 (m, CgP), 74.4-74.3 (m, CgP), 46.0-45.9 (m, CgP), 37.0 (CgP), 29.4-29.2 (m, CgP), 28.1 (CgP), 27.7 (CgP), 26.5-26.4 (m, CgP). $^{31}P\{^{1}H\}$ NMR (202.5 MHz, $CDCl_3$): δ -40.7. HRMS *m/z* ESI^+ found 529.1879 $[M + Na]^+$ calculated for $C_{26}H_{36}NaO_6P_2$ 529.1885.

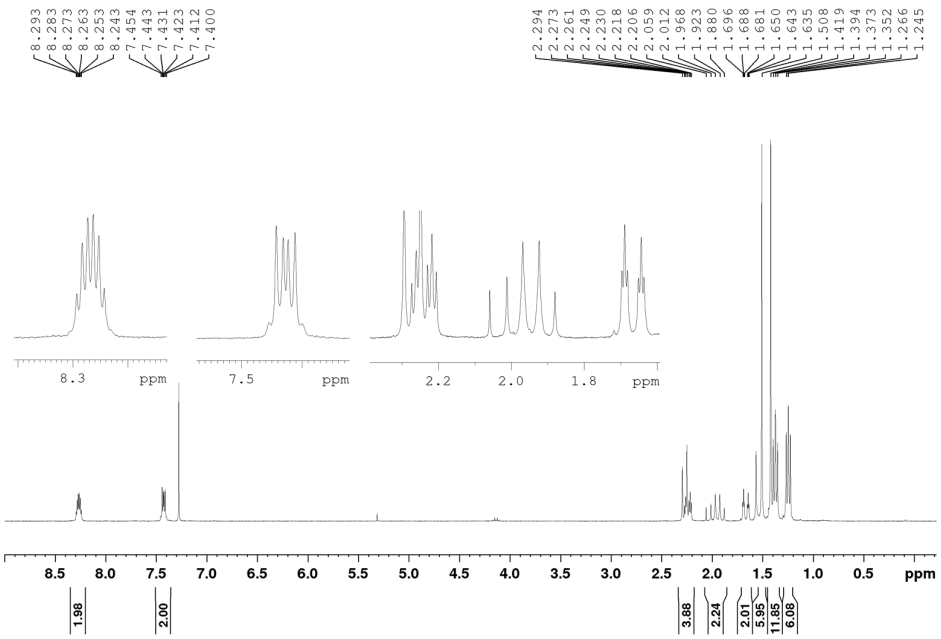

Figure 6-9. ^{1}H NMR Spectrum of ***meso-o*-PCg$_2$-benzene**, *meso*-**3-L1** ($CDCl_3$, 300 MHz)

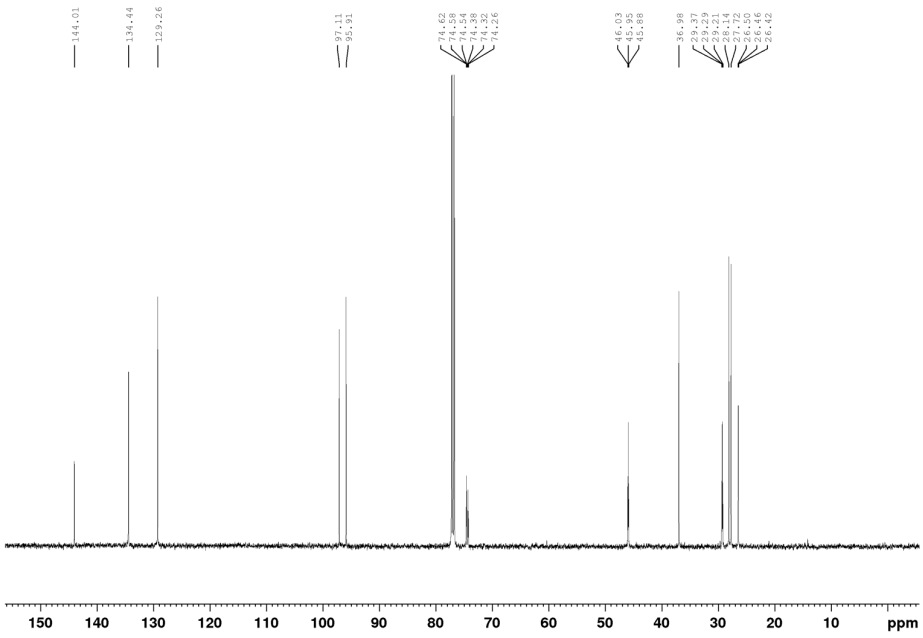

Figure 6-10. $^{13}C\{^{1}H\}$ UDEFT NMR Spectrum of *meso*-**3-L1** ($CDCl_3$, 125.8 MHz)

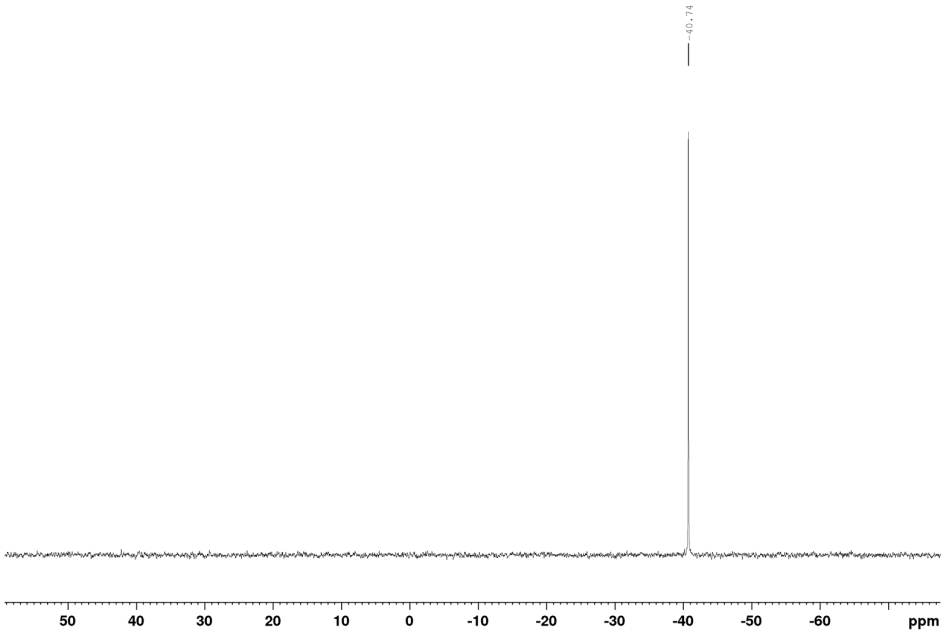

Figure 6-11. $^{31}P\{^{1}H\}$ NMR Spectrum of *meso*-**3-L1** ($CDCl_3$, 121.5 MHz)

Data for ***(o-PCg$_2$-benzene)Ni(o-tolyl)Cl*, 3-C1**: Anal. Calcd for $C_{33}H_{43}ClNiO_6P_2$: C, 57.30; H, 6.27; N, 0. Found: C, 57.41; H, 5.89; N, <0.5. Given the presence of *meso* and *rac* isomers of **3-L1**, as well as Ni-bound *ortho*-tolyl fragment rotamers, a total of 8 unique phosphorus NMR signals are expected. The ^{1}H and $^{13}C\{^{1}H\}$ solution NMR spectra for these complexes are sufficiently complex so as to preclude meaningful assignment (see Section 6.2). $^{31}P\{^{1}H\}$ NMR data for **3-C1** from **3-L1** (202.5 MHz; $CDCl_3$): δ 29.6 (s, *rac*-**3-C1** major), 28.7 (s, *meso*-**3-C1** major), 27.7 (s, *rac*-**3-C1** minor), 27.0 (s, *meso*-**3-C1** minor), 15.1 (s, *meso*-**3-C1** major), 14.1 (s, *meso*-**3-C1** minor), 13.2 (s, *rac*-**3-C1** major), 11.5 (s, *rac*-**3-C1** minor). *rac*-**3-C1**: $^{31}P\{^{1}H\}$ NMR (202.5 MHz; $CDCl_3$): δ 29.6 (s, major), 27.7 (s, minor), 13.2 (s, major), 11.5 (s, minor). *meso*-**3-C1**: $^{31}P\{^{1}H\}$ NMR (202.5 MHz; $CDCl_3$): δ 28.7 (s, major), 27.0 (s, minor), 15.2 (s, major), 14.1 (s, minor). NMR spectra for **3-C1** prepared from **3-L1** and *rac*-**3-C1** are found in the Appendix.

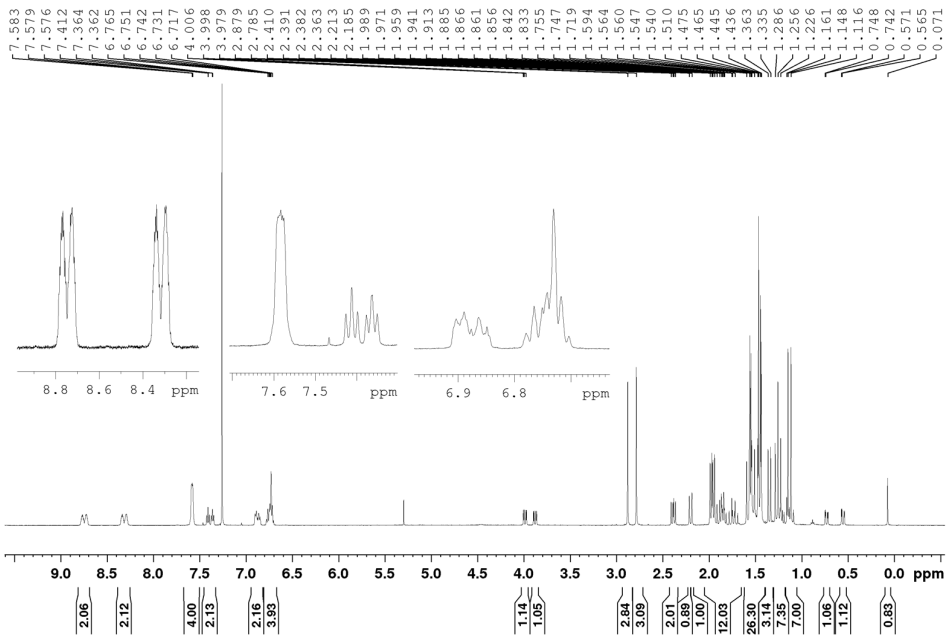

Figure 6-12. ^{1}H NMR Spectrum of *meso*-**3-C1** ($CDCl_3$, 500 MHz)

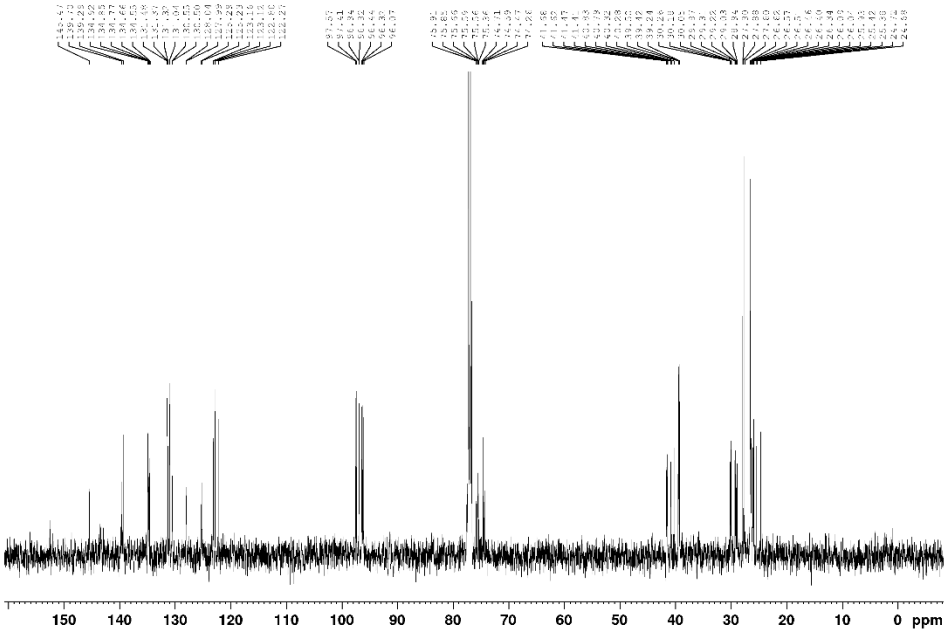

Figure 6-13. $^{13}C\{^{1}H\}$ UDEFT NMR Spectrum of *meso*-**3-C1** ($CDCl_3$, 125.8 MHz)

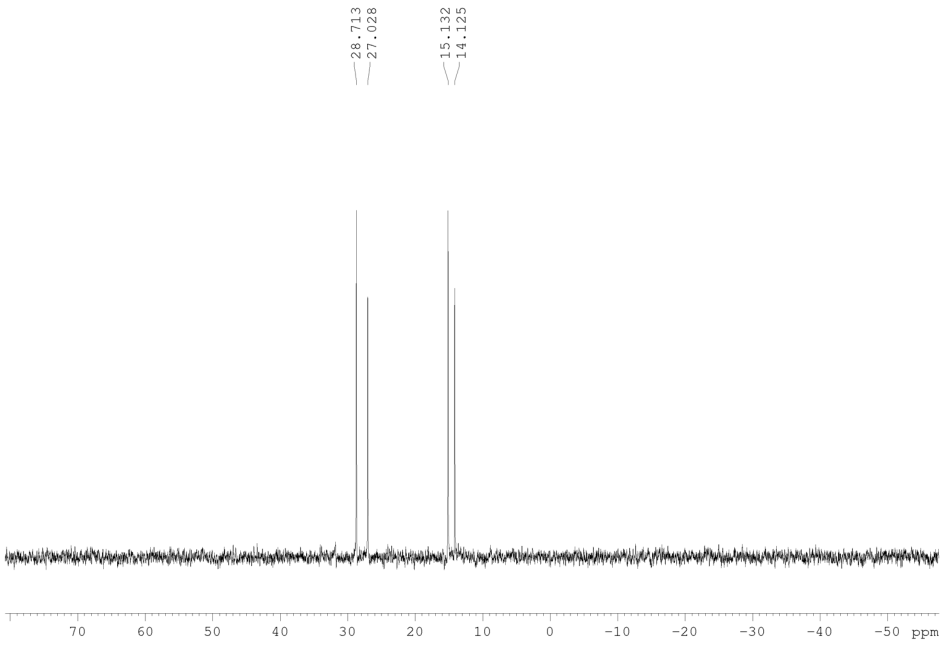

Figure 6-14. $^{31}P\{^{1}H\}$ NMR Spectrum of *meso*-**3-C1** ($CDCl_3$, 202.5 MHz)

Characterization data and spectra for all other aniline products, ligands, ligand precursors, and nickel complexes are found in the Appendix.

Chapter 7.0. Research Summaries and Future Directions

Section 7.1. Chapter 2 Conclusions and Future Directions

Three state-of-the-art ancillary ligands (PAd-DalPhos (**L0**), CyPF-Cy (**1-L1**) and DPPF) and their respective (*o*-tolyl)nickel(II) chloride pre-catalysts (**C0**, **1-C1**, and **1-C2**) were compared in nickel-catalyzed C(sp^2)-N cross-coupling reactions involving ammonia, linear and hindered primary alkylamines, and a dialkylamine. The goal of these catalytic surveys was to establish similarities, differences, and performance rankings within the structurally divergent ligand set, with hopes of elucidating structure-reactivity trends pertaining to the influence that ancillary ligands impart on catalysis. This series of surveys benchmarks **1-C1** as competitive with **C0** in room temperature cross-couplings of primary alkylamines and heated monoarylations of ammonia with (hetero)aryl chlorides. In select cases, contrasting reactivity was observed: higher turnover to *N*-(*sec*-butyl)naphthalen-1-amine (a hindered primary alkylamine coupled with a hindered electrophile) and 4-anisidine (ammonia monoarylation with a deactivated electrophile) is achieved using **C0**, whereas **1-C1** gives higher yields of benzo[*b*]thiophen-5-amine (ammonia monoarylation with a heterocyclic electrophile) and 4-morpholinobenzonitrile (a dialkylamine coupled with an activated electrophile). Experiments involving the direct competition of either two different electrophiles (ArCl vs. ArBr or ArOTs) or nucleophiles (NH_3 vs. $MeNH_2$) employing **C0** or **1-C1** revealed complementary selectivities. Preference for the alkylamine was observed when using **C0** whereas **1-C1** was selective for ammonia. A modest preference for aryl bromides and tosylates was displayed by **C0**, whereas **1-C1** exhibited a slight uptake of aryl chlorides. Additionally, **1-C1** appears to experience catalyst inhibition in the presence of aryl bromides, unlike **C0**. The DPPF-based pre-catalyst **1-C2** was distinguished from **C0** and **1-C1** by its inefficacy with ammonia and primary alkylamine substrates, and through its excellent turnover of the hindered dialkylamine morpholine.

In an effort to relate the catalytic similarities of structurally and electronically dissimilar **C0** and **1-C1**, revisiting the concept of remote steric bulk as a key ligand property for Ni-based cross-coupling may provide preliminary insight (Section 1.4). The complex **C0** features hindering fragments that are oriented toward the metal centre (methyl groups of the *o*-tolyl phosphine; *β*-methyl groups of PCg) which appears to contradict Doyle's observation that optimal Ni-based ligands should hold their steric bulk at a distance.[82]

However, the <90° bite angle generated by the smaller chelate of **C0** might allow for the phosphino substituents to be less invasive to the metal active site, whereas the >90° bite angle of **1-C1** may prove less hindering at the metal centre due to the flexibility of the cyclohexylphosphino fragments. These factors may give rise to similar steric profiles for **C0** and **1-C1**. On the other hand, the subtle contrast in reactivity observed with amines may be attributed to a more electrophilic Ni centre in the case of **C0**, leading to preferred binding of more nucleophilic amines, and a slightly more encumbered Ni centre in the case of **1-C1**, favouring smaller NH substrates. The reactivity differences with aryl halide substrates could indicate an inhibitory effect of **1-C1** with aryl bromides, where this complex may undergo comproportionation, generating potentially inactive Ni^{I} intermediates.

If the work in Chapter 2 were furthered, a deeper exploration into the divergent reactivity of **C0** and **1-C1** with aryl bromides would be of particular relevance to the current direction of this field. An increasing number of reports show the susceptibility of nickel complexes to undergo comproportionation pathways (Scheme 7-1A).[46-50, 52] Resultant Ni^{I} species from this reaction are cycle-terminating in select cases,[47, 49-51] and as such the design of ligands that dissuade this type of reactivity is highly desirable. Additionally, recent reports have shown that the isolation and stability of (DPPF)Ni^{II}ArBr complexes rely on the presence of *ortho*-substituted aryl ligands which dissuade comproportionation.[47, 48, 52, 130] Considering the above, attempting the isolation of **P₂**Ni^{II}ArBr complexes (where **P₂** = **L0** or **1-L1**) would provide insight into the stability of such species, or the potential for decomposition to **P₂**Ni^{I}Br. The results in Chapter 2 highlight **L0** and **1-L1** as excellent candidates for this stoichiometric study, where the tame reactivity of the former could be attributed to clean (**L0**)Ni^{II}ArBr formation, whereas the stalled reactivity of the latter may result from (**1-L1**)Ni^{I}Br by-products. Starting points for this research project could involve: syntheses of **P₂**Ni^{II}ArBr complexes *via* oxidative addition of aryl bromides to **P₂**Ni^{0}COD (where **P₂** = **L0** or **1-L1**) to identify which electrophiles give clean two electron oxidative addition events and yield stable, isolable nickel(II) species (Scheme 7-1B); subjecting stoichiometric **P₂**Ni^{II}ArBr to standard amination conditions (i.e., amine and base) and monitoring the reaction profiles by tracking **P₂**Ni^{X} intermediates *via* $^{31}P\{^{1}H\}$ NMR (Scheme 7-1C); evaluating the productivity of catalytic **P₂**Ni^{II}ArBr under standard amination conditions (Scheme 7-1C); and examining the potential reactivity of **P₂**Ni^{II}ArBr

with $\mathbf{P_2}Ni^0COD$, which could either lead to $\mathbf{P_2}Ni^IBr$ or unconsumed $\mathbf{P_2}Ni^{II}ArBr$ (Scheme 7-1D). Each of these modules can be conducted alongside analogous $\mathbf{P_2}Ni^{II}ArCl$ complexes to compare the propensity for comproportionation between nickel bromides and chlorides. This work would be impactful as it could shed light on the types of ligands that shield nickel catalysts from decomposition pathways and promote BHA-like Ni^0/Ni^{II} redox events.

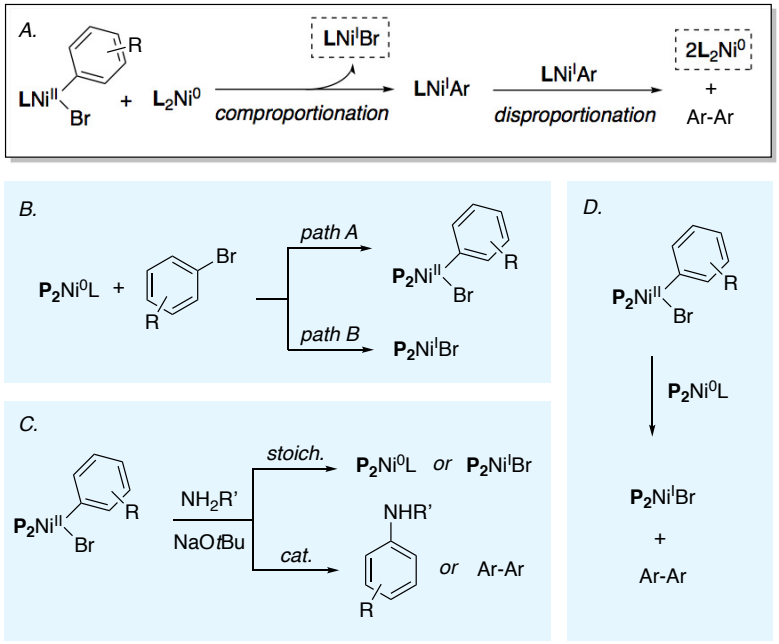

Scheme 7-1. Future work proposal for Chapter 2. *A*. Pathway from $\mathbf{L}Ni^{II}ArBr$ to $\mathbf{L}Ni^IBr$ and $\mathbf{L_2}Ni^0$ *via* comproportionation of Ni^{II} and Ni^0 to give $\mathbf{L}Ni^IBr$ and $\mathbf{L}Ni^IAr$. $\mathbf{L}Ni^IAr$ disproportionates with another equivalent of $\mathbf{L}Ni^IAr$ to give unstable $\mathbf{L}Ni^{II}Ar_2$, which undergoes C-C reductive elimination to generate 2 equiv $\mathbf{L_2}Ni^0$ and biaryl. Proposed research modules, where $\mathbf{P_2}$ = **L0** or **1-L1**: *B*. reaction of ArBr with Ni^0 either *via* two electron oxidative addition (path A) or comproportionation (path B); *C*. comparison of reaction outcomes when employing stoichiometric or catalytic Ni^{II} to standard amination conditions; *D*. reaction of Ni^{II} with Ni^0.

Section 7.2. Chapter 3 Conclusions and Future Directions

The ligand class 1,1'-bis(di(alkyl/aryl)phosphino)ferrocene was selected as a model framework to examine the effects of phosphino variation on catalytic reaction outcomes in Ni-catalyzed C(sp^2)-N cross-coupling. Ten variants (including parent DPPF, $\mathbf{L^{Ph}}$) were chosen for this comparative survey: three featured alkylphosphino fragments of varying steric bulk ($\mathbf{L^{iPr}}$, $\mathbf{L^{Cy}}$, $\mathbf{L^{tBu}}$); two *ortho*-substituted diarylphosphines with orthogonal

electronic properties ($\mathbf{L}^{o\text{-tol}}$, $\mathbf{L}^{1\text{-nap}}$); three *meta*-substituted diarylphosphines, including electron-rich ($\mathbf{L}^{\mathbf{OMe}}$), modestly electron-rich ($\mathbf{L}^{\mathbf{Me}}$), and electron-poor ($\mathbf{L}^{\mathbf{CF3}}$) variants; and an unhindered electron-poor diheteroarylphosphine ($\mathbf{L}^{\mathbf{fur}}$). The goal of this study was to elucidate structure-reactivity trends within the ligand family, with hopes of identifying key ligand characteristics that give rise to superlative catalysis. The ferrocenyl ligands were compared in C(sp^2)-N cross-couplings involving furfurylamine, morpholine, and indole with various (hetero)aryl chlorides using *in situ* derived catalyst systems (i.e., $\mathbf{L}^{\mathbf{X}}$ + $Ni(COD)_2$). This survey identified less hindered dialkylphosphines $\mathbf{L}^{i\mathbf{Pr}}$ and $\mathbf{L}^{\mathbf{Cy}}$, unsubstituted parent $\mathbf{L}^{\mathbf{Ph}}$, and *meta*-substituted diarylphosphines $\mathbf{L}^{\mathbf{CF3}}$, $\mathbf{L}^{\mathbf{OMe}}$, and $\mathbf{L}^{\mathbf{Me}}$ as the highest performing 1,1'-bis(di(alkyl/aryl)phosphino)ferrocenyl ligands for couplings involving all three nucleophiles. More rigorous screening of this superior crop revealed the greater efficacy of arylphosphino relative to alkylphosphino motifs. Notably, $\mathbf{L}^{\mathbf{CF3}}$ was the most widely effective in transformations involving indole, including the turnover of particularly challenging substrates such as 4-chloroanisole and 2-chloro-1,4-dimethylbenzene.

Particularly ineffective ligands for all transformations described herein included highly hindered $\mathbf{L}^{t\mathbf{Bu}}$, $\mathbf{L}^{o\text{-tol}}$, and $\mathbf{L}^{1\text{-nap}}$, and sterically compact $\mathbf{L}^{\mathbf{fur}}$. Interestingly, $\mathbf{L}^{t\mathbf{Bu}}$ and $\mathbf{L}^{o\text{-tol}}$ are effective BHA ligands,[100, 109, 110] which simultaneously highlights the divergent properties of nickel and palladium and the need for new ligands designed specifically for nickel. Whereas the synthesis of ($\mathbf{L}^{i\mathbf{Pr}}$)Ni(*o*-tolyl)Cl was straightforward, access to similar complexes comprising $\mathbf{L}^{t\mathbf{Bu}}$, $\mathbf{L}^{o\text{-tol}}$, $\mathbf{L}^{\mathbf{CF3}}$, and $\mathbf{L}^{\mathbf{OMe}}$ was denied due to synthetic challenges, which exposes a lack of general applicability associated with this pre-catalyst method.

The similar catalytic competencies of $\mathbf{L}^{\mathbf{Ph}}$, $\mathbf{L}^{\mathbf{CF3}}$, $\mathbf{L}^{\mathbf{Me}}$, and $\mathbf{L}^{\mathbf{OMe}}$ in cross-couplings involving furfurylamine, morpholine, and indole suggests that the electronic make-up of arylphosphino groups within this ligand framework does not greatly impact the behavior of nickel in this chemistry. This trend is congruent with the reactivity profiles of the ligands surveyed in Chapter 2, where the divergent electronic properties of PAd-DalPhos (**L0**) and CyPF-Cy (**1-L1**) do not appear to markedly influence the general effectiveness of the catalyst. The remote steric bulk associated with the mutual substitution pattern of $\mathbf{L}^{\mathbf{Me}}$, $\mathbf{L}^{\mathbf{CF3}}$, and $\mathbf{L}^{\mathbf{OMe}}$ may have a greater effect on reactivity, given that *meta*-substitution (regardless of electronic bias) in the $\mathbf{L}^{\mathbf{X}}$ family results in highly active nickel catalysts,

whereas more invasive *ortho*-substitution gives rise to ineffective catalysts in select nickel-based C(sp^2)-N cross-couplings. In line with these observations, Doyle and co-workers noted the contrasting performance between *meta*-substituted and *ortho*-substituted arylphosphines in nickel-catalyzed applications, with the former offering excellent productivity and the latter being catalytically inactive.[82] Notwithstanding the general efficacy of *meta*-substituted $\mathbf{L^{Ph}}$ variants, the superiority of $\mathbf{L^{CF3}}$ when paired with nickel for indole couplings may be attributed to a subtly electrophilic metal centre (induced by the ancillary ligand), which could enhance the more challenging C-N reductive elimination of nickel indolates.[103, 121]

The results from the indole screening experiments detailed in Scheme 3-4 could serve as a springboard for a future research project. The greater acidity and hindered nature of indole makes it a particularly challenging nucleophile for C(sp^2)-N cross-coupling, which is demonstrated by the limited disclosures of Ni-catalysts that effect this transformation. Existing reports feature indole cross-couplings with electronically activated (hetero)aryl chlorides and alkyl-substituted aryl chlorides;[69, 90] however, examples of deactivated aryl chlorides as coupling partners for indole is limited to one scope entry from Nicasio's report of an IPrNi(styrene)$_2$ catalyst.[69] The high-yielding cross-coupling of 4-chloroanisole and indole using $\mathbf{L^{CF3}}$/Ni(COD)$_2$ (91% isolated yield of **2.3h)** suggests that this ligand may be capable of accessing a wider scope of deactivated electrophiles. A project could be initiated through the development of a pre-catalyst bearing $\mathbf{L^{CF3}}$, which would likely offer improved catalytic efficacy and milder operating conditions relative to the *in situ* method employed in Chapter 3. The remarkably low solubility of the assumed product ($\mathbf{L^{CF3}}$)Ni(*o*-tolyl)Cl reported in Section 3.4 would warrant the preparation of other pre-catalyst scaffolds[92] that may offer improved solubility such that complex characterization could be achieved. For example, 1-naphthyl[92], 2-mesityl[90, 93], 2-methyl-4-methoxyphenyl or 2-methyl-4-trifluoromethylphenyl[130] could be used in place of an *o*-tolyl aryl ligand (Scheme 7-2). Ideally, *ortho*-substitution of aryl ligands would be retained to prevent complex decomposition.[130]

Pending the successful synthesis and characterization of an $\mathbf{L^{CF3}}$-based nickel(II) pre-catalyst ($\mathbf{C^{CF3}}$, Scheme 7-2), a preliminary catalytic screening of deactivated electrophiles coupled with indole employing $\mathbf{C^{CF3}}$ would be initiated (Scheme 7-3). In

addition to electron-rich aryl chlorides, other difficult substrates such as hindered aryl chlorides, 5-membered ring heteroaryl electrophiles, and phenol derived electrophiles would be included to identify which electrophile sub-category emerges as fruitful, from which a substrate scope could be pursued. This work would be impactful as it would push the boundaries of accessible substrates in the realm of nickel catalysis.

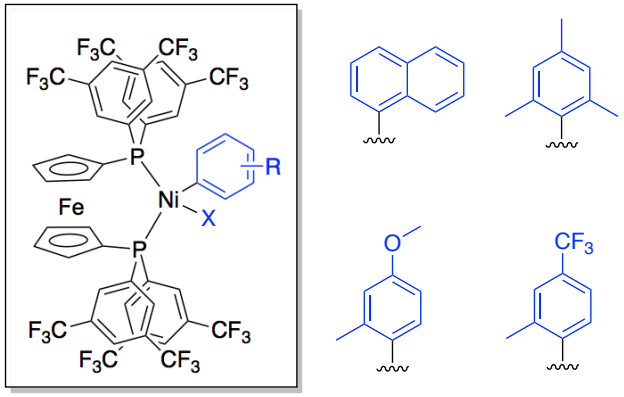

Scheme 7-2. Proposed $\mathbf{L}^{\mathbf{CF3}}$NiArX pre-catalyst ($\mathbf{C}^{\mathbf{CF3}}$). X = Cl or Br; candidates for aryl ligands are shown in blue.

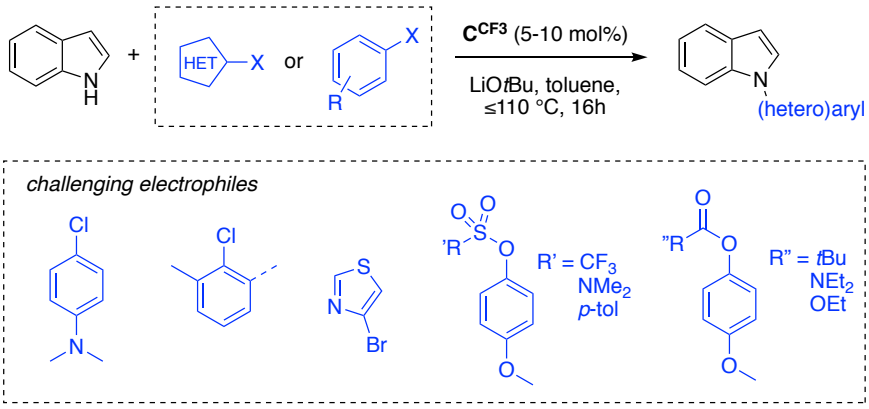

Scheme 7-3. Preliminary catalytic screen of $\mathbf{C}^{\mathbf{CF3}}$ with indole as a test nucleophile. Electrophiles would include 1-chloro-4-dimethylaminobenzene, 2-chlorotoluene, 2-chloro-*m*-xylene, 4-bromothiazole, and 4-(pseudohalo)anisole.

Section 7.3. Chapter 4 Conclusions and Future Directions

Chapter 4 explores the PAd-DalPhos (**L0**) framework through systematic variation of its ligand backbone and phosphino substitution pattern. This was achieved through the syntheses of seven new bisphosphines containing parent phosphino fragments (PCg and P(*o*-tolyl)$_2$) linked by thiophenyl or pyridyl backbones, some of which are regioisomeric

with respect to phosphino substitution. The effect of these manipulations was evaluated by comparing the outcomes of nickel-catalyzed amination reactions employing the new variants and the known ligands **L0**,[72] *o*-(P(*o*-tolyl)$_2$)$_2$benzene (**2-L1**),[115] and 3,4-(P(*o*-tolyl)$_2$)$_2$-thiophene (**2-L9**).[114] These screening reactions were conducted with *in situ* derived catalysts (i.e., **L** + Ni(COD)$_2$) and operated under challenging conditions to distinguish the performance of the catalysts. Whereas the variants did not outperform **L0** in transformations involving ammonia or benzamide, thiophenyl-linked bisphosphines, particularly those with 3,4-substitution, excelled in furfurylamine cross-couplings relative to **L0**. The 3,4-thiophenyl ligands **2-L8** and **2-L9** were carried forward into (**L**)Ni(*o*-tolyl)Cl pre-catalyst syntheses (yielding **2-C1** and **2-C2**, respectively), and were subsequently evaluated alongside the analogous **L0** complex, **C0**, in cross-couplings of furfurylamine and (hetero)aryl (pseudo)halides (i.e., Cl, Br, OTs) operating under exceptionally mild catalytic conditions (i.e., room temperature, 2.5 to 0.25 mol% catalyst). The pre-catalyst **2-C1** consistently provided product yields 20-40% greater than **C0**, and was capable of turning over aniline products (30-50% yields) employing 0.125 mol% catalyst at 80 °C. The scalability of this low loading protocol was demonstrated in a brief substrate scope, where mono-arylated primary alkylamine products containing quinaldine, quinoxaline, quinoline, and naphthalene cores were isolated in high yields (68-91%) employing elevated or room temperature conditions and 0.25 mol% **2-C1**. To understand the differences between **L0** and **2-L8**, DFT analysis comparing **L0** and **2-L8** in a representative C-N reductive elimination step (i.e., **L**Ni^{II}(Ph)(NH(CH$_2$-furyl) to **L**Ni^0(η^2-*N*-phenyl-furanmethanamine)) revealed identical transition state energies but a lower energy ground state for the resultant **2-L8**Ni^0 species (~4 kcal/mol less than **L0**Ni^0). It is possible that the greater stability of **2-L8**Ni^0 may be responsible for the enhanced productivity of **2-C1**. Reaction monitoring of the room temperature cross-coupling of 1-chloronaphthalene and furfurylamine (0.25 mol% **L0** or **2-L8**) showed no difference in early reaction progress or a pronounced induction period.

Speculation on the effect of replacing a phenylene backbone with thiophenyl[113, 114] is offered in the following scenarios. The more electron-donating phosphino groups of **2-L8** resulting from the thiophenyl linkage may accelerate C(sp^2)-Cl oxidative addition, which would reduce the relative amount of Ni^0 species available to react *via*

comproportionation with **L**Ni^{II}ArCl to create potentially inactive Ni^{I} species. The slightly larger bite angle observed in the crystal structure of **2-C1** may lead **2-L8**Ni^{0} species to dissuade comproportionation to a greater extent than related **L0** complexes through steric shielding, or prevent the formation of $(P_2)_2Ni^0$ species. Another means of slowing comproportionation could involve the different binding modes of Ni^{0} species with thiophenyl fragments compared to phenylene. It is possible that improved metal binding with a more π-basic heteroaryl backbone could deflect η^2-binding of the P(*o*-tolyl)$_2$ fragment (Scheme 7-4),[131] or the different ring-walking paths of nickel with thiophene and phenyl substrates[132] may be involved in disfavouring comproportionation mediated by arylphosphino/Ni^{0} π-interactions.[50]

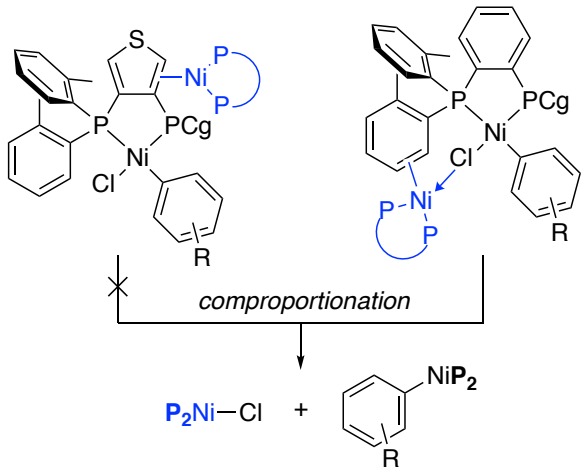

Scheme 7-4. Conjectured comproportionation pathway for **L0**Ni^{II}ArCl species.[50] Favoured Ni^{0}-thiophenyl binding in **2-L8**NiArCl species may dissuade dimer formation, preventing subsequent chloride abstraction.

Extension of the work featured in Chapter 4 could involve a deeper exploration into 5-membered ring heteroaryl backbones for PAd-DalPhos ligands. As it is unclear exactly how the 3,4-thiophenyl unit influences the catalyst, an assessment of similarly substituted furan and pyrrole based ligands may shed light on the influence of either the heteroatom identity or ligand backbone size. This work would be initiated through the syntheses of 3-PCg-4-P(*o*-tolyl)$_2$-furan (**4-L1**) and *N*-methyl-3-PCg-4-P(*o*-tolyl)$_2$-pyrrole (**4-L2**), which would allow the heteroatom identity to act as the sole variable within the ligand set (Scheme 7-5A). The new ligands **4-L1** and **4-L2** would be carried forward into **L**Ni(*o*-tolyl)Cl pre-catalyst syntheses, generating **4-C1** and **4-C2,** respectively (Scheme 7-5B). Comparison of

the catalytic outcomes of **2-C1**, **4-C1**, and **4-C2** in the room temperature cross-coupling of 1-chloronaphthalene and furfurylamine using ≤0.25 mol% catalyst loadings (Scheme 7-5C) could reveal the importance of the backbone's heteroatom identity if the pre-catalysts offered different outcomes, or the importance of the 5-membered ring linker if the pre-catalysts were equally competent. A more direct analysis of the influence of backbone ring size would involve a comparison of **L0** and an analogous cyclopentadienyl-linked ligand; however, this backbone is not aromatic and the basic catalytic conditions would likely deprotonate the backbone, as the driving force to restore aromaticity renders the cyclopentadienyl CH_2 fragment acidic. The results of this work would further our understanding of ligand design trends as they pertain to nickel-catalyzed amination.

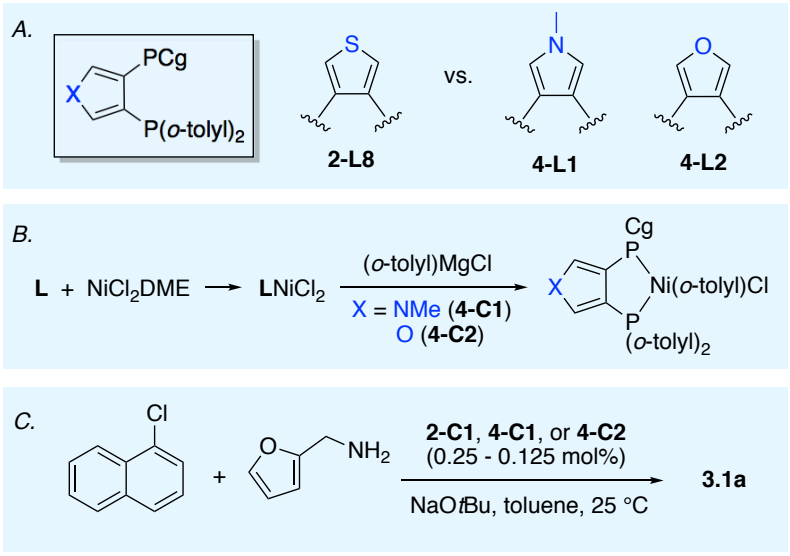

Scheme 7-5. Comparison of isosteric 5-membered ring heteroaryl variants of **2-L8**. *A.* Proposed ligand variants of **2-L8** comprise 3,4-substituted *N*-methylpyrrole (**4-L1**) and furan (**4-L2**). *B.* Syntheses of new (**L**)Ni(*o*-tolyl)Cl pre-catalysts **4-C1** and **4-C2**, featuring the new ligands **4-L1** and **4-L2**, respectively. *C.* Catalytic screen involving the cross-coupling of 1-chloronaphthalene and furfurylamine. In Scheme 4-4, 80% conversion to **3.1a** is achieved through the use of 0.25 mol% **2-C1** at room temperature, and 40% conversion to **3.1a** employing 0.125 mol% **2-C1** at 80 °C.

Section 7.4. Chapter 5 Conclusions and Future Directions

In response to the culmination of data emphasizing the importance of the PCg motif in ancillary ligand design (Chapter 4; Section 1.3.3), a new sub-category of PAd-DalPhos

ligands comprising two PCg fragments (i.e., 'double cage') were developed. Three double cage ligands with different (hetero)aryl backbones (phenylene (**3-L1,** PAd2-DalPhos), pyridine (**3-L2**), and quinoxaline (**3-L3**)) were synthesized using Pd-catalyzed P-C cross-coupling methods, and were incorporated into **L**Ni(*o*-tolyl)Cl complexes. Competitive reactivity surveys involving the cross-coupling of furfurylamine with several aryl chlorides were implemented to distinguish the catalytic performance of the double cage pre-catalysts and **L0**Ni(*o*-tolyl)Cl, (**C0**). The pre-catalysts featuring **3-L1** and **3-L2** were found to outperform **L0** and **3-L3**, and (**3-L1**)Ni(*o*-tolyl)Cl (**3-C1**) was selected for subsequent testing in the hitherto unknown Ni-catalyzed mono-arylation of 2-aminooxazole. An excellent yield of the arylated 2-aminooxazole product **4.2a** was obtained using **3-C1** whereas **C0** and other nickel pre-catalysts bearing CyPF-Cy, DPPF, and XantPhos ligands proved inferior. Superior catalytic performance of diastereomerically pure *meso*-**3-C1** versus *rac*-**3-C1** at lower catalyst loadings was noted in this preliminary screen. Notwithstanding this observation, the substrate scope of the diastereomeric catalyst mixture **3-C1** was explored. Challenging 5- and 6-membered ring heteroarylamino nucleophiles such as 2-aminooxazole, 2-aminothiazole, 5-amino-1,3-dimethyl-1H-pyrazole, 2-aminopyridine, and aminopyrazine were successfully coupled with a range of (hetero)aryl chlorides and a 5-membered ring heteroaryl bromide. Notably, a chemoselective example demonstrated a nucleophile preference of **3-C1** for a primary heteroarylamine over a secondary amide, and was conducted using benchtop techniques employing rudimentary nitrogen lines. PAd2-DalPhos represents the successful design of a ligand specifically intended for use with nickel, and has unveiled a new mode of reactivity in the context of Ni-catalyzed amination, namely the construction of heteroatom dense molecules *via* the monoarylation of primary heteroarylamines. The pre-catalyst **3-C1** not only operates under milder reaction temperatures compared with best-in-class palladium methods,[43] but rivals analogous BHA protocols with respect to catalyst loading and substrate scope.

The improvement seen in replacing the P(*o*-tolyl)$_2$ fragment with PCg within the PAd-DalPhos framework could be attributed to a modest increase of steric bulk at the nickel centre, which may enhance more challenging reductive eliminations of acidic amido reactive ligands,[103, 121] and/or better stabilize resultant Ni^0 species. It is also possible that the absence of arylphosphino appendages (disregarding the aryl backbone) of PAd2-

DalPhos prevents unwanted η^2-interactions of approaching Ni^0 species, a scenario where the consequential proximity of Ni^0 and Ni^{II} species can lead to chloride abstraction of the latter (Scheme 7-4).[50] This action would siphon productive Ni^{II} species *via* comproportionation into potentially inactive Ni^I species, which may be responsible for the higher catalyst loadings that are needed when employing **C0** relative to **3-C1**.

Although PAd2-DalPhos represents a breakthrough in nickel catalysis, limitations exist in the nickel-catalyzed arylation of acidic amines. Accessing deactivated electrophiles as cross-coupling partners with primary heteroarylamines (Chapter 5) and amides[73] remains an insurmountable task using existing nickel catalysts. This could be due to a stalled C-N bond forming step, as nickel is purported to suffer from a more challenging reductive elimination step,[44] and metal complexes with more electron-rich amido ligands and electron-poor aryl ligands undergo faster reductive elimination.[103, 121] To understand the principles governing the inertness of nickel catalysts with deactivated substrates, the work in Chapter 5 could be extended into a study of **3-L1** and **L0** ligated nickel amido complexes containing electron-rich aryl ligands (i.e., *p*-anisyl) and acidic amido ligands (i.e., 2-aminooxazole for **3-L1**, benzamide for **L0**) (Scheme 7-6).

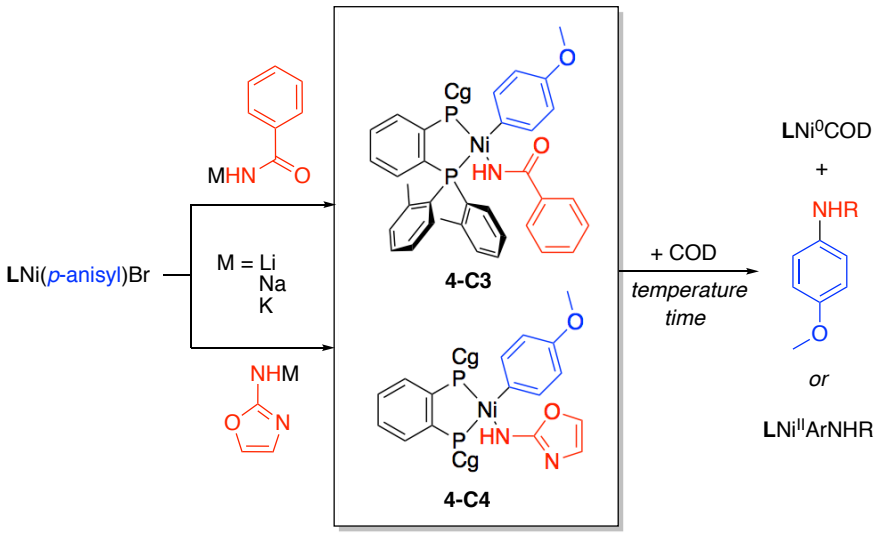

Scheme 7-6. Stoichiometric studies on the reductive elimination of **L**Ni(*p*-anisyl)NHR complexes. **L** = **L0** and R = carbonylbenzene, or **L** = **3-L3** and R = 2-oxazolyl. Syntheses of nickel amido complexes commence from transmetallation of **L**$NiBr_2$ with (*p*-anisyl)MgBr (not shown), followed by a second transmetallation with a metal amido to

generate **4-C3** and **4-C4**. Reductive elimination would be monitored by NMR or GC methods to detect COD-trapped **L**Ni^0, **L**Ni^{II}ArNHR, or aniline product.

If the supposition of a challenging reductive elimination were correct, the stability of these nickel amido species should allow for their straightforward isolation and characterization. The reductive elimination of **L**Ni^{II}ArNHR would be evaluated by monitoring the formation of **L**Ni^0COD through $^{31}P\{^1H\}$ NMR analysis, or the formation of the aniline product by either ^1H NMR or GC methods. Unconsumed **L**Ni^{II}ArNHR, or product turnover over longer time periods or at reaction temperatures greater than standard catalytic conditions (i.e., >16 hours; >80 °C for 1° heteroarylamines and >90 °C for 1° amides) would confirm the hypothesis of a stalled reductive elimination step. If this were the case, the design of a new ligand with properties that further promote this elementary step would be warranted. Conversely, clean turnover of **L**Ni^{II}ArNHR employing typical catalytic reaction temperatures and times would suggest that other factors preventing the coupling of these deactivated substrates are at play. In this scenario, further mechanistic studies could be implemented involving stoichiometric studies of various nickel intermediates that may exist within the catalytic cycle. This work would be particularly impactful as it would expose mechanistic insight pertaining to nickel-catalyzed amination and potentially lead to the rational design of a new ancillary ligand that may accommodate these challenging substrates, which would broaden the substrate scope for these nickel-based protocols even further.

Chapter 8. Conclusion

Methods to identify effective nickel catalysts are beginning to shift from the widespread screening of existing palladium-based ligands to the rational design of ligands created specifically for nickel. This is enabled by the recent growth of mechanistic data surrounding nickel-based cross-coupling manifolds, and the expansion of privileged ligand classes for nickel-based catalysts. These pursuits have begun to expose criteria for ancillary ligand design, thus enabling the development of new and improved ligands to address unmet reactivity challenges in the context of nickel-based cross-couplings.

The objective of my thesis work was to discover ancillary ligand characteristics that give rise to robust nickel-based catalysts for use in C(sp^2)-N cross-coupling, with an overarching intention to develop a new ligand guided by the information produced herein. These goals were met by gathering comparative data between high-performing ligand classes in a diverse array of C(sp^2)-N cross-couplings and extracting resultant structure-reactivity trends. Chapters 2-4 established ideal ligand properties for C(sp^2)-N cross-coupling Ni-catalysts, which guided the design of premier 'double cage' ligands disclosed in Chapter 5. The data from Chapters 2-3 suggest that the steric environment imparted by the ligand is more impactful on catalytic performance than the electronic properties of the ligand. The inclusion of both a thiophenyl linker and PCg moiety within a ligand framework was found to be critical for excellent reactivity in Chapter 4, potentially by offering more stable Ni^0 species and/or dissuading off-cycle pathways. These studies led to the development of PAd2-DalPhos and related double cage ligands, which may be appropriately hindered to stabilize Ni^0 species, facilitate reductive elimination, dissuade $(P_2)_2Ni^0$ formation and comproportionation, and exhibit subtle electronic properties which may balance the divergent characteristics needed for certain elementary steps. This highlights the advantage of rational ligand design through the meticulous examination of ligand effects in Ni-catalyzed aminations, given that PAd2-DalPhos has unveiled new reactivity in the domain of nickel catalysis, namely the hitherto unknown Ni-catalyzed cross-coupling of primary heterocyclic amines with (hetero)aryl chlorides.

The evolution of ancillary ligands for applications in nickel catalysis parallels the development of cutting-edge Buchwald Hartwig Amination (BHA) ligands. Since BHA is now a state-of-the-art protocol, this bodes well for the future of analogous nickel catalysis.

References

1. M. L. Crawley, B. M. Trost, *Applications of Transition Metal Catalysis in Drug Discovery and Development: An Industrial Perspective*. John Wiley & Sons **2012**.
2. B. G. Miller, R. Wolfenden, *Annu. Rev. Biochem.* **2002**, *71*, 847-885.
3. E. J. Corey, J. O. Link, *J. Am. Chem. Soc.* **1992**, *114*, 1906-1908.
4. E. J. Corey, S. Shibata, R. K. Bakshi, *J. Org. Chem.* **1988**, *53*, 2861-2863.
5. R. Noyori, *Adv. Synth. Catal.* **2003**, *345*, 15-32.
6. S. Akutagawa, *Topics in Catalysis* **1997**, *4*, 271-274.
7. M. Beller, C. Bolm, *Transition Metals for Organic Synthesis*. 2 ed.; Wiley-VCH **2004**; Vol. 1.
8. I. Chorkendorff, J. W. Niemantsverdriet, *Concept of Modern Catalysis and Kinetics*. Wiley-VCH GmbH & Co. KGaA **2003**.
9. G. L. Miessler, P. J. Fischer, D. A. Tarr, *Inorganic Chemistry*. 5 ed.; Pearson **2014**.
10. D. J. Cole-Hamilton, *Science* **2003**, *299*, 1702-1708.
11. M. Stradiotto, R. Lundgren, *Ligand Design in Metal Chemistry: Reactivity and Catalysis*. John Wiley & Sons, Ltd.: Hoboken, NJ, **2016**.
12. V. Vallet, U. Wahlgren, I. Grenthe, *J. Am. Chem. Soc.* **2003**, *125*, 14941-14950.
13. R. Hancock, *Comments Inorg. Chem.* **1988**, *6*, 237-284.
14. R. Noyori, T. Ohkuma, *Pure Appl. Chem.* **1999**, *71*, 1493-1501.
15. T. Ohkuma, M. Koizumi, H. Doucet, T. Pham, M. Kozawa, K. Murata, E. Katayama, T. Yokozawa, T. Ikariya, R. Noyori, *J. Am. Chem. Soc.* **1998**, *120*, 13529-13530.
16. L. M. Alcazar-Roman, J. F. Hartwig, A. L. Rheingold, L. M. Liable-Sands, I. A. Guzei, *J. Am. Chem. Soc.* **2000**, *122*, 4618-4630.
17. J. L. Klinkenberg, J. F. Hartwig, *J. Am. Chem. Soc.* **2010**, *132*, 11830-11833.
18. U. Christmann, R. Vilar, *Angew. Chem. Int. Ed.* **2005**, *44*, 366-374.
19. I. P. Beletskaya, A. V. Cheprakov, *Organometallics* **2012**, *31*, 7753-7808.
20. D. S. Surry, S. L. Buchwald, *Angew. Chem. Int. Ed.* **2008**, *47*, 6338-6361.

21. E. A. B. Kantchev, C. J. O'Brien, M. G. Organ, *Angew. Chem. Int. Ed.* **2007**, *46*, 2768-2813.

22. P. Ruiz-Castillo, S. L. Buchwald, *Chem. Rev.* **2016**, *116*, 12564-12649.

23. J. F. Hartwig, S. Shekhar, Q. Shen, F. Barrios-Ianderos, Synthesis of Anilines. In *The Chemistry of Anilines*, Rappoport, S., Ed. John Wiley and Sons Ltd. **2007**; pp 455-536.

24. F. Ullman, *Chem. Ber.* **1903**, *36*, 2382-2384.

25. I. Goldberg, *Chem. Ber.* **1906**, *39*, 1691-1692.

26. C. Sambiagio, S. P. Marsden, A. J. Blacker, P. C. McGowan, *Chem. Soc. Rev.* **2014**, *43*, 3525-3550.

27. G. Evano, N. Blanchard, *Copper-Mediated Cross-Coupling Reactions*. John Wiley & Sons, Inc. **2014**.

28. H. Yu, Y. Jiang, Y. Fu, L. Liu, *J. Am. Chem. Soc.* **2010**, *132*, 18078-18091.

29. M. Kosugi, M. Kameyama, T. Migita, *Chem. Lett.* **1983,** 927-928.

30. J. Louie, J. F. Hartwig, *Tetrahedron Lett.* **1995**, *36*, 3609-3612.

31. A. S. Guram, R. A. Rennels, S. L. Buchwald, *Angew. Chem. Int. Ed.* **1995**, *34*, 1348-1350.

32. M. S. Driver, J. F. Hartwig, *J. Am. Chem. Soc.* **1996**, *118*, 7217-7218.

33. J. P. Wolfe, S. Wagaw, S. L. Buchwald, *J. Am. Chem. Soc.* **1996**, *118*, 7215-7216.

34. M. Nishiyama, T. Yamamoto, Y. Koie, *Tetrahedron Lett.* **1998**, *39*, 617-620.

35. A. Ehrentraut, A. Zapf, M. Beller, *J. Mol. Catal. A: Chem* **2002**, *182-183*, 515-523.

36. N. Kataoka, Q. Shelby, J. P. Stambuli, J. F. Hartwig, *J. Org. Chem.* **2002**, *67*, 5553-5566.

37. J. Huang, G. Grasa, S. P. Nolan, *Org. Lett.* **1999**, *1*, 1307-1309.

38. J. F. Hartwig, *Acc. Chem. Res.* **2008**, *41*, 1534-1544.

39. R. J. Lundgren, B. D. Peters, P. G. Alsabeh, M. Stradiotto, *Angew. Chem. Int. Ed.* **2010**, *49*, 4071-4074.

40. S. M. Crawford, C. B. Lavery, M. Stradiotto, *Chem. Eur. J.* **2013**, *19*, 16760-16771.

41. C. W. Cheung, D. S. Surry, S. L. Buchwald, *Org. Lett.* **2013**, *15*, 3734-3737.

42. M. Su, S. L. Buchwald, *Angew. Chem. Int. Ed.* **2012**, *51*, 4710-4713.

43. E. P. K. Olsen, P. L. Arrechea, S. L. Buchwald, *Angew. Chem. Int. Ed.* **2017**, *56*, 10569-10572.

44. S. Z. Tasker, E. A. Standley, T. F. Jamison, *Nature* **2014**, *509*, 299-309.

45. J. Twilton, C. Le, P. Zhang, M. H. Shaw, R. W. Evans, D. W. C. MacMillan, *Nat. Rev. Chem.* **2017**, *1*, 0052.

46. L. M. Guard, M. M. Beromi, G. W. Brudvig, N. Hazari, D. J. Vinyard, *Angew. Chem. Int. Ed.* **2015**, *54*, 13352-13356.

47. G. Yin, I. Kalvet, U. Englert, F. Schoenebeck, *J. Am. Chem. Soc.* **2015**, *137*, 4164.

48. S. Bajo, G. Laidlaw, A. R. Kennedy, S. Sproules, D. J. Nelson, *Organometallics* **2017**, *36*, 1662-1672.

49. M. Mohadjer Beromi, G. Banerjee, G. W. Brudvig, N. Hazari, B. Q. Mercado, *ACS Catal.* **2018**, *8*, 2526-2533.

50. M. Mohadjer Beromi, A. Nova, D. Balcells, A. M. Brasacchio, G. W. Brudvig, L. M. Guard, N. Hazari, D. J. Vinyard, *J. Am. Chem. Soc.* **2017**, *139*, 922-936.

51. S. Z. Ge, R. A. Green, J. F. Hartwig, *J. Am. Chem. Soc.* **2014**, *136*, 1617-1627.

52. S. Bajo, G. Laidlaw, A. R. Kennedy, S. Sproules, D. J. Nelson, *Organometallics* **2017**, *36*, 1880-1880.

53. R. Norris Shreve, G. N. Vriens, D. A. Vogel, *Ind. Eng. Chem.* **1950**, *42*, 791-796.

54. M. Marin, R. J. Rama, M. C. Nicasio, *Chem. Rec.* **2016**, *16*, 1819-1832.

55. H. Cristau, J. Desmurs, *J. Ind. Chem.* **1995**, *7*, 240-263.

56. J. P. Wolfe, S. L. Buchwald, *J. Am. Chem. Soc.* **1997**, *119*, 6054-6058.

57. M. J. Iglesias, A. Prieto, M. C. Nicasio, *Adv. Synth. Catal.* **2010**, *352*, 1949-1954.

58. G. Manolikakes, A. Gavryushin, P. Knochel, *J. Org. Chem.* **2008**, *73*, 1429-1434.

59. C. Gao, L. Yang, *J. Org. Chem.* **2008**, *73*, 1624-1627.

60. T. Shimasaki, M. Tobisu, N. Chatani, *Angew. Chem. Int. Ed.* **2010**, *49*, 2929-2932.

61. M. Tobisu, T. Shimasaki, N. Chatani, *Chem. Lett.* **2009**, *38*, 710-711.

62. J. F. Hartwig, *Angew. Chem. Int. Ed.* **1998**, *37*, 2046-2067.

63. Y. Sunesson, E. Lime, S. Nilsson Lill, R. E. Meadows, P. Norrby, *J. Org. Chem.* **2014**, *79*, 11961-11969.

64. F. F. Yong, A. M. Mak, W. Wu, M. B. Sullivan, E. G. Robins, C. W. Johannes, H. Jong, Y. H. Lim, *ChemPlusChem* **2017**, *82*, 750-757.

65. S. G. Rull, I. Funes-Ardoiz, C. Maya, F. Maseras, M. R. Fructos, T. R. Belderrain, M. C. Nicasio, *ACS Catal.* **2018**, *8*, 3733-3742.

66. K. Matsubara, Y. Fukahori, T. Inatomi, S. Tazaki, Y. Yamada, Y. Koga, S. Kanegawa, T. Nakamura, *Organometallics* **2016**, *35*, 3281-3287.

67. C. M. Lavoie, R. McDonald, E. R. Johnson, M. Stradiotto, *Adv. Synth. Catal.* **2017**, *359*, 2972-2980.

68. N. H. Park, G. Teverovskiy, S. L. Buchwald, *Org. Lett.* **2014**, *16*, 220-223.

69. S. G. Rull, J. F. Blandez, M. R. Fructos, T. R. Belderrain, M. C. Nicasio, *Adv. Synth. Catal.* **2015**, *357*, 907.

70. R. A. Green, J. F. Hartwig, *Angew. Chem. Int. Ed.* **2015**, *54*, 3768-3772.

71. A. Borzenko, N. L. Rotta-Loria, P. M. MacQueen, C. M. Lavoie, R. McDonald, M. Stradiotto, *Angew. Chem. Int. Ed.* **2015**, *54*, 3773-3777.

72. C. M. Lavoie, P. M. MacQueen, N. L. Rotta-Loria, R. S. Sawatzky, A. Borzenko, A. J. Chisholm, B. K. V. Hargreaves, R. McDonald, M. J. Ferguson, M. Stradiotto, *Nat. Commun.* **2016**, *7*, 11073.

73. C. M. Lavoie, P. M. MacQueen, M. Stradiotto, *Chem. Eur. J.* **2016**, *22*, 18752-18755.

74. C. Li, Y. Kawamata, H. Nakamura, J. C. Vantourout, Z. Liu, Q. Hou, D. Bao, J. T. Starr, J. Chen, M. Yan, P. S. Baran, *Angew. Chem. Int. Ed.* **2017**, *56*, 13088-13093.

75. Y. Kawamata, J. C. Vantourout, D. P. Hickey, P. Bai, L. Chen, Q. Hou, W. Qiao, K. Barman, M. A. Edwards, A. F. Garrido-Castro, J. N. deGruyter, H. Nakamura, K. Knouse, C. Qin, K. J. Clay, D. Bao, C. Li, J. T. Starr, C. Garcia-Irizarry, N. Sach, H. S. White, M. Neurock, S. D. Minteer, P. S. Baran, *J. Am. Chem. Soc.* **2019**, *141*, 6392-6402.

76. E. B. Corcoran, M. T. Pirnot, S. Lin, S. D. Dreher, D. A. DiRocco, I. W. Davies, S. L. Buchwald, D. W. C. MacMillan, *Science* **2016**, *353*, 279-283.

77. C. M. Lavoie, M. Stradiotto, *ACS Catal.* **2018**, *8*, 7228-7250.

78. Y.-P. Zhou, S. Raoufmoghaddam, T. Szilvási, M. Driess, *Angew. Chem. Int. Ed.* **2016**, *55*, 12868-12872.

79. J. P. Tassone, P. M. MacQueen, C. M. Lavoie, M. J. Ferguson, R. McDonald, M. Stradiotto, *ACS Catal.* **2017**, *7*, 6048-6059.

80. J. P. Tassone, E. V. England, P. M. MacQueen, M. J. Ferguson, M. Stradiotto, *Angew. Chem. Int. Ed.* **2019**, *58*, 2485-2489.

81. A. V. Gatien, C. M. Lavoie, R. N. Bennett, M. J. Ferguson, R. McDonald, E. R. Johnson, A. W. H. Speed, M. Stradiotto, *ACS Catal.* **2018**, *8*, 5328−5339.

82. K. Wu, A. G. Doyle, *Nat. Chem.* **2017**.

83. P. M. MacQueen, M. Stradiotto, *Synlett* **2017**, *28*, 1652-1656.

84. J. Schranck, P. Furer, V. Hartmann, A. Tlili, *Eur. J. Org. Chem.* **2017**, 3496-3500.

85. L. Ackermann, R. Sandmann, W. Song, *Org. Lett.* **2011**, *13*, 1784-1786.

86. L. Ackermann, W. Song, R. Sandmann, *J. Organomet. Chem.* **2011**, *696*, 195-201.

87. N. Iranpoor, F. Panahi, *Adv. Synth. Catal.* **2014**, *356*, 3067-3073.

88. S. S. Kampmann, A. N. Sobolev, G. A. Koutsantonis, S. G. Stewart, *Adv. Synth. Catal.* **2014**, *356*, 1967-1973.

89. P. S. Hanley, T. P. Clark, A. L. Krasovskiy, M. S. Ober, J. P. O'Brien, T. S. Staton, *ACS Catal.* **2016**, *6*, 3515-3519.

90. R. S. Sawatzky, M. J. Ferguson, M. Stradiotto, *Synlett* **2017**, *28*, 1586-1591.

91. E. C. Hansen, D. J. Pedro, A. C. Wotal, N. J. Gower, J. D. Nelson, S. Caron, D. J. Weix, *Nat. Chem.* **2016**, *8*, 1126-1130.

92. N. Hazari, P. R. Melvin, M. M. Beromi, *Nat. Rev. Chem.* **2017**, *1*, 0025.

93. E. A. Standley, S. J. Smith, P. Müller, T. F. Jamison, *Organometallics* **2014**, *33*, 2012-2018.

94. M. Appl, *Ammonia: Principles and Industrial Practice*. Wiley-VCH Verlag GmbH: Weinheim, **1999**.

95. J. Schranck, J. Rotzler, *Org. Process Res. Dev.* **2015**, *19*, 1936-1943.

96. J. L. Klinkenberg, J. F. Hartwig, *Angew. Chem. Int. Ed.* **2011**, *50*, 86-95.

97. M. Stradiotto, Ancillary Ligand Design in the Development of Palladium Catalysts for Challenging Selective Monoarylation Reactions. In *New Trends in Cross-Coupling: Theory and Applications*, Colacot, T. J., Ed. The Royal Society of Chemistry: Cambridge, UK, **2014**; pp 228-253.

98. E. A. Standley, T. F. Jamison, *J. Am. Chem. Soc.* **2013**, *135*, 1585-1592.

99. S. S. Kampmann, B. W. Skelton, D. A. Wild, G. A. Koutsantonis, S. G. Stewart, *Eur. J. Org. Chem.* **2015**, 5995-6004.

100. B. C. Hamann, J. F. Hartwig, *J. Am. Chem. Soc.* **1998**, *120*, 3694-3703.

101. U. Jahn, *Top. Curr. Chem.* **2011**, *320*, 323-451.

102. V. P. Ananikov, *ACS Catal.* **2015**, *5*, 1964-1971.

103. J. F. Hartwig, *Inorganic Chemistry* **2007**, *46*, 1936-1947.

104. A. L. Clevenger, R. M. Stolley, N. D. Staudaher, N. Al, A. L. Rheingold, R. T. Vanderlinden, J. Louie, *Organometallics* **2018**, *37*, 3259-3268.

105. B. H. Lipshutz, H. Ueda, *Angew. Chem. Int. Ed.* **2000**, *39*, 4492-4494.

106. S. Tasler, B. H. Lipshutz, *J. Org. Chem.* **2003**, *68*, 1190-1199.

107. J. D. Shields, E. E. Gray, A. G. Doyle, *Org. Lett.* **2015**, *17*, 2166-2169.

108. J. E. Dander, N. A. Weires, N. K. Garg, *Org. Lett.* **2016**, *18*, 3934-3936.

109. B. C. Hamann, J. F. Hartwig, *J. Am. Chem. Soc.* **1998**, *120*, 7369-7370.

110. B. C. Hamann, J. F. Hartwig, *J. Am. Chem. Soc.* **1998**, *120*, 12706-12706.

111. Some confusion exists regarding the identity of what is claimed as **2.3g** in this report, in that the NMR, IR, and elemental analysis characterization data provided for this compound in the supporting information are identical to those listed for the isomeric product derived from 1-bromo-3,5-dimethylbenzene. In this regard, the ^{1}H and $^{13}C\{^{1}H\}$ NMR chemical shift data provided (in the absence of accompanying spectra) are inconsistent with the claimed structure of **2.3g**: Old, D. W.; Harris, M. C.; Buchwald, S. L. *Org. Lett.* **2000**, *2*, 1403-1406.

112. J. Magano, S. Monfette, *ACS Catal.* **2015**, *5*, 3120-3123.

113. R. Takise, K. Muto, J. Yamaguchi, K. Itami, *Angew. Chem. Int. Ed.* **2014**, *53*, 6791-6794.

114. J. Clifton, E. R. M. Habraken, P. G. Pringle, I. Manners, *Catal. Sci. Technol.* **2015**, *5*, 4350-4353.

115. M. Hashimoto, S. Igawa, M. Yashima, I. Kawata, M. Hoshino, M. Osawa, *J. Am. Chem. Soc.* **2011**, *133*, 10348-10351.

116. P. G. Pringle, M. B. Smith, Phosphatrioxa-adamantane Ligands. In *Phosphorus(III) Ligands in Homogeneous Catalysis: Design and Synthesis*, Kamer, P. C. J.; van Leeuwen, P. W. N. M., Eds. John Wiley & Sons Ltd. **2012**; pp 391-404.

117. J. H. Downing, J. Floure, K. Heslop, M. F. Haddow, J. Hopewell, M. Lusi, H. Phetmung, A. G. Orpen, P. G. Pringle, R. I. Pugh, D. Zambrano-Williams, *Organometallics* **2008**, *27*, 3216-3224.

118. The terms 'meso' (RS/SR) and 'rac' (RR/SS) reference the relative handedness of the PCg fragments within the ligands **3-L1** to **3-L3**. Complete experimental details and characterization data are provided in Chapter 6 and the Appendix, which contains the supplementary data for the crystallographic characterization of meso-**3-L1**, rac-**3-L1**, meso-**3-L2**, rac-**3-L2**, meso-**3-L3**, rac-**3-L3**, meso-**3-C1**, rac-**3-C1**, meso-**3-C2**, and meso-**3-C3**.

119. D. C. Blakemore, L. Castro, I. Churcher, D. C. Rees, A. W. Thomas, D. M. Wilson, A. Wood, *Nat. Chem.* **2018**, *10*, 383-394.

120. N. A. Meanwell, *J. Med. Chem.* **2011**, *54*, 2529-2591.

121. M. S. Driver, J. F. Hartwig, *J. Am. Chem. Soc.* **1997**, *119*, 8232-8245.

122. Y. Yamamoto, T. Koizumi, K. Katagiri, Y. Furuya, H. Danjo, T. Imamoto, K. Yamaguchi, *Org. Lett.* **2006**, *8*, 6103-6106.

123. T. Imamoto, K. Sugita, K. Yoshida, *J. Am. Chem. Soc.* **2005**, *127*, 11934-11935.

124. M. Oliverio, P. Costanzo, R. Paonessa, M. Nardi, A. Procopio, *RSC Adv.* **2013**, *3*, 2548-2552.

125. D. A. Wilson, C. J. Wilson, C. Moldoveanu, A. Resmerita, P. Corcoran, L. M. Hoang, B. M. Rosen, V. Percec, *J. Am. Chem. Soc.* **2010**, *132*, 1800-1801.

126. J. I. Kuroda, K. Inamoto, K. Hiroya, T. Doi, *Eur. J. Org. Chem.* **2009**, 2251-2261.

127. P. W. Clark, B. J. Mulraney, *J. Organomet. Chem.* **1981**, *217*, 51-59.

128. L. Qin, X. Ren, Y. Lu, Y. Li, J. Zhou, *Angew. Chem. Int. Ed.* **2012**, *51*, 5915-5919.

129. C. M. Reisinger, R. J. Nowack, D. Volkmer, B. Rieger, *Dalton Trans.* **2007**, 272-278.

130. M. Mohadjer Beromi, G. Banerjee, G. W. Brudvig, D. J. Charboneau, N. Hazari, H. M. C. Lant, B. Q. Mercado, *Organometallics* **2018**, *37*, 3943-3955.

131. A. K. Leone, P. K. Goldberg, A. J. McNeil, *J. Am. Chem. Soc.* **2018**, *140*, 7846-7850.

132. J. A. Bilbrey, A. N. Bootsma, M. A. Bartlett, J. Locklin, S. E. Wheeler, W. D. Allen, *J. Chem. Theory Comput.* **2017**, *13*, 1706-1711.

Appendices

"Investigating the Design of Bisphosphine Ligands for use in Nickel-catalyzed C(sp^2)-N Cross Coupling"

Jillian S. K. Clark

Table of Contents

NMR Integrated Yield Experiments

napthalen-1-amine **(1.1a)**

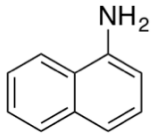

The title compound was synthesized from the corresponding chloride according to **GP2**, using 0.005 equiv **1-C1**, 5.0 equiv 0.5 M ammonia in 1,4-dioxane ([Ar-Cl] = 0.1 M), conducted at 110 °C, and purified according to Workup Method C using dodecane as an internal standard (0.2 equiv) which afforded the title product in a calculated 85% yield. Spectral data are consistent with literature.[A1]

3-methoxyaniline **(1.1b)**

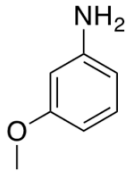

The title compound was synthesized from the corresponding chloride according to **GP2**, using 0.05 equiv **1-C1**, 7.0 equiv 0.5 M ammonia in 1,4-dioxane ([Ar-Cl] = 0.07 M), conducted at 110 °C, and purified according to Workup Method C using dodecane as an internal standard (0.2 equiv) which afforded the title product in a calculated 91% yield. Spectral data are consistent with literature. [A2]

4-methoxyaniline **(1.1c)**

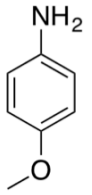

The title compound was synthesized from the corresponding chloride according to **GP2**, using 0.05 equiv **1-C1**, 7.0 equiv 0.5 M ammonia in 1,4-dioxane, 0.5 mL toluene ([Ar-Cl] = 0.07 M), conducted at 110 °C, and purified according to Workup Method C using dodecane as an internal standard (0.2 equiv) which afforded the title product in a calculated 51% yield. Spectral data are consistent with literature. [A2]

benzo[b]thiophen-5-amine **(1.1d)**

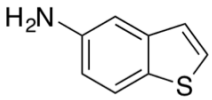

The title compound was synthesized from the corresponding chloride according to **GP2**, using 0.02 equiv **1-C1**, 7.0 equiv 0.5 M ammonia in 1,4-dioxane ([ArCl] = 0.07 M), conducted at 110 °C, and purified according to Workup Method C using dodecane as an internal standard (0.2 equiv) which afforded the title product in a calculated 75 % yield. Spectral data are consistent with literature. [A1]

N-(furan-2-ylmethyl)-2,5-dimethylaniline **(2.1f)**

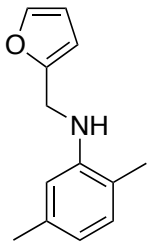

The title compound was synthesized from the corresponding chloride according to **GP1**, conducted at 110 °C using 10 mol% 1,1'-bis(diphenylphosphino)ferrocene, and purified according to Workup Method A. Purified by flash column chromatography on silica gel using a gradient of dichloromethane and hexanes which afforded the title product in a 47% isolated yield (45 mg, 0.22 mmol) as a yellow oil. The loss of material due to handling/compound volatility was confirmed on the basis of calibrated NMR experiments: Following Workup Method C the title product was produced in a 68% calculated yield using 20 mol% ferrocene as an internal standard. ^{1}H NMR (500 MHz, $CDCl_3$): δ 7.40-7.39 (m, 1H), 6.97-6.94 (m, 1H), 6.54-6.52 (m, 2H), 6.35-6.34 (m, 1H), 6.26-6.25 (m, 1H), 4.36 (s, 1H), 3.81 (br, 1H), 2.30 (s, 3H), 2.13 (s, 3H). ^{13}C{^{1}H} NMR (125.8 MHz, $CDCl_3$): δ 152.9, 145.5, 141.9, 136.7, 130.0, 119.4, 118.2, 111.1, 110.4, 106.9, 41.6, 21.5, 17.0. HRMS *m/z* ESI^+ found 224.1046 $[M + Na]^+$ calculated for $C_{13}H_{15}NNaO$ 224.1051.

N-1-naphthalenyl-2-pyridinamine **(4.2j)**

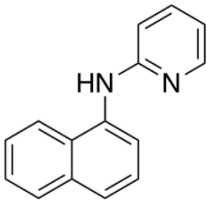

The title compound was synthesized from the corresponding aryl chloride (0.6 mmol) according to **GP6**, conducted at 80 °C using 5 mol% **C2**. The reaction mixture was diluted with ethyl acetate (ca. 30 mL), was washed with brine (3 × ca. 30 mL), and the organic layer was dried over sodium sulfate. The solvent was removed *in vacuo* and the compound was and purified according to Workup Method A. Purified by flash column chromatography on silica gel using 9:1 hexanes/ethyl acetate as eluent, to which dodecane (136.3 μL, 0.6 mmol) was added to afford the title product in an 80% calculated yield on the basis of NMR data. NMR integration analysis of yield is provided given the inability to rigorously obtain **4.2j** in spectroscopically pure form, free of aromatic impurities. ^{1}H NMR (500 MHz, $CDCl_3$): δ 8.21-8.20 (m, 1H, ArH), 8.07 (d, J = 7.4 Hz, 1H, ArH), 7.90-7.88 (m, 1H, ArH), 7.71 (d, J = 8.2 Hz, 1H, ArH), 7.58 (d, J = 7.4 Hz, 1H, ArH), 7.54-7.46 (m, 3H, ArH), 7.43-7.40 (m, 1H, ArH), 6.72-6.70 (m, 1H, ArH), 6.62 (d, J = 8.5 Hz, 1H, ArH), 1.27 (m, 25.3 H, dodecane-CH_2), 0.89 (t, J = 6.8 Hz, 7.5 H, dodecane-CH_3). Spectral data are in agreement with literature.[3]

***N-(furan-2-ylmethyl)-4-methylaniline and 4-butyl-N-(furan-2-ylmethyl)aniline using* 1-C1 (1.5a and 1.5b, from Scheme 2-8).** The title compounds were synthesized from the corresponding chloride and bromide according to **GP7**, using 0.05 equiv **1-C1** and Workup Method C. By NMR integration using ferrocene as an internal standard (0.2 equiv), the title products (N-(furan-2-ylmethyl)-4-methylaniline and 4-butyl-N-(furan-2-ylmethyl)aniline) were afforded in a calculated 43% yield and 25% yield respectively. Select line data for signals used in NMR integrated yield calculations: ^{1}H NMR (300 MHz, $CDCl_3$): δ 4.16 (s, 10H), 2.53-2.48 (t, J = 13 Hz, 2H), 2.24 (s, 3H).

***N-(furan-2-ylmethyl)-4-methylaniline and 4-butyl-N-(furan-2-ylmethyl)aniline using* C0 (1.5a and 1.5b, from Scheme 2-8).** The title compounds were synthesized from the corresponding chloride and bromide according to **GP7**, using 0.05 equiv **C0** and Workup Method C. By NMR integration using ferrocene as an internal standard (0.2 equiv), the

title products (N-(furan-2-ylmethyl)-4-methylaniline and 4-butyl-N-(furan-2-ylmethyl)aniline) were afforded in a calculated 24% yield and 76% yield respectively. Select line data for signals used in the NMR integration calculations: ^{1}H NMR (300 MHz, $CDCl_3$): δ 4.17 (m, 10H), 2.53-2.48 (m, 2H), 2.25 (s, 3H).

Characterization Data for Isolated Products, Ligands, and Complexes

Data for Aniline products:

***N-(furan-2-ylmethyl)naphthalen-1-amine* (1.2a)**

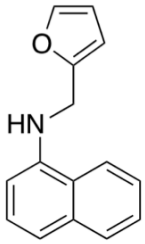

The title compound [A4] was synthesized from the corresponding chloride according to **GP1**, using 0.005 equiv **1-C2**, 1.1 equiv of furfurylamine, 3.75 mL toluene ([Ar-Cl] = 0.27 M), conducted at 25 °C, and purified according to Workup Method A. Purified by flash column chromatography on silica gel using (19:1) hexanes to ethyl acetate which afforded the title product in 62% isolated yield (138 mg, 0.62 mmol) as a light brown oil. ^{1}H NMR (500 MHz, $CDCl_3$): δ 7.86-7.84 (m, 2H), 7.51-7.46 (m, 3H), 7.42-7.39 (m, 1H), 7.34-7.32 (d, J = 8.2 Hz, 1H), 6.75-6.73 (d, J = 7.5 Hz, 1H), 6.40-6.35 (m, 2H), 4.73 (br s, 1H), 4.52 (s, 2H). ^{13}C{^{1}H} NMR (125.8 MHz, $CDCl_3$): δ 152.6, 143.0, 142.3, 134.5, 128.8, 126.7, 126.0, 125.0, 123.8, 120.1, 118.3, 110.6, 107.5, 105.1, 41.9.

***N-(furan-2-ylmethyl)-3-methoxyaniline* (1.2b)**

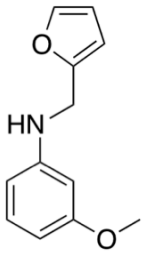

The title compound was synthesized from the corresponding chloride according to **GP1**, using 0.005 equiv **C0**, 1.1 equiv of furfurylamine, 4.17 mL toluene ([Ar-Cl] = 0.24 M), conducted at 25 °C, and purified according to Workup Method A. Purified by flash column

chromatography on silica gel using (5.7:1) hexanes to ethyl acetate which afforded the title product in 78% isolated yield (159 mg, 0.78 mmol) as a dark brown oil. ^{1}H NMR (500 MHz, $CDCl_3$): δ 7.37 (m, 1H), 7.12-7.08 (apparent t, J = 8.1 Hz, 1H), 6.33-6.29 (m, 3H), 6.25-6.24 (m, 2H), 4.31 (s, 2H), 4.07 (br s, 1H), 3.77 (s, 3H). ^{13}C{^{1}H} NMR (125.8 MHz, $CDCl_3$): δ 161.0, 152.8, 149.2, 142.1, 130.2, 110.5, 107.2, 106.5, 103.4, 99.5, 55.3, 41.6. Spectral data are consistent with literature. [A4]

N-(furan-2-ylmethyl)-4-methoxyaniline **(1.2c)**

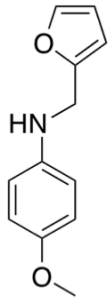

The title compound was synthesized from the corresponding chloride according to **GP1**, using 0.05 equiv **C0**, 1.1 equiv of furfurylamine, 4.17 mL toluene ([Ar-Cl] = 0.24 M), conducted at 25 °C, and purified according to Workup Method A. Purified by flash column chromatography on silica gel using (5.7:1) hexanes to ethyl acetate which afforded the title product in 90% isolated yield (182 mg, 0.90 mmol) as a dark brown oil. ^{1}H NMR (500 MHz, $CDCl_3$): δ 7.38-7.37 (m, 1H), 6.81-6.79 (m, 2H), 6.67-6.65 (m, 2H), 6.33-6.32 (m, 1H), 6.23 (m, 1H), 4.28 (s, 2H), 3.76 (s, 3H).^{13}C{^{1}H} NMR (125.8 MHz, $CDCl_3$): δ 153.2, 152.8, 142.0, 115.0, 114.8, 110.5, 107.1, 55.9, 42.6. Spectral data are consistent with literature. [A5]

N-(furan-2-ylmethyl)benzo[b]thiophen-5-amine **(1.2d)**

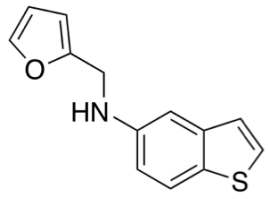

The title compound was synthesized from the corresponding chloride according to **GP1**, using 0.01 equiv **C0**, 1.1 equiv of furfurylamine, 6.25 mL toluene ([Ar-Cl] = 0.16 M), conducted at 25 °C, and purified according to Workup Method A. Purified by flash

column chromatography on silica gel using (5.7:1) hexanes to ethyl acetate which afforded the title product in 75% isolated yield (173 mg, 0.75 mmol) as a dark brown oil. ^{1}H NMR (500 MHz, $CDCl_3$): δ 7.66-7.64 (d, J = 8.7 Hz, 1H), 7.40-7.38 (m, 2H), 7.19-7.18 (m, 1H), 7.08-7.07 (m, 1H), 6.80-6.78 (m, 1H), 6.35-6.34 (m, 1H), 6.28-6.27 (m, 1H), 4.39 (s, 2H), 4.11 (br s, 1H). ^{13}C{^{1}H} NMR (125.8 MHz, $CDCl_3$): δ 152.9, 145.3, 142.1, 141.1, 130.2, 127.1, 123.6, 123.0, 114.3, 110.6, 107.2, 105.7, 42.1. HRMS *m/z* ESI$^+$ found 252.0454 $[M + Na]^+$ calculated for $C_{13}H_{11}NNaOS$ 252.0459.

N-(sec-butyl)naphthalen-1-amine **(1.3a)**

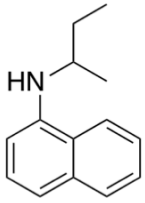

The title compound was synthesized from the corresponding chloride according to **GP1**, using 0.02 equiv **C0**, 1.1 equiv of *sec*-butylamine, 3.75 mL toluene ([Ar-Cl] = 0.16 M), conducted at 25 °C, and purified according to Workup Method A. Purified by flash column chromatography on silica gel using (9:1) hexanes to ethyl acetate which afforded the title product in 70% isolated yield (78 mg, 0.43 mmol) as a dark brown oil. ^{1}H NMR (500 MHz, $CDCl_3$): δ 7.83-7.80 (m, 2H), 7.48-7.43 (m, 2H), 7.39-7.36 (m, 1H), 7.24-7.22 (m, 1H), 6.65-6.64 (m, 1H), 4.23 (br s, 1H), 3.66-3.60 (m, 1H), 1.83-1.75 (m, 1H), 1.68-1.60 (m, 1H), 1.34-1.32 (d, J = 6.3 Hz, 3H), 1.07-1.04 (t, J = 7.5 Hz, 3H). ^{13}C{^{1}H} NMR (125.8 MHz, $CDCl_3$): δ 142.8, 134.8, 128.9, 126.8, 125.8, 124.7, 123.6, 120.0, 116.9, 104.9, 50.2, 29.7, 20.3, 10.6. HRMS *m/z* ESI$^+$ found 200.1434 $[M + H]^+$ calculated for $C_{14}H_{18}N$ 200.1439.

N-(sec-butyl)-3-methoxyaniline **(1.3b)**

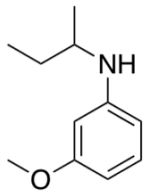

The title compound was synthesized from the corresponding chloride according to **GP1**, using 0.05 equiv **1-C1**, 1.1 equiv *sec*-butylamine, 8.3 mL toluene ([Ar-Cl] = 0.12 M),

conducted at 25 °C, and purified according to Workup Method A. Purified by flash column chromatography on silica gel using (23.5:1) hexanes to ethyl acetate which afforded the title product in 64% isolated yield (114 mg, 0.64 mmol) as a light brown oil. ^{1}H NMR (500 MHz, $CDCl_3$): δ 7.09-7.03 (apparent t, J = 8.1 Hz, 1H), 6.25-6.18 (m, 2H), 6.15-6.13 (apparent t, J = 2.3 Hz, 1H), 3.77 (s, 3H), 3.46-3.35 (m, 2H), 1.65-1.42 (m, 2H), 1.18-1.16 (d, J = 6.3 Hz, 3H), 0.98-0.93 (t, J = 7.4 Hz, 3H). ^{13}C{^{1}H} NMR (125.8 MHz, $CDCl_3$): δ 161.1, 149.4, 130.2, 106.6, 102.0, 99.3, 55.3, 50.1, 29.9, 20.5, 10.6. Spectral data are consistent with literature. [A6]

N-(sec-butyl)-4-methoxyaniline **(1.3c)**

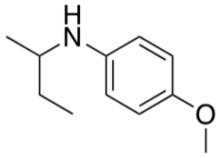

The title compound was synthesized from the corresponding chloride according to **GP1**, using 0.05 equiv **1-C1**, 1.1 equiv *sec*-butylamine, 5 mL toluene ([Ar-Cl] = 0.12 M), conducted at 110 °C, and purified according to Workup Method A. Purified by flash column chromatography on silica gel using (19:1) hexanes to ethyl acetate which afforded the title product in 59% isolated yield (63 mg, 0.35 mmol) as a light brown oil. ^{1}H NMR (300 MHz, $CDCl_3$): δ 6.80-6.74 (m, 2H), 6.58-6.53 (m, 2H), 3.75 (s, 3H), 3.37-3.26 (m, 1H), 3.14 (br s, 1H), 1.67-1.37 (m, 2H), 1.16-1.14 (d, J = 6.3 Hz, 3H), 0.97-0.92 (t, J = 7.4 Hz, 3H). ^{13}C{^{1}H} NMR (75.5 MHz, $CDCl_3$): δ 151.8, 142.0, 115.0, 114.7, 55.9, 50.8, 29.7, 20.3, 10.3. Spectral data are consistent with literature. [A7]

N-(sec-butyl)benzo[b]thiophen-5-amine **(1.3d)**

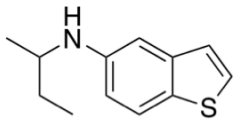

The title compound was synthesized from the corresponding chloride according to **GP1**, using 0.05 equiv **C2**, 1.1 equiv *sec*-butylamine, 5 mL toluene ([Ar-Cl] = 0.12 M), conducted at 25 °C, and purified according to Workup Method A. Purified by flash column chromatography on silica gel using (19:1) hexanes to ethyl acetate which afforded the title product in 61% isolated yield (85 mg, 0.41 mmol) as a light brown oil. ^{1}H NMR

(500 MHz, $CDCl_3$): δ 7.63-7.61 (d, *J* = 8.7 Hz, 1H), 7.37-7.36 (d, *J* = 5.4 Hz, 1H), 7.17-7.16 (d, *J* = 5.4 Hz, 1H), 6.99 (s, 1H), 6.73-6.71 (m, 1H), 3.68 (br s, 1H), 3.49-3.43 (m, 1H), 1.70-1.62 (m, 1H), 1.55-1.47 (m, 1H), 1.22-1.21 (d, *J* = 6.3 Hz, 3 H), 1.00-0.97 (t, *J* = 7.5 Hz, 3H).$^{13}C\{^1H\}$ NMR (125.8 MHz, $CDCl_3$): δ 145.1, 141.2, 129.0, 127.0, 123.5, 123.0, 114.6, 105.6, 50.6, 29.6, 20.3, 10.6. HRMS *m/z* ESI^+ found 206.0998 $[M + H]^+$ calculated for $C_{12}H_{16}NS$ 206.1003.

4-morpholinobenzonitrile **(1.4a)**

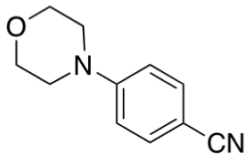

The title compound was synthesized according to **GP3**, using 0.05 equiv **1-C2** and purified according to Workup Method A. Purified by flash column chromatography on silica gel using (2.3:1) hexanes to ethyl acetate which afforded the title product in 94% isolated yield (176 mg, 0.94 mmol) as a light brown solid. ^1H NMR (500 MHz, $CDCl_3$): δ 7.52-7.50 (m, 2H), 6.87-6.85 (m, 2H), 3.86-3.84 (m, 4H), 3.29-3.27 (m, 4H). $^{13}C\{^1H\}$ NMR (125.8 MHz, $CDCl_3$): δ 153.7, 133.7, 120.0, 114.3, 101.3, 66.7, 47.6. Spectral data are consistent with literature. [A8]

4-(benzo[b]thiophen-5-yl)morpholine **(1.4b)**

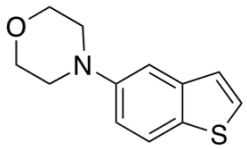

The title compound was synthesized according to **GP3**, using 0.05 equiv **1-C2** and purified according to Workup Method A. Purified by flash column chromatography on silica gel using (3:1) hexanes to ethyl acetate which afforded the title product in 72% isolated yield (157 mg, 0.94 mmol) as a white powder. ^1H NMR (500 MHz, $CDCl_3$): δ 7.76-7.75 (d, *J* = 8.8 Hz, 1H), 7.42-7.41 (d, *J* = 5.4 Hz, 1H), 7.29 (m, 1H), 7.25-7.24 (m, 1H), 7.08-7.06 (m, 1H), 3.92-3.90 (m, 4H), 3.20-3.18 (m, 4H). $^{13}C\{^1H\}$ NMR (125.8 MHz, $CDCl_3$): δ 149.4, 140.9, 132.3, 127.4, 123.9, 123.0, 116.4, 109.7, 67.2, 50.8. Spectral data are consistent with literature. [A9]

N-(furan-2-ylmethyl)-4-methylaniline **(1.5a)**

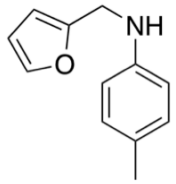

The title compound was synthesized from the corresponding chloride according to **GP1**, using 0.05 equiv **C0**, 1.1 equiv of furfurylamine, 8.33 mL toluene ([Ar-Cl] = 0.12 M), conducted at 25 °C, and purified according to Workup Method A. Purified by flash column chromatography on silica gel using (19:1) hexanes to ethyl acetate which afforded the title product in 72% isolated yield (134 mg, 0.72 mmol) as a light brown oil. ^{1}H NMR (500 MHz, $CDCl_3$): δ 7.41 (m, 1H), 7.07-7.05 (m, 2H), 6.66-6.64 (m, 2H), 6.37-6.36 (m, 1H), 6.27 (m, 1H), 4.34 (s, 2H), 3.89 (br s, 1H), 2.30 (s, 3H). ^{13}C{^{1}H} NMR (125.8 MHz, $CDCl_3$): δ 152.9, 145.3, 141.7, 129.5, 127.1, 113.3, 110.2, 106.8, 41.7, 20.3. Spectral data are consistent with literature. [A10]

4-butyl-N-(furan-2-ylmethyl)aniline **(1.5b)**

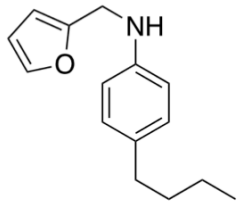

The title compound was synthesized from the corresponding bromide according to **GP1**, using 0.05 equiv **C0**, 1.1 equiv of furfurylamine, 8.33 mL toluene ([Ar-Cl] = 0.12 M), conducted at 25 °C, and purified according to Workup Method A. Purified by flash column chromatography on silica gel using (19:1) hexanes to ethyl acetate which afforded the title product in 72% isolated yield (166 mg, 0.72 mmol) as a light brown oil. ^{1}H NMR (500 MHz, $CDCl_3$): δ 7.40 (m, 1H), 7.06-7.05 (m, 2H), 6.67-6.65 (m, 2H), 6.37-6.36 (m, 1H), 6.27 (m, 1H), 4.33 (s, 2H), 3.92 (br s, 1H), 2.58-2.55 (t, J = 7.7 Hz, 2H), 1.64-1.58 (m, 2H), 1.44-1.36 (m, 2H), 1.00-0.96 (t, J = 7.4 Hz, 3H). ^{13}C{^{1}H} NMR (125.8 MHz, $CDCl_3$): δ 153.2, 145.7, 142.0, 132.7, 129.3, 113.4, 110.5, 107.0, 42.0, 34.9, 34.1, 22.5, 14.2. HRMS *m/z* ESI^{+} found 252.1359 $[M + Na]^{+}$ calculated for $C_{15}H_{19}NNaO$ 252.1364.

4-ethyl-N-(furan-2-ylmethyl)aniline **(1.5c)**

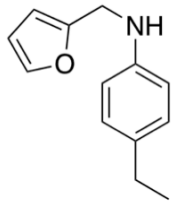

The title compound was synthesized for use as an authentic sample in competition studies (see Scheme 2-8) from the corresponding tosylate according to **GP1**, using 0.05 equiv **C0**, 1.1 equiv of furfurylamine, 6 mL toluene ([Ar-OTs] = 0.12 M), conducted at 25 °C, and purified according to Workup Method A. Purified by flash column chromatography on silica gel using (19:1) hexanes to ethyl acetate, which afforded the title product in 78% isolated yield (113 mg) as a light brown oil. ^{1}H NMR (500 MHz, $CDCl_3$): δ 7.38-7.37 (m, 1H), 7.05-7.03 (m, 2H), 6.64-6.63 (m, 2H), 6.33-6.32 (m, 1H), 6.24-6.23 (m, 1H), 4.31 (s, 2H), 3.90 (br s, 1H), 2.58-2.53 (q, *J* = 7.6 Hz, 2H), 1.22-1.19 (t, *J* = 7.6 Hz, 3H). ^{13}C{^{1}H} NMR (125.8 MHz, $CDCl_3$): δ 153.2, 145.8, 142.1, 134.1, 128.8, 113.6, 110.5, 107.1, 42.0, 28.1, 16.1. HRMS *m/z* ESI$^+$ found 224.1046 $[M + Na]^+$ calculated for $C_{13}H_{15}NNaO$ 224.1051.

N-(furan-2-ylmethyl)-2-methylquinolin-4-amine **(2.1e)**

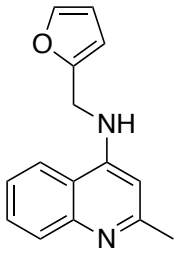

The title compound was synthesized from the corresponding chloride according to **GP1**, conducted at 25 °C using 6.7 mol% 1,1'-bis(diphenyl)phosphinoferrocene, and purified according to Workup Method A which afforded the title product in a 73% yield (175 mg) as a light brown powder. ^{1}H NMR (300 MHz, $CDCl_3$): δ 7.94-7.91 (m, 1H), 7.72-7.69 (m, 1H), 7.62-7.57 (m, 1H), 7.42-7.45 (m, 2H), 6.43 (s, 1H), 6.38-6.32 (m, 2H), 5.33 (br. s, 1H), 4.51-4.50 (d, *J* = 5.3 Hz, 2H), 2.62 (s, 3H). ^{13}C{^{1}H} NMR (125.8 MHz, $CDCl_3$): δ 159.7, 151.2, 149.4, 148.4, 142.7, 129.4, 129.3, 124.3, 119.4, 117.6, 110.7, 108.0, 99.7, 40.8, 25.9. HRMS *m/z* ESI$^+$ found 239.1179 $[M + H]^+$ calculated for $C_{15}H_{15}N_2O$ 239.1184.

***4-(naphthalen-1-yl)morpholine* (2.2a)**

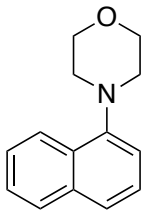

The title compound was synthesized from the corresponding chloride according to **GP3**, conducted at 100 °C using 5 mol% 1,1'-bis(diphenyl)phosphinoferrocene, and purified according to Workup Method A. Purified by flash column chromatography on silica gel using (19:1) hexanes/ethyl acetate which afforded the title product in 85% isolated yield (181 mg, 0.85 mmol) as a white solid. ^{1}H NMR (500 MHz, $CDCl_3$): δ 8.25-8.23 (m, 1H), 7.86-7.84 (m, 1H), 7.60-7.58 (d, J = 8.2 Hz, 1H), 7.52-7.47 (m, 2H), 7.44-7.41 (m, 1H), 7.12-7.10 (d, J = 7.4 Hz, 1H), 4.01-3.99 (m, 4H), 3.14-3.12 (m, 4H).^{13}C{^{1}H} NMR (125.8 MHz, $CDCl_3$): δ 149.6, 135.0 (2 signals), 129.0, 128.7, 126.1, 125.7, 124.0, 123.6, 114.9, 67.7, 53.7. Spectral data are in agreement with literature. [A11]

***4-(3-methoxyphenyl)morpholine* (2c)**

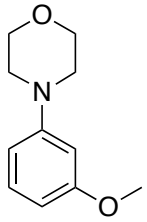

The title compound was synthesized from the corresponding chloride according to **GP3**, conducted at 100 °C using 5 mol% 1,1'-bis(diphenyl)phosphinoferrocene, and purified according to Workup Method A. Purified by flash column chromatography on silica gel using (9:1) hexanes/ethyl acetate which afforded the title product in 84% isolated yield (162 mg, 0.84 mmol) as a pale brown oil. ^{1}H NMR (300 MHz, $CDCl_3$): δ 7.22-7.16 (m, 1H), 6.55-6.52 (m, 1H), 6.46-6.43 (m, 2H), 3.87-3.84 (m, 4H), 3.80 (s, 3H), 3.17-3.14 (m, 4H). ^{13}C{^{1}H} NMR (75.5 MHz, $CDCl_3$): δ 160.7, 152.7, 129.9, 108.5, 104.8, 102.3, 66.9, 55.2, 49.3. Spectral data are in agreement with literature.[A12]

***4-(2-methylquinolin-4-yl)morpholine* (2.2e)**

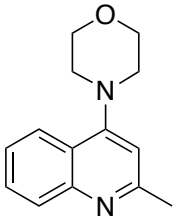

The title compound was synthesized from the corresponding chloride according to **GP3**, conducted at 25 °C using 6.7 mol% 1,1'-bis(diphenyl)phosphinoferrocene, and purified according to Workup Method A. Purified by flash column chromatography on silica gel using (1:4) hexanes/ethyl acetate which afforded the title product in 91% isolated yield (207 mg, 0.91 mmol) as a light brown solid. ^{1}H NMR (500 MHz, $CDCl_3$): δ 7.99-7.95 (m, 2H), 7.64-7.59 (m, 1H), 7.44-7.39 (m, 1H), 6.74 (s, 1H), 3.99-3.96 (m, 4H), 3.22-3.19 (m, 4H), 2.68 (s, 3H). ^{13}C{^{1}H} NMR (125.8 MHz, $CDCl_3$): δ 159.5, 156.7, 149.3, 129.3, 129.1, 124.7, 123.2, 121.7, 109.3, 67.0, 52.6, 25.7. Spectral data are consistent with literature. [A13]

***4-(4-(tert-butyl)phenyl)morpholine* (2.2f)**

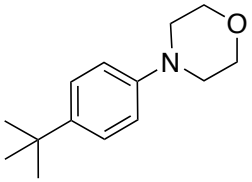

The title compound was synthesized from the corresponding bromide according to **GP3**, conducted at 100 °C using 5 mol% 1,1'-bis(diphenyl)phosphinoferrocene, and purified according to Workup Method A. Purified by flash column chromatography on silica gel using (19:1) hexanes/ethyl acetate which afforded the title product in 82% isolated yield (179 mg, 0.82 mmol) as an off-white solid. ^{1}H NMR (500 MHz, $CDCl_3$): δ 7.33-7.31 (d, J = 8.8 Hz, 2H), 6.89-6.87 (d, J = 8.8 Hz, 2H), 3.88-3.86 (m, 4H), 3.16-3.14 (m, 4H), 1.31 (s, 9H). ^{13}C{^{1}H} NMR (125.8 MHz, $CDCl_3$): δ 149.1, 143.0, 126.2, 115.6, 67.2, 49.8, 34.2, 31.7. Spectral data are consistent with literature. [A14]

4-(2,5-dimethylphenyl)morpholine **(2.2g)**

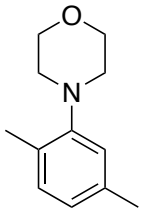

The title compound was synthesized from the corresponding chloride according to **GP3**, conducted at 100 °C using 5 mol% 1,1'-bis(diphenyl)phosphinoferrocene, and purified according to Workup Method A. Purified by flash column chromatography on silica gel using 24:1 hexanes/ethyl acetate which afforded the title product in a 16% yield (45 mg) as a light brown oil. ^{1}H NMR (300 MHz, $CDCl_3$): δ 7.09-7.06 (d, J = 8.8 Hz, 1H), 6.84-6.81 (m, 2H), 3.87-3.84 (m, 4H), 2.92-2.89 (m, 4H), 2.32 (s, 3H), 2.28 (s, 3H).^{13}C{^{1}H} NMR (125.8 MHz, $CDCl_3$): δ 151.4, 136.4, 131.2, 129.5, 124.2, 119.9, 67.7, 52.5, 21.4, 17.7. Spectral data are consistent with literature. [A15]

4-(4-methoxyphenyl)morpholine **(2.2h)**

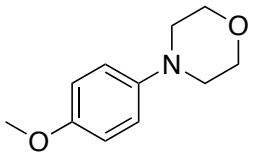

The title compound was synthesized from the corresponding chloride according to **GP3**, conducted at 100 °C using 6.7 mol% 1,1'-bis(diphenyl)phosphinoferrocene, and purified according to Workup Method A. Purified by flash column chromatography on silica gel using (9:1) hexanes/ethyl acetate which afforded the title product in 65% isolated yield (126 mg, 0.65 mmol) as a white solid. ^{1}H NMR (300 MHz, $CDCl_3$): δ 6.91-6.83 (m, 4H), 3.87-3.84 (m, 4H), 3.77 (s, 3H), 3.07-3.04 (m, 4H). ^{13}C{^{1}H} NMR (75.5 MHz, $CDCl_3$): δ 154.0, 145.7, 117.8, 114.5, 67.0, 55.6, 50.8. Spectral data are in agreement with literature values. [A11]

1-(naphthalen-1-yl)-1H-indole **(2.3a)**

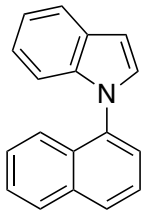

The title compound was synthesized from the corresponding chloride according to **GP4**, conducted at 110 °C using 5 mol% 1,1'-bis(di(bis-3,5-trifluoromethyl)phenyl)phosphinoferrocene, and purified according to Workup Method A. Purified by flash column chromatography on silica gel using (19:1) hexanes/ethyl acetate which afforded the title product in an 80% isolated yield (117 mg, 0.48 mmol) as an off-white solid. ^{1}H NMR (500 MHz, $CDCl_3$): δ 7.99-7.98 (m, 2H), 7.77-7.75 (d, J = 7.9 Hz, 1H), 7.61-7.53 (m, 3H), 7.48-7.46 (m, 1H), 7.43-7.40 (m, 1H), 7.37 (d, J = 3.2 Hz, 1H), 7.21-7.13 (m, 2H), 7.05-7.04 (m, 1H), 6.79-6.78 (d, J = 3.2 Hz, 1H). ^{13}C{^{1}H} NMR (125.8 MHz, $CDCl_3$): δ 138.2, 136.3, 134.7, 130.8, 130.0, 128.7, 128.5, 127.2, 126.9, 125.7, 125.4, 123.6, 122.4, 121.1, 120.3, 111.1, 103.1. Spectral data are in agreement with literature. [A16]

4-(1H-indol-1-yl)benzonitrile **(2.3b)**

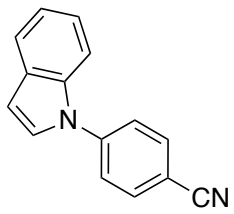

The title compound was synthesized from the corresponding chloride according to **GP4**, conducted at 110 °C using 5 mol% 1,1'-bis(diphenyl)phosphinoferrocene, and purified according to Workup Method A. Purified by flash column chromatography on silica gel using a gradient of 100:0 to 19:1 hexanes/ethyl acetate which afforded the title product in a quantitative isolated yield (213 mg, 0.98 mmol) as a light brown oil. ^{1}H NMR (500 MHz; CDCl3): δ 7.82-7.80 (m, 2H), 7.71-7.70 (m, 1H), 7.65-7.61 (m, 3H) 7.35 (d, J = 3.4 Hz, 1H), 7.30-7.22 (m, 2H), 6.76 (d, J = 3.4 Hz, 1H). ^{13}C{^{1}H} NMR (125.8 MHz; $CDCl_3$): δ 143.8, 135.4, 134.0, 130.2, 127.3, 124.1, 123.4, 121.8, 121.6, 118.6, 110.6, 109.6, 106.0. Spectral data are consistent with literature. [A17]

1-(benzo[b]thiophen-5-yl)-1H-indole **(2.3d)**

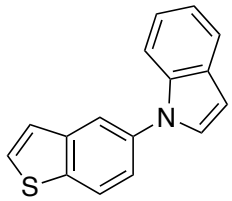

The title compound was synthesized from the corresponding chloride according to **GP4**, conducted at 110ºC using using 5 mol% 1,1'-bis(diphenyl)phosphinoferrocene, and purified according to Workup Method A. Purified by flash column chromatography on silica gel using hexanes which afforded the title product in 92 % isolated yield (229 mg, 0.92 mmol) as a yellow oil. ^{1}H NMR (500 MHz, $CDCl_3$): δ 8.06-8.04 (d, *J* = 8.5 Hz, 1H), 7.99 (m, 1H), 7.81-7.79 (d, *J* = 7.7 Hz, 1H), 7.66-7.62 (m, 2H), 7.58-7.55 (dd, *J* = 8.5 Hz, 2.0 Hz, 1H), 7.46-7.44 (m, 2H), 7.33-7.26 (m, 2H), 6.80-6.79 (d, *J* = 3.2 Hz, 1H). ^{13}C{^{1}H} NMR (125.8 MHz, $CDCl_3$): δ 140.9, 138.3, 137.1, 136.7, 129.7, 128.8, 124.3, 123.9, 122.8, 121.9, 121.6, 120.8, 119.7, 110.9, 103.9. HRMS *m/z* ESI^+ found 272.0504 $[M + Na]^+$ calculated for $C_{16}H_{11}NNaS$ 272.0510.

4-(1H-indol-1-yl)-2-methylquinoline **(2.3e)**

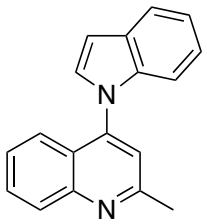

The title compound was synthesized from the corresponding chloride according to **GP4**, conducted at 110 °C using 5 mol% 1,1'-bis(diphenyl)phosphinoferrocene, and purified according to Workup Method A. Purified by flash column chromatography on silica gel using a gradient of 19:1 to 5.7:1 hexanes/ethyl acetate which afforded the title product in a 96 % isolated yield (247 mg, 0.96 mmol) as a white solid. ^{1}H NMR (500 MHz, $CDCl_3$): δ 8.19-8.18 (d, *J* = 8.5 Hz, 1H), 7.77-7.72 (m, 2H), 7.69-7.67 (d, *J* = 8.3 Hz, 1H), 7.43-7.40 (m, 1H), 7.37-7.36 (d, *J* = 3.3 Hz, 1H), 7.34 (s, 1H), 7.24-7.18 (m, 3H), 6.82-6.81 (d, *J* = 3.3 Hz, 1H), 2.82 (s, 3H). ^{13}C{^{1}H} NMR (125.8 MHz, $CDCl_3$): δ 159.7, 149.8, 144.5, 137.2, 130.3, 129.4, 129.1, 126.5, 123.6, 122.9, 121.4, 121.0, 119.2, 111.0, 104.7, 25.6.

HRMS *m/z* ESI$^+$ found 259.1230 [M + H]$^+$ calculated for $C_{18}H_{15}N_2$ 259.1235.

1-(4-(tert-butyl)phenyl)-1H-indole **(2.3f)**

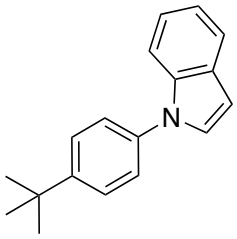

The title compound was synthesized from the corresponding bromide according to **GP4**, conducted at 110ºC using using 5 mol% 1,1'-bis(diphenyl)phosphinoferrocene, and purified according to Workup Method A. Purified by flash column chromatography on silica gel using a gradient of 99:1 to 49:1 hexanes/ethyl acetate which afforded the title product in a 64 % isolated yield (160 mg, 0.64 mmol) as a white solid. ^{1}H NMR (500 MHz, $CDCl_3$): δ 7.83-7.82 (d, *J* = 7.7 Hz, 1H), 7.71-7.70 (d, *J* = 8.2 Hz, 1H), 7.64-7.62 (m, 2H), 7.55-7.53 (m, 2H), 7.44-7.43 (d, *J* = 3.3 Hz, 1H), 7.36-7.28 (m, 2H), 6.80-6.79 (d, *J* = 3.2 Hz, 1H), 1.52 (s, 9H). ^{13}C{^{1}H} NMR (125.8 MHz, $CDCl_3$): δ 149.6, 137.4, 136.2, 129.4, 128.2, 126.6, 124.2, 122.4, 121.3, 120.4, 111.8, 103.4, 34.8, 31.6. Spectral data are consistent with literature. [A14]

1-(2,5-dimethylphenyl)-1H-indole **(2.3g)**

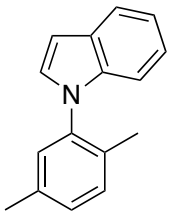

The title compound was synthesized from the corresponding bromide according to **GP4**, conducted at 110ºC using using 10 mol% 1,1'-bis(3,5-(bis-trifluoromethyl)phenyl)phosphinoferrocene, and purified according to Workup Method A. Purified by flash column chromatography on silica gel using 99:1 hexanes/ethyl acetate which afforded the title product in 67% isolated yield (89 mg, 0.40 mmol) as a light brown oil. ^{1}H NMR (500 MHz, $CDCl_3$): δ 7.79-7.75 (m, 1H), 7.33-7.31 (d, *J* = 7.8 Hz, 1H), 7.24-7.19 (m, 5H), 7.13-7.11 (m, 1H), 6.73-6.72 (m, 1H), 2.43 (s, 3H), 2.09 (s, 3H). ^{13}C{^{1}H} NMR (125.8 MHz, $CDCl_3$): 138.3, 137.2, 136.8, 132.7, 131.2, 129.1, 128.9, 128.8, 128.5, 122.2, 121.0, 120.0, 110.8, 102.6, 21.0, 17.4. Some confusion exists

regarding the identity of what is claimed as **2.3g** in this report, in that the NMR, IR, and elemental analysis characterization data provided for this compound in the supporting information are identical to those listed for the isomeric product derived from 1-bromo-3,5-dimethylbenzene. In this regard, the ^{1}H and ^{13}C NMR chemical shift data provided (in the absence of accompanying spectra) are inconsistent with the claimed structure of **2.3g**. [A18]

1-(4-methoxyphenyl)-1H-indole **(2.3h)**

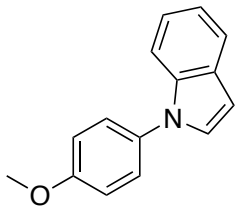

The title compound was synthesized from the corresponding chloride according to **GP4**, conducted at 110ºC using using 5 mol% 1,1'-bis(3,5-(bis-trifluoromethyl)phenyl)phosphinoferrocene, and purified according to Workup Method A. Purified by flash column chromatography on silica gel using 49:1 hexanes/ethyl acetate which afforded the title product in 91% isolated yield (203 mg, 0.91 mmol) as a yellow oil. ^{1}H NMR (500 MHz; $CDCl_3$): δ 7.79-7.77 (d, J = 7.7 Hz, 1H), 7.56-7.55 (d, J = 8.1 Hz, 1H), 7.50-7.47 (m, 2H), 7.36 (d, J = 3.2 Hz, 1H), 7.31-7.24 (m, 2H), 7.12-7.09 (m, 2H), 6.75 (d, J = 3.2 Hz, 1H), 3.95 (s, 3H).$^{13}C\{^{1}H\}$ NMR (125.8 MHz; $CDCl_3$): δ 158.6, 136.5, 133.0, 129.2, 128.5, 126.2, 122.3, 121.2, 120.3, 114.9, 110.6, 103.1, 55.8. Spectral data are in agreement with literature. [A1]

2-methyl-N-octyl-4-quinolinamine **(3.3a)**

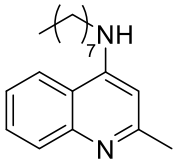

The title compound was synthesized from the corresponding aryl chloride (1.0 mmol) according to **GP1**, conducted at 80 °C using 0.25 mol% **2-C1**, and purified according to Workup Method A. Purified by flash column chromatography on silica gel using an ethyl acetate/methanol eluent gradient (100% ethyl acetate, 200 mL; 9:1, 800 mL) which afforded the title product in 68% isolated yield (184 mg, 0.68 mmol) as a light brown

solid. ^{1}H NMR (500 MHz; $CDCl_3$): δ 7.94 (d, 1H, *J* = 8.4 Hz), 7.73 (d, 1H, *J* = 8.3 Hz), 7.63-7.60 (m, 1H) 7.51-7.38 (m, 1H), 6.33 (s, 1H), 5.13 (br. s, 1H), 3.35-3.31 (m, 2H), 2.65 (s, 3H), 1.82-1.76 (m, 2H), 1.53-1.29 (m, 10H). ^{13}C{^{1}H} NMR (125.8 MHz; $CDCl_3$): δ 159.2, 150.0, 147.5, 129.2, 128.5, 123.9, 119.2, 117.2, 98.9, 43.3, 31.8, 29.3, 29.2, 28.9, 27.2, 25.3, 22.6, 14.1. HRMS *m/z* ESI^{+} found 271.2169 $[M + H]^{+}$ calculated for $C_{18}H_{27}N_2$ 271.2174.

N-(2-furanylmethyl)-6-quinoxalinamine **(3.3b)**

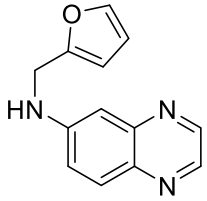

The title compound was synthesized from the corresponding aryl chloride (1.0 mmol) according to **GP1**, conducted at 80 °C using 0.5 mol% **2-C1**, and purified according to Workup Method A. Purified by flash column chromatography on silica gel using 1:1 ethyl acetate/hexanes eluent, which afforded the title product in a 91% yield (102 mg, 0.45 mmol) as a yellow solid. ^{1}H NMR (500 MHz, $CDCl_3$): δ 8.65 (d, 1H, *J* = 1.8 Hz), 8.53 (d, 1H, *J* = 1.8 Hz), 7.85 (d, 1H, *J* = 9.1 Hz), 7.39 (m, 1H), 7.17-7.15 (dd, 1H, J_1 = 2.6 Hz, J_2 = 9.1 Hz), 7.08 (d, 1H, *J* = 2.6 Hz), 6.34-6.33 (m, 2H), 4.63 (br. s, 1H), 4.47 (d, 2H, *J* = 5.1 Hz) ^{13}C{^{1}H} UDEFT NMR (125.8 MHz, $CDCl_3$): δ 151.3, 148.5 145.4, 145.0, 142.3, 140.7, 138.2, 130.2, 122.1, 110.5, 107.8, 104.5, 41.1. HRMS *m/z* ESI^{+} found 226.0975 $[M + H]^{+}$ calculated for $C_{13}H_{12}N_3O$ 226.0980.

N-***[(tetrahydro-2-furanyl)methyl]-2-quinolinamine*** **(3.3c)**

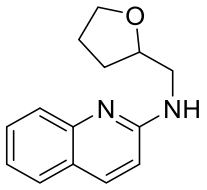

The title compound was synthesized from the corresponding aryl chloride (1.0 mmol) according to **GP1**, conducted at both 25 °C using 0.25 mol% **2-C1** and 80 °C using 0.125 mol% **2-C1**. The reactions were purified according to Workup Method A. Purified by flash column chromatography on silica gel using 3:2 hexanes/ethyl acetate eluent, which afforded the title product in an 86% isolated yield using 0.25 mol% at 25 °C (197 mg,

0.86 mmol) and in a 43% isolated yield using 0.125 mol% at 80 °C (98 mg, 0.43 mmol) as a yellow oil. ^{1}H NMR (500 MHz, $CDCl_3$): δ 7.81 (d, 1H, *J* = 8.9 Hz), 7.71 (d, 1H, *J* = 8.4 Hz), 7.60 (d, 1H, *J* = 7.9 Hz), 7.56-7.53 (m, 1H), 7.24-7.22 (m, 1H), 6.66 (d, 1H, *J* = 8.9 Hz), 5.09 (br. s, 1H), 4.22-4.17 (m, 1H), 3.97-3.81 (m, 3H), 3.51-3.46 (m, 1H), 2.12-1.92 (m, 3H), 1.77-1.70 (m, 1H). ^{13}C{^{1}H} NMR (125.8 MHz, $CDCl_3$): δ 156.9, 148.0, 137.1, 129.4, 127.4, 126.2, 123.5, 121.9, 112.1, 78.0, 68.0, 45.3, 28.8, 25.9. HRMS *m/z* ESI$^+$ found 229.1335 $[M + H]^+$ calculated for $C_{14}H_{17}N_2O$ 229.1341.

N-(naphthalen-1-ylmethyl)aniline **(3d)**

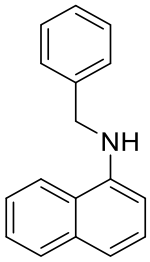

The title compound was synthesized from the corresponding aryl tosylate according to **GP1**, conducted at 80 °C using both 0.25 mol% **2-C1** (0.71 mmol aryl tosylate) and 0.5 mol% **2-C1** (1 mmol aryl tosylate). The reactions were purified according to Workup Method A. Purified by flash column chromatography on silica gel using 97:3 hexanes/ethyl acetate eluent, which afforded the title product in a 55% isolated yield using 0.25 mol% (91 mg, 0.39 mmol) and in an 87% isolated yield using 0.5 mol% (202 mg, 0.87 mmol) as a yellow oil. ^{1}H NMR (500 MHz, $CDCl_3$): δ 7.88-7.84 (m, 2H), 7.51-7.34 (m, 9H) 6.69 (d, 1H, *J* = 7.5 Hz), 4.74 (br. s, 1H), 4.55 (s, 2H). ^{13}C{^{1}H} NMR (125.8 MHz, $CDCl_3$): δ 143.2, 139.1, 134.3, 128.7 (two signals), 127.8, 127.4, 126.6, 125.7, 124.8, 123.4, 119.9, 117.7, 104.8, 48.7. Spectral data are in agreement with literature. [A19]

4-(2-oxazolylaminophenyl)phenyl-methanone **(4.2a)**

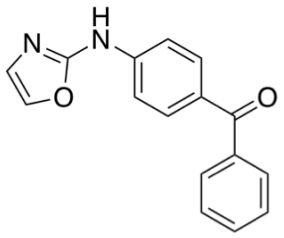

The title compound was synthesized from the corresponding aryl chloride (0.6 mmol) according to **GP6**, conducted at 80 °C using 5 mol% **3-C1**, and purified according to

Workup Method A. Purified by flash column chromatography on silica gel using a 7:3 hexanes/ethyl acetate eluent which afforded the title product in 87% isolated yield (138 mg, 0.52 mmol) as an off-white solid. ^{1}H NMR (500 MHz; $CDCl_3$): δ 8.21 (br. s, 1H, NH), 7.86 (d, *J* = 8.6 Hz, ArH, 2H), 7.77 (d, 2H, *J* = 7.5 Hz, ArH), 7.59-7.56 (m, 3H, ArH), 7.49-7.46 (m, 2H, ArH), 7.36 (s, 1H, ArH), 7.00 (s, 1H, ArH). ^{13}C{^{1}H} NMR (125.8 MHz; $CDCl_3$): δ 195.4 (C=O), 156.3 (ArC), 142.7 (ArC), 138.2 (ArC), 133.0 (ArC), 132.2 (ArC), 132.0 (ArC), 131.0 (ArC), 129.8 (ArC), 128.2 (ArC), 126.5 (ArC), 115.9 (ArC). HRMS *m/z* ESI$^+$ found 287.0791 $[M + Na]^+$ calculated for $C_{16}H_{12}N_2NaO_2$ 287.0796.

N-(2-oxazolyl)-6-quinoxalinamine **(4.2b)**

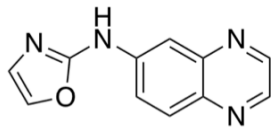

The title compound was synthesized from the corresponding aryl chloride (0.6 mmol) according to **GP6**, conducted at 80 °C using 5 mol% **3-C1**, and purified according to Workup Method A. Purified by flash column chromatography on silica gel using 4:1 ethyl acetate/hexanes eluent, which afforded the title product in a 73% yield (93 mg, 0.44 mmol) as a yellow solid. ^{1}H NMR (500 MHz, DMSO-d_6): δ 10.74 (br. s, 1H, NH), 8.83 (d, *J* = 1.6 Hz, 1H, ArH), 8.73 (d, *J* = 1.7 Hz, 1H, ArH), 8.53 (d, *J* = 2.4 Hz, 1H, ArH), 8.01 (d, *J* = 9.1 Hz, 1H ArH), 7.87 (dd, J_1 = 9.1 Hz, J_2 = 2.5 Hz, 1H, ArH), 7.76 (s, 1H, ArH), 7.12 (s, 1H, ArH). ^{13}C{^{1}H} UDEFT NMR (125.8 MHz, DMSO-d_6): δ 156.1 (ArC), 145.8 (ArC), 143.7 (ArC), 142.8 (ArC), 140.7 (ArC), 138.3 (ArC), 133.3 (ArC), 129.7 (ArC), 126.6 (ArC), 122.5 (ArC). HRMS *m/z* ESI$^+$ found 235.0590 $[M + Na]^+$ calculated for $C_{11}H_8N_4NaO$ 235.0596.

N-[(2-oxazolyl]-2-quinolinamine **(4.2c)**

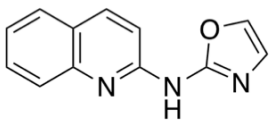

The title compound was synthesized from the corresponding aryl chloride (0.6 mmol) according to **GP6**, conducted at both 80 °C using 5 mol% **3-C1**, and purified according to Workup Method A. Purified by flash column chromatography on silica gel using 7:3

hexanes/ethyl acetate eluent, which afforded the title product as a yellow solid in a 79% crude isolated yield (0.100g, 0.47 mmol) containing an 8% (on a mole basis as determined by use of ^{1}H NMR spectroscopy) impurity of triarylamine byproduct (i.e., ***N-[(2-oxazolyl]-di(2-quinolinamine), confirmed on the basis of HPLC-MS data)*** resulting in a 72% (i.e., 79 x 92%) corrected isolated yield. Column fractions containing pure **4.2c** were collected to afford the title product in a 36% isolated yield, for which NMR line data are provided. The ^{1}H NMR spectrum is provided for the crude sample, and both ^{1}H and ^{13}C{^{1}H} UDEFT NMR spectra are provided for the pure sample. ^{1}H NMR (300 MHz, $CDCl_3$): δ 13.9 (br. s, 1H, NH), 7.67 (d, J = 9.4 Hz, 1H, ArH), 7.54-7.48 (m, 2H, ArH), 7.38-7.36 (m, 2H, ArH), 7.23-7.21 (m, 1H, ArH), 7.07 (s, 1H, ArH), 6.91 (d, J = 9.4 Hz, 1H, ArH). ^{13}C{^{1}H} UDEFT NMR (125.8 MHz, $CDCl_3$): δ 164.2 (ArC), 152.9 (ArC), 137.5 (ArC), 136.8 (ArC), 133.0 (ArC), 130.5 (ArC), 127.7 (ArC), 125.5 (ArC), 123.5 (ArC), 121.5 (ArC), 116.5 (ArC). HRMS *m/z* ESI$^+$ found 212.0818 $[M + H]^+$ calculated for $C_{12}H_{10}N_3O$ 212.0824.

N-(2-thiazolyl)-6-quinoxalinamine **(4.2d)**

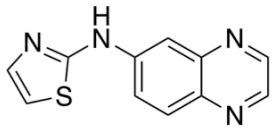

The title compound was synthesized from the corresponding aryl chloride (0.6 mmol) according to **GP6**, conducted at 80 °C using 5 mol% **3-C1**, and purified according to Workup Method A. Purified by flash column chromatography on silica gel using 30:19:1 ethyl acetate/hexanes/triethylamine eluent, which afforded the title product in an 83% yield (114 mg, 0.50 mmol) as a yellow solid. ^{1}H NMR (500 MHz, DMSO-d_6): δ 10.8 (br. s, 1H, ArH), 8.82 (d, J = 1.6 Hz, 1H, ArH), 8.72 (d, J = 1.6 Hz, 1H, ArH), 8.65 (d, J = 2.4 Hz, 1H, ArH), 8.00 (d, J = 9.1 Hz, 1H ArH), 7.82 (dd, J_1 = 9.1 Hz, J_2 = 2.5 Hz, 1H, ArH), 7.41 (d, J = 3.7 Hz, 1H, ArH), 7.08 (d, J = 3.6 Hz, 1H, ArH). ^{13}C{^{1}H} NMR (125.8 MHz, DMSO-d_6): δ 163.4 (ArC), 146.2 (ArC), 144.3 (ArC), 143.1 (ArC), 142.6 (ArC), 139.5 (ArC), 138.8 (ArC), 130.1 (ArC), 123.3 (ArC), 111.6 (ArC), 110.5 (ArC). HRMS *m/z* ESI$^+$ found 251.0362 $[M + Na]^+$ calculated for $C_{11}H_8N_4NaS$ 251.0367.

4-(2-thiazolylamino)-benzonitrile **(4.2e)**

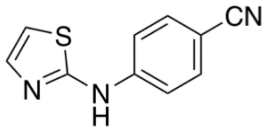

The title compound was synthesized from the corresponding aryl chloride (1.0 mmol) according to **GP6**, with the exception of tetrahydrofuran used as solvent, and a mixture of sodium *tert*-butoxide and phenol (1.2 equiv each) pre-dissolved in tetrahydrofuran used in place of sodium phenoxide. The reaction was conducted at 80 °C using 5 mol% **3-C1**, and purified according to Workup Method A. Purified by flash column chromatography on silica gel using 4:1 hexanes/ethyl acetate eluent, which afforded the title product in an 83% isolated yield (0.169 g, 0.83 mmol) as a light yellow solid. ^{1}H NMR (300 MHz, DMSO-d_6): δ 10.73 (br. s, 1H, ArH), 7.82-7.71 (m, 4H, ArH), 7.35 (d, J = 3.7 Hz, 1H, ArH), 7.07 (d, J = 3.7 Hz, 1H, ArH). ^{13}C{^{1}H} NMR (125.8 MHz, DMSO-d_6): δ 163.1 (ArC), 145.5 (ArC), 139.4 (ArC), 133.9 (ArC), 120.0 (C(*sp*)N), 117.0 (ArC), 110.8 (ArC), 102.4 (ArC). Spectral data are agreement with literature. [A20]

4-(2-thiazolylamino)-quinaldine **(4.2f)**

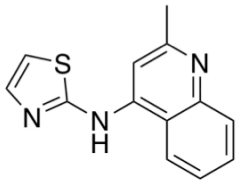

The title compound was synthesized from the corresponding aryl chloride (0.61 mmol) according to **GP6**, conducted at 80 °C using 5 mol% **3-C1**, and purified according to Workup Method A. Purified by flash column chromatography on silica gel using 19:1 ethyl acetate/hexanes eluent. Despite exhaustive trituration and exposure to vacuum at elevated temperature, this material was found to tenaciously hold onto trace amounts of ethyl acetate. The title product was afforded as a yellow solid in a 96% crude isolated yield (142 mg, 0.59 mmol) containing 6% ethyl acetate on a mole basis, resulting in a 90% corrected isolated yield (i.e., 96 x 94%). ^{1}H NMR (500 MHz, DMSO-d_6): δ 10.49 (br. s, 1H, NH), 8.44-8.42 (m, 2H, ArH), 7.85 (br. s, 1H, ArH), 7.69-7.66 (m, 2H, ArH), 7.51-7.46 (m, 2H, ArH), 7.15 (br. s, 1H, ArH), 2.57 (br. s, 3H, CH_3). ^{13}C{^{1}H} UDEFT NMR (125.8 MHz, DMSO-d_6): δ 163.4 (ArC), 159.6 (ArC), 148.7 (ArC), 144.0 (ArC),

139.2 (ArC), 129.6-129.2 (m, ArC), 124.9 (ArC), 122.0 (ArC), 118.2 (ArC), 112.1 (ArC), 106.7 (ArC), 25.9 (CH_3). HRMS *m/z* ESI^+ found 242.0746 $[M + H]^+$ calculated for $C_{13}H_{12}N_3S$ 242.0752.

2-[(1,3-dimethyl-1H-pyrazol-5-yl)amino]-benzothiazole **(4.2g)**

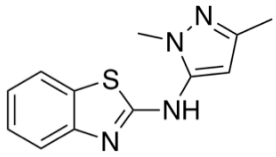

The title compound was synthesized from the corresponding aryl chloride (0.6 mmol) according to **GP6**, conducted at 80 °C using 5 mol% **3-C1**, and purified according to Workup Method A. Purified by flash column chromatography on silica gel using 13:7 ethyl acetate/hexanes eluent, which afforded the title product in an 83% isolated yield (0.122 g, 0.50 mmol) as a white solid. ^1H NMR (500 MHz, $CDCl_3$): δ 9.88 (br. s, 1H, NH), 7.57 (d, *J* = 7.9 Hz, 1H, ArH), 7.33-7.29 (m, 2H, ArH), 7.16-7.13 (m, 1H, ArH), 6.11 (s, 1H, ArH), 3.73 (s, 3H, CH_3), 2.31 (s, 3H, CH_3). $^{13}C\{^1H\}$ NMR (125.8 MHz, $CDCl_3$): δ 166.1 (ArC), 148.2 (ArC), 147.8 (ArC), 140.3 (ArC), 128.9 (ArC), 126.5 (ArC), 122.6 (ArC), 121.4 (ArC), 117.3 (ArC), 98.6 (ArC), 34.8 (CH_3), 14.2 (CH_3). HRMS *m/z* ESI^+ found 245.0855 $[M + H]^+$ calculated for $C_{12}H_{13}N_4S$ 245.0861.

2-[(1,3-dimethyl-1H-pyrazol-5-yl)amino]-quinoline **(4.2h)**

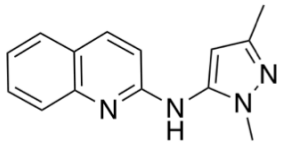

The title compound was synthesized from the corresponding aryl chloride (0.6 mmol) according to **GP6**, conducted at 80 °C using 5 mol% **3-C1**, and purified according to Workup Method A. Purified by flash column chromatography on silica gel using ethyl acetate as eluent, which afforded the title product in a 92% isolated yield (0.132 g, 0.55 mmol) as a white solid. ^1H NMR (500 MHz, $CDCl_3$): δ 7.95 (d, *J* = 8.9 Hz, 1H, ArH), 7.67-7.56 (m, 3H, ArH), 7.32-7.30 (m, 2H, ArH/NH), 6.76 (d, *J* = 8.9 Hz, 1H, ArH), 6.04 (s, 1H, ArH), 3.69 (s, 3H, CH_3), 2.29 (s, 3H, CH_3). $^{13}C\{^1H\}$ NMR (125.8 MHz, $CDCl_3$): δ 155.4 (ArC), 147.7 (ArC), 147.3 (ArC), 138.7 (ArC), 138.4 (ArC), 130.2 (ArC), 127.6 (ArC), 126.3 (ArC), 124.3 (ArC), 123.5 (ArC), 109.6 (ArC), 100.5 (ArC), 34.8 (CH_3),

14.1 (CH_3). HRMS *m/z* ESI^+ found 239.1291 $[M + H]^+$ calculated for $C_{14}H_{15}N_4$ 239.1297.

4-[(1,3-dimethyl-1H-pyrazol-5-yl)amino]-quinaldine **(4.2i)**

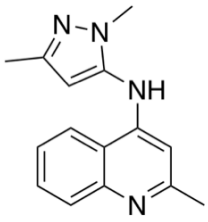

The title compound was synthesized from the corresponding aryl chloride (1.0 mmol) according to **GP6**, conducted at 80 °C using 5 mol% **3-C1**, and purified according to Workup Method A. Purified by flash column chromatography on silica gel using 19:1 ethyl acetate/methanol as eluent, and the resultant product was dissolved in dichloromethane and dried over magnesium sulfate. The drying agent was filtered and the solvent was removed *in vacuo* to afford the title product in a 90% isolated yield (0.215 g, 0.90 mmol) as a white solid. ^1H NMR (500 MHz, $CDCl_3$): 7.99 (d, J = 8.4 Hz, 1H, ArH), 7.87 (d, J = 8.3 Hz, 1H, ArH), 7.69-7.66 (m, 1H, ArH), 7.49-7.46 (m, 1H, ArH), 6.38-6.25 (m, 2H, ArH/NH), 5.97 (s, 1H, ArH), 3.65 (s, 3H, CH_3), 2.56 (s, 3H, CH_3), 2.31 (s, 3H, CH_3). $^{13}C\{^1H\}$ NMR (125.8 MHz, $CDCl_3$): δ 159.7 (ArC), 148.4 (ArC), 148.0-147.9 (m, ArC), 137.9 (ArC), 129.6-129.3 (m, ArC), 124.9 (ArC), 119.1 (ArC), 117.2 (ArC), 102.5 (ArC), 101.2 (ArC), 34.9 (CH_3), 25.5 (CH_3), 14.1 (CH_3). HRMS *m/z* ESI^+ found 253.1448 $[M + H]^+$ calculated for $C_{15}H_{17}N_4$ 253.1453.

N-(1,1'-biphenyl)-4-yl-2-pyridinamine **(4.2k)**

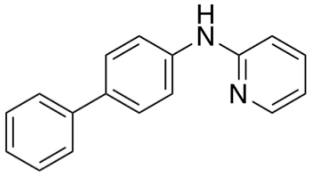

The title compound was synthesized from the corresponding aryl chloride (0.6 mmol) according to **GP6**, conducted at 80 °C using 5 mol% **3-C1**, and purified according to Workup Method A. Purified by flash column chromatography on silica gel using 4:1 hexanes/ethyl acetate as eluent, which afforded the title product in an 89% isolated yield (0.131 g, 0.53 mmol) as a white solid. ^1H NMR (500 MHz, DMSO-d_6): δ 9.13 (br. s, 1H, NH), 8.19-8.17 (m, 1H, ArH), 7.79 (d, J = 8.7 Hz, 2H, ArH), 7.64-7.56 (m, 5H, ArH), 7.44-7.41 (m, 2H, ArH), 7.30-7.27 (m, 1H, ArH), 6.87 (d, J = 8.4 Hz, 1H), 6.77-6.74 (m,

1H, ArH). $^{13}C\{^{1}H\}$ NMR (125.8 MHz, DMSO-d_6): δ 161.0 (ArC), 152.5 (ArC), 146.5 (ArC), 145.3 (ArC), 142.4 (ArC), 137.1 (ArC), 134.0 (ArC), 132.0 (ArC), 131.7 (ArC), 131.1 (ArC), 123.4 (ArC), 119.6 (ArC), 116.1 (ArC). Spectral data are consistent with literature (spectral data reported in $CDCl_3$). [A21]

N-(4-phenyl-2-thiazolyl)-2-pyridinamine **(4.2l)**

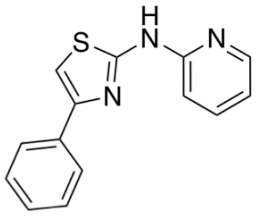

The title compound was synthesized from the corresponding aryl chloride (0.6 mmol) according to **GP6**, conducted at 80 °C using 5 mol% **3-C1**, and purified according to Workup Method A. Purified by flash column chromatography on silica gel using 17:3 hexanes/ethyl acetate as eluent, which afforded the title product in a 95% isolated yield (0.144 g, 0.57 mmol) as a white solid. When conducted on a 3.65 mmol scale of aryl chloride, the product was obtained in a 72% isolated yield (0.666 mg 2.63 mmol) as a white solid. ^{1}H NMR (500 MHz, $CDCl_3$): δ 10.14 (br. s, 1H, NH), 8.34-8.33 (m, 1H, ArH), 7.90 (d, J = 7.3 Hz, 2H, ArH), 7.39-7.34 (m, 3H, ArH), 7.30-7.27 (m, 1H, ArH), 7.05 (s, 1H, ArH), 6.82-6.79 (m, 1H, ArH), 6.50 (d, J = 8.4 Hz, 1H, ArH). $^{13}C\{^{1}H\}$ NMR (125.8 MHz, $CDCl_3$): δ 161.1 (ArC), 151.4 (ArC), 149.5 (ArC), 146.7 (ArC), 137.4 (ArC), 134.8 (ArC), 128.7 (ArC), 127.7 (ArC), 126.2 (ArC), 116.2 (ArC), 110.6 (ArC), 105.7 (ArC). Spectral data are in agreement with literature. [A22]

N-methyl-4-(pyrazin-2-ylamino)pyridine-2-carboxamide **(4.2m)**

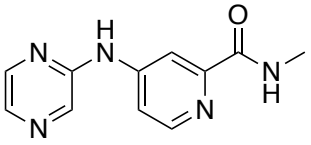

On the benchtop in air, a microwave vial containing a magnetic stirbar was charged with **3-C1** (0.05 equiv), 4-chloro-*N*-methylpicolinamide (0.53 mmol, 1.0 equiv), NaOPh (1.2 equiv), and aminopyrazine (1.2 equiv). The microwave vial was sealed via crimping using a cap featuring a PTFE septum, and the vial was alternately purged with nitrogen and evacuated three times by way of a needle line that was inserted into the septum. After refilling with nitrogen, anhydrous tetrahydrofuran (used as-purchased without further

purification; 0.24 M aryl chloride) was added to the microwave vial *via* syringe, and the vial was placed in a temperature-controlled aluminum heating block set to 80 °C for 16 h under the influence of magnetic stirring. After cooling to room-temperature, the reaction mixture was concentrated *in vacuo*, dissolved in DMSO, and purified via reverse-phase flash chromatography using the following gradient of acetonitrile/water, both containing 0.1% formic acid as eluent: 0% (4CV), 10-100% (18CV), 100% (3CV). The relevant column fractions were combined and lyophilized to afford the target product **4.2m** in 83% yield (101 mg, 0.44 mmol) as a white solid. ^{1}H NMR (400 MHz, DMSO-d_6 + 0.05% $SiMe_4$) δ 10.21 (s, 1H, NH), 8.75–8.63 (m, 1H, NH), 8.40 (d, J = 5.6 Hz, 1H, ArH), 8.35–8.31 (m, 1H, ArH), 8.31–8.25 (m, 2H, ArH), 8.11 (d, J = 2.8 Hz, 1H, ArH), 7.93 (dd, J = 5.6, 2.3 Hz, 1H, ArH), 2.82 (d, J = 4.8 Hz, 3H, CH_3). ^{13}C{^{1}H} NMR (100.6 MHz, DMSO-d_6 + 0.05% $SiMe_4$) δ 164.6 (C=O), 151.4 (ArC), 150.9 (ArC), 149.0 (ArC), 148.5 (ArC), 141.1 (ArC), 136.0–135.5 (m, ArC), 113.5 (ArC), 110.2 (ArC), 25.9 (CH_3). HRMS *m/z* ESI$^+$ found 252.0864 $[M + Na]^+$ calculated for $C_{11}H_{11}N_5NaO$ 252.0856.

Data for Ligands and Ligand Precursors:

Data for P2 (1-P(*o*-tol)$_2$-2-bromobenzene): ^{1}H NMR (500 MHz, $CDCl_3$): δ 7.63-7.60 (m, 1H, ArH), 7.33-7.19 (m, 6H, ArH), 7.11-7.08 (m, 2H, ArH), 6.75-6.73 (m, 3H, ArH), 2.42 (s, 6H, CH_3). ^{13}C{^{1}H} NMR (125.8 MHz, $CDCl_3$): δ 143.1-142.9 (d, $J_{C\text{-}P}$ = 27.2 Hz, ArC), 138.0-137.9 (d, $J_{C\text{-}P}$ = 10.6 Hz, ArC), 134.9 (ArC), 134.3-134.2 (d, $J_{C\text{-}P}$ = 11.4 Hz, ArC), 133.4-133.3 (m, ArC), 130.9-130.7 (m, ArC), 130.5-130.3 (m, ArC), 129.2 (ArC), 127.8 (ArC), 126.5 (ArC), 21.5-21.3 (d, $J_{C\text{-}P}$ = 22.6 Hz, CH_3). ^{31}P{^{1}H} NMR (202.5 MHz, $CDCl_3$): δ -19.7 (s).

Data for P3 (2-PCg-3-bromopyridine). ^{1}H NMR (500 MHz, $CDCl_3$): δ 8.70-8.69 (dd, 1H, J_1 = 1.5 Hz, J_2 = 4.6 Hz, ArH), 7.86-7.83 (ddd, 1H, J_1 = 1.5 Hz, J_2 = 3.8 Hz, J_3 = 8.2 Hz, ArH), 7.11-7.08 (dd, 1H, J_1 = 4.6 Hz, J_2 = 8.1 Hz, ArH), 2.80-2.77 (d, 1H, J = 13.1 Hz, CgP), 2.17-2.13 (m, 1H, CgP), 1.95-1.89 (m, 1H, CgP), 1.57-1.54 (m, 1H, CgP), 1.49-1.41 (m, 12H, CH_3). ^{13}C{^{1}H} NMR (125.8 MHz, $CDCl_3$): δ 159.0 (d, $J_{C\text{-}P}$ = 31.5 Hz, ArC), 148.5 (ArC), 140.1 (ArC), 131.4 (d, $J_{C\text{-}P}$ = 39.0 Hz, ArC), 124.2 (ArC), 97.2 (CgP), 96.5 (CgP), 74.9 (d, $J_{C\text{-}P}$ = 7.5 Hz, CgP), 74.5 (d, $J_{C\text{-}P}$ = 26.4 Hz, CgP), 46.0 (d, $J_{C\text{-}P}$ = 18.9 Hz, CgP), 37.2 (CgP), 28.8 (d, $J_{C\text{-}P}$ = 20.1 Hz, CgP), 28.2-28.0 (m, CgP), 27.5 (d, $J_{C\text{-}P}$ = 10.1 Hz, CgP). ^{31}P{^{1}H} NMR (202.5 MHz, $CDCl_3$): δ -26.0 (s). HRMS *m/z* ESI$^+$ found

394.0178 $[M + Na]^+$ calculated for $C_{15}H_{19}BrNNaOP$ 394.0184.

Data for P4 (2-P(*o*-tol)$_2$-3-bromopyridine). ^1H NMR (300 MHz, $CDCl_3$): δ 8.57 (dd, 1H, J_1 = 1.4 Hz, J_2 = 4.6 Hz, ArH), 7.84-7.80 (ddd, 1H, J_1 = 1.5 Hz, J_2 = 4.1 Hz, J_3 = 8.0 Hz, ArH), 7.33-7.25 (m, 4H, ArH), 7.14-7.06 (m, 3H, ArH), 6.85-6.82 (m, 2H, ArH), 2.45 (s, 6H, CH_3). $^{13}C\{^1H\}$ UDEFT NMR (75.4 MHz, $CDCl_3$): δ 162.1 (d, J_{C-P} = 6.1 Hz, ArC), 148.8 (ArC), 143.2 (d, J_{C-P} = 26.5 Hz, ArC), 139.5-139.4 (m, ArC), 133.6-133.5 (m, ArC), 130.0 (m, ArC), 129.1 (ArC), 128.5 (d, J_{C-P} = 39.6 Hz, ArC) , 126.1 (ArC), 123.4 (ArC), 110.0 (ArC), 21.4 (d, J_{C-P} = 21.2 Hz, CH_3). $^{31}P\{^1H\}$ NMR (202.5 MHz, $CDCl_3$): δ -12.0 (s). HRMS *m/z* ESI^+ found 370.0355 $[M + H]^+$ calculated for $C_{19}H_{18}BrNP$ 370.0360.

Data for P5 (**2-PCg-3-bromothiophene).** ^1H NMR (500 MHz, $CDCl_3$): δ 7.62-7.61 (dd, 1H, J_1 = 1.5 Hz, J_2 = 5.2 Hz, ArH), 7.14-7.12 (dd, 1H, J_1 = 2.6 Hz, J_2 = 5.2 Hz, ArH), 2.12-2.08 (m, 2H, CgP), 2.04-1.96 (m, 1H, CgP), 1.59-1.55 (m, 1H, CgP), 1.50-1.39 (m, 12H, CH_3). $^{13}C\{^1H\}$ NMR (125.8 MHz, $CDCl_3$): δ 133.3 (ArC), 131.3 (ArC), 127.8 (d, J_{C-P} = 49.1 Hz, ArC), 123.7 (d, J_{C-P} = 31.5 Hz, ArC), 97.0 (CgP), 96.5 (CgP), 74.3 (d, J_{C-P} = 8.8 Hz, CgP), 73.1 (d, J_{C-P} = 17.6 Hz, CgP), 45.0 (d, J_{C-P} = 18.9 Hz, CgP), 37.2 (CgP), 28.3 (d, J_{C-P} = 21.4 Hz, CgP), 28.1 (CgP), 27.9 (CgP), 27.4 (d, J_{C-P} = 10.1 Hz, CgP). $^{31}P\{^1H\}$ NMR (202.5 MHz, $CDCl_3$): δ -37.6 (s). HRMS *m/z* ESI^+ found 398.9790 $[M + Na]^+$ calculated for $C_{14}H_{18}BrNaO_3PS$ 398.9795.

Data for P6 (2-P(*o*-tol)$_2$-3-bromothiophene). ^1H NMR (300 MHz, $CDCl_3$): δ 7.50-7.48 (dd, 1H, J_1 = 1.6 Hz, J_2 = 5.1 Hz, ArH), 7.34-7.29 (m, 2H, ArH), 7.26-7.22 (m, 2H, ArH), 7.18-7.12 (m, 3H, ArH), 6.89-6.85 (m, 2H, ArH), 2.44 (d, J = 1.3 Hz, CH_3). $^{13}C\{^1H\}$ NMR (125.8 MHz, $CDCl_3$): δ 142.4 (d, J_{C-P} = 27.1 Hz, ArC), 134.4 (d, J_{C-P} = 9.6 Hz, ArC), 132.6 (ArC), 132.3 (ArC), 132.2 (ArC), 130.5-130.4 (m, ArC), 129.5 (ArC), 126.4 (ArC), 119.8 (d, J_{C-P} = 30.2 Hz, ArC), 21.3 (d, J_{C-P} = 21.4 Hz, CH_3). $^{31}P\{^1H\}$ NMR (121.5 MHz, $CDCl_3$): δ -35.2 (s). HRMS *m/z* ESI^+ found 374.9966 $[M + H]^+$ calculated for $C_{18}H_{17}BrPS$ 374.9972.

Data for P7 (3-P(*o*-tol)$_2$-4-bromothiophene). ^1H NMR (500 MHz, $CDCl_3$): δ 7.42-7.41 (m, 1H, ArH), 7.30-7.27 (m, 2H, ArH), 7.25-7.22 (m, 2H, ArH), 7.14-7.11 (m, 2H, ArH), 6.82-6.79 (m, 2H, ArH), 6.61-6.60 (d, 1H, J = 3.4 Hz, ArH), 2.44 (s, 6H, CH_3). $^{13}C\{^1H\}$ NMR (125.8 MHz, $CDCl_3$): δ 142.6 (d, J_{C-P} = 27.1 Hz, ArC), 136.9 (d, J_{C-P} = 13.0 Hz,

ArC), 134.4 (d, $J_{C\text{-}P}$ = 9.9 Hz, ArC), 133.1 (ArC), 131.7 (ArC), 130.4 (d, $J_{C\text{-}P}$ = 4.8 Hz, ArC), 129.2 (ArC), 126.5 (ArC), 124.7 (m, ArC), 116.4 (d, $J_{C\text{-}P}$ = 33.3 Hz, ArC), 21.3 (d, $J_{C\text{-}P}$ = 22.0 Hz, CH_3). $^{31}P\{^1H\}$ NMR (202.5 MHz, $CDCl_3$): δ -32.6 (s). HRMS *m/z* ESI^+ found 374.9966 $[M + H]^+$ calculated for $C_{18}H_{17}BrPS$ 374.9972.

Data for P8 (2-chloro-3-PCg-pyridine). ^1H NMR (500 MHz, $CDCl_3$): δ 8.61-8.59 (m, 1H, ArH), 8.38 (dd, 1H, J_1 = 4.7 Hz, J_2 = 1.9 Hz, ArH), 7.27-7.25 (m, 1H, ArH), 2.10-2.06 (m, 1H, CgP), 1.99-1.91 (m, 1H, CgP), 1.71 (d, 1H, J = 13.6 Hz, CgP), 1.56-1.52 (dd, 1H, J_1 = 13.6 Hz, J_2 = 4.1 Hz, CgP), 1.48-1.41 (m, 12H, CgP). $^{13}C\{^1H\}$ UDEFT NMR (125.8 MHz, $CDCl_3$): δ 157.9 (d, $J_{C\text{-}P}$ = 31.0 Hz, ArC), 150.1 (ArC), 143.9 (d, $J_{C\text{-}P}$ = 2.7 Hz, ArC), 130.8 (d, $J_{C\text{-}P}$ = 36.8 Hz, ArC), 122.4 (m, ArC), 96.8 (CgP), 96.0 (CgP), 74.2 (d, $J_{C\text{-}P}$ = 10.1 Hz, CgP), 73.3 (d, $J_{C\text{-}P}$ = 24.2 Hz, CgP), 45.3 (d, $J_{C\text{-}P}$ = 18.9 Hz, CgP), 36.4 (m, CgP), 28.5 (d, $J_{C\text{-}P}$ = 19.2 Hz, CgP), 27.9 (CgP), 27.6 (CgP), 26.5 (d, $J_{C\text{-}P}$ = 10.8 Hz, CgP).$^{31}P\{^1H\}$ NMR (202.5 MHz, $CDCl_3$): δ -38.2 (s). HRMS *m/z* ESI^+ found 350.0683 $[M + Na]^+$ calculated for $C_{15}H_{19}ClNNaO_3P$ 350.0689.

Data for P9 (2-chloro-3-PCg-quinoxaline). ^1H NMR (500 MHz, $CDCl_3$): δ 8.11-8.09 (m, 1H, ArH), 8.00-7.98 (m, 1H, ArH), 7.81-7.76 (m, 2H, ArH), 3.20 (d, J = 13.2 Hz, 1H, CgP), 2.26-2.22 (m, 1H, CgP), 2.01-1.93 (m, 1H, CgP), 1.70 (dd, J_1 = 13.2 Hz, J_2 = 5.0 Hz, 1H, CgP), 1.55-1.51 (m, 6H, CgP), 1.45 (s, 3H, CgP), 1.38 (s, 3H, CgP). $^{13}C\{^1H\}$ NMR (125.8 MHz, $CDCl_3$): δ 156.3 (d, $J_{C\text{-}P}$ = 41.5 Hz, ArC), 152.0 (d, $J_{C\text{-}P}$ = 34.6 Hz, ArC), 141.2 (ArC), 140.5 (ArC), 131.6 (ArC), 130.2 (ArC), 129.3 (ArC), 128.3 (ArC), 97.0 (CgP), 96.3 (CgP), 75.1 (d, $J_{C\text{-}P}$ = 28.4 Hz, CgP), 74.4 (d, $J_{C\text{-}P}$ = 8.0 Hz, CgP), 45.9 (d, $J_{C\text{-}P}$ = 19.9 Hz, CgP), 37.1 (CgP), 28.3 (d, $J_{C\text{-}P}$ = 19.7 Hz, CgP), 28.0 (d, $J_{C\text{-}P}$ = 8.6 Hz, CgP), 27.9 (CgP), 27.8 (CgP). $^{31}P\{^1H\}$ NMR (202.5 MHz, $CDCl_3$): δ -28.3 (s). HRMS *m/z* ESI^+ found 401.0792 $[M + Na]^+$ calculated for $C_{18}H_{20}ClN_2NaO_3P$ 401.0798.

Data for 2-L2 (2-PCg-3-P(*o*-tolyl)$_2$-pyridine). ^1H NMR (500 MHz, $CDCl_3$): δ 8.73 (m, 1H, ArH), 7.27-7.21 (m, 4H, ArH), 7.11-7.05 (m, 4H, ArH) 6.70-6.66 (m, 2H, ArH), 3.18 (m, 1H, CgP), 2.39-2.38 (m, 6H, CgP), 2.07-2.03 (m, 1H, CgP), 1.88-1.82 (m, 1H, CgP), 1.56-1.53 (m, 1H, CgP), 1.47 (s, 3H, CH_3), 1.38 (s, 3H, CH_3), 1.26-1.19 (m, 6H, CH_3). $^{13}C\{^1H\}$ UDEFT NMR (125.8 MHz, $CDCl_3$): δ 164.1-163.7 (m, ArC), 149.6 (ArC), 144.3-143.8 (dd, $J_{C\text{-}P}$ = 17.2 Hz, $J_{C\text{-}P}$ = 38.9 Hz, ArC), 142.5-142.2 (dd, $J_{C\text{-}P}$ = 11.6 Hz, $J_{C\text{-}P}$ = 27.1 Hz, ArC), 140.2 (d, $J_{C\text{-}P}$ = 7.5 Hz, ArC), 134.9-134.6 (m, ArC), 133.7 (ArC),

130.3-130.2 (m, ArC), 128.9 (ArC), 128.8 (ArC), 126.1 (ArC), 123.3 (ArC), 97.1 (CgP), 96.4 (CgP), 74.4-74.3 (m, CgP), 73.7-73.7 (dd, $J_{C\text{-}P}$ = 6.3 Hz, $J_{C\text{-}P}$ = 26.3 Hz, CgP), 45.7 (d, $J_{C\text{-}P}$ = 19.2 Hz, CgP), 37.0 (CgP), 28.0-27.8 (m, CgP/CH_3), 26.6 (d, $J_{C\text{-}P}$ = 9.9 Hz, CgP), 21.4-21.2 (m, CgP/CH_3). $^{31}P\{^1H\}$ NMR (202.5 MHz, $CDCl_3$): δ -29.5 (d, J_{PP} = 158.0 Hz), -34.4 (d, J_{PP} = 156.0 Hz). HRMS *m/z* ESI^+ found 506.2008 $[M + H]^+$ calculated for $C_{29}H_{34}NO_3P_2$ 506.2014.

Data for 2-L3 (2-P(*o*-tolyl)$_2$-3-PCg-pyridine). ^1H NMR (500 MHz, $CDCl_3$): δ 8.62-8.61 (m, 1H, ArH), 8.52-8.51 (m, 1H, ArH), 7.24-7.17 (m, 5H, ArH), 7.08-7.03 (m, 2H, ArH), 6.87-6.85 (m, 1H, ArH), 6.72-6.70 (m, 1H, ArH), 2.39 (m, 6H, CgP), 2.05-1.81 (m, 3H, CgP), 1.56-1.53 (d, 1H, J_1 = 4.1 Hz, J_2 = 13.5 Hz, CgP), 1.43 (s, 3H, CH_3), 1.39 (s, 3H, CH_3), 1.32-1.30 (m, 3H, CH_3), 1.15 (d, 3H, J = 12.5 Hz, CH_3). $^{13}C\{^1H\}$ UDEFT NMR (125.8 MHz, $CDCl_3$): δ 170.9-170.6 (dd, $J_{1\ C\text{-}P}$ = 6.7 Hz, $J_{2\ C\text{-}P}$ = 34.1 Hz, ArC), 150.9 (ArC), 142.7-142.3 (m, ArC), 140.7 (m, ArC), 137.5-136.9 (m, ArC), 135.9-135.8 (m, ArC), 134.8-134.6 (m, ArC), 133.8 (ArC), 129.8-139.7 (m, ArC), 128.6 (ArC), 128.5 (ArC), 125.9 (ArC), 125.7 (ArC), 122.1 (ArC), 96.9 (CgP), 95.9 (CgP), 74.2-73.7 (m, CgP), 45.6 (d, $J_{C\text{-}P}$ = 19.1 Hz, CgP), 36.3 (CgP), 28.1-27.7 (m, CgP/CH_3), 26.0 (d, $J_{C\text{-}P}$ = 11.4 Hz, CgP/CH_3), 21.6-21.4 (m, CgP/CH_3). $^{31}P\{^1H\}$ NMR (202.5 MHz, $CDCl_3$): δ -16.6 (d, J_{PP} = 149.9 Hz), -41.6 (d, J_{PP} = 149.9 Hz). HRMS *m/z* ESI^+ found 506.2008 $[M + H]^+$ calculated for $C_{29}H_{34}NO_3P_2$ 506.2014.

Data for 2-L4 (2,3-(P(*o*-tolyl)$_2$)$_2$-pyridine). ^1H NMR (500 MHz, $CDCl_3$): δ 8.63 (m, 1H, ArH), 7.21-7.07 (m, 10H, ArH), 7.02-6.95 (m, 4H, ArH), 6.90-6.88 (m, 2H, ArH), 6.67-6.65 (m, 2H, ArH), 2.24-2.21 (m, 12H, CH_3).$^{13}C\{^1H\}$ UDEFT NMR (125.8 MHz, $CDCl_3$): δ 168.0-167.7 (m, ArC), 150.5 (ArC), 142.8 (d, $J_{C\text{-}P}$ = 26.2 Hz, ArC), 142.5 (d, $J_{C\text{-}P}$ = 27.1 Hz, ArC), 140.7 (d, $J_{C\text{-}P}$ = 7.0 Hz, ArC), 139.8-139.4 (m, ArC), 134.7 (m, ArC), 134.3-134.1 (m, ArC) 133.8 (ArC), 133.4 (ArC), 130.1 (d, $J_{C\text{-}P}$ = 4.7 Hz, ArC), 129.7 (d, $J_{C\text{-}P}$ = 5.1 Hz, ArC) 128.7 (ArC), 128.5 (ArC), 125.9 (ArC), 125.7 (ArC), 122.8 (ArC), 21.3-20.8 (overlapping signals, CH_3). $^{31}P\{^1H\}$ NMR (202.5 MHz, $CDCl_3$): δ -20.4 (d, J_{PP} = 148.0 Hz), -31.2 (d, J_{PP} = 148.1 Hz). HRMS *m/z* ESI^+ found 504.2004 $[M + H]^+$ calculated for $C_{33}H_{32}NP_2$ 504.2010.

Data for 2-L5 (2-PCg-3-P(*o*-tolyl)$_2$-thiophene). ^1H NMR (500 MHz, $CDCl_3$): δ 7.62 (d, 1H, J = 5.0 Hz, ArH), 7.28-7.19 (m, 4H, ArH), 7.12-7.07 (m, 2H, ArH), 6.85-6.83 (m,

1H, ArH), 6.74-6.72 (m, 1H, ArH), 6.63-6.62 (m, 1H, ArH), 2.44 (s, 3H, CgP), 2.35-2.33 (m, 4H, CgP), 2.13-2.09 (m, 1H, CgP), 2.01-1.93 (m, 1H, CgP), 1.61-1.57 (m, 2H, CgP), 1.51 (s, 3H, CgP/CH_3), 1.41 (s, 3H, CgP/CH_3), 1.36 (d, 3H, $J_{H\text{-}P}$ = 12.8 Hz, CgP/CH_3), 1.10 (d, 3H, $J_{H\text{-}P}$ = 13.4 Hz, CgP/CH_3). $^{13}C\{^1H\}$ UDEFT NMR (125.8 MHz, $CDCl_3$): δ 149.4-149.1 (dd, $J_{C\text{-}P}$ = 13.0 Hz, $J_{C\text{-}P}$ = 30.3 Hz, ArC), 142.3 (d, $J_{C\text{-}P}$ = 26.9 Hz, ArC), 141.8 (d, $J_{C\text{-}P}$ = 25.7 Hz, ArC), 138.9-138.1 (m, ArC), 136.4-136.4 (m, ArC), 135.7-135.6 (m, ArC), 133.2-133.1 (m, ArC), 132.6 (ArC), 131.8 (ArC), 131.0 (m, ArC), 130.1 (m, ArC), 128.6 (ArC), 128.4 (ArC), 126.0 (ArC), 125.8 (ArC), 96.9 (ArC), 96.2 (ArC), 73.6 (d, $J_{C\text{-}P}$ = 8.8 Hz, CgP), 73.3-73.1 (dd, $J_{C\text{-}P}$ = 7.8 Hz, $J_{C\text{-}P}$ = 19.1 Hz, CgP), 44.8 (d, $J_{C\text{-}P}$ = 17.9 Hz, CgP), 37.3 (CgP), 27.9-26.7 (m, CgP/CH_3), 26.8 (d, $J_{C\text{-}P}$ = 10.9 Hz, CgP/CH_3), 21.3-21.0 (m, CgP/CH_3). $^{31}P\{^1H\}$ NMR (202.5 MHz, $CDCl_3$): δ -38.4 (d, J_{PP} = 134.9 Hz), 42.0 (d, J_{PP} = 135.1 Hz). HRMS *m/z* ESI^+ found 533.1440 $[M + Na]^+$ calculated for $C_{28}H_{32}NaNO_3P_2S$ 533.1445.

Data for 2-L6 (2-P(*o*-tolyl)$_2$-3-PCg-thiophene). ^1H NMR (500 MHz, $CDCl_3$): δ 7.84-7.82 (dd, 1H, J_1 = 2.5 Hz, J_2 = 5.1 Hz, ArH), 7.61-7.60 (m, 1H, ArH), 7.32-7.23 (m, 3H, ArH), 7.21-7.19 (m, 2H, ArH), 7.14-7.08 (m, 2H, ArH), 6.97-6.95 (m, 1H, ArH), 6.73-6.71 (m, 1H, ArH), 2.49 (s, 3H, CgP), 2.33 (s, 3H, CgP), 2.10-2.06 (m, 1H, CgP), 1.98-1.90 (m, 2H, CgP), 1.60-1.59 (m, 1H, CgP), 1.48 (s, 3H, CH_3), 1.40 (s, 3H, CH_3), 1.33 (d, 3H, J_{HP} = 12.7 Hz, CH_3), 1.19 (d, 3H, J_{HP} = 12.9 Hz, CH_3). $^{13}C\{^1H\}$ NMR (125.8 MHz, $CDCl_3$): δ 141.8-141.6 (m, ArC), 136.0 (m, ArC), 134.2 (m, ArC), 133.4 (ArC), 132.5 (ArC), 131.8 (ArC), 130.1 (ArC), 129.1 (ArC), 128.7 (ArC), 126.0 (ArC), 125.8 (ArC), 96.9 (ArC), 96.1 (ArC), 73.6 (m, CgP), 45.3 (d, $J_{C\text{-}P}$ = 18.3 Hz, CgP), 37.5 (CgP), 28.1-27.7 (m, CgP/CH_3), 26.7-26.5 (m, CgP/CH_3), 21.3-20.9 (m, CgP/CH_3). $^{31}P\{^1H\}$ NMR (202.5 MHz, $CDCl_3$): δ -39.0 (d, J_{PP} = 127.1 Hz), -44.8 (d, J_{PP} = 127.1 Hz). HRMS *m/z* ESI^+ found 533.1440 $[M + Na]^+$ calculated for $C_{28}H_{32}NaNO_3P_2S$ 533.1445.

Data for 2-L7 (2,3-(P(*o*-tolyl)$_2$)$_2$-thiophene). ^1H NMR (500 MHz, $CDCl_3$): δ 7.49-7.47 (m, 1H, ArH), 7.24-6.99 (m, 12H, ArH), 6.87-6.85 (m, 4H, ArH), 6.69-6.67 (m, 1H, ArH), 2.33-2.29 (m, 12H, CH_3). $^{13}C\{^1H\}$ NMR (125.8 MHz, $CDCl_3$): 145.4-145.0 (m, ArC), 144.4-144.1 (dd, $J_{C\text{-}P}$ = 8.2 Hz, $J_{C\text{-}P}$ = 24.1 Hz, ArC), 142.5-142.2 (m, ArC), 136.1 (d, $J_{C\text{-}P}$ = 9.9 Hz, ArC), 135.8 (d, $J_{C\text{-}P}$ = 8.5 Hz, ArC), 134.1 (m, ArC), 132.9 (m, ArC), 132.0 (ArC), 130.2 (ArC), 129.0 (ArC), 128.6 (ArC), 126.0 (ArC), 21.4-21.3

(overlapping signals, CH_3). $^{31}P\{^1H\}$ NMR (202.5 MHz, $CDCl_3$): δ -40.4 (second order pattern). HRMS *m/z* ESI^+ found 509.1616 $[M + H]^+$ calculated for $C_{32}H_{31}P_2S$ 509.1622.

Data for 2-L8 (3-PCg-4-P(*o*-tolyl)$_2$-thiophene, ThioPAd-DalPhos). ^1H NMR (500 MHz, $CDCl_3$): δ 8.19-8.17 (m, 1H, ArH), 7.25-7.16 (m, 4H, ArH), 7.08-7.04 (m, 2H, ArH), 6.82-6.80 (m, 1H, ArH), 6.70-6.69 (m, 1H, ArH), 6.64-6.61 (m, 1H, ArH), 2.45 (s, 3H, CgP), 2.32 (s, 3H, CgP), 2.10-2.08 (m, 1H, CgP), 2.00-1.96 (m, 1H, CgP), 1.91-1.83 (m, 1H, CgP), 1.55-1.52 (m, 1H, CgP), 1.45 (s, 3H, CgP/CH_3), 1.37 (s, 3H, CgP/CH_3), 1.29-1.26 (m, 6H, CgP/CH_3). $^{13}C\{^1H\}$ NMR (125.8 MHz, $CDCl_3$): δ 143.7-143.3 (dd, J_{C-P} = 13.8 Hz, J_{C-P} = 35.5 Hz, ArC), 142.6 (d, J_{C-P} = 27.7 Hz, ArC), 136.8-136.3 (m, ArC), 136.0 (d, J_{C-P} = 11.3 Hz, ArC), 135.5-135.4 (m, ArC), 133.7 (ArC), 133.4-133.3 (m, ArC), 133.1 (ArC), 131.4 (m, ArC), 130.3-130.2 (m, ArC), 129.0 (ArC), 128.7 (ArC), 125.4 (ArC), 125.9 (ArC), 97.1 (ArC), 96.3 (ArC), 73.9-73.5 (m, CgP), 45.6 (d, J_{C-P} = 18.1 Hz, CgP), 36.7 (CgP), 28.4-28.0 (m, CgP/CH_3), 26.6 (d, J_{C-P} = 11.1 Hz, CgP/CH_3), 21.5-21.3 (m, CgP/CH_3). $^{31}P\{^1H\}$ NMR (202.5 MHz, $CDCl_3$): δ -36.4 (d, J_{PP} = 98.4 Hz), -44.7 (d, J_{PP} = 98.4). HRMS *m/z* ESI^+ found 511.1620 $[M + H]^+$ calculated for $C_{28}H_{33}O_3P_2S$ 511.1626.

Data for 2-L9 (3,4-(P(*o*-tolyl)$_2$)$_2$-thiophene). ^1H NMR (500 MHz, $CDCl_3$): δ 7.22-7.19 (m, 4H, ArH), 7.16-7.14 (m, 4H, ArH), 7.04-7.01 (m, 4H, ArH), 6.85-6.84 (m, 2H, ArH), 6.81-6.79 (m, 4H, ArH), 2.27 (s, 12H, CH_3). $^{13}C\{^1H\}$ NMR (125.8 MHz, $CDCl_3$): δ 142.7-142.5 (m, ArC), 140.8-140.6 (m, ArC), 135.6 (ArC), 133.3 (ArC), 132.7 (ArC), 130.1 (ArC), 128.7-128.5 (m, ArC), 126.0 (ArC), 21.4-21.2 (overlapping signals, CH_3). $^{31}P\{^1H\}$ NMR (202.5 MHz, $CDCl_3$): δ -38.0 (s). While **2-L9** is a known compound that was prepared *via* dilithiation and quench of 3,4-dibromothiophene using bis(2-methylphenyl)chlorophosphine and purified *via* sublimation using a Kugelrohr apparatus, an alternative synthesis is reported herein; spectral data are in agreement with literature**.** [A23]

Data for 3-L2 (2,3-PCg$_2$-pyridine). *rac*-**3-L2**: ^1H NMR (500 MHz, $CDCl_3$): δ 8.60 (d, *J* = 4.6 Hz, 1H, ArH), 8.58-8.52 (m, 1H, ArH), 7.20-7.18 (m, 1H, ArH), 3.96 (d, *J* = 12.7 Hz, 1H, CgP), 2.28-2.24 (m, 1H, CgP), 2.13-2.10 (m, 1H, CgP), 1.99-1.87 (m, 2H, CgP), 1.79 (d, *J* = 13.6 Hz, 1H, CgP), 1.66-1.62 (m, 1H, CgP), 1.46-1.37 (m, 26H, CgP). $^{13}C\{^1H\}$ UDEFT NMR (125.8 MHz, $CDCl_3$): δ 166.9-166.4 (m, ArC), 149.4 (ArC),

141.0-140.7 (m, ArC), 140.4 (m, ArC), 122.5 (ArC), 97.1 (CgP), 96.8 (CgP), 96.5 (CgP), 95.9 (CgP), 74.9-74.6 (m, CgP), 74.0 (d, $J_{C\text{-}P}$ = 14.1 Hz, CgP), 73.7 (d, $J_{C\text{-}P}$ = 13.9 Hz, CgP), 45.9 (d, $J_{C\text{-}P}$ = 19.2 Hz, CgP), 45.6 (d, $J_{C\text{-}P}$ = 19.4 Hz, CgP), 37.8 (CgP), 35.8 (CgP), 28.1-27.6 (m, CgP), 26.3 (d, $J_{C\text{-}P}$ = 11.0 Hz, CgP). $^{31}P\{^{1}H\}$ NMR (202.5 MHz, $CDCl_3$): δ -31.9 (d, J_{PP} = 148.4 Hz), -44.2 (d, J_{PP} = 148.6 Hz). HRMS *m/z* ESI^+ found 530.1832 $[M + Na]^+$ calculated for $C_{25}H_{35}NNaO_6P_2$ 530.1837. *meso*-**3-L2**: ^{1}H NMR (500 MHz, $CDCl_3$): δ 8.76 (d, $J_{C\text{-}P}$ = 4.6 Hz, 1H, ArH), 8.57-8.54 (m, 1H, ArH), 7.22-7.19 (m, 1H, ArH), 2.13-2.04 (m, 3H, CgP), 1.98-1.89 (m, 2H, CgP), 1.81 (d, 1H, *J* = 13.6 Hz, CgP), 1.46-1.39 (m, 26H, CgP). $^{13}C\{^{1}H\}$ UDEFT NMR (125.8 MHz, $CDCl_3$): δ 168.2-167.8 (m, ArC), 150.4 (ArC), 141.4-140.8 (m, ArC), 140.4 (m, ArC), 122.5 (ArC), 96.9-96.8 (m, CgP), 96.0-95.9 (m, CgP), 74.9 (d, $J_{C\text{-}P}$ = 9.4 Hz, CgP), 74.6 (d, $J_{C\text{-}P}$ = 11.1 Hz, CgP), 73.8 (dd, $J_{1\ C\text{-}P}$ = 28.0 Hz, $J_{2\ C\text{-}P}$ = 14.6 Hz, CgP), 73.3 (dd, $J_{1\ C\text{-}P}$ = 26.8 Hz, $J_{2\ C\text{-}P}$ = 15.9 Hz, CgP), 46.0-45.7 (m, CgP), 36.4 (CgP), 35.9 (CgP), 28.3-27.7 (m, CgP), 26.4-26.3 (m, CgP). $^{31}P\{^{1}H\}$ NMR (202.5 MHz, $CDCl_3$): δ -35.1 (d, J_{PP} = 152.1 Hz), -44.4 (d, J_{PP} = 152.0 Hz). HRMS *m/z* ESI^+ found 508.2012 $[M + H]^+$ calculated for $C_{25}H_{36}NO_6P_2$ 508.2018.

Data for 3-L3 (2,3-PCg$_2$-quinoxaline). ^{1}H NMR (500 MHz, $CDCl_3$): δ 8.10-8.01 (m, 2H, ArH), 7.77-7.74 (m, 2H, ArH), 3.79 (d, *J* = 12.9 Hz, 1H, CgP), 3.03 (d, *J* = 13.0 Hz, 1H, CgP), 2.30-2.21 (m, 2H, CgP), 2.00-1.91 (m, 2H, CgP), 1.72-1.68 (m, 1H, CgP), 1.59-1.56 (m, 1H, CgP), 1.54 (s, 3H, CgP), 1.50-1.43 (m, 20H, CgP), 1.39 (s, 3H, CgP).$^{13}C\{^{1}H\}$ UDEFT NMR (125.8 MHz, $CDCl_3$): δ 162.9 (d, $J_{C\text{-}P}$ = 4.9 Hz, ArC), 162.5 (d, $J_{C\text{-}P}$ = 5.6 Hz, ArC), 141.1 (ArC), 140.9 (ArC), 130.6 (ArC), 130.5 (ArC), 129.7 (ArC), 129.4 (ArC), 97.2 (CgP), 97.1 (CgP), 96.4 (CgP), 96.2 (CgP), 75.1-74.8 (m, CgP), 74.5-74.3 (m, CgP), 45.9-45.7 (m, CgP), 37.7 (CgP), 36.9 (CgP), 28.3-28.1 (m, CgP), 27.9-27.8 (m, CgP), 27.5-27.4 (m, CgP). $^{31}P\{^{1}H\}$ NMR (202.5 MHz, $CDCl_3$): δ -34.8 (s), -35.7 (s). HRMS *m/z* ESI^+ found 581.1941 $[M + Na]^+$ calculated for $C_{28}H_{36}N_2NaO_6P_2$ 581.1946.

Data for Nickel Complexes:

Data for 1-C1 ((CyPF-Cy)Ni(o-tolyl)Cl): ^{1}H NMR (300 K, 500 MHz, $CDCl_3$): δ 6.95 (s, 1H, ArH), 6.84 (s, 1H, ArH), 6.73 (m, 2H, ArH), 4.81 (s, 1H, Cp-P), 4.51 (s, 1H, Cp-P), 4.44 (s, 1H, Cp-P), 4.25 (s, 5H, C_5H_5), 3.23-3.03 (m, 6H, CH_3 and CH), 2.42-0.96 (m,

46H, CH_2 and CH), 0.32-0.30 (m, 1H, CH); $^{13}C\{^1H\}$ NMR (300 K, 125.8 MHz, $CDCl_3$): δ 144.6 (br m), 135.7 (br m), 128.0, 123.9, 122.2, 93.7 (br m), 73.0, 70.5 (br m), 69.2, 68.7, 68.4, 38.5 (d, J_{CP} = 15.1 Hz), 34.3 (br m), 32.0 (br m), 31.3, 30.5, 29.9 (m), 28.7-26.0 (overlapping m), 16.1. $^{31}P\{^1H\}$ NMR (300 K, 202.5 MHz, $CDCl_3$): δ 47.3 (br m), 7.9 (apparent d, J_{PP} = 34.4 Hz). $^{31}P\{^1H\}$ NMR (200 K, 121.4 MHz, $CDCl_3$): δ 46.9 (d, J_{PP} = 34.0 Hz), 7.3 (d, J_{PP} = 34.0 Hz). Anal. Calcd for $C_{43}H_{63}Cl_1Fe_1Ni_1P_2$: C, 65.22; H, 8.02; N, 0. Found: C, 64.84; H, 7.93; N < 0.3.

Data for (L^{iPr})Ni(o-tolyl)Cl: ^1H NMR (500 MHz; $CDCl_3$): δ 7.17 (m, 1H), 6.74-6.70 (m, 3H), 4.64-4.36 (m, 8H), 3.61 (s, 3H), 3.09 (m, 2H), 1.69 (m, 2H), 1.50-1.48 (m, 6H), 1.10-0.97 (m, 12H), 0.38-0.36 (m, 6H). $^{13}C\{^1H\}$ NMR (125.8 MHz; $CDCl_3$; quaternary carbons not observed despite prolonged acquisition times): δ 136.0, 125.9, 124.0, 122.0, 72.8, 71.7, 70.8, 69.7, 27.0, 25.1-24.9 (overlapping), 24.0, 21.1, 19.6, 17.5. $^{31}P\{^1H\}$ NMR (202.5 MHz; $CDCl_3$): δ 0.26 (s). Anal. Calcd for $C_{29}H_{43}Cl_1Fe_1Ni_1P_2$: C, 57.71; H, 7.18; N, 0. Found: C, 57.33; H, 6.80; N < 0.5.

Data for 2-C1 ((3-PCg-4-P(*o*-tolyl)$_2$-thiophene)Ni(*o*-tolyl)Cl): $^{31}P\{^1H\}$ NMR (202.5 MHz; $CDCl_3$): δ 12.8-12.7 (m), 12.1-12.0 (m), 11.3-11.1 (m, major species), 10.7 (d, J = 11.1 Hz, minor species), 5.2 (d, J = 10.9 Hz, minor species), 4.5 (d, J = 11.5 Hz, major species). On the basis of the observed positional disorder associated with the Ni-bound *ortho*-tolyl fragment within the X-ray structure of **2-C1**, arising from Ni-C(tolyl) bond rotation (57:43 occupancy ratio), the major and minor species are interpreted as being rotamers of this type. Anal. Calcd for $C_{35}H_{39}ClNiO_3P_2S$: C, 60.41; H, 5.65; N, 0. Found: C, 60.59; H, 5.58; N, <0.3.

Data for 2-C2 ((3,4-(P(*o*-tolyl)$_2$)$_2$-thiophene)Ni(*o*-tolyl)Cl): $^{31}P\{^1H\}$ NMR (202.5 MHz; $CDCl_3$): δ 30.6 (m), 28.9 (m), 26.3-25.1 (m), 6.6-6.1 (m), 5.2 (m). Anal. Calcd for $C_{39}H_{37}ClNiP_2S$: C, 67.51; H, 5.38; N, 0. Found: C, 67.22; H, 5.20; N, <0.3.

Data for 3-C2 ((2,3-PCg$_2$-pyridine)Ni(*o*-tolyl)Cl): Anal. Calcd for $C_{32}H_{42}ClNNiO_6P_2$: C, 55.48; H, 6.11; N, 2.02 Found: C, 55.46; H, 5.94; N, 2.17. Given the presence of *meso* and *rac* isomers of **3-L2**, Ni-bound *ortho*-tolyl fragment rotamers, as well as cis/trans disposed Ni-bound *ortho*-tolyl fragments, a total of 16 unique phosphorus NMR signals are expected; 12 broad signals are observed. Pairs of signals are assigned on the basis of $^{31}P\{^1H\}$-$^{31}P\{^1H\}$ COSY NMR data. $^{31}P\{^1H\}$ NMR (202.5 MHz; CD_2Cl_2): δ 25.3 (isomer

A), 23.4 (no label), 19.1 (isomer B), 18.7 (isomer C), 17.4 (isomer D), 16.8 (isomer E), 12.0 (isomer B), 10.9 (isomer D), 9.8 (isomer C), 8.0 (isomer E), 1.3 (isomer A), -0.5 (no label).

Data for 3-C3 ((2,3-PCg$_2$-quinoxaline)Ni(*o*-tolyl)Cl): Anal. Calcd for $C_{35}H_{43}ClN_2NiO_6P_2$: C, 56.52; H, 5.83; N, 3.77. Found: C, 56.29; H, 5.96; N, 3.52. Given the presence of *meso* and *rac* isomers of **3-L3**, as well as Ni-bound *ortho*-tolyl fragment rotamers, a total of eight unique phosphorus NMR signals are expected. Pairs of signals are assigned on the basis of $^{31}P\{^1H\}$-$^{31}P\{^1H\}$ COSY NMR data. $^{31}P\{^1H\}$ NMR (202.5 MHz; $CDCl_3$): δ 13.7 (d, $J_{P\text{-}P}$ = 18.8 Hz, isomer A), 13.0 (d, $J_{P\text{-}P}$ = 17.0 Hz, isomer B), 12.0 (d, $J_{P\text{-}P}$ = 16.5 Hz, isomer C), 11.4 (d, $J_{P\text{-}P}$ = 15.1 Hz, isomer D), -3.5 (d, $J_{P\text{-}P}$ = 19.0 Hz, isomer A), -4.5 (d, $J_{P\text{-}P}$ = 16.6 Hz, isomer C), -5.3 (d, $J_{P\text{-}P}$ = 16.9 Hz, isomer B), -6.2 (d, $J_{P\text{-}P}$ =15.0 Hz, isomer D).

NMR Spectra

^{1}H NMR Spectrum of ***N-(furan-2-ylmethyl)-4-methylaniline*** *and* ***4-butyl-N-(furan-2-ylmethyl)aniline*****, 1.5a** *and* **1.5b** *from Scheme 2-8 using* **1-C1** ($CDCl_3$, 300 MHz)

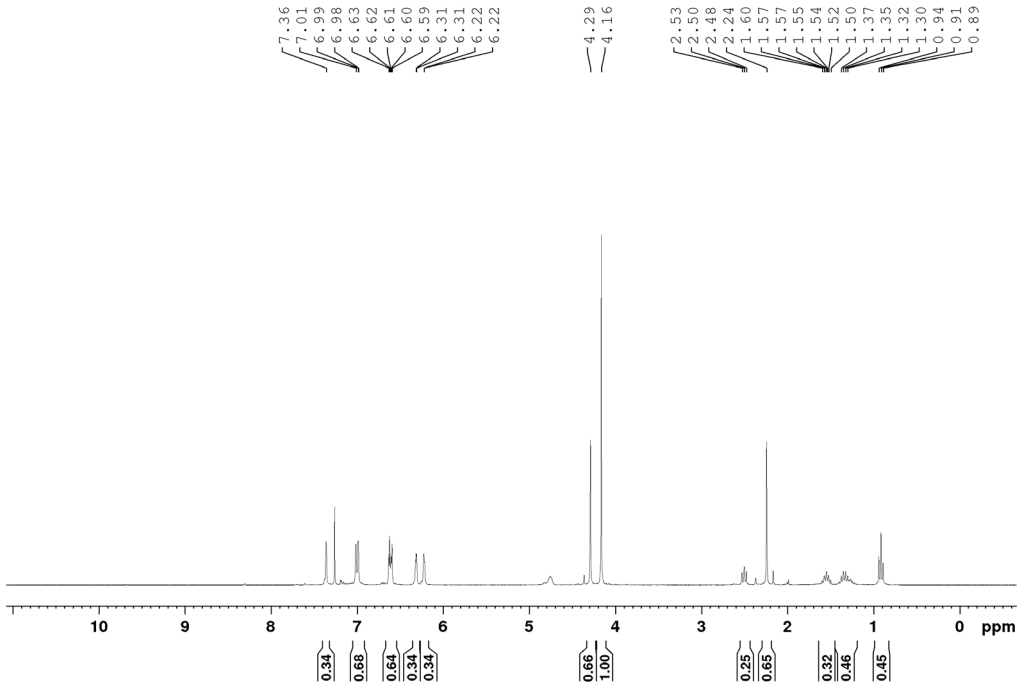

^{1}H NMR Spectrum of ***N-(furan-2-ylmethyl)-4-methylaniline*** *and* ***4-butyl-N-(furan-2-ylmethyl)aniline*** **1.5a** *and* **1.5b** *from Scheme 2-8 using* **C0** ($CDCl_3$, 300 MHz)

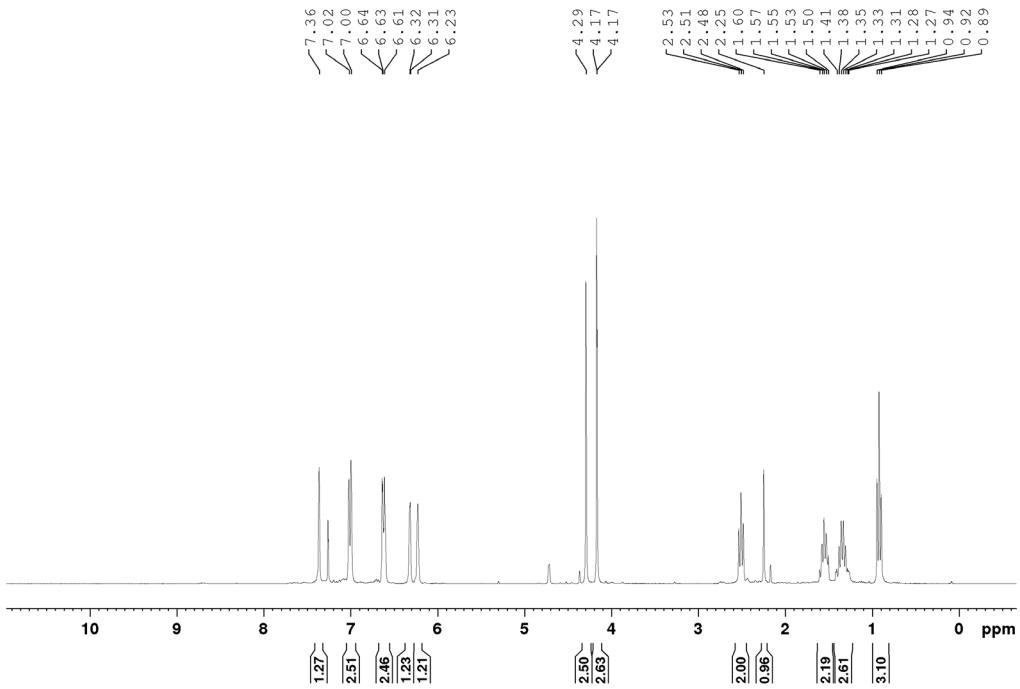

^{1}H NMR Spectrum of ***N-(furan-2-ylmethyl)naphthalen-1-amine*, 1.2a** ($CDCl_3$, 500 MHz)

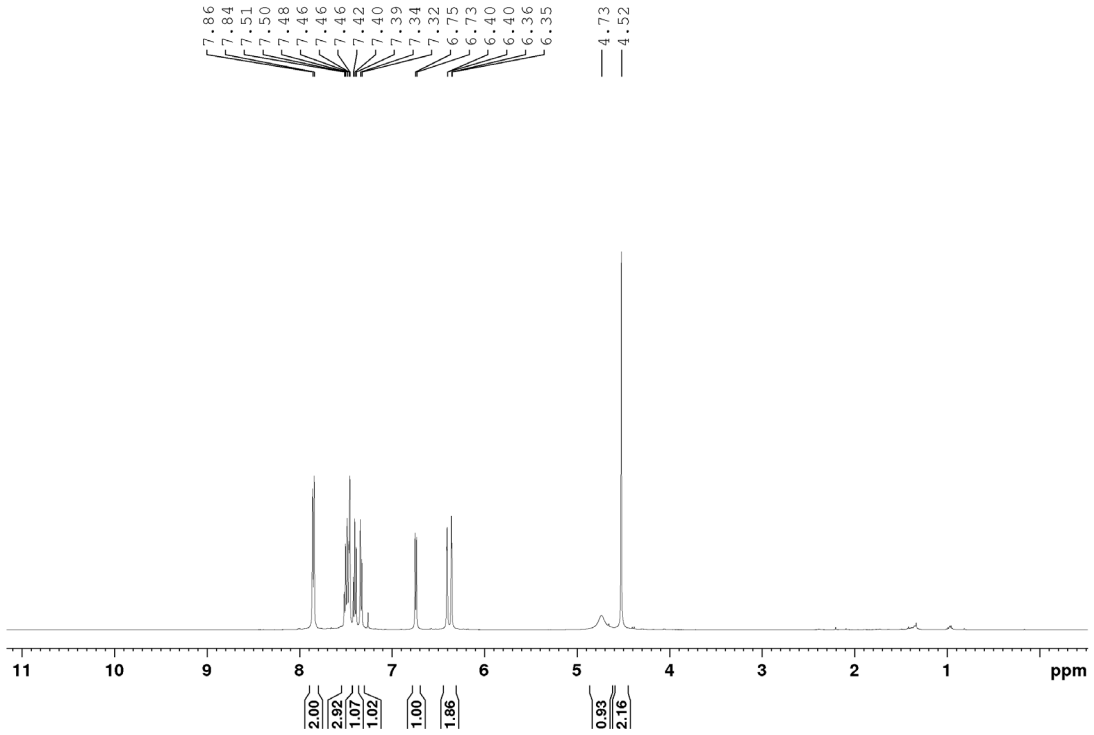

^{13}C{^{1}H} NMR Spectrum of **1.2a** ($CDCl_3$, 125.8 MHz)

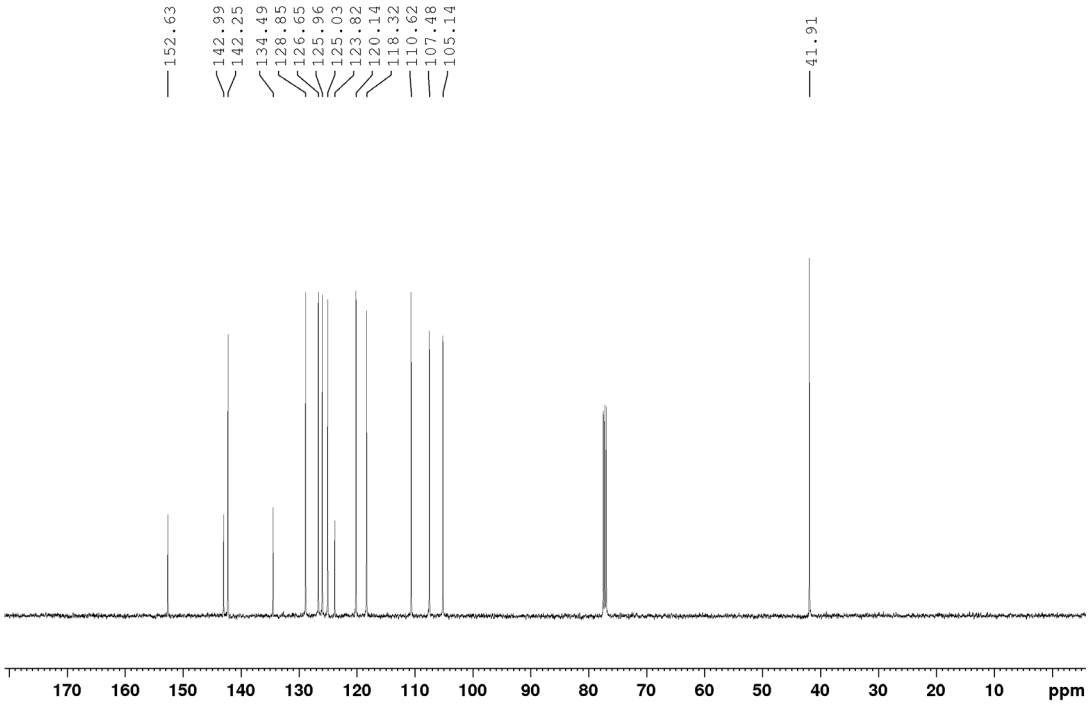

^{1}H NMR Spectrum of ***N-(furan-2-ylmethyl)-3-methoxyaniline***, **1.2b** ($CDCl_3$, 500 MHz)

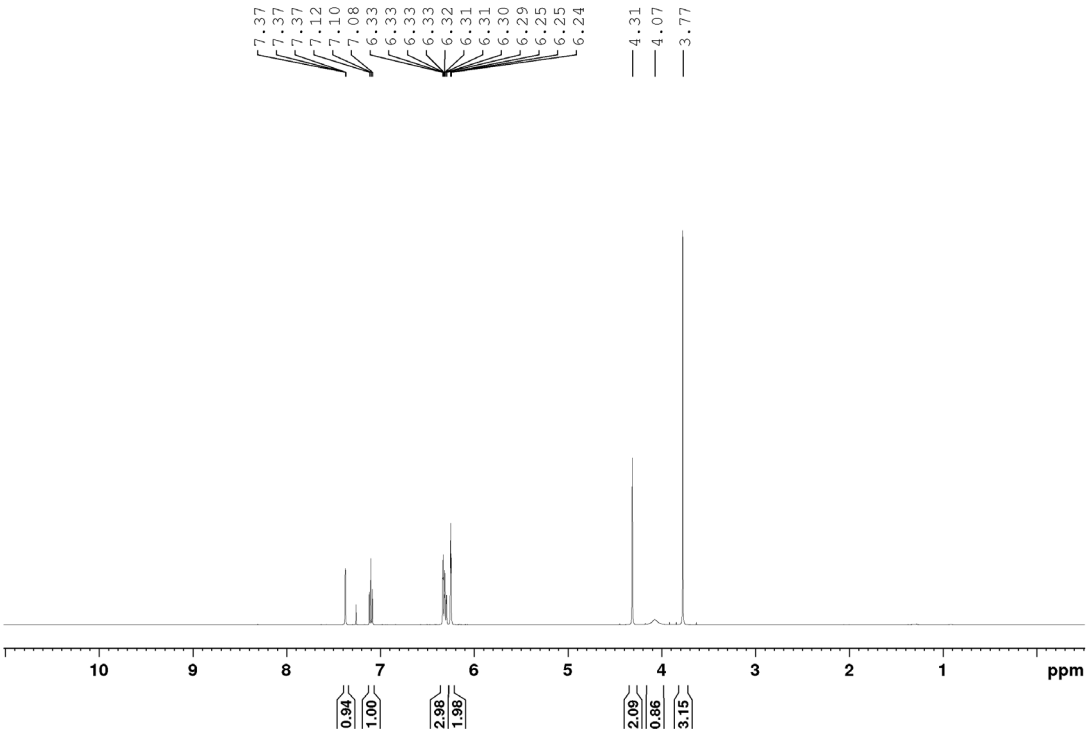

^{13}C{^{1}H} NMR Spectrum of **1.2b** ($CDCl_3$, 125.8 MHz)

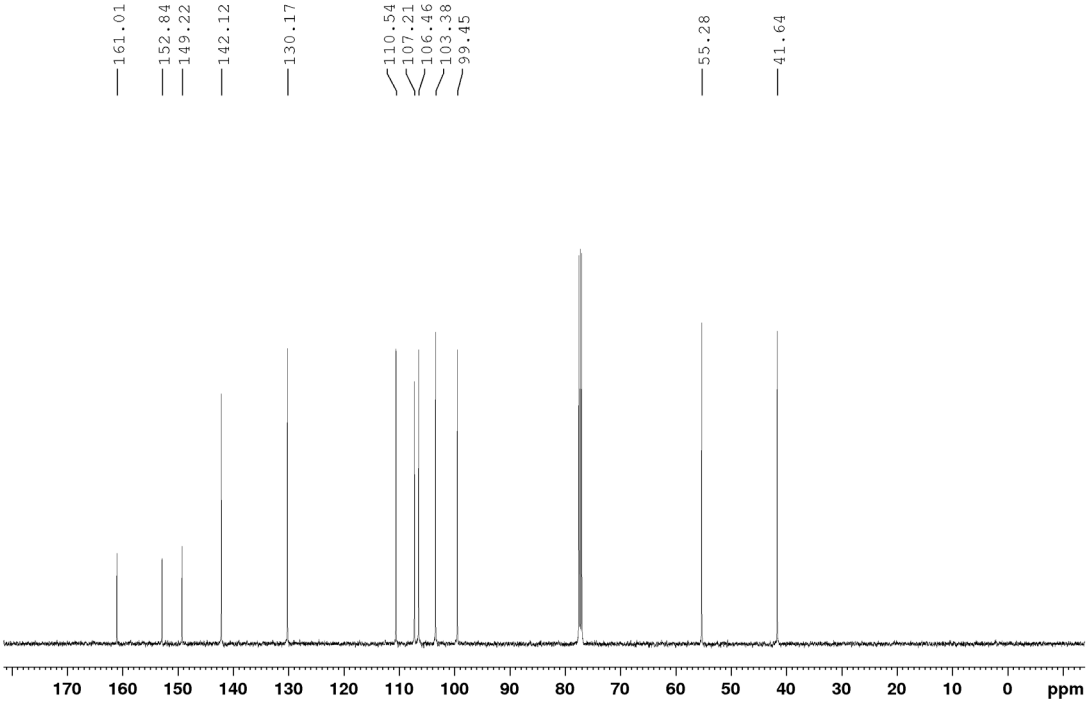

^{1}H NMR Spectrum of ***N-(furan-2-ylmethyl)-4-methoxyaniline*, 1.2c** ($CDCl_3$, 500 MHz)

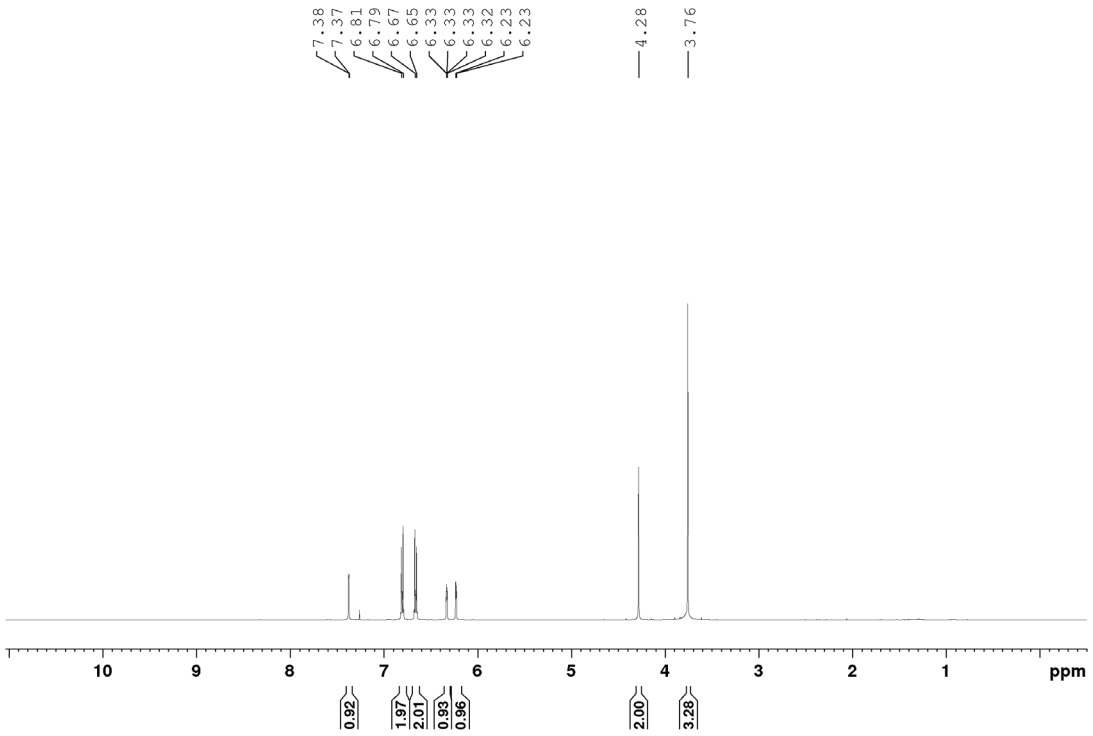

^{13}C{^{1}H} NMR Spectrum of **1.2c** ($CDCl_3$, 125.8 MHz)

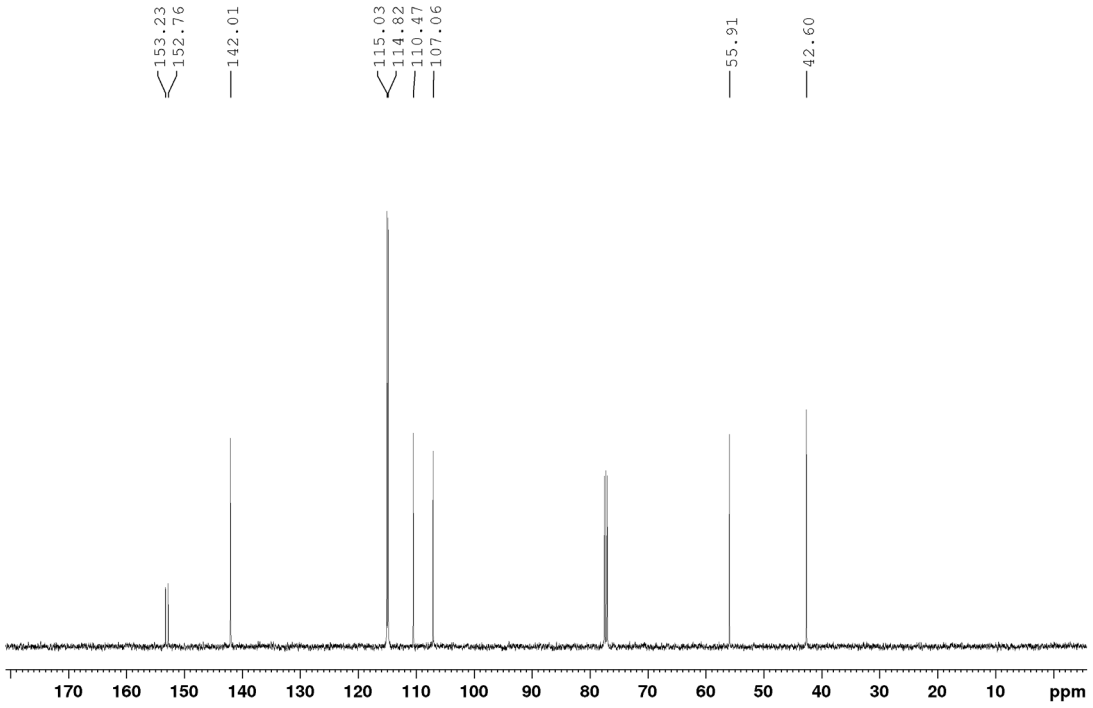

^{1}H NMR Spectrum of ***N-(furan-2-ylmethyl)benzo[b]thiophen-5-amine*, 1.2d** ($CDCl_3$, 500 MHz)

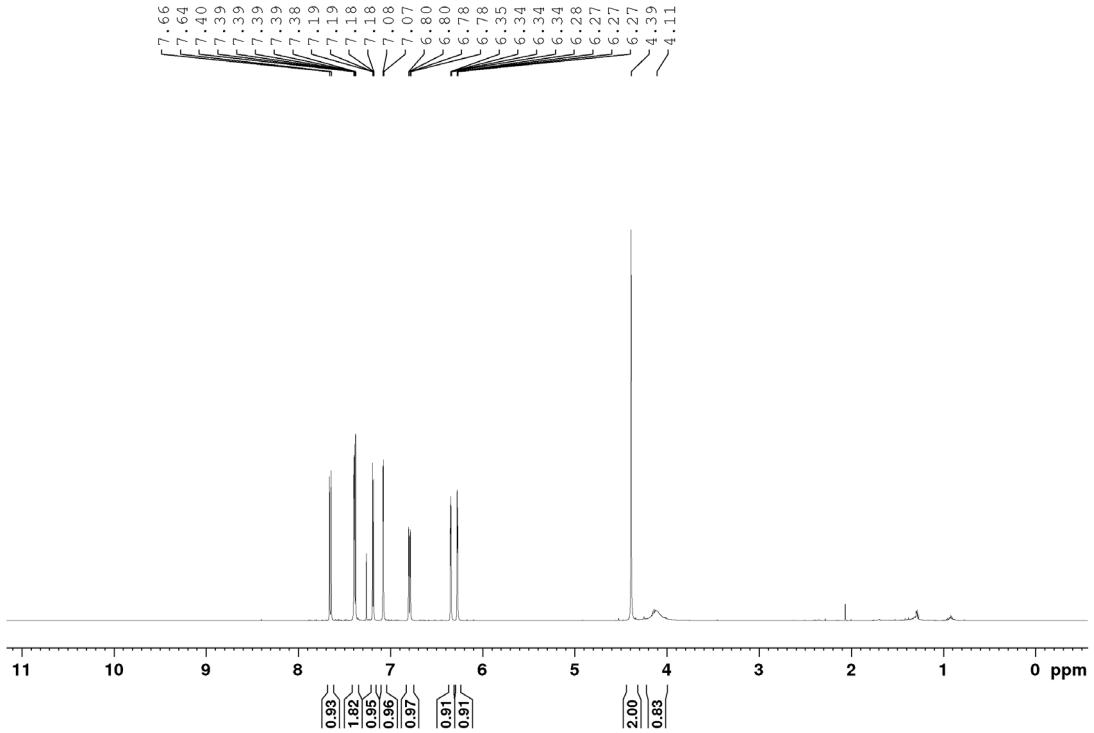

^{13}C{^{1}H} NMR Spectrum of **1.2d** ($CDCl_3$, 125.8 MHz)

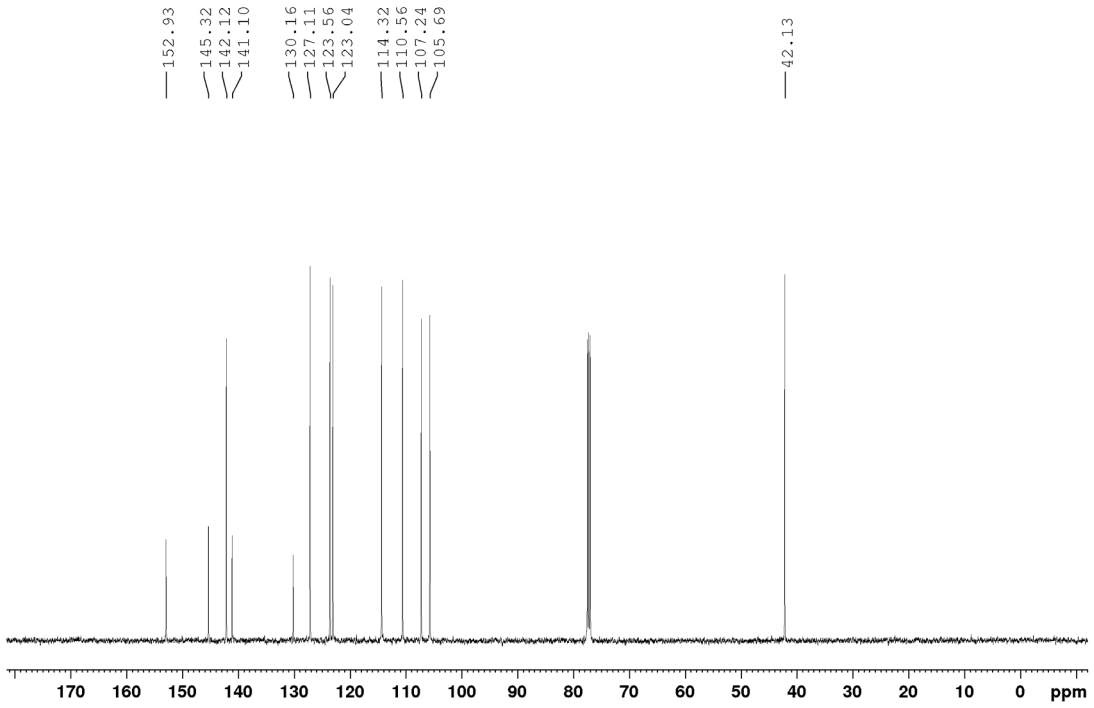

^{1}H NMR Spectrum of ***N-(sec-butyl)naphthalen-1-amine,*** **1.3a** ($CDCl_3$, 500 MHz)

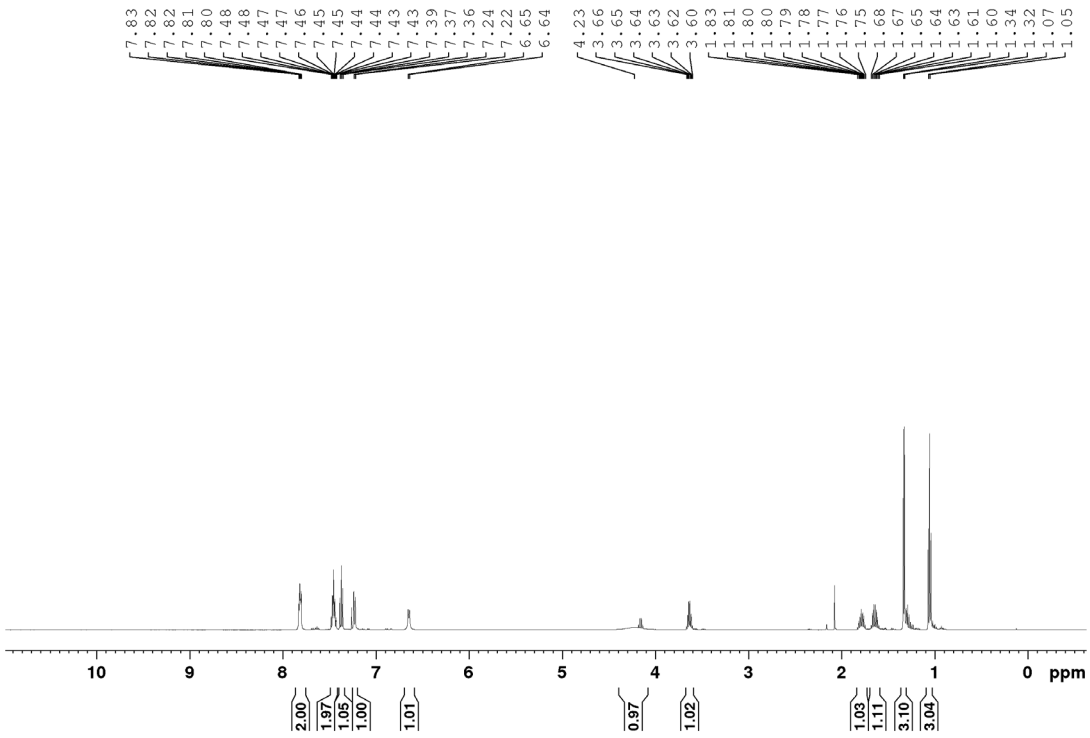

^{13}C{^{1}H} NMR Spectrum of **1.3a** ($CDCl_3$, 125.8 MHz)

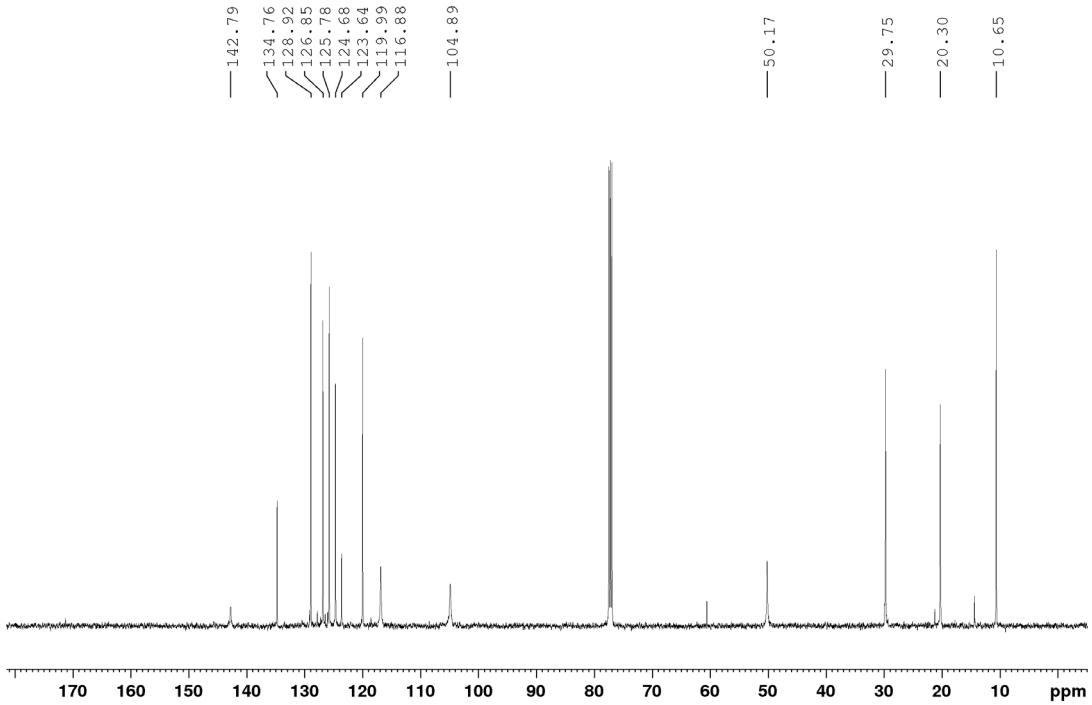

^{1}H NMR Spectrum of ***N-(sec-butyl)-3-methoxyaniline***, **1.3b** ($CDCl_3$, 300 MHz)

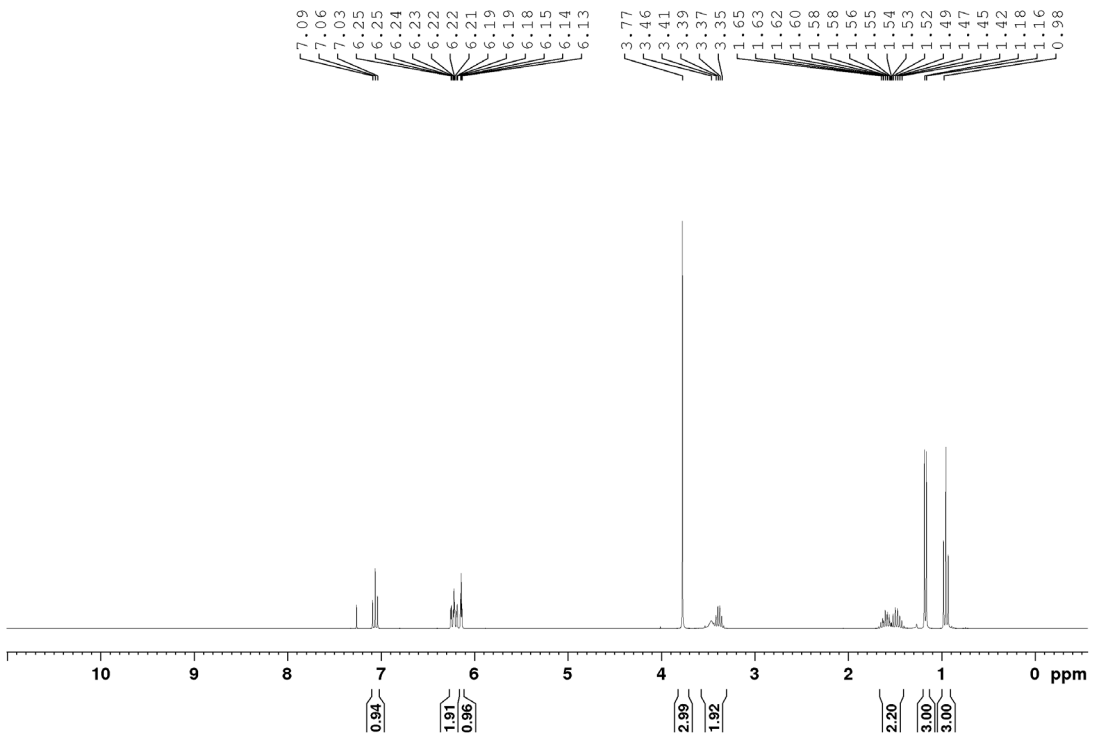

^{13}C{^{1}H} NMR Spectrum of **1.3b** ($CDCl_3$, 125.8 MHz)

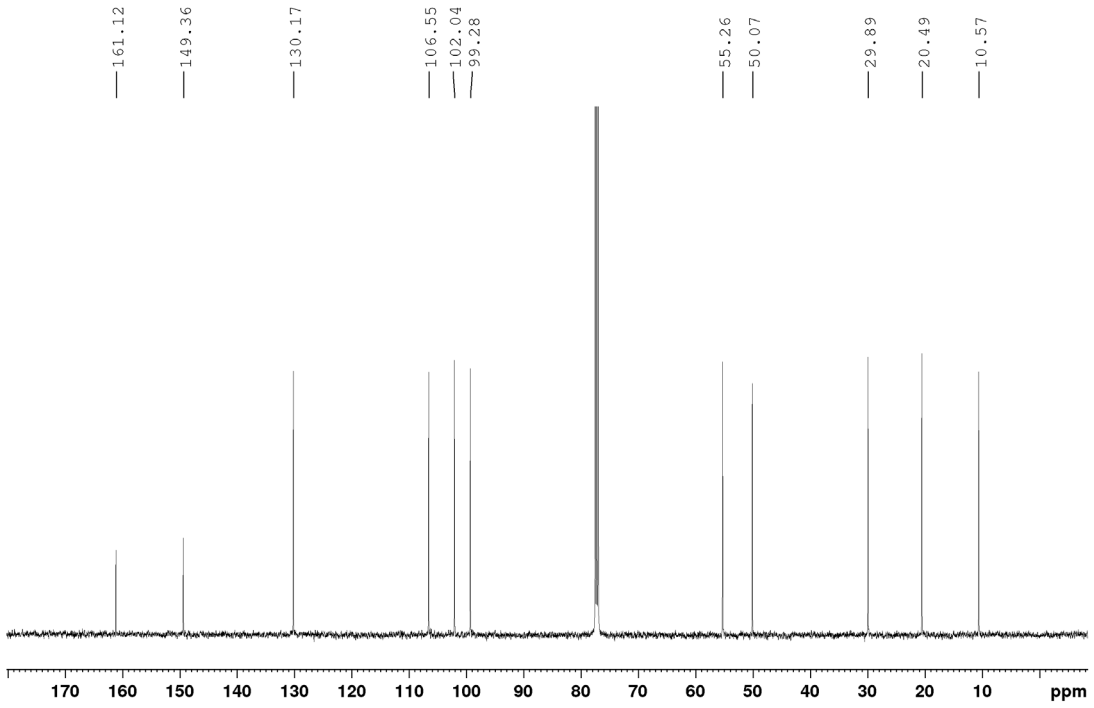

^{1}H NMR Spectrum of ***N-(sec-butyl)-4-methoxyaniline*, 1.3c** ($CDCl_3$, 300 MHz)

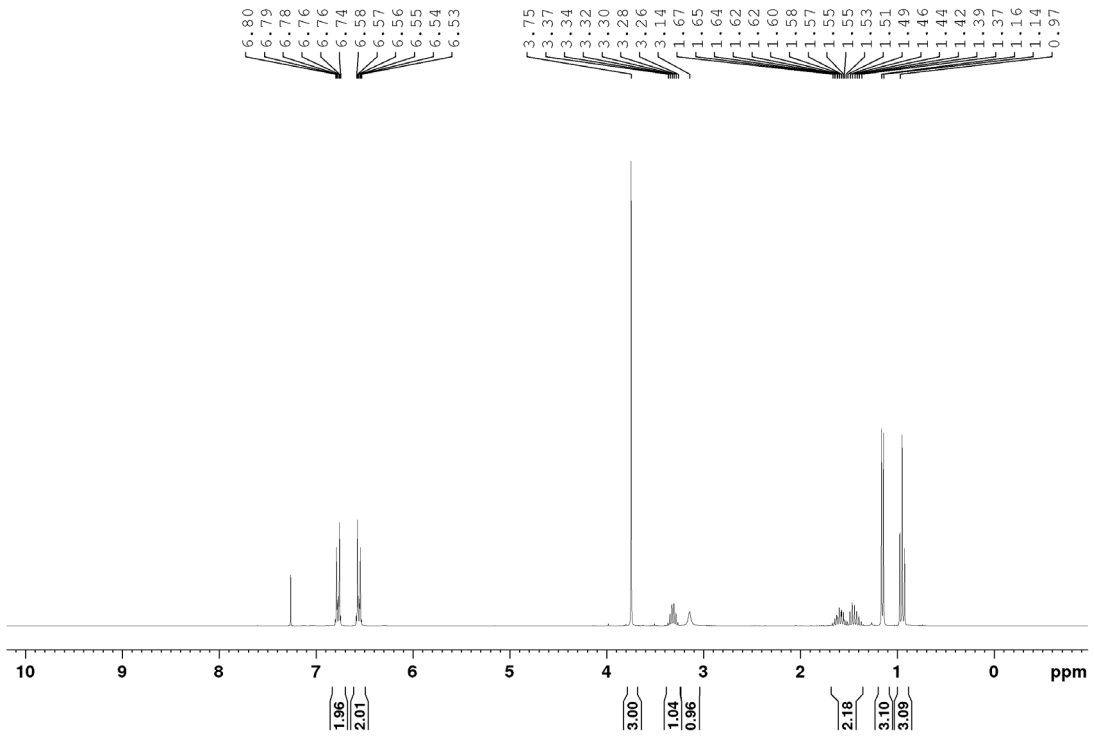

^{13}C{^{1}H} NMR Spectrum of **1.3c** ($CDCl_3$, 75.5 MHz)

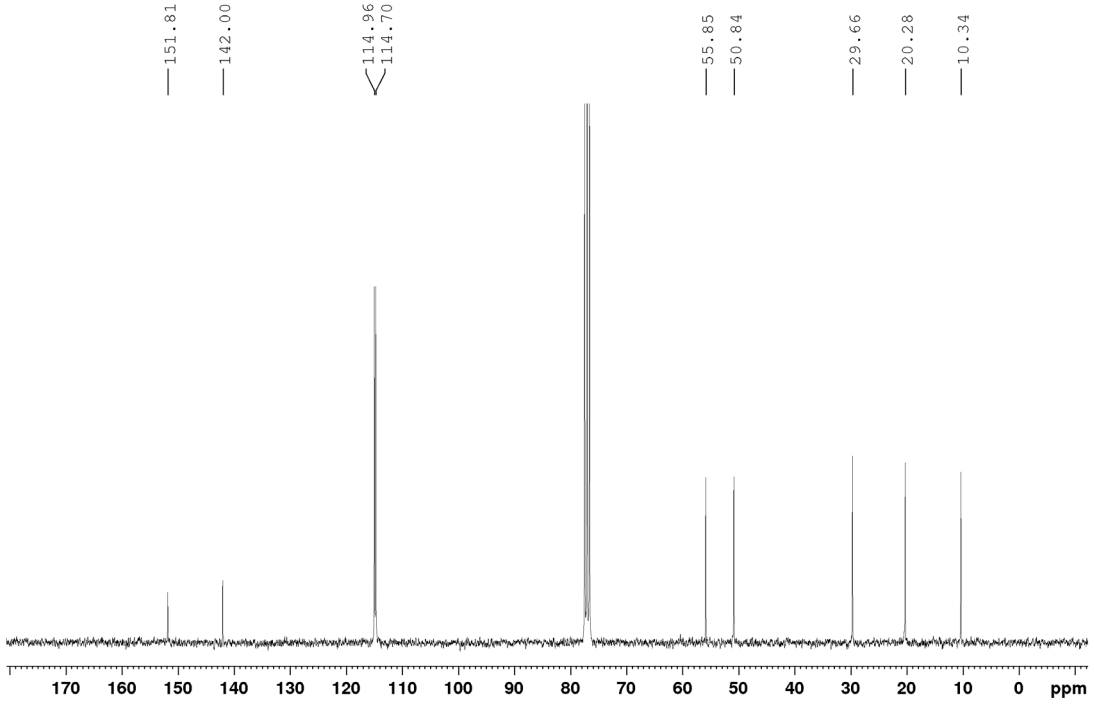

^{1}H NMR Spectrum of ***N-(sec-butyl)benzo[b]thiophen-5-amine***, **1.3d** ($CDCl_3$, 500 MHz)

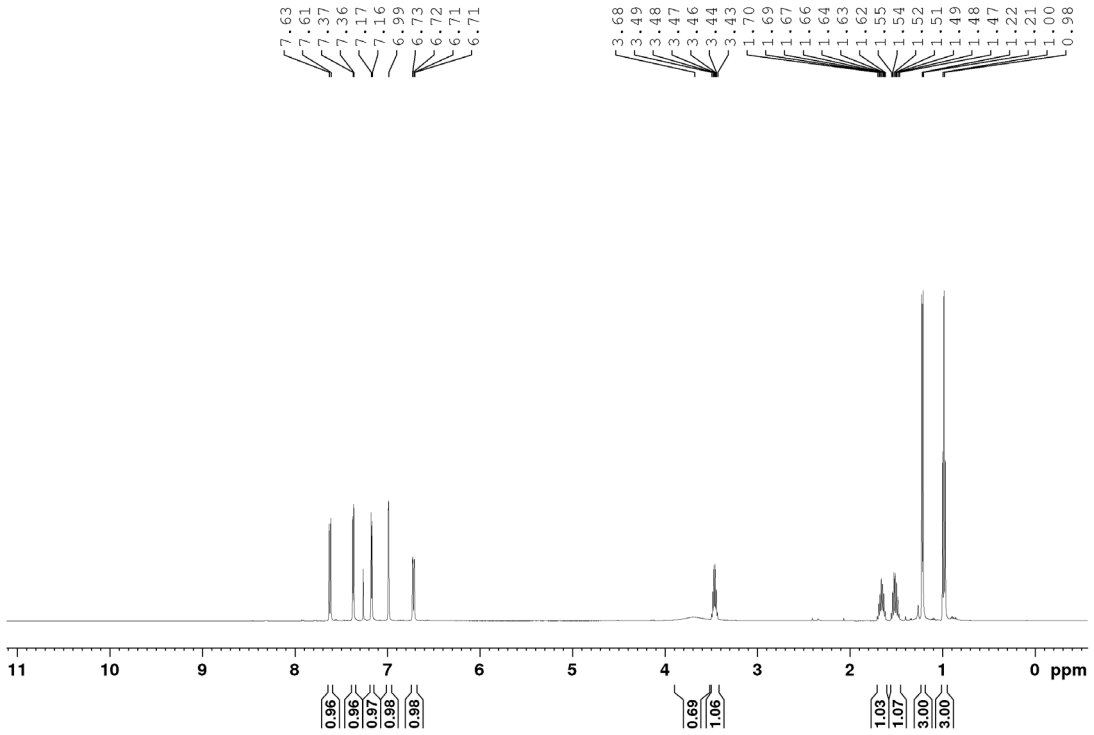

^{13}C{^{1}H} NMR Spectrum of **1.3d** ($CDCl_3$, 125.8 MHz)

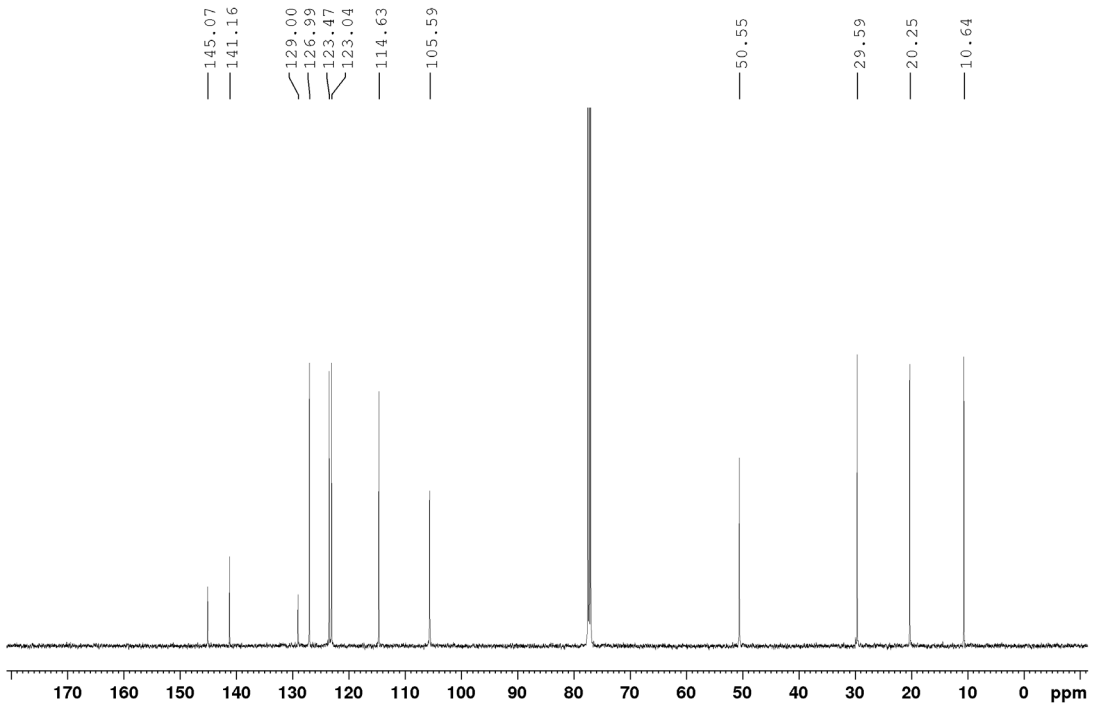

^{1}H NMR Spectrum of ***4-morpholinobenzonitrile*, 1.4a** ($CDCl_3$, 500 MHz)

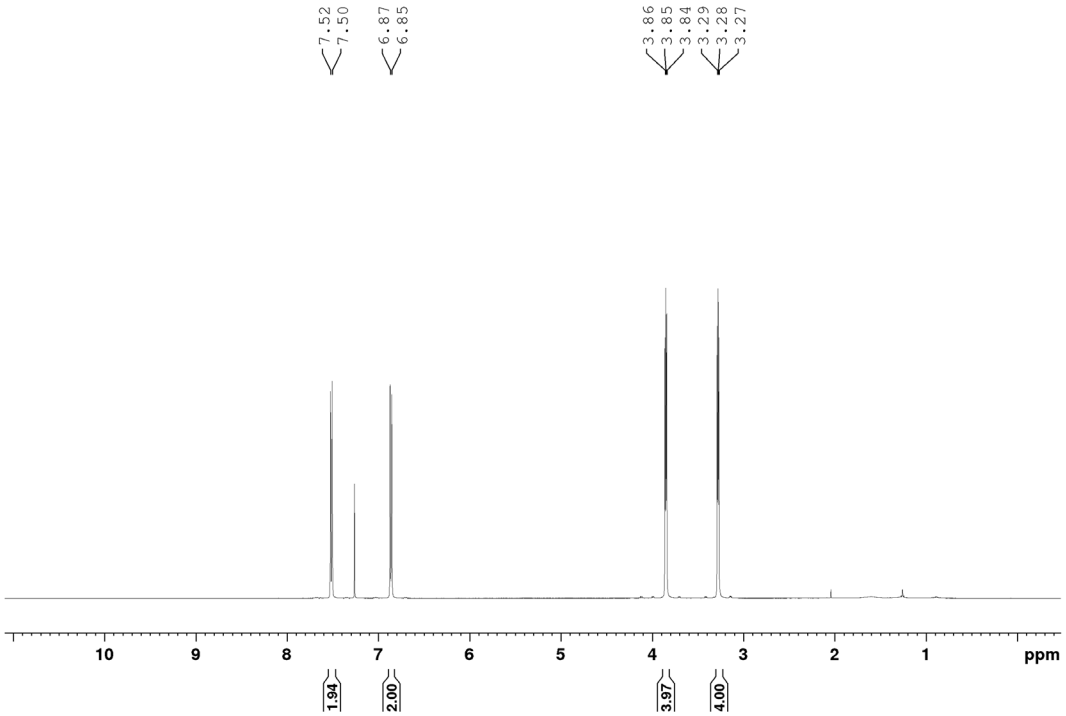

^{13}C{^{1}H} NMR Spectrum of **1.4a** ($CDCl_3$, 125.8 MHz)

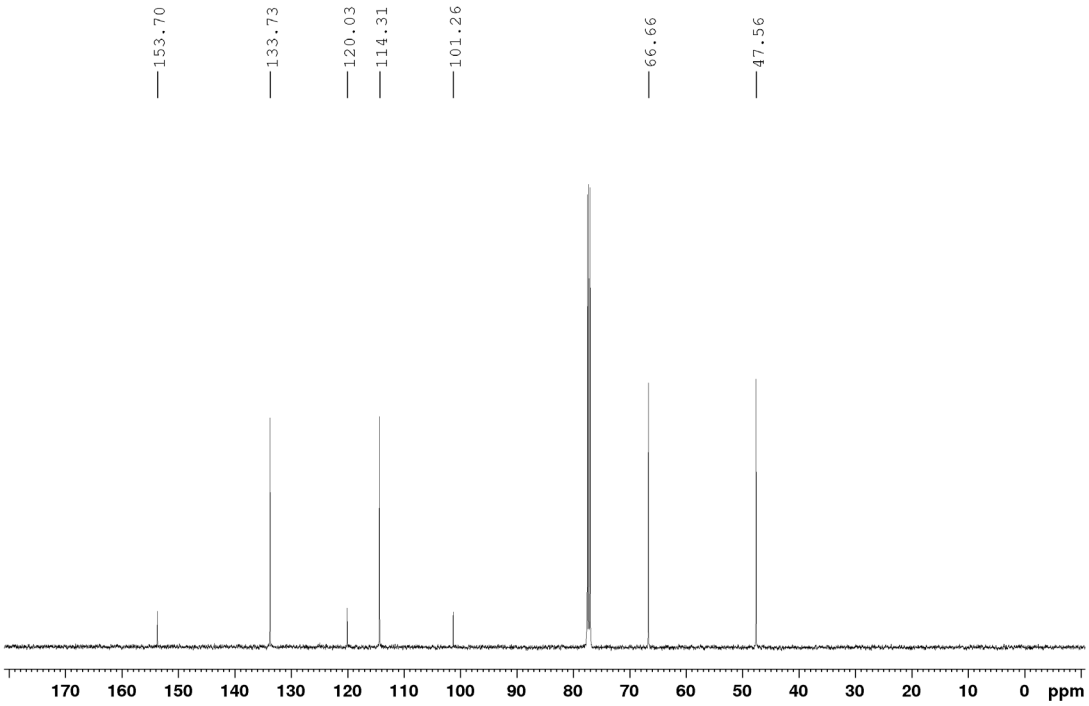

^{1}H NMR Spectrum of ***4-(benzo[b]thiophen-5-yl)morpholine*, 1.4b** ($CDCl_3$, 500 MHz)

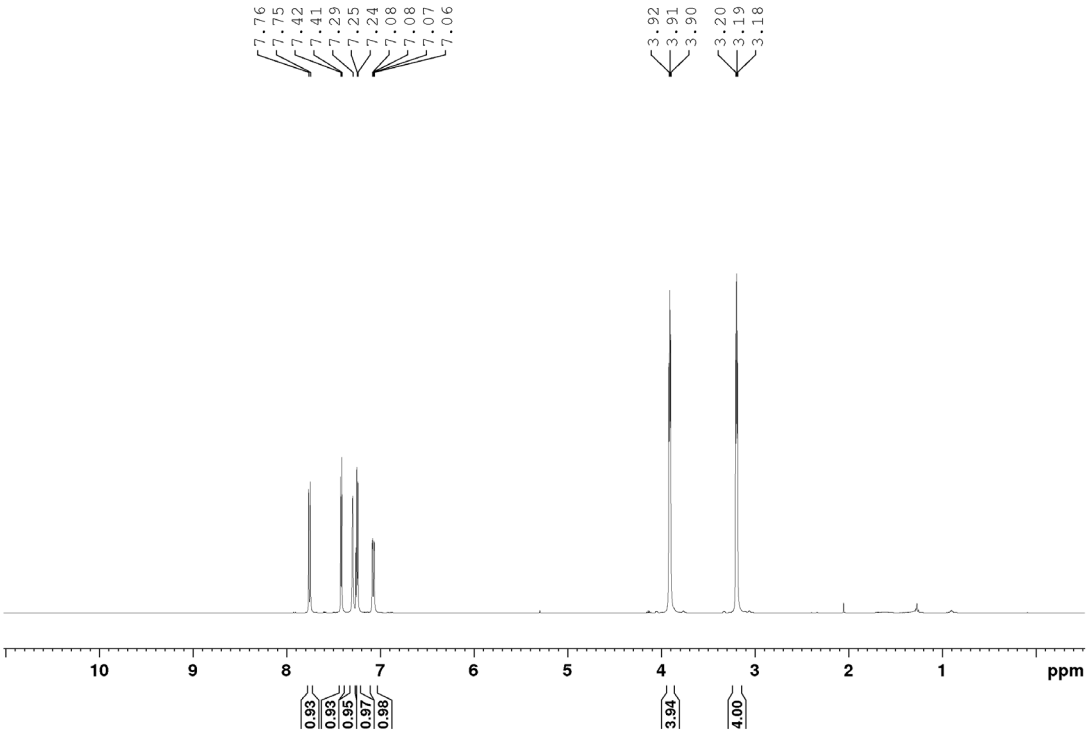

^{13}C{^{1}H} NMR Spectrum of **1.4b** ($CDCl_3$, 125.8 MHz)

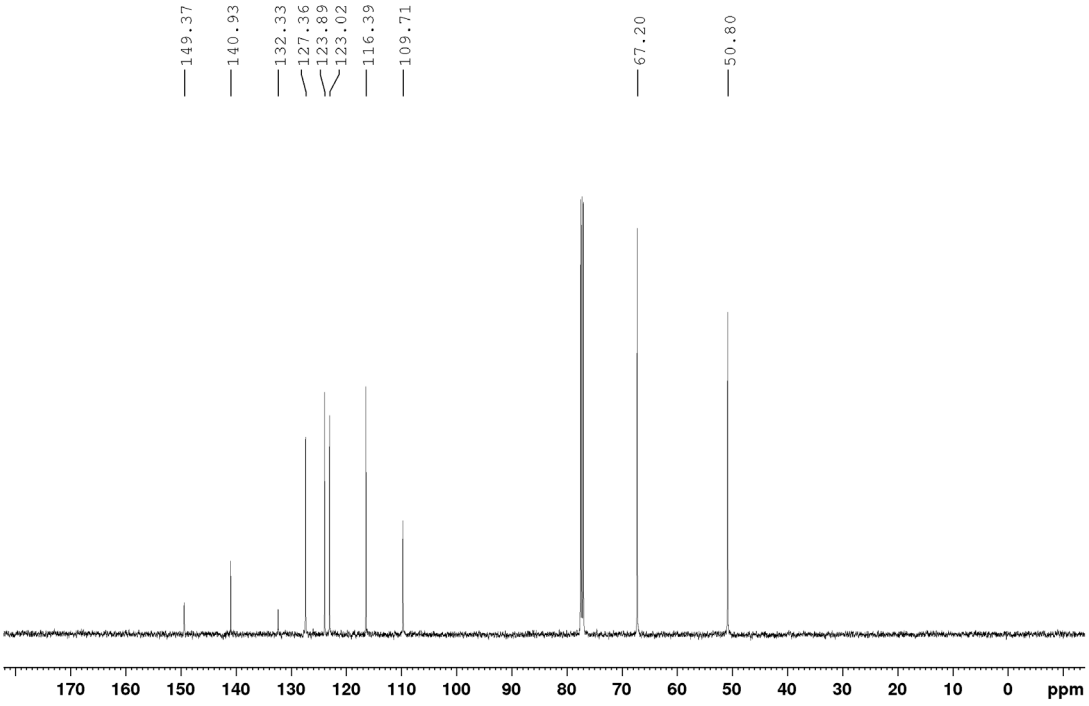

^{1}H NMR Spectrum of ***N-(furan-2-ylmethyl)-4-methylaniline,*** **1.5a** ($CDCl_3$, 500 MHz)

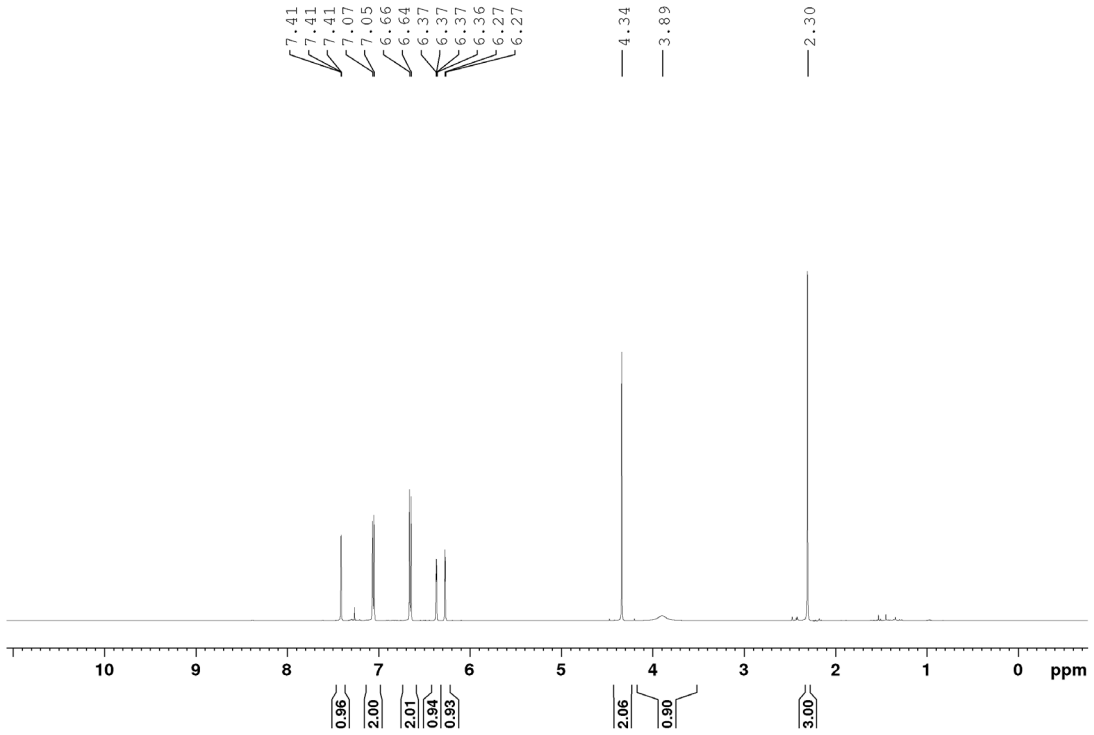

^{13}C{^{1}H} NMR Spectrum of **1.5a** ($CDCl_3$, 125.8 MHz)

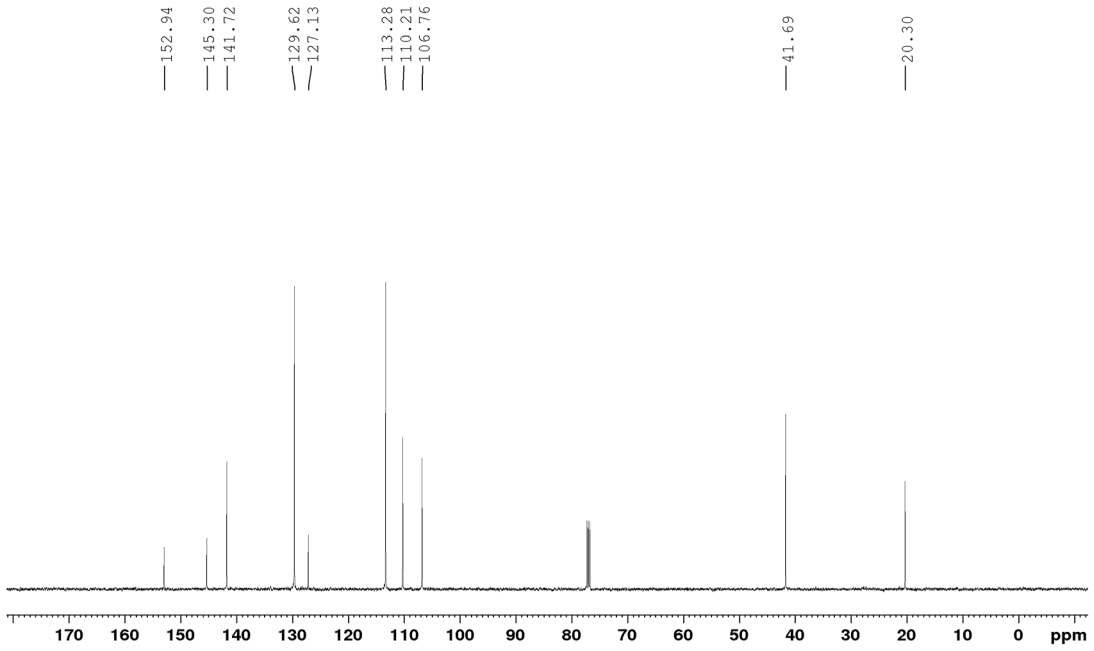

^{1}H NMR Spectrum of ***4-butyl-N-(furan-2-ylmethyl)aniline*, 1.5b** ($CDCl_3$, 500 MHz)

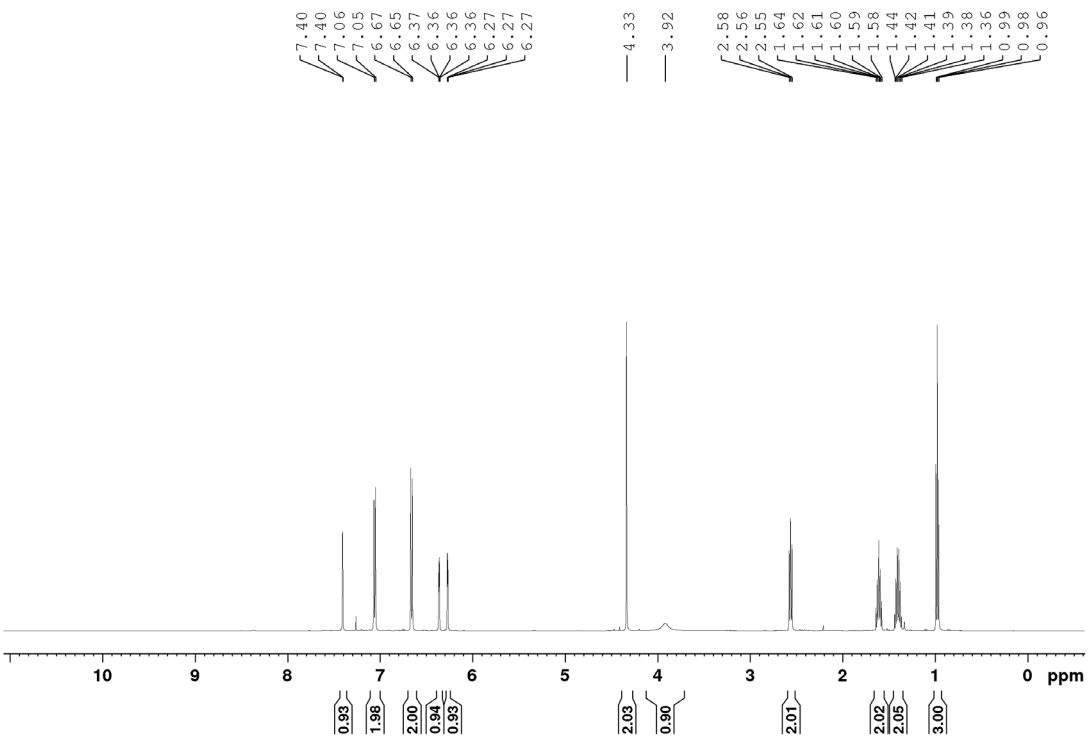

^{13}C{^{1}H} NMR Spectrum of **1.5b** ($CDCl_3$, 125.8 MHz)

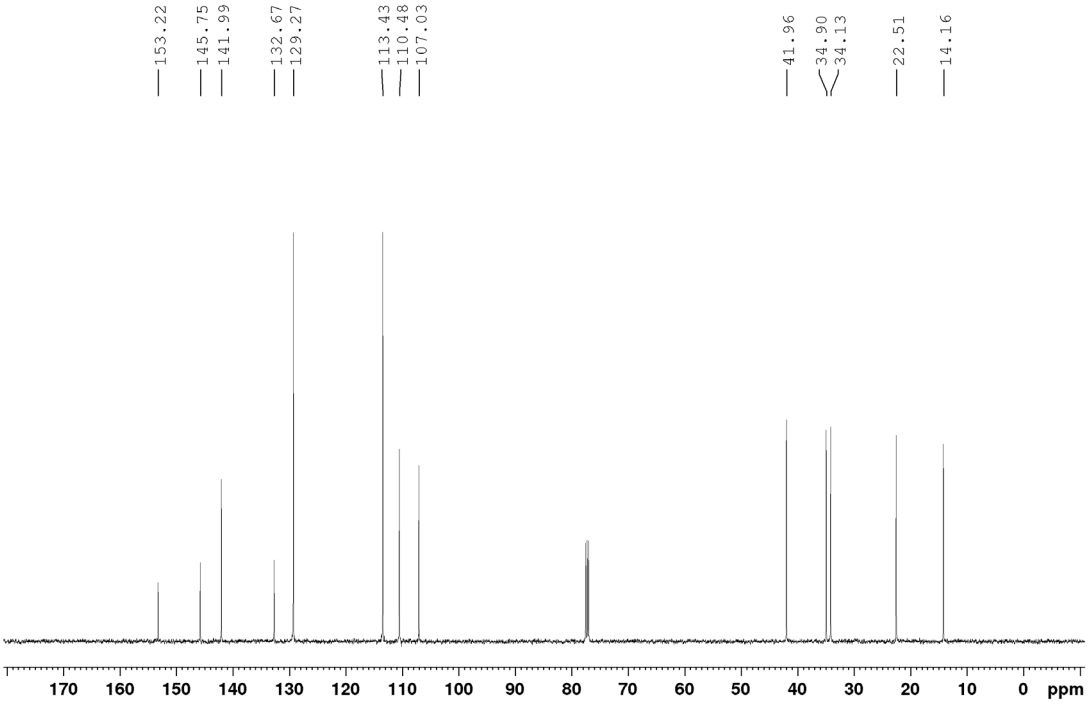

^{1}H NMR Spectrum of ***4-ethyl-N-(furan-2-ylmethyl)aniline*, 1.5c** ($CDCl_3$, 500 MHz)

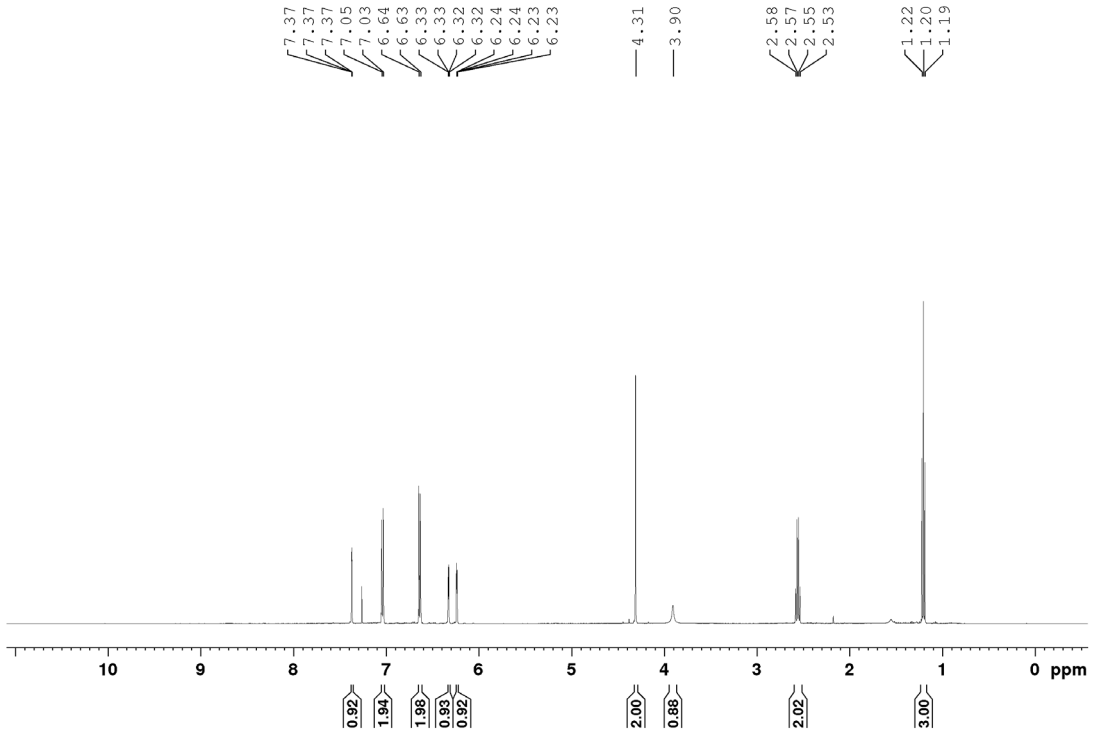

^{13}C{^{1}H} NMR Spectrum of **1.5c** ($CDCl_3$, 125.8 MHz)

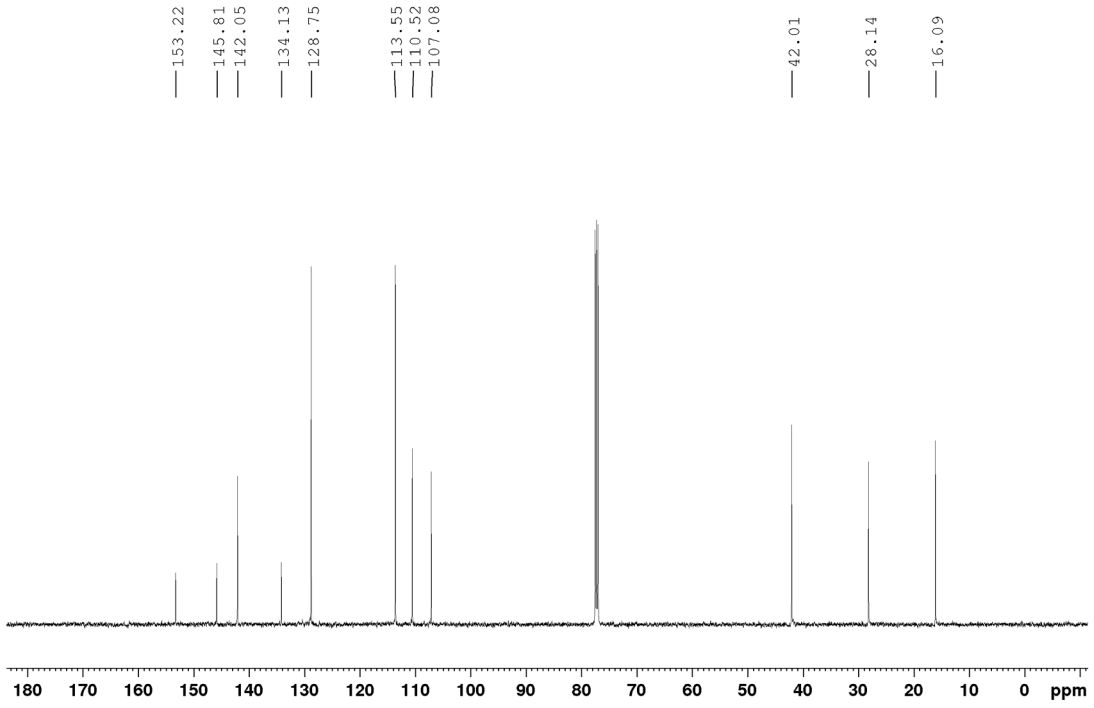

^{1}H NMR Spectrum of ***4-((furan-2-ylmethyl)amino)benzonitrile***, **2.1b** ($CDCl_3$, 500 MHz)

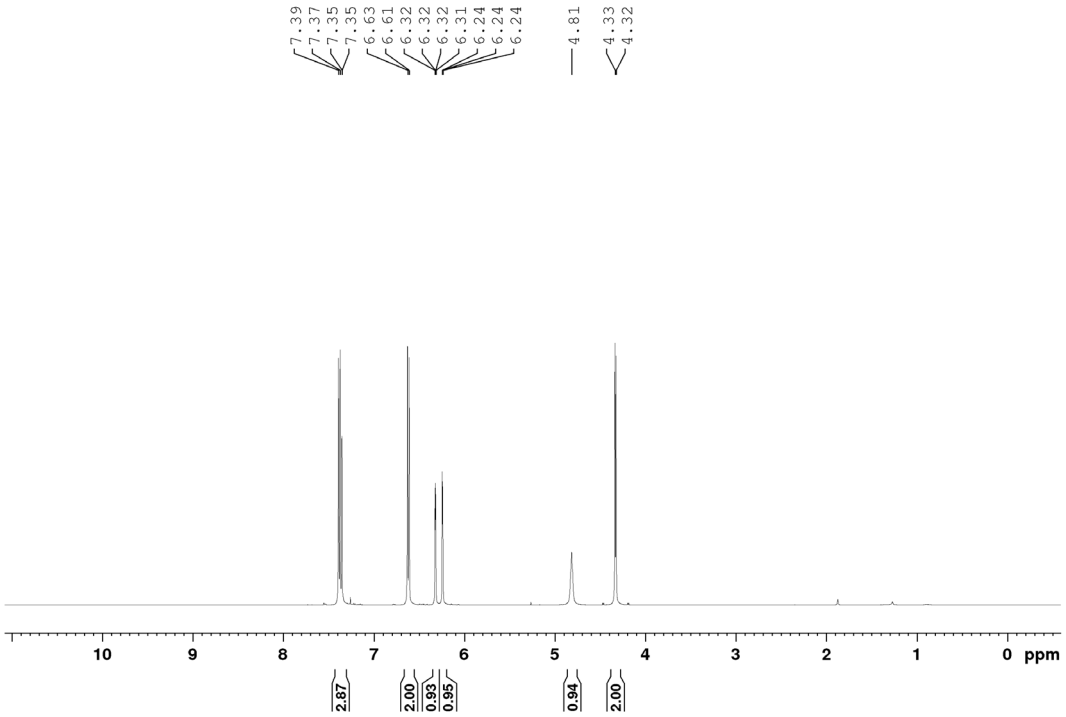

^{13}C{^{1}H} NMR Spectrum of **2.1b** ($CDCl_3$, 125.8 MHz)

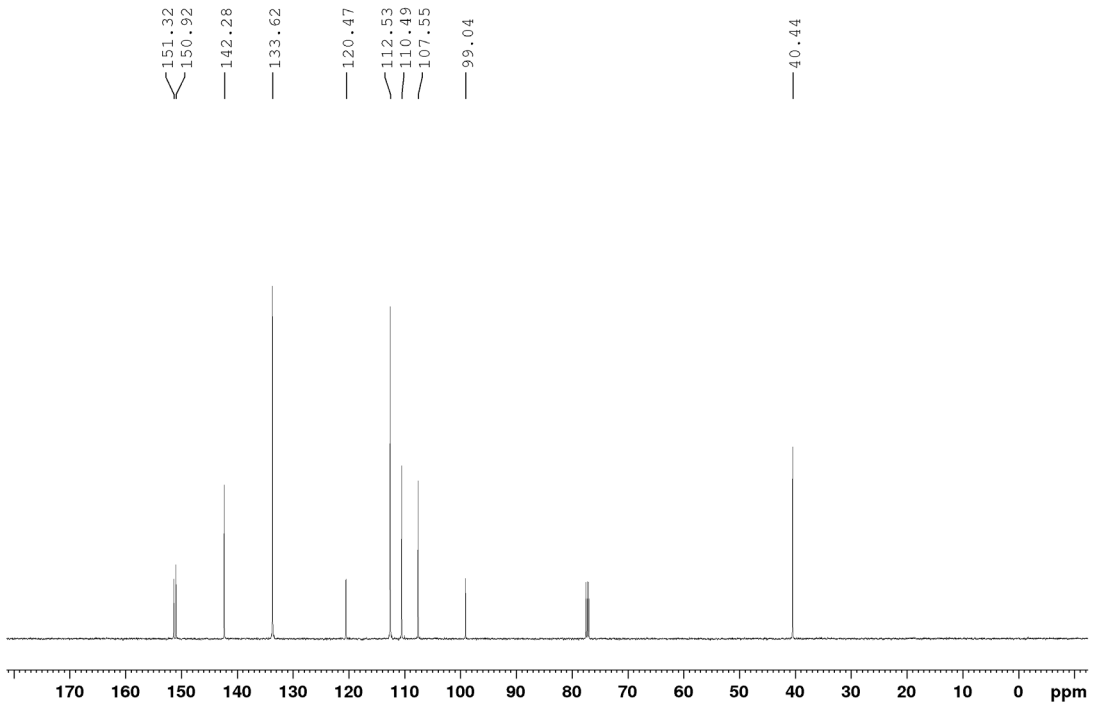

^{1}H NMR Spectrum of ***N-(furan-2-ylmethyl)-2-methylquinolin-4-amine***, **2.1e** ($CDCl_3$, 500 MHz)

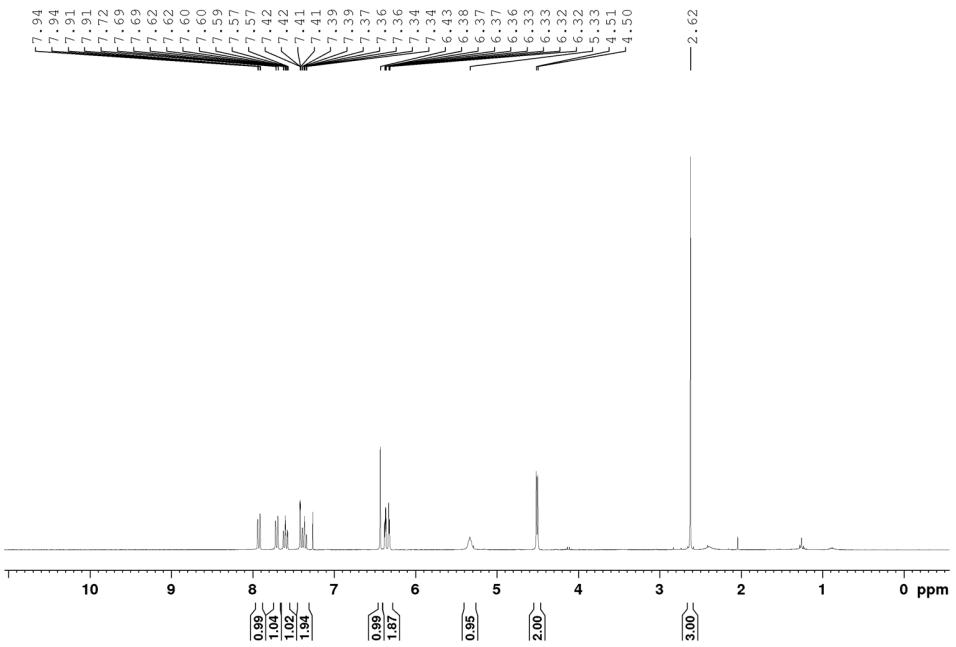

^{13}C{^{1}H} NMR of **2.1e** ($CDCl_3$, 125.8 MHz)

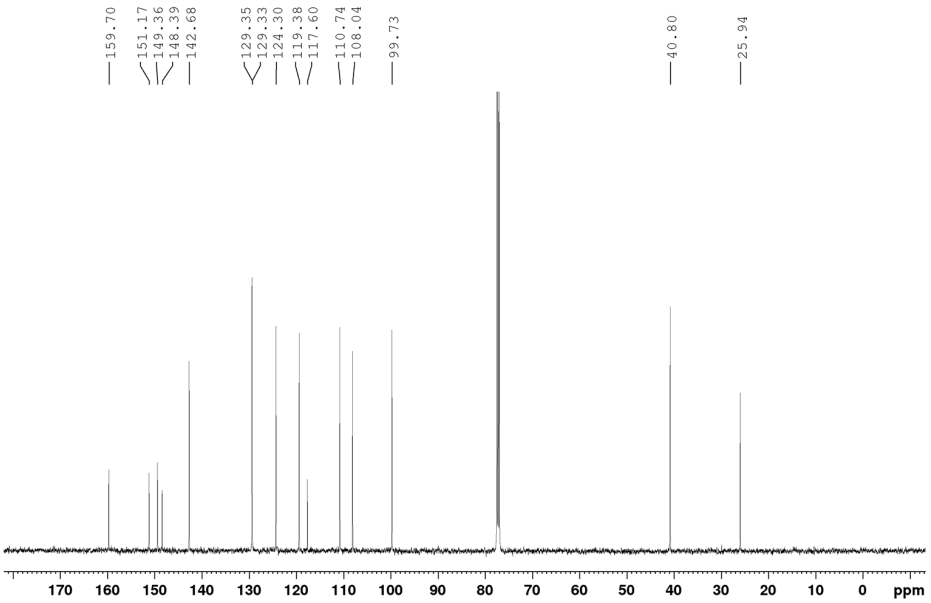

^{1}H NMR Spectrum of ***N-(furan-2-ylmethyl)-2,5-dimethylaniline***, **2.1f** ($CDCl_3$, 300 MHz)

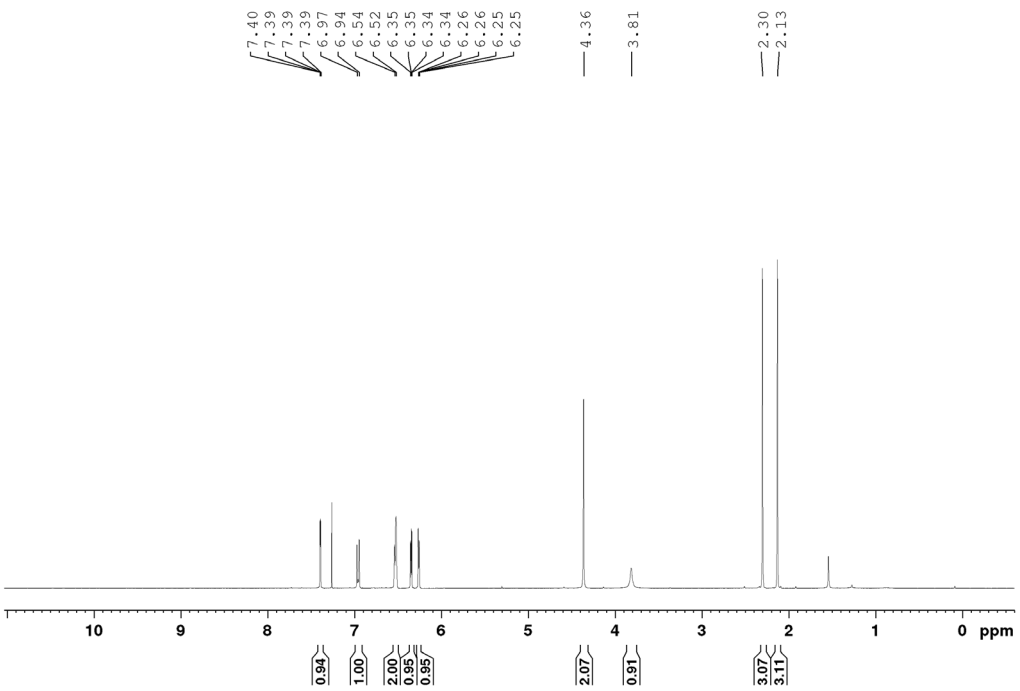

^{13}C{^{1}H} NMR Spectrum of **2.1f** ($CDCl_3$, 125.8 MHz)

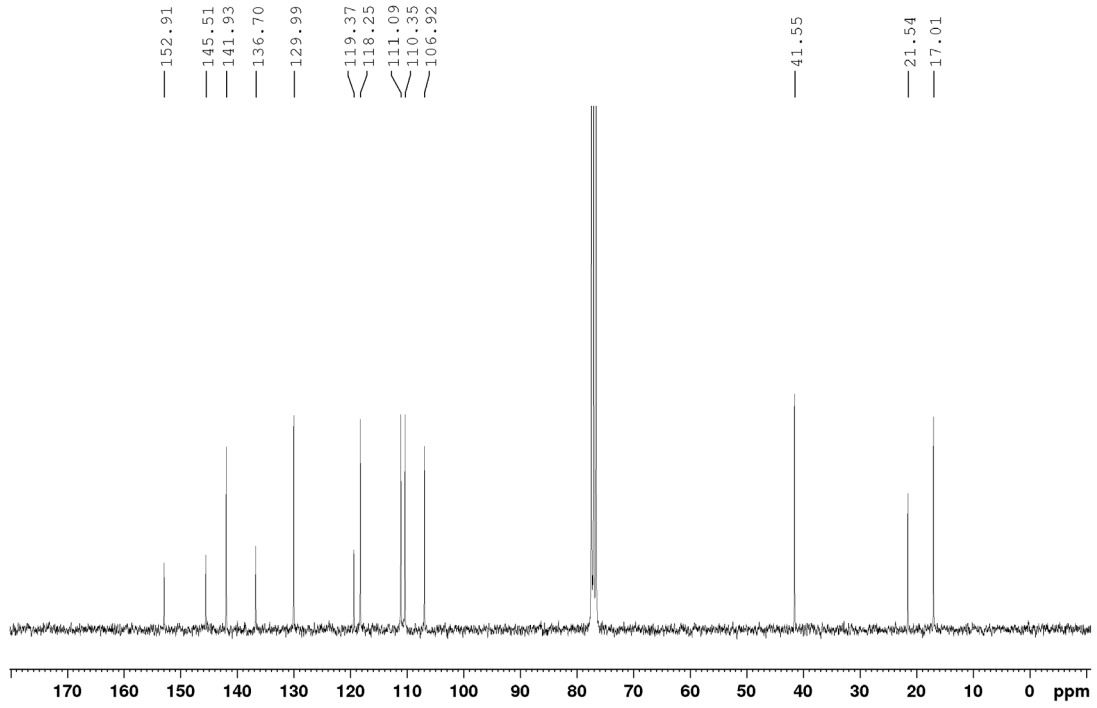

^{1}H NMR Spectrum of ***4-(naphthalen-1-yl)morpholine***, **2.2a** (CDCl3, 500 MHz)

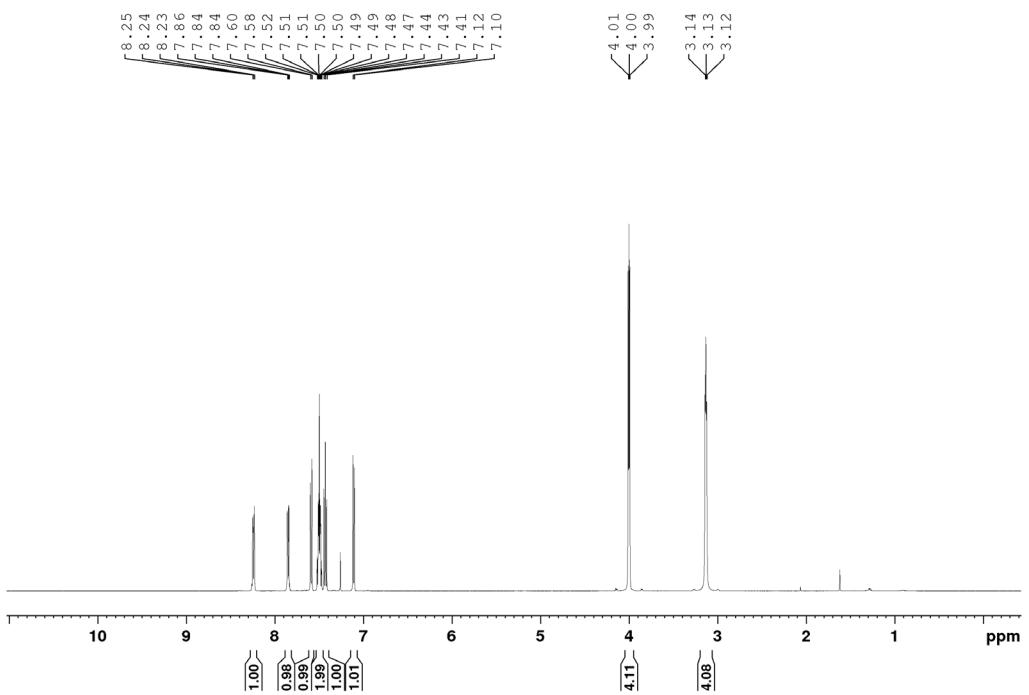

^{13}C{^{1}H} NMR Spectrum of **2.2a** ($CDCl_3$, 500 MHz)

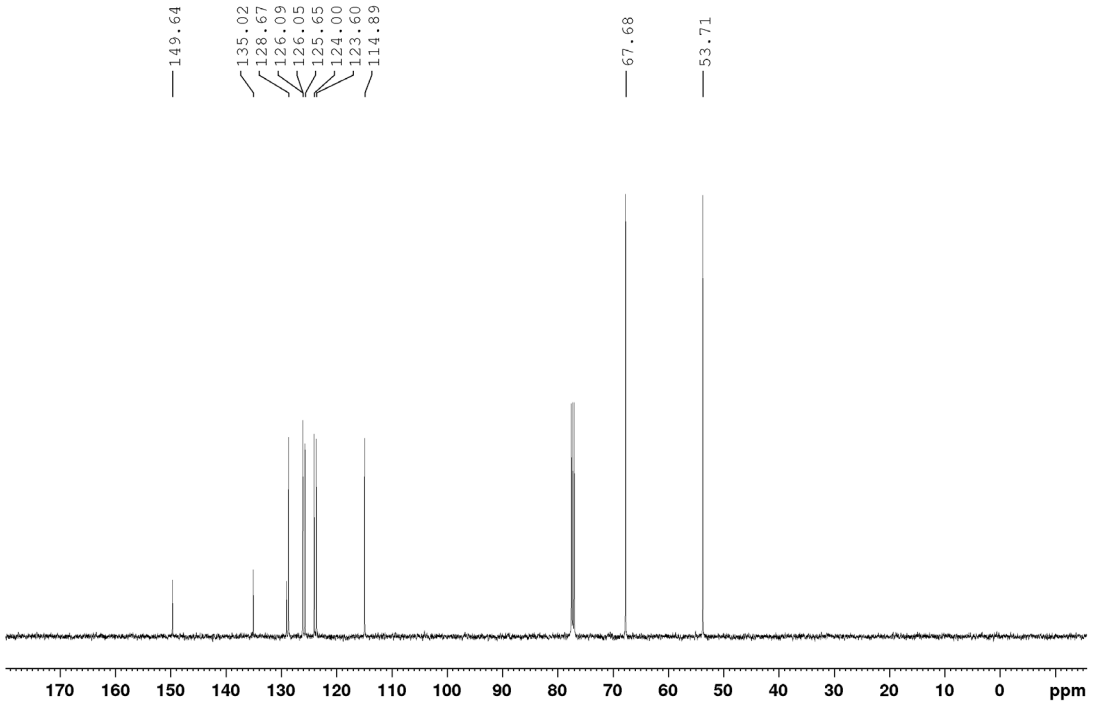

^{1}H NMR Spectrum ***4-(3-methoxyphenyl)morpholine***, **2.2c** ($CDCl_3$, 300 MHz)

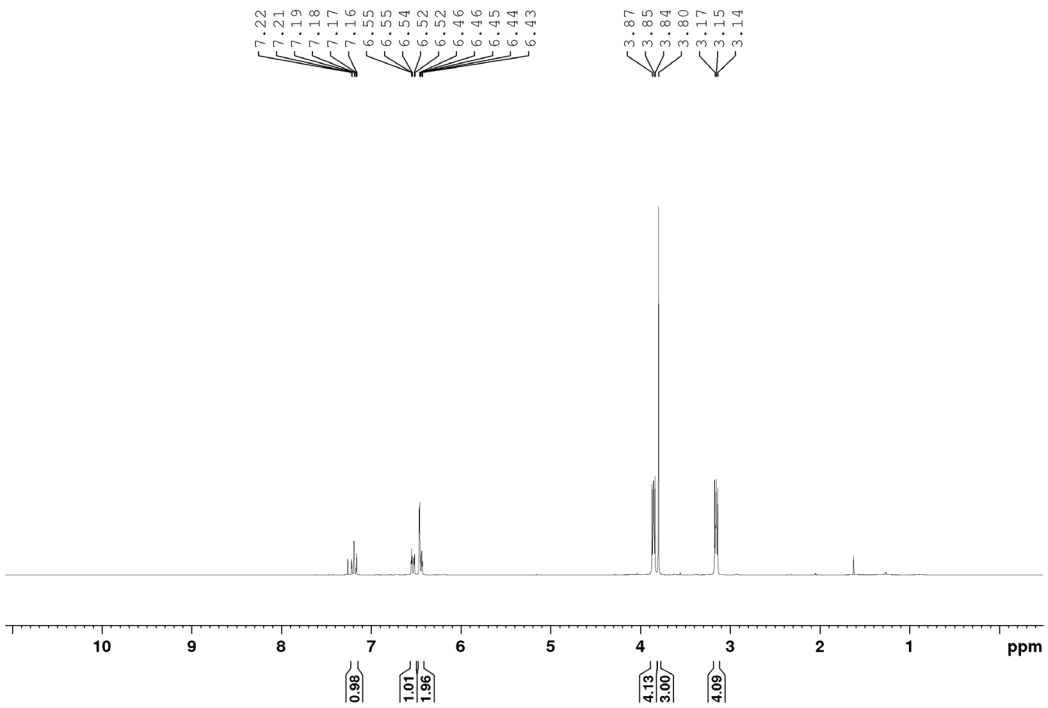

^{13}C{^{1}H} NMR Spectrum **2.2c** ($CDCl_3$, 75.5 MHz)

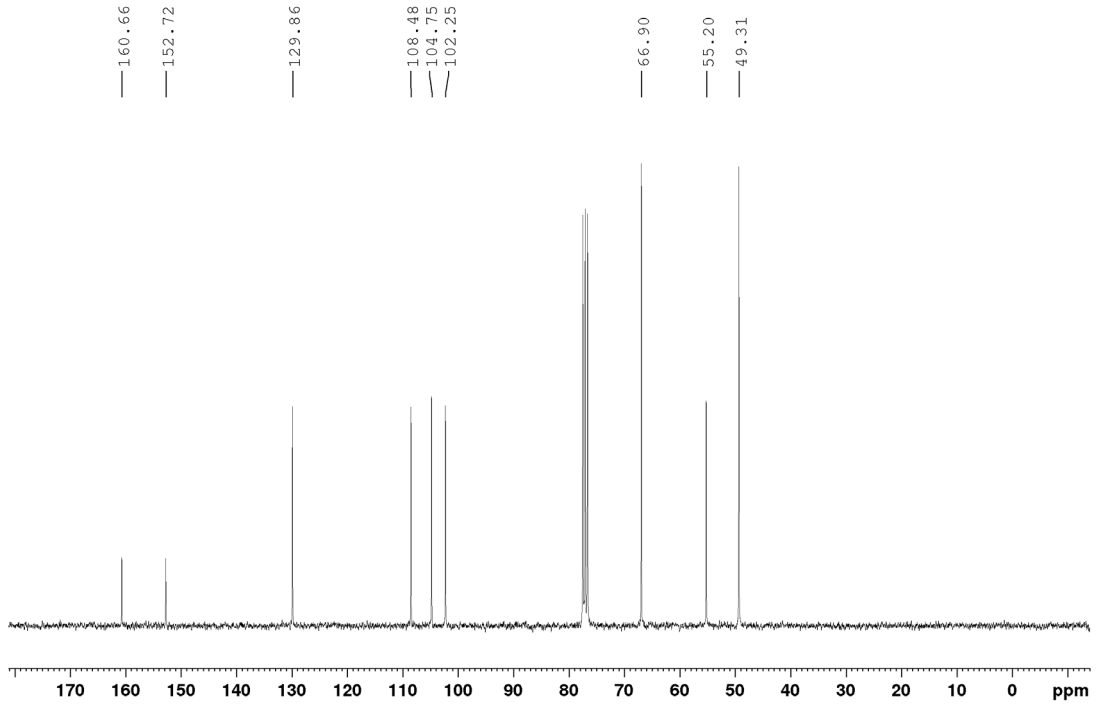

^{1}H NMR Spectrum of ***4-(2-methylquinolin-4-yl)morpholine***, **2.2e** ($CDCl_3$, 300 MHz)

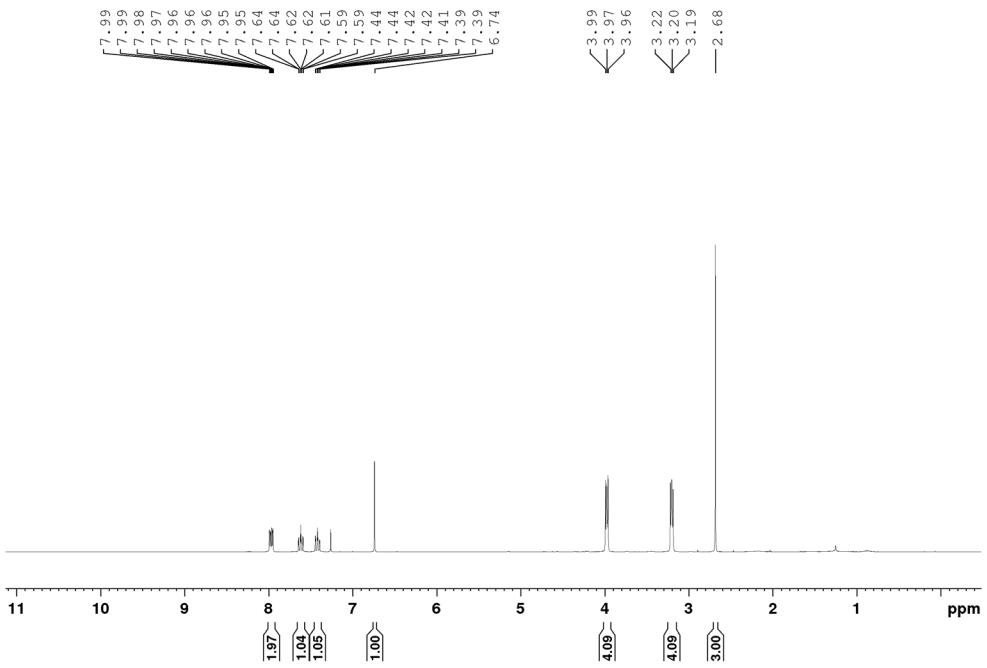

^{13}C{^{1}H} NMR Spectrum of **2.2e** ($CDCl_3$, 75.5 MHz)

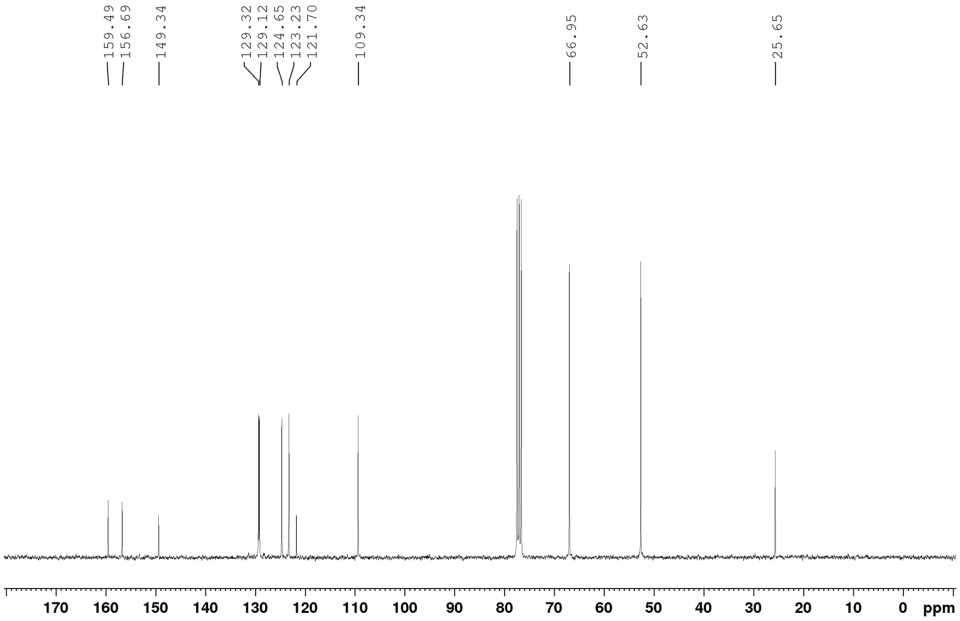

^{1}H NMR Spectrum of ***4-(4-(tert-butyl)phenyl)morpholine***, **2.2f** ($CDCl_3$, 500 MHz)

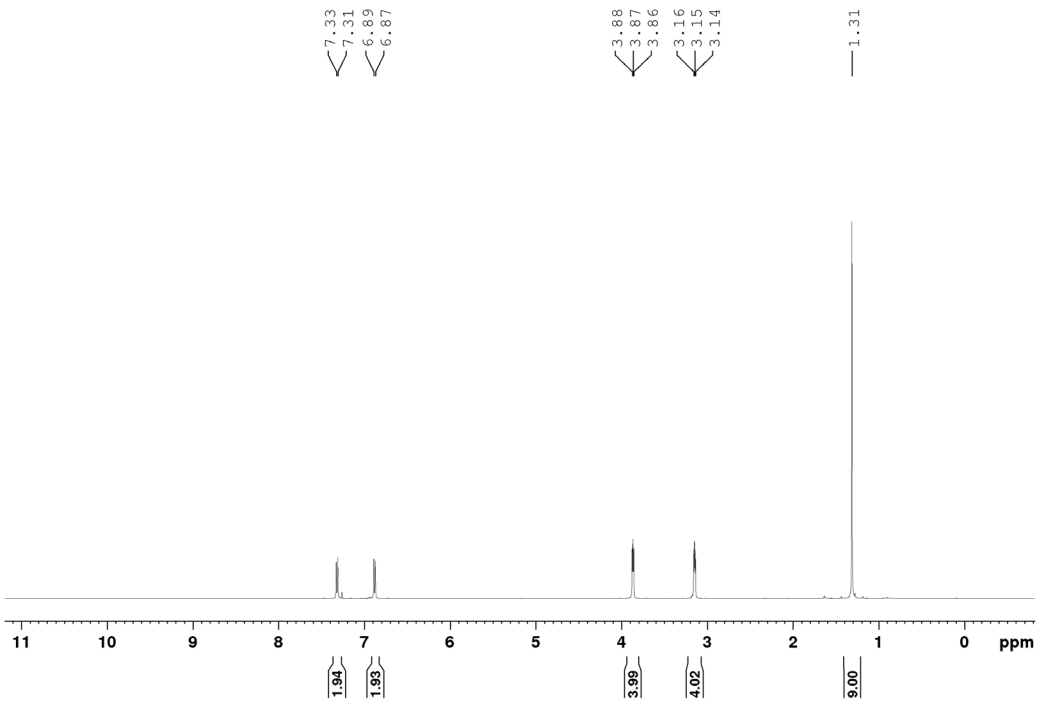

^{13}C{^{1}H} NMR Spectrum of **2.2f** ($CDCl_3$, 125.8 MHz)

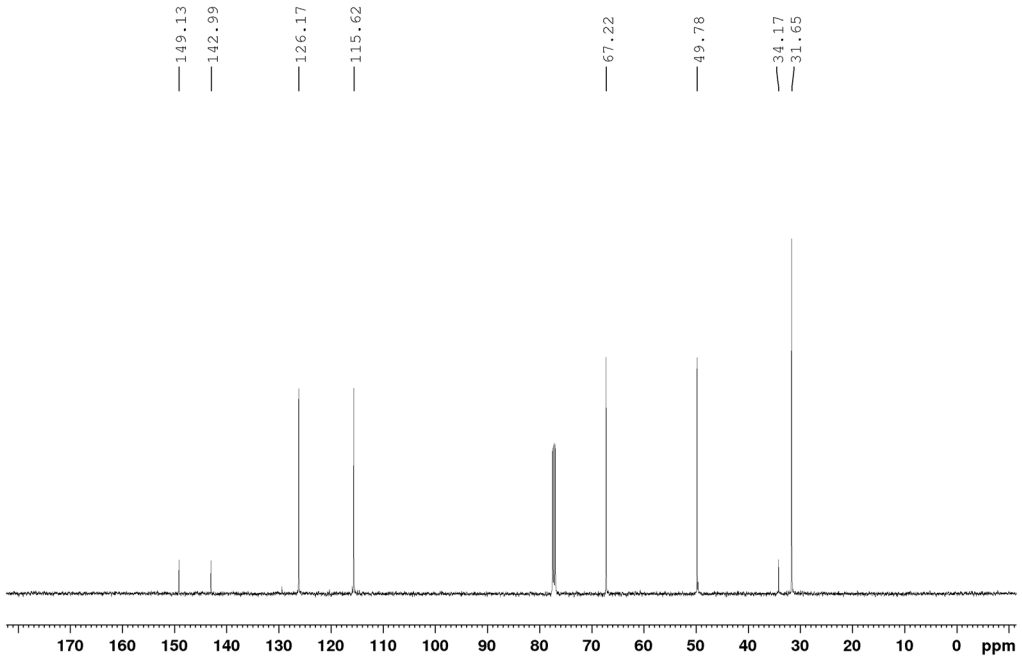

^{1}H NMR Spectrum of ***4-(2,5-dimethylphenyl)morpholine***, **2.2g** ($CDCl_3$, 300 MHz)

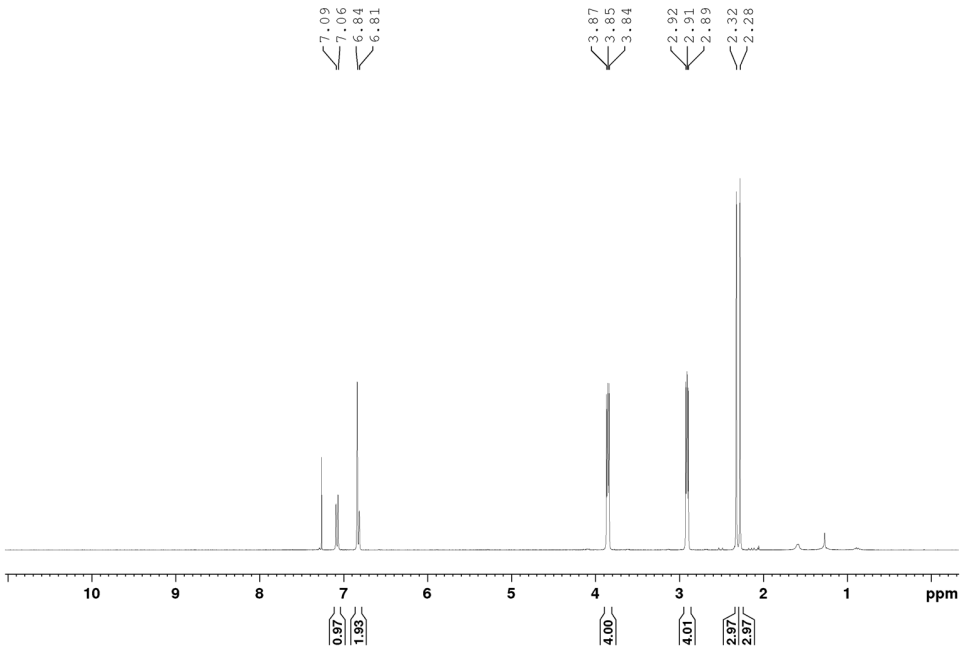

^{13}C{^{1}H} NMR Spectrum of **2.2g** ($CDCl_3$, 125.8 MHz)

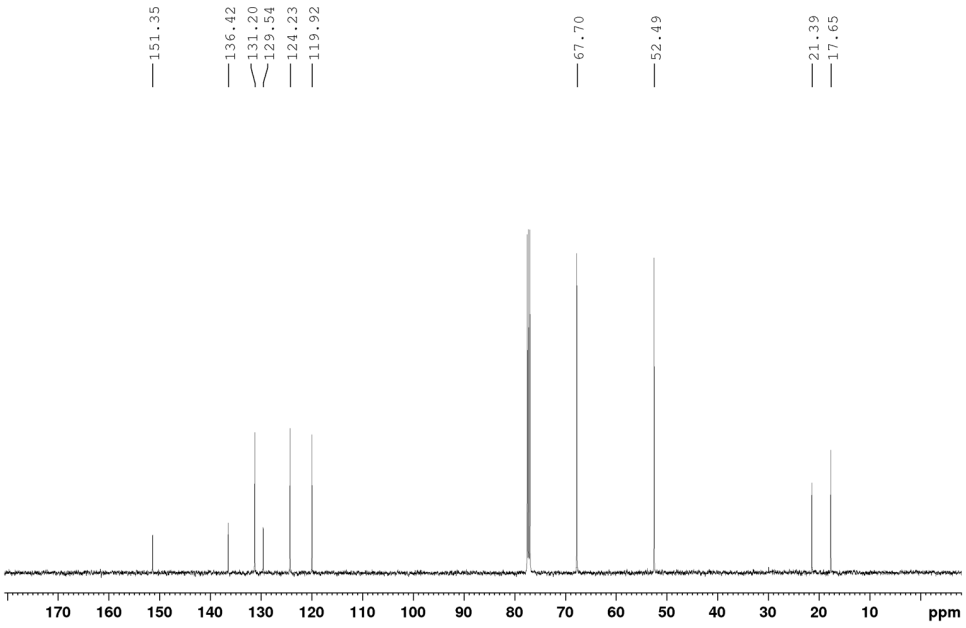

^{1}H NMR Spectrum of ***4-(4-methoxyphenyl)morpholine***, **2.2h** ($CDCl_3$, 300 MHz)

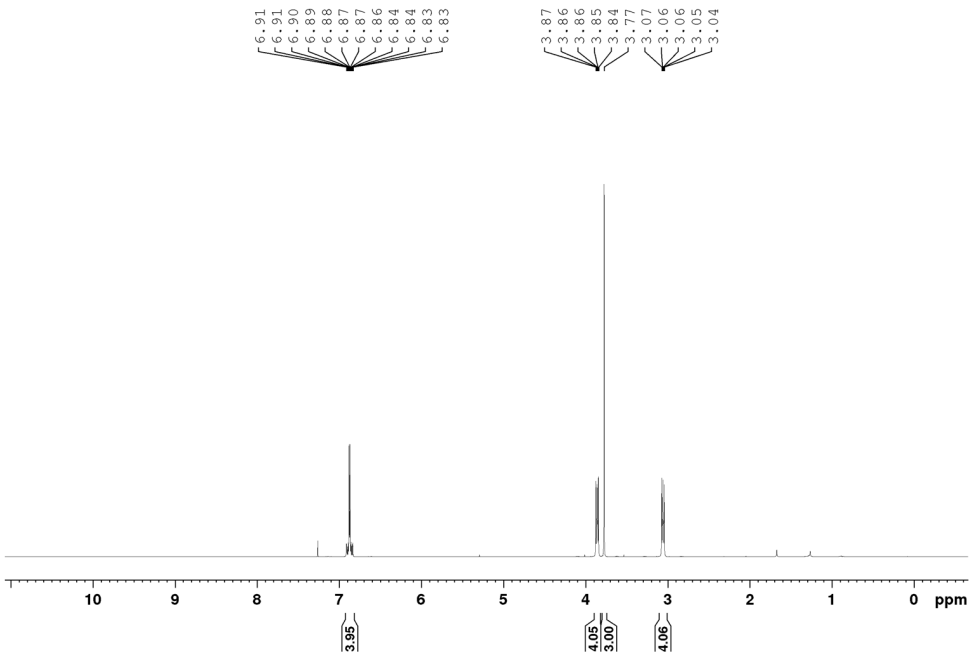

^{13}C{^{1}H} NMR Spectrum of **2.2h** ($CDCl_3$, 75.5 MHz)

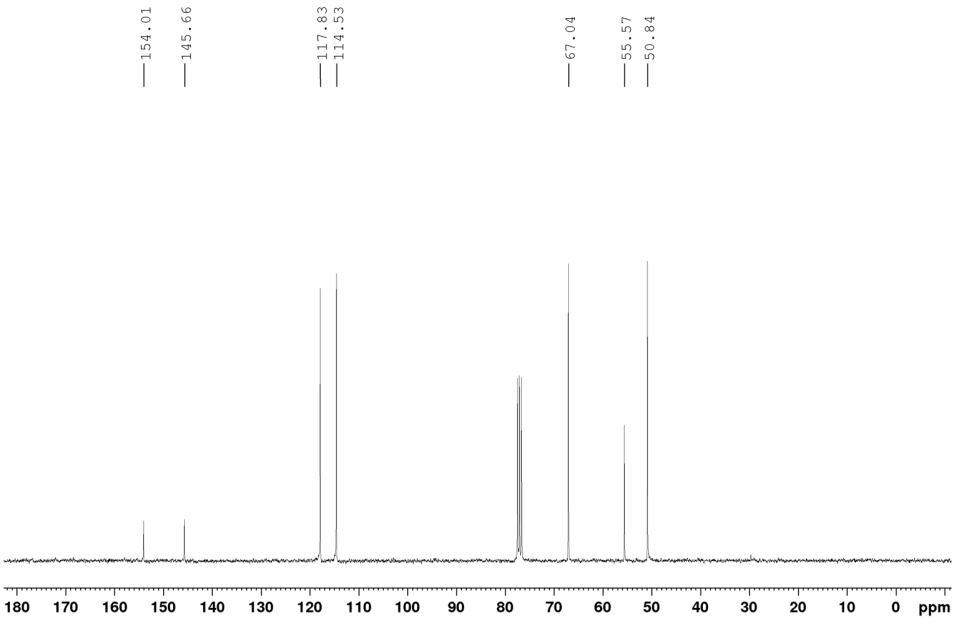

^{1}H NMR Spectrum of ***1-(naphthalen-1-yl)-1H-indole***, **2.3a** ($CDCl_3$, 500 MHz)

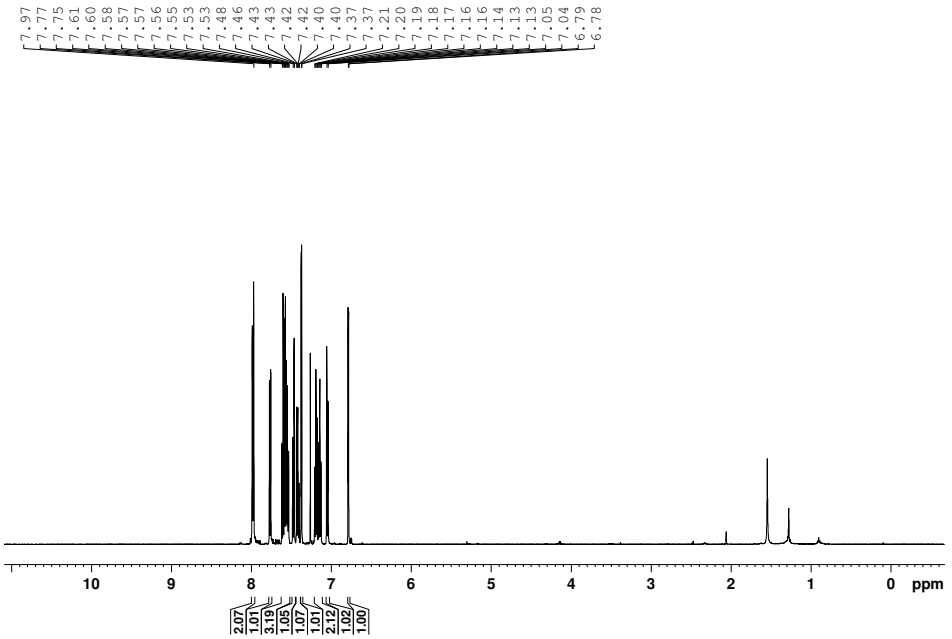

^{13}C{^{1}H} NMR Spectrum of **2.3a** ($CDCl_3$, 125.8 MHz)

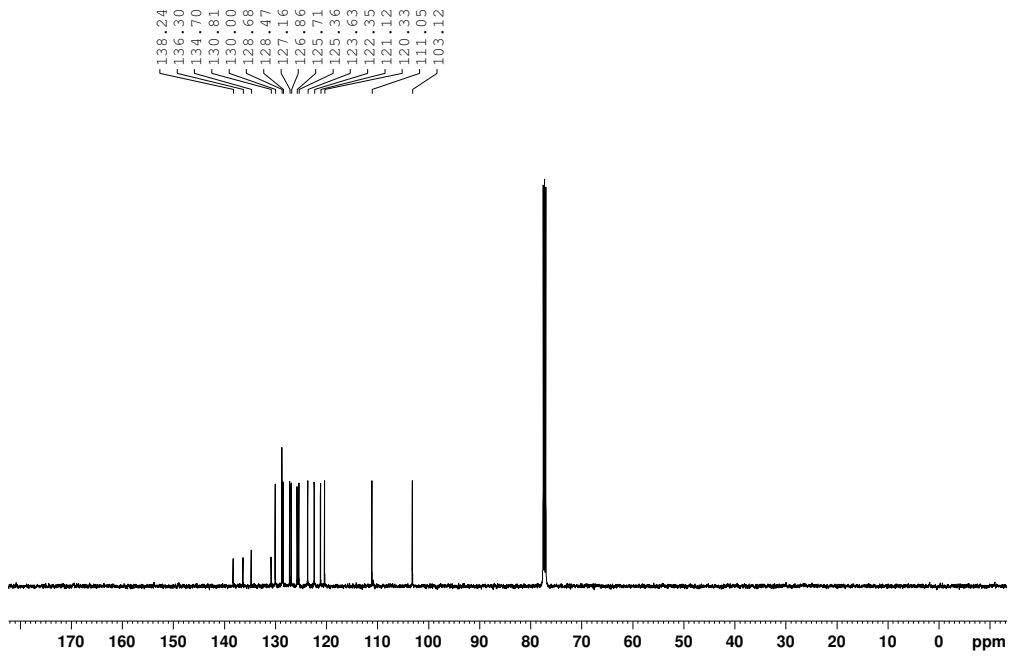

^{1}H NMR Spectrum of ***4-(1H-indol-1-yl)benzonitrile***, **2.3b** ($CDCl_3$, 500 MHz)

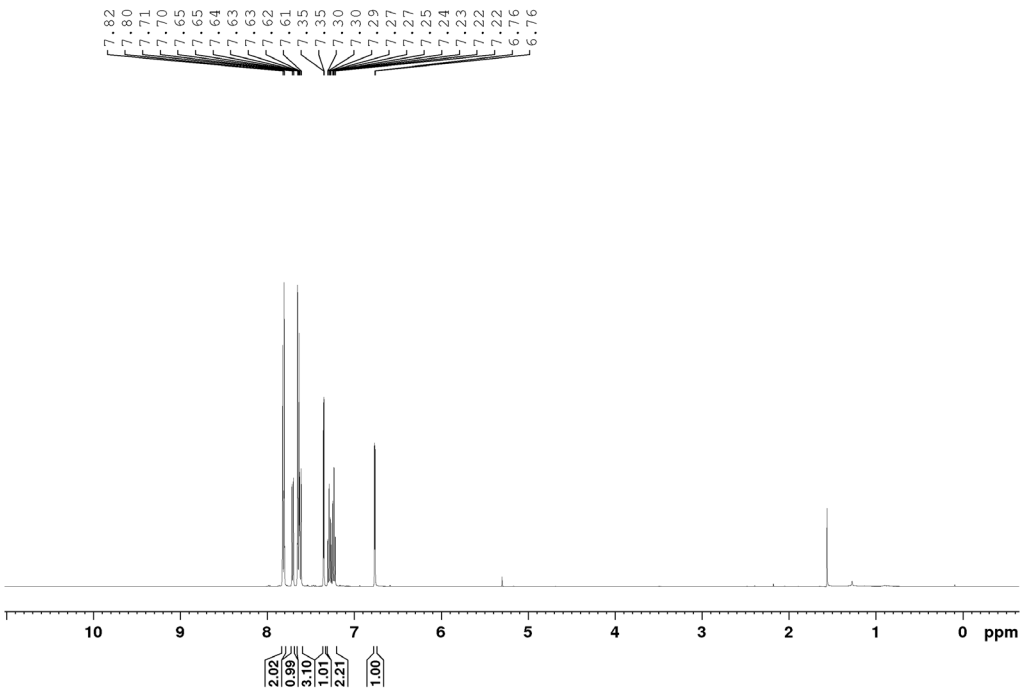

^{13}C{^{1}H} NMR Spectrum of **2.3b** ($CDCl_3$, 125.8 MHz)

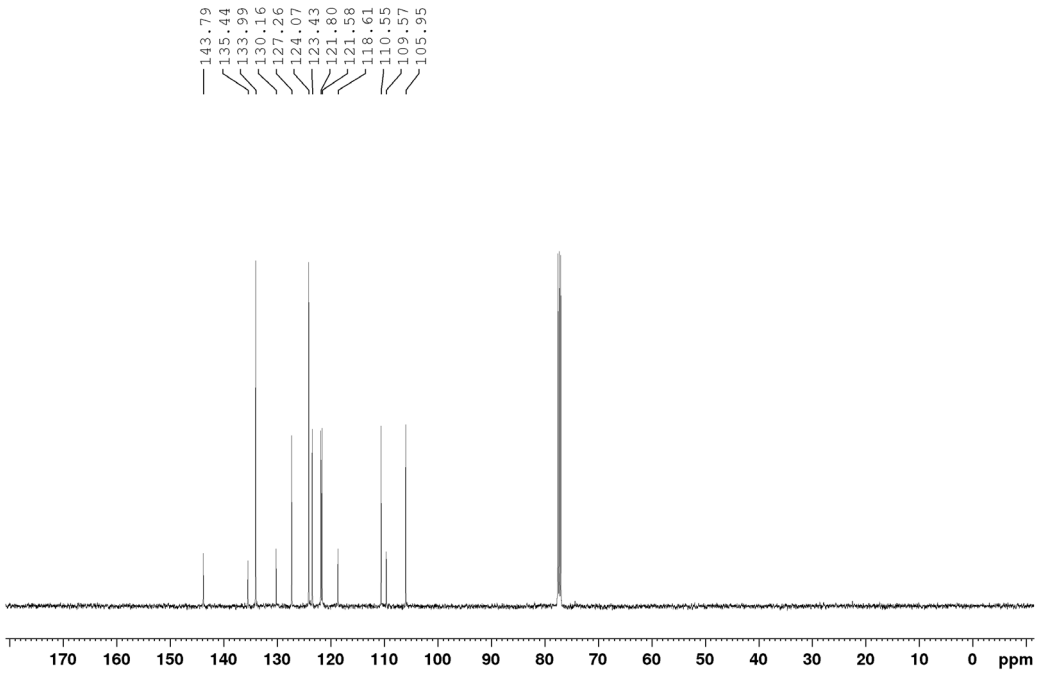

^{1}H NMR Spectrum of ***1-(benzo[b]thiophen-5-yl)-1H-indole***, **2.3d** ($CDCl_3$, 500 MHz)

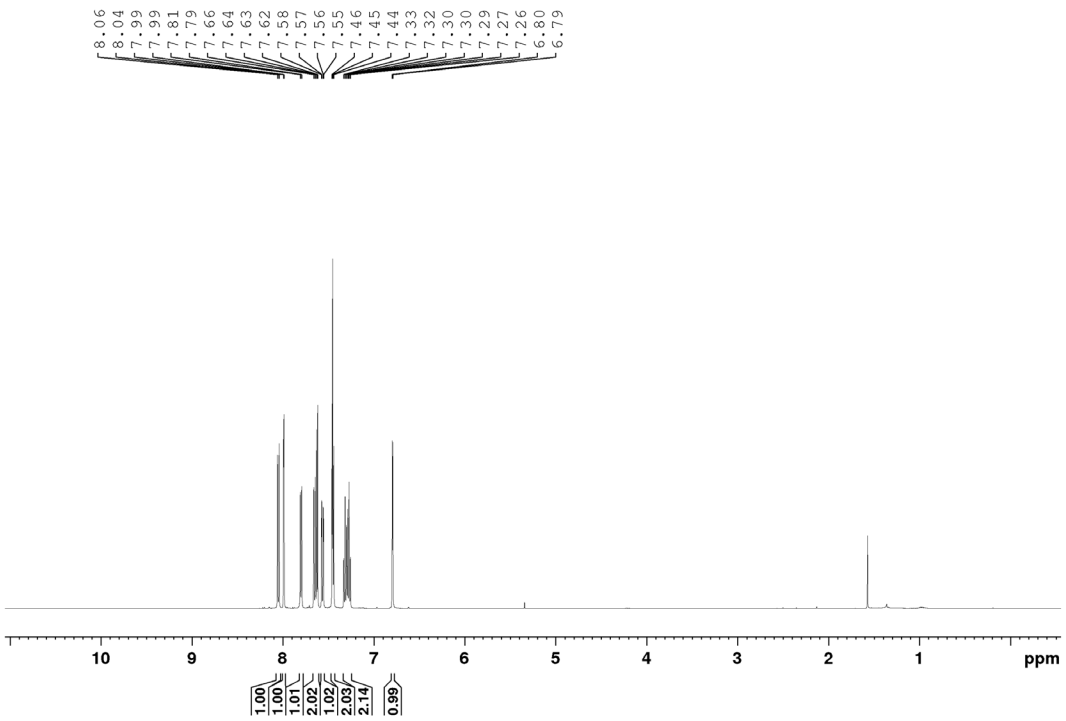

^{13}C{^{1}H} NMR Spectrum of **2.3d** ($CDCl_3$, 125.8 MHz)

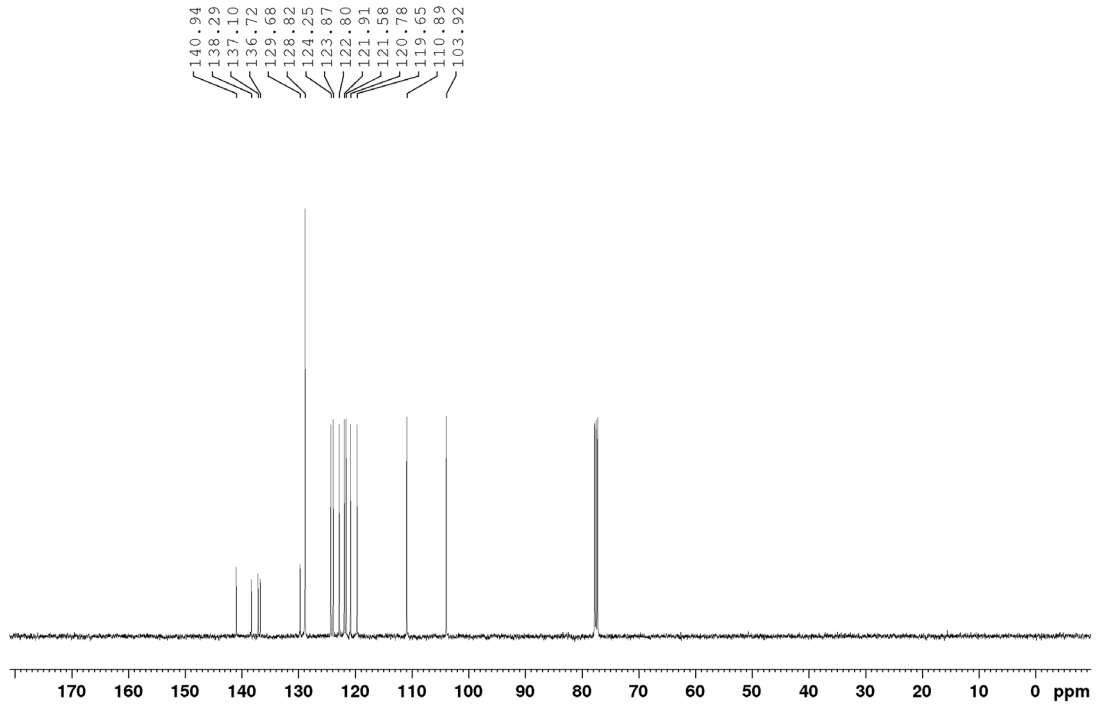

^{1}H NMR Spectrum of ***4-(1H-indol-1-yl)-2-methylquinoline***, **2.3e** ($CDCl_3$, 500 MHz)

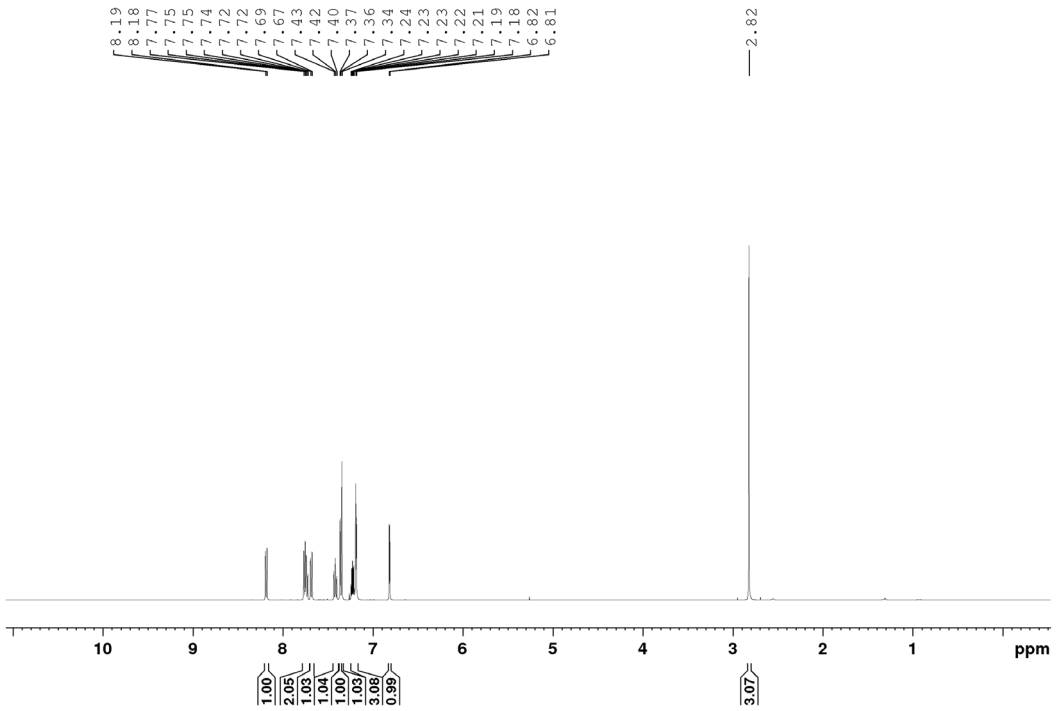

^{13}C{^{1}H} NMR Spectrum of **2.3e** ($CDCl_3$, 125.8 MHz)

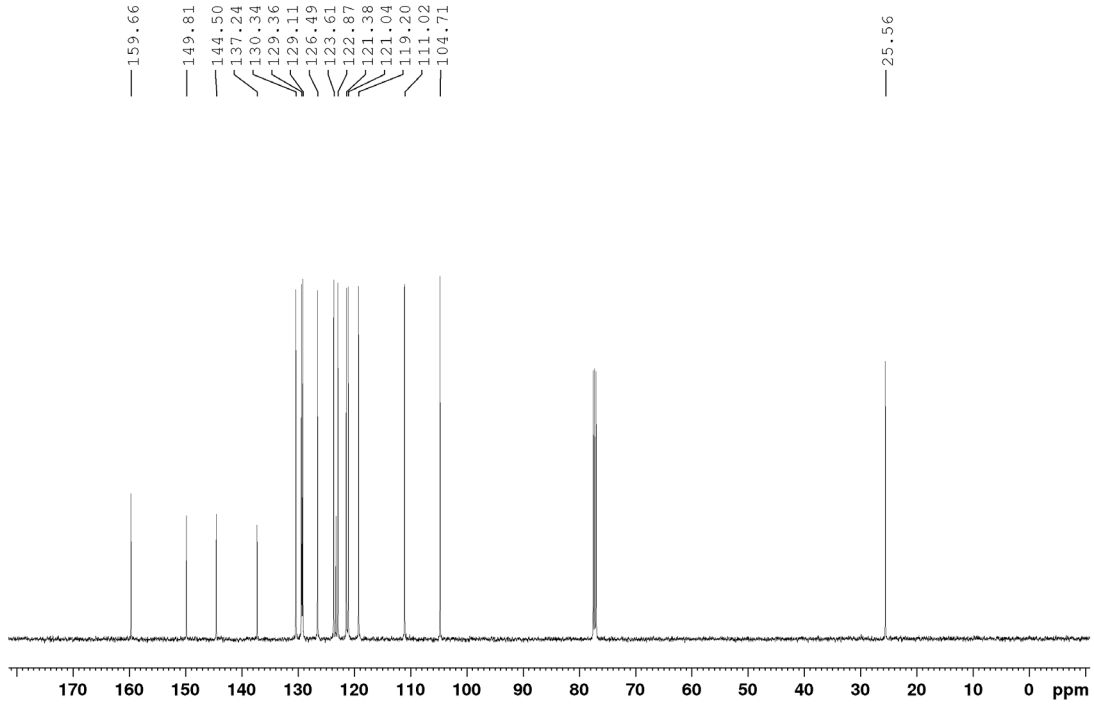

^{1}H NMR Spectrum of ***1-(4-(tert-butyl)phenyl)-1H-indole***, **2.3f** ($CDCl_3$, 500 MHz)

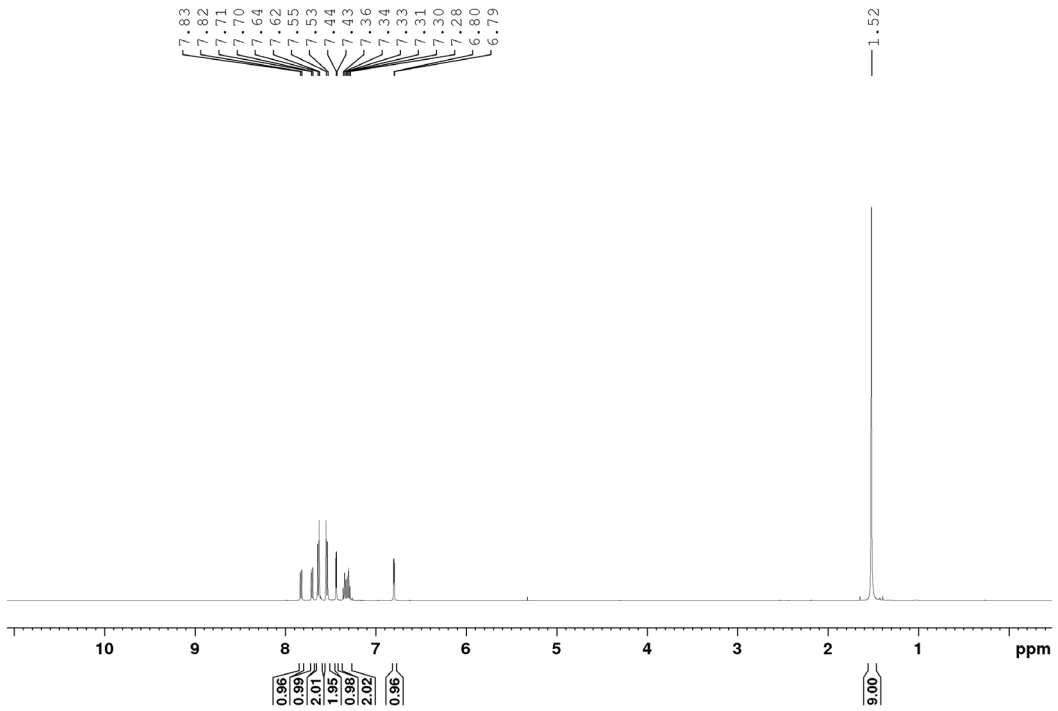

^{13}C{^{1}H} NMR Spectrum of **2.3f** ($CDCl_3$, 125.8 MHz)

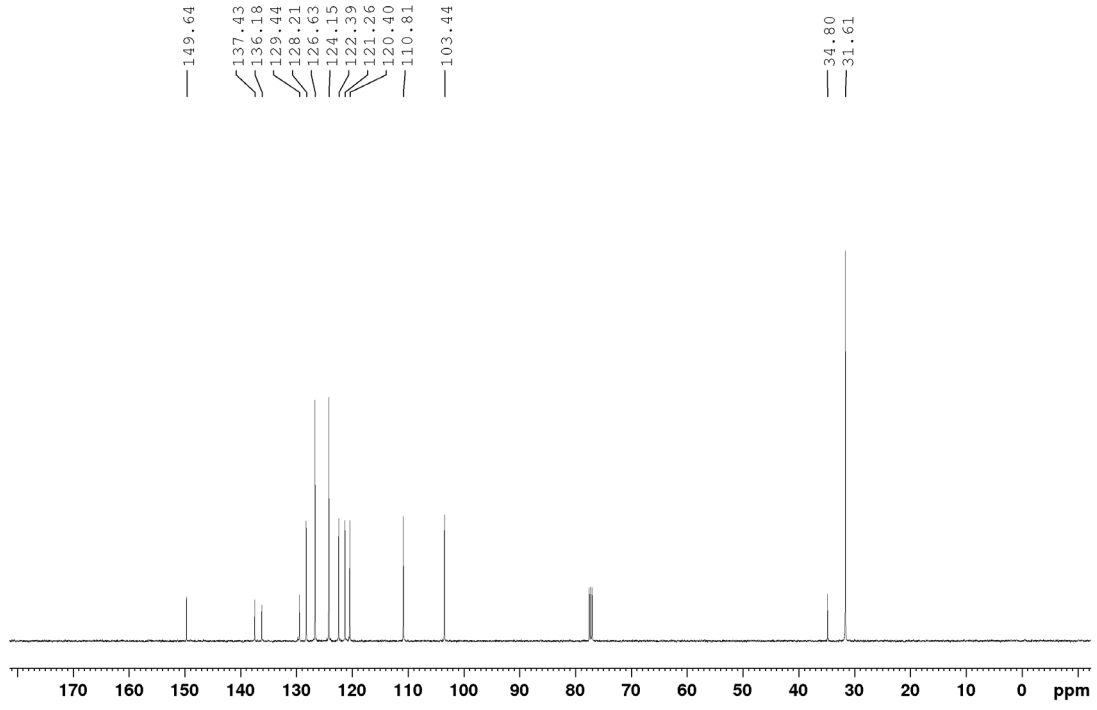

^{1}H NMR Spectrum of ***1-(2,5-dimethylphenyl)-1H-indole***, **2.3g** ($CDCl_3$, 500 MHz)

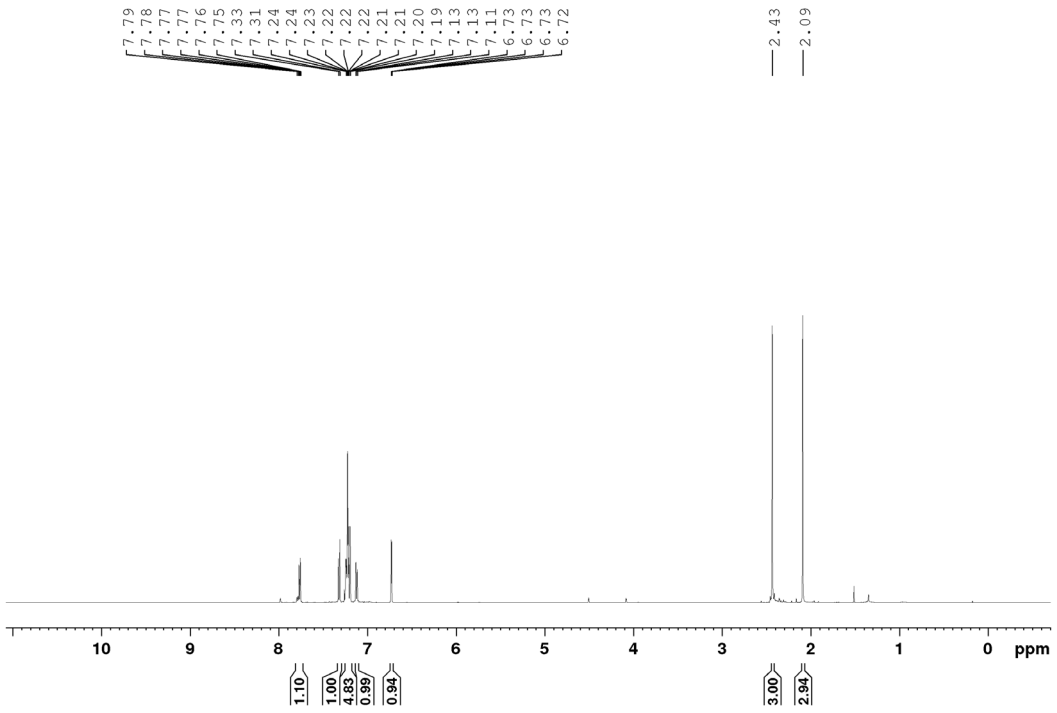

^{13}C{^{1}H} NMR Spectrum of **2.3g** ($CDCl_3$, 125.8 MHz)

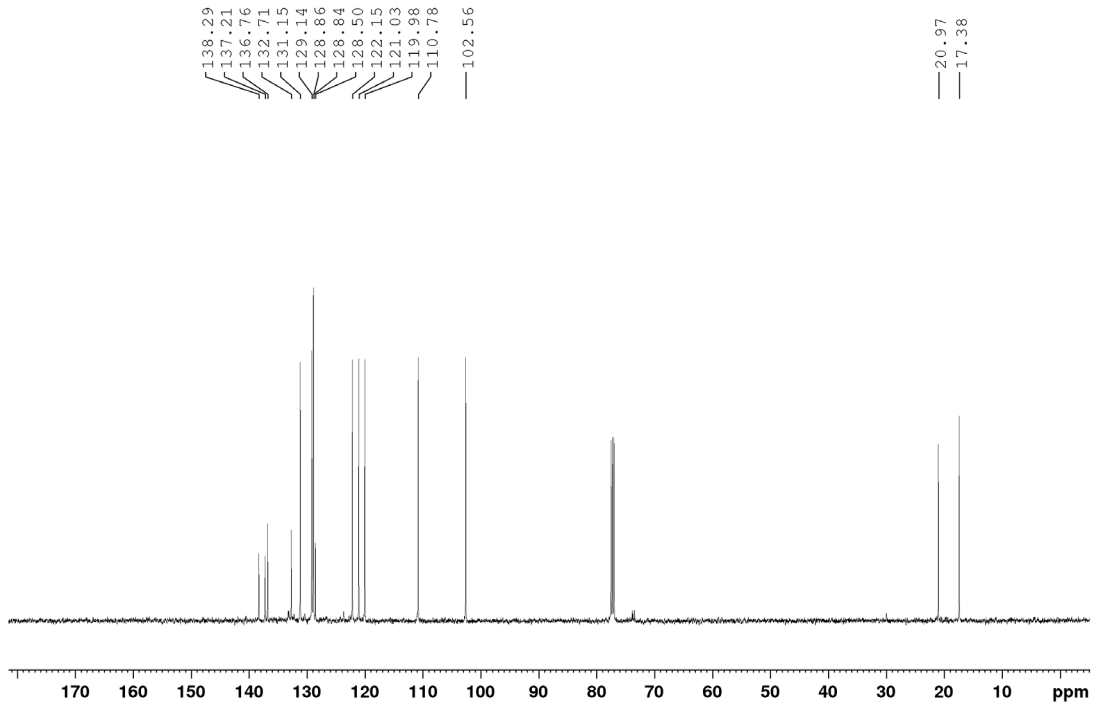

^{1}H NMR of Spectrum ***1-(4-methoxyphenyl)-1H-indole***, **2.3h** ($CDCl_3$, 500 MHz)

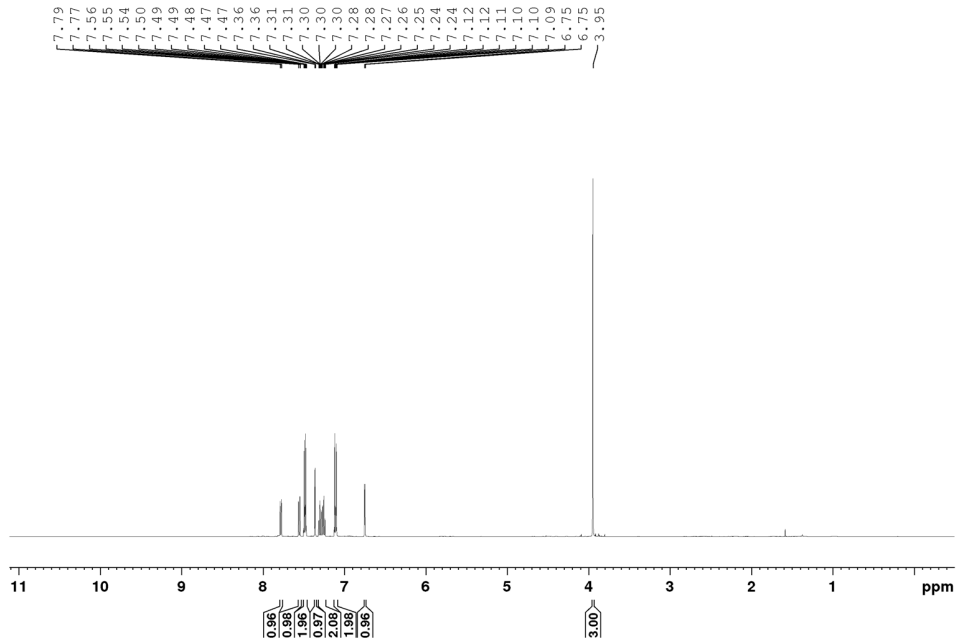

^{13}C{^{1}H} NMR Spectrum of **2.3h** ($CDCl_3$, 125.8 MHz)

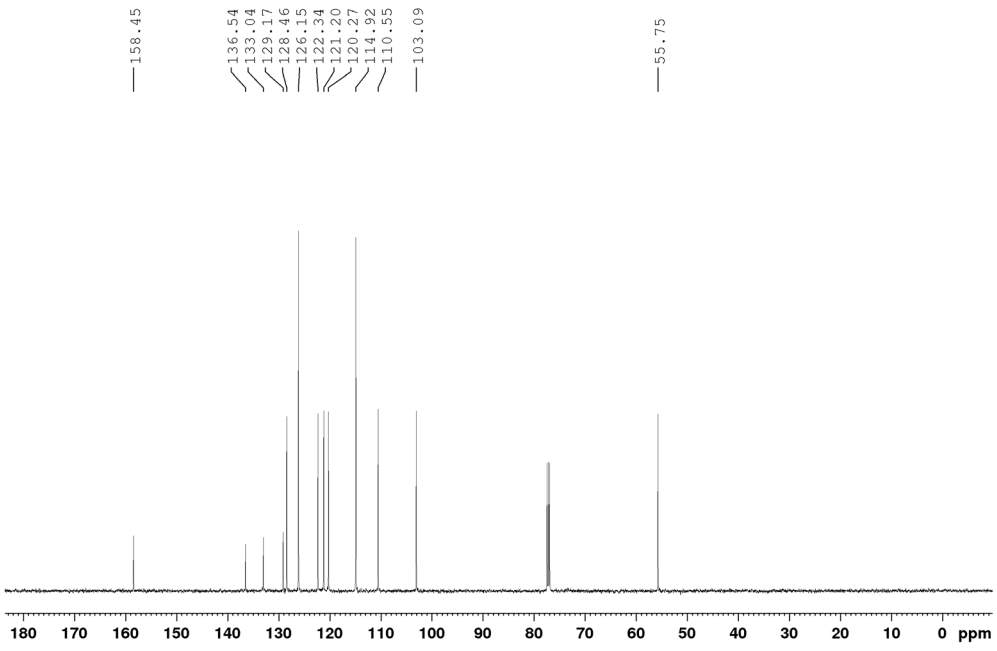

^{1}H NMR Spectrum of ***2-methyl-N-octyl-4-quinolinamine***, **3.3a** ($CDCl_3$, 500 MHz)

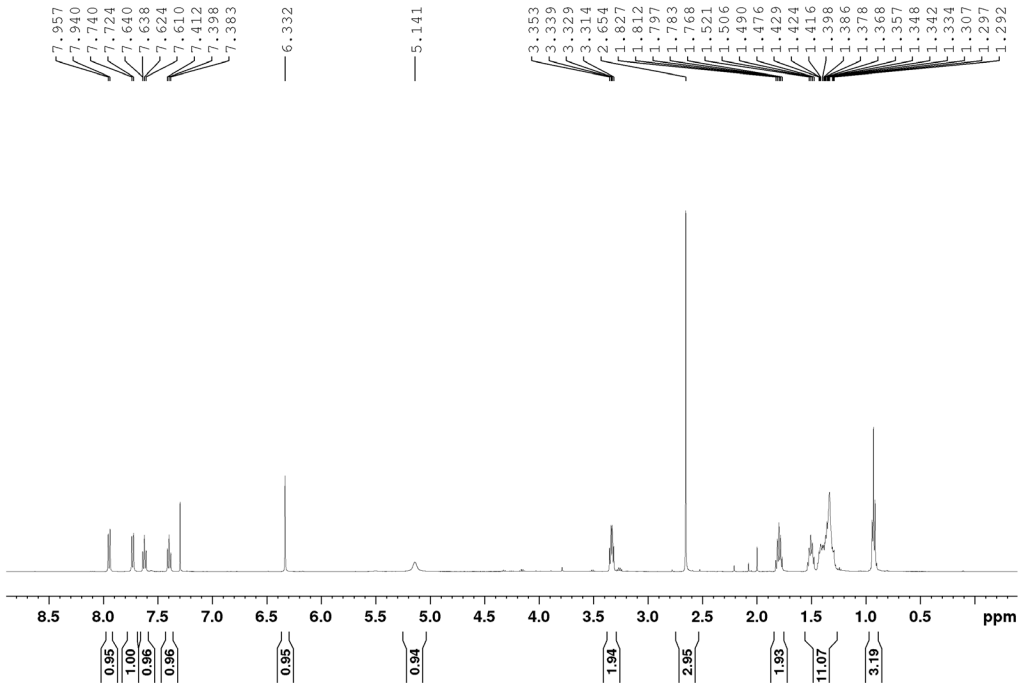

^{13}C{^{1}H} UDEFT NMR Spectrum of **3.3a** ($CDCl_3$, 125.8 MHz)

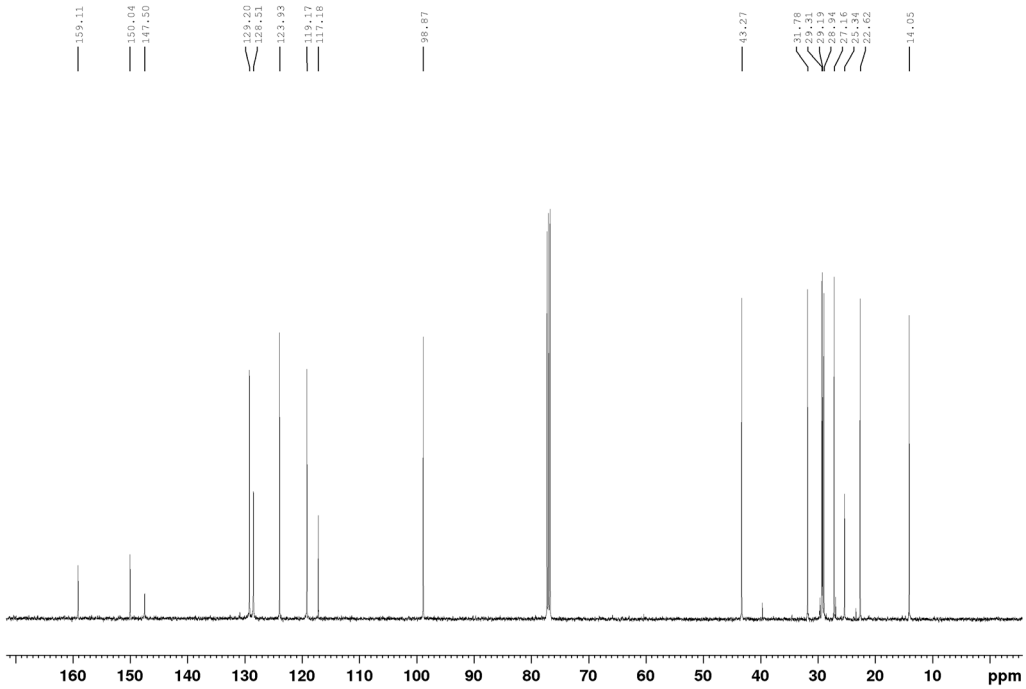

^{1}H NMR Spectrum of ***N-(2-furanylmethyl)-6-quinoxalinamine***, **3.3b** ($CDCl_3$, 500 MHz)

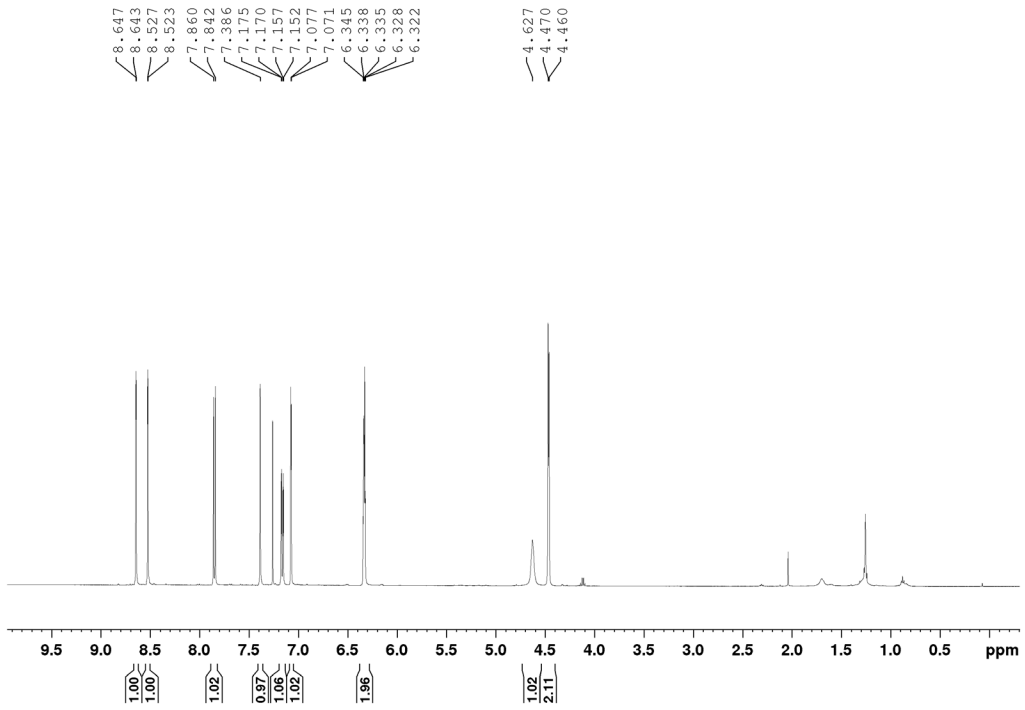

^{13}C{^{1}H} UDEFT NMR Spectrum of **3.3b** ($CDCl_3$, 125.8 MHz)

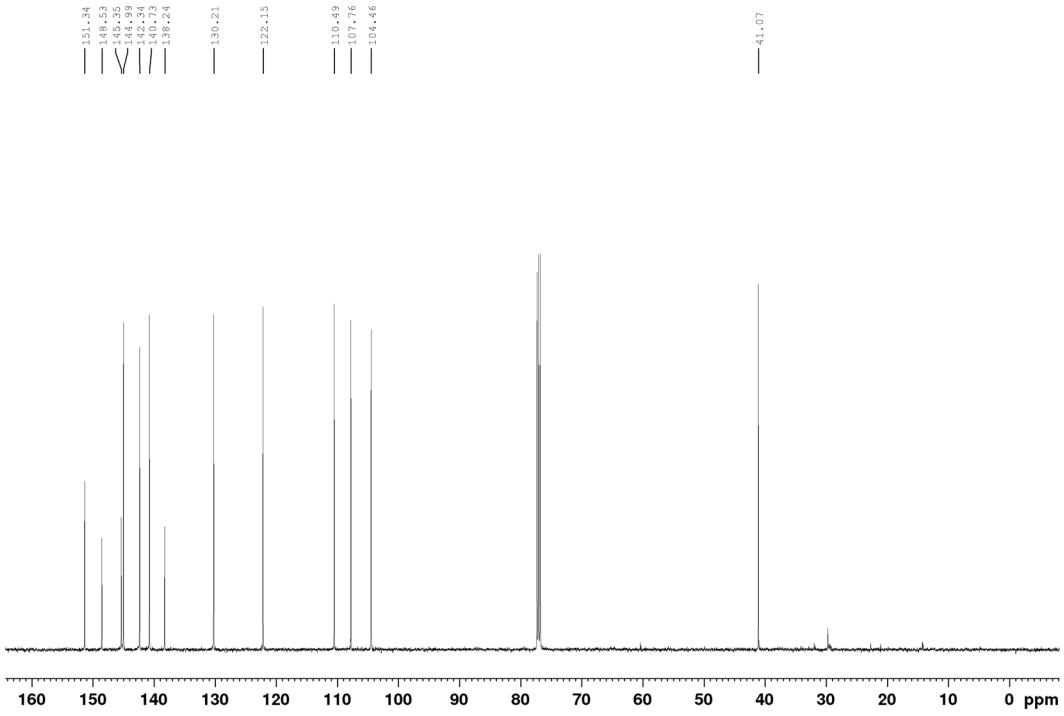

^{1}H NMR Spectrum of *N-[(tetrahydro-2-furanyl)methyl]-2-quinolinamine*, **3.3c** ($CDCl_3$, 500 MHz)

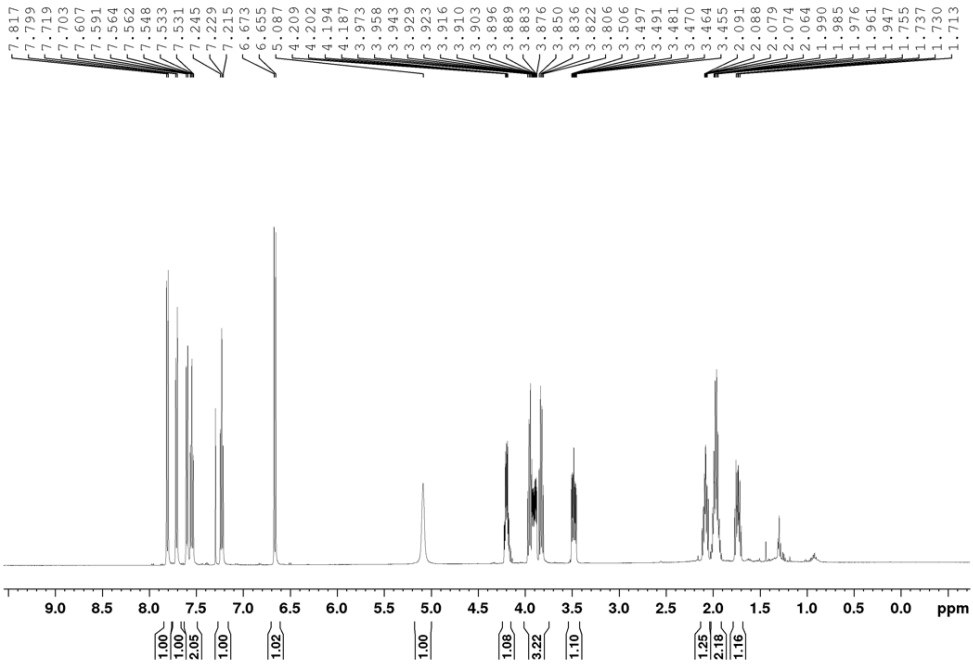

^{13}C{^{1}H} UDEFT NMR Spectrum of **3.3c** ($CDCl_3$, 125.8 MHz)

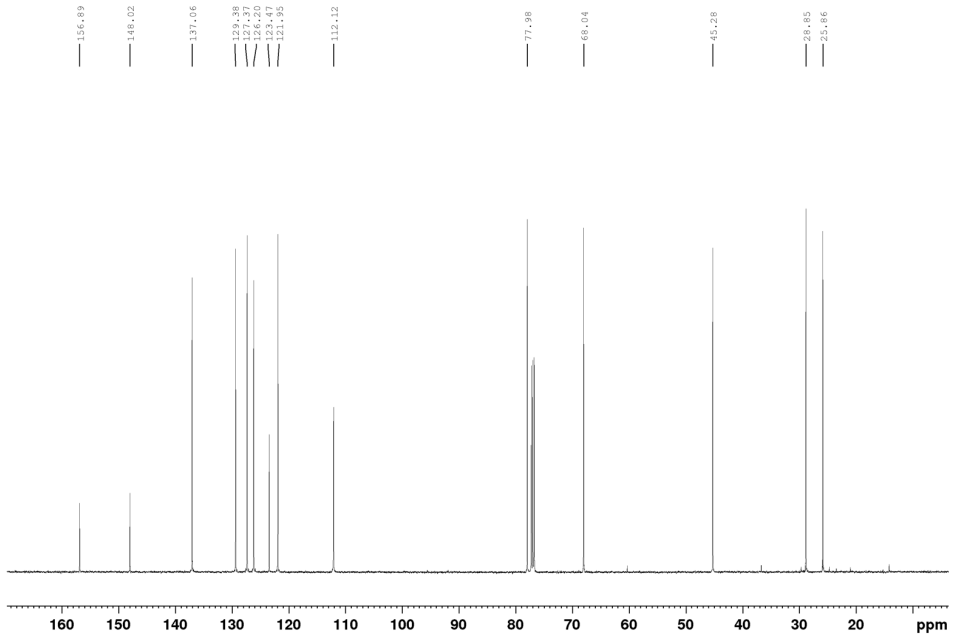

^{1}H NMR Spectrum of *N-(naphthalen-1-ylmethyl)aniline*, **3.3d** (CDCl3, 500 MHz)

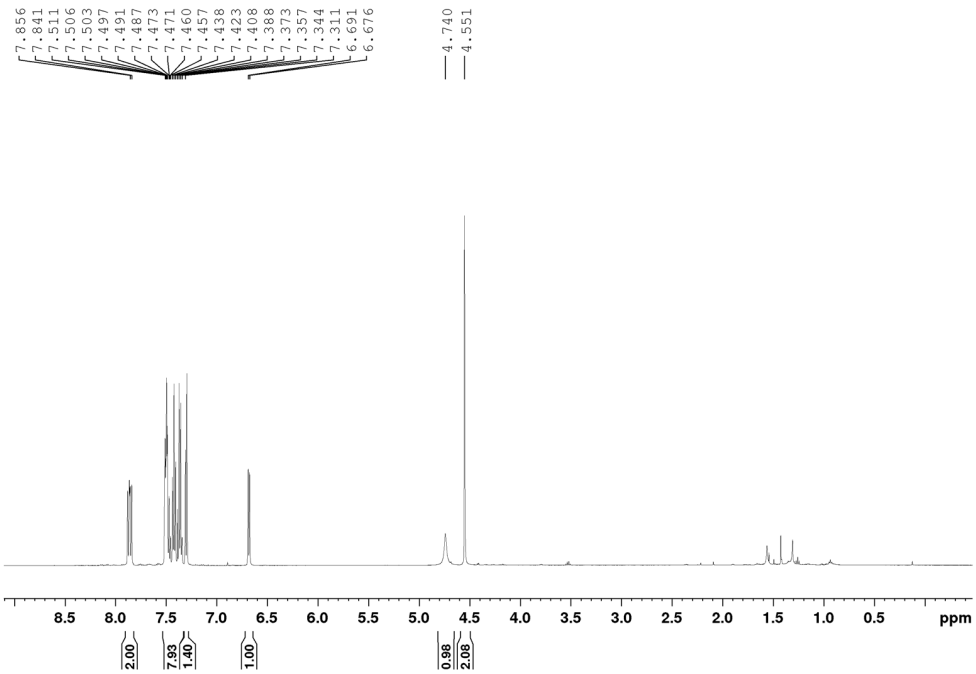

^{13}C{^{1}H} UDEFT NMR Spectrum of **3.3d** (CDCl3, 125.8 MHz)

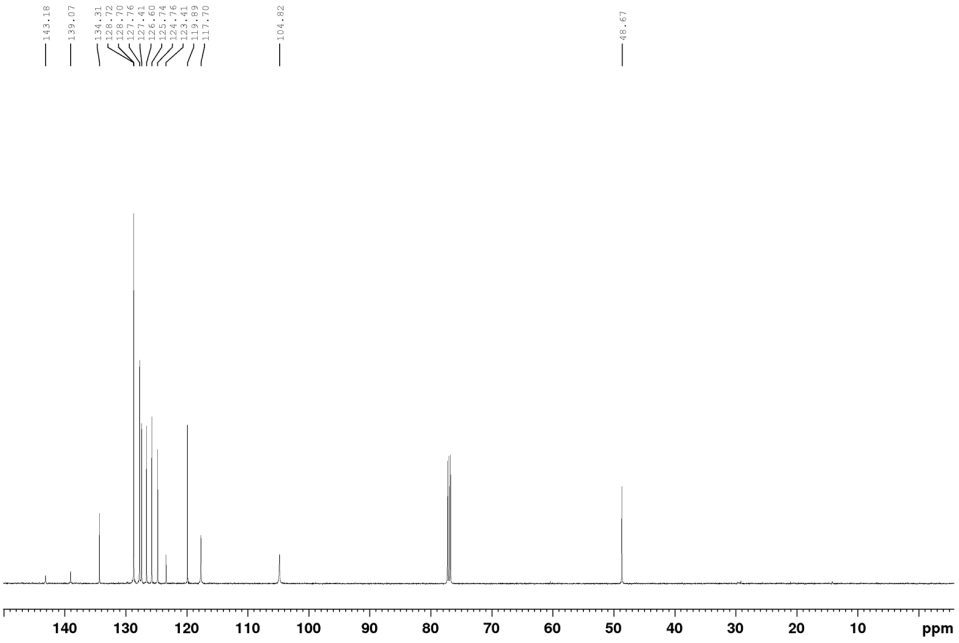

^{1}H NMR Spectrum of ***4-(2-oxazolylaminophenyl)phenyl-methanone,*** **4.2a** ($CDCl_3$, 500 MHz)

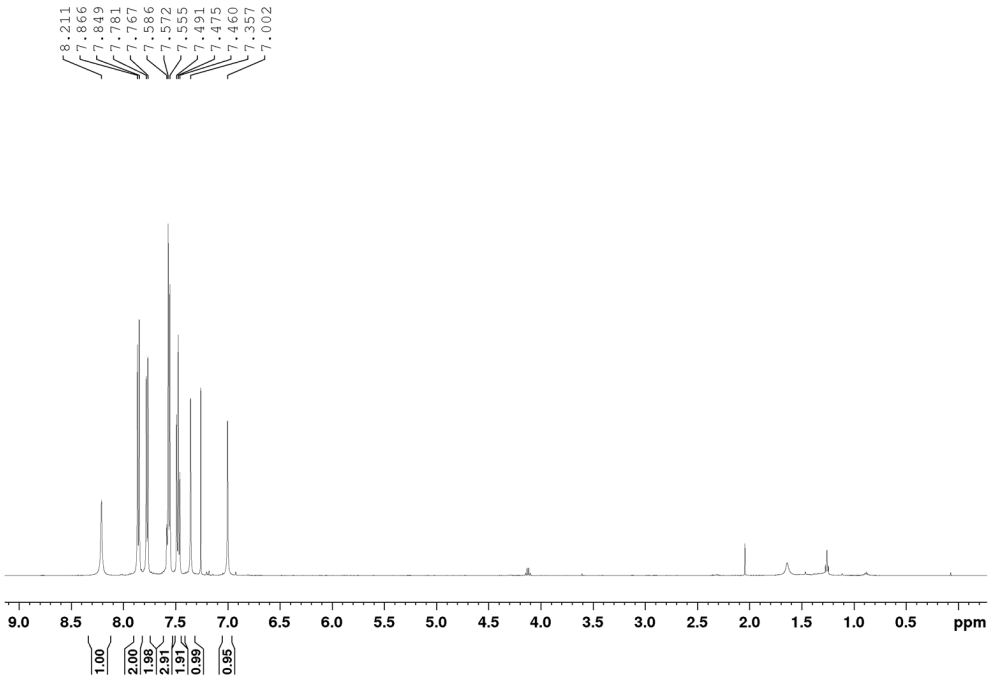

^{13}C{^{1}H} UDEFT NMR Spectrum of **4.2a** ($CDCl_3$, 125.8 MHz)

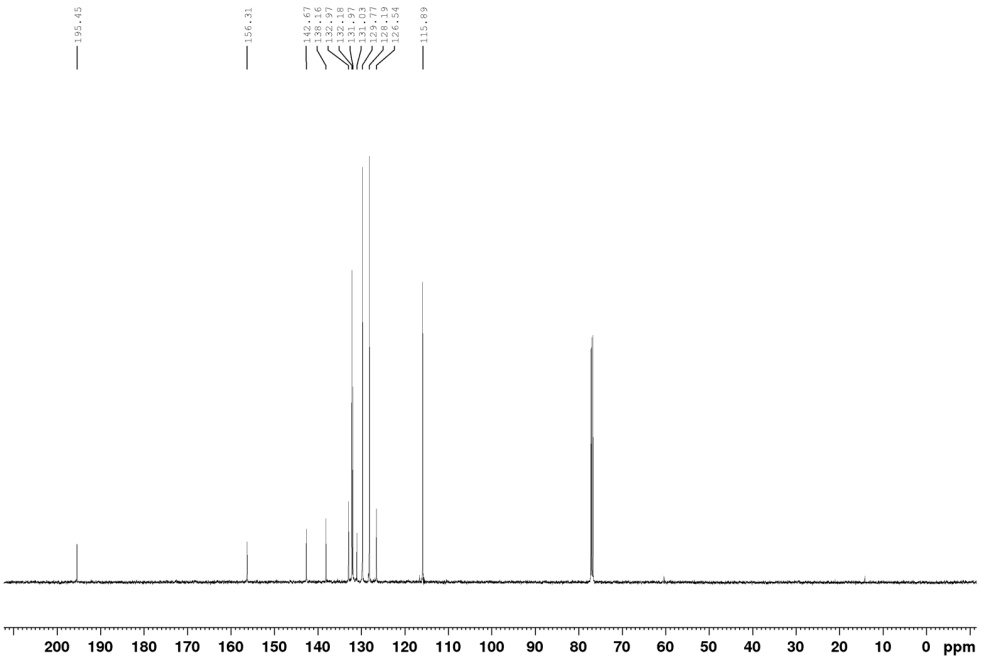

^{1}H NMR Spectrum of ***N-(2-oxazolyl)-6-quinoxalinamine***, **4.2b** (DMSO-d_6, 500 MHz)

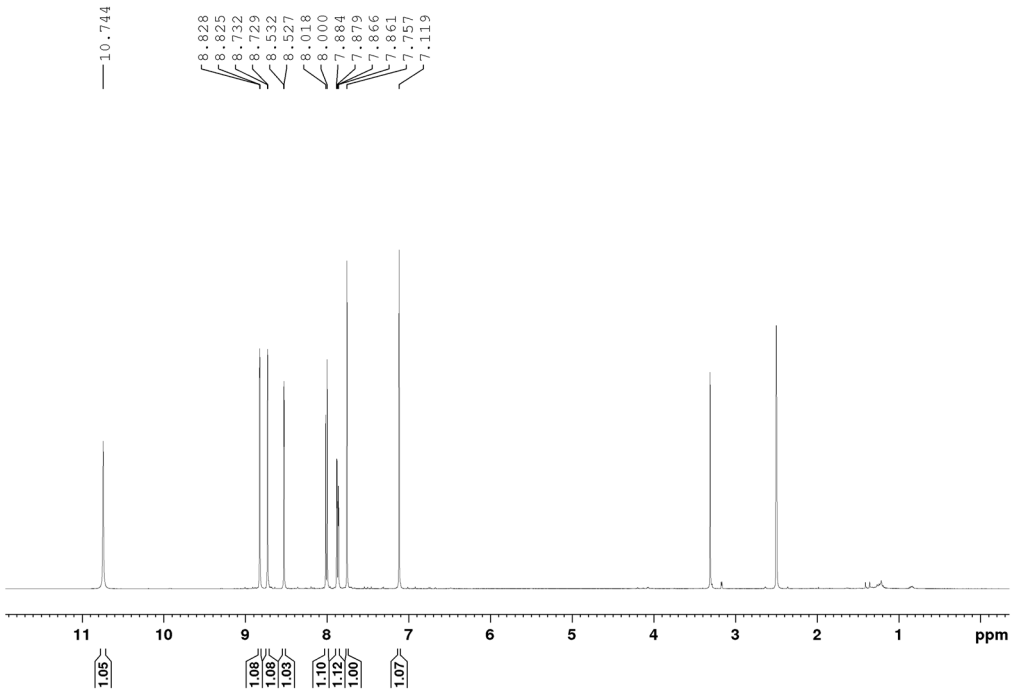

^{13}C{^{1}H} UDEFT NMR Spectrum of **4.2b** (DMSO-d_6, 125.8 MHz)

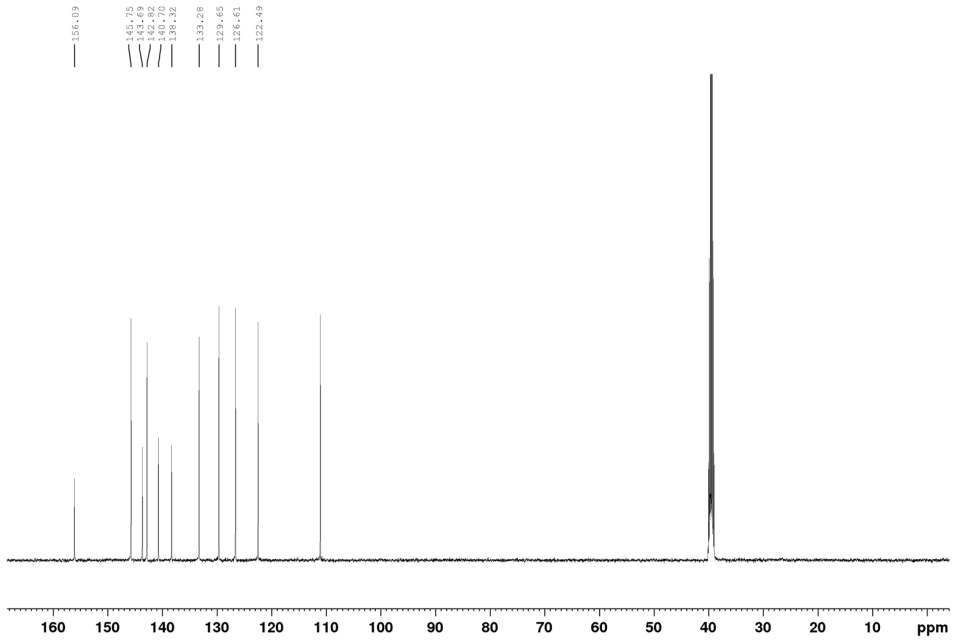

^{1}H NMR Spectrum of *N-[(2-oxazolyl]-2-quinolinamine*, **4.2c**, entire sample ($CDCl_3$, 500 MHz)

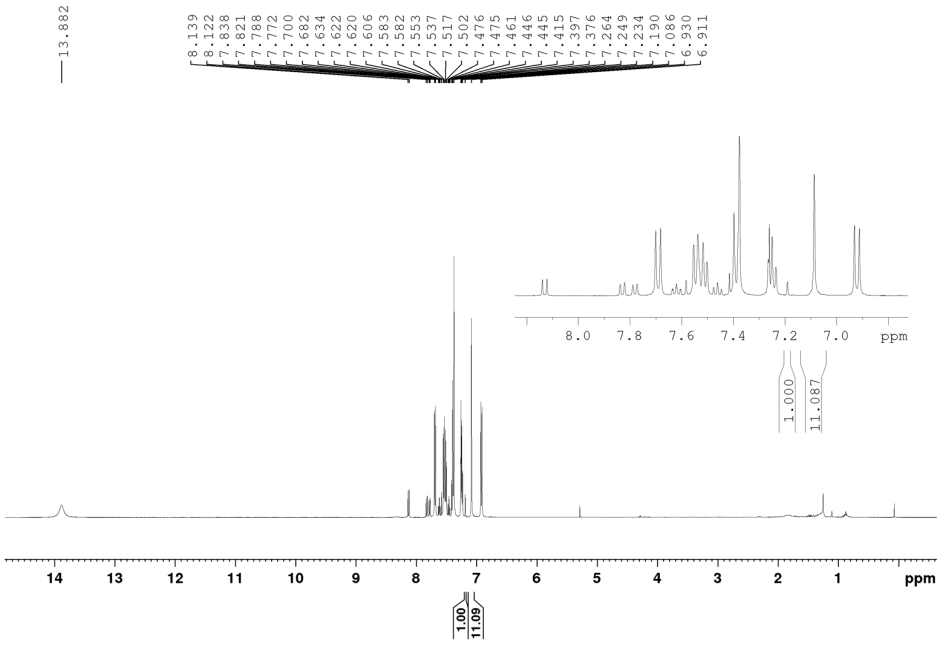

^{1}H NMR Spectrum of **4.2c**, purified material ($CDCl_3$, 500 MHz)

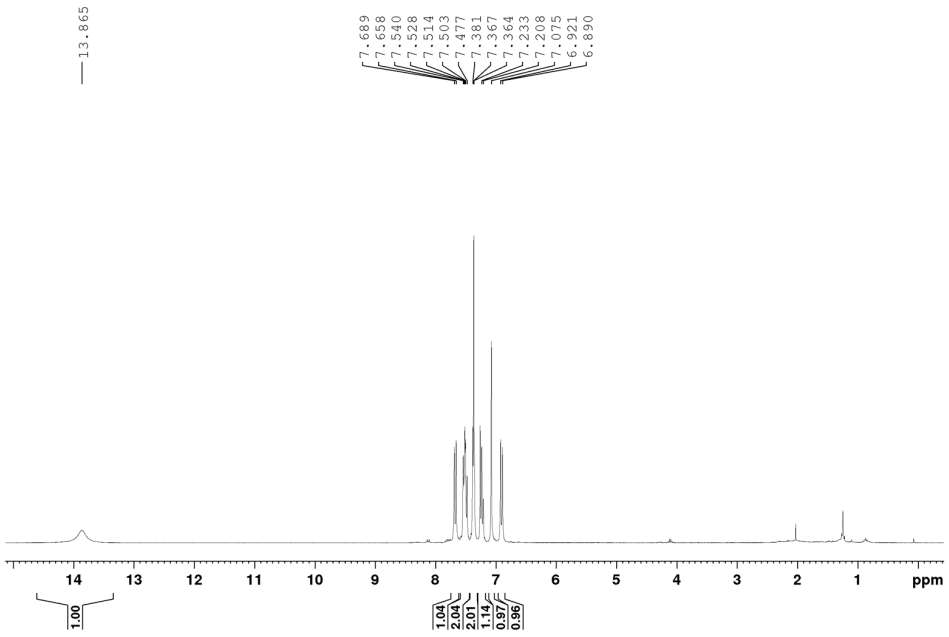

$^{13}C\{^{1}H\}$ UDEFT NMR Spectrum of **4.2c**, purified material (DMSO-d_6, 500 MHz)

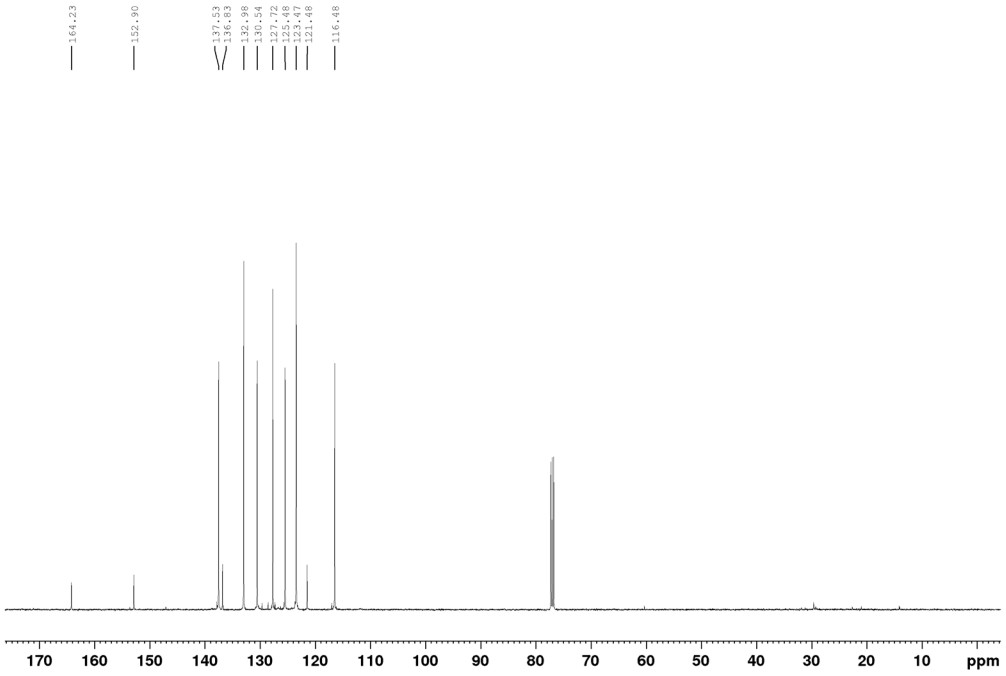

^{1}H NMR Spectrum of ***N-(2-thiazolyl)-6-quinoxalinamine***, **4.2d** (DMSO-d_6, 500 MHz)

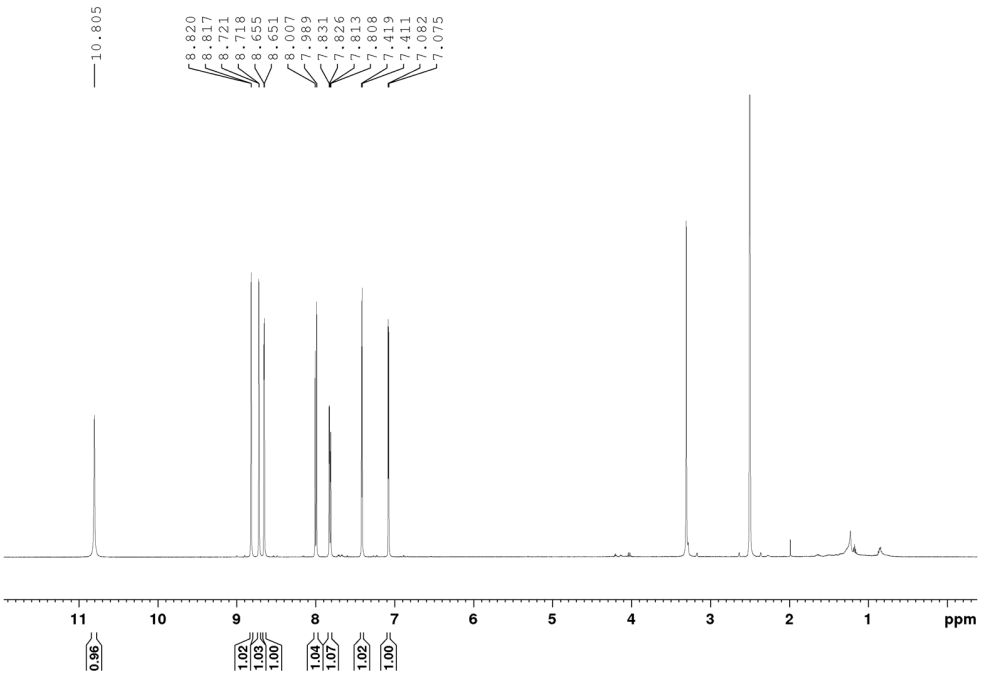

$^{13}C\{^{1}H\}$ UDEFT NMR Spectrum of **4.2b** (DMSO-d_6, 125.8 MHz)

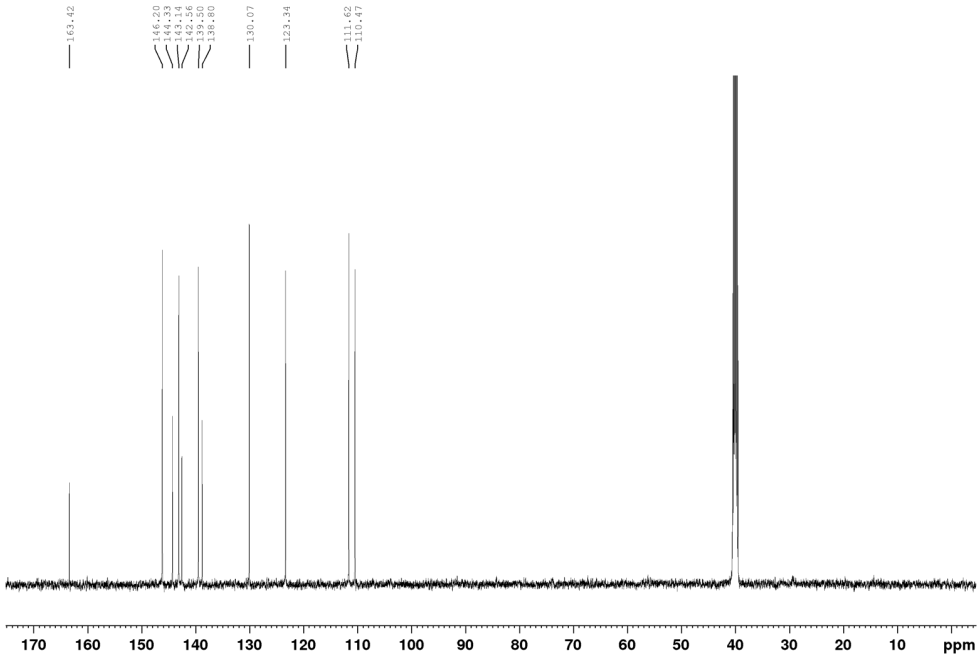

^{1}H NMR Spectrum of *4-(2-thiazolylamino)-benzonitrile*, **4.2e** (DMSO-d_6, 300 MHz)

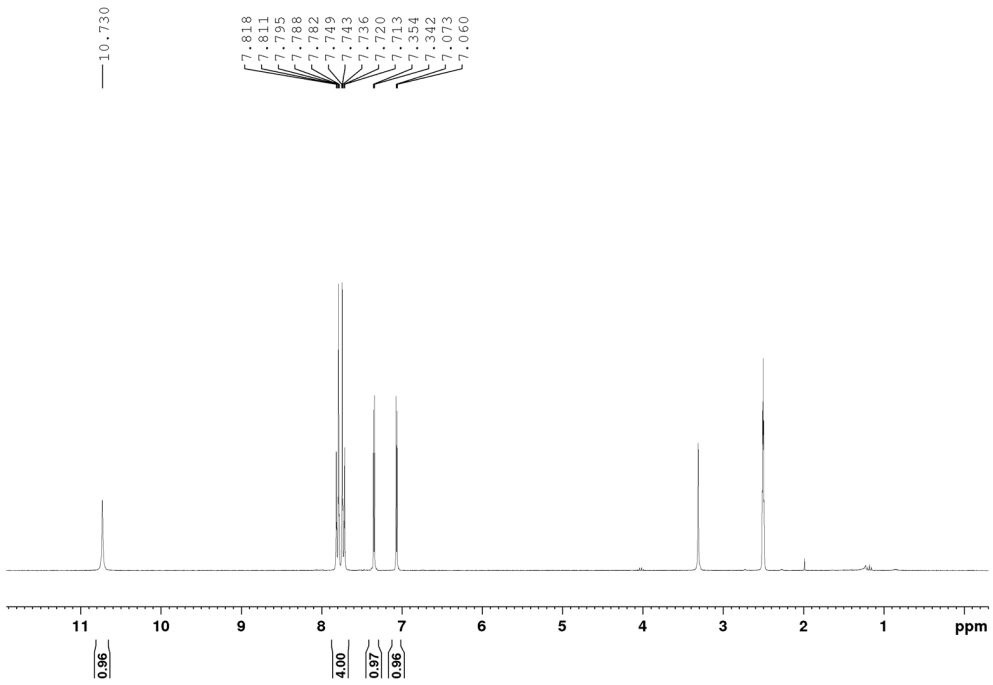

$^{13}C\{^{1}H\}$ NMR Spectrum of **4.2e** (DMSO-d_6, 125.8 MHz)

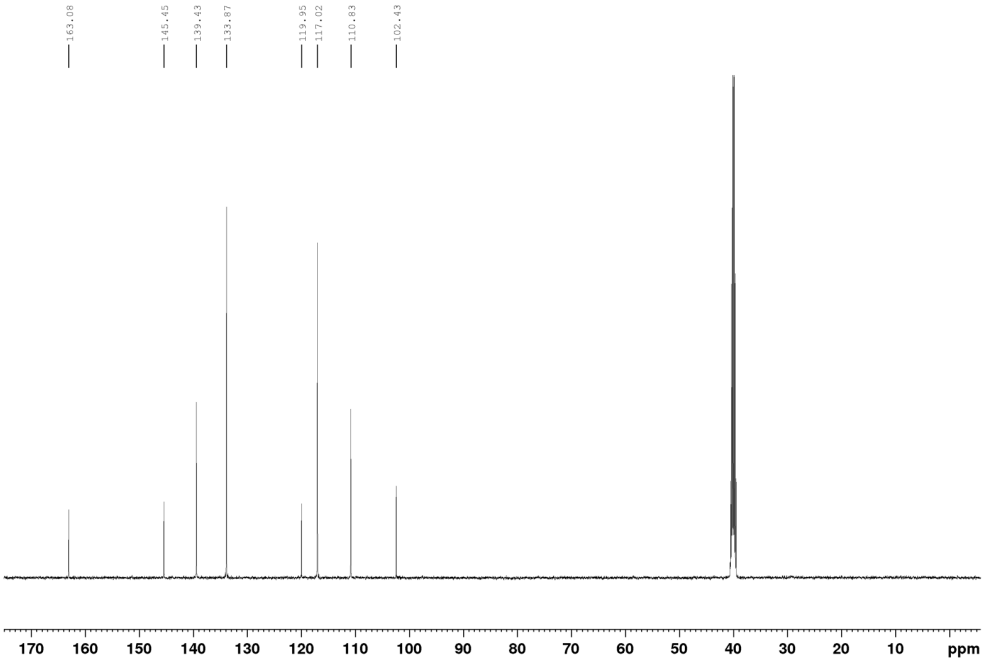

^{1}H NMR Spectrum of *4-(2-thiazolylamino)-quinaldine*, **4.2f** (DMSO-d_6, 300 MHz)

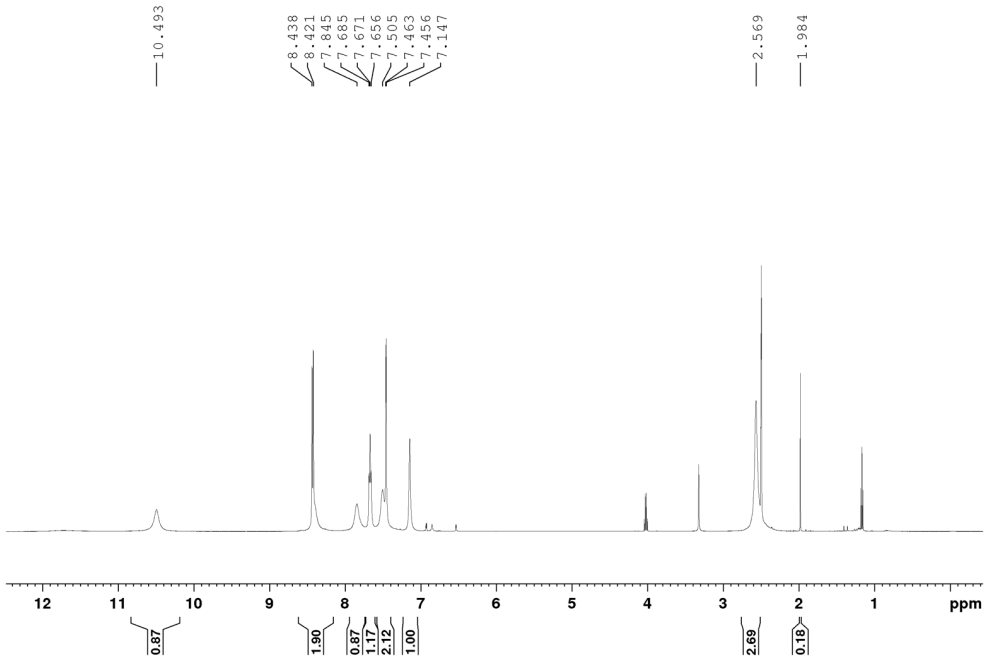

$^{13}C\{^{1}H\}$ UDEFT NMR Spectrum of **4.2f** (DMSO-d_6, 125.8 MHz)

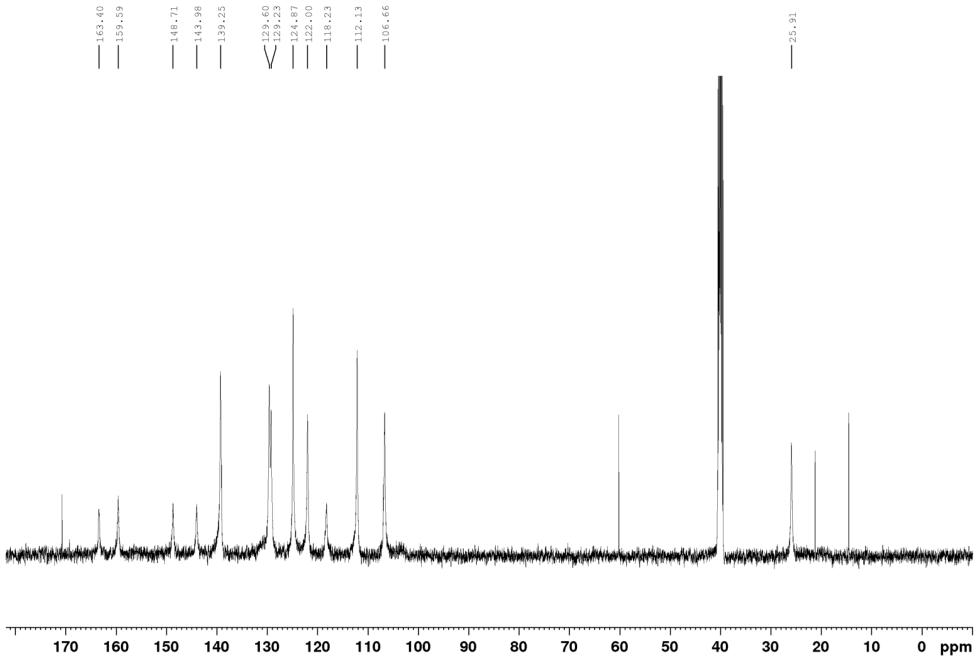

^{1}H NMR Spectrum of *2-[(1,3-dimethyl-1H-pyrazol-5-yl)amino]-benzothiazole*, **4.2g** ($CDCl_3$, 500 MHz)

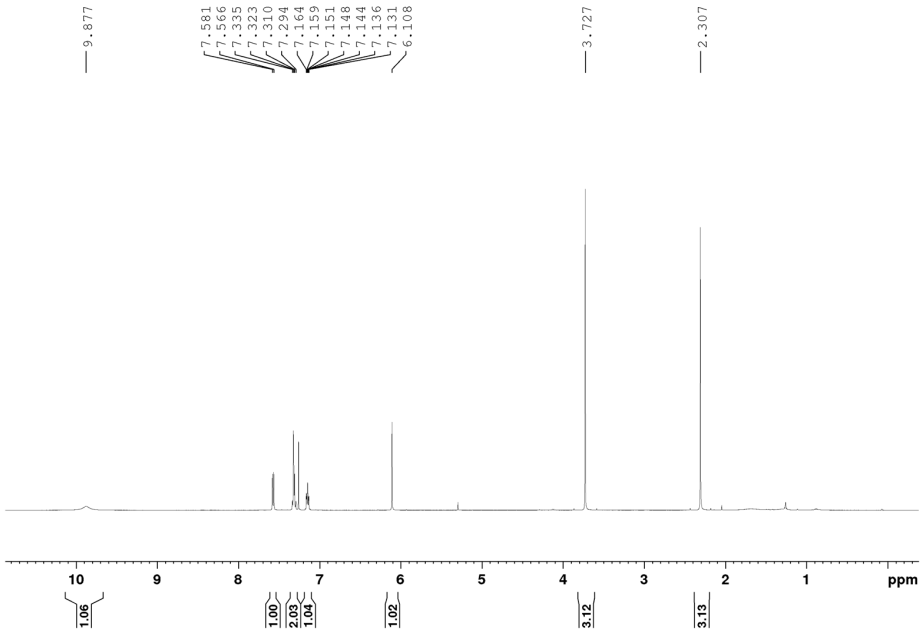

$^{13}C\{^{1}H\}$ UDEFT NMR Spectrum of **4.2g** ($CDCl_3$, 125.8 MHz)

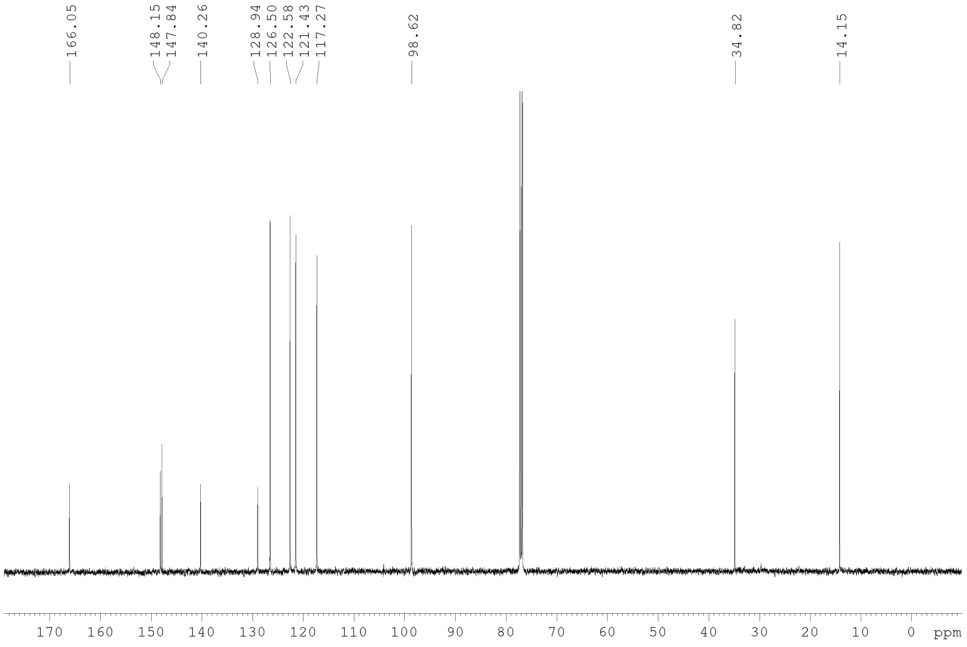

^{1}H NMR Spectrum of *2-[(1,3-dimethyl-1H-pyrazol-5-yl)amino]-quinoline*, **4.2h** ($CDCl_3$, 500 MHz)

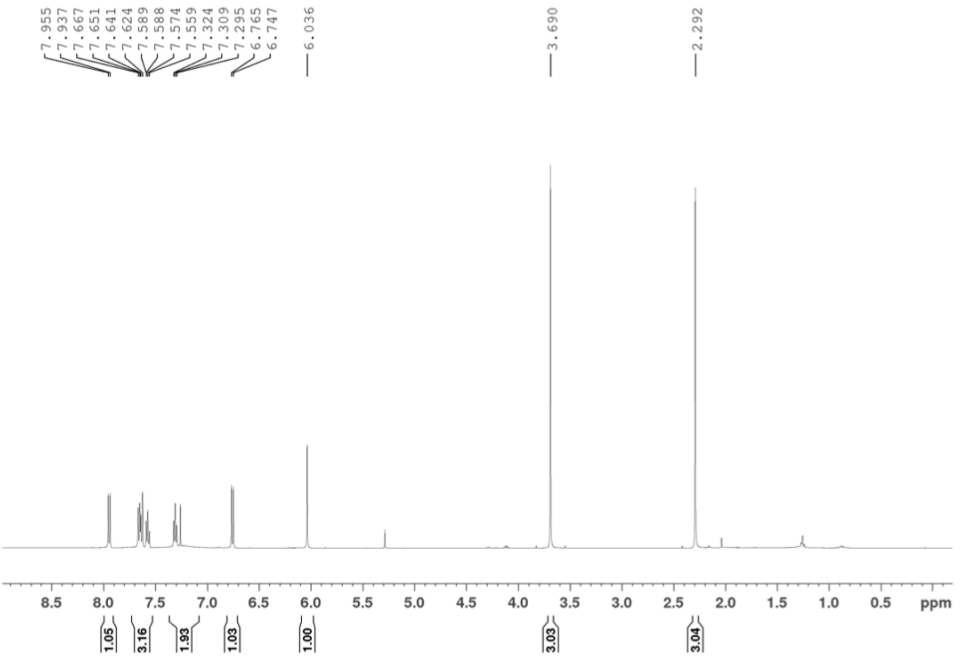

$^{13}C\{^{1}H\}$ UDEFT NMR Spectrum of **4.2h** ($CDCl_3$, 125.8 MHz)

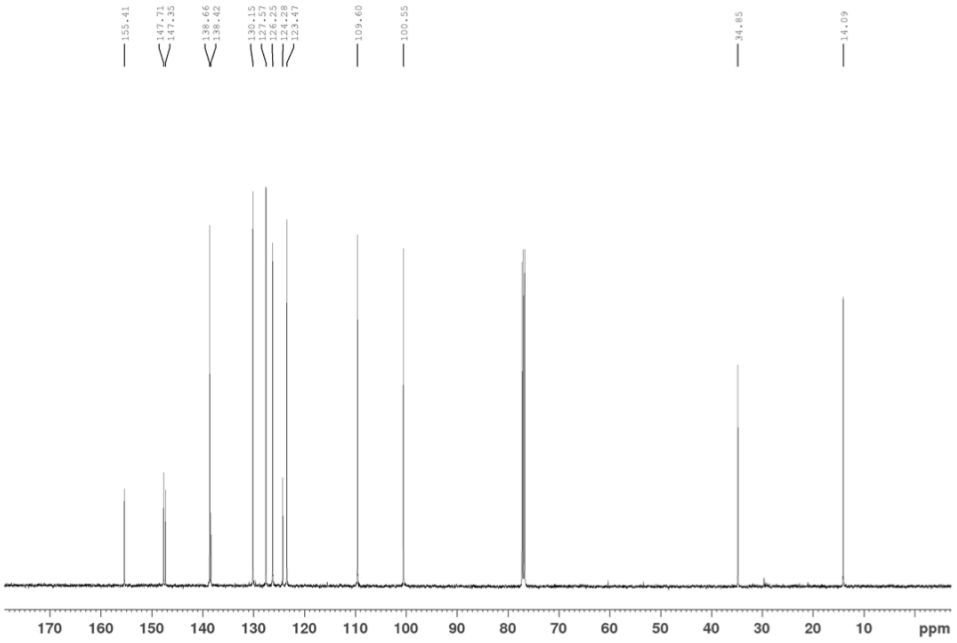

^{1}H NMR Spectrum of *4-[(1,3-dimethyl-1H-pyrazol-5-yl)amino]-quinaldine*, **4.2i** ($CDCl_3$, 500 MHz)

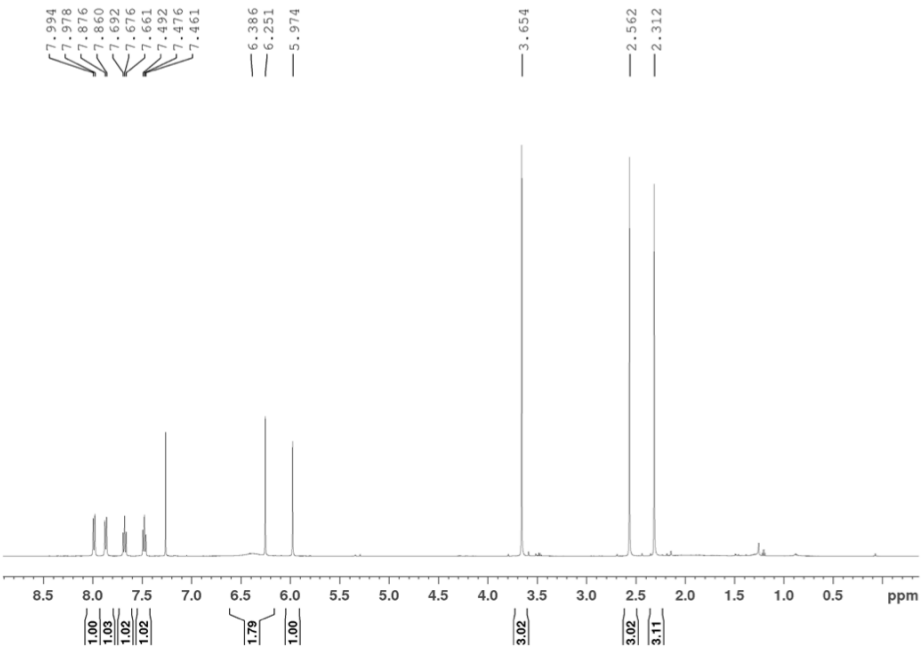

$^{13}C\{^{1}H\}$ UDEFT NMR Spectrum of **4.2i** ($CDCl_3$, 125.8 MHz)

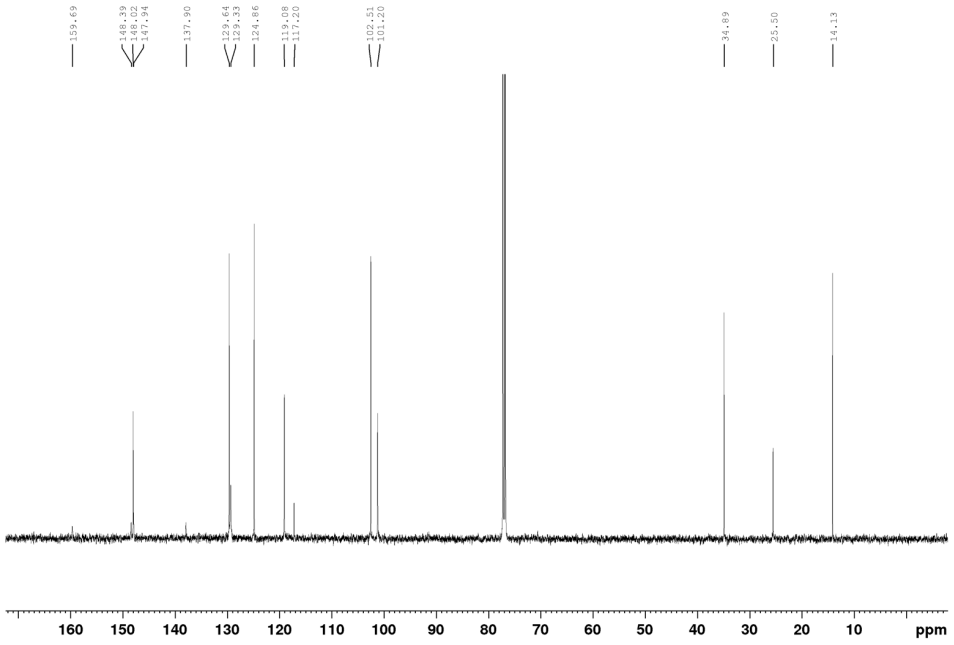

^{1}H NMR Spectrum of *N-1-naphthalenyl-2-pyridinamine* (**4.2j**) with dodecane internal standard ($CDCl_3$, 500 MHz)

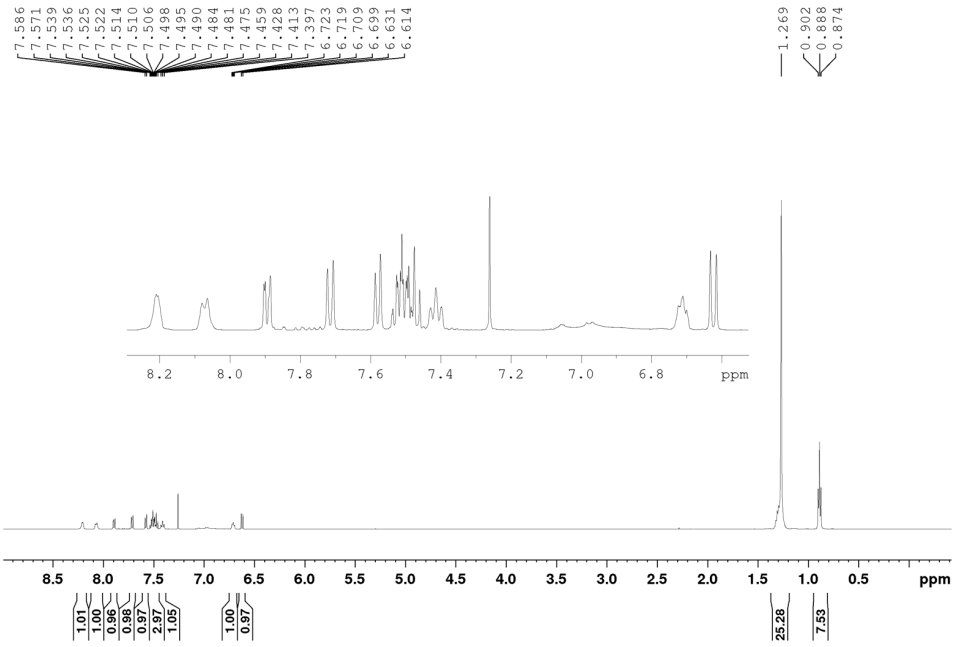

^{1}H NMR Spectrum of *N-(1,1'-biphenyl)-4-yl-2-pyridinamine*, **4.2k** (DMSO-d_6, 500 MHz)

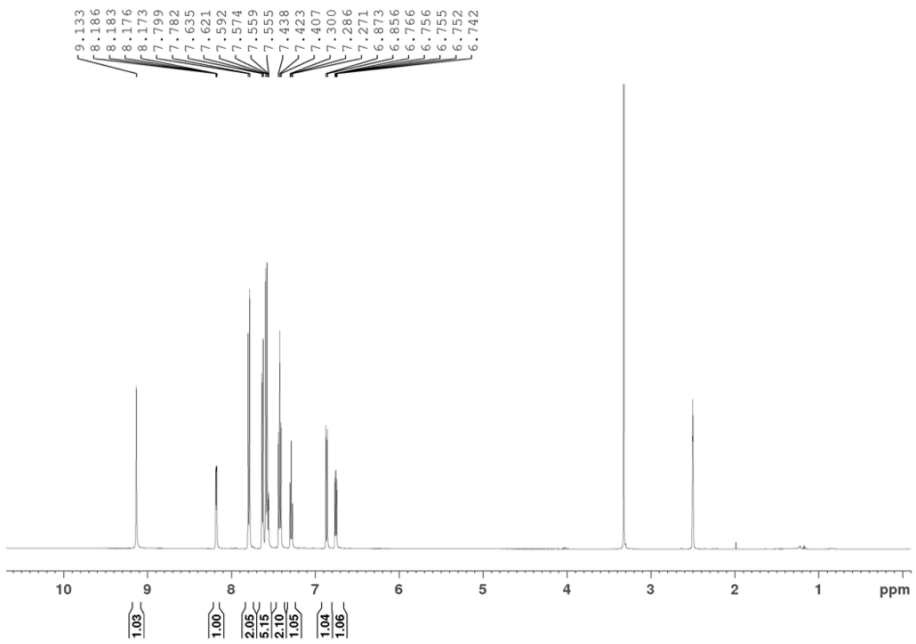

^{13}C{^{1}H} UDEFT NMR Spectrum of **4.2k** (DMSO-d_6, 125.8 MHz)

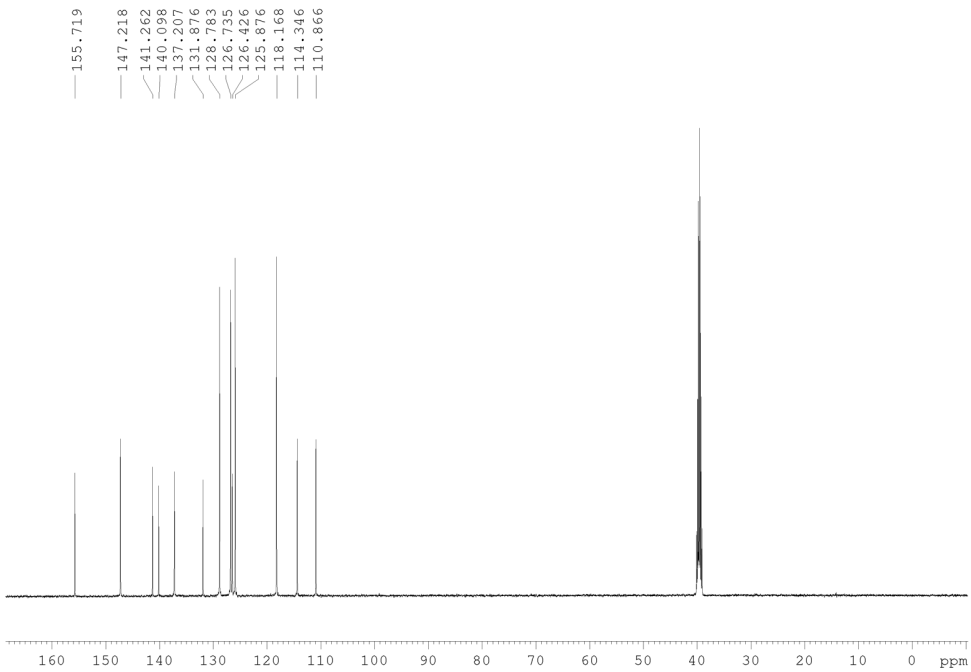

^{1}H NMR Spectrum of *N-(4-phenyl-2-thiazolyl)-2-pyridinamine*, **4.2l** ($CDCl_3$, 500 MHz)

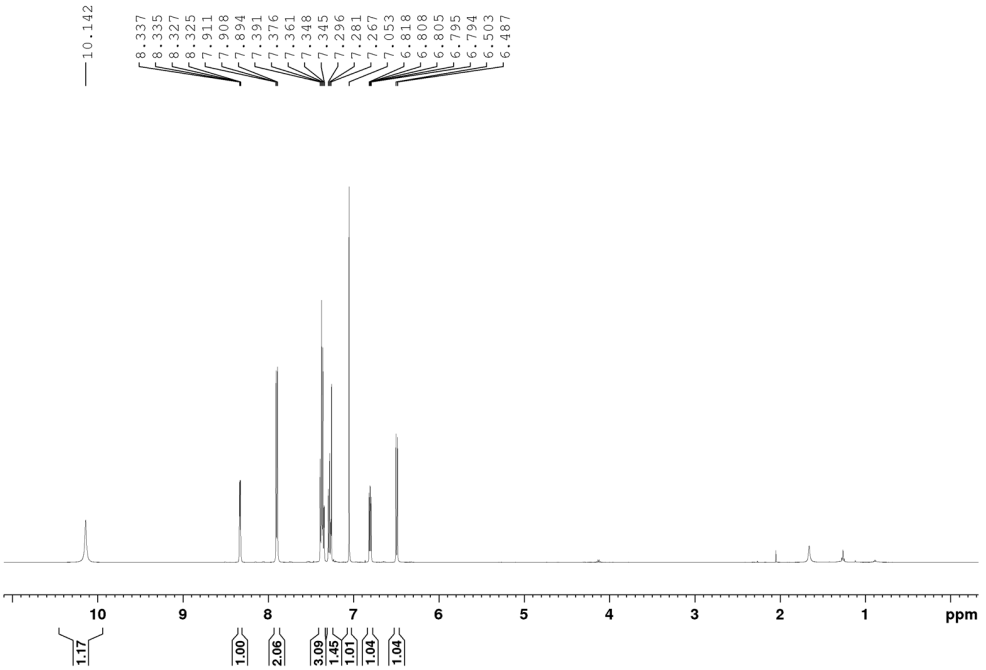

^{13}C{^{1}H} UDEFT NMR Spectrum of **4.2l** (DMSO-d_6, 125.8 MHz)

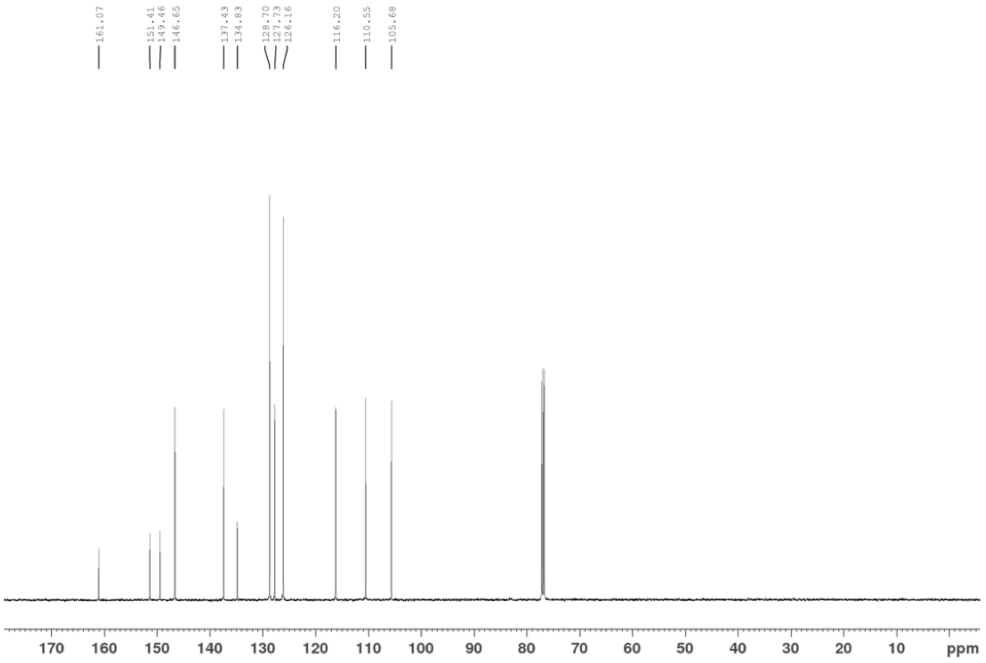

^{1}H NMR Spectrum of ***N-methyl-4-(pyrazin-2-ylamino)pyridine-2-carboxamide***, **4.2m** (DMSO-d_6 + 0.05% $SiMe_4$, 400 MHz)

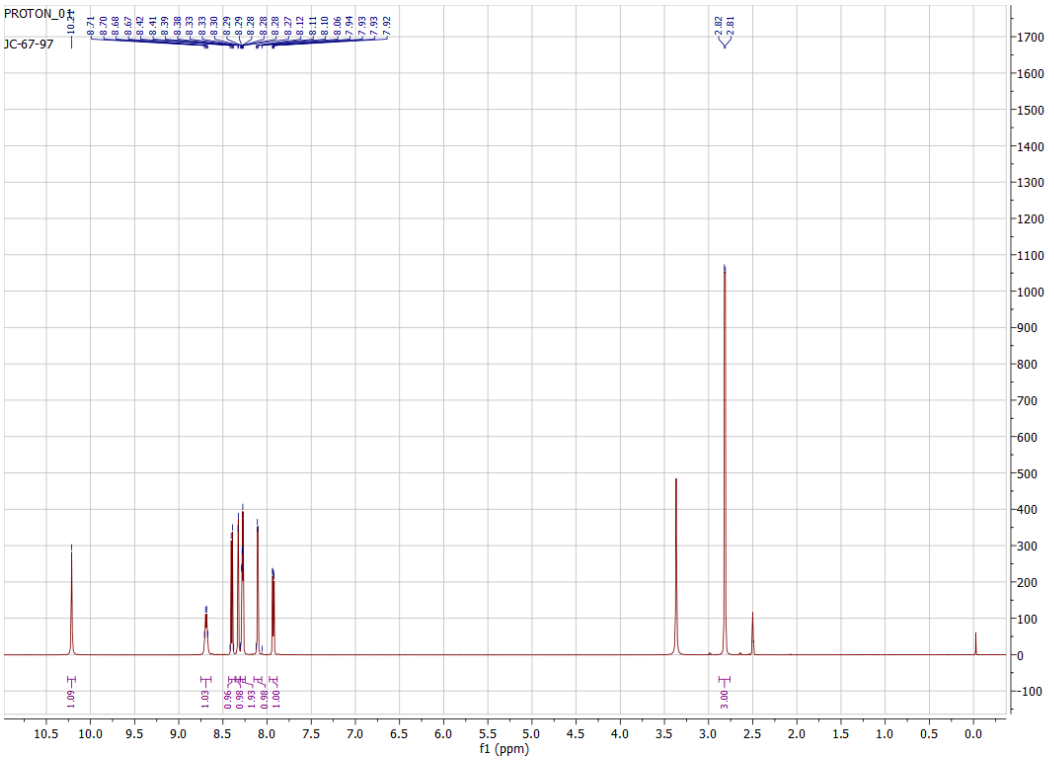

^{13}C{^{1}H} NMR Spectrum of **4.2m** (DMSO-d_6 + 0.05% $SiMe_4$, 100.6 MHz)

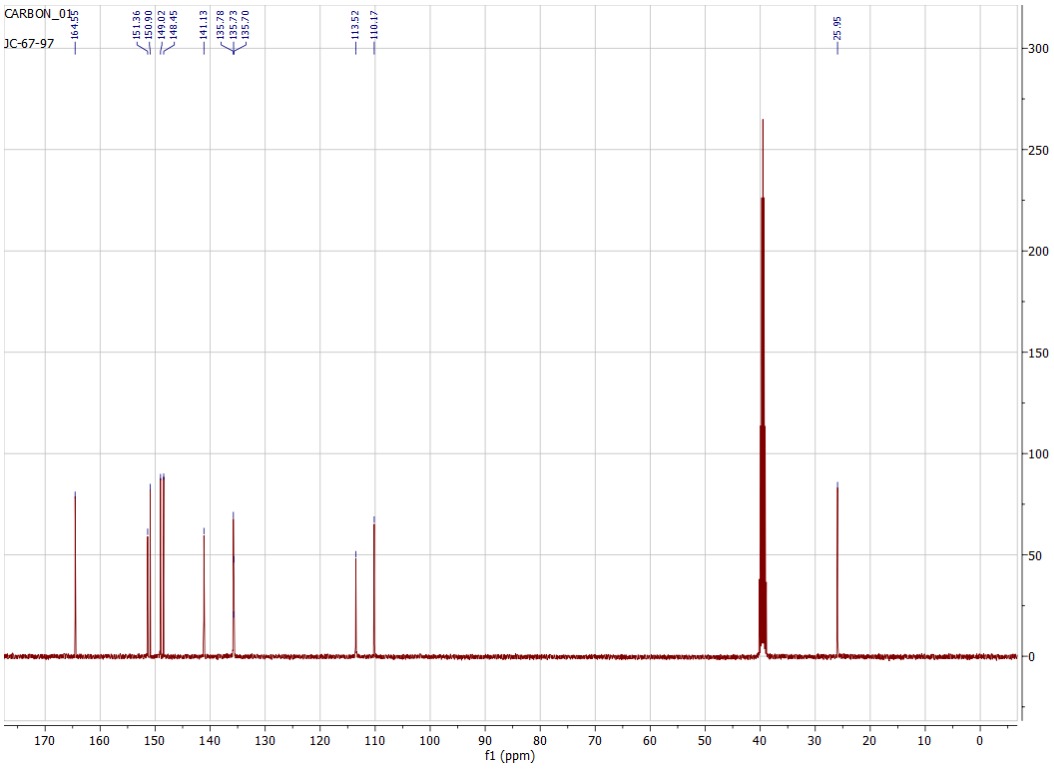

^{1}H NMR Spectrum of ***1,1'-(bis(3,5-xylyl)phosphino)ferrocene***, $\mathbf{L^{Me}}$ ($CDCl_3$, 500 MHz)

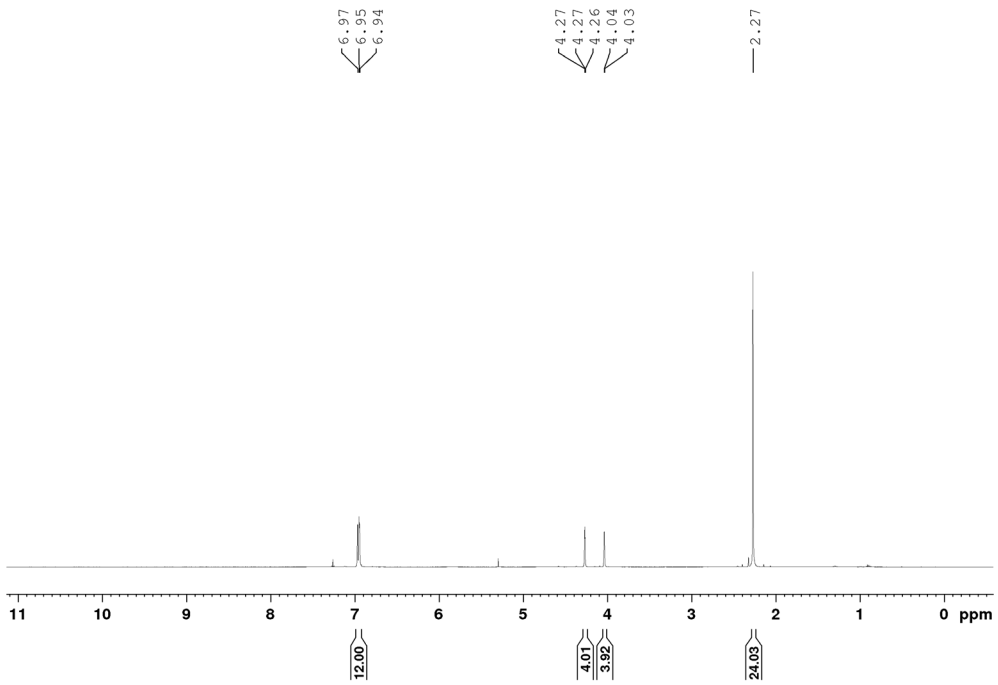

^{13}C{^{1}H} NMR Spectrum of $\mathbf{L^{Me}}$ ($CDCl_3$, 125.8 MHz)

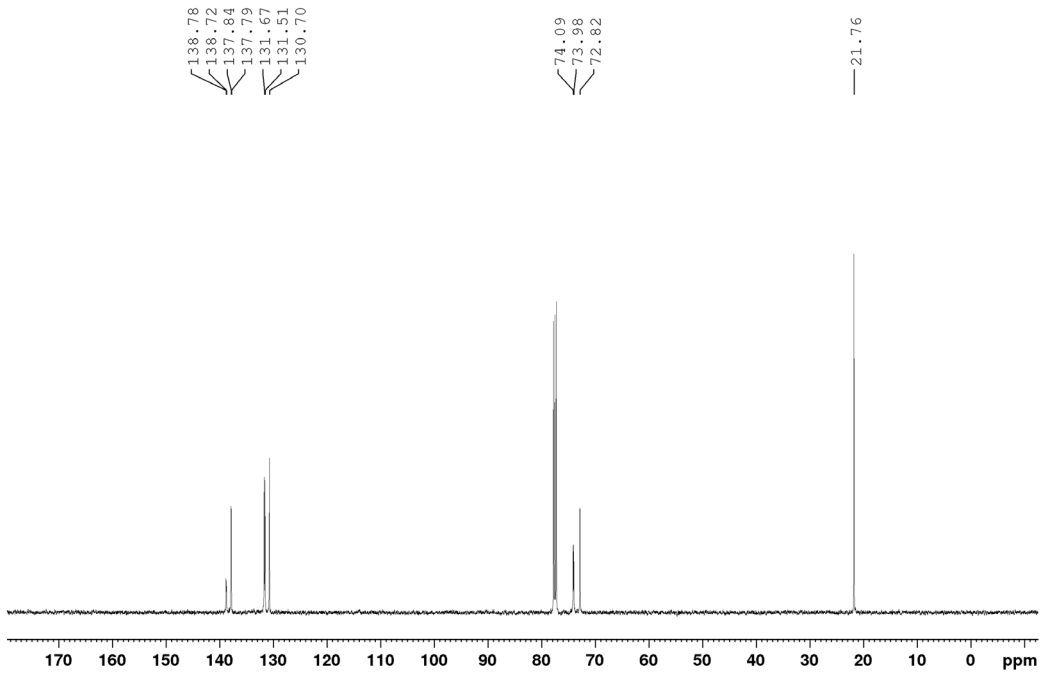

$^{31}P\{^{1}H\}$ NMR Spectrum of $\mathbf{L^{Me}}$ ($CDCl_3$, 202.5 MHz)

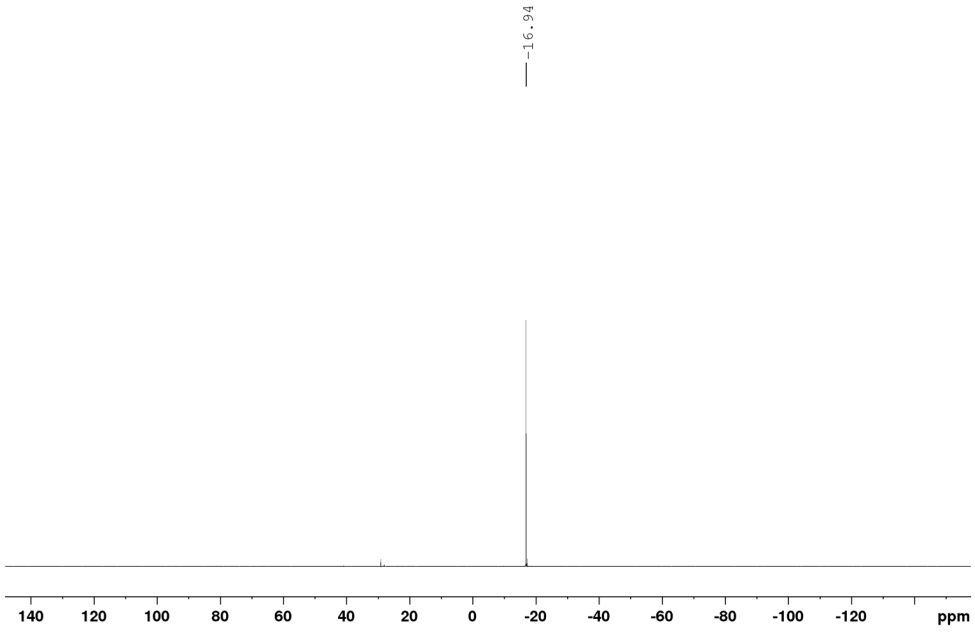

^{1}H NMR Spectrum of ***1,1'-(bis(di-(3,5-dimethyl-4-anisyl))phosphino)ferrocene***, $\mathbf{L^{OMe}}$ ($CDCl_3$, 500 MHz)

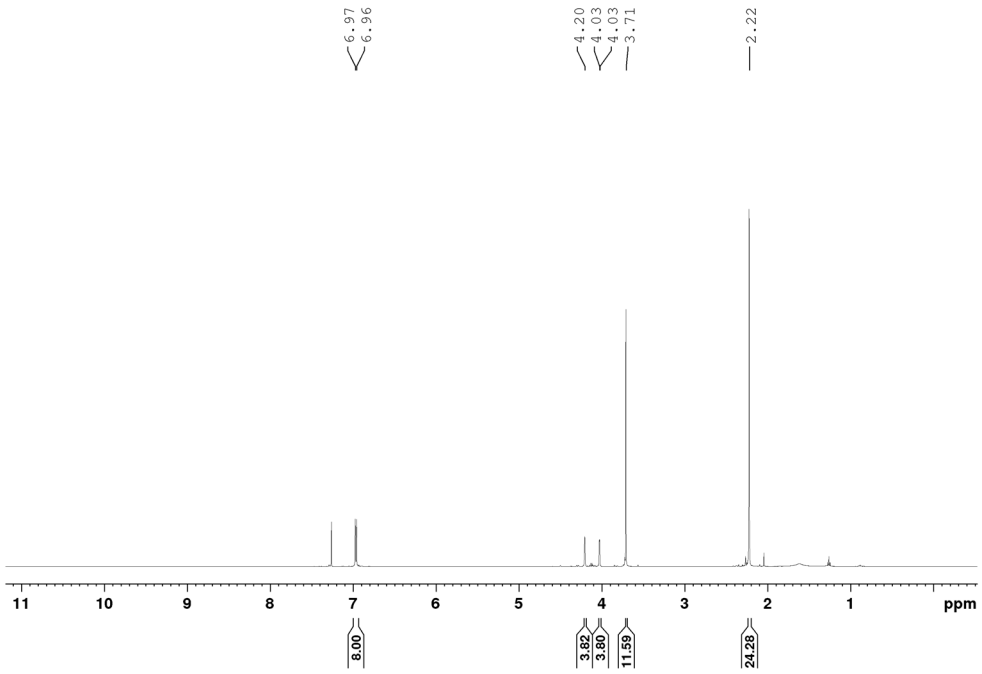

$^{13}C\{^{1}H\}$ NMR Spectrum of $\mathbf{L^{OMe}}$ ($CDCl_3$, 125.8 MHz)

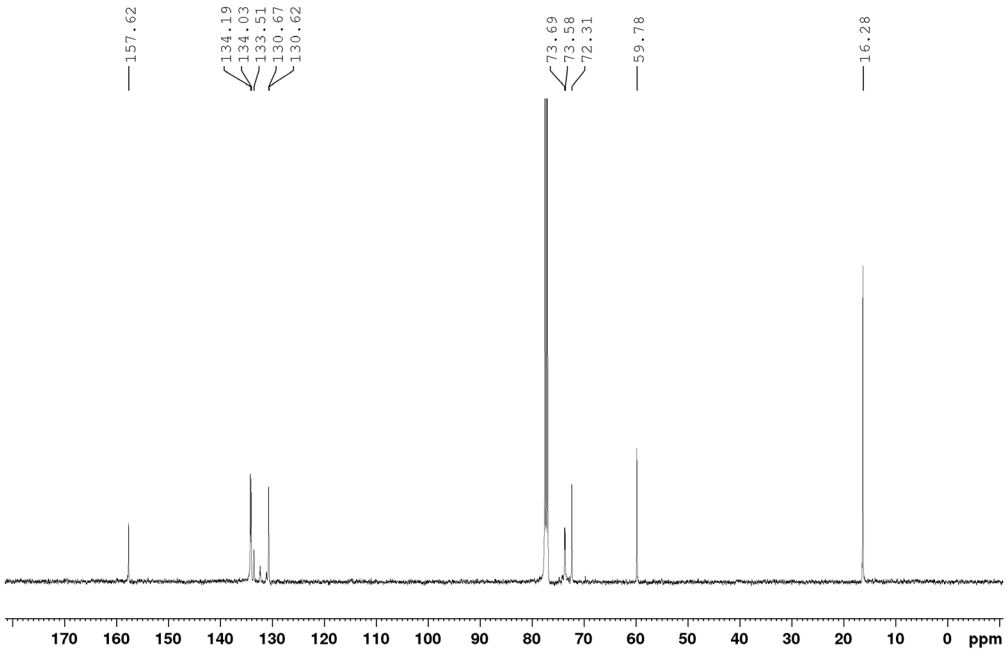

$^{31}P\{^{1}H\}$ NMR Spectrum of $\mathbf{L^{OMe}}$ ($CDCl_3$, 202.5 MHz)

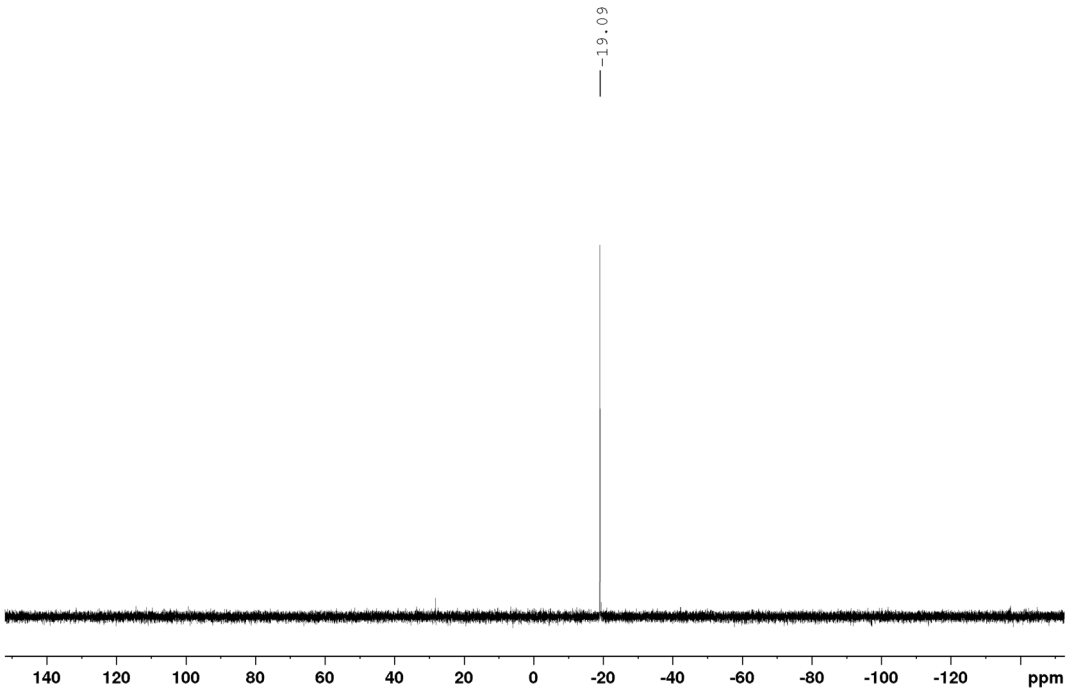

^{1}H NMR Spectrum of ***1-P(o-tol)$_2$-2-bromobenzene***, **P2** ($CDCl_3$, 500 MHz)

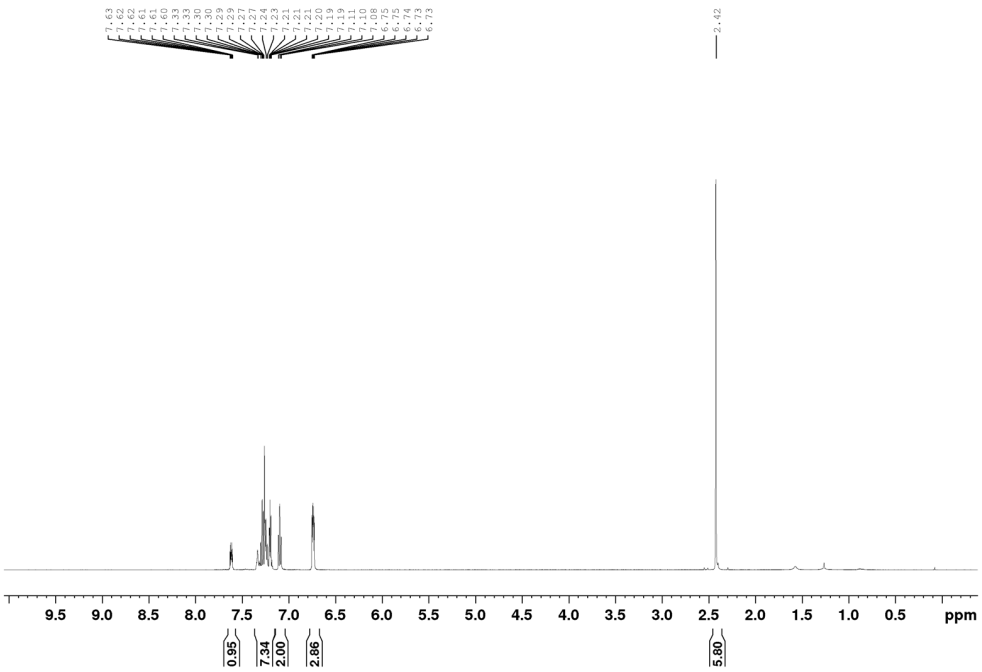

$^{13}C\{^{1}H\}$ NMR Spectrum of **P2**, ($CDCl_3$, 125.8 MHz)

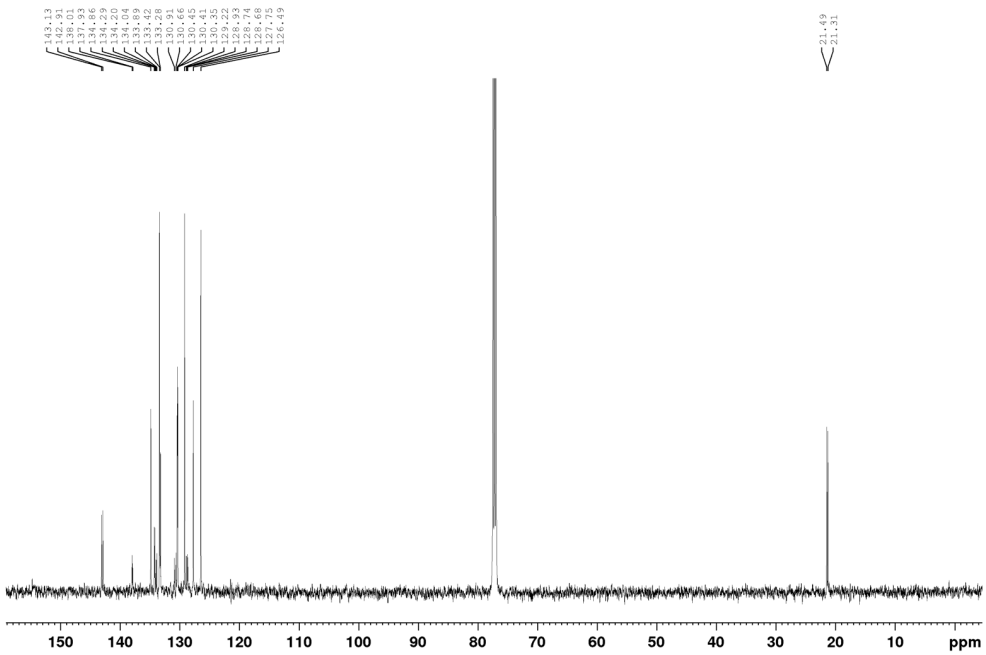

$^{31}P\{^{1}H\}$ NMR Spectrum of **P2**, ($CDCl_3$, 202.5 MHz)

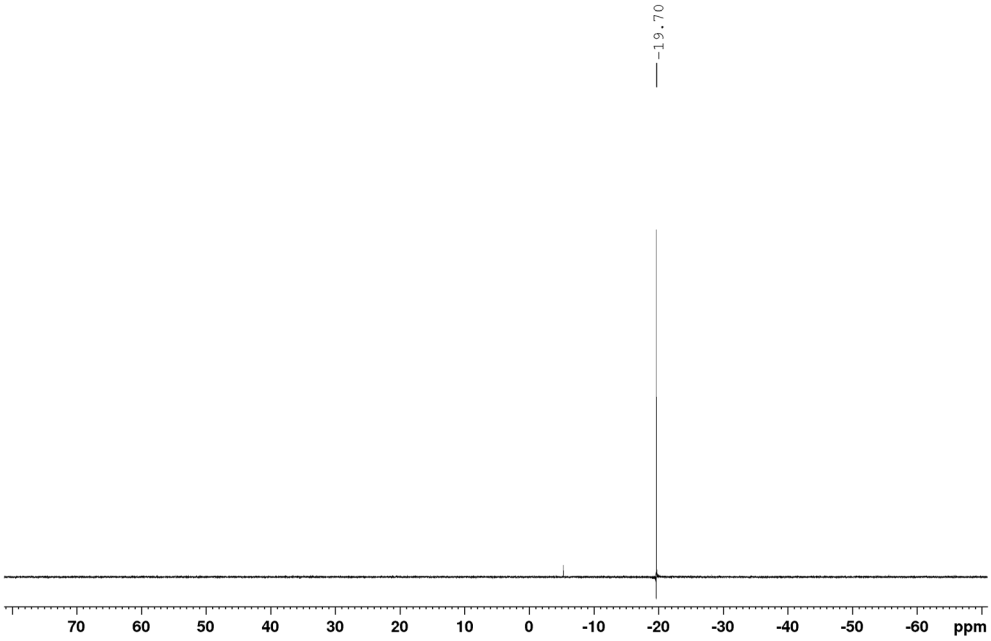

^{1}H NMR Spectrum of ***2-PCg-3-bromopyridine***, **P3** ($CDCl_3$, 500 MHz)

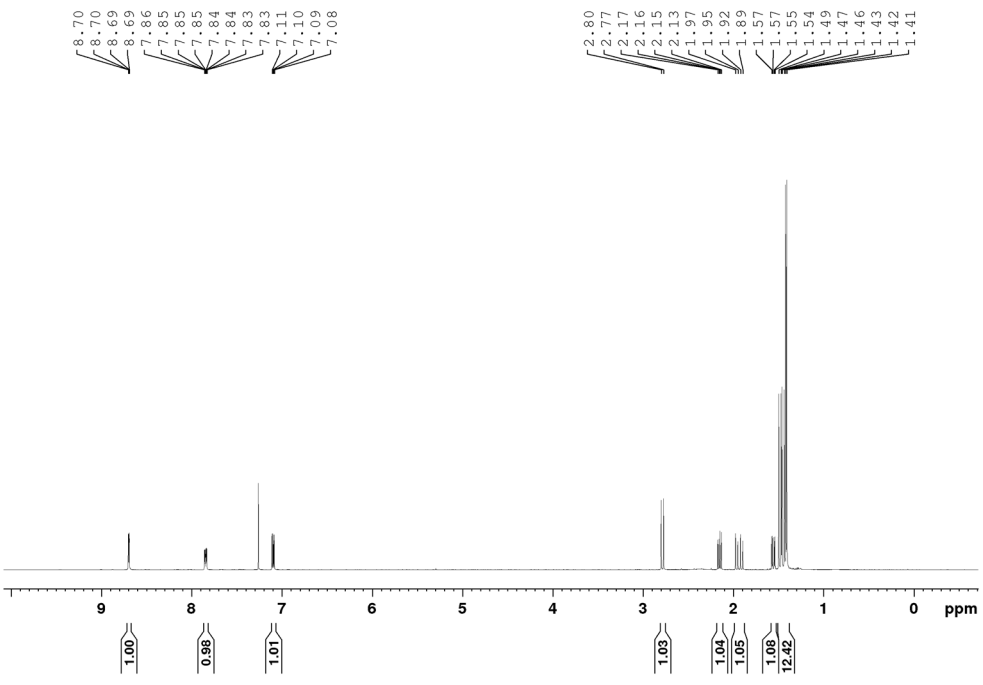

$^{13}C\{^{1}H\}$ NMR Spectrum of **P3**, ($CDCl_3$, 125.8 MHz)

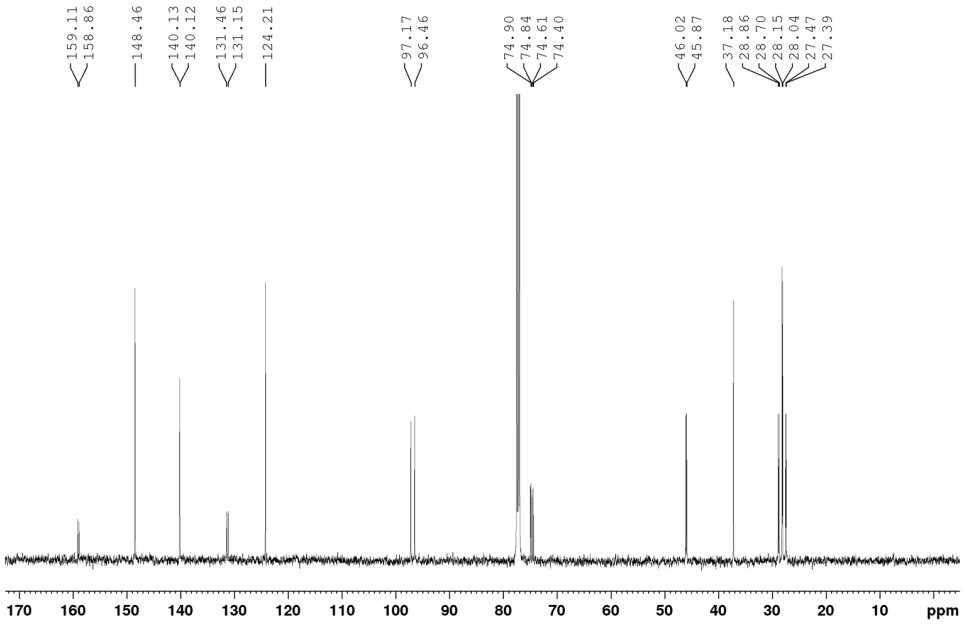

$^{31}P\{^{1}H\}$ NMR Spectrum of **P3**, ($CDCl_3$, 202.5 MHz)

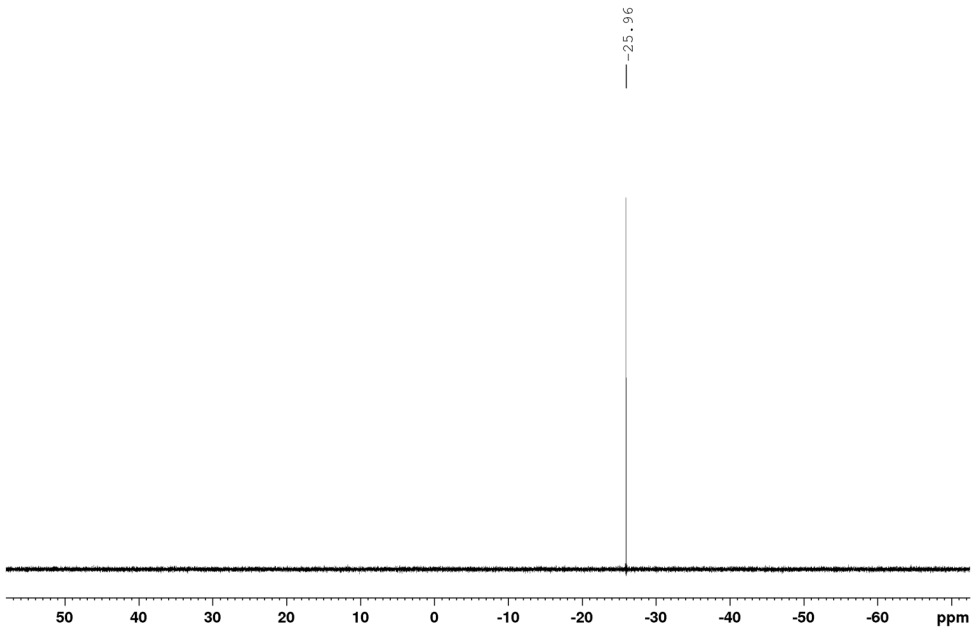

^{1}H NMR Spectrum of ***2-P(o-tol)$_2$-3-bromopyridine***, **P4** ($CDCl_3$, 300 MHz)

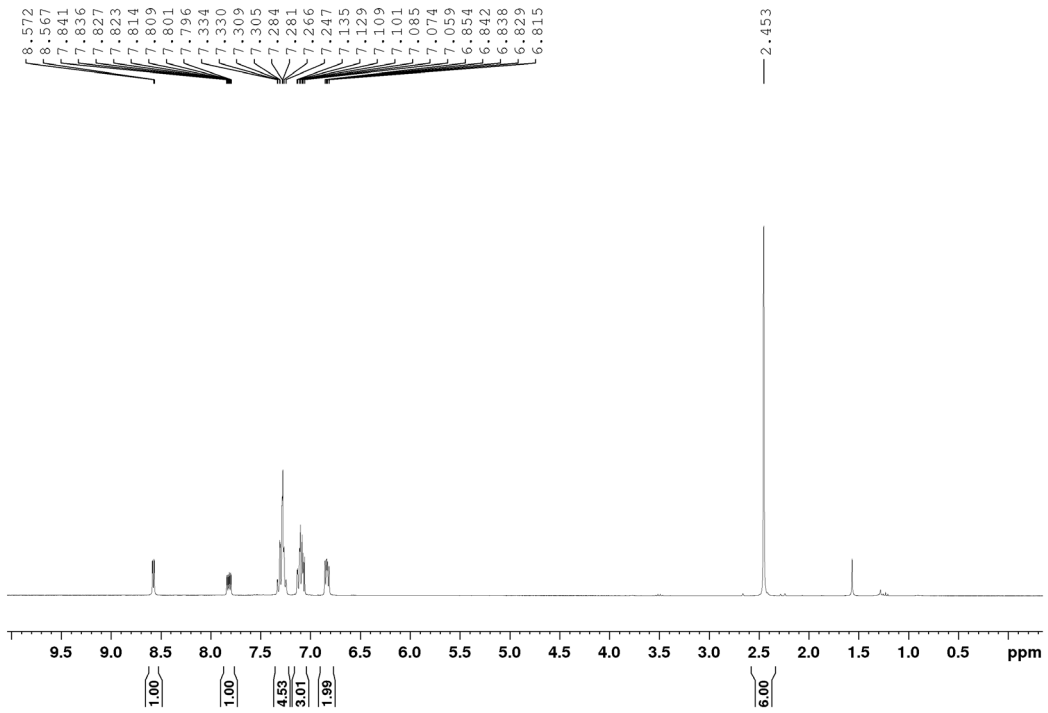

^{13}C{^{1}H} NMR Spectrum of **P4**, ($CDCl_3$, 125.8 MHz)

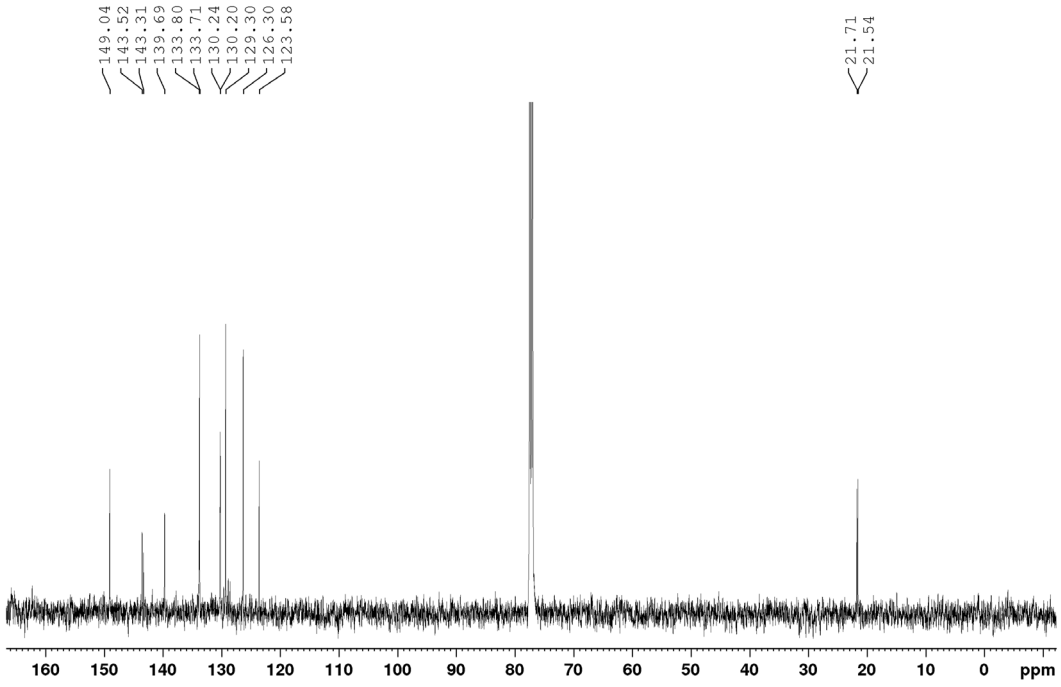

$^{13}C\{^{1}H\}$ UDEFT NMR Spectrum of **P4**, ($CDCl_3$, 75.4 MHz)

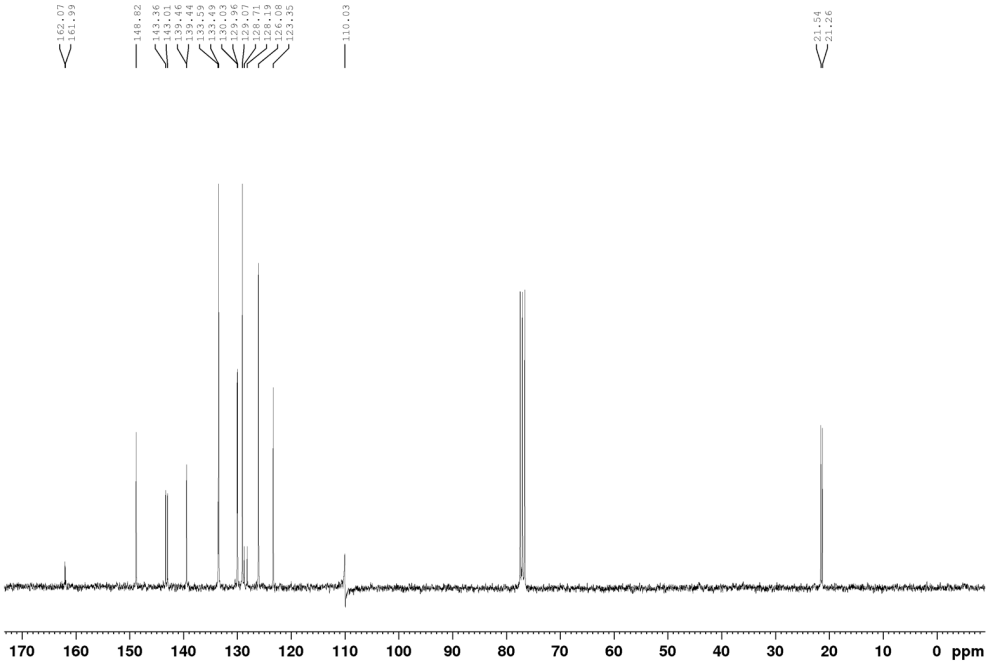

$^{31}P\{^{1}H\}$ NMR Spectrum of **P4**, ($CDCl_3$, 202.5 MHz)

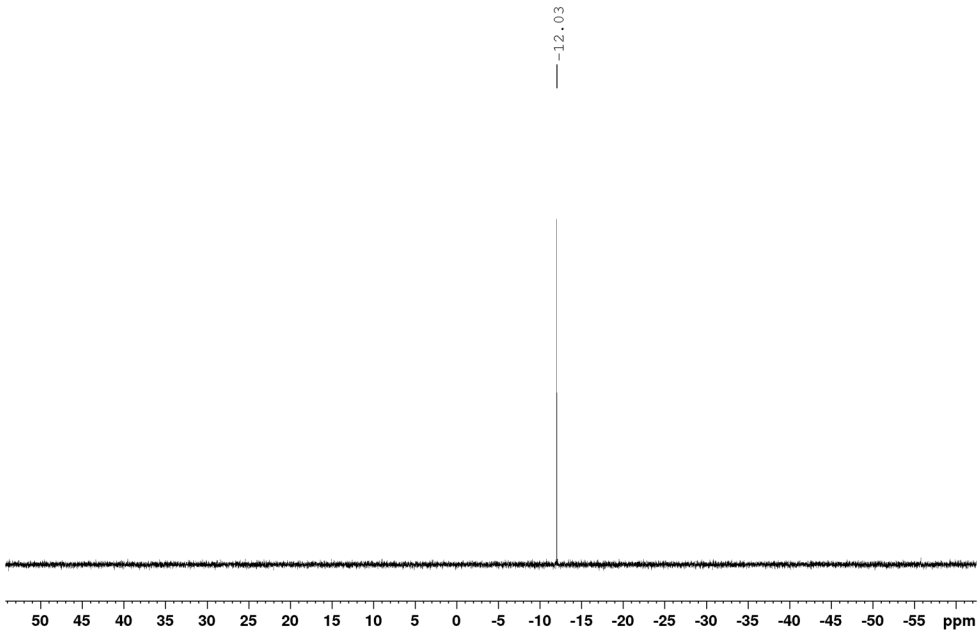

^{1}H NMR Spectrum of ***2-PCg-3-bromothiophene***, **P5** ($CDCl_3$, 500 MHz)

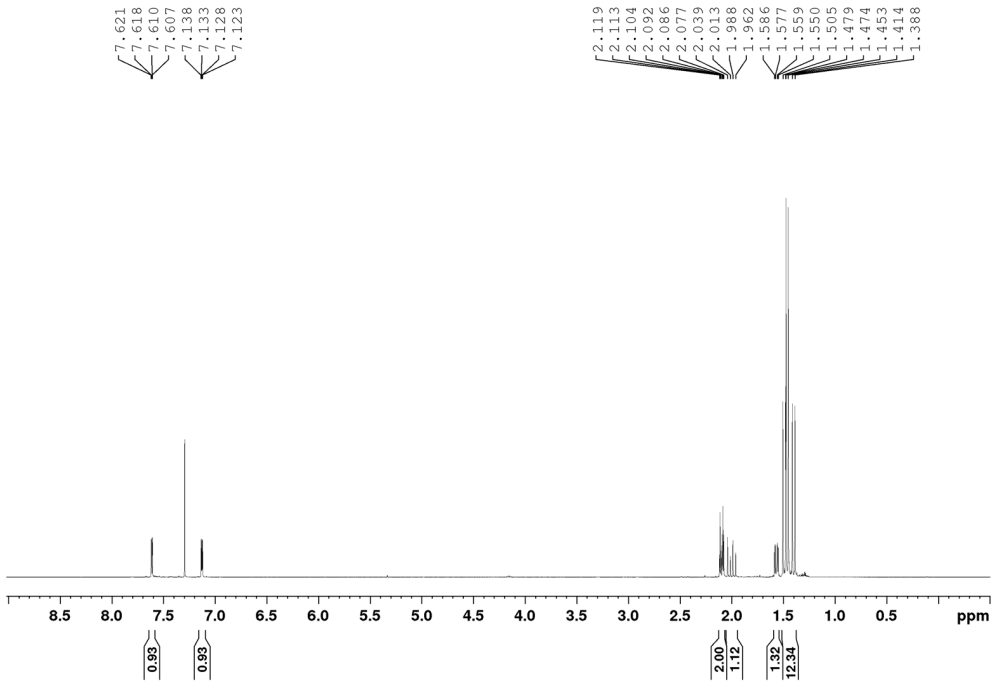

^{13}C{^{1}H} NMR Spectrum of **P5**, ($CDCl_3$, 125.8 MHz)

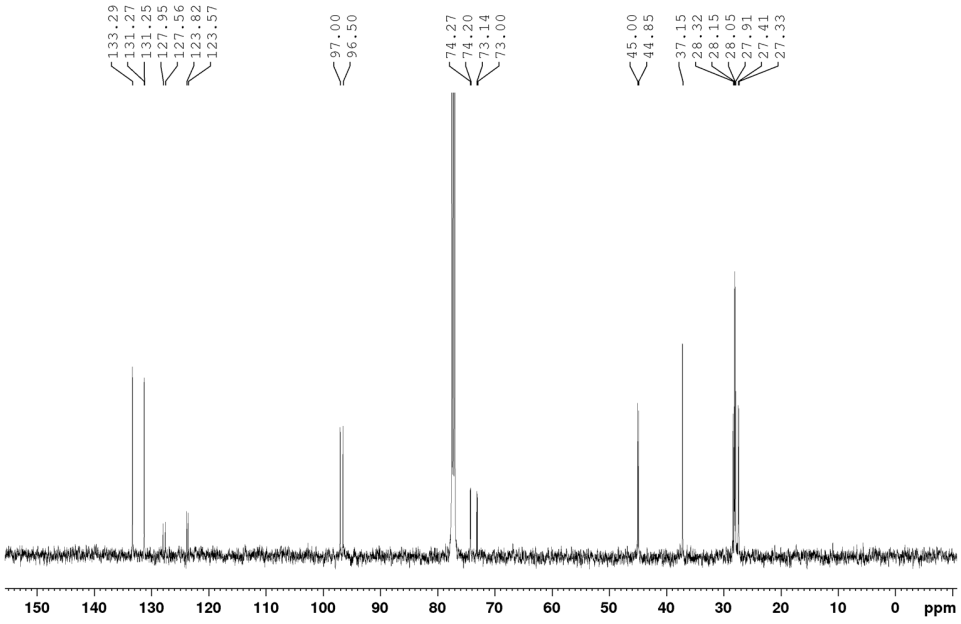

$^{31}P\{^{1}H\}$ NMR Spectrum of **P5**, ($CDCl_3$, 202.5 MHz)

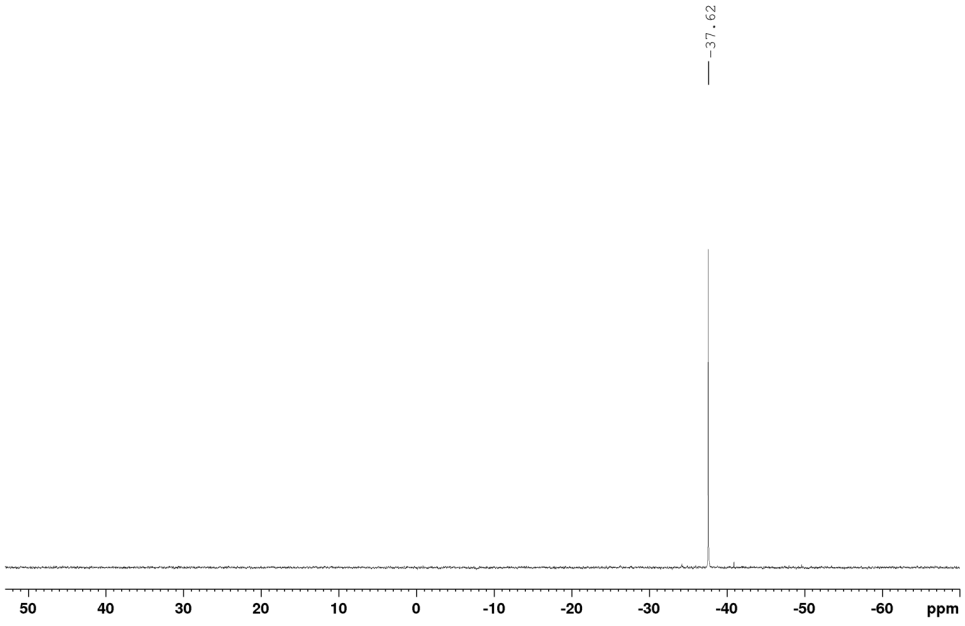

^{1}H NMR Spectrum of ***2-P(o-tol)$_2$-3-bromothiophene,*** **P6** ($CDCl_3$, 300 MHz)

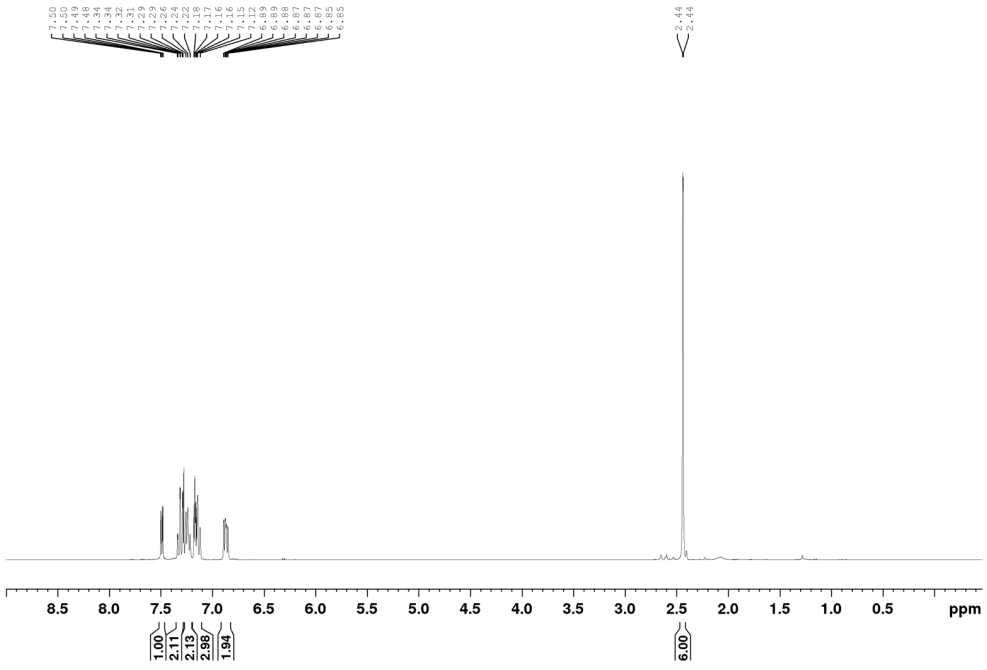

$^{13}C\{^{1}H\}$ NMR Spectrum of **P6**, ($CDCl_3$, 125.8 MHz)

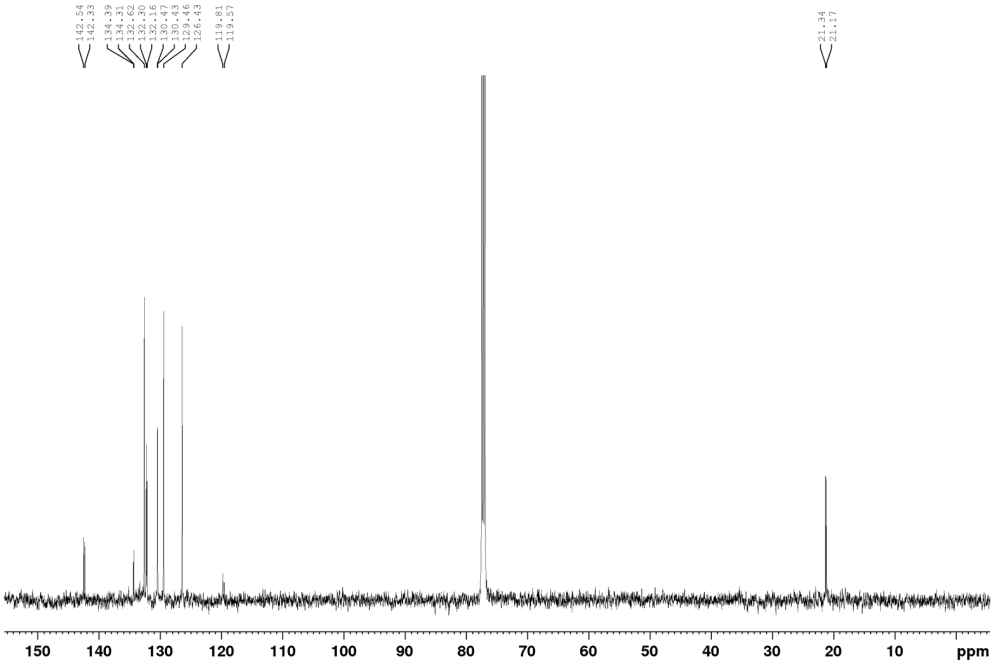

^{31}P NMR Spectrum of **P6**, ($CDCl_3$, 121.5 MHz)

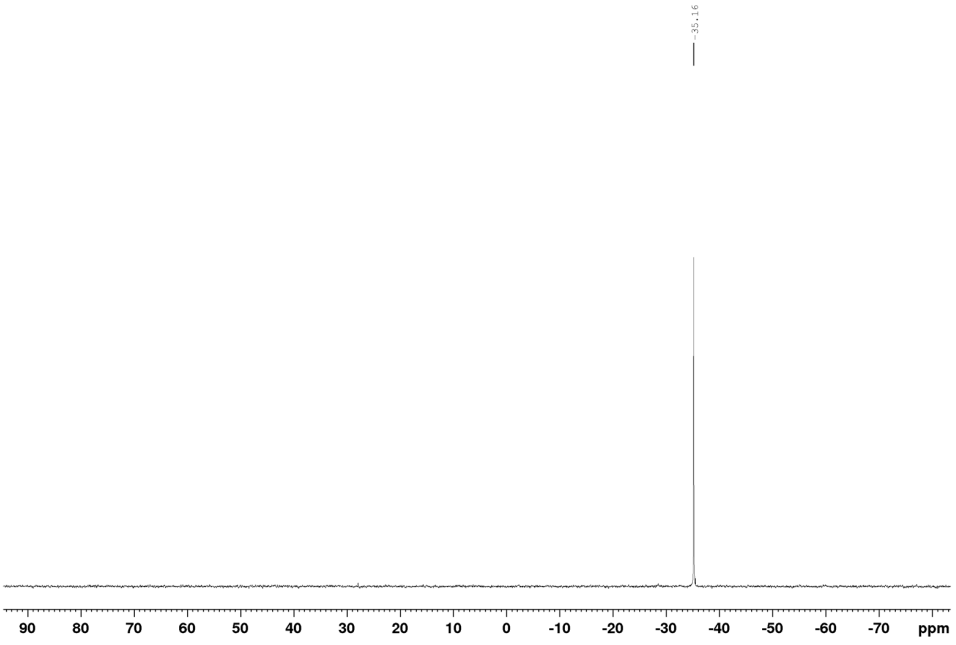

^{1}H NMR Spectrum of ***3-P(o-tol)$_2$-4-bromothiophene***, **P7** ($CDCl_3$, 500 MHz)

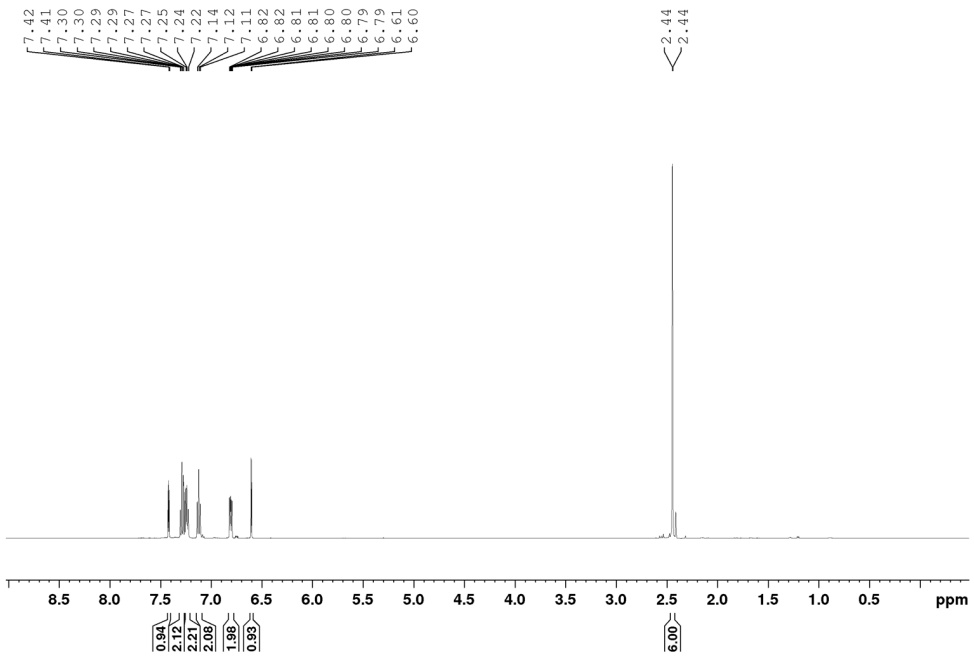

^{13}C{^{1}H} NMR Spectrum of **P7**, ($CDCl_3$, 125.8 MHz)

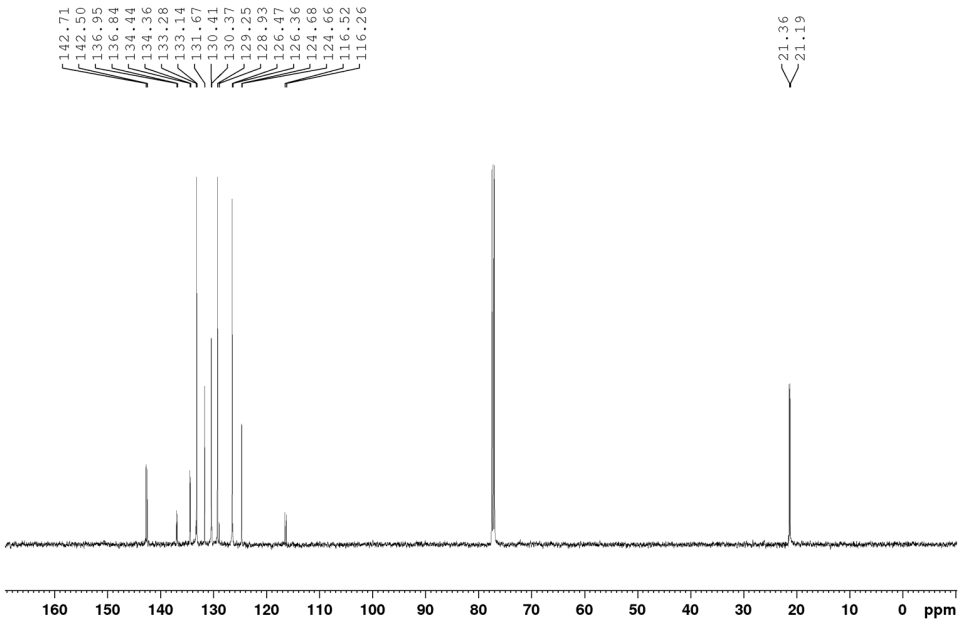

$^{31}P\{^{1}H\}$ NMR Spectrum of **P7**, ($CDCl_3$, 202.5 MHz)

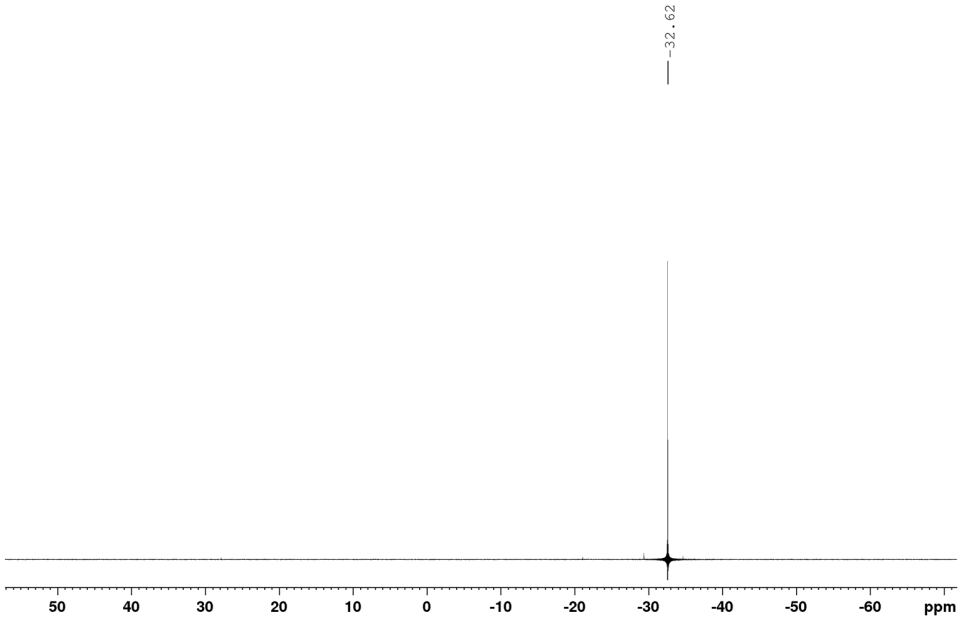

^{1}H NMR Spectrum of ***2-chloro-3-PCg-pyridine***, **P8** ($CDCl_3$, 500 MHz)

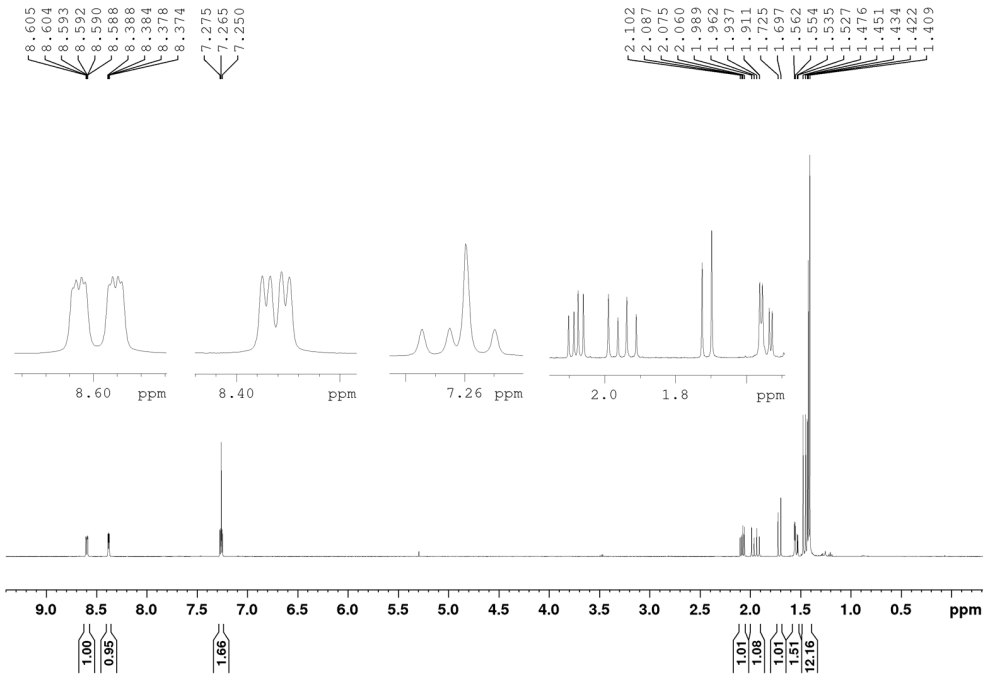

$^{13}C\{^{1}H\}$ UDEFT NMR Spectrum of **P8** ($CDCl_3$, 125.8 MHz)

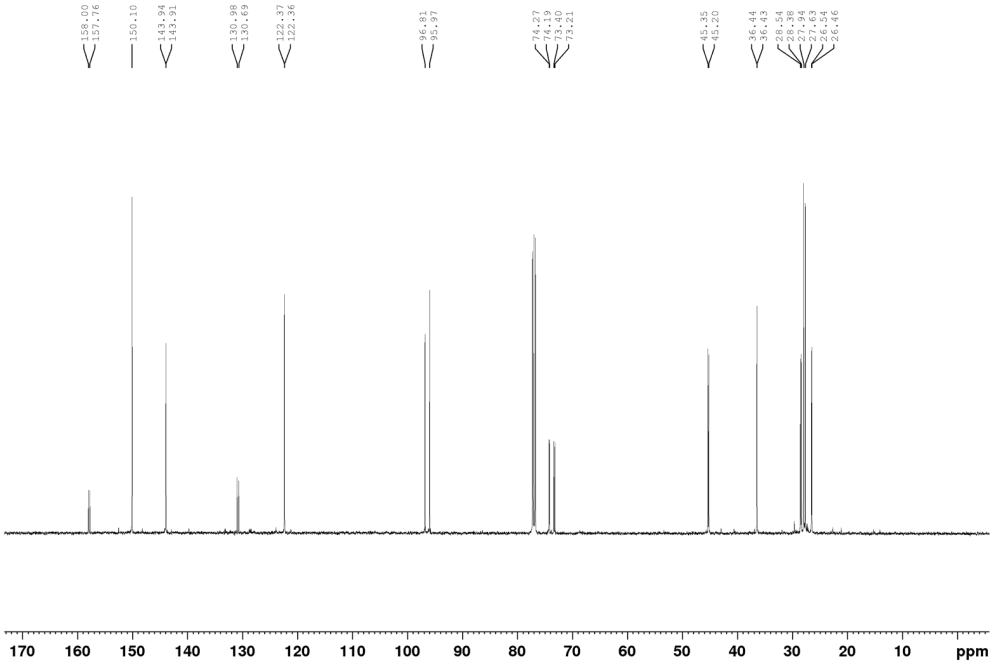

$^{31}P\{^{1}H\}$ NMR Spectrum of **P8** ($CDCl_3$, 202.5 MHz)

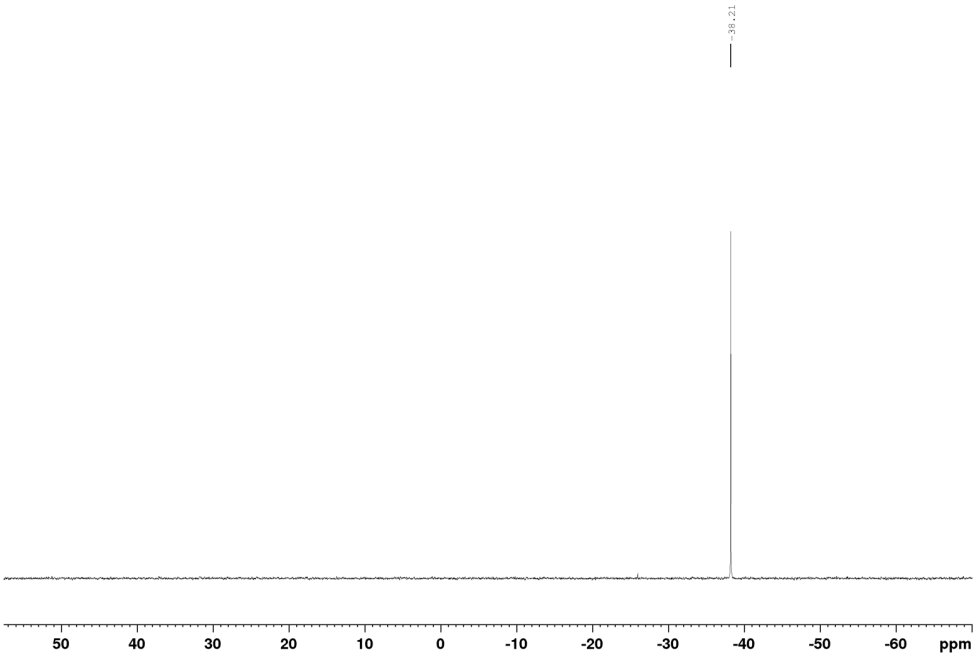

^{1}H NMR Spectrum of ***2-chloro-3-PCg-quinoxaline***, **P9** ($CDCl_3$, 500 MHz)

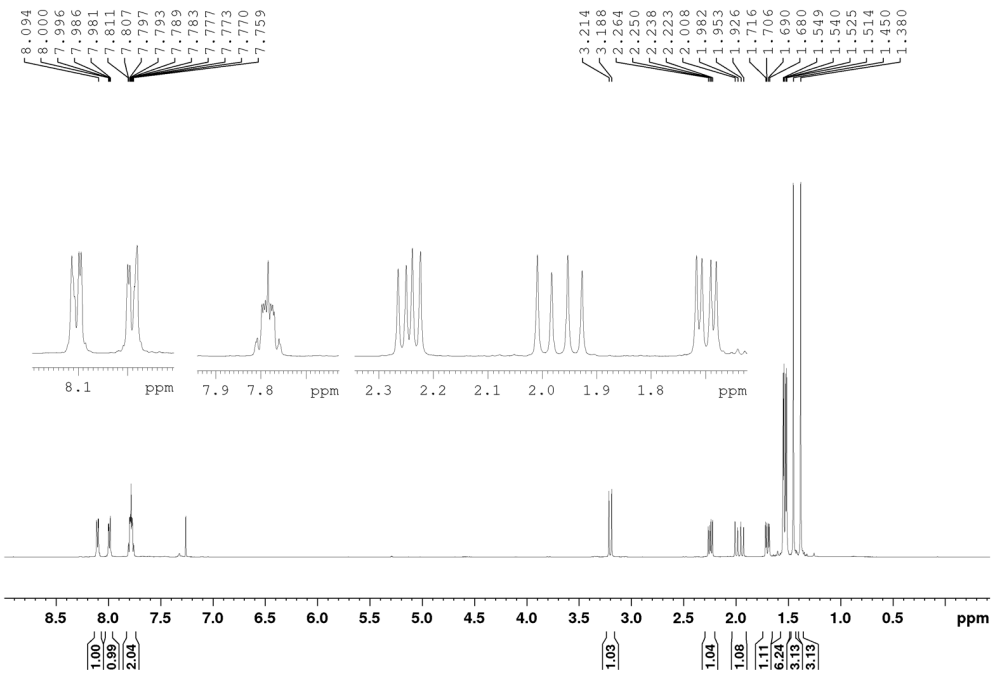

^{13}C{^{1}H} UDEFT NMR Spectrum of **P9** ($CDCl_3$, 125.8 MHz)

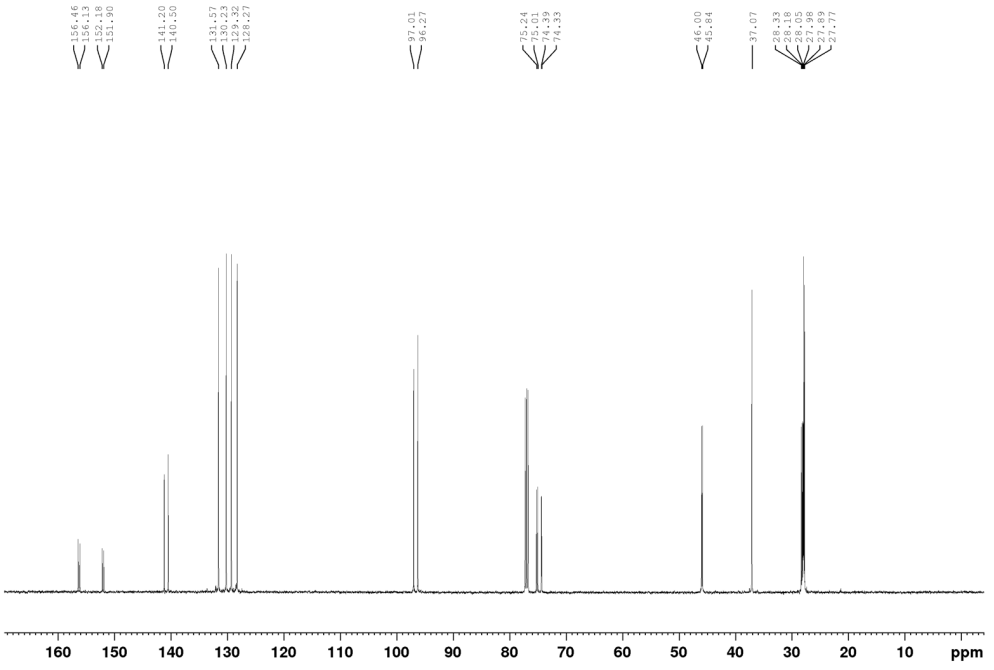

$^{31}P\{^{1}H\}$ NMR Spectrum of **P9** ($CDCl_3$, 202.5 MHz)

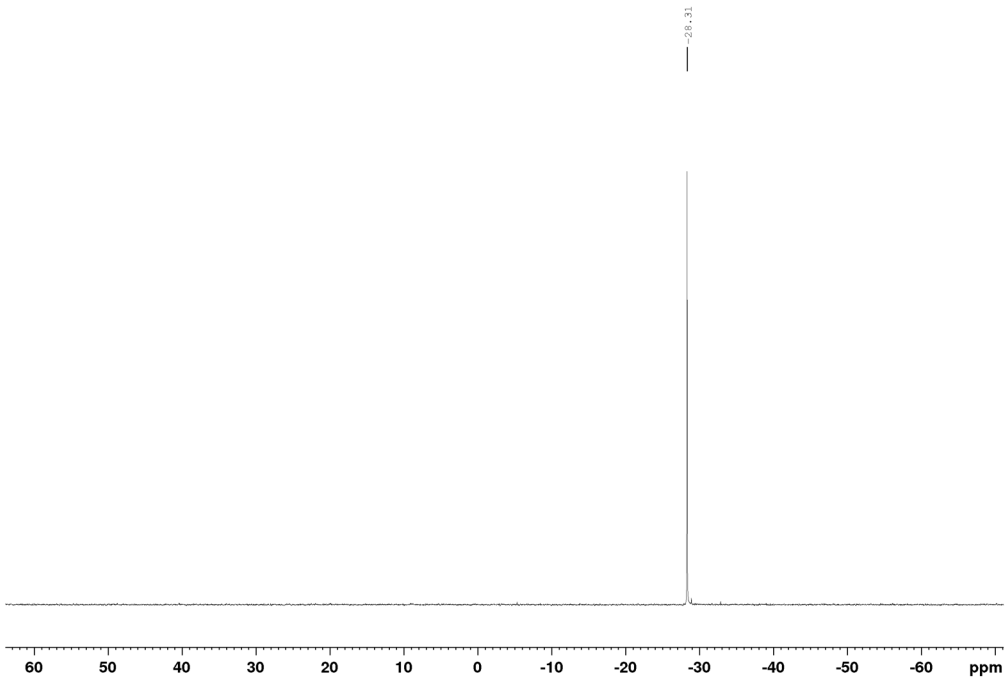

^{1}H NMR Spectrum of ***o-(P(o-tolyl)$_2$)$_2$benzene***, **2-L1** ($CDCl_3$, 500 MHz)

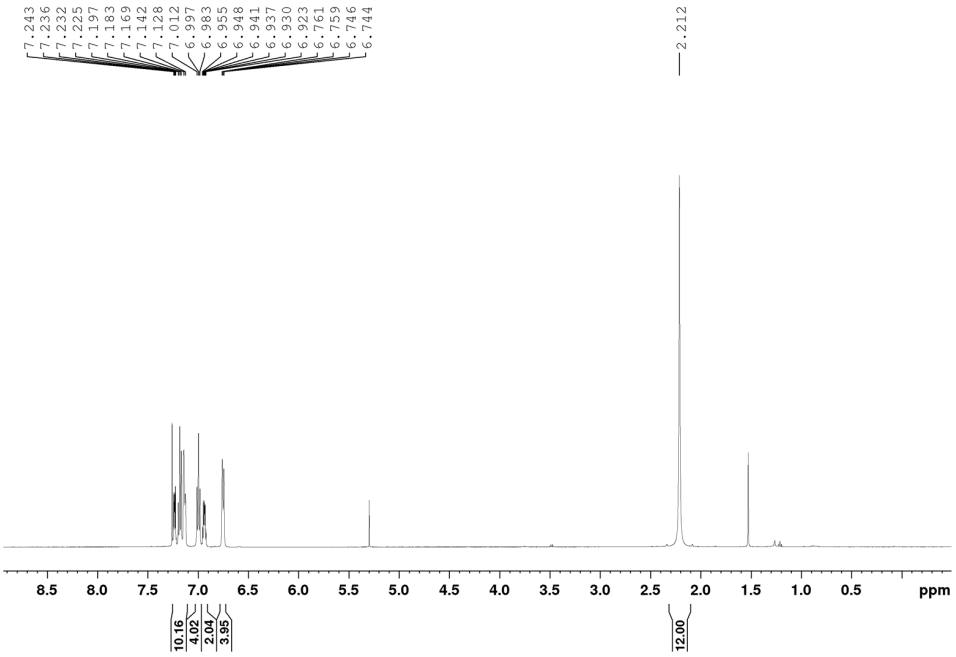

$^{13}C\{^{1}H\}$ NMR Spectrum of **2-L1**, ($CDCl_3$, 125.8 MHz)

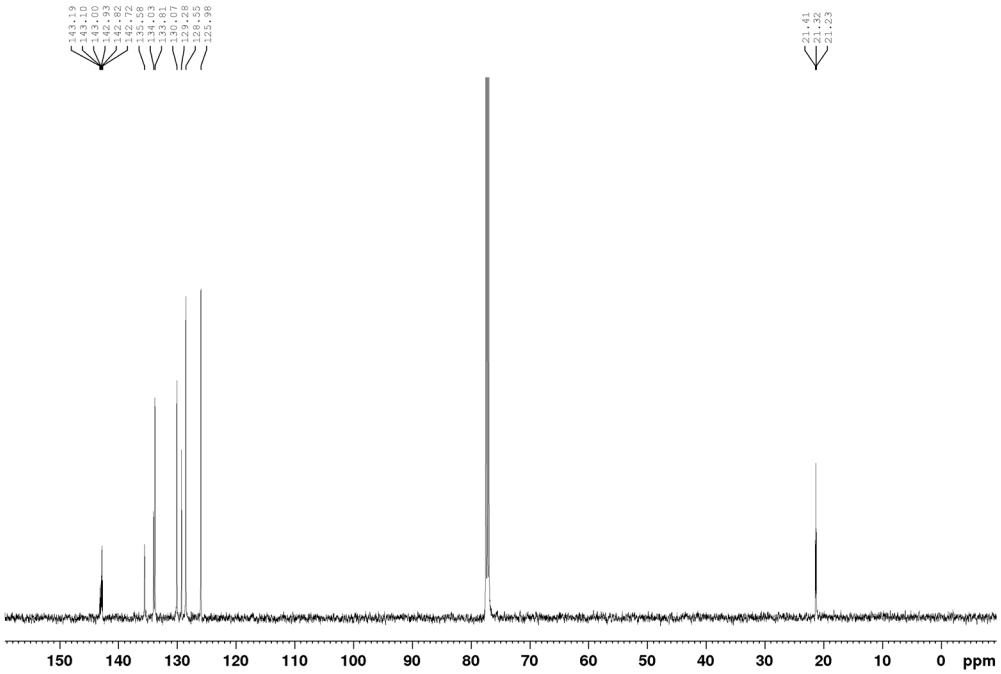

$^{13}C\{^{1}H\}$ UDEFT NMR Spectrum of **2-L1**, ($CDCl_3$, 125.8 MHz)

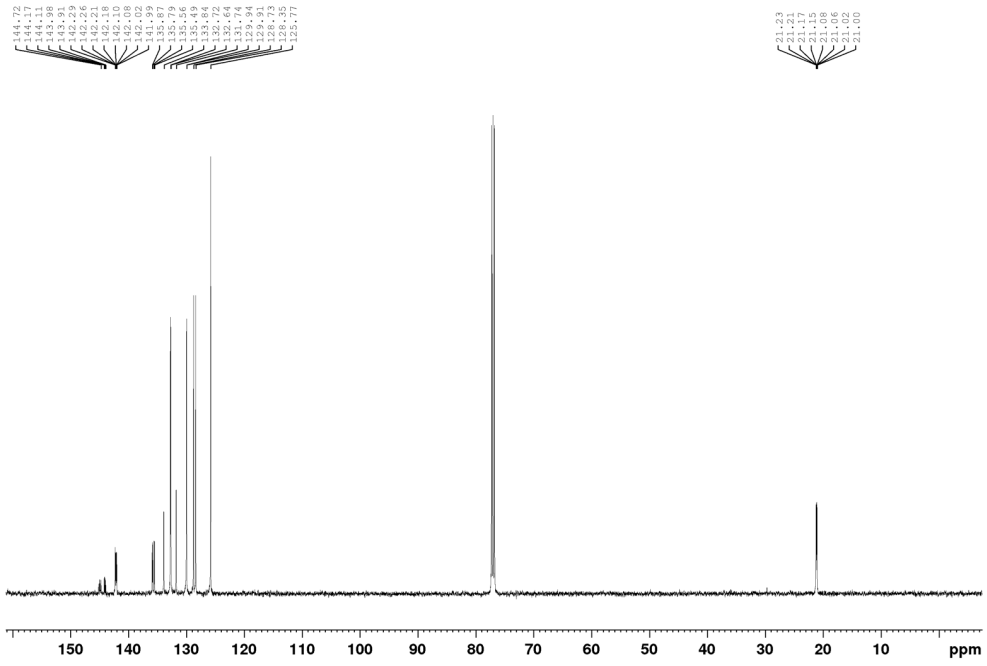

$^{31}P\{^{1}H\}$ NMR Spectrum of **2-L1**, ($CDCl_3$, 121.5 MHz)

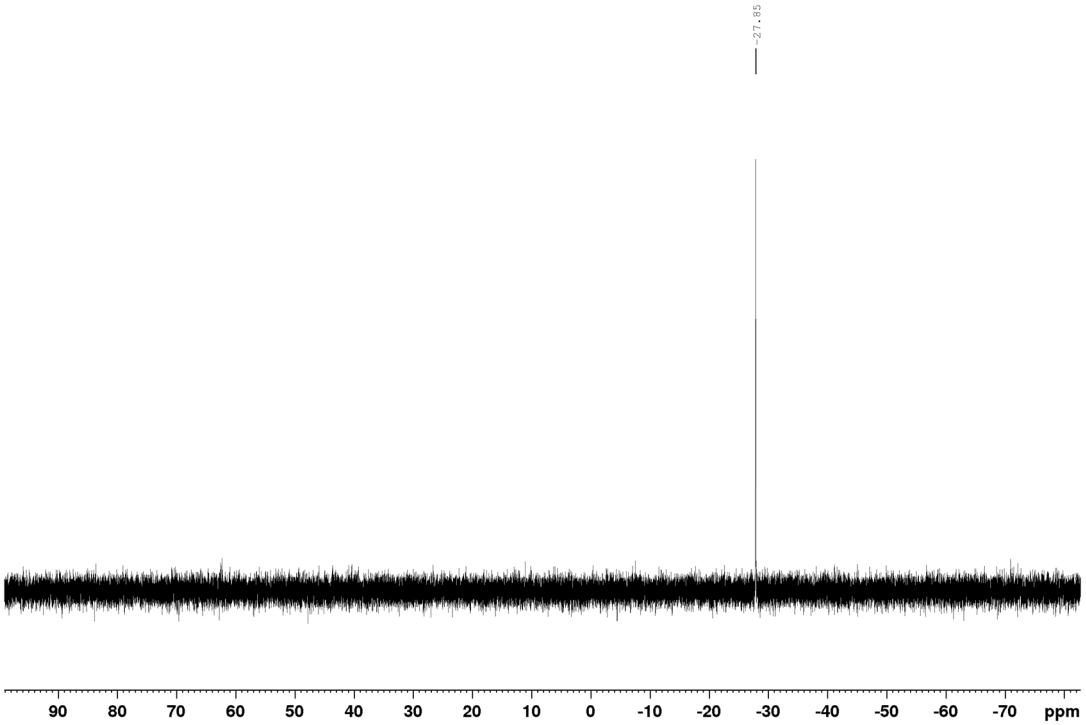

^{1}H NMR Spectrum of ***2-PCg-3-P(o-tolyl)$_2$-pyridine***, **2-L2** ($CDCl_3$, 500 MHz)

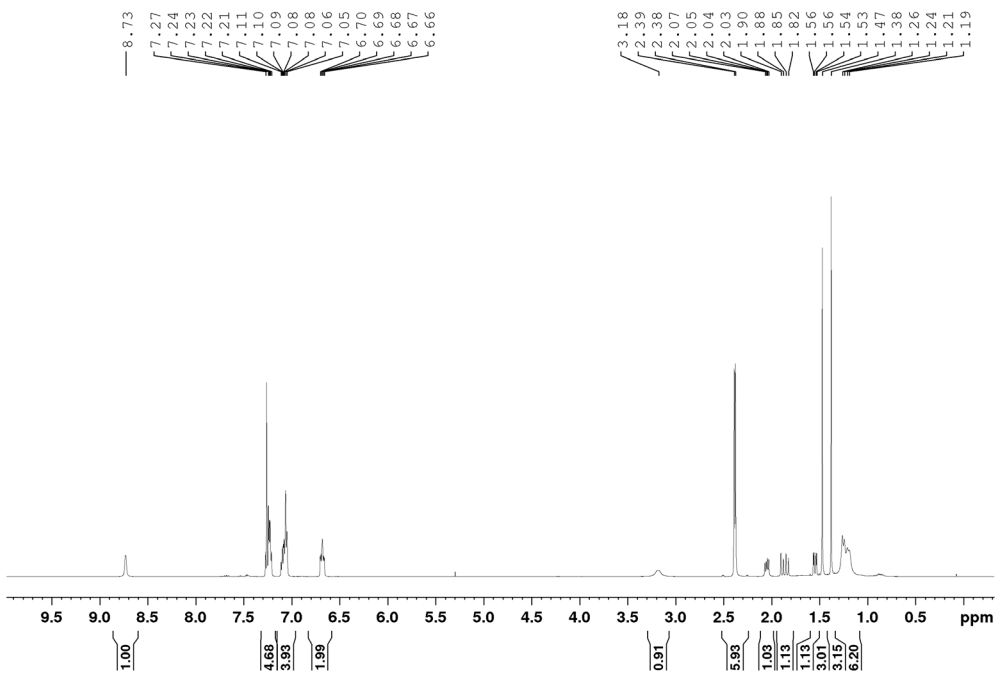

$^{13}C\{^{1}H\}$ NMR Spectrum of **2-L2**, ($CDCl_3$, 125.8 MHz)

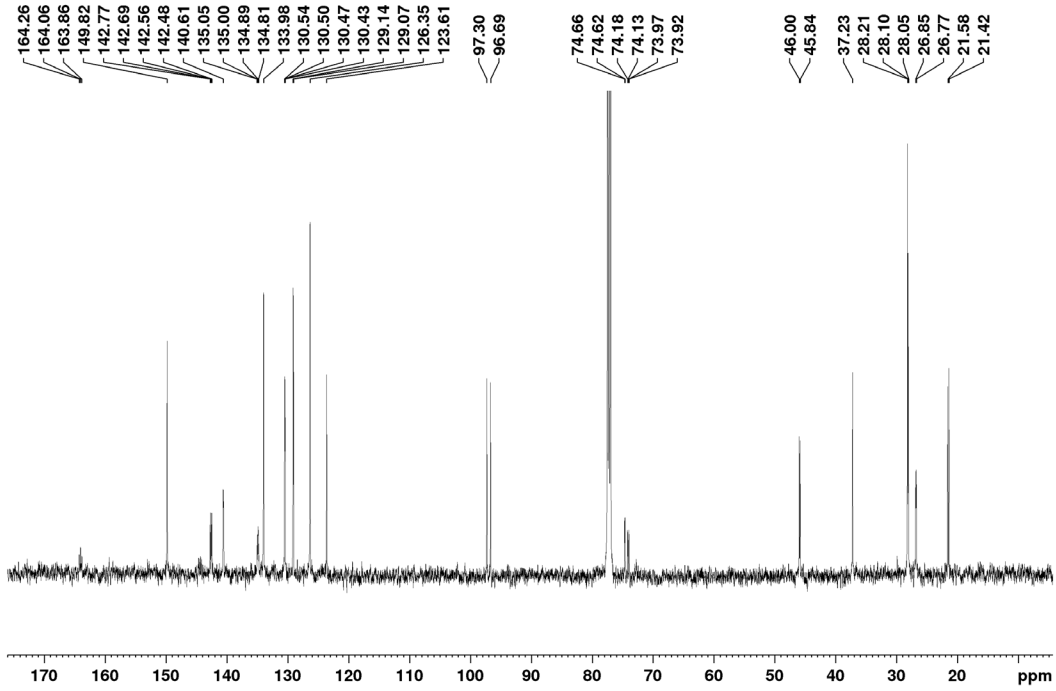

$^{13}C\{^{1}H\}$ UDEFT NMR Spectrum of **2-L2**, ($CDCl_3$, 125.8 MHz)

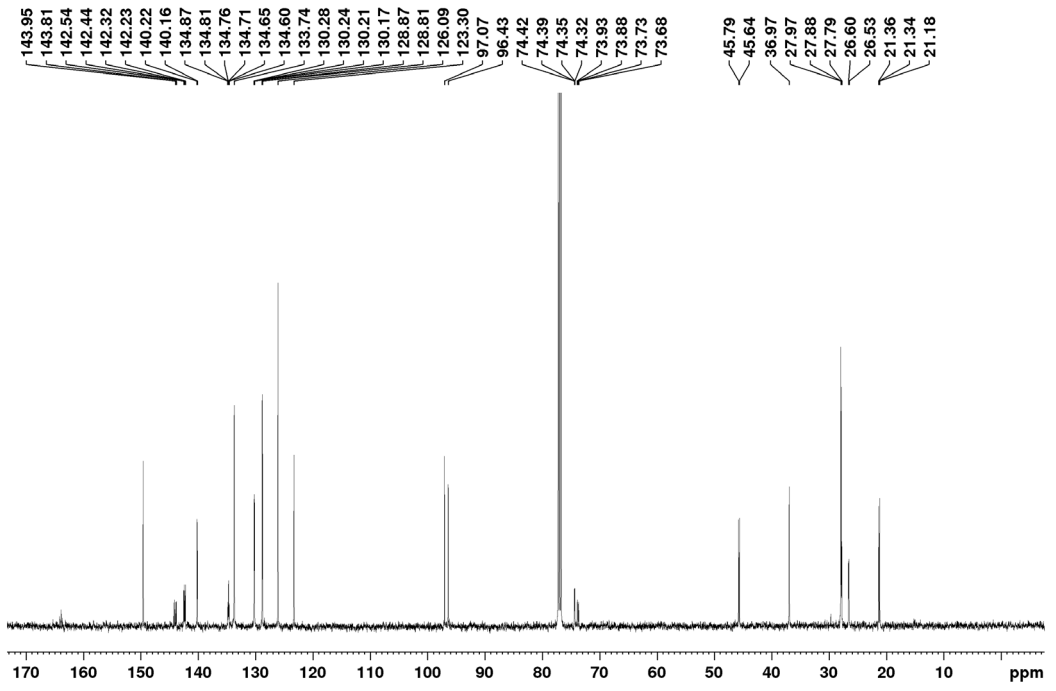

$^{31}P\{^{1}H\}$ NMR Spectrum of **2-L2**, ($CDCl_3$, 202.5 MHz)

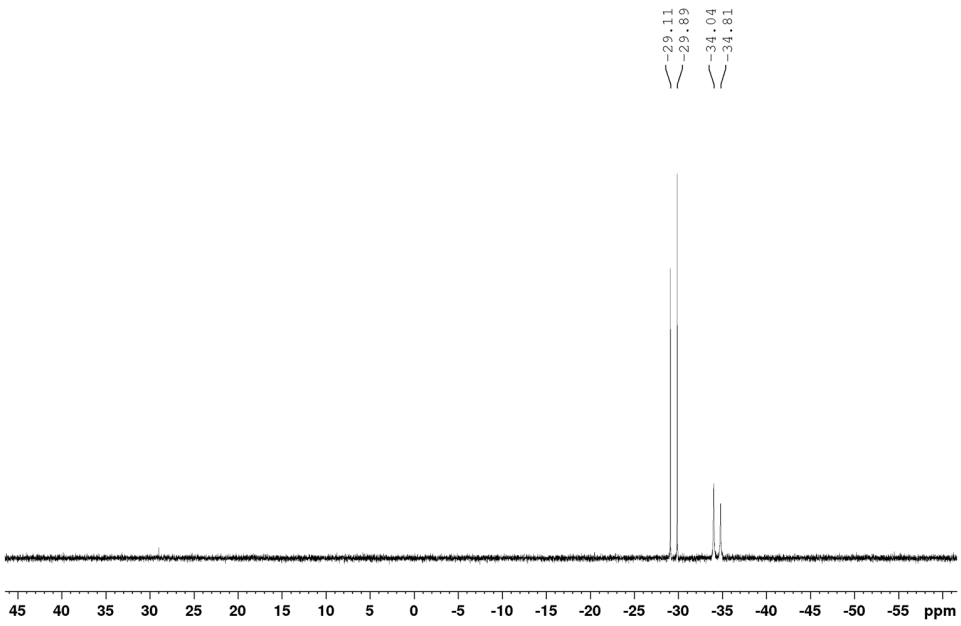

^{1}H NMR Spectrum of ***2-P(o-tolyl)$_2$-3-PCg-pyridine***, **2-L3**, ($CDCl_3$, 500 MHz)

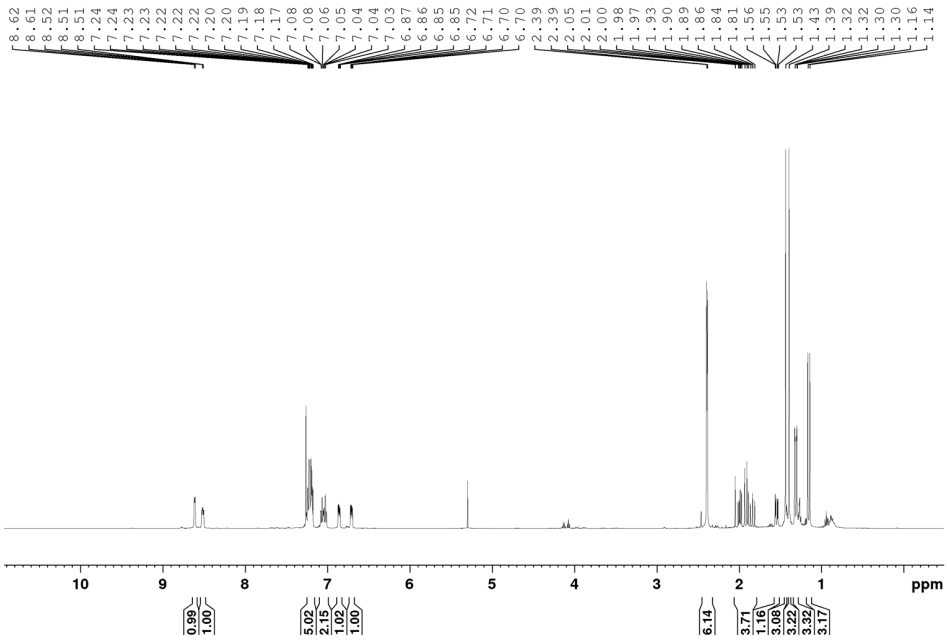

$^{13}C\{^{1}H\}$ NMR Spectrum of **2-L3**, ($CDCl_3$, 125.8 MHz)

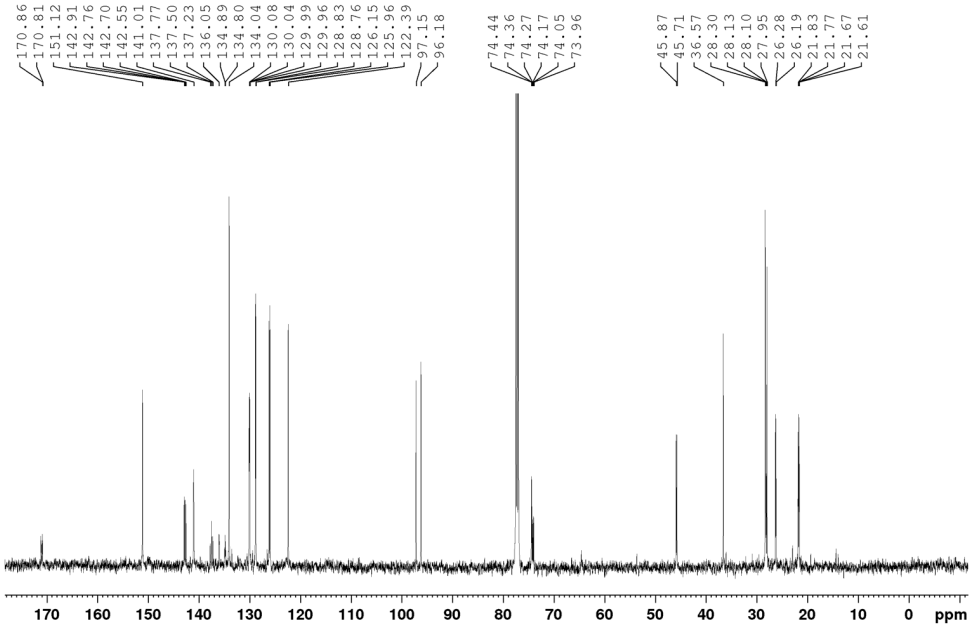

$^{13}C\{^{1}H\}$ UDEFT NMR Spectrum of **2-L3**, ($CDCl_3$, 125.8 MHz)

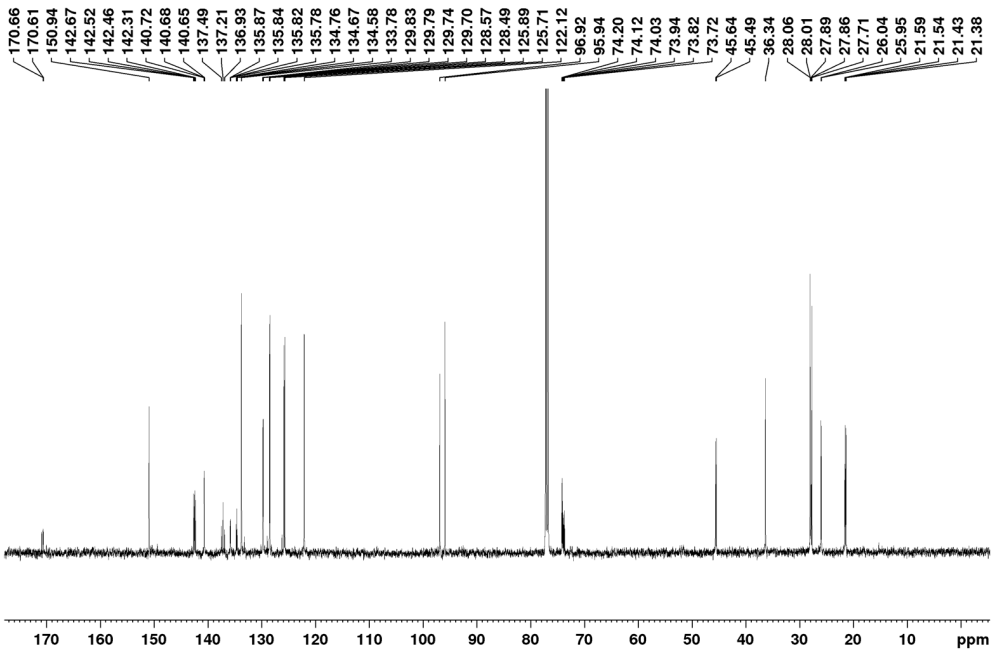

$^{31}P\{^{1}H\}$ NMR Spectrum of **2-L3**, ($CDCl_3$, 202.5 MHz)

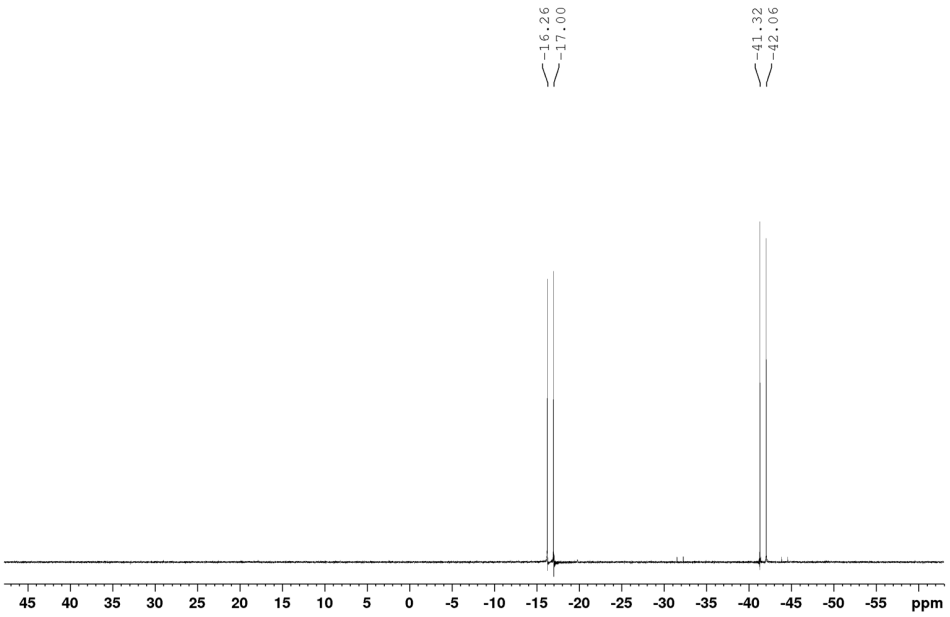

^{1}H NMR Spectrum of ***2,3-(P(o-tolyl)$_2$)$_2$-pyridine***, **2-L4** ($CDCl_3$, 500 MHz)

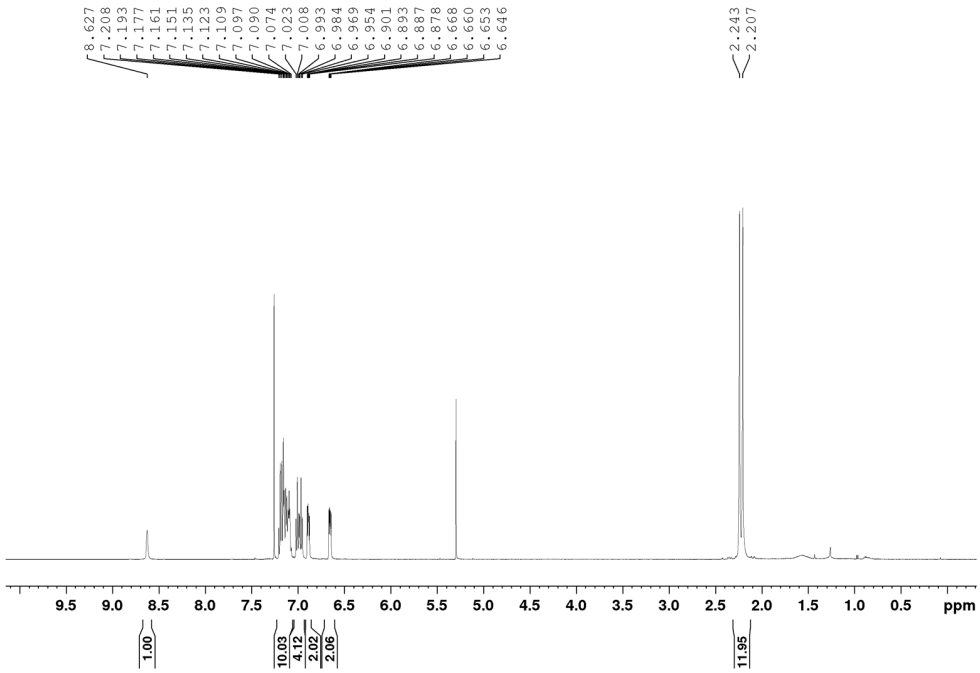

$^{13}C\{^{1}H\}$ NMR Spectrum of **2-L4**, ($CDCl_3$, 125.8 MHz)

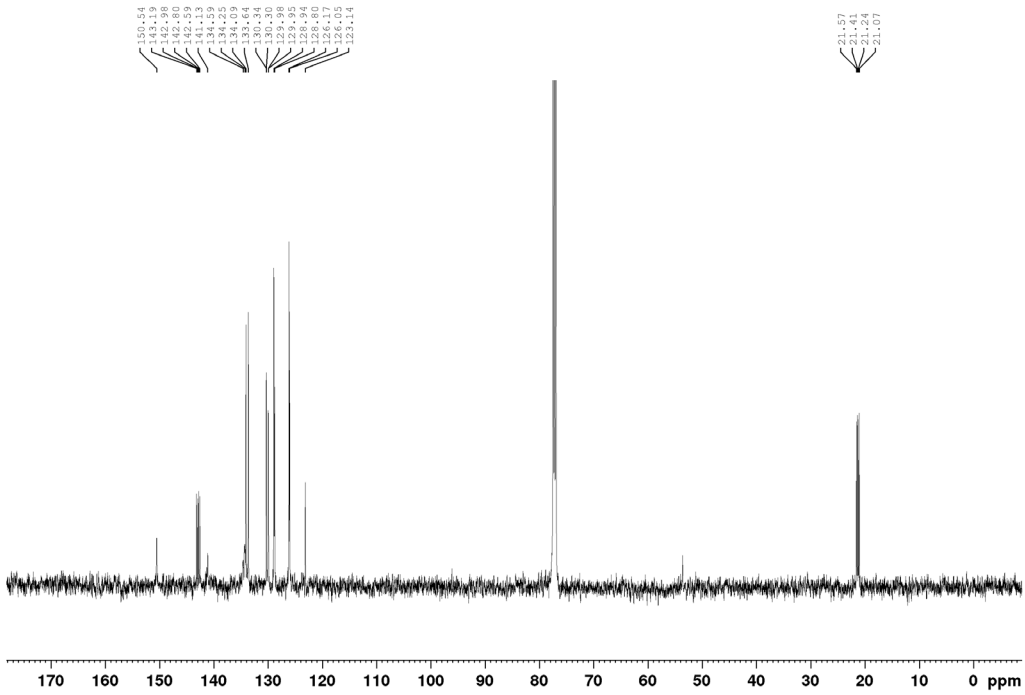

$^{13}C\{^{1}H\}$ UDEFT NMR Spectrum of **2-L4**, ($CDCl_3$, 125.8 MHz)

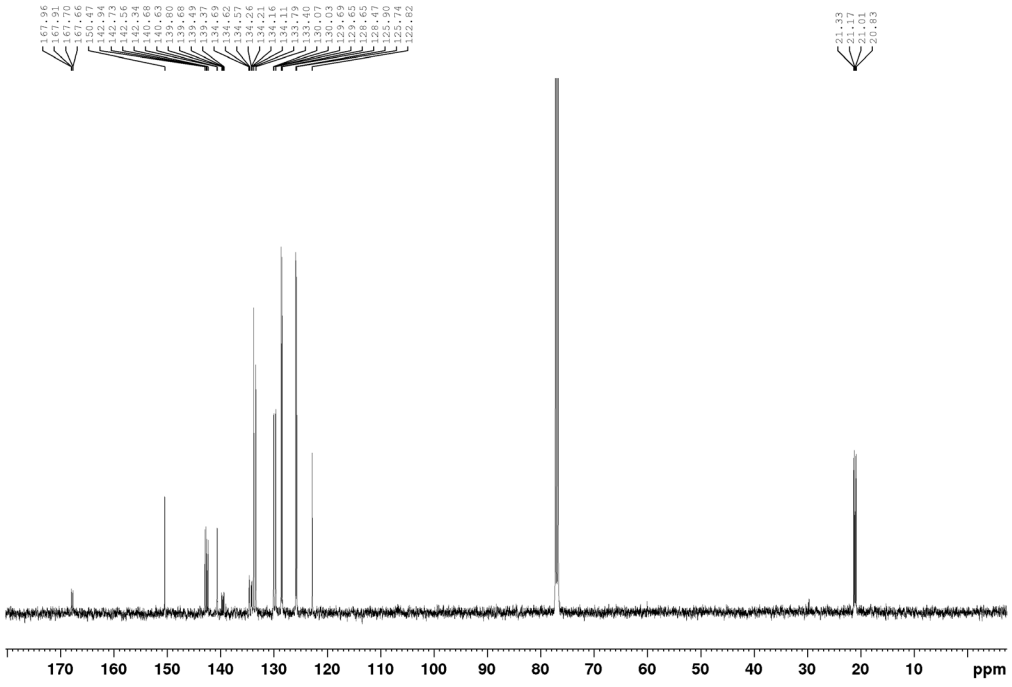

$^{31}P\{^{1}H\}$ NMR Spectrum of **2-L4**, ($CDCl_3$, 202.5 MHz)

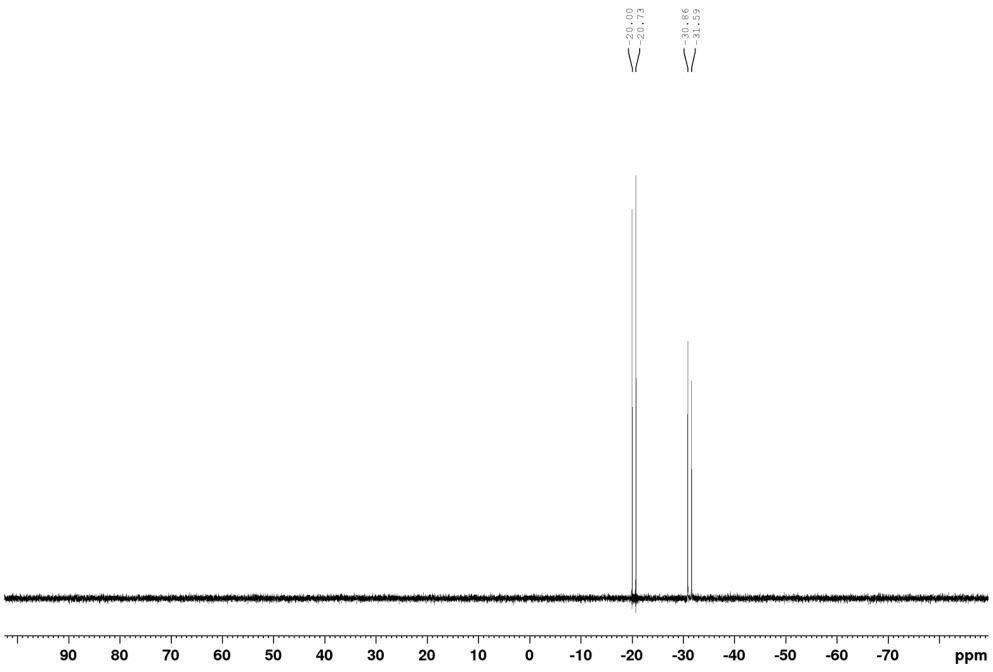

^{1}H NMR Spectrum of ***2-PCg-3-P(o-tolyl)$_2$-thiophene***, **2-L5** ($CDCl_3$, 500 MHz)

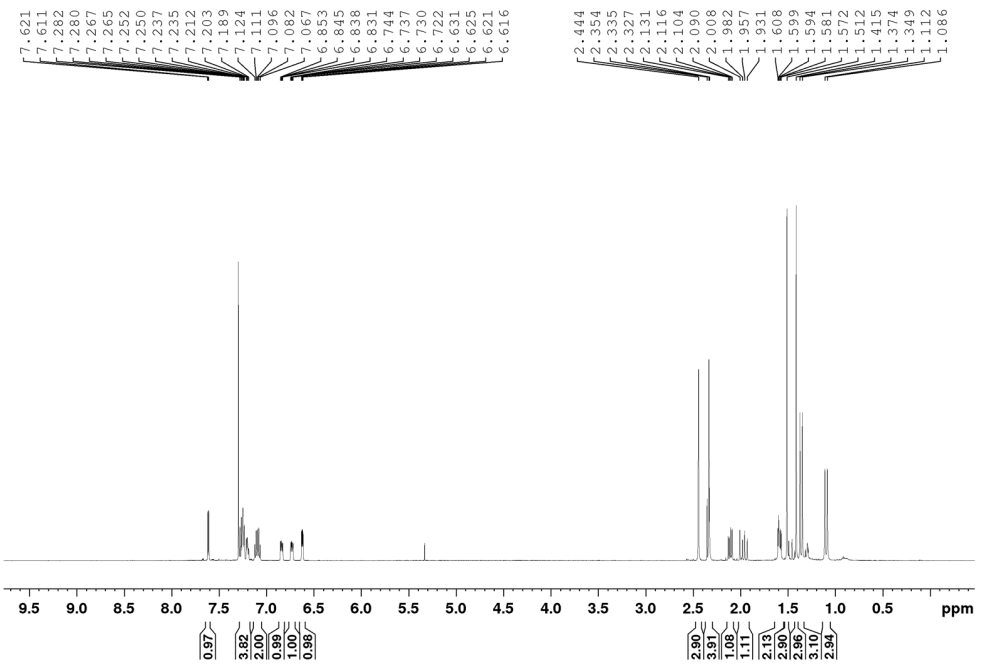

$^{13}C\{^{1}H\}$ NMR Spectrum of **2-L5**, ($CDCl_3$, 125.8 MHz)

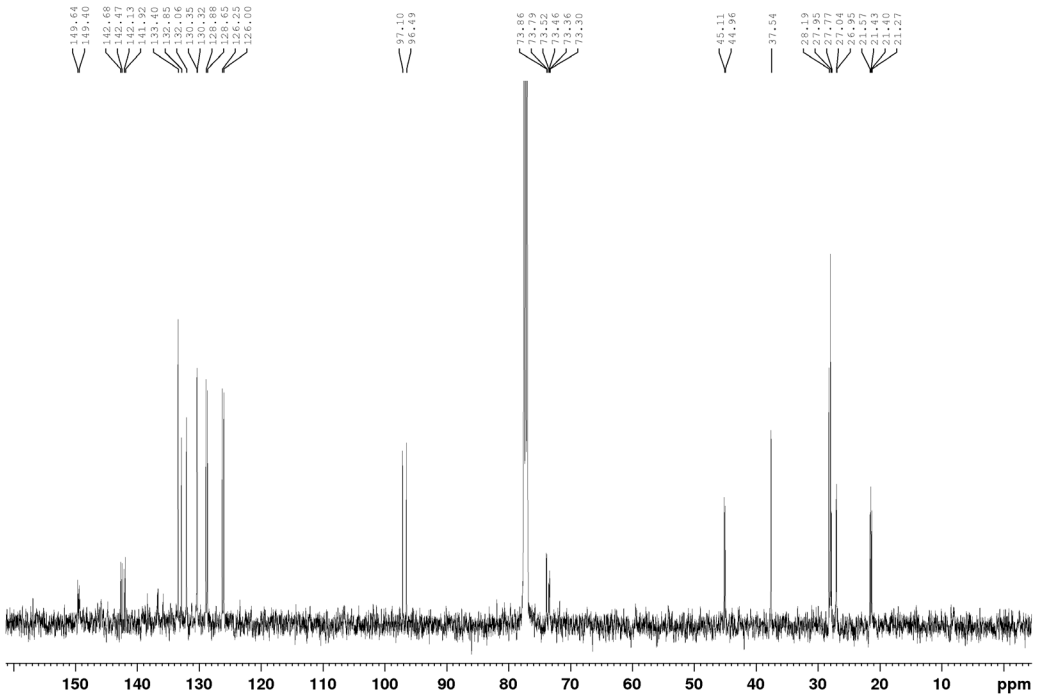

$^{13}C\{^{1}H\}$ UDEFT NMR Spectrum of **2-L5**, ($CDCl_3$, 125.8 MHz)

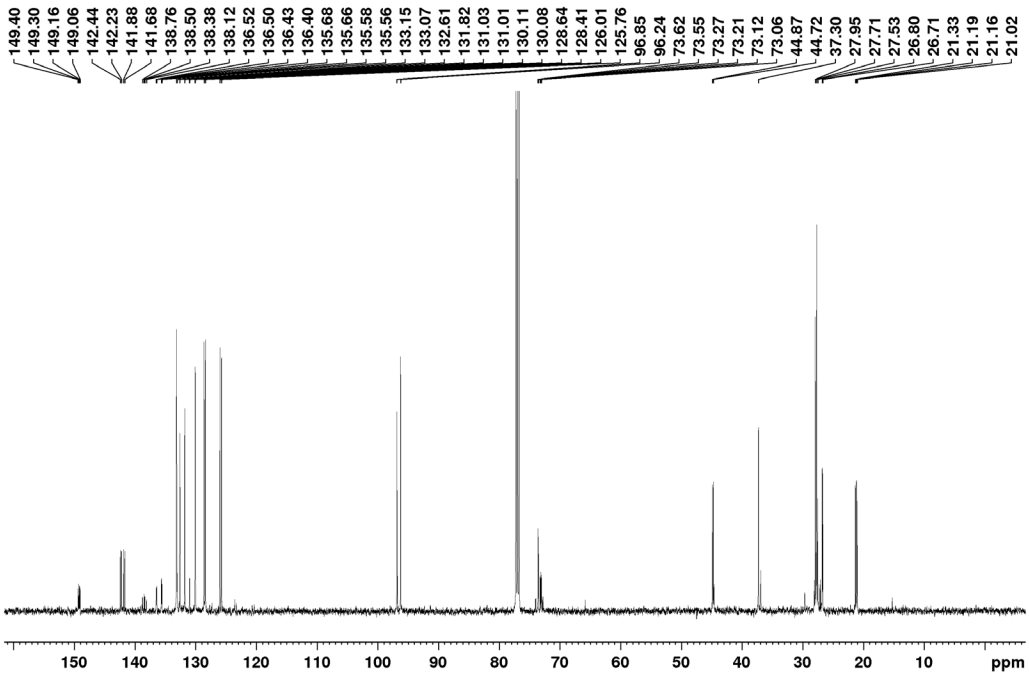

$^{31}P\{^{1}H\}$ NMR Spectrum of **2-L5**, ($CDCl_3$, 202.5 MHz)

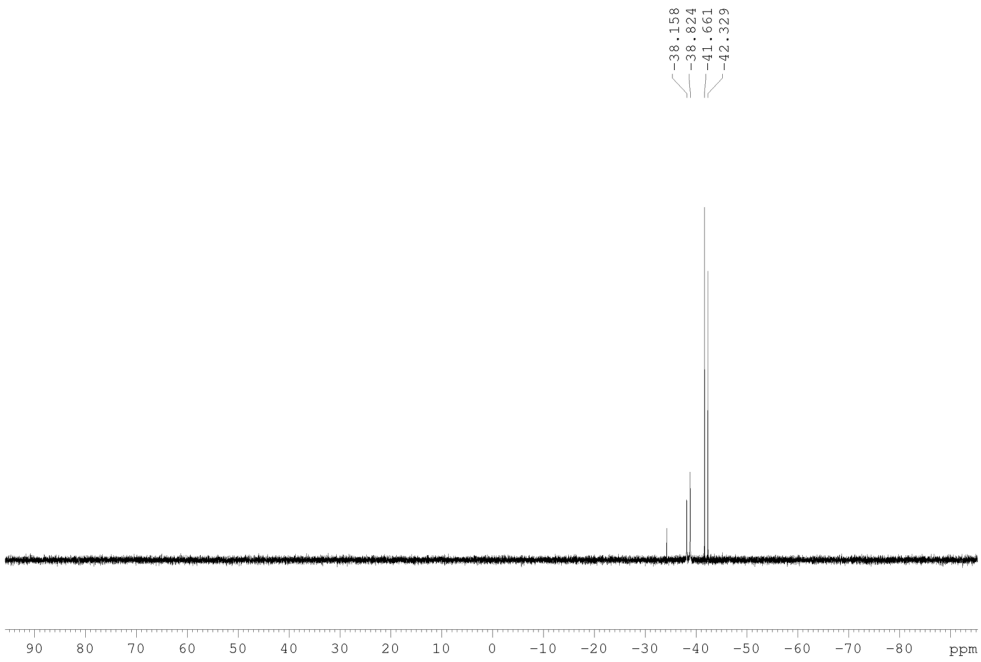

^{1}H NMR Spectrum of ***2-P(o-tolyl)$_2$-3-PCg-thiophene***, **2-L6** ($CDCl_3$, 500 MHz)

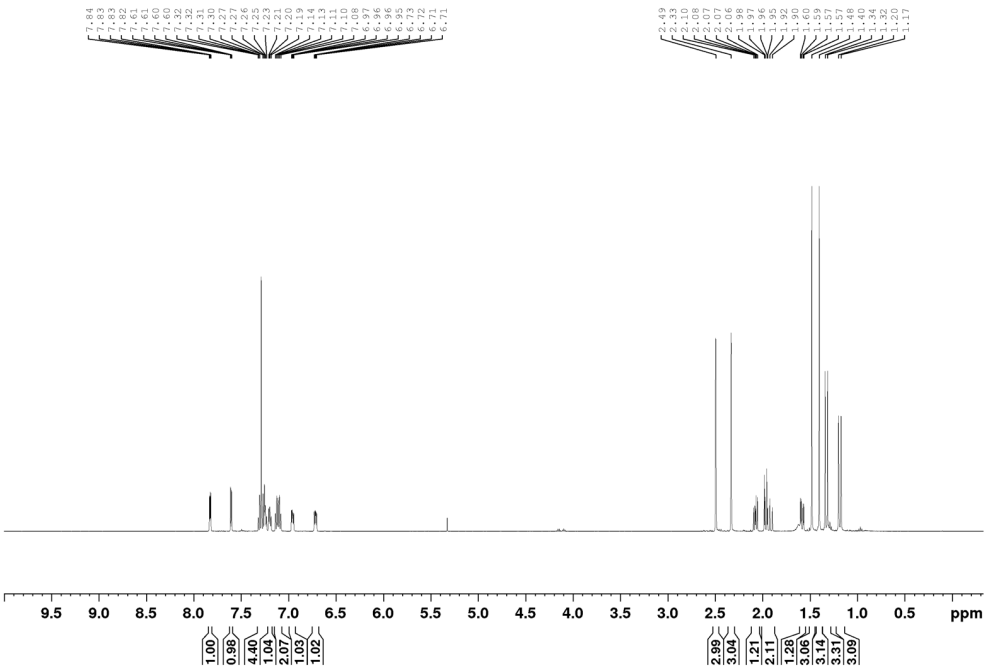

$^{13}C\{^{1}H\}$ NMR Spectrum of **2-L6**, ($CDCl_3$, 125.8 MHz)

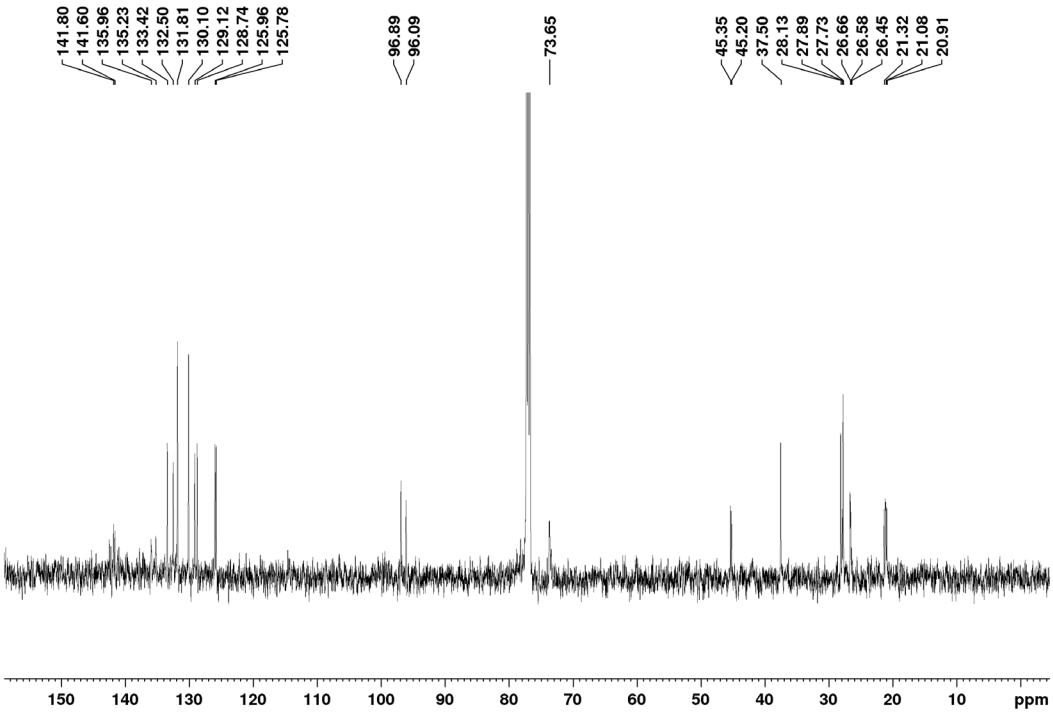

$^{31}P\{^{1}H\}$ NMR Spectrum of **2-L6**, ($CDCl_3$, 202.5 MHz)

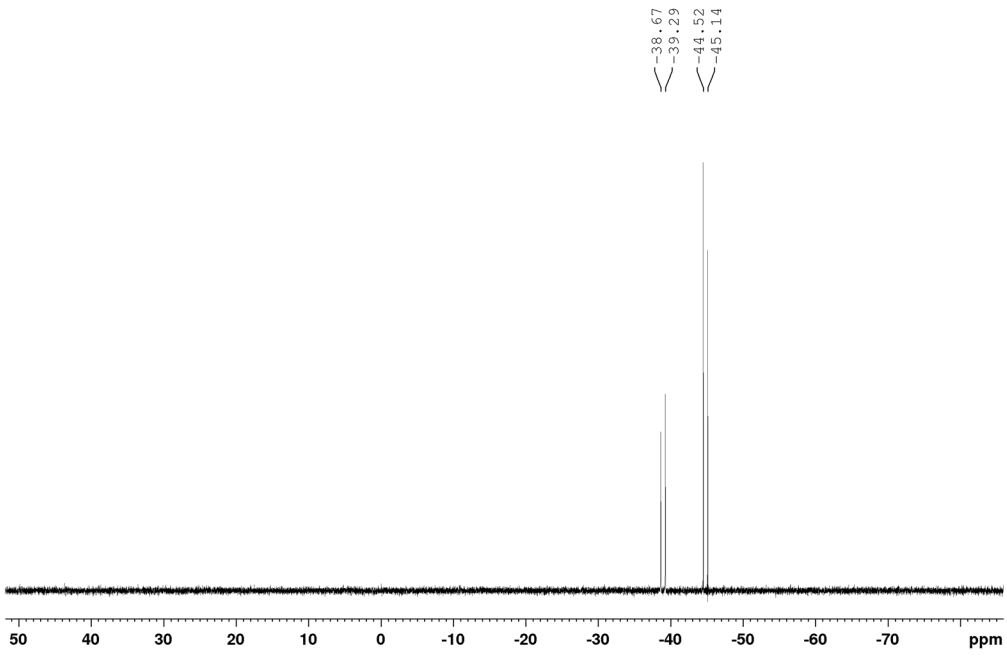

^{1}H NMR Spectrum of ***2,3-(P(o-tolyl)$_2$)$_2$-thiophene***, **2-L7** ($CDCl_3$, 500 MHz)

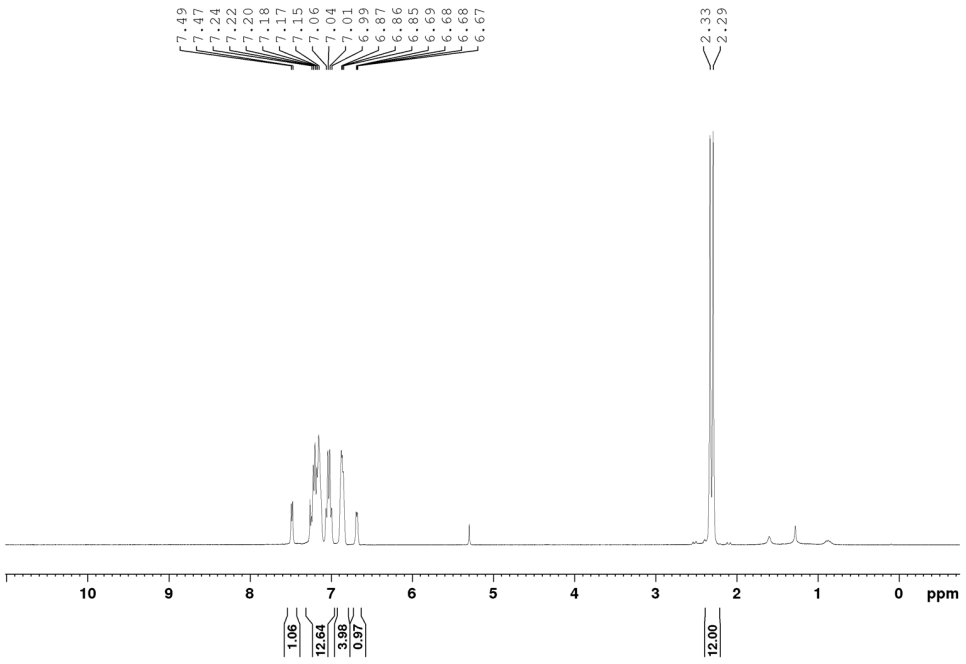

^{13}C{^{1}H} NMR Spectrum of **2-L7** ($CDCl_3$, 125.8 MHz)

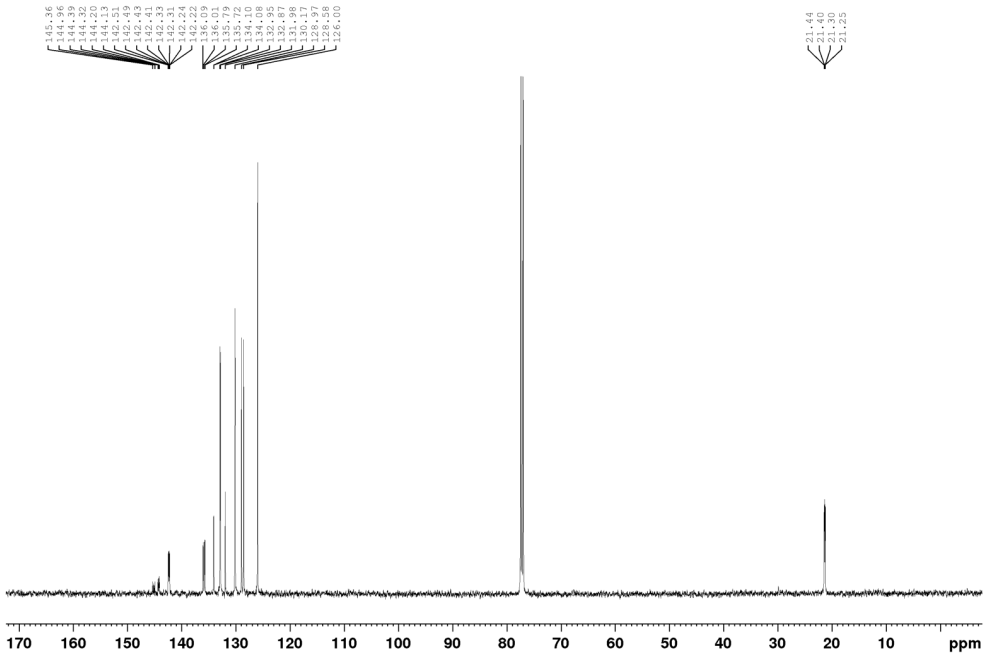

$^{31}P\{^{1}H\}$ NMR Spectrum of **2-L7** ($CDCl_3$, 202.5 MHz)

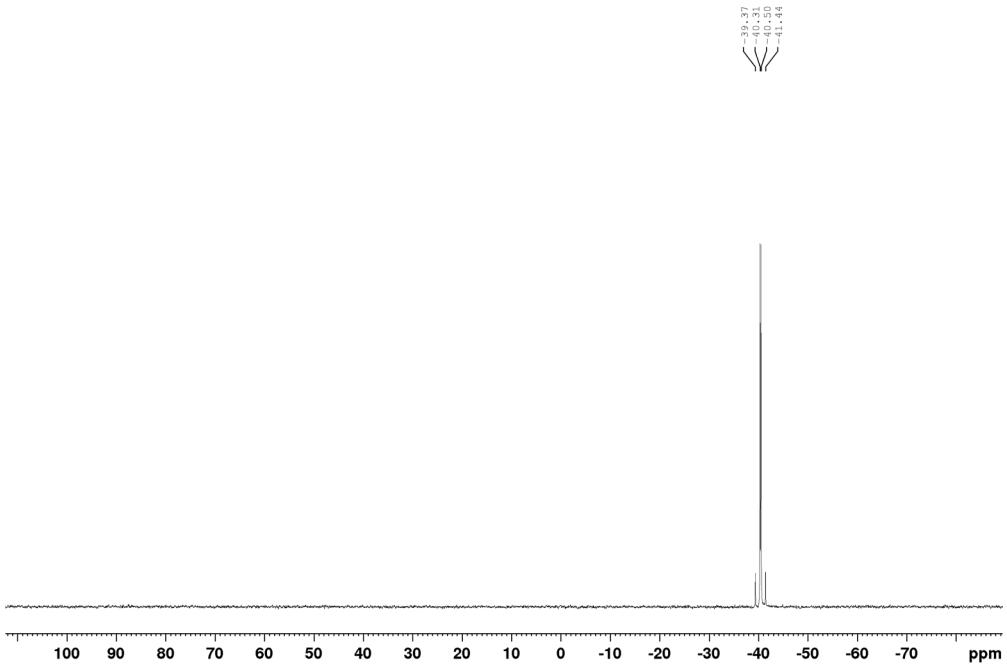

$^{31}P\{^{1}H\}$ NMR Spectrum of **2-L7**, expansion of region -26 to -52 ppm ($CDCl_3$, 202.5 MHz)

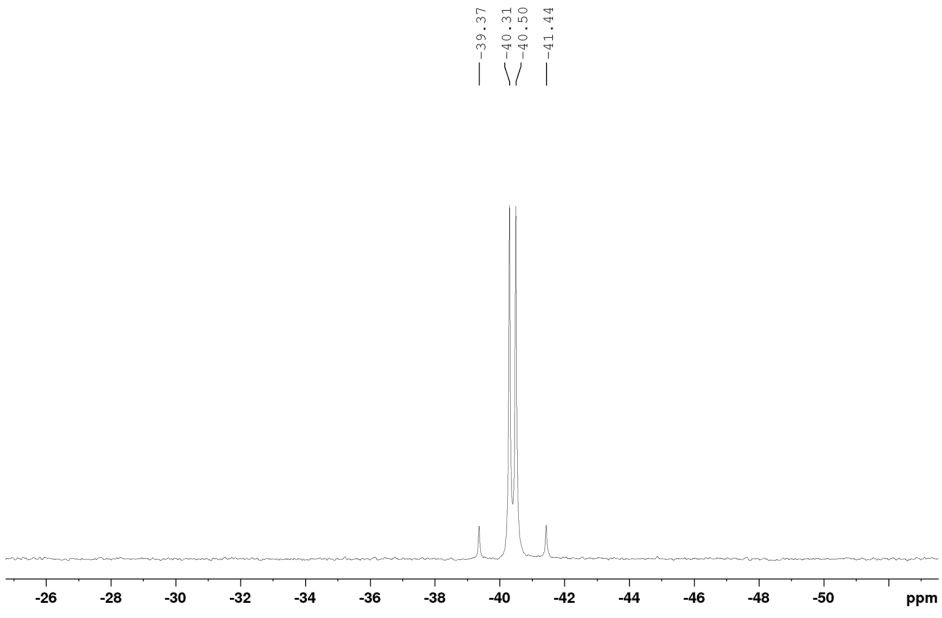

^{1}H NMR Spectrum of ***3-PCg-4-P(o-tolyl)$_2$-thiophene***, **2-L8,** ($CDCl_3$, 500 MHz)

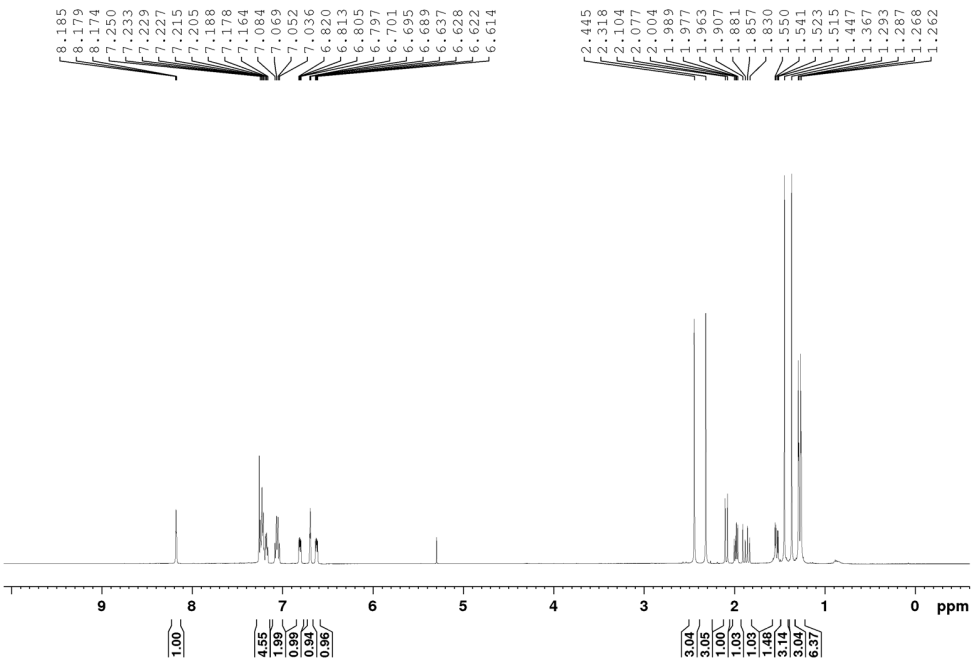

^{13}C{^{1}H} NMR Spectrum of **2-L8**, ($CDCl_3$, 125.8 MHz)

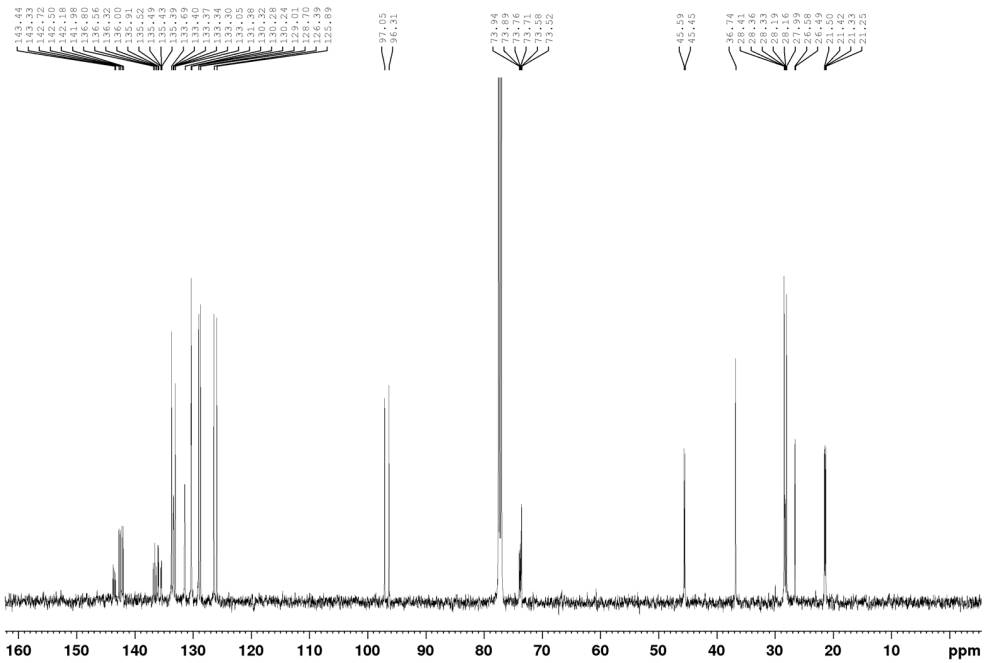

$^{31}P\{^{1}H\}$ NMR Spectrum of **2-L8**, ($CDCl_3$, 202.5 MHz)

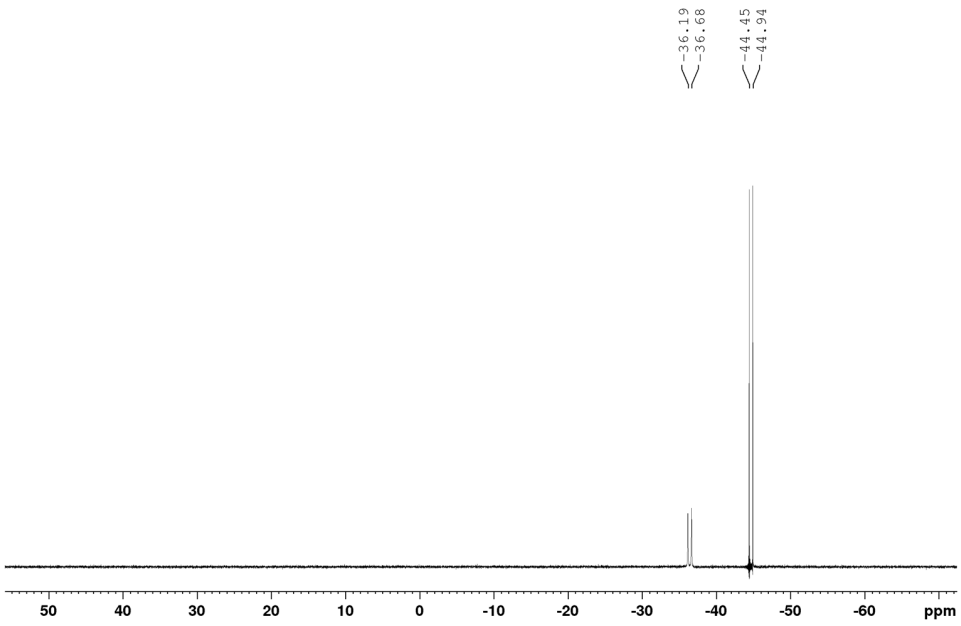

^{1}H NMR Spectrum of ***3,4-(P(o-tolyl)$_2$)$_2$-thiophene***, **2-L9** ($CDCl_3$, 500 MHz)

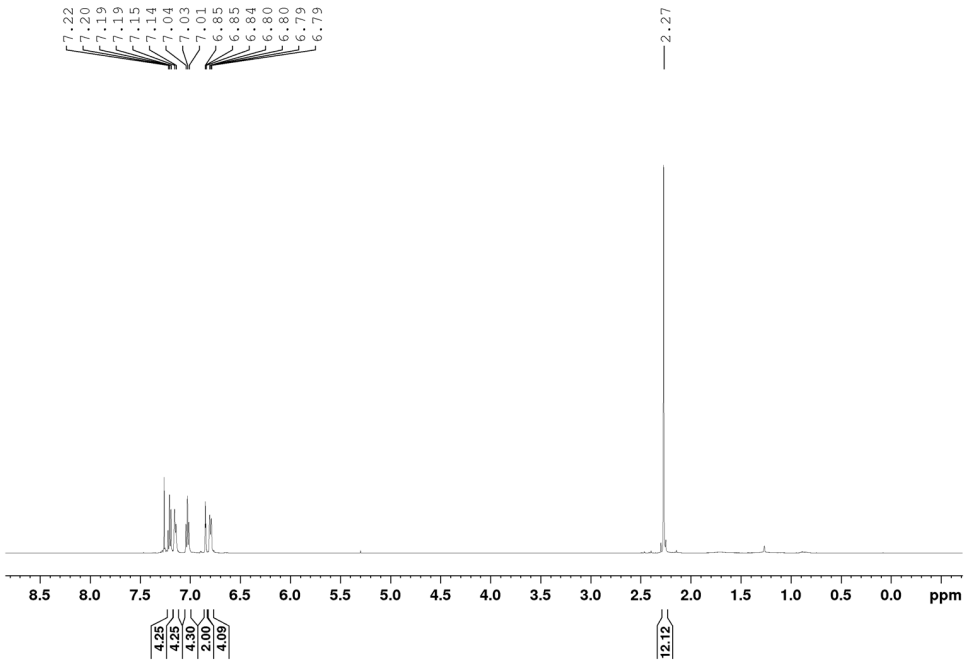

$^{13}C\{^{1}H\}$ NMR Spectrum of **2-L9**, ($CDCl_3$, 125.8 MHz)

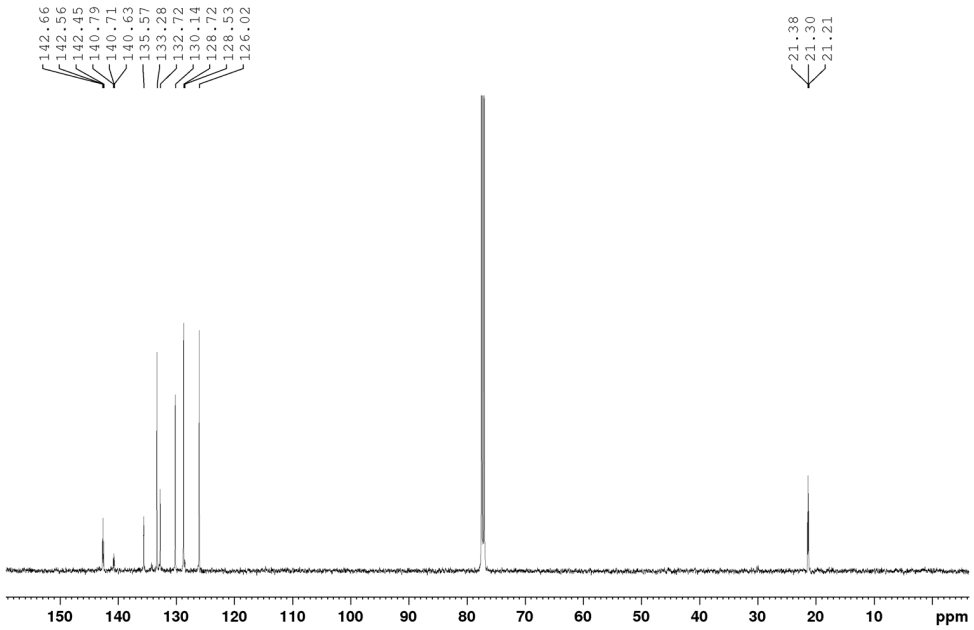

$^{31}P\{^{1}H\}$ NMR Spectrum of **2-L9**, ($CDCl_3$, 202.5 MHz)

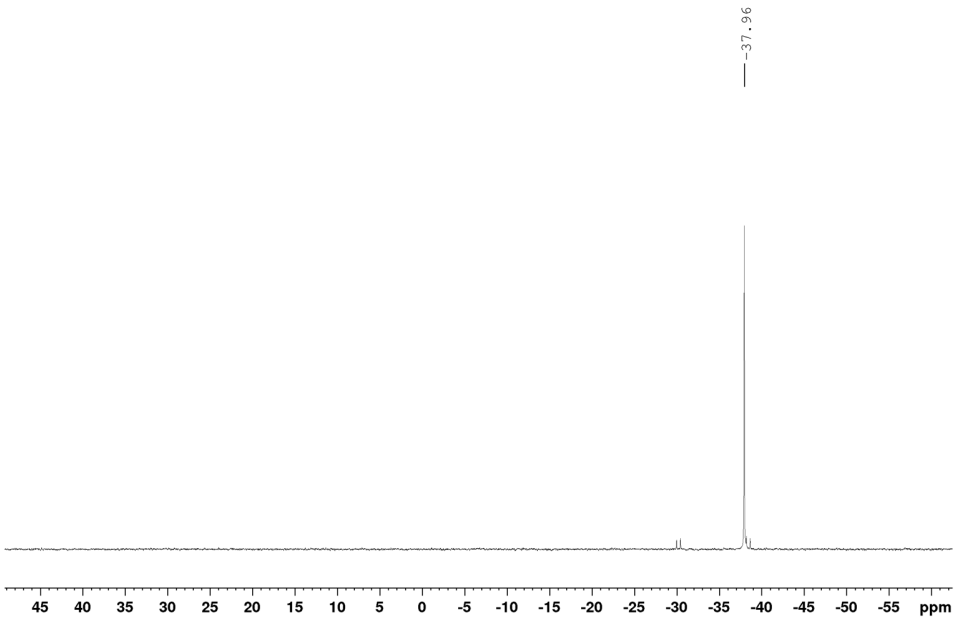

^{1}H NMR Spectrum of ***rac-(o-PCg$_2$-benzene),*** *rac*-**3-L1** ($CDCl_3$, 300 MHz)

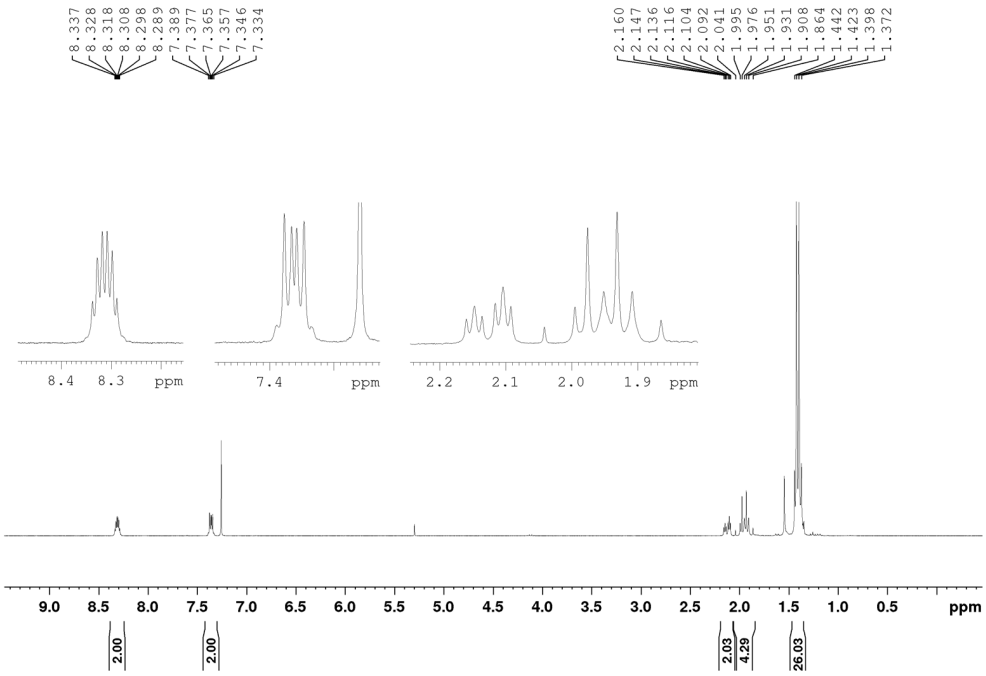

^{13}C{^{1}H} UDEFT NMR Spectrum of *rac*-**3-L1** ($CDCl_3$, 125.8 MHz)

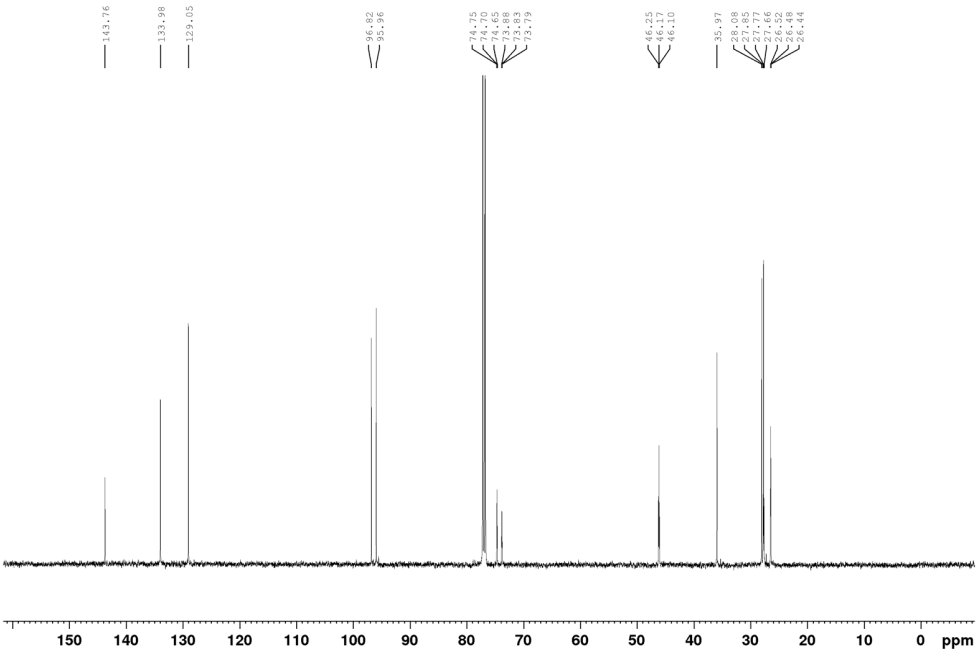

$^{31}P\{^{1}H\}$ NMR Spectrum of *rac*-**3-L1** ($CDCl_3$, 121.5 MHz)

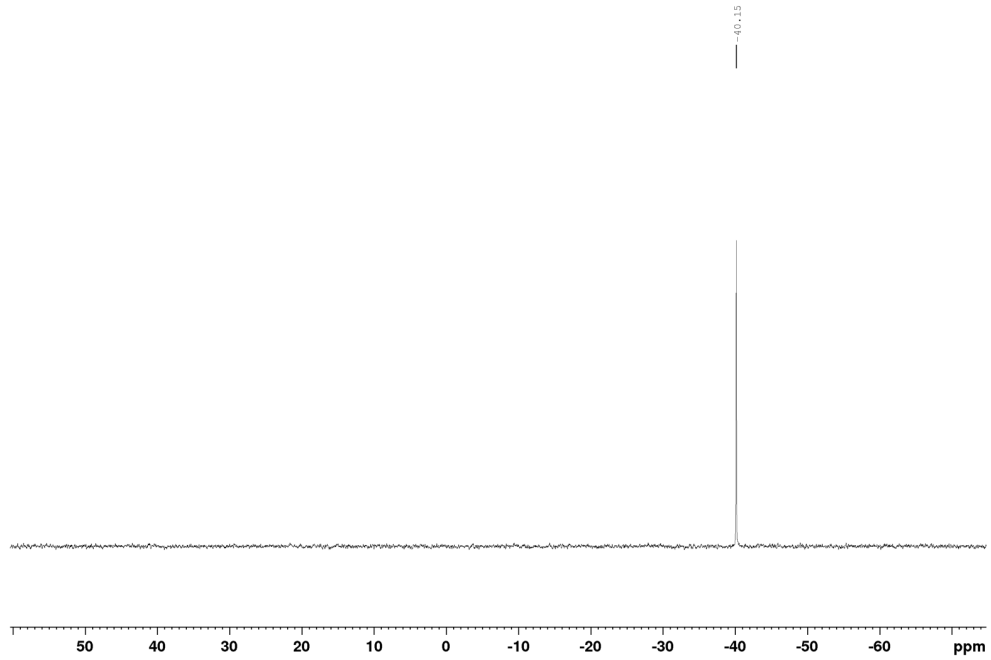

^{1}H NMR Spectrum of ***rac-2,3-PCg$_2$-pyridine***, *rac*-**3-L2** ($CDCl_3$, 500 MHz)

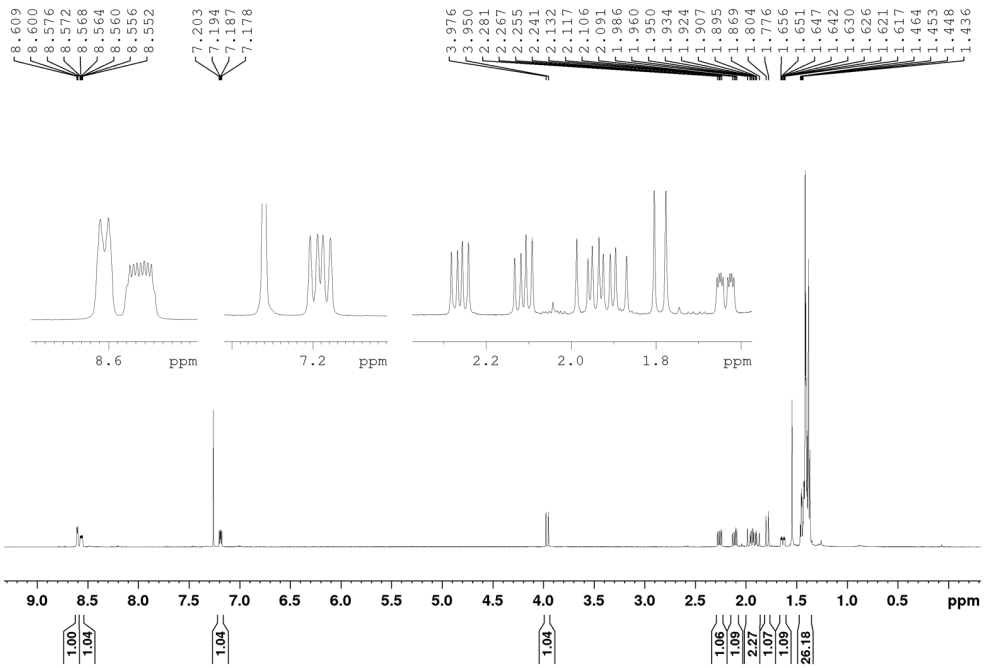

$^{13}C\{^{1}H\}$ UDEFT NMR Spectrum of *rac*-**3-L2** ($CDCl_3$, 125.8 MHz)

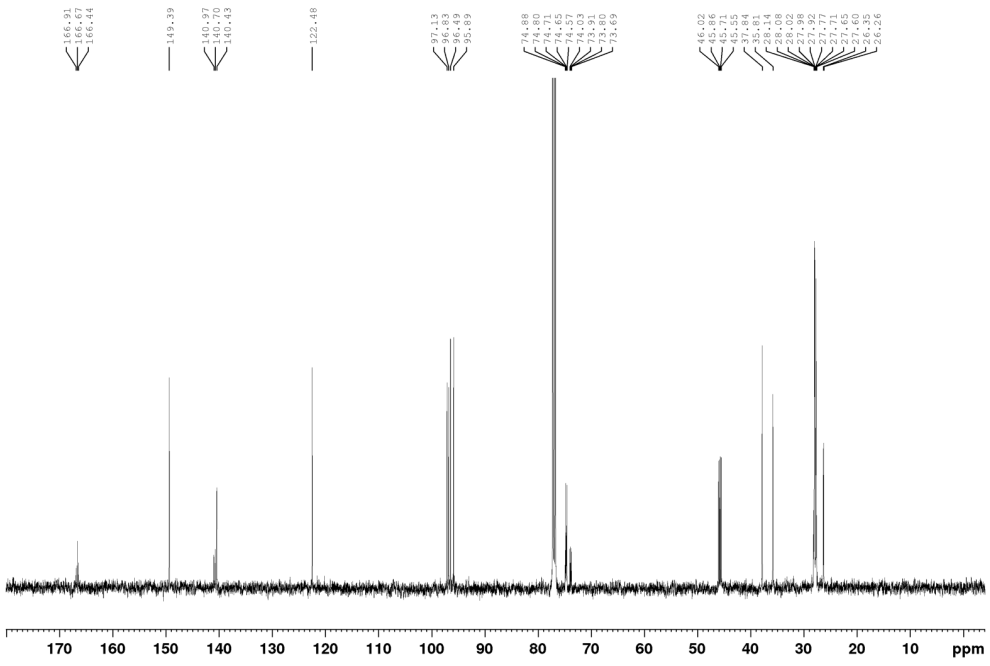

$^{31}P\{^{1}H\}$ NMR Spectrum of *rac*-**3-L2** ($CDCl_3$, 202.5 MHz)

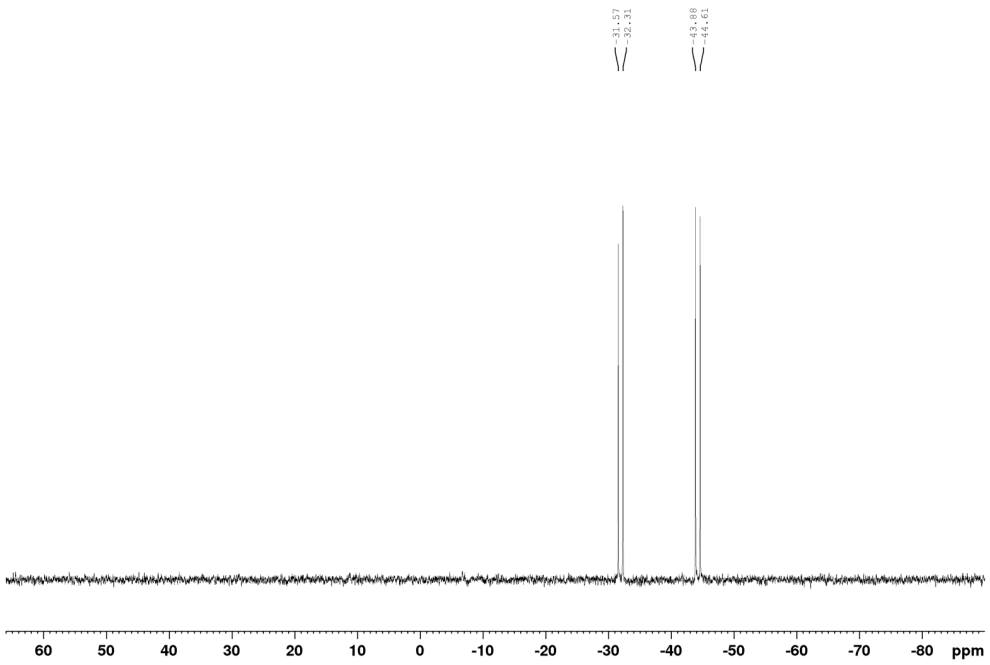

^{1}H NMR Spectrum of ***meso-2,3-PCg$_2$-pyridine***, *meso*-**3-L2** ($CDCl_3$, 500 MHz)

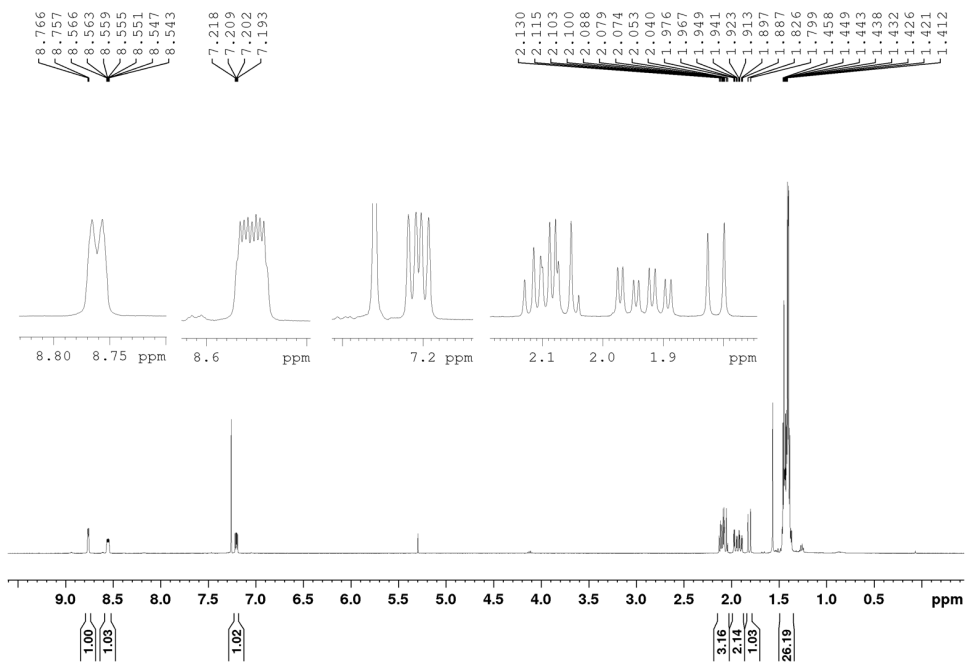

^{13}C{^{1}H} UDEFT NMR Spectrum of *meso*-**3-L2** ($CDCl_3$, 125.8 MHz)

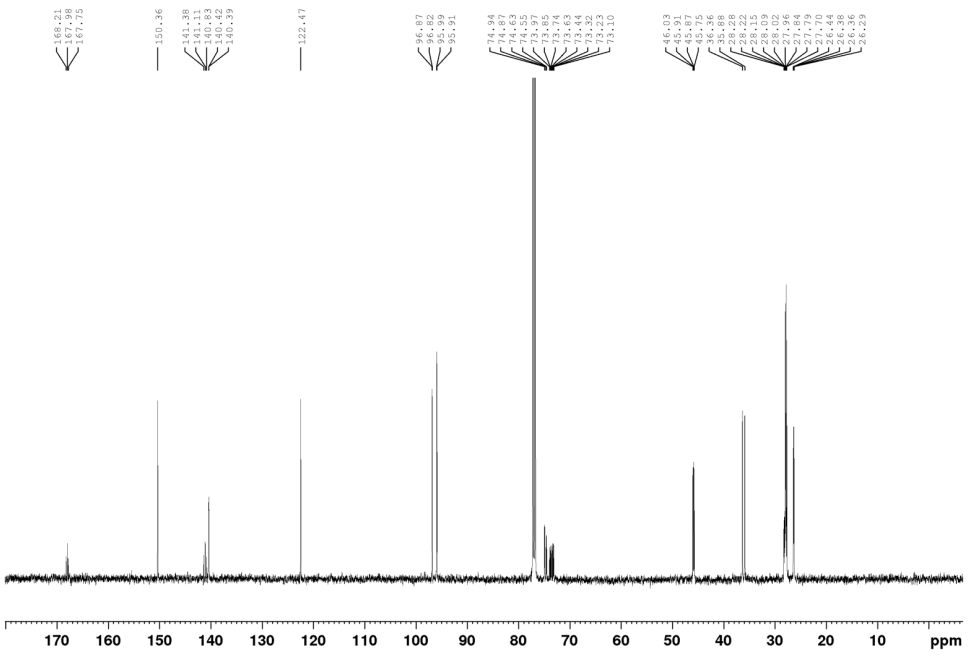

$^{31}P\{^{1}H\}$ NMR Spectrum of *meso*-**3-L2** ($CDCl_3$, 202.5 MHz)

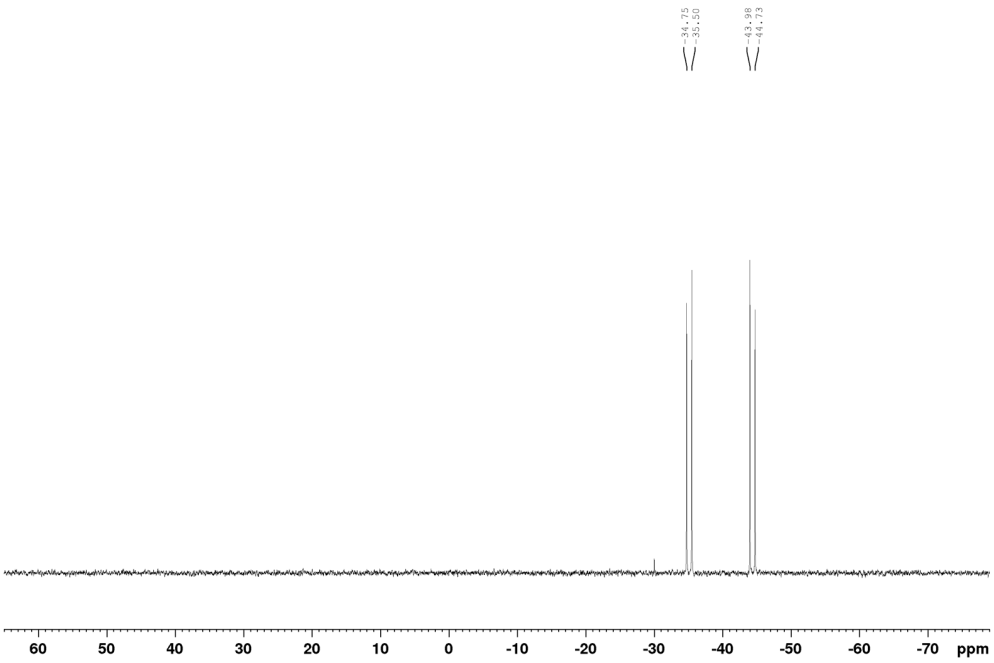

^{1}H NMR Spectrum of ***2,3-PCg$_2$-quinoxaline***, **3-L3** ($CDCl_3$, 500 MHz)

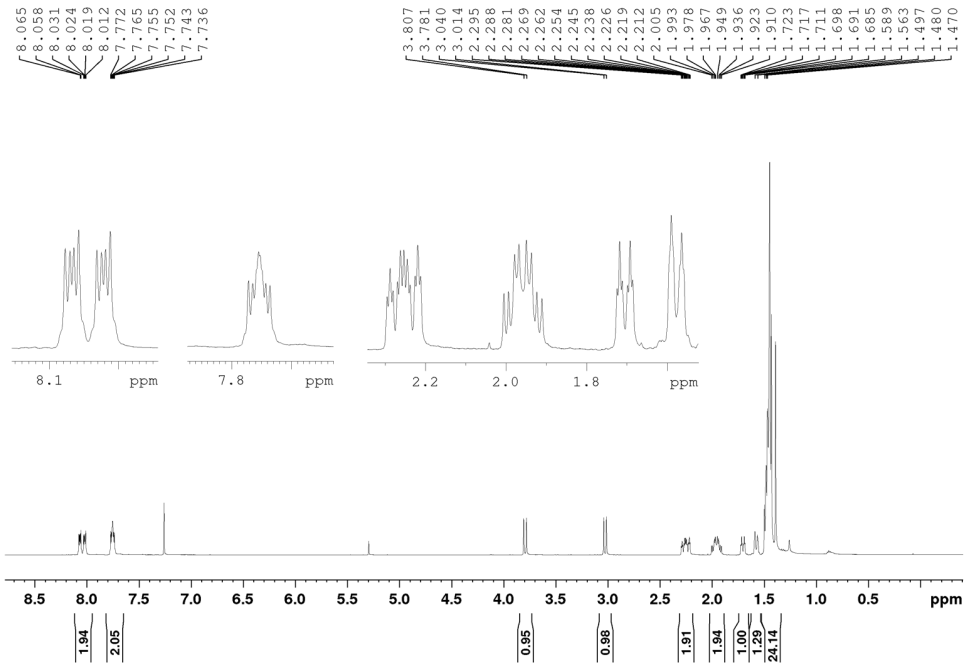

$^{13}C\{^{1}H\}$ UDEFT NMR Spectrum of **3-L3** ($CDCl_3$, 125.8 MHz)

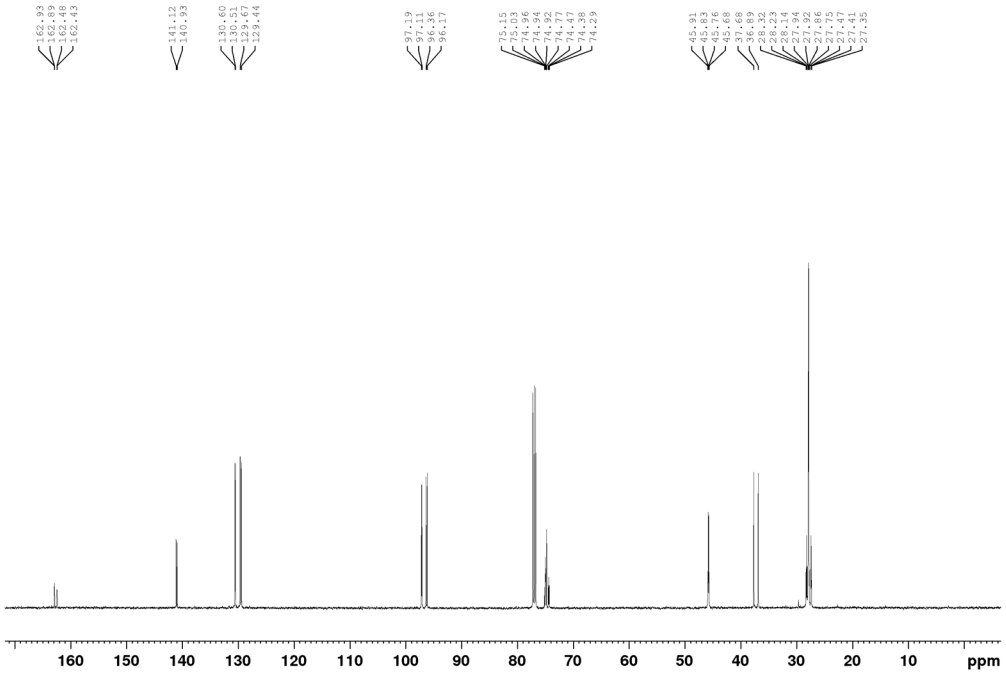

$^{31}P\{^{1}H\}$ NMR Spectrum of **3-L3** ($CDCl_3$, 202.5 MHz)

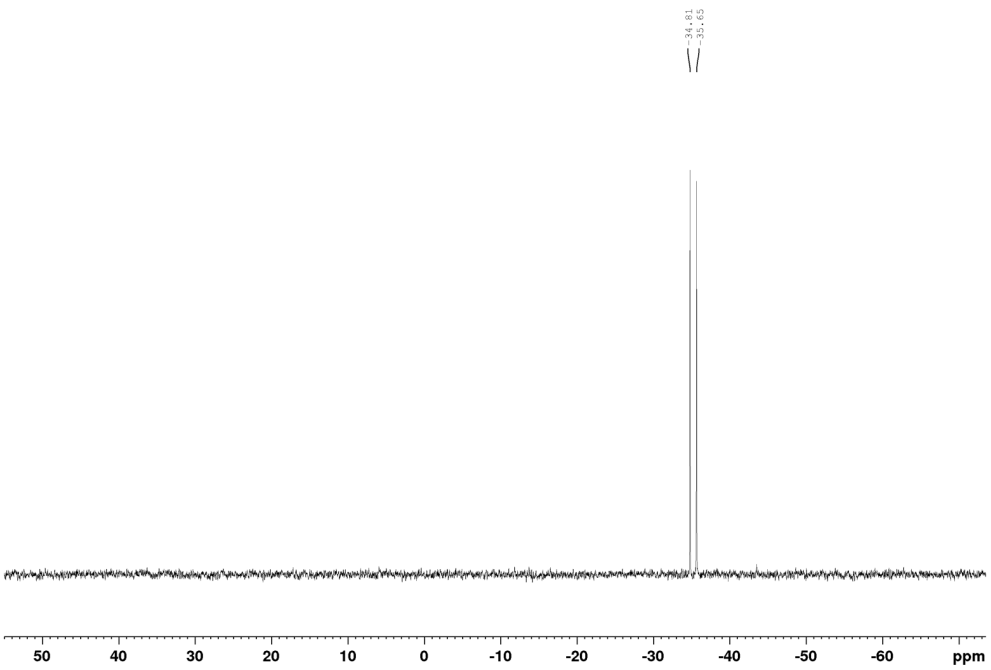

^{1}H NMR Spectrum of ***(CyPF-Cy)Ni(o-tolyl)Cl***, **1-C1** ($CDCl_3$, 500 MHz)

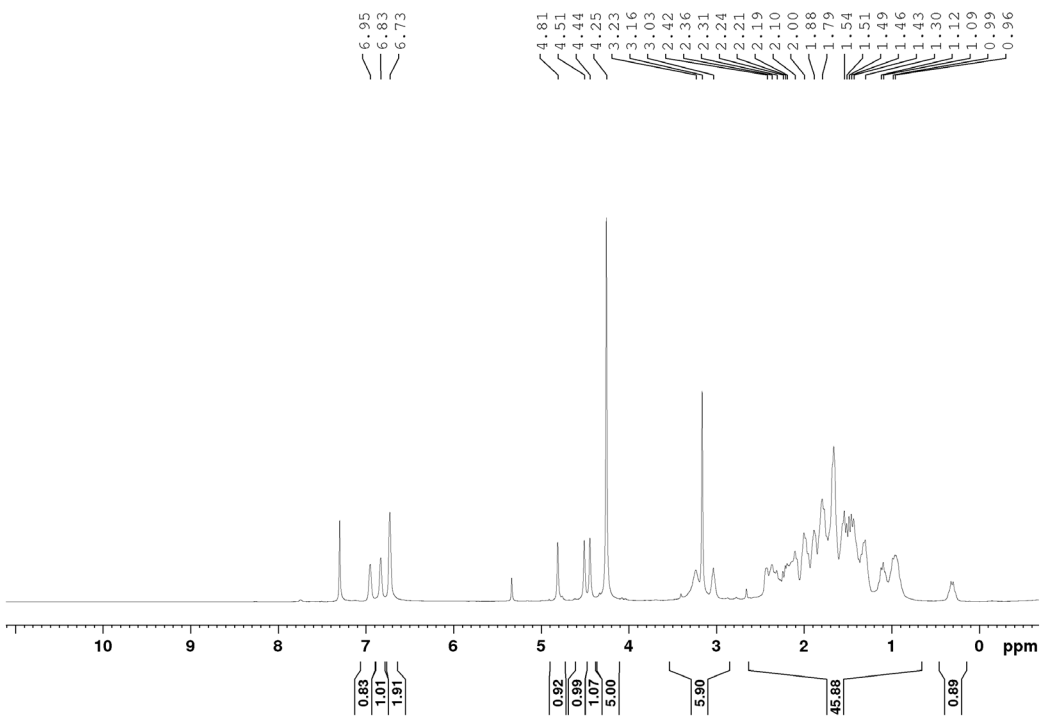

^{31}P{^{1}H} NMR Spectrum of **1-C1,** ($CDCl_3$, 202.5 MHz)

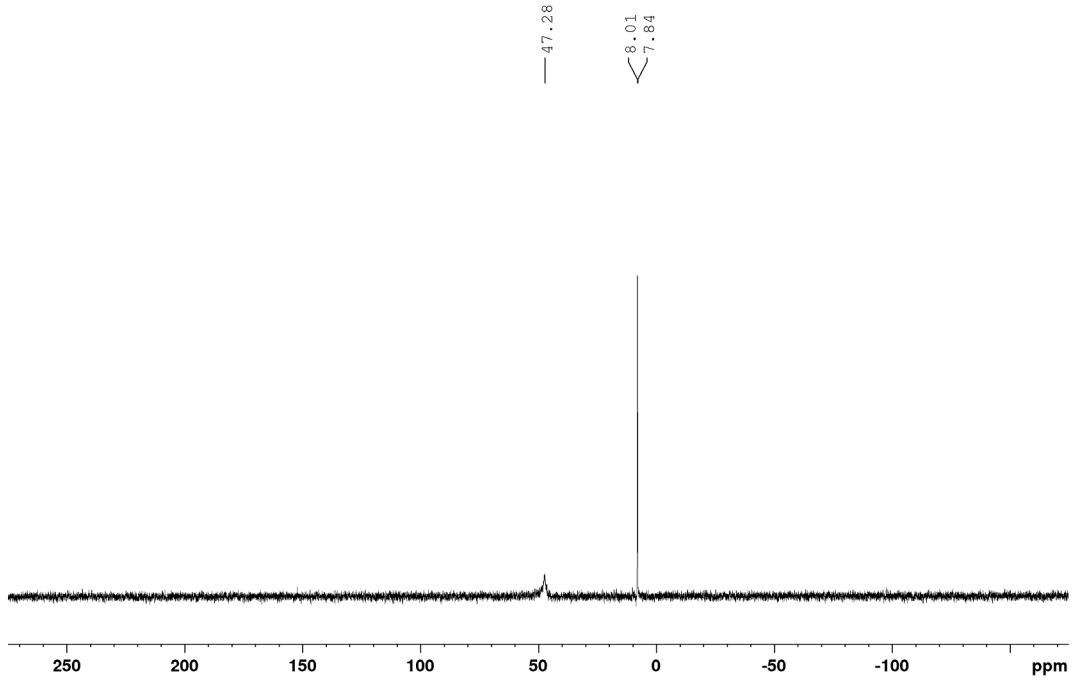

$^{31}P\{^{1}H\}$ NMR Spectrum of **1-C1,** (220 K, $CDCl_3$, 121.4 MHz)

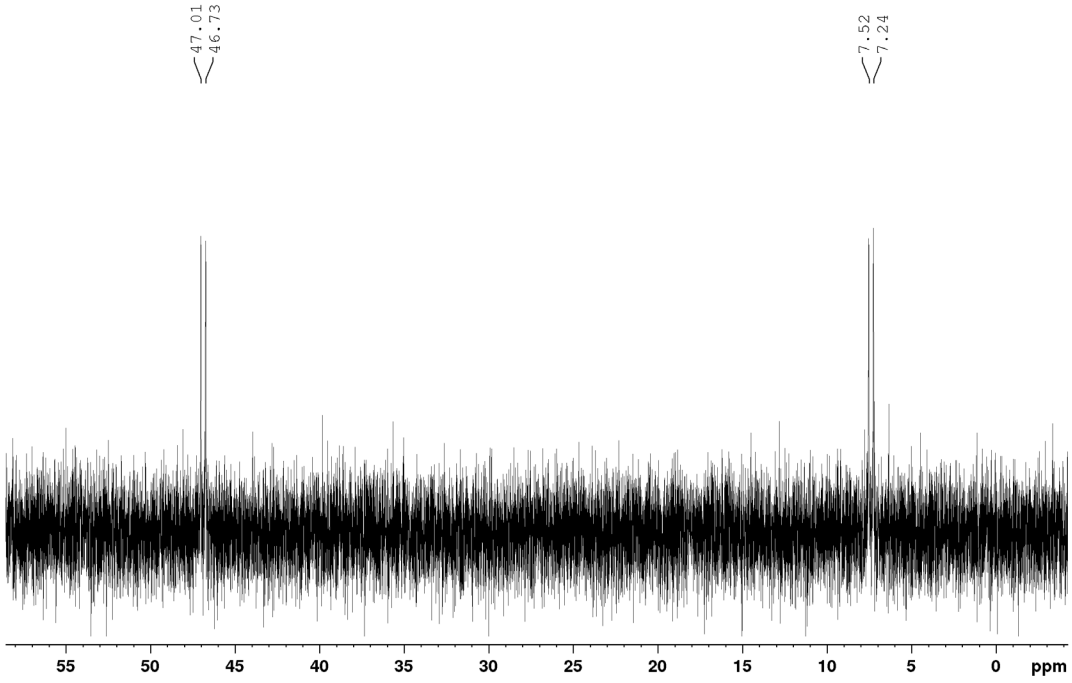

^{1}H NMR Spectrum of ***(L^{iPr})Ni(o-tolyl)Cl*** ($CDCl_3$, 500 MHz)

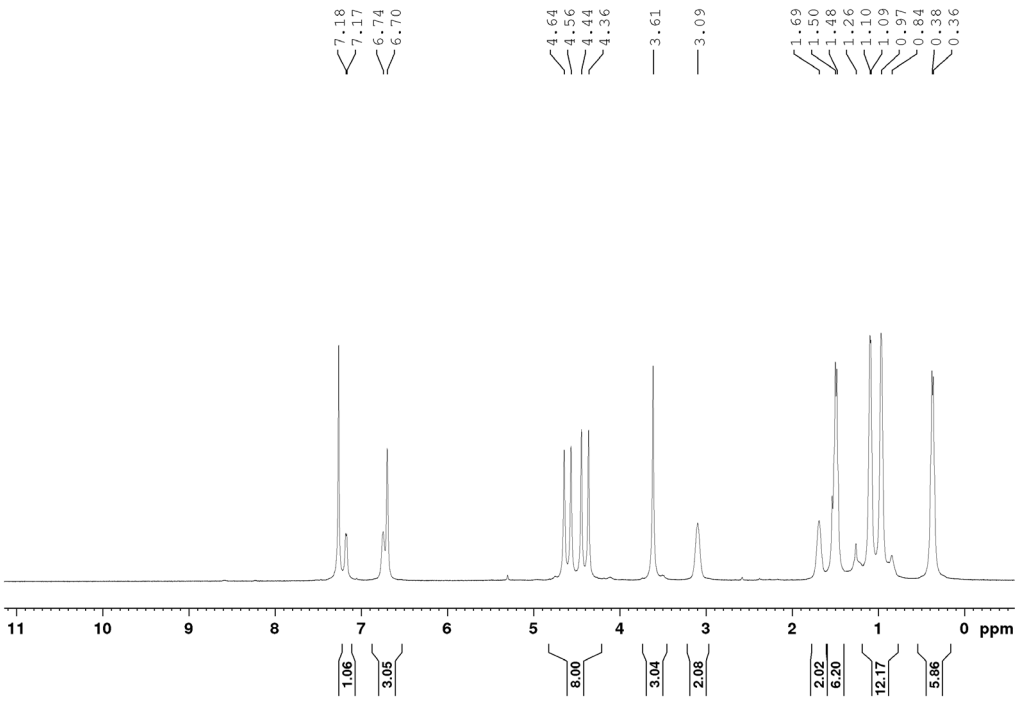

$^{13}C\{^{1}H\}$ NMR Spectrum of ***(L^{iPr})Ni(o-tolyl)Cl*** ($CDCl_3$, 125.8 MHz)

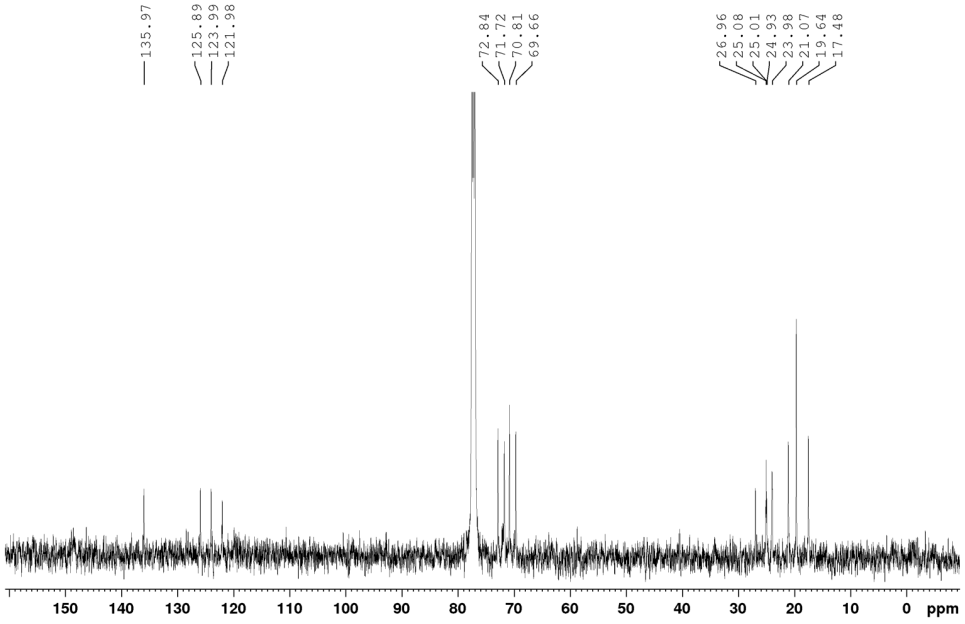

$^{31}P\{^{1}H\}$ NMR Spectrum of ***(L^{iPr})Ni(o-tolyl)Cl*** ($CDCl_3$, 202.5 MHz)

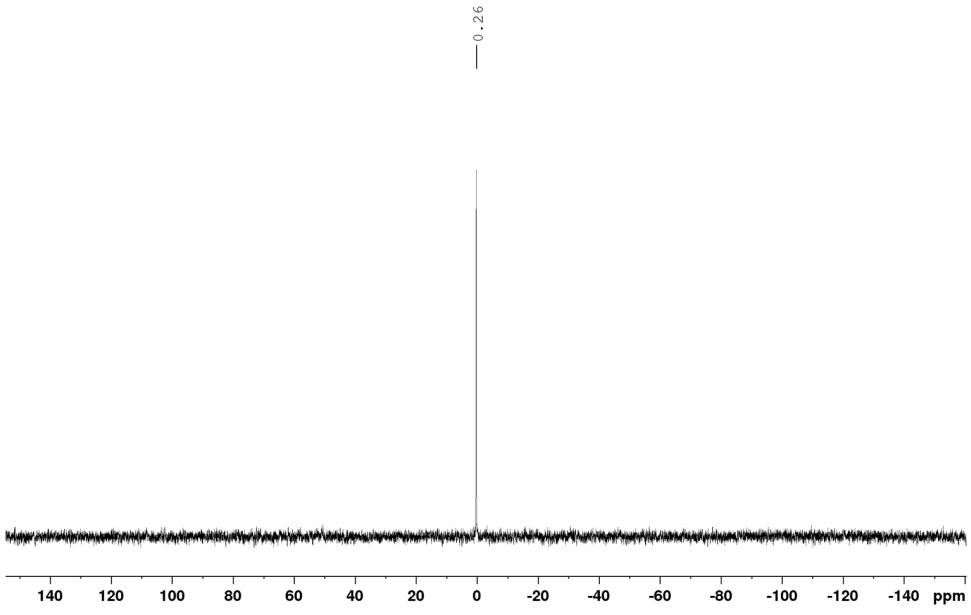

$^{31}P\{^{1}H\}$ NMR Spectrum of ***(3-PCg-4-P(o-tolyl)$_2$-thiophene)Ni(o-tolyl)Cl***, **2-C1** ($CDCl_3$, 202.5 MHz)

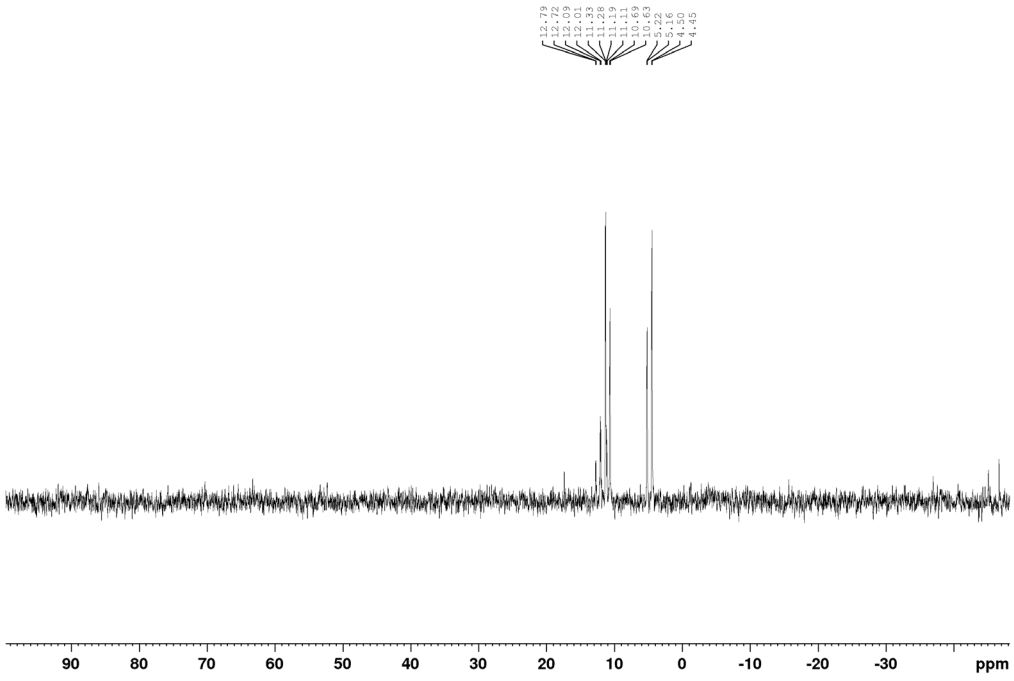

$^{31}P\{^{1}H\}$-$^{31}P\{^{1}H\}$ COSY NMR Spectrum of **2-C1**, ($CDCl_3$, 202.5 MHz)

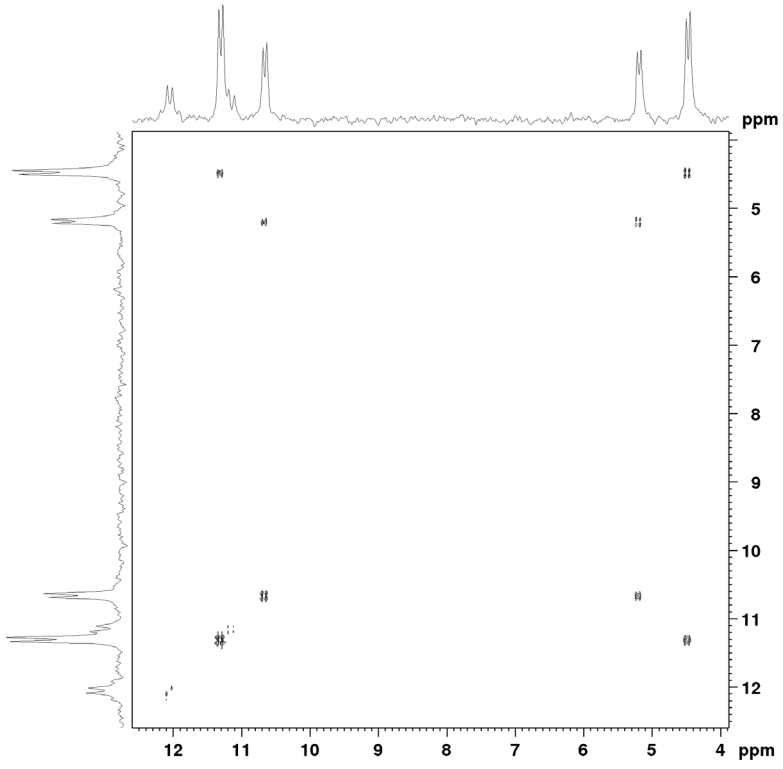

$^{31}P\{^{1}H\}$ NMR Spectrum of ***(3,4-(P(o-tolyl)$_2$)$_2$-thiophene)Ni(o-tolyl)Cl***, **2-C2** ($CDCl_3$, 202.5 MHz)

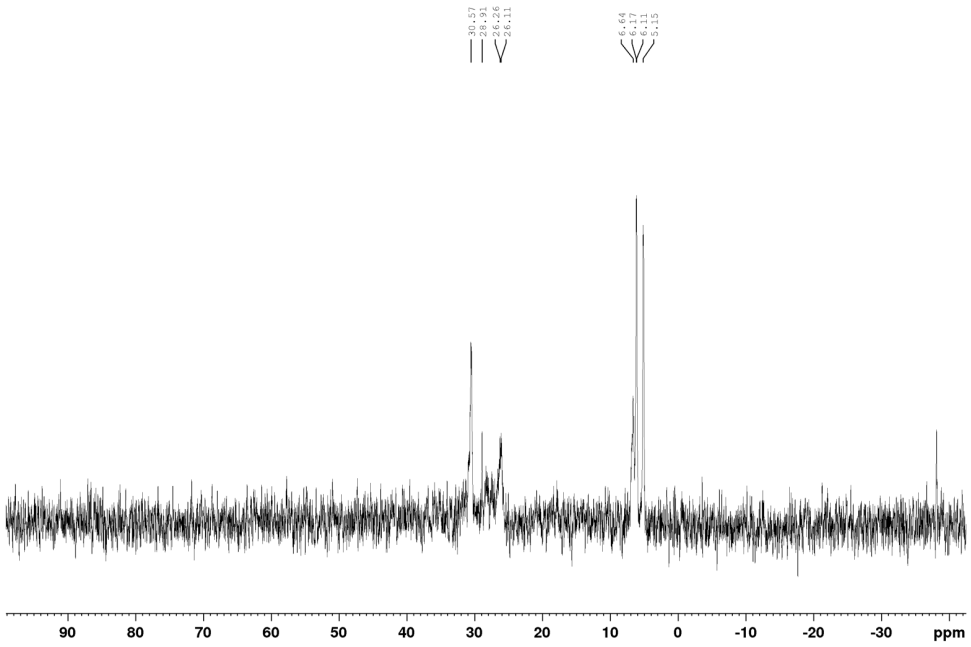

^{1}H NMR Spectrum of ***rac-(o-PCg$_2$-benzene)Ni(o-tolyl)Cl,*** *rac*-**3-C1** ($CDCl_3$, 500 MHz)

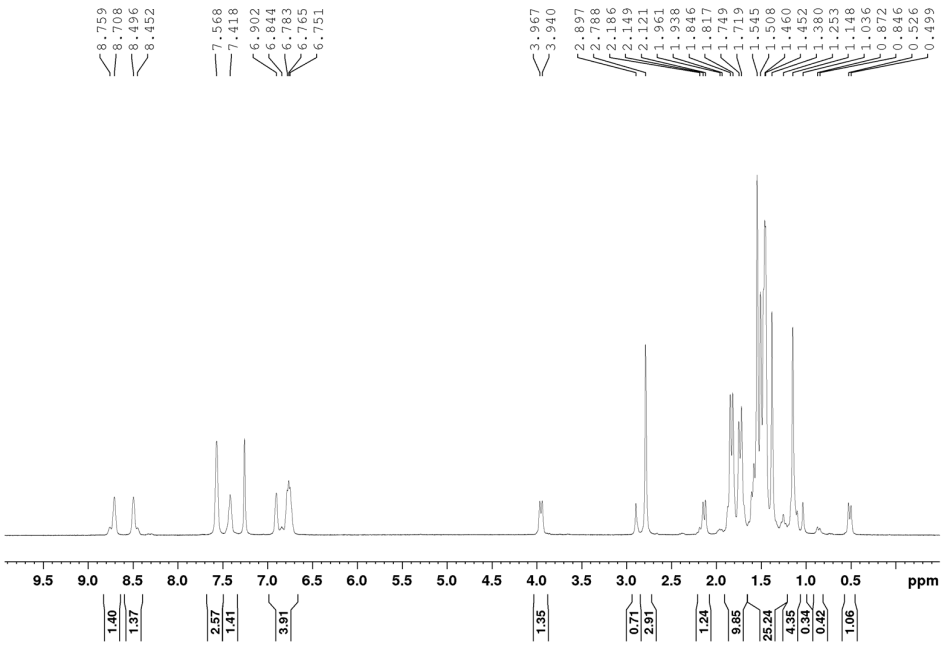

$^{13}C\{^{1}H\}$ UDEFT NMR Spectrum of *rac*-**3-C1** ($CDCl_3$, 125.8 MHz)

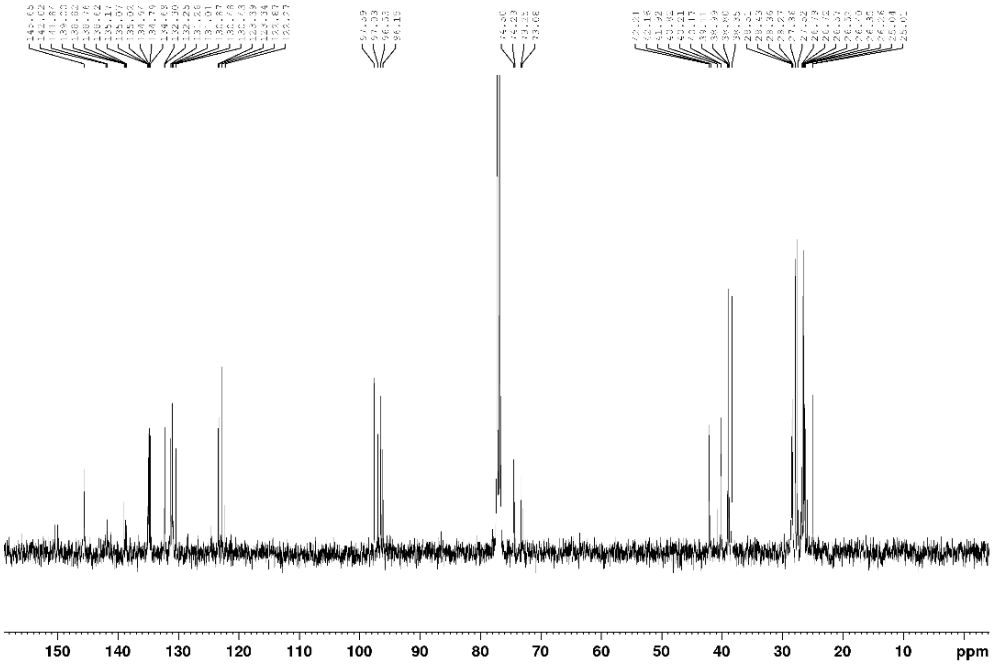

$^{31}P\{^{1}H\}$ NMR Spectrum of *rac*-**3-C1** ($CDCl_3$, 202.5 MHz)

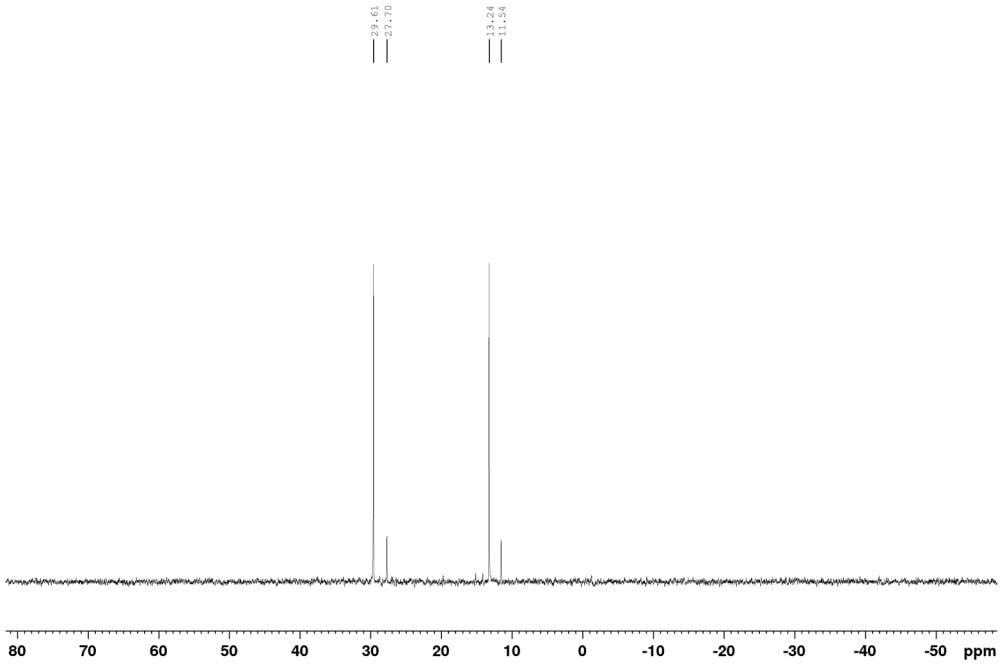

$^{31}P\{^{1}H\}$ NMR Spectrum of **3-C1** prepared from **3-L1** ($CDCl_3$, 202.5 MHz)

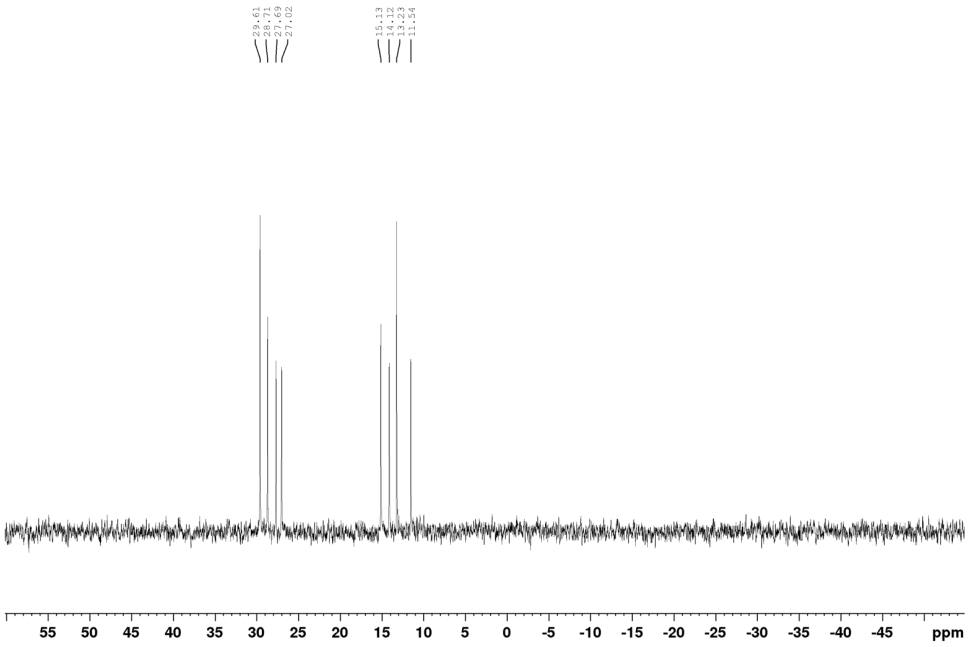

^{1}H NMR Spectrum of ***(2,3-PCg$_2$-pyridine)Ni(o-tolyl)Cl***, **3-C2** ($CDCl_3$, 500 MHz)

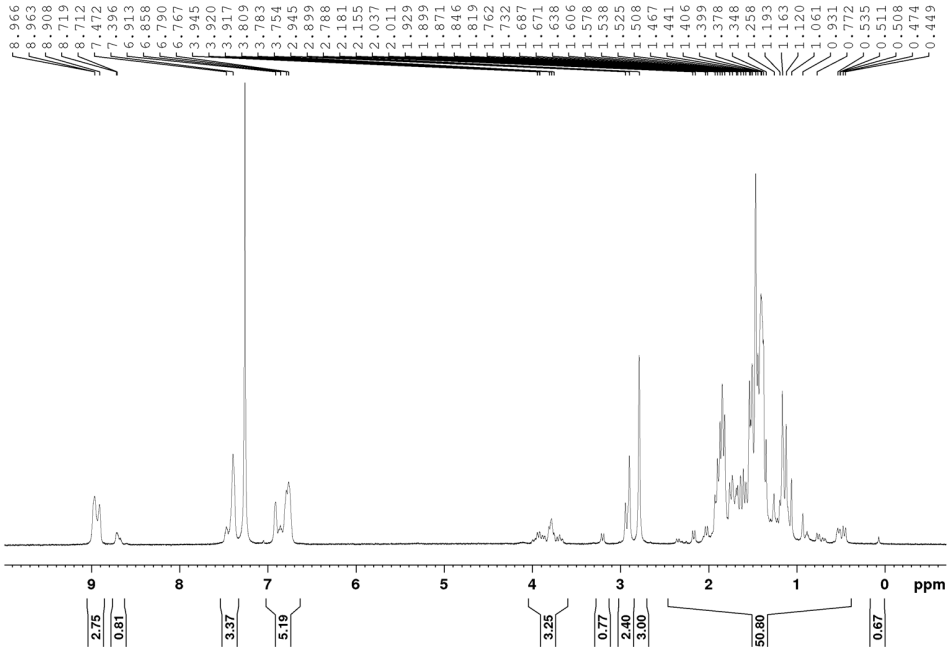

$^{13}C\{^{1}H\}$ UDEFT NMR Spectrum of **3-C2** (CD_2Cl_2, 125.8 MHz)

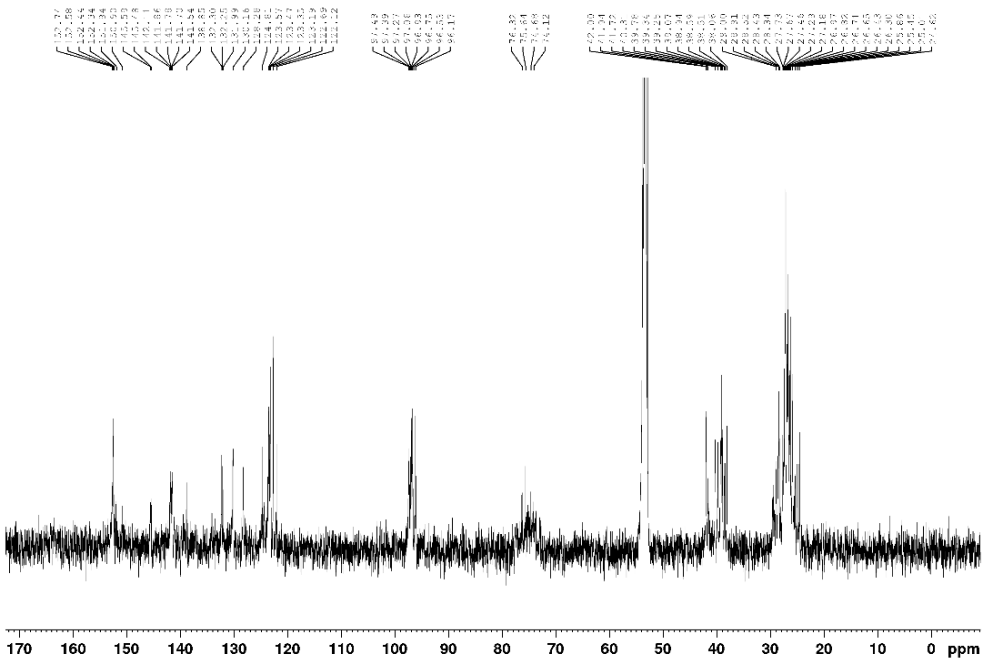

$^{31}P\{^{1}H\}$ NMR Spectrum of **3-C2** (CD_2Cl_2, 202.5 MHz)

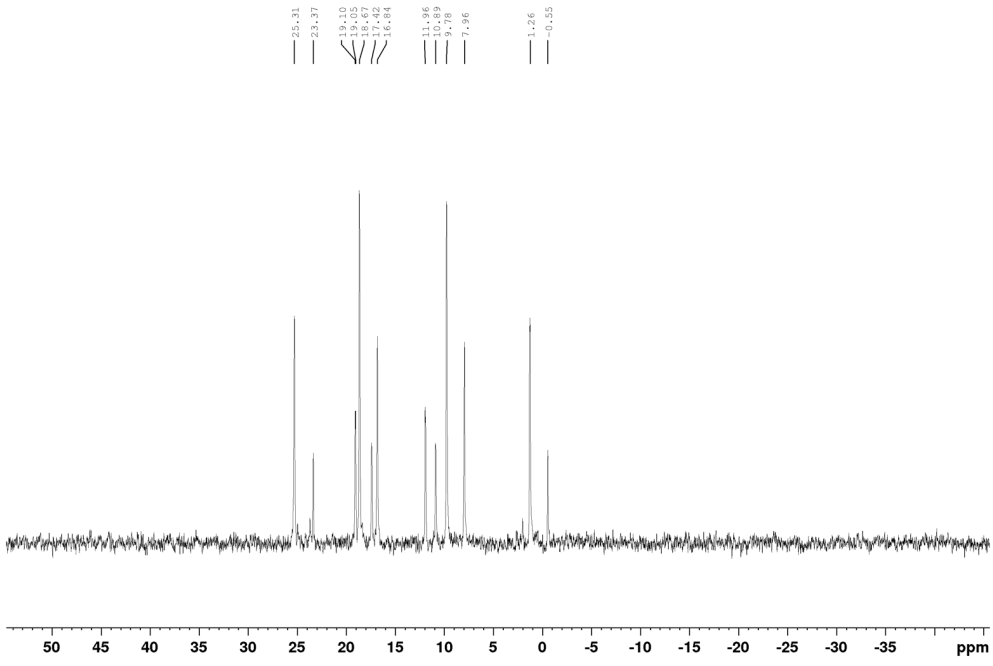

$^{31}P\{^{1}H\}$-$^{31}P\{^{1}H\}$ COSY NMR Spectrum of **3-C2** ($CDCl_3$, 202.5 MHz)

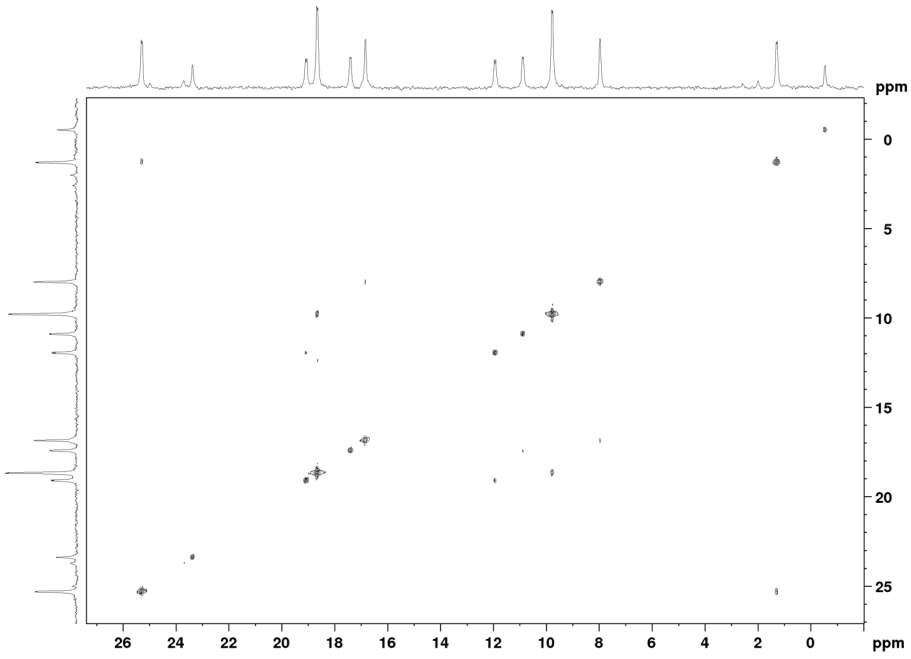

^{1}H NMR Spectrum of ***(2,3-PCg$_2$-quinoxaline)Ni(o-tolyl)Cl***, **3-C3** ($CDCl_3$, 500 MHz)

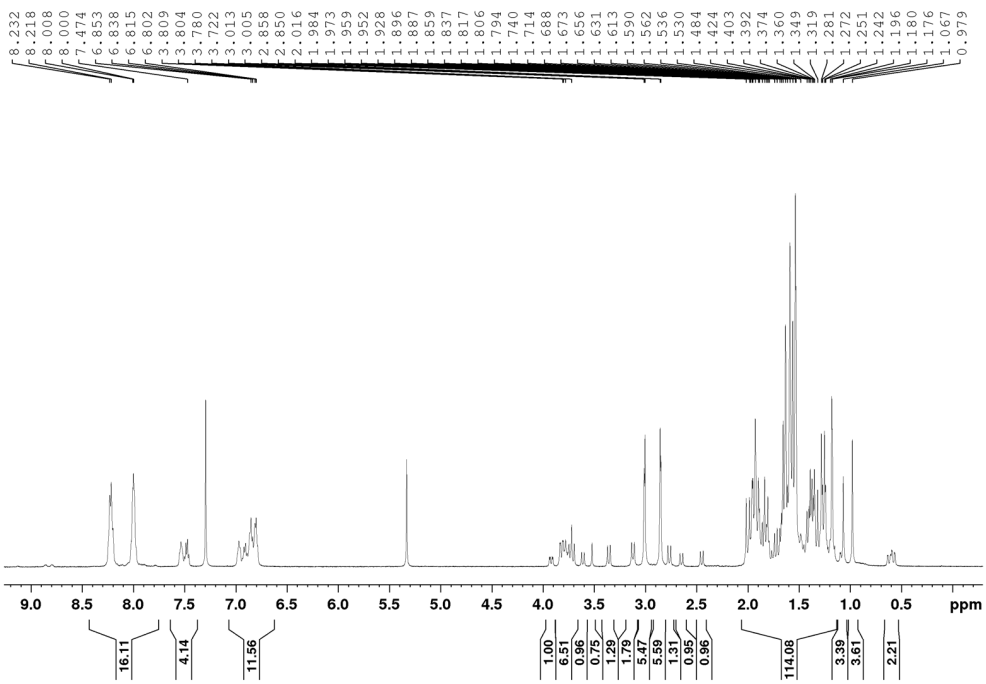

$^{13}C\{^{1}H\}$ UDEFT NMR Spectrum of **3-C3** ($CDCl_3$, 125.8 MHz)

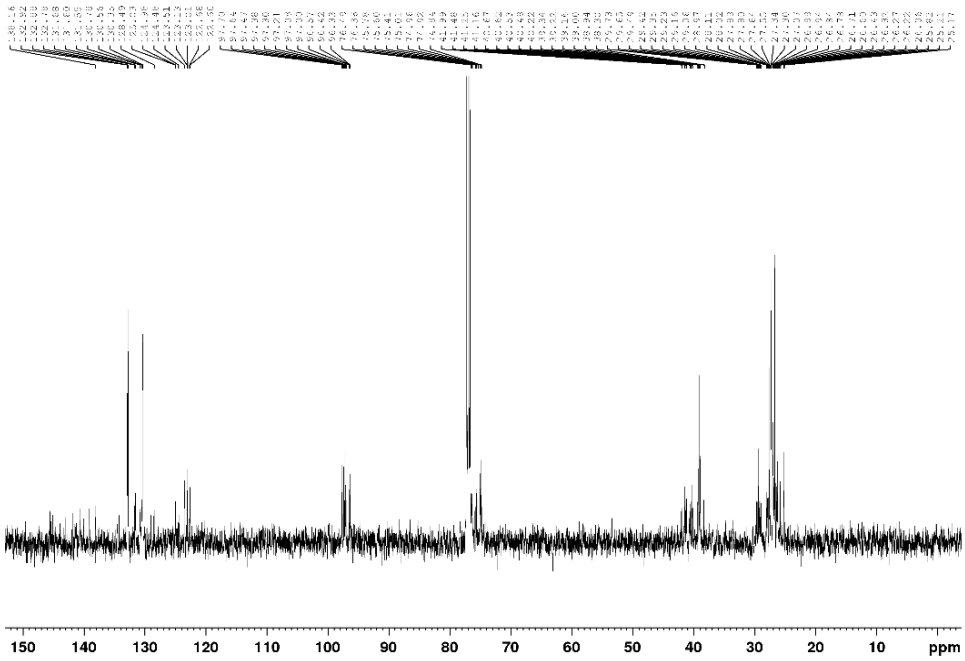

$^{31}P\{^{1}H\}$ NMR Spectrum of **3-C3** (CD_2Cl_2, 202.5 MHz)

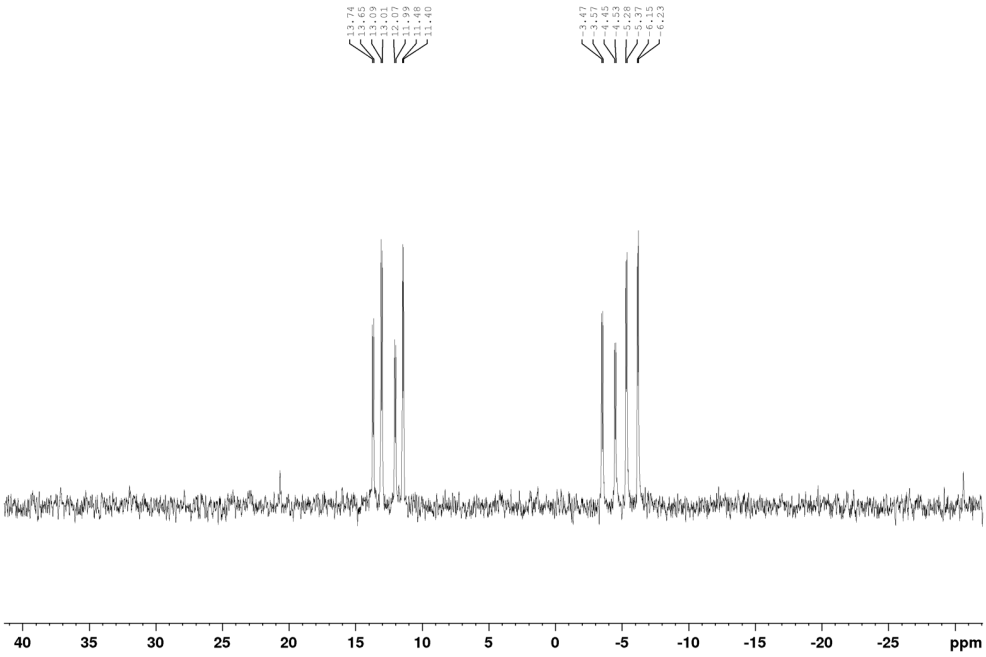

$^{31}P\{^{1}H\}$-$^{31}P\{^{1}H\}$ COSY NMR Spectrum of **3-C3** ($CDCl_3$, 202.5 MHz)

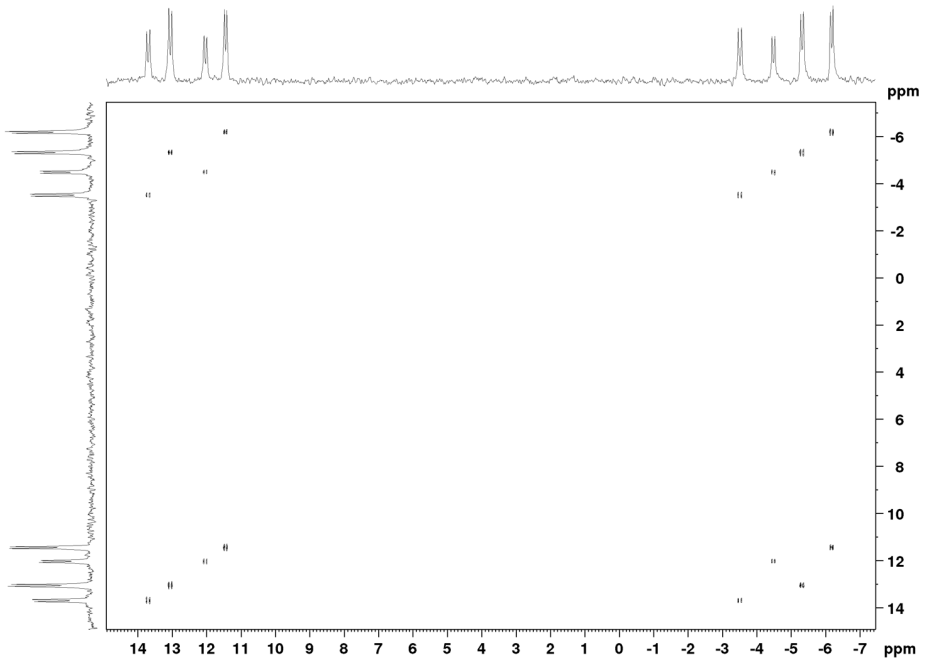

Crystallographic Solution and Refinement Details

Crystallographic data for **1-C1**, (**L**$^{i\mathbf{Pr}}$)Ni(o-tolyl)Cl, **2-L2**, **2-C1**, **2-C2**, **3-L2**, *meso*-**3-L1**, *rac*-**3-L1**, *meso*-**3-L2**, *rac*-**3-L2**, *meso*-**3-L3**, *rac*-**3-L3**, *meso*-**3-C1**, *rac*-**3-C1**, *meso*-**3-C2**, and *meso*-**3-C3** were obtained at or below -80 °C on a Bruker D8/APEX II CCD diffractometer equipped with a CCD area detector using: graphite-monochromated Mo Kα (α = 0.71073 Å) radiation for **1-C1**, **2-C2**, *meso*-**3-L1**, *rac*-**3-L1**, *meso*-**3-L3**, and *rac*-**3-L3**; Cu Kα (α = 1.54178 Å) (microfocus source) radiation for (**L**$^{i\mathbf{Pr}}$)Ni(o-tolyl)Cl, **2-L2, 2-C1**, **3-L2**, *meso*-**3-L2**, *rac*-**3-L2**, *meso*-**3-C1**, *rac*-**3-C1**, *meso*-**3-C2**, and *meso*-**3-C3**, employing samples that were mounted in inert oil and transferred to a cold gas stream on the diffractometers. Data reduction, correction for Lorentz polarization, and absorption correction (Gaussian integration; face-indexed) were each performed. Structure solution by using intrinsic phasing was carried out, followed by least-squares refinement on F^2. All non-hydrogen atoms were refined with anisotropic displacement parameters, while all hydrogen atoms were added at calculated positions and refined by use of a riding model employing isotropic displacement parameters based on the isotropic displacement parameter of the attached atom. In the case of **2-C1**, attempts to refine peaks of residual electron density as disordered or partial-occupancy solvent chloroform chlorine or carbon atoms were unsuccessful. The data were corrected for disordered electron density through use of the SQUEEZE procedure as implemented in *PLATON*.[A24] A total solvent-accessible void volume of 1665 Å^3 with a total electron count of 419 (consistent with 7 molecules of solvent chloroform, or 0.875 molecules per formula unit of the nickel complex) was found in the unit cell. In the case of **2-C2**, the crystal used for data collection was found to display non-merohedral twinning. Both components of the twin were indexed with the program *CELL_NOW* (Bruker AXS Inc., Madison, WI, 2004). The second twin component can be related to the first component by 180º rotation about the [1 0 0] axis in real space and about the [1 0 -1/3] axis in reciprocal space. Integrated intensities for the reflections from the two components were written into a *SHELXL-2014* HKLF 5 reflection file with the data integration program *SAINT* (version 8.38A), using all reflection data (exactly overlapped, partially overlapped and non-overlapped). The refined value of the twin fraction (*SHELXL-2014* BASF parameter) was 0.3422(9). In the case of *rac*-**3-L3**, primed atoms are related to unprimed ones via the crystallographic

twofold rotational axis ($^1/4$, *y*, 0) that passes through the midpoints of the C1–C1', C2–C2', and C4–C4' bonds. In the case of *meso*-**3-C3**, only the major orientation of the disordered tolyl group is shown; attempts to refine peaks of residual electron density as disordered or partial-occupancy solvent chloroform chlorine or carbon atoms were unsuccessful and the data were corrected for disordered electron density through use of the SQUEEZE procedure as implemented in *PLATON,* [A24] whereby a total solvent-accessible void volume of 310 $Å^3$ with a total electron count of 109 (consistent with 2 molecules of solvent chloroform, or 1 additional molecule per formula unit of the Ni complex) was found in the unit cell.

Copyright Agreements

Content in Chapter 2 is reproduced with permission from J. S. K. Clark, C. M. Lavoie, P. M. MacQueen, M. J. Ferguson, M. Stradiotto. *Organometallics*, **2016**, *35*, 3248-3254. Copyright 2016 American Chemical Society.
Content in Chapter 3 is reproduced with permission from J. S. K. Clark, C. N. Voth, M. J. Ferguson, M. Stradiotto. *Organometallics*, **2017**, *36*, 679-686. Copyright 2017 American Chemical Society.
Content in Chapter 4 is reproduced with permission from J. S. K. Clark, R. T. McGuire, C. M. Lavoie, M. J. Ferguson, M. Stradiotto. *Organometallics*, **2019**, *38*, 167-175. Copyright 2019 American Chemical Society.

JOHN WILEY AND SONS LICENSE
TERMS AND CONDITIONS

Dec 05, 2019

This Agreement between Dalhousie University -- Jillian Clark ("You") and John Wiley and Sons ("John Wiley and Sons") consists of your license details and the terms and conditions provided by John Wiley and Sons and Copyright Clearance Center.

License Number	4722441224497
License date	Dec 05, 2019
Licensed Content Publisher	John Wiley and Sons
Licensed Content Publication	Angewandte Chemie International Edition
Licensed Content Title	PAd2-DalPhos Enables the Nickel-Catalyzed C–N Cross-Coupling of Primary Heteroarylamines and (Hetero)aryl Chlorides
Licensed Content Author	Jillian S. K. Clark, Michael J. Ferguson, Robert McDonald, et al
Licensed Content Date	Apr 1, 2019
Licensed Content Volume	58
Licensed Content Issue	19
Licensed Content Pages	5
Type of Use	Dissertation/Thesis
Requestor type	Author of this Wiley article
Format	Print and electronic
Portion	Full article
Will you be translating?	No
Title of your thesis / dissertation	Investigating the Design of Bisphosphine Ligands for use in Nickelcatalyzed C(sp2)-N Cross-Coupling
Expected completion date	May 2020
Expected size (number of pages)	245

Appendix References

A1. C. M. Lavoie, P. M. MacQueen, N. L. Rotta-Loria, R. S. Sawatzky, A. Borzenko, A. J. Chisholm, B. K. V. Hargreaves, R. McDonald, M. J. Ferguson, M. Stradiotto, *Nat. Commun.* **2016,** *7*, 11073.

A2. S. Voth, J. W. Hollett, J. A. McCubbin, *J. Org. Chem.* **2015,** *80*, 2545-2553.

A3. Q. Shen, T. Ogata, J. F. Hartwig, *J. Am. Chem. Soc.* **2008,** *130*, 6586-6596.

A4. S. Z. Ge, R. A. Green, J. F. Hartwig, *J. Am. Chem. Soc.* **2014,** *136*, 1617-1627.

A5. D. Weickmann, W. Frey, B. Plietker, *Chem. Eur. J.* **2013,** *19*, 2741-2748.

A6. Q. Shen, J. F. Hartwig, *Org. Lett.* **2008,** *10*, 4109-4112.

A7. J. W. Park, Y. K. Chung, *ACS Catal.* **2015,** *5*, 4846-4850.

A8. D. Mendoza-Espinosa, R. González-Olvera, C. Osornio, G. E. Negrón-Silva, A. Álvarez-Hernández, C. I. Bautista-Hernández, O. R. Suárez-Castillo, *J. Organomet. Chem.* **2016,** *803*, 142-149.

A9. N. F. F. Nathel, J. Kim, L. N. Hie, X. Y. Jiang, N. K. Garg, *ACS Catal.* **2014,** *4*, 3289-3293.

A10. A. Heydari, A. Arefi, M. Esfandyari, *J. Mol. Catal. A: Chem* **2007,** *274*, 169-172.

A11. M. A. Topchiy, P. B. Dzhevakov, M. S. Rubina, O. S. Morozov, A. F. Asachenko, M. S. Nechaev, *Eur. J. Org. Chem.* **2016,** *2016*, 1908-1914.

A12. S. Zhou, Z. Yang, X. Chen, Y. Li, L. Zhang, H. Fang, W. Wang, X. Zhu, S. Wang, *J. Org. Chem.* **2015,** *80*, 6323-6328.

A13. L. Strekowski, S. E. Patterson, L. Janda, R. L. Wydra, D. B. Harden, M. Lipowska, M. T. Cegla, *J. Org. Chem.* **1992,** *57*, 196-201.

A14. C. M. So, Z. Zhou, C. P. Lau, F. Y. Kwong, *Angew. Chem. Int. Ed.* **2008,** *47*, 6402-6406.

A15. S. Doherty, J. G. Knight, J. P. McGrady, A. M. Ferguson, N. A. B. Ward, R. W. Harrington, W. Clegg, *Adv. Synth. Catal.* **2010,** *352*, 201-211.

A16. S. M. Crawford, C. B. Lavery, M. Stradiotto, *Chem. Eur. J.* **2013,** *19*, 16760-16771.

A17. B. S. Lane, D. Sames, *Org. Lett.* **2004,** *6*, 2897-2900.

A18. D. W. Old, M. C. Harris, S. L. Buchwald, *Org. Lett.* **2000,** *2*, 1403-1406.

A19. M. Vellakkaran, K. Singh, D. Banerjee, *ACS Catal.* **2017,** *7*, 8152-8158.

A20. M. A. McGowan, J. L. Henderson, S. L. Buchwald, *Org. Lett.* **2012,** *14*, 1432-1435.

A21. D. P. Wang, D. Z. Kuang, F. X. Zhang, Y. Liu, S. H. Ning, *Tetrahedron Lett.* **2014,** *55*, 7121-7123.

A22. T. J. Donohoe, M. A. Kabeshov, A. H. Rathi, I. E. D. Smith, *Org Biomol Chem* **2012,** *10*, 1093-1101.

A23. J. Clifton, E. R. M. Habraken, P. G. Pringle, I. Manners, *Catal. Sci. Technol.* **2015,** *5*, 4350-4353.

A24. A. L. Spek, *Acta Crystallogr C* **2015,** *C71*, 9-18.